UNIVERSITÉ DE CAEN BASSE-NORMANDIE

Mémoire d'habilitation

Contribution à l'analyse asymptotique des coques élastiques minces. Homogénéisation et modélisation des microstructures complexes

présenté par

Philippe Karamian

le 28 novembre 2014

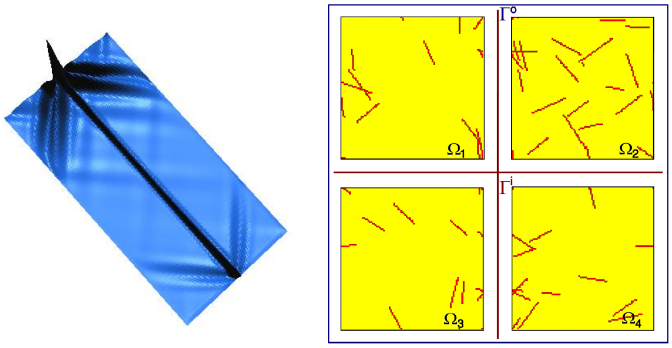

Rapporteurs:

Mme. Hélène Dumontet , Professeur, Université Paris VI, IJLRDA,

M. Nicolas Forcadel , Professeur, INSA de Rouen, LMI,

M. Olivier Polit , Professeur, Université Paris X, LEME EA Nanterre,

Examinateurs:

M. Alain Campbell, Professeur émérite, UCBN Caen, LMNO,

M. Franck Delvare , Professeur, UCBN Caen, LMNO,

M. Évariste Sanchez-Palencia, Directeur de recherche CNRS émérite Université Paris VI, IJLRDA,

Remerciements

En premier lieu, je tiens à exprimer toute ma gratitude envers le Professeur émérite Alain Campbell, qui a été mon enseignant puis un collègue et maintenant un ami, et qui a su me faire entièrement confiance pour encadrer son étudiant en thèse Willy Leclerc.

Le Professeur Alain Campbell a suivi ces travaux et a rédigé le rapport qui a ouvert la voie de cette habilitation. Je tiens également à remercier Madame le Professeur Sanchez-Hubert qui m'a ouvert les portes de la recherche en étant tour à tour mon enseignant et mon directeur de thèse.

Durant ces années, le travail de recherche que j'ai effectué au sein du LMNO, Laboratoire de Mathématiques Nicolas Oresme, est le fruit d'une collaboration avec Madame le Professeur Jacqueline Sanchez-Hubert, Monsieur le directeur de recherche Evariste Sanchez-Palencia, Monsieur Alexandre Vivet et celui de doctorants et des étudiants en Master effectuant leurs projets de recherche au sein de notre laboratoire - que je remercie et dont les travaux ont contribué à la conception de ce mémoire.

Je remercie vivement Madame le Professeur Hélène Dumontet, Messieurs les Professeurs Nicolas Forcadel et Olivier Polit qui ont accepté d'évaluer l'ensemble de mes travaux de recherche.

Je tiens également à remercier tous les membres du jury qui me font l'honneur de participer à la soutenance, et encore une fois les rapporteurs qui ont pris la peine de lire avec intérêt les articles présentés ainsi que le mémoire.

Je souhaite remercier tous mes collègues et amis et en particulier, Nathalie Leblond, Adil Ridha, André Sesboüé et Daniel Choi ... et tous les autres, trop nombreux pour être tous cités ici, avec lesquels j'ai eu le plaisir de collaborer depuis une douzaine d'années. Je remercie le personnel du secrétariat pour leur aide, leur disponibilité et leur gentillesse.

Enfin, je tiens tout particulièrement à remercier ma famille pour leur soutien, l'affection et l'amour qu'ils me témoignent chaque jour et aussi pour la joie et le bonheur qu'ils m'apportent. Je leur dédie ce mémoire et qu'ils puissent y voir tout mon amour, l'admiration et l'affection que j'éprouve pour eux.

À mes chers parents,

À Patricia, Emma et Baptiste

Table des matières

Avant-propos

Ce mémoire retrace mes activités de recherche depuis ma soutenance de thèse intervenue en mai 1999 au sein du laboratoire de Mécanique de l'Université de Caen Basse-Normandie. Ce travail porte sur l'étude des coques élastiques minces hyperboliques. Par la suite, j'ai bénéficié d'une bourse de l'académie des sciences pour poursuivre les travaux que j'avais initiés sur le phénomène de pseudo-reflexion des singularités dans les coques minces.

Désireux d'évoluer et de découvrir d'autres aspects de la recherche appliquée, j'ai décidé d'effectuer un post-doctorat au sein du GIN (Groupe d'Imagerie Neurofonctionnelle). L'objectif du postdoc était de traiter une grande base de données d'images du cerveau humain acquises par l'IRM (Imagerie par Résonance Magnétique). Il s'agissait de mettre en place une procédure de détection et de classification automatique des différentes lésions tels que HSB, AVC, (hyper substance blanche, accident vasculaire cérébral de nature ischémique) du cerveau et de participer à la conception et l'élaboration d'un outil d'aide au diagnostic pour les radiologues d'une part et d'autre part de mener une étude épistémiologique d'une tranche de la population française agée de plus de 65 ans afin d'établir d'éventuelles corrélations entre différents facteurs tels que l'hypertension, le sexe, l'âge, les traitements médicamenteux et l'apparition des lésions au sein du cerveau.

Parallèlement j'ai continué à travailler sur la théorie des coques minces en collaboration avec Madame Sanchez-Hubert et Monsieur Sanchez-Palencia, ce qui m'a permis dans un premier temps d'être recruté sur un poste d'ATER en mécanique dans le laboratoire de Mécanique de l'Université de Caen en 2001 puis d'y être nommé maître de conférences en 2002. Cette collaboration intense a permis d'étudier de manière approfondie les couches limites, les couches internes, la propagation des singularités dans les coques élastiques minces. Suite à mes travaux sur la notion de pseudo-réfexion introduite dans ma thèse, une approche beaucoup plus théorique du phénomène de pseudo-réflexion a été entamée pour mieux comprendre et cerner ce mécanisme qui ressemble à de la réflexion mais qui n'en est pas une.

Durant ma thèse, j'ai développé un code de calcul adapté pour effectuer des calculs concernant le problème limite réduit dans le cas où les forces extérieures sont convenablement choisies, c'est-à-dire satisfaisant des critères relatifs aux espaces fonctionnels issus du problème membranaire. Ce code est écrit en langage C++. Dès lors j'ai poursuivi son développement pour traiter des problèmes thermiques, élastiques, et des structures minces comme les plaques et les coques ainsi que les outils pour le calcul des coefficients homogénéisés des matériaux composites.

En outre, je continue à étudier à la fois d'un point de vue théorique et numérique le phénomène de réfraction en présence de plis dans les coques élastiques minces. Je poursuis le développement des outils informatiques nécessaires pour effectuer les simulations numériques afin d'exhiber les phénomènes de réfraction numérique. Ce travail m'a conduit à soumettre un article dont je suis seul auteur dans European Journal of Mechanics-A/Solids.

Ma volonté de mener une recherche plus appliquée, mes préoccupations environnementales, sociétales et l'idée d'être plus proche des préoccupations du citoyen m'ont conduit à collaborer avec des chercheurs et des partenaires industriels dans l'étude de nouveaux matériaux de haute technologie, bio-sourcés qui sont au centre des préoccupations des scientifiques et des enjeux technologiques et industriels. Cette approche m'a amené à co-encadrer une thèse avec Alexandre Vivet du CIMAP (Centre de Recherche sur les ions Lourds, les Matériaux et la Photonique) sous la direction du professeur Alain Campbell. Cette thèse a été soutenue le 7 novembre 2013. Cette collaboration de par la mutualisation de nos compétences respectives fut fructueuse, comme en témoignent les publications qui en découlent.

L'expérience acquise dans le domaine de la modélisation, la conception de VER (Volume Élémentaire Représentatif) et l'évaluation numérique des propriétés mécaniques des composites renforcés en fibres courtes par les techniques d'homogénéisation double-échelle et la maîtrise des outils de simulation m'ont ouvert les portes du milieu industriel. Je pense en particulier au projet ACCEA (Amélioration des Conductivités des Composites pour les Équipements Aéronautiques) financé par des partenariats industriels tels que Zodiac aerospace, Safran, Arkema, Dedienne, Thales, Lifco, Adcis et le FUI (Fonds unique interministériel). Aussi ai-je pu obtenir dans le cadre de ce projet le financement d'une thèse sur trois ans et d'un postdoctorat de deux ans que j'encadre en collaboration avec Monsieur Daniel Choi du LMNO. Nous avons travaillé en binôme sur le contrat de la socité CMEG (Cooperative Métropolitaine Entreprise Générale) pour réaliser une étude d'interaction sol-structure d'un ouvrage à la demande du GANIL (Grand Accélérateur National de Ions Lourds) sous chargement sismique.

Ce manuscrit est divisé en deux parties. Les deux parties sont totalement indépendantes, les problématiques sont de prime abord assez théoriques, du moins dans la première partie, alors que la seconde partie est plus une approche de modélisation et de simulation numérique laquelle peut trouver aussi bien un écho auprès du milieu académique qu'industriel. Enfin, le manuscrit se termine par un bilan et les perspectives de mon travail. En annexe, se trouve dans l'ordre chronologique les articles publiés dans des revues internationales sur lesquels s'appuie le mémoire.

Introduction générale

La modélisation et la simulation numérique des structures minces telles que les coques et celles des composites ont depuis plusieurs décennies suscité l'engouement et la mobilisation de nombreux chercheurs. L'avènement des nouveaux matériaux composites et l'usage des structures ultra-minces, permettront de concevoir entre autres les moyens de transport de demain, ultra-légers, robustes et moins énergivores ce qui intéresse tout particulièrement les secteurs de l'automobile, aéronautique et spatial. Les premières répercussions sont déjà palpables pour le consommateur, je pense notamment au secteur du sport et des loisirs (raquettes de tennis, cadres de vélo, planches à voile en fibres biosourcées comme le lin). Il nous faut donc être capable de concevoir des modèles suffisamment précis, fiables et robustes. Récemment, les méthodes asymptotiques ont été employées avec succès pour justifier de manière rigoureuse la théorie des coques minces linéaire et non linéaire à partir de l'élasticité tridimensionnelle [61, 62] d'une part et d'autre part la démarche en double-échelle introduite par Sanchez-Palencia pour l'homogénéisation des matériaux composites a été très féconde. En parallèle, les récents progrès enregistrés par les moyens de calcul et l'accès au centre de calcul haute performance et des logiciels de plus en plus performants permettent aujourd'hui d'entrevoir la possibilité d'appréhender des modèles numériques de plus en plus complexes et ambitieux capables de relever les défis et les enjeux que représentent les structures ultra-minces et les nouveaux matériaux.

Le mémoire est organisé en deux parties. Chaque partie est traitée par ordre chronologique. Le premier axe de recherche traite des coques élastiques minces et de leur traitement numérique. Nous nous intéressons plus particulièrement aux cas des coques hyperbolique et parabolique en présence de données singulières. Ces dernières sont à l'origine des couches internes, de la propagation des singularités et du phénomène de pseudo-réflexion, dont l'étude nécessite de faire appel aux développements asymptotiques. Le second axe aborde les études des matériaux composites à microstructures complexes. Cela va de la mise en place et la conception informatique des échantillons pour fabriquer en vue d'un traitement numérique par la méthode des échelles multiples pour évaluer les propriétés effectives des matériaux.

Chaque partie correspond respectivement à cinq articles publiés que l'on trouvera dans l'annexe A. Les références bibliographiques ont été regroupées et les renvois dans le texte sont indiqués par un numéro.

Mon travail de recherche depuis la thèse concerne deux thématiques distinctes bien qu'il existe plusieurs points communs entre elles. Un des points communs est l'usage des méthodes et techniques de développement asymptotiques pour étudier l'influence des petits paramètres aussi bien pour la théorie des coques minces que pour l'étude des matériaux composites par la méthode double-échelle introduite par Sanchez-Palencia [58]. L'autre aspect également non négligeable est l'usage des techniques numériques comme les éléments finis, la décomposition de domaine ou le calcul parallèle pour accélérer la résolution des équations aux dérivées partielles qui régissent le comportement des coques minces et des matériaux composites.

Le premier paragraphe de mon introduction rappelle quelques-unes des problématiques concernant les coques élastiques minces inhibées en flexion lorsque l'épaisseur de la coque est faible et les difficultés rencontrées lors des simulations numériques. Le second paragraphe s'intéresse plus particulièrement aux composites à microstructures complexes. La complexité se situe à deux niveaux : l'hétérogénéité seule d'une part, et d'autre part le réseau associé.

Étude des coques élastiques minces : cas des surfaces réglées

En mécanique, le terme, coque mince, désigne communément une structure tridimensionnelle pour laquelle une des dimensions, qualifiée d'épaisseur, est très petite vis à vis des deux autres. Il est d'usage de représenter une coque mince comme étant un corps élastique de petite épaisseur dont la forme est proche d'une surface mathématique. De par la légèreté qu'offrent ces structures minces, due à leur faible épaisseur, et la rigidité que leur confère leur courbure intrinsèque, l'industrie automobile, aéronautique, aérospatiale et même l'architecture moderne et contemporaine en font un grand usage pour concevoir des moyens de transport ultra-légers, résistants ainsi que des prouesses architecturales.

Un des enjeux majeurs concernant les coques minces voire même très minces est de disposer de modèles fiables, efficaces, faciles à mettre en oeuvre et peu coûteux en temps de calcul pour que le milieu industriel puisse s'en saisir. En conséquence il est important de disposer de modèles précis permettant de faire des simulations et des calculs numériques fiables des déplacements et des déformations sous l'action des forces extérieures supposées suffisamment petites pour que la coque déformée reste proche de son état naturel.

Lorsque l'épaisseur de la coque est faible, son comportement mécanique est assez bien décrit par celui de sa surface moyenne, ce qui en théorie asymptotique revient à dire qu'il est voisin du comportement de la coque lorsque son épaisseur ε tend vers zéro [59, 60]. En outre, le comportement de la coque mince est très différente selon que sa surface moyenne est ou non géométriquement rigide, on parle alors de coques inhibées ou non inhibées selon la terminologie introduite dans [62]. Nous rappelons que la rigidité géométrique d'une surface, au sens qui convient en théorie

des coques, consiste en la non existence de déplacements inextensionnels. Gardons à l'esprit que pour une surface non inhibée, la structure présente de grandes faiblesses tant et si bien que lors des simulations numériques ces faiblesses peuvent passer inaperçues. Dans le cas d'une coque dont la surface moyenne est inhibée, ce qui est le coeur de ma thématique de recherche, le problème limite est bien posé, on parle plus couramment de *coques membranaires*, mais on observe dans ce cas une perte de régularité des solutions liée à l'existence des couches limites, des couches internes, et à l'apparition des phénomènes de propagation des singularités et de la notion de pseudo-réflexion [28] que j'ai introduite lors de ma thèse.

Cependant, pour certaines géométries des coques même inhibées, le problème limite peut conduire à la sensitivité [18, 44] relativement aux données. De par le fait que ces problèmes sont mal posés, ils rendent du même coup la simulation numérique de ce type de coques très difficile voire impossible dans certains cas. On ne peut observer qu'une approximation qualitative voire quantitative du comportement des coques sensitives mais aucune garantie ne peut être apportée sur la fiabilité des résultats numériques. Le seul attrait de la simulation numérique est qu'elle conforte les résultats théoriques et vient compléter en terme d'illustration les effets de la sensitivité.

Pour éclairer le lecteur, il convient d'avoir à l'esprit certaines idées fondamentales. Dans le cas qui me préoccupe, un point fondamental dans les coques inhibées, est que contrairement à ce que l'on pourrait croire, la convergence des solutions numériques vers la solution appartenant à l'espace de travail V n'est pas uniforme par rapport à l'épaisseur de la coque (ε). Ceci est dû au fait, qu'au mieux, la solution exacte converge vers un élément de l'espace V^0 associé à la forme membranaire, ce qui se traduit mathématiquement par le fait que la norme $||u^\varepsilon||_V$ n'est pas bornée dans V car si tel était le cas, sa limite appartiendrait à V. En d'autres termes, puisque $u^\varepsilon \to u^0$ dans V^0 avec $u^0 \notin V$, aussi u^ε exhibe des couches limites où, dans une petite épaisseur $\delta(\varepsilon)$, la fonction ou certaines de ses dérivées présentent de fortes et brutales variations qui tendent vers l'infini. En conséquence pour bien approximer la solution, il est nécessaire de raffiner suffisamment le maillage dans les couches limites. En dehors des couches limites un maillage plus grossier suffit. En conséquence on voit la dépendance du pas de maillage par rapport à l'épaisseur ε. En outre, le calcul correct dans la couche est nécessaire pour avoir un calcul correct de la solution à l'extérieur de cette couche, autrement dit, les erreurs se propagent de la couche vers l'extérieur de la couche. La connaissance des couches apparaît donc fondamentale pour construire des maillages efficaces.

Tout ces points qui viennent d'être évoqués, nous ont amené à étudier de près les couches limites et les couches internes pour différents types de coques, ainsi que la propagation des singularitées et le phénomène de pseudo-réflexion pour les coques hyperboliques. L'ensemble de ce travail a fait l'objet de plusieurs publications dans des revues spécialisées.

Dans un premier temps, le travail a donc consisté à concevoir un problème modèle pour étudier le phénomène de couches limites lesquelles apparaissent dans la

théorie de coques élastiques minces quand l'épaisseur ε tend vers zéro. Pour $\varepsilon = 0$, il s'agit d'un problème parabolique, en conséquence cela concerne les surfaces développables. À partir de ce problème modèle, on met en évidence les couches internes associées à la propagation des singularités le long des caractéristiques. De par la particularité du problème limite on exhibe des solutions qui présentent des singularités lesquelles font intervenir des distributions le long des caractéristiques. Les couches le long des caractéristiques ont une structure particulière incluant des sous-espaces ; les multiplicateurs de Lagrange correspondants sont mis en évidence. Les calculs numériques montrent l'avantage de l'utilisation de maillages adaptés dans ce type de problèmes. [31]. Les résultats issus du problème modèle ont été appliqués aux cas des coques élastiques minces dont la surface moyenne est développable [32], en d'autres termes les coques paraboliques.

Dans un second temps, une étude consacrée à la propagation des singularités et l'étude des structures des couches internes dans le cas des coques hyperboliques est abordée. Une attention toute particulière est donnée aux couches internes associées à la propagation des singularités le long des caractéristiques. L'étude a permis de déterminer l'ordre de grandeur de l'épaisseur des couches internes aussi bien dans le cas des courbes caractéristiques que non caractéristiques. Ainsi la connaissance des structures des couches internes qu'elles soient ou non caractéristiques nous permet de mailler efficacement et de procéder ainsi à de l'adaptation de maillage. Il en résulte encore une fois, que l'approximation par les éléments finis ne peut pas être uniforme et qu'elle dépend bien de l'épaisseur ε de la coque [33]. Enfin, la notion de pseudo-réflexion introduite pendant ma thèse, a été étudiée de manière plus approfondie et généralisée. Il s'agissait d'étudier le phénomène qui ressemble à une réflexion lorsqu'une singularité se propage le long d'une caractéristique et lorsque celle-ci intercepte une frontière. Nous verrons que selon la nature de la singularité et de son support celle-ci se retrouve réfléchie selon l'autre direction caractéristique tout en gagnant un degré de régularité. C'est ce phénomène que je qualifie de pseudo-réflexion [35].

Matériaux composites à microstructures complexes

Pour estimer les propriétés d'un matériau composite on peut effectuer des mesures expérimentales par divers essais mécaniques comme la traction, la compression, la flexion ... Pour un certain matériau composite envisagé, le coût de fabrication élevé des éprouvettes et l'impossibilité de faire un très grand nombre d'essais en réduisent la portée notamment dans le cadre des composites dont la répartition spatiale des renforts est hétérogène. Pour le scientifique comme pour l'industriel, il est plus intéressant de disposer d'outils pour anticiper les propriétés mécaniques, thermiques, électriques d'un composite avant sa fabrication. Outre, le fait qu'un tel outil permet de se focaliser sur des questions d'optimisation, il permet également de jouer avec différents paramètres comme les dimensions des renforts ou leur répartition spatiale lesquelles influent sur la réponse mécanique, la conduction thermique ou électrique ce qui est inenvisageable dans un contexte expérimental. Ajoutons à cela que l'étude des nanocomposites pour lesquelles les échelles mises en jeu altèrent la fiabilité des

mesures expérimentales conduisent à concevoir des modèles analytique et numérique ouvrant ainsi la voie à la prédiction à priori des propriétés mécaniques de diverses sortes de composite.

Un autre moyen pour estimer les propriétés d'un matériau composite est l'approche analytique. L'approche analytique s'appuie sur des lois empiriques permettant ainsi de décrire le comportement mécanique des matériaux. L'idée sous-jacente est que les efforts intérieurs sont reliés aux déformations. Plusieurs modèles et bornes ont été imaginés, parmi lesquels citons les plus célèbres d'entre elles, les bornes de Voigt et Reuss, de Hashin-Shtrikman [22] et le modèle de Mori-Tanaka [52]. Certaines approches analytiques se contentent de donner des bornes et les autres modèles analytiques sont dédiés à des configurations simples et par conséquent, ils ne pouvent se transposer tels quels à des composites ayant une microstructure complexe, plus réaliste tout en faisant intervenir également des échelles différentes.

Les contraintes, les limitations et la non universalité des approches analytiques et expérimentales nous conduisent donc tout naturellement vers une troisième voie qu'est la simulation numérique dont le principal objectif est de surmonter les écueils des deux précédentes approches. Dans une telle approche, la question qui taraude le scientifique est la validité du ou des modèles sous-jacents relative aux simulations numériques. De par la complexité du réseau au sein des composites, il semble illusoire d'approcher la morphologie et le comportement du milieu hétérogène car cela demande une modélisation très fine et par conséquent cela devient très gourmand en temps de calcul. En dépit des performances qu'affichent les nouveaux ordinateurs et les moyens mis à la disposition des chercheurs par le biais des centres de calcul haute performance pour effectuer des simulations numériques, nous sommes contraints de reconnaître qu'il faut opérer des simplifications et par voie de conséquence nous essayons de bâtir un ou des modèles numériques avec toute la cohorte d'imperfections que cela implique. Cependant, le fait de pouvoir jouer avec les différents paramètres laisse entrevoir la possibilité de créer, de modifier, de corriger donc d'améliorer le ou les modèles pour mieux coller à la réalité et à la complexité du problème.

Je m'intéresse essentiellement à des composites à microstructures complexes. Puisqu'il est quasi impossible d'étudier la totalité du matériau composite, les scientifiques se sont donc tournés vers la notion de volume élémentaire. Le plus souvent il s'agit d'un motif périodique ou non, représentant la géométrie de la microstrucure du composite. Se posent alors les questions relatives aux *bonnes* dimensions que doit avoir cet échantillon pour représenter toute la diversité, la richesse et l'hétérogénéité de la microstructure. Ceci nous amène au concept de volume élémentaire représentatif qui doit être vu comme la brique élémentaire susceptible de générer le matériau composite. Pour la conception des volumes élémentaires représentatifs, j'ai fait le choix de les concevoir à partir d'un jeu de paramètres morphologiques sur lesquels j'ai une totale maîtrise. Ainsi, nous avons la possibilité de jouer avec différents paramètres tels que la répartition spatiale du réseau, les dimensions et le taux de chargement des hétérogénéités. Cette approche me permet donc d'engendrer de manière automatisée un grand nombre de petits volumes élémentaires représentatifs. L'idée sous-jacente est de pouvoir générer pour tout type d'hétérogénéités et

diverses complexités envisagées, une géométrie et un maillage fiables permettant une estimation efficace des propriétés mécaniques du composite par homogénéisation.

Pourquoi une telle démarche me direz-vous ? L'idée est de mieux comprendre le rôle exact de chacun des paramètres d'une part, et d'autre part être en mesure d'estimer l'impact de phénomènes physiques qui reste à ce jour mal compris en dépit de nombreuses études. Je pense plus particulièrement à la décohésion à l'interface entre les hétérogénéités et la matrice, les perturbations locales de la matrice dans la zone d'interphase entourant les hétérogénéités. Une conjecture, demandant à être validée, est que l'interface et la zone d'interphase seraient à l'origine du mauvais transfert des contraintes entre la matrice et le renfort. Par ailleurs, une meilleure connaissance des rôles joués par les différents paramètres morphologiques et phénoménologiques conduirait à mieux comprendre l'impact réel de ces phénomènes selon leurs caractéristiques. En outre, dans un cadre industriel il n'est pas illusoire de penser qu'une configuration optimale pourrait se dégager pour les paramètres morphologiques.

Je me suis donc attaché tout particulièrement à mettre en place une stratégie efficace pour répondre à la problématique de l'évaluation fiable et automatisée des propriétés élastique, thermique ou électrique de milieux à microstructures complexes. Dans les articles, nous nous sommes bornés aux propriétés mécaniques mais il va de soi que cela s'applique également à d'autres problèmes tels que la conductivité thermique et électrique sans grande difficulté. Pour déterminer les tenseurs homogénéisés, le choix s'est tout naturellement porté sur la technique d'homogénéisation multi-échelle développée par Sanchez-Palencia [58] elle-même résolue par la méthode des éléments finis. Le processus s'avère puissant dans la prise en compte de la morphologie, des contrastes, de la répartition spatiale des hétérogénéités ainsi que la complexité du réseau constituant le milieu. Outre le fait que la méthode reste sensible aux dimensions du volume élémentaire ainsi qu'à la nature des conditions aux limites une bonne approximation de l'interface est nécessaire pour une meilleure estimation des champs de gradients pour une meilleure estimation du tenseur de rigidité du composite.

Il est d'usage d'utiliser un panel de données statistiques pour générer la microstructure au sein d'un motif représentatif. À ce titre, deux écoles s'affrontent, l'une d'entre elles est basée sur des contraintes spécifiques de non contact et non interpénétrabilité entre les hétérogénéités, il s'agit de la méthode d'adsorption séquentielle aléatoire. Dans l'approche alternative, on s'affranchit de ces contraintes et on autorise l'interpénétration tout comme l'enchevêtrement. Cette dernière approche est moins coûteuse tout en respectant les lois statistiques décrivant les réseaux d'hétérogénéités. C'est cette approche qui a retenu mon attention car moins étudiée. Par ailleurs, l'approche aléatoire a été retenue pour générer efficacement et de façon automatique les microstructures.

La méthode d'homogénéisation multi-échelle retenue pour déterminer les tenseurs homogénéisés conduit à la résolution d'une série d'équations aux dérivées partielles dont les solutions sont approchées par la méthode des éléments finis. Dans une telle approche, nous devons donc générer les maillages des volumes élémentaires

représentatifs. La réponse est fournie par la méthode d'approximation par grille, plus connue sous les termes de pixelisation en 2D et de voxelisation en 3D [53]. Cette méthode permet de traiter la complexité des microstructures présentes au sein des composites en vue d'une résolution par éléments finis, néanmoins elle nécessite des adaptations pour la rendre plus efficace [7].

Dans un but d'efficacité le calcul parallèle est une stratégie efficace dans la réduction des coûts de calcul. Afin de décupler les effets du calcul parallèle je me suis tout naturellement orienté vers la décomposition de domaine. En effet, dans le contexte des techniques de décomposition de domaine, la parallélisation peut être menée de front sur deux niveaux. On commence par partitionner en plusieurs sous-domaines chaque volume élémentaire représentatif lesquels sont maillés de façon indépendante, ensuite on effectue l'estimation des propriétés mécaniques de chaque sous-domaine tout en intégrant la résolution d'un problème d'interface. Mon choix s'est porté sur le complément de Schur [1] et Feti [55].

Il s'agit d'un travail collaboratif entre des étudiants que j'ai encadrés durant leur projet de recherche et en particulier avec Willy Leclerc. La contribution de Willy Leclerc a permis à l'équipe de mettre en place des stratégies efficaces et optimisées dans la génération de maillage des volumes élémentaires représentatifs sous Castem [8]. De par son envie d'apprendre et son ouverture d'esprit aux nouvelles techniques et technologies, Il a su être d'une aide précieuse dans la programmation de la méthode de décomposition de domaine, de même quand il a fallu passer à la parallélisation des codes de calcul écrit en C++. Par ailleurs, nous avons pu disposer de créneaux de calcul auprès d'un mésocentre de calcul dénommé CRIHAN qui est basé à Rouen. Sans celui-ci nous n'aurions pas pu exploiter toutes les performances qu'offrent le décomposition de domaine et le calcul parallèle.

Les différents articles présentés dans mon mémoire d'habilitation à diriger des recherches, concernent les difficultés et les approches proposées liés à la complexité des géométries, à la génération des maillages, au fort taux de contraste des propriétés d'une part, et, d'autre part la résolution des équations aux dérivées partielles qui sont un obstacle pour une mise en place d'une procédure fiable et automatisé de l'estimation des propriétés des différents composantes du tenseur de rigidité.

Un premier travail dans la génération aléatoire des géométries a été mis en place. L'objectif est de pouvoir prendre en compte tout type de microstructure et ce de manière fiable et automatisée [37, 42].

Dans un second temps, une étude sur l'influence des paramètres morphologiques et phénoménologiques dans la réponse mécanique d'un composite renforcé en fibre courte a été faite [40]. L'impact des répartitions spatiales des fibres au sein de la matrice du composite a fait également l'objet d'une étude basée sur la modélisation du phénomène d'hétérogénéité spatiale [39].

Enfin, la résolution des équations aux dérivées partielles par la méthode des éléments finis s'avère coûteuse dès que la taille du volume élémentaire représentatif est

conséquent, que le nombre d'hétérogénéités devient important ou que l'on souhaite raffiner le maillage. La technique de décomposition de domaine s'est alors tout naturellement imposée laquelle, combinée avec le calcul parallèle via une architecture distribuée, permet d'obtenir un gain assez significatif en temps de calcul pourvu que la communication entres les processeurs soit optimisée. Ce travail à fait l'objet d'une publication [38].

Liste des publications présentées

[1] Karamian-Surville P., Sanchez-Hubert J., Sanchez Palencia É., 2000. A model problem for boundary layers of thin elastic shells. Math. Modell. Num. Anal. 34, N^0 1, 2000, 1-30.

[2] Karamian-Surville P., Sanchez-Hubert J., 2002 Boundary layers in thin elastic shells with developable middle surface. European Journal of Mechanics - A/Solids, Volume 21, Issue 1, 2002, 13-47.

[3] Karamian-Surville P., Sanchez-Hubert J., Sanchez Palencia É., 2002. Propagation of singularities and structure of layers in shells : Hyperbolic case. Computers & Structures, Volume 80, Issues 9–10, 2002, 747-768.

[4] Karamian-Surville P., Sanchez-Hubert J., Sanchez Palencia É., 2002. Nonsmothness in the asymptotics thin shells and propagation of singularities. Hyperbolic case. International Journal of Applied Mathematics and Computer Sciences, vol.12, $N^0$1, 2002, 81-90.

[5] Karamian-Surville P., Sanchez-Hubert J., Sanchez Palencia É., 2003. Pseudoreflection phenomena for singularities in thin elastic shells. Mathematical Models and Methods in Applied Sciences,Vol. 26, 17, 2003, 1451-1485.

[6] Leclerc W., Karamian, P., Vivet, A., Campbell, A., 2012. Numerical evaluation of the effective elastic properties of 2D overlapping random fibre composites. Tech. Mech. 32, 2012, 358-368.

[7] Leclerc, W., Karamian-Surville, P., Vivet, 2013. An efficient stochastic and double-scale model to evaluate the effective elastic properties of 2D overlapping random fibre composites. Comput. Mater. Sci. 69, 2013, 481-493.

[8] Leclerc, W., Karamian-Surville, P. 2013. Domain decomposition methods to evaluate effective elastic properties of random fibre composites in the framework of the double-scale homogenization. Int. J. Solids Struct. 50(18), 2013, 2808-2816.

[9] Leclerc, W., Karamian-Surville, P. 2013 Effects of fibre dispersion on the effective elastic properties of 2D overlapping random fibre composites. Computational Materials Science,79, 2013, 674-683

[10] Leclerc, W., Karamian-Surville, P., Vivet, 2013 Influence of morphological parameters of a 2D random short fibre composite on its effective elastic properties Mechanics & Industry, Volume 14, Issue 05, 2013, 361-365

Première partie

Étude des coques élastiques minces : cas des surfaces réglées

Chapitre 1

Étude des couches limites dans les coques élastiques minces : cas parabolique

Travaux publiés dans, Mathematical Modelling and Numerical Analysis [31] et dans European Journal of Mechanics A/ Solids [32]

1 Objectifs

Dans ce chapitre nous présentons les résultats de Karamian et al. [31,32] dont les deux principaux objectifs sont d'étudier et de comprendre le phénomène des couches limites et des couches internes dans le cadre du modèle linéaire des coques minces de Koïter lorsque l'épaisseur relative de la coque, notée ε, tend vers zéro.

Dans un premier temps, pour étudier les couches limites nous proposons de travailler sur un problème simplifié que nous qualifions de problème modèle, lequel modèle est à coefficients constants et à géométrie moins complexe. Pour $\varepsilon = 0$, le problème modèle est de nature parabolique. C'est donc un problème modèle pour étudier des coques dont la surface moyenne est développable, c'est-à-dire les coques paraboliques.

Dans un second temps, les résultats théoriques obtenus dans le cadre du problème modèle sont appliqués et exploités pour le cas des coques dont la surface moyenne est développable. Il en résulte, une série de simulations numériques lesquelles viennent étayer l'ensemble des travaux théoriques portant sur les couches limites et les couches internes. Ajoutons à cela que dans certains cas, de par la structure particulière du problème modèle et donc aussi pour celui des coques paraboliques, les solutions présentent des singularités faisant intervenir des solutions au sens des distributions le long des caractéristiques.

Rappelons qu'une coque est un corps élastique mince d'épaisseur 2ε, assez proche d'une surface S et dont les frontières sont soumises à des conditions aux limites. Le comportement de la coque est alors décrit par deux formes bilinéaires notées respectivement par $a(u, v)$ et $\varepsilon^2 b(u, b)$ correspondant à la déformation intrinsèque de la

métrique et de la variation de la courbure de la coque. Elles sont plus couramment dénommée forme membranaire et de flexion respectivement. Il est à noter que la seconde forme, laquelle est précédée du facteur ε^2, présente de ce fait une faible rigidité à la flexion. Ce fait entraîne des propriétés asymptotiques très particulières notamment quand l'épaisseur relative de la coque est très petite [9, 19, 63].

Dans la suite, l'étude ne concerne que les coques inhibées. Il est possible d'inhiber les flexions d'une coque par le truchement de certaines conditions aux limites de nature cinématique lesquelles rendent la surface moyenne de la coque géométriquement rigide. Notons par A et B les deux opérateurs relatifs à la forme membranaire et de flexion, il ressort alors que le système étudié est de la forme $A + \varepsilon^2 B$ avec B un opérateur elliptique et A un opérateur dont la nature est étroitement liée à la classification de la surface moyenne S de la coque, c'est-à-dire elliptique, parabolique ou hyperbolique. L'opérateur A est de nature parabolique puisqu'on s'intéresse au cas d'une surface développable. Par ailleurs, l'ordre de dérivation de l'opérateur B étant supérieur à celui de l'opérateur A alors lorsque ε tend vers zéro nous nous trouvons en présence d'un problème de perturbation singulière.

Gardons à l'esprit que pour tout $\varepsilon > 0$, l'espace d'énergie V assure la continuité et la coercivité de la forme bilinéaire $a+\varepsilon^2 b$, alors que le problème limite, correspondant au cas où $\varepsilon = 0$, induit un nouvel espace d'énergie noté V_a assurant la continuité et la coercivité de la forme bilinéaire a seulement. Dans les faits V_a est le complété de V pour la nouvelle norme induite par la forme d'énergie membranaire. Lors du passage à la limite, c'est-à-dire $\varepsilon \searrow 0$, le problème devient singulier dans la mesure où nous partons d'un problème elliptique pour tendre vers un problème parabolique, ce qui se traduit notamment par l'existence des couches limites aux frontières puisqu'on ne peut pas satisfaire la totalité des conditions aux limites du problème initial.

Il va de soi que l'espace V_a contient des fonctions elles-mêmes beaucoup moins régulières que celles vivant dans l'espace V. La conséquence est que u^ε appartient à V mais lorsque ε tend vers zéro, celle-ci devient de moins en moins régulière donnant naissance à des couches limites. Outre cet aspect, il existe une autre raison encore plus importante à la présence des couches limites. Ceci tient au fait que les forces appliquées à la coque bien qu'appartenant à l'espace dual V' cessent d'appartenir à $V_a^{'}$ et donc u^ε présente de fortes variations. Il en résulte que la solution du problème limite n'est pas dans V_a et donc les solutions sont des distributions singulières [43] entraînant dans leur sillage des couches limites.

Insistons sur le fait que la non-régularité des solutions du problème limite a un impact direct sur le calcul par éléments finis de u^ε quand ε est très petit. Lorsque la donnée des forces extérieures n'appartient pas à $V_a^{'}$ alors la convergence de la solution par éléments finis ne converge pas de manière uniforme par rapport à ε, [28–30]. En d'autres termes, plus ε est petit plus il faut raffiner pour avoir une bonne approximation de la solution numérique.

À notre connaissance, les couches limites ont été peu étudiées ; tout au plus trouve-t-on une mention faisant référence aux effets de frontières et une sorte de

catalogue de solutions analytiques dans Rutten [56] mais dont l'utilisation à des cas spécifiques n'est pas évidente. C'est pourquoi nous considérons un problème modèle pour lequel l'opérateur associé au problème limite est parabolique. Il s'agit d'un modèle simplifié à coefficients constants dans lequel figurent deux inconnues u_1 et u_2 jouant tour à tour le rôle de la composante tangentielle et normale des déplacements dans les coques.

2 Problème modèle et critères d'appartenance de $f \in V'_a$

2.1 problème P(ε) avec ε fixé non nul

Le problème modèle noté $P(\varepsilon)$ est défini de la manière suivante. Soit un domaine $\Omega = (0, a_1) \times (0, a_2)$ du plan cartésien. Les conditions aux limites se décomposent en deux parties disjointes Γ_0 et Γ_1 correspondant respectivement à une partie encastrée et une partie libre. Alors l'espace d'énergie V est défini par :

$$V = \{v \in H^1(\Omega) \times H^2(\Omega);\ \text{tel que } v_1 = v_2 = \partial_n v_2 = 0 \text{ sur } \Gamma_0\} \tag{1.1}$$

On considère les deux formes bilinéaires suivantes :

$$a(u,v) = \int_\Omega [\partial_1 u_1 \partial_1 v_1 + (\partial_2 u_1 - u_2)(\partial_2 v_1 - v_2)]dx \tag{1.2}$$

$$b(u,v) = \int_\Omega \sum_{|\alpha| \le 2} \partial_\alpha u_2 \partial_\alpha v_2 dx \equiv (u_2, v_2). \tag{1.3}$$

On se donne un chargement $f \in V'$, alors la formulation variationnelle du problème $P(\varepsilon)$ s'écrit :

$$\begin{cases} \text{Trouvez } u^\varepsilon \text{ tel que } \forall v \in V \\ a(u^\varepsilon, v) + \varepsilon^2 b(u^\varepsilon, v) =< f, v >_{V,V'} \end{cases} \tag{1.4}$$

Ce problème rentre dans le champ d'application du théorème de Lax-Milgram qui en assure l'existence et l'unicité de la solution pour tout ε fixé non nul, cependant il est à noter que la constante de coercivité laquelle dépend de ε^2 s'annule à mesure que ε tend vers zéro. Les équations aux dérivées partielles associées aux formes bilinéaires sont :

$$\begin{cases} -\Delta u_1^\varepsilon + \partial_2 u_2^\varepsilon = f_1 \\ -\partial_2 u_1^\varepsilon + u_2^\varepsilon + \varepsilon^2(\Delta^2 u_2^\varepsilon - \Delta u_2^\varepsilon + u_2^\varepsilon) = f_2 \end{cases} \tag{1.5}$$

avec les conditions aux limites correspondant aux frontières Γ_0 et Γ_1

$$\begin{cases} \partial_n u_1^\varepsilon - n_2 u_2^\varepsilon = F_1 \\ \varepsilon^2[\partial_n u_2^\varepsilon - \partial_n \Delta u_2^\varepsilon - \partial_t \partial_{nt} u_2^\varepsilon] = F_2 \\ \varepsilon^2 \partial_{nn} u_2^\varepsilon = C \end{cases} \tag{1.6}$$

Dans la suite pour simplifier l'exposé on fixe $F_1 = F_2 = C = 0$

2.2 problème P(0)

On définit le problème $P(0)$ au sens variationnel de la manière suivante :

$$\begin{cases} \text{Trouver } u^0 \in V_a \text{ tel que } \forall v \in V_a \\ a(u^0, v) =< f, v >_{V_a, V_a'} \text{ pour toute donnée } f \in V_a' \end{cases} \tag{1.7}$$

Ce problème est continu et coercif sur V_a où V_a est le complété de V pour la norme induite par la forme bilinéaire $||u||_{V_a} = \sqrt{a(u,u)}$. Le théorème de Lax-Milgram assure l'existence et l'unicité de la solution pourvu que la donnée f appartienne au dual de V_a. Dans l'article nous énonçons le critère d'appartenance de $f \in V_a'$ sous forme d'un théorème qui donne les conditions nécessaires et suffisantes :

Théorème 1 *La fonctionnelle définie par $l_f(v) = \int_\Omega (f_1 v_1 + f_2 v_2) d\Omega$ peut être prolongée par continuité dans V'_a, (ce qui revient à dire que $f \in V'_a$) si et seulement si il existe $T = (T^1, T^2) \in L^2(\Omega) \times L^2(\Omega)$ tel que :*

$$l_f(v) = \int_\Omega (f_1 v_1 + f_2 v_2) d\Omega = \int_\Omega (T^1 \gamma_1(v) + T^2 \gamma_2(v)) d\Omega \quad \forall v \in V$$

avec

$$\begin{cases} \gamma_1(u) \equiv \partial_1 u_1 \\ \gamma_2(u) \equiv \partial_2 u_1 - u_2 \end{cases} \tag{1.8}$$

2.3 Critère énergétique

Comme il est d'usage, on identifie l'espace $L^2(\Omega)$ à son propre dual, l'espace V est à injection continue et dense dans V_a de sorte que l'on a $V_a' \subset V'$. Lorsque la donnée f est dans V_a' cela conduit à établir la convergence dans les espaces classiques (cf. le théorème 2). Dans l'éventualité où la donnée f cesse d'être dans V_a' tout en étant dans V', alors on ne peut plus établir de théorème de convergence et la solution u^0 du problème limite $P(0)$ n'appartient pas à l'espace V_a comme le suggère le théorème 3.

Théorème 2 *Soit $f \in V_a'$ la donnée extérieure ne dépendant pas de ε. Soit u^ε et u^0 les solutions de (1.4) et (1.7) respectivement. Alors*

$$u^\varepsilon \longrightarrow u^0 \text{ dans } V \text{ fortement} \tag{1.9}$$

et il existe une constante C telle que

$$E(u^\varepsilon) = \frac{1}{2}[a(u^\varepsilon, u^\varepsilon) + \varepsilon^2 b(u^\varepsilon, u^\varepsilon)] \leq C. \tag{1.10}$$

Théorème 3 *Soit $f \in V'$ la donnée extérieure ne dépendant pas de ε. Soit u^ε la solution de 1.4, alors*

1. *une condition nécessaire et suffisante pour que $E(u^\varepsilon)$ reste bornée pour $\varepsilon \searrow 0$ est que $f \in V_a'$.*
2. *si $f \notin V_a'$, alors $E(u^\varepsilon)$ diverge $\varepsilon \searrow 0$*

Grâce à ces deux théorèmes nous disposons d'un critère pour savoir si la donnée extérieure appartient ou non à l'espace V_a'.

3 Caractérisation des couches limites et des couches internes

Pour étudier les couches limites aussi bien le long des courbes caractéristiques que des courbes non-caractéristiques, nous utilisons la technique de la mise à l'échelle basée sur le comportement asymptotique des solutions exponentielles. Pour décrire les structures des couches limites, il est d'usage d'effectuer un changement de variables suivie d'une dilatation de la variable normale à la couche limite. Par ailleurs, afin d'obtenir un système consistant, une remise à l'échelle des inconnues est aussi nécessaire. L'approche qui a été choisie est la même que celle de l'article de Pitkaranta et al. [54]. Le tableau 1.1 issue de l'article Karamian et al. [31] synthétise les principaux résultats dont vous trouverez ci-dessous les principales caractéristiques.

Premièrement, dans le cadre général d'un problème parabolique, l'ordre de grandeur de l'épaisseur des couches limites le long des frontières caractéristiques est en $\eta(\varepsilon) = \varepsilon^{\frac{1}{3}}$ alors que dans le cas des frontières non-caractéristiques l'épaisseur de la couche limite est en $\eta(\varepsilon) = \varepsilon^{\frac{1}{2}}$. En ce qui concerne les couches internes l'ordre de grandeur de la couche limite le long des courbes caractéristiques est identique à celle des couches limites des frontières caractéristiques, c'est-à-dire en $\eta(\varepsilon) = \varepsilon^{\frac{1}{3}}$

Deuxièmement, nous sommes en mesure de donner les ordres de grandeur des composantes tangentielle et normale de sorte que le rapport entre la composante normale et tangentielle est en $O(\eta^{-1})$. Outre cette première remarque, une étude est également réalisée selon que la frontière caractéristique est ou non encastrée. Dans l'éventualité où la frontière n'est pas encastrée, nous distinguons deux cas car les conclusions ne sont pas les mêmes suivant que la donnée des forces extérieures s'annule on non sur la portion de la frontière caractéristique. Il ressort que dans le cas où la donnée des forces extérieures est à trace nulle sur la frontière caractéristique ou bien si on impose l'encastrement, les développements asymptotiques sont identiques et les énergies sont finies, à l'inverse du cas où la donnée extérieure n'est pas à trace nulle. Dans le cas d'une frontière non-caractéristique, les choses sont plus simples à gérer car il n'y a pas de cas particulier à distinguer et nous avons un développement asymptotique dans lequel les énergies restent finies.

Troisièmement, dans le cas des couches internes, dans l'éventualité où la donnée extérieure présente une singularité, celle-ci engendre une réponse en certain point analogue aux cas des frontières caractéristiques dont le développement asymptotique est identique ainsi que l'ordre de grandeur des énergies.

4 Analyse par éléments finis et simulations numériques : problème modèle

Afin de confronter nos résultats théoriques avec des simulations numériques, à l'aide des éléments finis il a fallu coder le problème modèle. Lors de ma thèse, j'ai développé un code en éléments finis pour traiter le problème limite réduit dans le cas des coques hyperboliques. À partir des éléments de ce code j'ai pu y greffer le

Tableau 1.1 –

Couches	Comportement	Énergie
Caractéristique épaisseur : $\eta(\varepsilon) = \varepsilon^{\frac{1}{3}}$	$\frac{v_2^\varepsilon}{v_1^\varepsilon} = \mathcal{O}(\eta^{-1})$	
encastrement	$\begin{cases} v_1^\varepsilon \cong U_1^0(x_1, y_2) \\ v_2^\varepsilon \cong \eta^{-1} U_2^0(x_1, y_2) \end{cases}$	$E_C = \mathcal{O}(\eta)$
bord libre $f_2(x_1, 0) = 0$	$\begin{cases} v_1^\varepsilon \cong U_1^0(x_1, y_2) \\ v_2^\varepsilon \cong \eta^{-1} U_2^0(x_1, y_2) \end{cases}$	$E_C = \mathcal{O}(\eta)$
bord libre $f_2(x_1, 0) \neq 0$	$\begin{cases} v_1^\varepsilon \cong \eta^{-1} U_1^0(x_1, y_2) \\ v_2^\varepsilon \cong \eta^{-2} U_2^0(x_1, y_2) \end{cases}$	$E_C = \mathcal{O}(\eta^{-1})$
Non-caractéristique épaisseur : $\eta(\varepsilon) = \varepsilon^{\frac{1}{2}}$	$\frac{v_2^\varepsilon}{v_1^\varepsilon} = \mathcal{O}(\eta^{-1})$ $\begin{cases} v_1^\varepsilon \cong \eta U_1^0(x_1, y_2) \\ v_2^\varepsilon \cong U_2^0(x_1, y_2) \end{cases}$	$E_C = \mathcal{O}(\eta)$
Caractéristique interne épaisseur : $\eta(\varepsilon) = \varepsilon^{\frac{1}{3}}$ avec discontinuité de f_2 en $x_2 = 0$	$\frac{v_2^\varepsilon}{v_1^\varepsilon} = \mathcal{O}(\eta^{-1})$ $\begin{cases} v_1^\varepsilon \cong \eta^{-1} U_1^0(x_1, y_2) \\ v_2^\varepsilon \cong \eta^{-2} U_2^0(x_1, y_2) \end{cases}$	$E_C = \mathcal{O}(\eta^{-1})$

problème modèle pour réaliser des simulations numériques. Le code permet entre autre de choisir différents types d'éléments finis, notamment les éléments finis P1, P2, Q1, Q2, Hermite, Hermite réduit et enfin les éléments finis de Bell. Pour les simulations numériques nous avons utilisé les éléments finis Hermite réduits.

Dans la suite nous exhibons des simulations numériques pour les différents cas de figures énumérés dans le tableau 1.1 de la section précédente. Nous adoptons différents types de configuration de maillages, des maillages réguliers et uniformes, et d'autres maillages présentant des raffinements spécifiques et localisés en fonction du contexte étudié. La figure 1.1 illustre trois types de configuration de maillage utilisés pour effectuer les simulations numériques. À travers les simulations, nous montrons qu'il est nécessaire de faire appel à des maillages adaptés pour obtenir des solutions numériques fiables et de qualité.

4.1 Encastrement total

Dans la simulation présentée l'épaisseur $\varepsilon = 0.001$, les courbes caractéristiques sont parallèles à l'axe x_2. D'après le tableau 1.1, l'ordre de grandeur de la couche limite est $\eta(\varepsilon) = \varepsilon^{\frac{1}{3}} = 0.1$ alors que celle des courbes non-caractéristiques est en $\eta(\varepsilon) = \varepsilon^{\frac{1}{2}} = 0.0316$ et en ce qui concerne les ordres de grandeur des énergies nous avons respectivement $O(\eta(\varepsilon)) = 0.1$ et $O(\eta(\varepsilon)) = 0,032$, mais les premiers termes du développement asymptotique diffèrent dans la mesure où pour le cas des courbes caractéristiques nous avons $(u_1^\varepsilon, u_2^\varepsilon) = (u_1^0, \eta^{-1} u_2^0)$ c'est-à-dire $(u_1^\varepsilon, u_2^\varepsilon) = (u_1^0, 10u_2^0)$ d'une part, et d'autre part pour les courbes non-caractéristiques $(u_1^\varepsilon, u_2^\varepsilon) = (\eta u_1^0, u_2^0)$ c'est-à-dire $(u_1^\varepsilon, u_2^\varepsilon) = (0,0316u_1^0, u_2^0)$. Ce qui explique pourquoi nous observons les

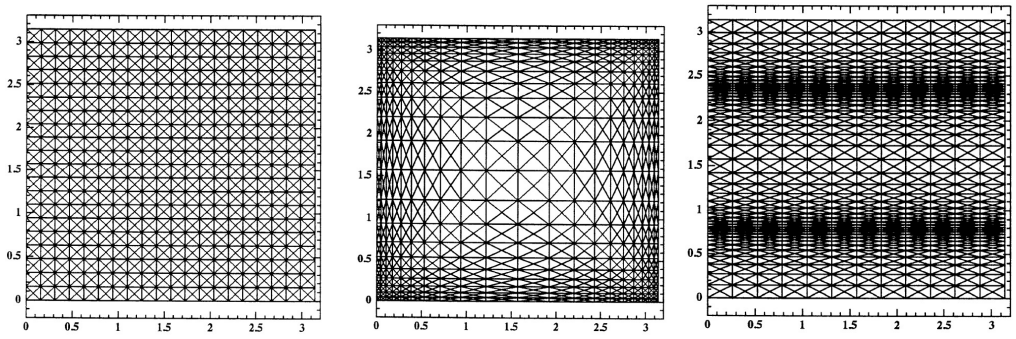

FIGURE 1.1 – De gauche à droite, maillage uniforme et maillage raffiné

boursouflures au niveau des frontières parallèles aux courbes caractéristiques et donc aussi à l'apparition des couches limites. La simulation numérique est conforme à ce qui a été annoncé par la théorie.

Par ailleurs, avec un maillage uniforme la simulation numérique donne un résultat correct. Néanmoins un maillage non uniforme avec des mailles de taille différente permet d'obtenir un très bon résultat pourvu que l'on raffine correctement la zone de la couche limite. Une bonne connaissance de l'épaisseur de la couche limite donne une indication sur la taille et le nombre de mailles qu'il faut mettre pour avoir de très bons résultats sans être prohibitif en temps de calcul.

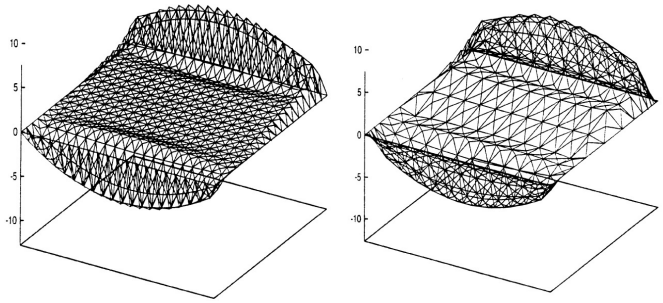

FIGURE 1.2 – Visualisation de la seconde composante de la solution à la fois pour le maillage uniforme et non uniforme

4.2 Cas de la frontière caractéristique avec une donnée extérieure $f_2 \neq 0$

Dans cette simulation nous fixons toujours l'épaisseur ε à 0.001. À la différence du cas précédent, ici la donnée extérieure ne s'annule pas sur la frontière caractéristique pour laquelle nous n'imposons aucune condition aux limites. D'après le tableau, l'ordre de grandeur de la couche limite est $\eta(\varepsilon) = \varepsilon^{\frac{1}{3}} = 0.1$ alors que celle des courbes non-caractéristiques est en $\eta(\varepsilon) = \varepsilon^{\frac{1}{2}} = 0.0316$ et en ce qui concerne les ordres de grandeur des énergies nous avons respectivement $O(\eta(\varepsilon)) = 10$ et $O(\eta(\varepsilon)) = 0,032$, mais les premiers termes du développement asymptotique diffèrent dans la mesure

où pour le cas des courbes caractéristiques nous avons $(u_1^\varepsilon, u_2^\varepsilon) = (\eta^{-1}u_1^0, \eta^{-2}u_2^0)$ c'est-à-dire $(u_1^\varepsilon, u_2^\varepsilon) = (10u_1^0, 100u_2^0)$ d'une part, et d'autre part pour les courbes non-caractéristiques $(u_1^\varepsilon, u_2^\varepsilon) = (\eta u_1^0, u_2^0)$ c'est-à-dire $(u_1^\varepsilon, u_2^\varepsilon) = (0,0316u_1^0, u_2^0)$. Il est clair que les ordres de grandeur ne sont plus du tout les mêmes ce qui explique une plus grande amplitude de la solution le long de la frontière caractéristique. La simulation numérique est conforme à ce qui a été prédit par la théorie.

Comme dans le cas précédent, nous remarquons qu'il est préférable de faire appel à un maillage adapté car plus économe en temps de calcul tout en étant aussi précis et fiable.

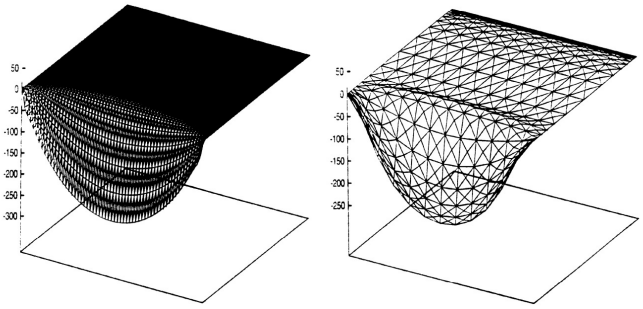

FIGURE 1.3 – Visualisation de la seconde composante de la solution à la fois pour le maillage uniforme et non uniforme

4.3 Couches internes

À présent on considère le cas d'une couche interne avec une donnée singulière de type Heaviside et nous fixons toujours l'épaisseur ε à 0.001. D'après le tableau, nous sommes comme dans la situation précédente en ce qui concerne les ordres de grandeur des énergies et des premiers termes du développement asymptotique. La simulation numérique exhibe bien ce qui a été prédit par la théorie et comme précédemment l'usage d'un maillage adapté permet d'obtenir des résultats fiables et précis avec un gain de temps de calcul appréciable.

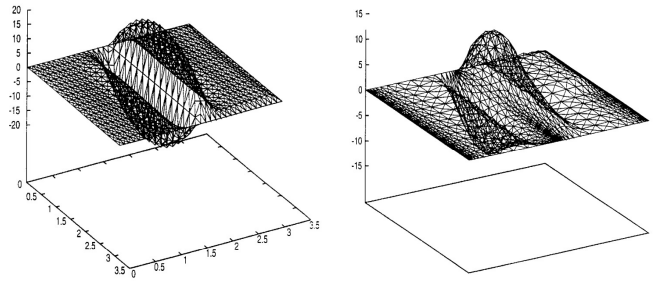

FIGURE 1.4 – Visualisation de la seconde composante de la solution à la fois pour le maillage uniforme et non uniforme

5 Cas des coques développables

Le travail effectué pour le cas du problème modèle se transpose modulo quelques adaptations aux cas des coques dont la surface moyenne est développable (cf. article Karamian et al. [32]). Dans cette section le problème noté $P(\varepsilon)$ est défini de la manière suivante. Soit un domaine $\Omega = (0, l_1) \times (0, l_2)$ du plan cartésien de coordonnées (y^1, y^2). Pour mémoire, un point P de la surface possède deux directions, également désignées directions asymptotiques, lesquelles sont tangentes à la surface moyenne de la coque. Le point P est qualifié d'elliptique, hyperbolique ou parabolique, quand les directions asymptotiques sont respectivement imaginaires, réelles et distinctes ou réelles et doubles. On dit qu'une surface est développable dès lors que tous ses points sont paraboliques. Dans la suite nous privilégions le dernier cas. Les conditions aux limites se décomposent en deux parties disjointes Γ_0 et Γ_1 correspondant respectivement à une partie encastrée et libre. L'espace d'énergie V est définie par :

$$V = \{v \in H^1(\Omega) \times H^1(\Omega) \times H^2(\Omega);\ \text{tel que } v_1 = v_2 = v_3 = \partial_n v_3 = 0 \text{ sur } \Gamma_0\} \quad (1.11)$$

On considère les deux formes bilinéaires suivantes représentant respectivement l'énergie de déformation en membrane et en flexion :

$$a_m(u, v) = \int_\Omega A^{\alpha\beta\lambda\nu} \gamma_{\lambda\nu}(u) \gamma_{\alpha\beta}(v) \sqrt{a} dx \quad (1.12)$$

$$a_f(u, v) = \int_\Omega \frac{1}{12} A^{\alpha\beta\lambda\nu} \rho_{\lambda\nu}(u) \rho_{\alpha\beta}(v) \sqrt{a} dx \quad (1.13)$$

où les coefficients $A^{\alpha\beta\lambda\nu}$ sont les coefficients de l'élasticité qui dépendent des variables (y^1, y^2) et satisfont aux propriétés de symétrie et de positivité. Les composantes covariantes $\gamma_{\lambda\nu}(u)$ et $\rho_{\lambda\nu}(u)$ représentent respectivement le tenseur de déformation et la variation de la courbure. Pour un chargement donnée, telle que $f \in V'$, la formulation variationnelle du problème $P(\varepsilon)$ s'écrit :

$$\begin{cases} \text{Trouvez } u^\varepsilon \text{ tel que } \forall v \in V \\ a_m(u^\varepsilon, v) + \varepsilon^2 a_f(u^\varepsilon, v) = < f, v >_{V,V'} \end{cases} \quad (1.14)$$

Ce problème rentre dans le champ d'application du théorème de Lax-Milgram [6] qui en assure l'existence et l'unicité de la solution pour tout ε fixé non nul, cependant la constante de coercivité dépend de ε^2 de sorte qu'elle s'annule à mesure que ε tend vers zéro.

5.1 Critère d'appartenance de $f \in V'_m$

Comme pour le problème modèle, nous sommes en mesure d'énoncer des critères énergétiques et un critère d'appartenance de la donnée extérieure pour que les théorèmes soient valides. Nous identifions l'espace $L^2(\Omega)$ à son propre dual, l'espace V est à injection continue et dense dans V_m de sorte que l'on a $V'_m \subset V'$. V_m est le complété de V pour la norme induite par la forme bilinéaire $a_m(v, v)$. Lorsque la donnée f est dans V'_m cela conduit à établir la convergence dans les espaces classiques (cf. le théorème 4). Dans l'éventualité où la donnée f cesse d'être dans V'_m tout en étant

dans V', alors on ne peut établir de théorème de convergence et la solution u^0 du problème limite n'appartient pas à l'espace V_m (cf. le théorème 5).

Théorème 4 *Soit $f \in V'_m$ la donnée extérieure ne dépendant pas de ε. Soit u^ε et u^0 les solutions de (2.6) respectivement. Alors*

$$u^\varepsilon \longrightarrow u^0 \text{ dans } V \text{ fortement} \tag{1.15}$$

et il existe une constante C telle que

$$E(u^\varepsilon) = \frac{1}{2}[a_m(u^\varepsilon, u^\varepsilon) + \varepsilon^2 a_f(u^\varepsilon, u^\varepsilon)] \leq C. \tag{1.16}$$

Théorème 5 *Soit $f \in V'$ la donnée extérieure ne dépendant pas de ε. Soit u^ε la solution de 2.6, alors*

1. *une condition nécessaire et suffisante pour que $E(u^\varepsilon)$ reste bornée pour $\varepsilon \searrow 0$ est que $f \in V'_m$.*
2. *si $f \notin V'_m$, alors $E(u^\varepsilon)$ diverge $\varepsilon \searrow 0$*

Grâce à ces deux théorèmes nous disposons d'un critère pour savoir si la donnée extérieure appartient ou non à l'espace V'_m.

5.2 Caractérisation des couches limites et couches internes

Nous procédons comme dans le cas du problème modèle, pour décrire et étudier les couches limites et les couches internes. De cette étude il ressort principalement que l'ordre de grandeur de l'épaisseur de la couche limite et de la couche interne le long de courbes caractéristiques et des frontières caractéristiques est en $\eta(\varepsilon) = \varepsilon^{\frac{1}{4}}$ alors que dans le cas des frontières non caractéristiques l'épaisseur de la couche limite est en $\eta(\varepsilon) = \varepsilon^{\frac{1}{2}}$. Nous sommes également en mesure de donner les ordres de grandeur des composantes tangentielles et normale aussi bien pour le cas des courbes caractéristiques que non-caractéristiques. Le tableau 1.2 récapitule les principaux résultats à retenir dans le cas des coques paraboliques.

6 Simulations numériques

Dans cette section nous présentons quelques simulations numériques pour illustrer les résultats des sections précédentes appliquées aux cas des coques paraboliques. Nous considérons le cas d'une surface developpable qui est une partie d'un cône (cf. la figure 1.5). La carte locale est définie par $(\Omega, \overrightarrow{\psi}(y^1, y^2))$ avec $\Omega = [0, 1] \times [0, \frac{1}{2}]$ et l'application $\overrightarrow{\psi}(y^1, y^2)$ définie de la manière suivante :

$$\overrightarrow{\psi}(y^1, y^2) = \begin{cases} y^1 \\ (y^1 + 2)\sin(2\pi y^2) \\ (y^1 + 2)\cos(2\pi y^2) \end{cases} \tag{1.17}$$

Couches	Comportement	Énergie
Caractéristique épaisseur : $\eta(\varepsilon) = \varepsilon^{\frac{1}{4}}$	$\frac{v_2^\varepsilon}{v_1^\varepsilon} = \mathcal{O}(\eta^{-1})$ et $\frac{v_3^\varepsilon}{v_1^\varepsilon} = \mathcal{O}(\eta^{-2})$	
encastrement	$\begin{cases} v_1^\varepsilon \cong U_1^0(y^1, y^2) \\ v_2^\varepsilon \cong \eta^{-1} U_2^0(y^1, y^2) \\ v_3^\varepsilon \cong \eta^{-2} U_3^0(y^1, y^2) \end{cases}$	$E_C = \mathcal{O}(\eta)$
bord libre $f_3(x_1, 0) \neq 0$	$\begin{cases} v_1^\varepsilon \cong \eta^{-2} U_1^0(y^1, y^2) \\ v_2^\varepsilon \cong \eta^{-3} U_2^0(y^1, y^2) \\ v_3^\varepsilon \cong \eta^{-4} U_3^0(y^1, y^2) \end{cases}$	$E_C = \mathcal{O}(\eta^{-1})$
couche interne avec f_3 discontinue	$\begin{cases} v_1^\varepsilon \cong \eta^{-2} U_1^0(y^1, y^2) \\ v_2^\varepsilon \cong \eta^{-3} U_2^0(y^1, y^2) \\ v_3^\varepsilon \cong \eta^{-4} U_2^0(y^1, y^2) \end{cases}$	$E_C = \mathcal{O}(\eta^{-1})$
Non-caractéristique épaisseur : $\eta(\varepsilon) = \varepsilon^{\frac{1}{2}}$	$\frac{v_2^\varepsilon}{v_1^\varepsilon} = \mathcal{O}(\eta^{-1})$ et $\frac{v_3^\varepsilon}{v_1^\varepsilon} = \mathcal{O}(\eta^{-2})$	
	$\begin{cases} v_1^\varepsilon \cong \eta^2 U_1^0(y^1, y^2) \\ v_2^\varepsilon \cong \eta U_2^0(y^1, y^2) \\ v_3^\varepsilon \cong U_3^0(y^1, y^2) \end{cases}$	$E_C = \mathcal{O}(\eta)$

Tableau 1.2 –

6.1 Exemple 1 : cas d'une couche limite

Pour cet exemple, nous considérons le chargement $\overrightarrow{f} = (0, 0, 1)$. La portion de frontière Γ_0 encastrée est la droite d'équation $y^1 = 1$ et le reste de la frontière est libre de toutes conditions aux limites. Notons que les frontières caractéristiques sont les droites d'équations $y^2 = 0$ et $y^2 = \frac{1}{2}$. Par ailleurs, la composante normale du chargement ne s'annule pas sur les frontières caractéristiques, en conséquence conformément à la théorie, cela entraîne la présence d'une couche limite le long des frontières caractéristiques comme l'atteste la figure 1.6. Sur cette figure, nous avons représenté le graphe de la composante normale du déplacement de la coque ainsi

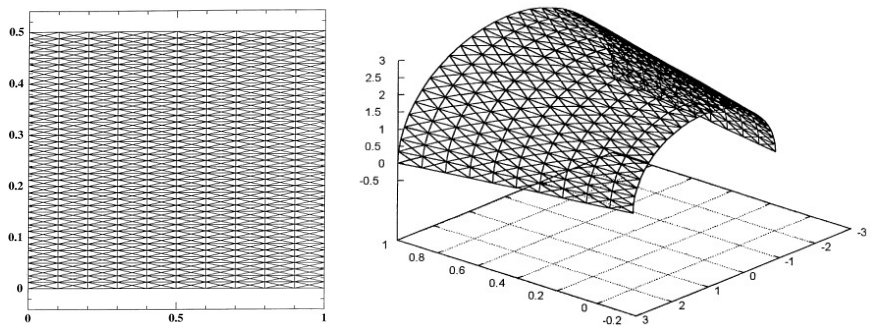

FIGURE 1.5 – De gauche à droite. Maillage uniforme et image de la surface moyenne de la coque.

,

qu'une coupe de celle-ci pour $y^1 = 0$.

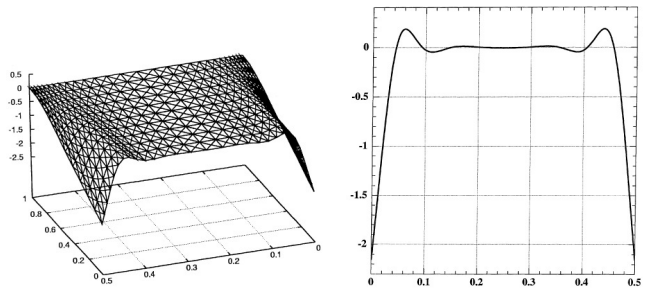

FIGURE 1.6 – De gauche à droite, visualisation de u_3 sur la totalité du domaine. Représentation graphique d'une section de u_3 pour $y^1 = 0$

6.2 Exemple 2 : cas d'une couche interne

Dans cet exemple, nous considérons le chargement $\overrightarrow{f} = (0, 0, H(y^2 - \frac{1}{4}))$ où H représente la distribution de Heaviside. Les portions de frontière Γ_0 encastrées sont les droites d'équation $y^1 = 1$, $y^2 = 0$ et $y^2 = \frac{1}{2}$. Comme nous le remarquons, le chargement possède une discontinuité de première espèce le long de la caractéristique $y^2 = \dfrac{1}{4}$. La figure 1.7 met en évidence la couche interne qui apparait le long de la courbe caractéristique.

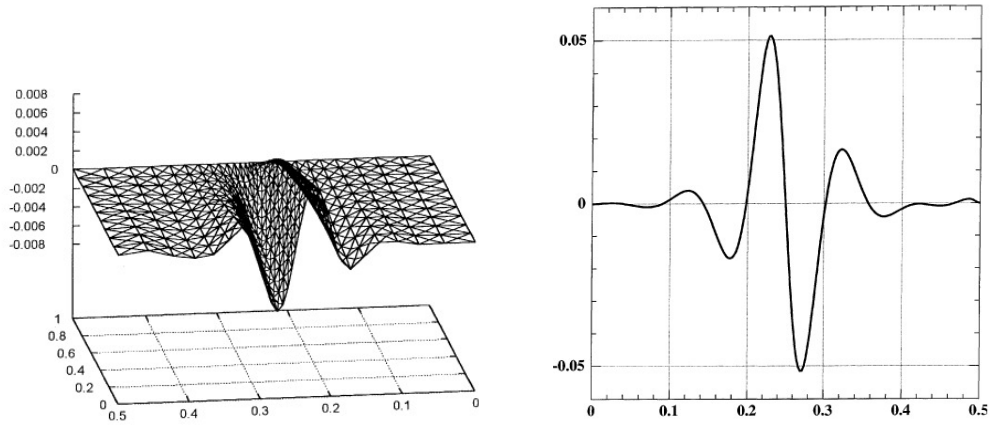

FIGURE 1.7 – De gauche à droite, Visualisation de u_3 sur la totalité du domaine. Représentation graphique d'une section de u_3 pour $y^1 = 0$

7 Bilan

Dans le cadre de la théorie linéaire des coques minces de Koïter pour laquelle la surface moyenne est parabolique, les principaux résultats sont résumés dans le tableau 1.2. Ce tableau donne l'ordre de grandeur de l'épaisseur des couches limites, la structure et les premiers termes du développement asymptotique appropriés. Il

ressort que l'énergie tend vers l'infini lorsque l'épaisseur $\varepsilon \searrow 0$ pour deux cas : cas des frontières caractéristiques lorsque la charge ne s'y annule pas et lorsque le long d'une caractéristique interne celle-ci supporte une donnée singulière. Il va de soi que l'énergie en dehors des régions liées aux caractéristiques est de l'ordre de l'unité ce qui est en accord avec les théorèmes. Cependant, il faut noter que la structure asymptotique montre également que l'énergie a tendance à être confinée dans la zone très étroite qu'est la couche limite ou la couche interne.

Chapitre 2

Étude de la propagation des singularités et notion de pseudo-réflexion dans les coques minces hyperboliques

Travaux publiés dans Computers and Structures [33], International Journal of Applied Mathematics and Computer Science [34] et Mathematical Models and Methods in Applied Sciences [35]

1 Objectifs

À l'instar des coques paraboliques, les coques hyperboliques présentent des particularités qui leur sont propres et qui, de prime abord, semblent pathologiques. Lors de certaines simulations numériques que j'ai réalisées, et ce pour certains chargements et conditions aux limites cinématiques, lesquelles assurent l'inhibition de la coque, c'est-à-dire que la surface moyenne de la coque est géométriquement rigide, il nous est arrivé d'observer des résultats numériques qui paraissent étranges et pour lesquels nous n'avions pas d'explications simples à formuler.

Pour mémoire, ce chapitre concerne les coques dont les surfaces moyennes sont hyperboliques, et comme nous l'avons déjà mentionné, dans le cas inhibé lorsque l'épaisseur de la coque devient très petite, le comportement de celle-ci est assez bien décrite par le système membranaire. La nature elliptique, parabolique ou hyperbolique de ce système, est intimement liée à la classification même de la surface moyenne de la coque. Comme nous traitons une coque dont la surface moyenne est hyperbolique, il en résulte que le système des équations aux dérivées partielles que nous devons résoudre est lui aussi hyperbolique. Par ailleurs, nous savons que dans les systèmes hyperboliques la propagation des singularités se manifeste exclusivement le long des caractéristiques, ce qui se traduit par la présence d'une sorte de zone mince ou des couches fines dans lesquelles nous observons de très fortes et brutales variations des solutions, et ce pour des très petites valeurs de l'épaisseur ε de la coque. En effet, il arrive que les solutions présentent des degrés de singularité plus élevés que le degré de la singularité du chargement ce qui entraîne une concentration

de l'énergie dans les couches fines le long des caractéristiques.

Dans ce chapitre nous présentons les principaux résultats obtenus pour les coques hyperboliques cf. Karamian et al. [33, 34]. Les deux principaux objectifs sont d'étudier la propagation des singularités le long des caractéristiques et l'écart qui existe entre le degré de la singularité du chargement et celui des solutions ; selon que le support du chargement est porté ou non par les courbes caractéristiques, cet écart est différent. Comme nous le verrons, cela s'explique par la nature hyperbolique du système membranaire.

Outre cet aspect, un autre phénomène s'observe lors des propagations des singularités, notamment, lorsque celles-ci rencontrent des frontières non-caractéristiques. Ce phénomène s'apparente à de la réflexion sans en être au sens premier du terme. En effet, la singularité incidente, une fois qu'elle rencontre une des frontières se propage selon la seconde direction caractéristique faisant penser au phénomène de réflexion mais la comparaison s'arrête là. Lors de ce processus, nous observons que la singularité a perdu en intensité et a même gagné en régularité. Je qualifie de pseudo-réflexion [28] ce phénomène.

Il existe une grande analogie avec le précédent chapitre dans la manière d'aborder le problème des coques hyperboliques. Nous posons, A_m et A_f les opérateurs associés aux deux formes bilinéaires a_m et a_f, alors l'opérateur $A_m + \varepsilon^2 A_f$ est elliptique pour tout $\varepsilon > 0$. L'opérateur A_m est hyperbolique comme la surface moyenne. Les caractéristiques sont réelles et distinctes. Elles coïncident avec les lignes asymptotiques de la surface moyenne. On parle aussi de surface à courbures principales de signe opposé. En outre, rappelons que l'ordre de dérivation de A_f est supérieur à A_m. En conséquence, lorsque $\varepsilon \searrow 0$ nous avons affaire à un problème de perturbation singulière. Ce qui se traduit par la présence des couches limites.

Pour tout $\varepsilon > 0$, l'espace d'énergie V est défini tel que la forme bilinéaire $a_m + \varepsilon^2 a_f$ y soit continue et coercive, ce qui n'est pas le cas du problème limite lequel induit un nouvel espace d'énergie V_m, associé à la forme bilinéaire membranaire, pour lequel la forme membranaire a_m y est continue et coercive. Dans les faits, V_m est le complété de V pour la norme induite par $\sqrt{a_m(.,.)}$ puisque la coque est inhibée.

Il est clair que l'espace V_m contient des fonctions beaucoup moins regulières que celle de V. Il en résulte que lors du passage à la limite, les solutions u^ε appartiennent à V pour tout $\varepsilon > 0$ mais que leurs limites correspondant à $\varepsilon \searrow 0$ le sont moins et présentent alors des couches limites et des couches internes. Un autre point très important est le fait que $V'_m \subset V'$. En conséquence, les forces usuelles qui appartiennent à V' peuvent, et c'est souvent le cas, ne pas être dans V'_m. La conséquence directe est que les solutions sont des distributions singulières lesquelles entraînent l'apparition des couches internes avec son cortège de fortes et brutales variations dans les solutions numériques.

La conséquence directe de la non régularité des solutions lorsque l'épaisseur ε tend vers zéro est que cela complique singulièrement le calcul par éléments finis pour

les petites valeurs de l'épaisseur de la coque. Il en résulte que lorsque le chargement $\vec{f} \notin V'_m$, la convergence de l'approximation de la solution numérique par éléments finis n'est pas uniforme par rapport à l'épaisseur et que plus ε est petit plus le maillage doit être fin et donc dense. Cela se traduit par la nécessité de faire du raffinement de maillage pour obtenir des bonnes approximations numériques des déformations.

2 Propagation des singularités dans les coques hyperboliques

Dans cette partie, nous considérons une coque dont la surface moyenne est hyperbolique. Soit un domaine $\Omega = (0, a_1) \times (0, a_2)$ du plan cartésien de coordonnées (y^1, y^2). Dans le cas présent les droites d'équations $y^1 = Const.$ et $y^2 = Const.$ sont les lignes asymptotiques, ce qui correspond à une paramétrisation de la surface moyenne de la coque pour laquelle les coefficients de la seconde forme fondamentale valent respectivement $b_{11} = b_{22} = 0$ et $b_{12} \neq 0$.

On pose $P(0)$ le problème limite. Les équations sont alors données par :

$$\begin{cases} D_\alpha T^{\alpha\beta} + f^\beta = 0, \\ 2b_{12}T^{12} + f^3 = 0. \end{cases} \tag{2.1}$$

où D_α représente la dérivée covariante. Ce système s'écrit encore sous la forme suivante :

$$\begin{cases} -\partial_1 T^{11} - (2\Gamma^1_{11} + \Gamma^2_{12})T^{11} - \Gamma^1_{22}T^{22} = \partial_2 T^{12} + (3\Gamma^1_{12} + \Gamma^2_{22})T^{12} + f^1, \\ -\partial_2 T^{22} - (2\Gamma^2_{22} + \Gamma^1_{12})T^{22} - \Gamma^2_{11}T^{11} = \partial_1 T^{12} + (3\Gamma^2_{12} + \Gamma^1_{11})T^{12} + f^2, \\ -2b_{12}T^{12} = f^3. \end{cases} \tag{2.2}$$

les composantes du déplacement sont solutions du système :

$$\gamma_{\alpha\beta} = \frac{1}{2}(D_\alpha u_\beta + D_\beta u_\alpha) - b_{\alpha\beta} = B_{\alpha\beta\lambda\nu}T^{\lambda\nu} \tag{2.3}$$

soit encore :

$$\begin{cases} \partial_1 u_1 - \Gamma^1_{11}u_1 - \Gamma^2_{11}u_2 = B_{11\alpha\beta}T^{\alpha\beta}, \\ \partial_2 u_2 - \Gamma^1_{22}u_1 - \Gamma^2_{22}u_2 = B_{22\alpha\beta}T^{\alpha\beta}, \\ \frac{1}{2}(\partial_1 u_2 + \partial_2 u_1) - \Gamma^1_{12}u_1 - \Gamma^2_{12}u_2 - b_{12}u_3 = B_{12\alpha\beta}T^{\alpha\beta}. \end{cases} \tag{2.4}$$

où les coefficients $B_{\alpha\beta\lambda\nu}$ sont les composantes du tenseur de souplesse. Dans la suite, pour étudier les singularités, nous considérons 6 inconnues $T^{\alpha\beta}$ et u_i lesquelles satisfont respectivement à (2.1) ou(2.2) et (2.3) ou (2.4). Les deux systèmes sont hyperboliques et les caractéristiques sont les droites d'équation $y^1 = Const.$ et $y^2 = Const.$. Les conditions aux limites sont choisies de manière à assurer l'inhibition de la coque. Le reste de la frontière est libre d'effort. Nous présentons deux cas particuliers, d'une part on s'intéresse à une donnée extérieure qui présente une discontinuité le long des caractéristiques et d'autre part on considère une donnée dont le support de la singularité n'est pas caractéristique.

2.1 Cas où le support du chargement est porté par une caractéristique

Considérons le chargement ayant comme particularité d'avoir un support rectangulaire dont les bords sont caractéristiques voir la figure 2.1.

$$\vec{f} = \begin{cases} f^1 = 0, \\ f^2 = 0, \\ f^3 = Y(y^2 - \frac{a_2}{2}) I_{[l^1,l^2]}(y^1). \end{cases} \tag{2.5}$$

où Y est la fonction de Heaviside, $I_{[a^1,b^1]}$ la fonction indicatrice sur l'intervalle $[l^1, l^2] \subset [0, a^1]$. En résolvant le système (2.1), nous remarquons que :

$$T^{12} = -\frac{Y(y^2 - \frac{a_2}{2}) I_{[l^1,l^2]}(y^1)}{2b_{12}(y^1, y^2)}$$

En reportant ceci dans les équations régissant T^{11} et T^{22} nous obtenons les relations suivantes :

$$\begin{cases} \partial_1 T^{11} - (2\Gamma^1_{11} + \Gamma^2_{12}) T^{11} - \Gamma^1_{22} T^{22} = \delta(y^2 - \frac{a_2}{2}) F_1(y^1) + \dots, \\ \partial_2 T^{22} - (2\Gamma^2_{22} + \Gamma^1_{12}) T^{22} - \Gamma^2_{11} T^{11} = Y(y^2 - \frac{a_2}{2}) F_2(y^1) + \dots. \end{cases} \tag{2.6}$$

Nous sommes donc concernés par la propagation des singularités dans les systèmes hyperboliques. Nous renvoyons le lecteur intéressé à l'ouvrage suivant [12] et aux articles suivants [31, 64]. Dans ce contexte, à l'ordre dominant et en tenant compte des singularités qui apparaissent dans le second membre du système d'équations (2.6), nous sommes amenés à rechercher pour les inconnues T^{11} et T^{22} des solutions sous la forme suivante :

$$\begin{cases} T^{11} = \tau^{11}(y^1) \delta(y^2 - \frac{a^2}{2}) + \dots, \\ T^{22} = \tau^{22}(y^1) Y(y^2 - \frac{a^2}{2}) + \dots. \end{cases} \tag{2.7}$$

où τ^{11} est solution d'une équation différentielle du premier ordre à coefficients non constants que l'on peut entièrement déterminer, et τ^{22} satisfait à une relation algébrique voir la section 2 de Karamian et al. [33]. À présent on s'intéresse au système d'équations concernant les composantes du déplacement. En reportant les expressions T^{11}, T^{12}, T^{22} dans (2.3) (ou 2.4) à l'ordre dominant nous obtenons le système suivant :

$$\begin{cases} \partial_1 u_1 - \Gamma^1_{11} u_1 - \Gamma^2_{11} u_2 = \delta(y^2 - \frac{a^2}{2}) B_{1111} \tau^{11}(y^1), \\ \partial_2 u_2 - \Gamma^1_{22} u_1 - \Gamma^2_{22} u_2 = \delta(y^2 - \frac{a^2}{2}) B_{2211} \tau^{11}(y^1), \\ \frac{1}{2}(\partial_1 u_2 + \partial_2 u_1) - \Gamma^1_{12} u_1 - \Gamma^2_{12} u_2 - b_{12} u_3 = \delta(y^2 - \frac{a^2}{2}) B_{1211} \tau^{11}(y^1) \end{cases} \tag{2.8}$$

ce qui suggère de rechercher des solutions sous la forme suivante :

$$\begin{cases} u_1 = \delta(y^2 - \frac{a^2}{2}) U_1(y^1) + \dots \\ u_2 = Y(y^2 - \frac{a^2}{2}) U_2(y^1) + \dots \\ u_3 = \delta'(y^2 - \frac{a^2}{2}) U_3(y^1) + \dots \end{cases} \tag{2.9}$$

où $U_1(y^1)$ est solution d'une équation différentielle du premier ordre à coefficients non constants, laquelle est résoluble et entièrement déterminée à partir des conditions aux limites. Les composantes $U_2(y^1)$ et $U_2(y^1)$ satisfont une relation algébrique

voir la section 2 de Karamian et al. [33].

Nous constatons que le degré de singularité de la troisième composante est de 2 degrés plus élevé que la singularité initiale et que cette singularité se propage non seulement dans la direction du support de la donnée initiale qui est caractéristique mais aussi dans l'autre direction caractéristique.

2.2 Cas où le support Σ du chargement est non-caractéristique

Considérons le chargement suivant dont la particularité est d'avoir un support non caractéristique (cf. figure 2.3). L'intérêt d'un tel choix est que cela ressemble à un chargement de type distribution de Dirac dont le support n'est pas caractéristique et comme nous allons le voir, les solutions vont présenter des singularités, qui vont se propager le long des caractéristiques mais pas dans le prolongement du support de la donnée. Contrairement au cas précédent, les solutions sont moins singulières, cela tient au fait que contrairement au cas précédent le support Σ du chargement n'est pas caractéristique.

$$\vec{f} = \begin{cases} f^1 = 0, \\ f^2 = 0, \\ f^3 = \delta(y^1 - y^2). \end{cases} \tag{2.10}$$

Pour étudier correctement ce cas de charge, nous devons procéder à un changement de variable. On pose comme nouvelles coordonnées l'abscisse curviligne ξ^1 le long du support Σ et ξ^2 la coordonnée normale à ξ^1 orientée dans le sens direct. Il en résulte que pour ce nouveau choix de coordonnées, les droites d'équations $\xi^2 = Const.$ ne sont pas des caractéristiques et par conséquent, avec la nouvelle paramétrisation les coefficients de la seconde forme fondamentale sont telles que $b_{11} \neq 0$ et $b_{22} \neq 0$. Nous avons alors la relation suivante :

$$T^{12} = -\frac{\delta(\xi^2)}{2b_{12}(\xi^1,0)} + \frac{b_{11}(\xi^1,0)}{2b_{12}(\xi^1,0)}T^{11} + \frac{b_{22}(\xi^1,0)}{2b_{12}(\xi^1,0)}T^{22}$$

En reportant cette nouvelle relation dans le système (2.1), à l'ordre dominant nous devons rechercher les solutions de la forme suivante :

$$\begin{cases} T^{11} = \tau^{11}(\xi^1)\delta(\xi^2) + \dots \\ T^{12} = \tau^{12}(\xi^1)\delta(\xi^2) + \dots \\ T^{22} = \tau^{22}(\xi^1)\delta(\xi^2) \dots . \end{cases} \tag{2.11}$$

En ce qui concerne les composantes du déplacement nous obtenons :

$$\begin{cases} \partial_1 u_1 - \Gamma^1_{11}u_1 - \Gamma^2_{11}u_2 - b_{11}u_3 = \delta(\xi^2)B_{11\alpha\beta}\tau^{\alpha\beta}(\xi^1), \\ \partial_2 u_2 - \Gamma^1_{22}u_1 - \Gamma^2_{22}u_2 - b_{22}u_3 = \delta(\xi^2)B_{22\alpha\beta}\tau^{\alpha\beta}(\xi^1), \\ \frac{1}{2}(\partial_1 u_2 + \partial_2 u_1) - \Gamma^1_{12}u_1 - \Gamma^2_{12}u_2 - b_{12}u_3 = \delta(\xi^2)B_{12\alpha\beta}\tau^{\alpha\beta}(\xi^1) \end{cases} \tag{2.12}$$

Ce qui nous amène à rechercher les solutions sous la forme suivante :

$$\begin{cases} u_1 = Y(\xi^2)U_1(\xi^1) + \dots \\ u_2 = Y(\xi^2)U_2(\xi^1) + \dots \\ u_3 = \delta(\xi^2)U_3(\xi^1) + \dots \end{cases} \tag{2.13}$$

Comme nous l'avions annoncé, dans le cas où le support de la singularité n'est pas caractéristique, les solutions sont moins singulières que dans le cas d'un chargement de type Heaviside et les singularités restent confinées sur Σ.

3 Etude asymptotique

À partir des exemples que nous avons présentés, nous pouvons déduire des renseignements sur les ordres de grandeur des couches caractéristiques et non-caractéristiques ainsi que sur le développement asymptotique des composantes du déplacement. Notre objectif est de décrire les couches internes au voisinage d'une caractéristique $y^2 = \frac{a^2}{2}$ mais également le long d'un segment non-caractéristique. Pour cela, nous allons nous servir des deux exemples que nous avons présentés dans la section précédente. Pour obtenir un développement asymptotique dans une couche nous commençons par faire un changement de variable avec mise à l'échelle. Posons respectivement pour une couche caractéristique

$$z^2 = \frac{y^2 - \frac{a^2}{2}}{\eta(\varepsilon)}, \quad \eta(\varepsilon) \searrow 0 \quad \text{quand} \quad \varepsilon \searrow 0$$

et pour une couche non-caractéristique

$$z^2 = \frac{\xi^2}{\eta(\varepsilon)}, \quad \eta(\varepsilon) \searrow 0 \quad \text{quand} \quad \varepsilon \searrow 0$$

où $\eta(\varepsilon)$ est l'ordre de grandeur de l'épaisseur de la couche interne. On postule l'allure du développement asymptotique des composantes du déplacement $\vec{u}^\varepsilon$ sous la forme suivante :

$$u_i^\varepsilon = \sum_k \eta^k(\varepsilon) u_i^k(y^1, \frac{y^2 - \frac{a^2}{2}}{\eta(\varepsilon)}) \quad \text{pour le cas caractéristique}$$

et

$$u_i^\varepsilon = \sum_k \eta^k(\varepsilon) u_i^k(\xi^1, \frac{\xi^2}{\eta(\varepsilon)}) \quad \text{pour le cas non-caractéristique}$$

En conséquence, comme le comportement des composantes du déplacement solution du problème limite $P(0)$ sont

$$\begin{cases} u_1 = \delta(y^2 - \frac{a^2}{2}) U_1(y^1) + \dots \\ u_2 = Y(y^2 - \frac{a^2}{2}) U_2(y^1) + \dots \\ u_3 = \delta'(y^2 - \frac{a^2}{2}) U_3(y^1) + \dots \end{cases}$$

au sein de la couche interne au voisinage de $y^2 = \dfrac{a^2}{2}$, nous devons donc chercher un développement asymptotique des composantes du déplacement quand $\varepsilon \searrow 0$ de la forme suivante :

$$\begin{cases} u_1^\varepsilon = \eta^{-1} U_1^\eta(y^1, y^2 - \frac{a^2}{2}) + \dots \\ u_2^\varepsilon = \eta^0 U_2^\eta(y^1, y^2 - \frac{a^2}{2}) + \dots \\ u_3^\varepsilon = \eta^{-2} U_3^\eta(y^1, y^2 - \frac{a^2}{2}) + \dots \end{cases} \tag{2.14}$$

De la même façon, pour le cas non-caractéristique, un raisonnement analogue nous conduit à postuler le développement asymptotique des composantes du déplacement quand $\varepsilon \searrow 0$ de la forme suivante :

$$\begin{cases} u_1^\varepsilon = \eta^0 U_1^\eta(y^1, y^2 - \frac{a^2}{2}) + \dots \\ u_2^\varepsilon = \eta^0 U_2^\eta(y^1, y^2 - \frac{a^2}{2}) + \dots \\ u_3^\varepsilon = \eta^{-1} U_3^\eta(y^1, y^2 - \frac{a^2}{2}) + \dots \end{cases} \tag{2.15}$$

Posons $\mathcal{V} = \{v = (v_1, v_2, v_3) \in H^1 \times H^1 \times H^2; v_1 = v_2 = v_3 = \partial_n v_3 = 0 \quad \text{sur} \quad \Gamma_0\}$ alors le problème des coques s'énonce ainsi.

$$\begin{cases} \text{Trouver } u^\varepsilon \in \mathcal{V} \quad \text{tel que} \\ a^m(u^\varepsilon, v) + \varepsilon^2 a^f(u^\varepsilon, v) =< f, v > \quad \forall v \in \mathcal{V} \end{cases} \tag{2.16}$$

En substituant (2.14) dans la formulation variationnelle (2.16) du problème des coques hyperboliques inhibées et en prenant une fonction test dépendant de η et réordonnant les termes nous obtenons une nouvelle expression voir la section 4 de l'article Karamian et al. [33].

$$\frac{1}{\eta^2} a_2^m(U^\eta, V) + \frac{1}{\eta} a_1^m(U^\eta, V) + a_0^m(U^\eta, V) + \frac{\varepsilon^2}{\eta^6} a^f(U^\eta, V) =< f, V >$$

Nous choisissons η de sorte que $\dfrac{\varepsilon^2}{\eta^6} = O(1)$, ce qui conduit alors à poser $\eta(\varepsilon) = \varepsilon^{\frac{1}{3}}$.

Nous procédons de manière similaire dans le cas non-caractéristique, si bien qu'en reportant (2.15) dans la formulation variationnelle (2.16) du problème des coques hyperboliques inhibées et en prenant une fonction test dépendant de η et réordonnant les termes nous obtenons une nouvelle expression voir la section 5 de l'article Karamian et al. [33].

$$a(U^\eta, V) + \frac{\varepsilon^2}{\eta^4} a^f(U^\eta, V) =< f, V >$$

Nous choisissons η de sorte que $\dfrac{\varepsilon^2}{\eta^4} = O(1)$, ce qui conduit alors à poser $\eta(\varepsilon) = \varepsilon^{\frac{1}{2}}$.
Le tableau 2.1 synthétise les différents cas qui peuvent se présenter pour des coques hyperboliques.

4 Estimation de l'erreur d'approximation numérique par les éléments finis isotropes versus anisotropes

Dans cette section nous énonçons deux propositions démontrant l'intérêt d'utiliser les éléments finis anisotropes dans le cas des couches limites et des couches internes. En effet, il est intéressant de tirer profit des particularités de la structure du développement asymptotique des solutions pour trouver une estimation de l'erreur dans le cadre d'une approximation par élément finis. Dans cette optique, nous nous bornons aux ordres dominants du développement asymptotique des solutions dans le cas des couches internes caractéristiques. Nous partons de la formulation

Couche interne	Comportement
Caractéristique épaisseur : $\eta(\varepsilon) = \varepsilon^{\frac{1}{3}}$	$\frac{v_2^\varepsilon}{v_1^\varepsilon} = \mathcal{O}(\eta^1)$ et $\frac{v_3^\varepsilon}{v_1^\varepsilon} = \mathcal{O}(\eta^{-1})$
avec f_3 discontinue	$\begin{cases} v_1^\varepsilon \cong \eta^{-1} U_1^0(y^1, y^2) \\ v_2^\varepsilon \cong \eta^0 U_2^0(y^1, y^2) \\ v_3^\varepsilon \cong \eta^{-2} U_2^0(y^1, y^2) \end{cases}$
Non-caractéristique épaisseur : $\eta(\varepsilon) = \varepsilon^{\frac{1}{2}}$	$\frac{v_2^\varepsilon}{v_1^\varepsilon} = \mathcal{O}(1)$ et $\frac{v_3^\varepsilon}{v_1^\varepsilon} = \mathcal{O}(\eta^{-1})$
	$\begin{cases} v_1^\varepsilon \cong U_1^0(y^1, y^2) \\ v_2^\varepsilon \cong U_2^0(y^1, y^2) \\ v_3^\varepsilon \cong \eta^{-1} U_3^0(y^1, y^2) \end{cases}$

Tableau 2.1 –

variationnelle du problème des coques (2.16).

Outre le fait que les solutions ne sont pas bornées et qu'il est préférable de raisonner en erreur relative, nous devons aussi faire face à un problème de pénalisation. En effet, les formes bilinéaires sont affectées respectivement des facteurs η^{-2}, η^{-1} et η^0. La conséquence est que les estimations d'erreur dans le cadre d'une approximation de Galerkin sont proportionnelles à η^{-1} entraînant dans son sillage des phénomènes de verrouillage numérique.

Puisque dans le développement asymptotique, l'ordre principal $U^0(y^1, z^2)$ est indépendant de η, nous allons considérer des estimations pour le cas des maillages avec des éléments finis isotropes en les variables y^1 et z^2 et nous posons $O(H)$ le pas de maillage dans les deux directions. Nous pouvons en déduire des estimations correspondant aux éléments finis en les variables y^1 et y^2 lesquelles deviennent anisotropes par la mise à l'échelle $z^2 = \dfrac{y^2}{\eta}$. Ceci conduit à des mailles anisotropes dont le pas de maillage dans les deux directions sont respectivement en $O(H)$ et en $O(\eta H)$. D'un point de vue géométrique cela revient à dire que les mailles sont très allongées dans la direction de la caractéristique. Nous sommes alors en mesure d'énoncer les deux propositions suivantes.

Proposition 1 *Soient k_1, k_2 les degrés des polynômes utilisés respectivement pour approximer les composantes tangentielles et normale du déplacement. Dans le cadre d'une approximation par la méthode de Galerkin, pour un maillage avec des éléments finis isotropes, c'est-à-dire que le pas de maillage en $O(h)$ est identique dans les deux directions, les estimations d'erreur sont données par les relations suivantes :*

$$\begin{cases} ||\delta_H \partial_1 u_1^\varepsilon||_{L^2} \leq C(\dfrac{h}{\eta})^{inf(k_1, k_2-1)} \eta^{-\frac{3}{2}} \\ ||\delta_H \partial_2 u_2^\varepsilon||_{L^2} \leq C(\dfrac{h}{\eta})^{inf(k_1, k_2-1)} \eta^{-\frac{3}{2}} \\ ||\delta_H \partial_2^2 u_3^\varepsilon||_{L^2} \leq C(\dfrac{h}{\eta})^{inf(k_1, k_2-1)} \eta^{-\frac{9}{2}} \end{cases} \tag{2.17}$$

Proposition 2 *Soient k_1, k_2 les degrés des polynômes utilisés respectivement pour approximer les composantes tangentielles et normale du déplacement. Dans le cadre d'une approximation par la méthode de Galerkin, pour un maillage avec des éléments finis anisotropes, c'est-à-dire que le pas de maillage n'est pas identique dans les deux directions $(H, \eta H)$, les estimations d'erreur sont données par les relations suivantes :*

$$\begin{cases} \dfrac{||\delta_H \partial_1 u_1^\varepsilon||_{L^2}}{||\partial_1 u_1^\varepsilon||_{L^2}} \leq C(H)^{inf(k_1,k_2-1)}\eta^{-1} \\ \dfrac{||\delta_H \partial_2 u_2^\varepsilon||_{L^2}}{||\partial_2 u_2^\varepsilon||_{L^2}} \leq C(H)^{inf(k_1,k_2-1)}\eta^{-1} \\ \dfrac{||\delta_H \partial_2^2 u_3^\varepsilon||_{L^2}}{||\partial_2^2 u_3^\varepsilon||_{L^2}} \leq C(H)^{inf(k_1,k_2-1)}\eta^{-1} \end{cases} \tag{2.18}$$

Il est à noter que dans le cas très particulier où $h = \eta H$ les estimations d'erreur du cas isotrope donnent précisément ceux du cas anisotrope. En outre, dans ce cas nous remarquons que le rapport des aires des triangles isotropes sur les aires des triangles anisotropes est en $O(\eta)$.

D'après les deux propositions, pour de très petites valeurs de ε, la conclusion est que pour les simulations numériques, dans l'éventualité où des couches internes apparaissent lesquelles se confondent avec les caractéristiques, il vaut mieux utiliser des mailles très allongées dans la direction des caractéristiques car cela n'altère en rien la qualité de l'approximation numérique tout en garantissant la convergence des solutions.

5 Simulations Numériques

Dans cette section, nous donnons quelques simulations numériques pour illustrer les résultats des sections précédentes pour le cas des coques hyperboliques soumises à des chargements singuliers. La carte locale est définie par $(\Omega, \overrightarrow{\psi}(y^1, y^2))$ avec $\Omega = [0, \pi] \times [0, \pi]$ et l'application $\overrightarrow{\psi}(y^1, y^2)$ définie de la manière suivante :

$$\overrightarrow{\psi}(y^1, y^2) = \begin{cases} y^1 \\ y^2 \\ y^1 y^2 \end{cases} \tag{2.19}$$

Pour l'ensemble des simulations, Γ_0 désigne les portions de frontière encastrées correspondant aux droites d'équations $y^1 = \pi$ et $y^2 = \pi$. En outre, pour les simulations numériques nous avons fixé le module de Young à $28500 Nm^{-2}$, le coefficient de Poisson est fixé à 0.4 et l'épaisseur ε de la coque est prise à 10^{-4}.

5.1 Cas des couches internes caractéristiques

Pour cet exemple, nous considérons le chargement $\overrightarrow{f} = (0, 0, f^3)$ avec

$$f^3 = \begin{cases} 1 \text{ sur } [\frac{\pi}{4}, \frac{\pi}{2}][\frac{\pi}{2}, \pi] \\ 0 \text{ ailleurs} \end{cases} \tag{2.20}$$

La figure 2.1 illustre de gauche à droite le support d'application du chargement et le maillage non uniforme utilisé pour la simulation numérique. La connaissance a priori des caractéristiques et de la structure des solutions nous aident à concevoir un maillage lequel est raffiné aux endroits où les singularités se propagent.

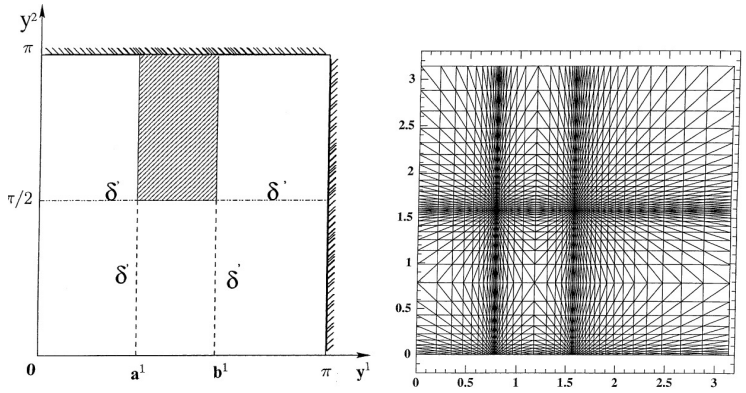

FIGURE 2.1 – De gauche à droite. Visualisation du support et la nature du chargement. Maillage raffiné correspondant

,

La figure 2.2 illustre de gauche à droite la troisième composante du déplacement ainsi qu'une coupe de cette même solution le long de la droite d'équation $y^2 = \dfrac{3\pi}{8}$. Comme cela a déjà été vu dans la section 2.1 la solution numérique exhibe trois singularités lesquelles se propagent respectivement le long des courbes caractéristiques d'équations $y^1 = \frac{\pi}{4}$, $y^1 = \frac{\pi}{2}$ et enfin $y^2 = \frac{\pi}{2}$. Comme nous pouvons le voir l'allure de la solution numérique est semblable à une distribution δ' comme cela a été établi.

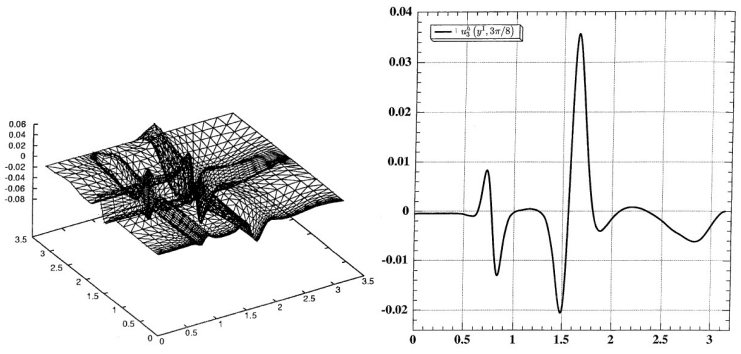

FIGURE 2.2 – De gauche à droite. Graphe de u_3 sur tout le domaine. Visualisation d'une coupe de u_3 pour $y^2 = \frac{3\pi}{8}$ qui illustre la propagation des singularités au voisinage de $y^1 = \frac{\pi}{4}$ et $y^1 = \frac{\pi}{2}$. L'allure de la solution numérique est semblable à δ'

,

5.2 Cas des couches internes non-caractéristiques

Pour cet exemple, nous considérons le chargement $\overrightarrow{f} = (0, 0, f^3)$ avec

$$f^3 = \begin{cases} 50 \text{ sur } \{0 < y^1 < \frac{\pi}{2}, |y^1 - y^2| < 0.02\} \\ 0 \text{ ailleurs} \end{cases} \tag{2.21}$$

La figure 2.3 illustre de gauche à droite le support Σ d'application du chargement et le maillage non uniforme utilisé pour la simulation numérique. La connaissance a priori des caractéristiques et de la structure des solutions nous aident à concevoir un maillage lequel est raffiné aux endroits où les singularités se propagent.

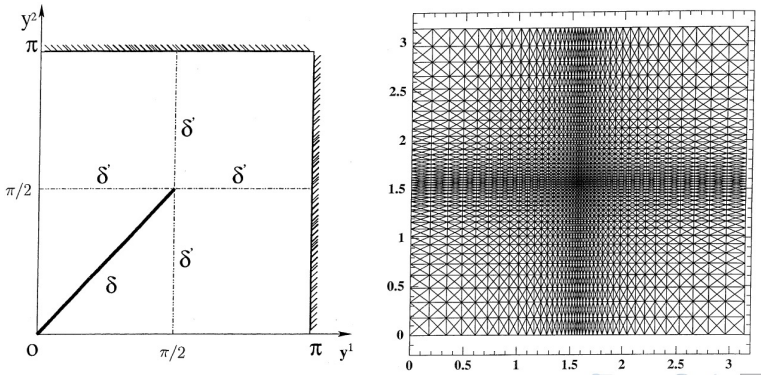

FIGURE 2.3 – De gauche à droite. Visualisation du support et la nature du chargement. Maillage raffiné correspondant

,

La figure 2.4 illustre de gauche à droite la troisième composante du déplacement ainsi qu'une coupe de cette même solution le long de la droite d'équation $y^2 = \dfrac{3\pi}{8}$. Comme cela a déjà été vu dans la section 2.1 la solution numérique exhibe deux singularités qui se propagent respectivement le long des courbes caractéristiques d'équations $y^1 = \frac{\pi}{2}$, $y^1 = \frac{\pi}{2}$. Comme nous pouvons le voir l'allure de la solution numérique est semblable à une distribution δ' comme cela a été établi dans la section 2.1.

La figure 2.5 montre une coupe de cette même solution le long de la droite d'équation $y^2 = \dfrac{17\pi}{20}$. Comme nous pouvons le voir l'allure de la solution numérique est semblable à une distribution δ comme cela a été établi dans la section 2.2.

6 Problème de réflexion dans les coques : notion de pseudo-réflexion

Dans cette section nous abordons la notion de pseudo-réflexion que j'ai introduite pour la première fois dans [28]. Nous insistons sur le fait que cela concerne uniquement le problème membranaire. Le principal objectif est d'étudier l'éventualité d'une réflexion des singularités quand ces dernières interceptent une frontière non-caractéristique. Ce point est essentiel. Un point important à retenir est que les

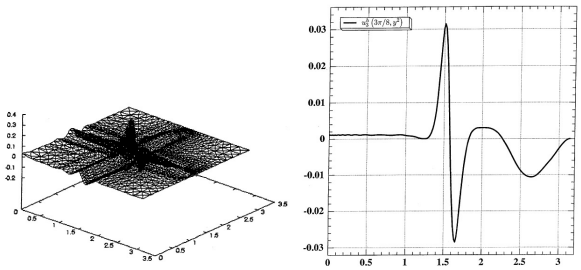

FIGURE 2.4 – De gauche à droite. Graphe de u_3 sur tout le domaine. Visualisation d'une coupe de u_3 pour $y^2 = \frac{3\pi}{8}$ ce qui illustre la propagation des singularités au voisinage du point $y^1 = \frac{\pi}{2}$ et $y^2 = \frac{\pi}{2}$. L'allure de la solution numérique est semblable à δ'

,

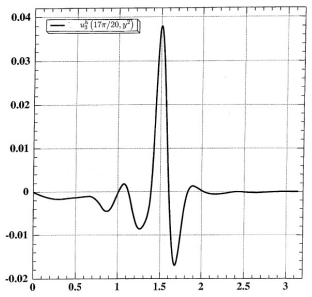

FIGURE 2.5 – Visualisation d'une coupe de u_3 pour $y^2 = \frac{17\pi}{20}$ qui illustre le confinement de la singularité sur le support de Σ. L'allure de la solution numérique est semblable à δ

,

conditions aux limites que l'on prescrit sur les frontières ne sont pas exactement celles conduisant à la notion de réflexion qui s'applique classiquement aux équations hyperboliques.

Rappelons que nous nous intéressons au phénomène de réflexion sur les portions de frontière Γ qui ne sont pas parallèles aux caractéristiques. Ces frontières peuvent être soit libres de toutes conditions aux limites voire satisfaire à des conditions de fixation mais ce uniquement pour les composantes tangentielles. En effet, dans le problème membranaire la composante normale du déplacement intervient en tant qu'inconnue principale et non sa dérivée. Ce qui explique pourquoi nous n'avons pas besoin d'imposer de conditions aux limites pour cette inconnue.

Nous choisissons les lignes asymptotiques comme lignes coordonnées. Les coefficients de la seconde forme fondamentale sont $b_{11} = b_{22} = 0$, $b_{12} \neq 0$. Après elimination de T^{12}, les équations et les conditions aux limites prennent la forme suivante :

$$\begin{cases} \partial_1 T^{11} + (2\Gamma^1_{11} + \Gamma^2_{12})T^{11} + \Gamma^1_{22}T^{22} = -f^1 + \partial_2(\dfrac{f^3}{2b_{12}}) + \dfrac{3\Gamma^1_{12} + \Gamma^2_{22}}{2b_{12}} f^3 \\ \partial_2 T^{22} + (2\Gamma^2_{22} + \Gamma^1_{12})T^{22} + \Gamma^2_{11}T^{11} = -f^2 + \partial_1(\dfrac{f^3}{2b_{12}}) + \dfrac{3\Gamma^2_{12} + \Gamma^1_{11}}{2b_{12}} f^3 \\ T^{11}n_1 = \dfrac{f^3}{2b_{12}} n_2 \quad , \quad T^{22}n_2 = \dfrac{f^3}{2b_{12}} n_1 \quad \text{sur une partie } \Gamma_1 \text{ de la frontière} \end{cases} \tag{2.22}$$

De même après élimination de u_3 nous obtenons

$$\begin{cases} \partial_1 u_1 + \Gamma^1_{11}u_1 + \Gamma^2_{11}u_2 = B_{11\alpha\beta}T^{\alpha\beta} \\ \partial_2 u_2 + \Gamma^1_{22}u_1 + \Gamma^2_{22}u_2 = B_{22\alpha\beta}T^{\alpha\beta} \\ (u_1, u_2) = (0,0) \quad \text{sur une partie } \Gamma_0 \text{ de la frontière} \end{cases} \tag{2.23}$$

où les $\Gamma^\alpha_{\beta\delta}$ sont les symboles de Christoffel et les $B_{\alpha\beta\delta\nu}$ sont les coefficients de souplesse.

Definition 1 (pseudo-reflexion) *Considérons les deux systèmes différentiels 2.22 et 2.23 lesquelles sont de nature hyperbolique avec données de Cauchy sur des courbes non caractéristiques ; à ce titre ils sont le siège de propagation des singularités le long des caractéristiques dès lors que les données extérieures sont singulières. Nous dirons qu'il y a pseudo-réflexion si la singularité qui intercepte une frontière non caractéristique sur laquelle y est prescrite des conditions de Cauchy celle-ci est réfléchie selon la seconde caractéristique en gagnant un degré de régularité lors de la réflexion. C'est à dire que la singularité réfléchie est moins singulière que la singularité incidente.*

Nous distinguons deux cas. Le cas où le chargement $\overrightarrow{f}$ est régulier au voisinage de la frontière d'une part et d'autre part le cas où le chargement présente des singularités. Ainsi avons nous étudié une série de 6 variantes qui sont :

1. frontière libre Γ_1 avec une donnée $\overrightarrow{f}$ régulière dans un voisinage d'un point $A \in \Gamma_1$

2. frontière fixé Γ_0 avec une donnée $\overrightarrow{f}$ régulière dans un voisinage d'un point $A \in \Gamma_0$
3. frontière libre Γ_1 avec une donnée $\overrightarrow{f}$ singulière le long d'une caractéristique au voisinage de tout point $A \in \Gamma_1$
4. frontière fixé Γ_0 avec une donnée $\overrightarrow{f}$ singulière le long d'une caractéristique au voisinage de tout point $A \in \Gamma_0$
5. frontière libre Γ_1 avec une donnée $\overrightarrow{f}$ singulière sur une courbe non-caractéristique au voisinage de tout point $A \in \Gamma_1$
6. frontière fixé Γ_0 avec une donnée $\overrightarrow{f}$ singulière sur une courbe non-caractéristique au voisinage de tout point $A \in \Gamma_0$

Il est facile de voir que le premier cas ne conduit pas à de la réflexion. En effet, comme la donnée $\overrightarrow{f}$ est régulière et que nous n'imposons aucune condition aux limites sur Γ_1 toutes les inconnues du système membranaire sont régulières et donc elles ne présentent aucune singularité, par conséquent il n'y a pas de réflexion. Quant aux autres cas les choses se passent différemment. Pour le détail des 5 autres cas nous renvoyons le lecteur aux sections 6 et 7 dans [35].

Les deux propositions qui suivent résument les principaux résultats obtenus dans l'étude des pseudo-réflexions.

Proposition 3 (cas caractéristique) *Étant donné un chargement dont la composante normale notée f^3 a une singularité d'ordre δ (ou de manière équivalente, les composantes tangentielles f^α ont une singularité d'ordre δ') le long d'une caractéristique. Alors, la composante normale du déplacement u_3 présente une singularité d'ordre δ'' le long de la caractéristique. Celle-ci jouit de propriétés de propagation et lorsqu'elle intercepte une frontière, elle se propage selon l'autre direction caractéristique en gagnant un degré de régularité, ce qui revient à dire que u_3 a une singularité d'ordre δ'. Cependant, il existe un cas particulier. Il s'agit du cas où la frontière est libre de toutes conditions aux limites et dont le support de la singularité de f^3 n'atteint pas la frontière. Dans ce cas et uniquement dans ce cas il n'y a aucune réflexion qui se produise. Le processus se poursuit jusqu'à la rencontre de la prochaine frontière, gagnant à chaque étape un degré de régularité entraînant l'évanescence de la singularité.*

Proposition 4 (cas non-caractéristique) *Étant donné un chargement dont la composante normale notée f^3 a une singularité d'ordre δ (ou de manière équivalente, les composantes tangentielles f^α ont une singularité d'ordre δ') le long d'un support non-caractéristique. Alors, la composante normale du déplacement u_3 présente une singularité d'ordre δ le long du support non-caractéristique. Dans l'éventualité où le support non-caractéristique de la donnée singulière intercepte une frontière avec ou sans conditions aux limites, alors la composante u_3 a une singularité d'ordre δ et δ' respectivement tout en se propageant le long des caractéristiques issues de la frontière et le phénomène de pseudo-réflexion est observé selon les règles de la proposition précédente.*

7 Simulations Numériques

Dans cette section, afin d'illustrer par des simulations numériques le phénomène de pseudo-réflexion, nous allons considérer un domaine Ω représenté par la figure 2.6. Il s'agit d'un domaine rectangulaire dont les coordonnées des sommets sont respectivement $A = (-4, 0)$, $B = (0, -4)$, $C = (6, 2)$, $D = (2, 6)$. La surface moyenne de la coque est paramétrée à l'aide de l'application $\overrightarrow{\psi}(y^1, y^2)$ définie de la manière suivante :

$$\overrightarrow{\psi}(y^1, y^2) = \begin{cases} y^1 \\ y^2 \\ y^1 y^2 \end{cases} \tag{2.24}$$

Ainsi les lignes asymptotiques sont les droites d'équation $y^1 = Const.$ et $y^2 = Const.$. La coque est encastrée sur les portions de frontière d'équation $y^1 - y^2 = 4$ et $y^1 - y^2 = -4$ respectivement. Sur la figure 2.6, les portions de frontière encastrées sont matérialisées en gras. Il est à noter que de par le choix des conditions aux limites la coque est inhibée.

Nous considérons un chargement de la forme suivante :

$$\overrightarrow{f}(y^1, y^2) = \begin{cases} 0 \\ 0 \\ \delta(y^2 + 2) \end{cases} \tag{2.25}$$

ce qui revient à considérer une force concentrée le long de la droite d'équation $y^2 = -2$ qui de surcroît est une caractéristique. Pour la simulation numérique cette force est appliquée aux noeuds présents sur la droite d'équation $y^2 = -2$. D'après ce qui précède de l'étude des propagations des singularités et les conséquences de la pseudo-réflexion, la singularité va se propager le long des courbes caractéristiques qui dans le cas présent sont $y^2 = -2$, $y^1 = \pm 2$ et $y^2 = 2$.

La figure 2.7 illustre bien le phénomène de pseudo-réflexion sur la troisième composante du déplacement. Il est clair que la solution est plus singulière (δ'') sur la caractéristique $y^2 = -2$ que sur les caractéristiques $y^1 = \pm 2$ (δ') et $y^2 = 2$ (δ).

La figure 2.8 montre des coupes de la solution u_3^ε et met en avant la structure en δ'' et δ' des solutions.

La figure 2.9 est une illustration de la proposition 4

8 Bilan

Les solutions des équations qui décrivent les coques minces de type hyperbolique, comme nous avons pu le constater, jouissent de propriétés particulières qui sont le siège de phénomènes complexes. Il s'agit du phénomène de propagation des singularités le long des caractéristiques lesquelles coïncident avec les lignes asymptotiques de la surface moyenne. Il ressort que pour des petites valeurs de l'épaisseur ε, nous

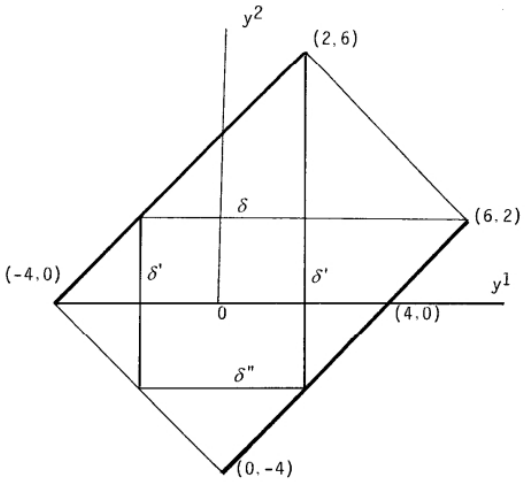

FIGURE 2.6 – Visualisation du domaine Ω et matérialisation du support des singularités et des pseudo-reflexions. Les symboles $\delta'', \delta', \delta$ représentent le degré des singularités de la composante normale du déplacement pour la donnée $\vec{f} = (0, 0, \delta(y^2 + 2))$.

,

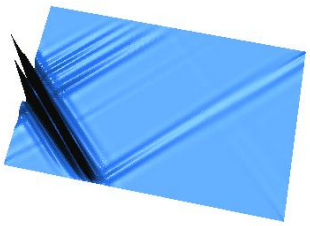

FIGURE 2.7 – Graphe de u_3^ε pour la totalité du domaine

,

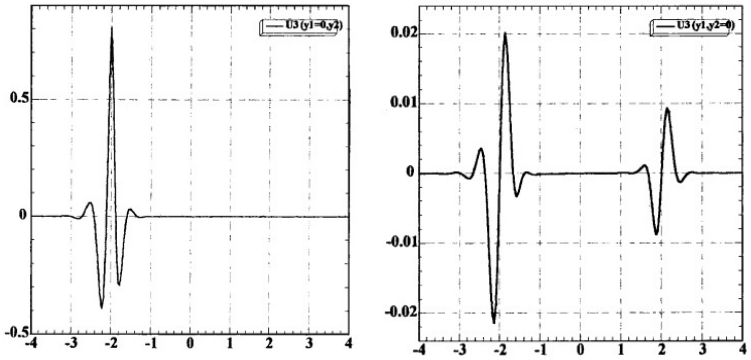

FIGURE 2.8 – De gauche à droite. Coupe de u_3^ε le long des sections d'équation $y^1 = 0$ et $y^2 = 0$

,

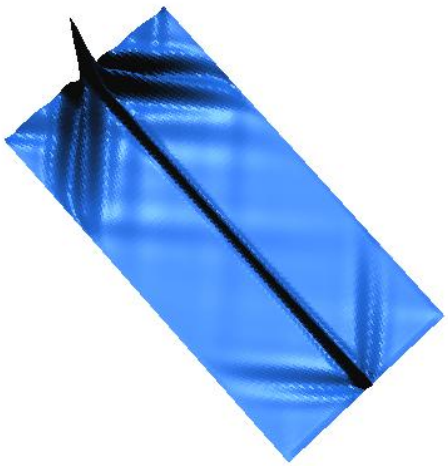

FIGURE 2.9 – Visualisation de u_3^ε sur la totalité du domaine Ω

,

observons des zones ou des bandes très étroites qui sont le siège de forte et brutale variation pour les composantes du déplacement. De cette étude il en résulte que dans le cas des coques hyperboliques, le degré de singularités des solutions est plus élevé que celui de la donnée elle-même. Au travers de cette étude nous avons pu mettre en évidence les ordres de grandeur des couches internes caractéristique ou non caractéristique qui sont respectivement en $O\left(\varepsilon^{\frac{1}{3}}\right)$ et $O\left(\varepsilon^{\frac{1}{2}}\right)$, ainsi que la structure des solutions et les ordres principaux dans le développement asymptotique pour chacun des cas de figure (cf. le tableau 2.1). Par ailleurs, dans le cadre de la méthode de Galerkin, nous avons établi des estimations d'erreur pour la méthode des éléments finis isotropes et anisotropes. Enfin, le phénomène de pseudo-réflexion nous conduit à énoncer des lois générales de réflexion au travers de deux propositions.

Deuxième partie

Matériaux composites à microstructures complexes

Chapitre 3

Modélisation 2D, étude et évaluation numérique des propriétés élastiques des composites à fibres courtes

Travaux publiés dans Technische Mechanik [36] et Computational Materials Science [37]

1 Objectifs

Dans cette section nous cherchons à concevoir une modélisation numérique pour étudier les composites à microstructures complexes laquelle a fait l'objet de deux publications [36, 37].

Dans un premier temps, nous abordons le problème de la génération des VER (volume élémentaire représentatif) ainsi que la manière dont nous procédons pour engendrer les microstructures au sein des VER et comment nous sommes parvenus à les mailler.

Dans un second temps nous utilisons la technique d'homogénéisation double-échelle et une approche stochastique dans le traitement des données puis nous comparons notre approche et nos résultats avec ceux existants dans la littérature.

2 Problématique

Les composites à fibres courtes suscitent un grand intérêt pour le secteur industriel tel que l'automobile, l'aérospatiale et l'aéronautique. À performance mécanique égale, ces derniers permettent de concevoir des structures très légères à un faible coût de production.

Il faut donc être en mesure d'évaluer les propriétés élastiques des milieux hétérogènes, notamment en ce qui concerne les inclusions à fibres courtes. De par les fluctuations des hétérogénéités et les contrastes élevés des propriétés mécaniques,

l'usage des bornes habituelles de Voigt et Reuss, et ceux de Hashin-Shtrikman [22] sont à écarter. C'est pourquoi une nouvelle approche est proposée pour mener une étude numérique liée à la génération d'un grand nombre de volumes élémentaires représentatifs (VER). Le VER doit satisfaire plusieurs contraintes à savoir, suffisamment grand pour prendre en compte la nature de la microstructure du milieu et limiter le coût de calcul et respecter un rapport d'échelle minimal avec le milieu macroscopique. Le lecteur intéressé peut se référer à l'article [11] sur ce sujet. La notion de VER a une importance cruciale dans le domaine des milieux hétérogènes et exige une détermination précise en fonction de la configuration matérielle.

Il faut savoir qu'un unique VER de grande taille peut être choisi aussi bien que plusieurs VER de petite taille à condition que les dimensions choisies pour les VER n'entraînent pas de biais relativement aux conditions aux limites. Il s'avère que les conditions aux limites périodiques donnent de meilleurs résultats. Par la suite, sauf mention explicite du contraire, ce choix sera toujours fait. Pour procéder à une évaluation asymptotique des propriétés nous avons considéré un grand nombre de VER de petite taille et périodique. Quant à l'évaluation des propriétés mécaniques, la méthode double-échelle décrite par [58] et [4] est employée.

Outre les considérations sus-mentionnées, la démarche adoptée pour appréhender et étudier ces composites est basée sur l'emploi d'une approche stochastique décrite par Kanit et al. [27]. L'idée est de concevoir un échantillonage de motifs périodiques représentatifs du composite étudié ayant des dimensions plus petites, donc plus adapté à la simulation numérique intense. L'ensemble des échantillons constitue une base de données, laquelle est exploitée pour déterminer les propriétés mécaniques effectives du composite. Ainsi, les propriétés effectives ne sont pas évaluées sur un seul VER mais sur l'ensemble des échantillons. Une des difficultés à laquelle il a fallut faire face était de constituer cette base de données. Dans cette optique, les VER ont été fabriqués de toute pièce selon une approche de Monte-Carlo, dans laquelle un jeu de paramètres décrivant la morphologie du composite, tels que la longueur des fibres, le diamètre des fibres et leur orientation, est tiré aléatoirement selon des lois de distribution préalablement définies. Dans cette modélisation, l'entrelacement, le contact et le chevauchement entre les hétérogénéités sont autorisés contrairement aux méthodes d'adsorption séquentielle aléatoire (ASA) [57]. Ce choix de modéliser les contacts est motivé pour prendre en compte l'impact de la percolation des hétérogénéités sur les propriétés mécaniques des composites à fibres courtes [23].

Une possibilité pour évaluer des propriétés mécaniques des matériaux composites est l'usage de la méthode des éléments finis bien qu'une approche par transformée de Fourier soit également envisageable, je pense notamment à la méthode développée par Moulinec et Suquet [51]. Ce n'est pas le choix fait par la suite. Une fois les VER conçus, il faut les mailler. Cette étape est cruciale. Elle doit être la plus automatisée et la plus fiable possible, ce qui est un véritable défi. C'est pourquoi une approche dite par grille a été choisie pour laquelle les hétérogénéités sont générées à partir d'une grille d'hexaèdres réguliers. Outre cette approche, un processus de raffinement local de type multi-grille est proposé, lequel permet une réduction significative du

coût de calcul des VER en vue d'un traitement par éléments finis.

3 Génération stochastique des VER, maillage sous Cast3M

Le logiciel Cast3M a été retenu pour la conception et l'étape de maillage des VER pour constituer la base de données avec laquelle les évaluations des propriétés mécaniques et l'étude des différents paramètres morphologiques ont été menées. Dans cette optique, les hétérogénéités 2D et 3D au sein du composite sont générées à l'aide d'une approche Monte-Carlo. Pour décrire les hétérogénéités au sein du composite, les paramètres morphologiques tels que la longueur, le diamètre, l'orientation, la localisation spatiale des fibres sont pris en compte lesquels sont considérés comme des variables aléatoires réelles obéissant à des lois de distribution classique comme la loi uniforme, la loi normale, la loi log-normale ... D'autres paramètres morphologiques ont été aussi introduits pour estimer leur impact et les effets sur l'évaluation des propriétés mécaniques. Je pense, notamment, à la tortuosité des fibres, la largeur de la zone d'interphase laquelle peut se voir comme une altération des propriétés locales entre le renfort et la matrice d'une part, et, d'autre part, la décohésion de l'interface entre la matrice et le renfort.

L'algorithme de génération des hétérogénéités peut se résumer de la sorte : engendrer une cellule parallélépipédique, le plus souvent un cube en 3D ou un carré en 2D. Décider les lois de distribution des paramètres morphologiques comme la longueur, l'orientation, l'élancement, le diamètre, la localisation des fibres. Fixer la quantité des hétérogénéités pour atteindre la fraction volumique ou surfacique désirées des fibres courtes. Ensuite pour chaque fibre effectuer un tirage aléatoire de localisation spatiale, de l'orientation, de la longueur et de l'élancement et construire à l'aide des commandes de Cast3M la représentation dans l'espace ou dans le plan de l'enveloppe des hétérogénéités. L'étape suivante, toujours sous Cast3M, consiste à mailler les VER ainsi générés en respectant les frontières géométriques le chevauchement des hétérogénéités [37, 41]. Deux approches peuvent être envisagées. Une méthode qualifiée de conforme à la géométrie d'une part, et, d'autre part, une méthode dite non-conforme. Dans la première approche, chaque hétérogénéité est maillée indépendamment les unes des autres selon un degré de raffinement souhaité, ensuite la matrice est à son tour maillée en s'appuyant sur les frontières du réseau des hétérogénéités. Les inconvénients d'une telle approche sont multiples, temps de calcul prohibitif, manque de fiabilité dans la génération des VER et, dans certains cas, défauts dans la construction même du maillage annihilant dans la foulée la possibilité de faire du Monte-Carlo.

La seconde approche est empruntée à la technique de l'imagerie à partir d'une acquisition d'image, il s'agit d'utiliser la notion de pixelisation en 2D ou voxelisation en 3D. (cf. Mishnaevsky [48, 49, 53]). D'autres auteurs [7] l'ont utilisée dans le calcul d'homogénéisation pour l'évaluation des propriétés mécaniques. L'idée consiste à approximer la géométrie réelle des hétérogénéités à l'aide d'une grille de qua-

drangles dans le plan ou d'hexaèdres dans l'espace. Ainsi, le centre de gravité de chaque élément sert de critère pour la sélection des quadrangles ou des hexaèdres pour délimiter la frontière des hétérogénéités. À son tour, cette approche présente un inconvénient majeur dans la prise en compte des frontières du réseau des hétérogénéités.

Pour contourner cette difficulté tout en conservant l'avantage de la pixelisation ou de la voxelisation la technique de raffinement de maillage adaptatif est utilisée [5]. Lorsque la taille du VER devient importante la méthode perd de son intérêt et donc nécessite de mettre en place une autre approche. Nous proposons une autre voie baptisée à géométrie d'ordre n et développée au sein de l'équipe (cf. section 2.3.2 [41]) pour procéder au calcul des tenseurs homogénéisés de rigidité et de souplesse afin de déterminer les propriétés mécaniques effectives des composites à fibres courtes .

Une étude comparative des résultats en temps de calcul CPU a été menée selon une approche conforme versus une approche non-conforme des géométries des hétérogénéités. De cette étude, il ressort qu'à faible taux de fraction surfacique des hétérogénéités, le temps de calcul CPU pour concevoir, mailler et calculer les tenseurs homogénéisés de rigidité et de souplesse ne varie pas de manière significative aussi bien dans l'approche qualifiée de conforme que non-conforme. L'intérêt de la méthode à géométrie d'ordre n se manifeste pour des taux de fraction surfacique supérieure à 10%.

4 Évaluation des propriétés mécaniques du composite : homogénéisation double-échelle

Dorénavant, les hypothèses suivantes sont supposées êtres vérifiées pour l'évaluation des propriétés mécaniques des composites. Les VER contiennent un nombre suffisant d'informations sur les hétérogénéités telles que les vides, les fibres courtes, les inclusions, les grains etc... Les dimensions des VER sont finies et bornées inférieurement et supérieurement par la taille de la plus grosse hétérogénéité et par les dimensions du milieu macroscopique respectivement. Les VER sont statistiquement représentatifs du milieu macroscopique. C'est-à-dire que le principe d'ergodicité du milieu n'est pas violé. Différents tests empruntés à la théorie statistique ont été employés pour vérifier cette hypothèse et ainsi valider la conception de nos VER. Les VER sont soumis aux conditions aux limites périodiques car ce sont elles qui induisent le moins de biais sur les résultats. Enfin, les tailles des VER sont ajustées en fonction de la nature des microstructures et de la fraction volumique ou surfacique des hétérogénéités. Il ne faut pas perdre de vue que la base de données des VER est entièrement générée et contrôlée par un jeu de paramètres, considérés comme des variables aléatoires obéissant à des lois de distribution classique. Le maillage des VER est alors issu de l'approche non-conforme basée sur une approximation géométrique d'ordre n des frontières des hétérogénéités.

L'évaluation proprement dite des propriétés mécaniques des composites se fait par la méthode d'homogénéisation double-échelle introduite par Sanchez-Palencia [58]. Le processus asymptotique formel, qui se justifie mathématiquement après coup,

appliqué à l'équation fondamentale de la statique en mécanique, fournit un moyen efficace pour déterminer le tenseur homogénéisé de rigidité et de souplesse, permettant ainsi d'avoir accès aux différentes propriétés effectives des composites. En effet, le processus une fois mené à son terme conduit à résoudre une équation aux dérivées partielles, dénommée équation microscopique, laquelle se résout par les éléments finis. Cependant, il n'est pas judicieux de traiter directement cette équation aux dérivées partielles, il est préférable de la retravailler. Debordes [10] a été le premier à fournir une technique fort élégante pour résoudre l'équation aux dérivées partielles en introduisant la notion de noeud fictif d'une part, et, d'autre part, une fois la résolution effectuée celle-ci donne directement le tenseur de rigidité homogénéisé du composite et donc donne accès aux propriétés mécaniques du composite. Une fois l'équation aux dérivées partielles discrétisée par les éléments finis et après avoir pris en compte les conditions aux limites périodiques, celle-ci conduit à la résolution d'un système linéaire de la forme suivante.

$$\begin{bmatrix} K & KE^t \\ KE & E \end{bmatrix} \begin{bmatrix} \boldsymbol{\omega}^{kl} \\ P_{ij}^{kl} \end{bmatrix} = \begin{bmatrix} \mathbf{0}^{kl} \\ \delta_i^k \delta_j^l \end{bmatrix} \tag{3.1}$$

où la matrice K désigne la matrice de rigidité associée aux différentes hétérogénéités. La matrice KE ainsi que sa transposée KE^t est une matrice issue de la forme linéaire de la dérivée au sens des distributions du tenseur de rigidité du milieu et la matrice E représente la moyenne du tenseur de rigidité du milieu. Les $\boldsymbol{\omega}^{kl}$ et P_{ij}^{kl} représentent nos inconnues correspondant respectivement au champ des déformations locales et une matrice que, par abus de langage, je dénommerai matrice de souplesse homogénéisée effective ; la dépendance aux indices $\{k, l\}$ correspond respectivement aux trois directions $\{1,1\}, \{2,2\}, \{1,2\}$ dans le plan et aux 6 directions $\{1,1\}, \{2,2\}, \{3,3\}, \{1,2\}, \{1,3\}, \{2,3\}$ dans l'espace. Dans l'hypothèse où le comportement macroscopique du matériau est isotrope, ce qui n'est pas tout à fait le cas, désignons par $\boldsymbol{S}$ le tenseur de souplesse, alors le module de Young, le coefficient de Poisson, le module de compressibilité et le module de cisaillement dans le plan ont pour expressions :

$$\begin{aligned} E &= \frac{1}{2} \sum_{\alpha \leq 2} \frac{1}{\boldsymbol{S}_{\alpha\alpha\alpha\alpha}} \\ \nu &= -\frac{1}{2} \sum_{\alpha,\beta \leq 2_{\alpha \neq \beta}} \frac{\boldsymbol{S}_{\alpha\alpha\beta\beta}}{\boldsymbol{S}_{\beta\beta\beta\beta}} \\ K &= \frac{1}{4} \sum_{\alpha,\beta \leq 2} \boldsymbol{C}_{\alpha\alpha\beta\beta} \\ \mu &= \frac{1}{\boldsymbol{S}_{3333}} \end{aligned}$$

5 Validation du modèle numérique et comparaison avec d'autres modèles analytiques

Proposer une modélisation pour étudier et évaluer les propriétés des composites à microstructures complexes reste toujours un point délicat. Encore, faut-il que cette

modélisation soit cohérente, et espérer qu'elle soit féconde pour aborder d'autres aspects que les précédentes modélisations n'ont pas pu appréhender.

5.1 Modèle à géométrie conforme versus géométrie non-conforme

Pour valider la modélisation, la conception et la génération des VER par la méthode de Monte-Carlo faisant appel à un jeu de paramètres stochastiques et d'un processus de maillage géométrique d'ordre n précédemment évoqué, différents tests et cas de figure ont été élaborés. Dans un premier temps, l'influence sur les résultats numériques de l'approximation géométrique d'ordre n, pour $n \in [0, 1, 2]$ a été testée. Pour ce faire, différentes fractions surfaciques de fibre ont été choisies pour comparer avec le modèle à géométrie conforme versus le modèle à géométrie non-conforme. Les figures 3.1 illustrent de ce point vue la convergence du module de Young et le coefficient de cisaillement en fonction de l'ordre d'approximation de la géométrie. De cette étude il ressort que plus l'ordre d'approximation est élevé moins les valeurs numériques des propriétés mécaniques divergent de celles obtenues avec le modèle à géométrie conforme. Dans un second temps, une comparaison a été effectuée en utilisant la méthode FE^2 laquelle a été développée par Feyel [16]. Les résultats sont en totale concordance avec ceux obtenus avec la technique d'homogénéisation en double-échelle développée par Sanchez-Palencia [60]. Dans un troisième temps, un test numérique sous Cast3M simulant le test de traction uniaxial a été mené. Les figures 3.2 exhibent parfaitement la totale cohérence entre ces différents cas test proposés, ce qui permet de conclure que le modélisation proposée est admissible.

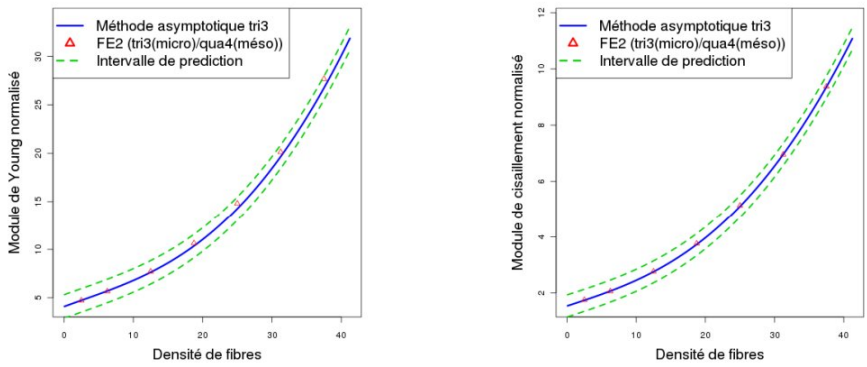

FIGURE 3.1 – Comparaison FE2/ méthode double-échelle : Cas du module de Young et du module de cisaillement

5.2 Modèle analytique versus modèle numérique proposé

Il nous reste à comparer le modèle numérique proposé avec les modèles analytiques pour étudier les composites à microstructures complexes. Dans un premier temps, une comparaison est effectuée avec les bornes micromécaniques classiques tirées de la littérature des milieux hétérogènes. Il s'agit des bornes de Voigt et Reuss (VR), lesquelles s'obtiennent par la loi des mélanges dans des directions parallèle et

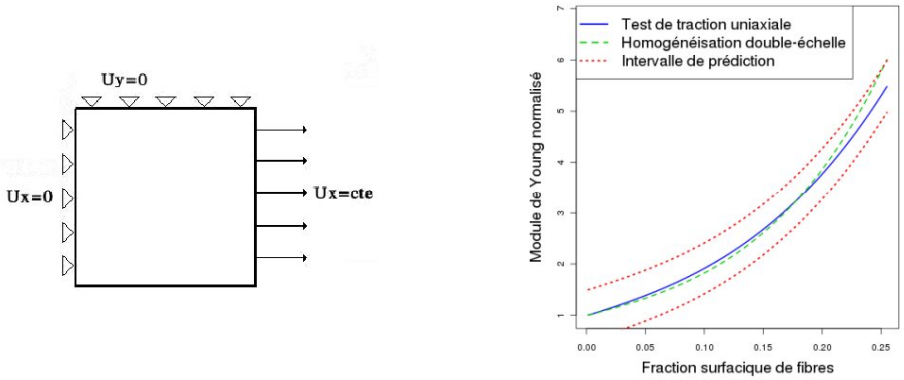

FIGURE 3.2 – test de traction uniaxiale et conditions aux limites associées

transverse. Dans un second temps, les estimations de Halpin-Tsai (HT) [21] sont évaluées ; ce modèle permet d'obtenir respectivement les bornes supérieur et inférieur pour les modules de Young transverse et le module de Young longitudinal. Dans un troisième temps, les bornes de Hashin-Shrtickmam (HS) [22, 67] sont également évaluées et sont usuellement utilisé dans les milieux à deux phases pour le cas tridimensionnel. Une adaption s'avère être nécessaire car les renforts dans le cas considéré sont isotropes transverses et de plus bidimensionnels. Les figures 3.3, 3.4, 3.5 illustrant les résultats numériques montrent qu'ils sont tous situés entre les bornes supérieure et inférieure de Hashin-Shrtickmam, il en resulte que la modélisation numérique proposée et l'usage de la technique d'homogénéisation double-échelle ne viole pas les bornes issues des modèles analytiques.

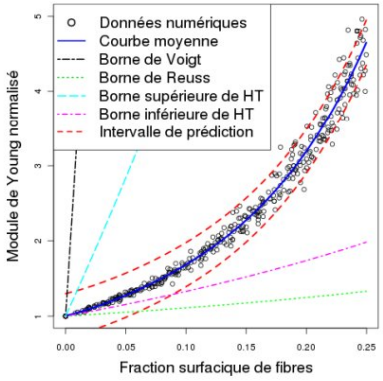

FIGURE 3.3 – Comparaison module de Young versus bornes de Hashin-Tsai

Un autre grand classique des modèles analytiques intéressant à prendre en compte est celui de Mori-Tanaka [52]. Sa validité à notre modélisation est mise en cause dans la mesure où notre modèle tient compte de l'entrelacement des hétérogénéités est que le modèle de Mori-Tanaka est précisément conçu pour le cas inverse. Cependant dans le cas d'un faible taux de fraction surfacique il peut être exploité pour effectuer une série de comparaison. La figure 3.5 illustre bien ce phénomène et permet

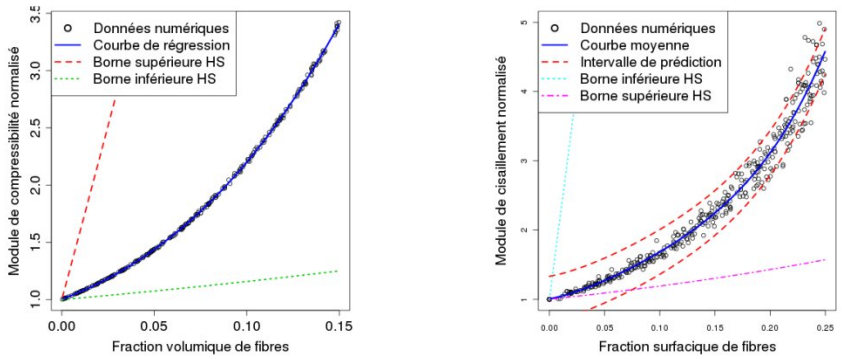

FIGURE 3.4 – Comparaison module de copressibilité versus bornes de Hashin-Shtrikmann

d'observer la divergence entre les résultats issus de simulation numérique et ceux prédits par le modèle de Mori-Tanaka.

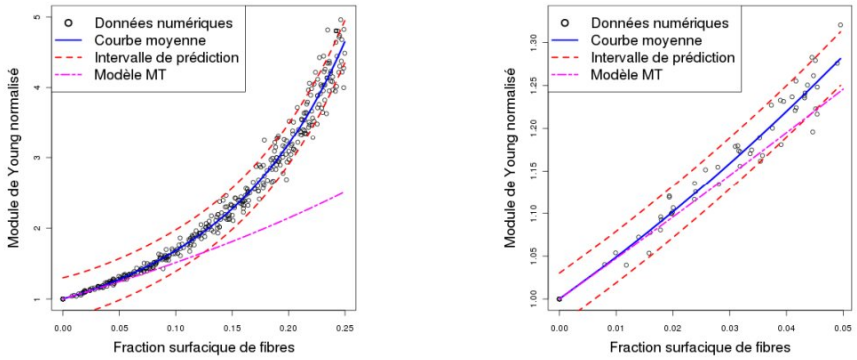

FIGURE 3.5 – Module de Young versus Modèle Mori-Tanaka. Agrandissement sur une fraction surfacique inférieure à 5%

6 Bilan

À ce stade, les outils sont en place pour étudier numériquement les composites à microstructures complexes en vue de l'évaluation des propriétés mécaniques des composites par la technique d'homogénéisation en double-échelle. Il s'agit d'une procédure stochastique, automatisée, fiable, robuste et efficace dans la génération des hétérogénéités en dépit de la complexité du réseau des hétérogénéités qui est de plus entrelacé. Les paramètres morphologiques sont des variables aléatoires régies par des lois de distribution usuelles, telles que la loi uniforme et la loi normale. La méthode de Monte-Carlo est utilisée pour la génération des VER. Le maillage des VER est assuré par l'approximation géométrique d'ordre n non-conforme. Le modèle proposé permet de retrouver les résultats obtenus par d'autres modélisation et ne viole pas les résultats des modèles analytiques.

Chapitre 4

Effets et influence de la dispersion spatiale des hétérogénéités sur les propriétés mécaniques

Article publié dans Computational Materials Science [39] et Mechanics et Industry [40]

1 Objectifs

Diverses études attestent que la fraction surfacique ou volumique des hétérogénéités joue un rôle fondamental dans la réponse mécanique d'un composite. Outre ce paramètre, il en existe bien d'autres pour expliquer les propriétés effectives d'un composite. Je pense tout particulièrement à la morphologie des hétérogénéités et leur réseau, c'est-à-dire la manière dont ils se répartissent au sein des composites. Ces paramètres jouent un rôle prépondérant pour étudier et expliquer certaines propriétés mécaniques et la manière dont les composites sont ou peuvent être sollicités.

La dispersion spatiale des hétérogénéités au sein de la matrice, certes d'un tout autre enjeu, a également des répercussions aussi importantes que les phénomènes morphologiques et ne peut pas être écartée. Aussi est-il reconnu que pour un composite dans lequel les hétérogénéités forment des agrégats, celui-ci tend à avoir des propriétés mécaniques moindres. Les questions relatives à l'impact et l'influence de la distribution spatiale des hétérogénéités sont plus délicates et complexes qu'il n'y paraît. Parmi les récents travaux portant sur cette question citons ceux de Seidel [66] et Jeulin [23–25]. Ce dernier a introduit le concept de schéma booléen pour simuler la notion de dispersion spatiale non-homogène de sphères et de sphéro-cylindres. Cette approche est relativement féconde et efficace car facile à mettre en œuvre d'une part, et, d'autre part elle agit sur plusieurs paramètres conduisant à la modélisation de diverses hétérogénéités dans la dispersion spatiale permettant ainsi de considérer les situations des plus simples aux plus complexes. Certaines des configurations étudiées présentent le phénomène de percolation relatif au réseau des hétérogénéités ce qui permet de les comparer à des cas de distribution homogène.

La percolation joue un rôle très important dans la conduction thermique et élec-

trique des composites. Cependant, dans un contexte mécanique le caractère non diffusif des équations de l'élasticité laisse à penser que la percolation n'est pas de nature phénoménologique. En effet, dans la communauté des expérimentateurs il est connu que la formation d'agglomérats ou agrégats agit comme un concentrateur de contraintes inhibant le bénéfice des renforts [20, 45]. À l'inverse, une répartition homogène des hétérogénéités a tendance à améliorer les propriétés mécaniques du matériau.

Les travaux récents de Fralick et al. [17] apportent un nouvel éclairage sur la percolation dans le cadre mécanique dans la mesure où les auteurs montrent que sous l'hypothèse d'un fort taux de contraste des propriétés, rapport entre matrice et renfort supérieur à 10^7, alors un effet plus que significatif sur la réponse mécanique du composite est observé.

Bon nombre de mécaniciens, dont Jeulin et Moreaud, conjecturent l'idée selon laquelle un milieu présentant une percolation verrait ses propriétés mécaniques drastiquement améliorées. Bien que ce fait soit assez bien observé et qu'il puisse s'expliquer par la nature diffusive des équations aux dérivées partielles de la conduction thermique et électrique, j'y apporte toute fois une réserve car il me semble encore prématuré de conclure qu'un réseau nécessairement percolant conduise invariablement à une augmentation des propriétés mécaniques. À mon humble avis, il faut aussi tenir compte du fait que le transfert des charges au sein même du réseau n'est pas parfait, donnant naissance à des zones de concentration de contraintes, tendant ainsi à dégrader les propriétés du composite et par ricochet atténuer l'effet escompté de la percolation. Cette observation ne contredit pas les travaux de Fralick et al. dans la mesure où si les taux de contraste et le taux de fraction surfacique ou volumique sont élevés, ce n'est pas la percolation qui améliore les propriétés mécaniques mais justement c'est le fait qu'il y ait un grand nombre d'hétérogénéités à fort taux de contraste qui expliquerait les améliorations. L'argument de la percolation est souvent mis en avant dans ce genre de situation car il y a plus de chance de l'observer mais il n'est pas rare de trouver des situations où la percolation a lieu sans pour autant observer une augmentation des propriétés mécaniques du composite comme cela sera illustré plus tard.

2 Modèle numérique adopté

Pour générer la distribution des fibres au sein des VER, nous faisons appel au schéma booléen de cercles, la transcription 2D de la version 3D des travaux de Jeulin [23–25]. Il s'agit de jouer sur deux facteurs d'échelle, une première échelle relative à la dimension des fibres et une seconde échelle plus importante liée à la dimension des agglomérats pour concevoir les inclusions. Nous introduisons trois paramètres : le facteur d'échelle, lequel représente le rapport entre le diamètre des cercles et la longueur des fibres, la densité de fibres présentes dans les disques et enfin la fraction surfacique des cercles au sein du VER.

La figure 4.1 illustre un exemple de VER construit sur le principe du schéma

booléen de cercles à deux niveaux. L'idée est toujours la même, les cercles sont engendrés de façon aléatoire, ensuite les centres des fibres sont elles-mêmes réparties aléatoirement au sein des disques. Pour terminer le maillage est fait à l'aide de l'approximation géométrique d'ordre n=0. Comme le suggère les figures, les fibres forment de petits îlots indépendants.

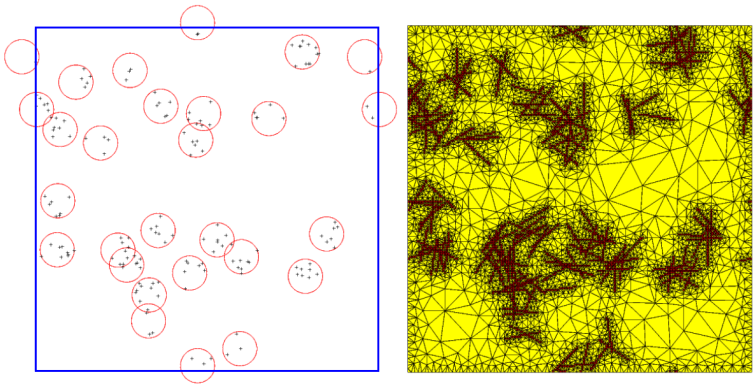

FIGURE 4.1 – De gauche à droite : schéma booléen de cercles à deux échelles avec positionnement des centres des fibres. Illustration finalisée du VER après maillage

3 Étude de la percolation dans le cadre d'une approche géométrique d'ordre n

En présence d'une forte concentration des hétérogénéités au sein de la matrice il peut se former des chemins par le contact successif de plusieurs hétérogénéités. Il est alors possible de constater que deux bords opposés du VER sont reliés, ce phénomène porte le nom de percolation. Dans la suite, les études présentées concernent un réseau de VER 2D percolant dans lequel les chemins de percolation sont selon une direction privilégiée, laquelle peut être soient parallèles aux axes de coordonnées (ox) ou (oy). La notion de seuil de percolation a une importance fondamentale dans le domaine des schémas booléens puisque la notion de percolation existe à différentes échelles. Encore faut-il être capable d'évaluer ce seuil de percolation. Il existe essentiellement deux manières d'évaluer le seuil de percolation. La première approche est de nature analytique [2, 3]. La seconde fondée sur une approche numérique développée par Jeulin et Moreaud [24, 46]. Dans l'article [39] une autre approche numérique pour évaluer le seuil de percolation est proposée et présentée dans la section suivante.

3.1 Méthode proposée pour l'évaluation de la percolation

Le principe de la méthode est basé sur l'étiquetage avec partitionnement de domaine pour optimiser le temps de calcul. La méthode est récursive et dichotomique. Il faut disposer d'une subdivision efficace pour minimiser le coût de l'étape de la connexion. Le processus est réalisé en q étapes, où q est l'ordre du partitionnement en puissance de 4 pour le cas bidimensionnel. Ainsi, pour $q = 2$ la subdivision engendre 16 sous-domaines voir figure 4.2, ce qui correspond à l'étape $i = 0$. Une subdivision

dichotomique en 2^q sous-domaines est effectuée (ici $i = 1$). Pour chaque étape $i > 0$, on pose $p = i - 1$ et une nouvelle subdivision dichotomique en 4^p domaines est réalisée et ce jusqu'à ce que $p = 0$, ce qui représente le VER dans sa globalité. La seconde étape consiste à effectuer les connexions par groupe de 4 sous-domaines au sein de chaque domaine. Le processus est répété tant que $i \neq q$. La figure 4.2 résume le diagramme décrivant le processus de partitionnement dichotomique et récursif des connexions entre sous-domaines avec $q = 2$.

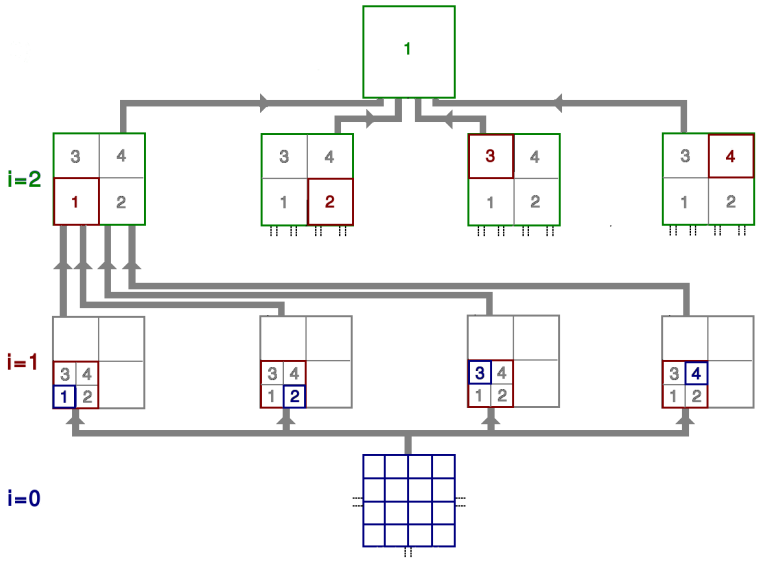

FIGURE 4.2 – Diagramme du processus de partitionnement dichotomique et récursif des connexions entre sous-domaines avec $q = 2$

Le tableau 4.1 illustre le temps de calcul afin de vérifier la percolation sur un VER à l'aide de la technique de partitionnement dichotomique et récursive. Le choix de l'ordre q est donc déterminant pour optimiser les temps de calcul. Dans le cas d'une étude avec des fibres courtes, où l désigne la longueur de la fibre, alors il s'avère qu'un choix optimal pour q est donné par la partie entière de $\log_2(l)$. Nous constatons que pour un taux de fraction surfacique supérieur ou égale à 10%, et pour la longueur des fibres que nous considérons il vaut mieux prendre $q = 2$ pour avoir un gain de temps substantiel dans l'évaluation de la percolation.

fraction surfacique	5%	10%	15%	20%	25%
q = 0	0'16"70	0'48"04	1'30"30	2'09"23	2'50"36
q = 1	0'14"31	0'32"20	0'48"67	1'03"24	1'17"05
q = 2	0'18"02	0'31"03	0'41"53	0'50"46	0'57"28
q = 3	0'31"44	1'00"51	1'07"62	1'11"74	1'11"86

Tableau 4.1 – Temps de calcul CPU : méthode de partitionnement dichotomique et récursive

4 Effets de la dispersion des fibres aléatoirement réparties

Une étude sur la distribution hétérogène des fibres a été conduite. Dans les sections suivantes les principaux résultats pour le seuil de percolation et les propriétés mécaniques sont présentés relativement au degré d'agglomération qui est un paramètre soit de la densité de fibres au sein des agrégats circulaires soit de la fraction surfacique de cercles présents dans le VER.

4.1 Impact de la densité moyenne des fibres

Une première étude de l'influence de la densité de fibres dans les inclusions circulaires est menée. Il s'agit de quantifier l'influence du degré d'agglomération sur les propriétés mécaniques. Les graphiques de la figure 4.3 montrent l'influence de la densité des fibres à l'intérieur des inclusions circulaires à la fois sur le module de Young et le module de cisaillement. Il ressort qu'au fur et à mesure que la densité augmente, cela se traduit par une perte des propriétés mécaniques. En résumé, une distribution hétérogène des agglomérats de même dimension que les fibres a un impact plutôt négatif. Ce résultat est corroboré par des mesures expérimentales.

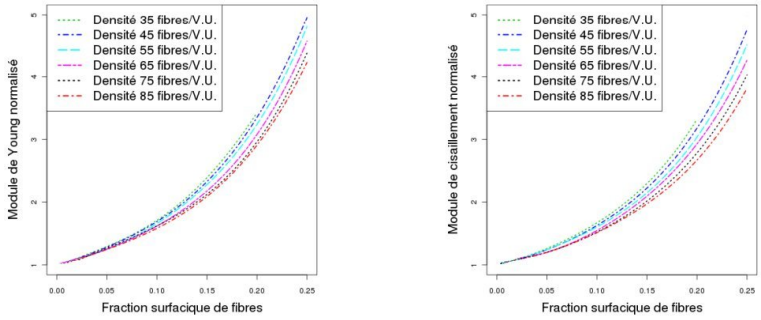

FIGURE 4.3 – De gauche à droite : influence de la densité de fibres sur le module de Young et le module de cisaillement

Le tableau 4.2 illustre l'influence de la densité de fibres sur le module de Young et le module de cisaillement ainsi que le seuil de percolation des fibres. Il ressort que les propriétés mécaniques faiblissent et que ce phénomène s'accompagne d'une augmentation du seuil de percolation dès lors que le taux de fibres est important.

Densité (/U.R.)	35	45	55	65	75	85
E (25%,GPa)	20.81	20.80	20.11	19.17	18.44	17.63
G (25%,GPa)	8.02	7.32	6.97	6.61	6.12	5.85
Seuil de percolation	0.1973	0.2081	0.2211	0.2370	0.2500	0.2609

Tableau 4.2 – Influence de la densité de fibres à la fois sur les propriétés mécaniques et le seuil de percolation du composite

4.2 Impact du facteur d'échelle sur le seuil de percolation

Afin de montrer l'influence et l'impact d'une dispersion hétérogène de fibres une étude dans le cadre d'un facteur d'échelle supérieur à 1 est présentée. Deux cas de figure sont pris en compte, d'une part la densité des fibres au sein des inclusions, et, d'autre part, la fraction surfacique des cercles au sein du VER. Le but est de mettre en évidence le lien qui pourrait exister entre le seuil de percolation et le renforcement des propriétés mécaniques du composite.

Le premier graphe de la figure 4.4 permet d'illustrer l'influence de la densité de fibres sur le seuil de percolation pour les trois facteurs d'échelles différent. Sur la figure de gauche, la ligne discontinue en rouge matérialise le seuil de percolation d'une distribution homogène de fibres. Il ressort des courbes que pour une densité de fibres inférieure à 45 fibres par VER unitaire, plus le facteur d'échelle est grand et plus le seuil de percolation est faible et inversement pour une densité de fibres supérieure à 45 fibres par VER unitaire. Ce phénomène s'explique par l'influence des dimensions du VER, car dans le cas d'un facteur d'échelle plus grand, les dimensions du VER le sont également afin de respecter le rapport entre les dimensions du motif et le diamètre des cercles ce qui conduit à des résultats plus précis.

Le second graphique de la figure 4.4 montre l'influence de la fraction surfacique de cercles sur le seuil de percolation pour les mêmes facteurs d'échelle considérés précédemment. La ligne discontinue en violet matérialise le seuil de percolation d'un réseau de cercles distribués de manière homogène. Pour les trois courbes, le seuil de percolation minimal est obtenu lorsque la fraction surfacique de cercles est égale à 100%. En d'autres termes, pour avoir le plus faible taux de percolation il faut avoir une distribution des fibres qui soit la plus homogène possible. Cependant, il ne faut pas exclure une possible réduction du seuil de percolation pour une fraction surfacique de cercles moindre et un facteur d'échelle strictement supérieur à 4. Par manque de ressources informatiques suffisantes, la conjecture n'a pu être vérifiée.

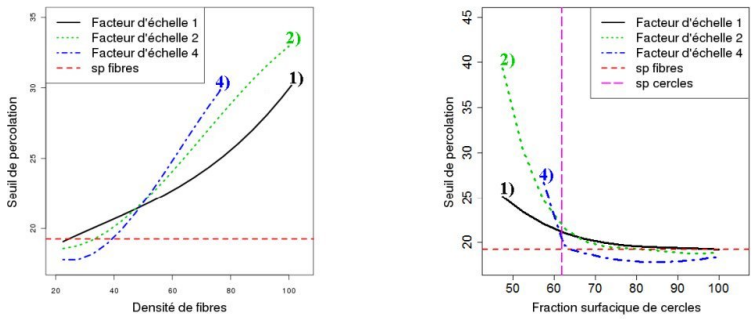

FIGURE 4.4 – De gauche à droite : influence de la densité de fibres et de la fraction surfacique de cercles sur le seuil de percolation

4.3 Impact du facteur d'échelle sur les propriétés effectives du module de Young

D'après ce qui précède une distribution homogène de fibres s'accompagne d'un seuil de percolation plus faible que dans le cas d'une distribution hétérogène. Ce seuil peut aussi être abaissé pour des distributions faiblement hétérogènes mais avec des facteurs d'échelle plus importants. Mais quelle répercussion cela a-t-il sur les propriétés mécaniques lorsque le seuil de percolation présente des fluctuations à la hausse ou à la baisse ? Les graphiques de la figure 4.5 montrent l'évolution du module de Young en fonction de la fraction surfacique de cercles et pour deux facteurs d'échelle. Il ressort de cette étude que dans les deux situations le module de Young diminue selon l'importance de l'agglomération et ce quels que soient la fraction surfacique de fibres et le seuil de percolation. La conclusion est que la percolation n'est pas une garantie à elle seule pour assurer de meilleures performances mécaniques des composites.

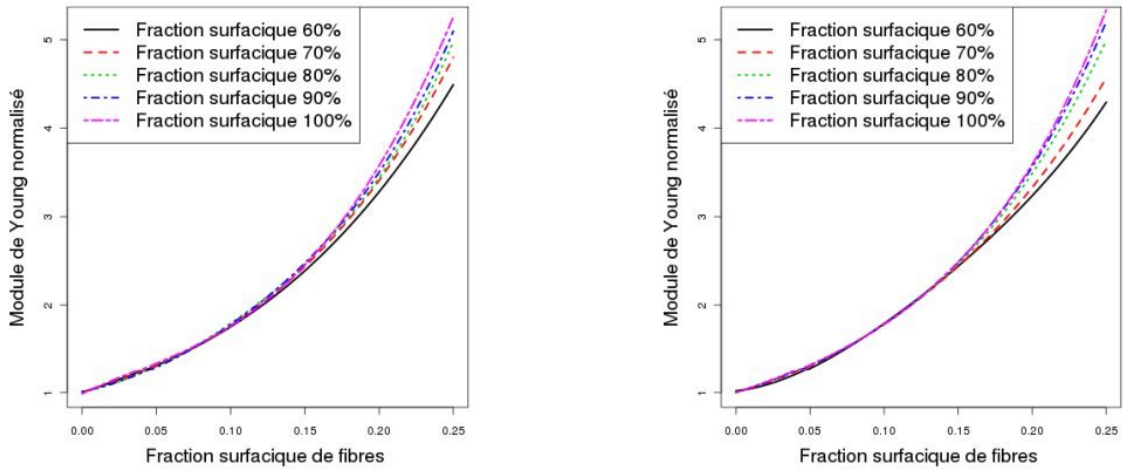

FIGURE 4.5 – De gauche à droite : influence de la fraction surfacique de cercles sur le module de Young avec un facteur d'échelle fixé respectivement à 2 et 4

le tableau 4.3 permet de se rendre compte de l'influence du facteur d'échelle sur le module de Young et le seuil de percolation pour les 3 facteurs d'échelles pris en considération pour cette étude.

	Fraction surfacique de cercles (%)	60	70	80	90	100
Echelle=1	E (25%,GPa)	20.43	21.02	21.61	21.87	21.91
	Seuil de percolation	0.2154	0.1991	0.2026	0.1916	0.1928
	Nombre de réalisations	16180	22756	21035	37557	25430
	Ecart-type	0.0015	0.0010	0.0016	0.0007	0.0004
Echelle=2	E (25%,GPa)	18.86	20.16	20.89	21.40	22.07
	Seuil de percolation	0.2329	0.1963	0.1920	0.1897	0.1882
	Nombre de réalisations	6867	7602	7960	11310	13516
	Ecart-type	0.0042	0.0017	0.0008	0.0006	0.0004
Echelle=4	E (25%,GPa)	18.03	19.19	20.96	21.85	22.41
	Seuil de percolation	0.2956	0.1847	0.1793	0.1810	0.1810
	Nombre de réalisations	701	1790	2258	3812	4096
	Ecart-type	0.0137	0.0033	0.0007	0.0003	0.0002

Tableau 4.3 – Influence du facteur d'échelle à la fois sur le module de Young et seuil de percolation d'un matériau composite

5 Impact mutuel de la dispersion et de la morphologie des fibres

Afin d'étudier l'influence conjuguée de l'orientation et de l'élancement de la dispersion des fibres sur les propriétés mécaniques, une approche par schéma booléen de cercles à deux échelles a été mise en place. Deux études disjointes sont réalisées, la première porte sur l'impact d'un réseau de fibres alignées, la seconde est dédiée à l'étude de l'élancement des fibres.

5.1 Alignement des fibres

Pour étudier l'alignement des fibres un réseau de fibres aléatoirement orientées est engendré. Dans cette configuration, il ressort que plus la fraction surfacique de fibres est importante, plus le module de Young augmente et plus le seuil de percolation diminue. Le tableau 4.5 réprésente l'influence de la fraction surfacique de cercles sur les modules de Young et de cisaillement ainsi que sur le seuil de percolation du composite étudié.

Fraction surfacique de cercles (%)	60	70	80	90	100
E (Fraction surfacique 25%)	40.62	45.59	49.82	52.02	53.69
G (Fraction surfacique 25%)	2.48	2.43	2.43	2.42	2.40
Seuil de percolation	0.3262	0.3150	0.3112	0.3074	0.3047

Tableau 4.4 – Influence de la fraction surfacique de cercles à la fois sur le modules de Young et de cisaillement et le seuil de percolation dans le cadre de fibres alignées

5.2 Élancement des fibres

Il ressort que plus la fraction surfacique de cercles est importante, plus le module de Young augmente et que le seuil de percolation des fibres et du module de

cisaillement est abaissé. La conclusion est que le phénomène d'agglomération altère le renforcement du composite. Le tableau 4.5 résume l'effet de la fraction surfacique des cercles sur le module de Young ainsi que sur le seuil de percolation des fibres.

Fraction surfacique de cercles (%)	60	70	80	90	100
E (25%, Elancement 10)	14.54	14.93	15.16	15.34	15.45
s (Elancement 10)	0.3015	0.2877	0.2768	0.2751	0.2753
E (25%, Elancement 20)	20.43	21.02	21.61	21.87	21.91
s (Elancement 20)	0.2229	0.2006	0.2007	0.1916	0.1928
E (25%, Elancement 50)	30.12	33.04	36.58	38.24	39.44
s (Elancement 50)	0.1124	0.1043	0.1012	0.0983	0.0968
E (25%, Elancement 100)	39.58	45.20	49.49	52.67	55.11
s (Elancement 100)	0.0630	0.0581	0.0556	0.0549	0.0531

Tableau 4.5 – Influence de la fraction surfacique de cercles sur le module de Young et le seuil de percolation pour différentes valeurs du rapport d'aspect

6 Bilan

Dans le cadre de l'étude numérique qui a été conduite, il ressort que la percolation joue un rôle négligeable sur les propriétés mécaniques du composite. L'existence d'un, deux ou plusieurs chemins de percolation reliant deux bords du VER ne permet pas d'observer une amélioration significative des propriétés mécaniques. Notons qu'un réseau de fibres agglomérées conduit à des propriétés mécaniques plus faibles que dans le cas d'une distribution uniforme des fibres dans le composite d'une part, et, d'autre part le seuil de percolation se trouve être plus élevé.

Les travaux menés par Fralick et al. [17], suggèrent que pour observer un effet notoire des renforts, le taux de contraste entre ces derniers et la matrice doit être très élevé. Cette conjecture reste à vérifier et croiser avec des études en rapport avec la percolation à fort taux de contraste.

Outre le fait que dans le contexte de cette étude, il en résulte que quels que soient l'élancement et l'orientation des fibres, les propriétés mécaniques du composite sont moindres, cette étude permet néanmoins de retrouver les résultats de Jeulin et Moreaud [23–26, 46] dans le cas où les fibres sont réparties de manière hétérogène avec des facteurs d'échelle respectivement égaux à 2 et 4.

Chapitre 5

Décomposition de domaine dans le cadre de l'homogénéisation double-échelle

Article publié dans International Journal of Solids and Structures [38]

1 Objectifs

Pourquoi adapter la méthode de décomposition de domaine à l'homogénéisation me direz-vous ? Pour accélérer le calcul des propriétés effectives de milieux hétérogènes me rétorquerez-vous ! Mais l'enjeu majeur est tout autre. En effet, dans le cadre bidimensionnel, l'étude d'une distribution hétérogène de fibres engendrée par un schéma booléen de cercle avec facteur d'échelle élevé est un exemple qui nécessite des VER de grandes dimensions. Dans le cas tridimensionnel, il s'avère quasi-impossible de traiter une base de données dont les VER ont de grandes dimensions. Cependant ces propos sont à nuancer dans le cadre tridimensionnel du fait que la nature et le degré de finesse des hétérogénéités à étudier peuvent eux-mêmes réduire la portée de l'apport de la décomposition de domaine. Vous l'aurez compris, le principal objectif est de réduire le temps de calcul CPU afin de rendre possible une étude bi et tridimensionnel des VER de grandes dimensions. Le calcul multi-processeurs est la voie qu'il faut prendre pour contourner ces difficultés qui surgissent dans l'étude des VER de grandes dimensions. L'idée est donc de mettre en place une stratégie de parallélisation des procédures à tous les niveaux. En ce sens, la décomposition de domaine fournit une base solide et relativement facile à mettre en oeuvre. Il existe différentes méthodes pour aborder la méthode de décomposition de domaine. Elle se scinde en deux familles, les méthodes dite avec et sans recouvrement. De par leur robustesse les méthodes sans recouvrement ont été privilégiées pour étudier les VER de grandes tailles. Les deux principales méthodes sont donc celles du complément de Schur [1] et de FETI (Finite Element Tearing and Interconnect) [13, 14, 55].

Afin de procéder à l'évaluation des propriétés effectives des matériaux composites avec la technique de décomposition de domaine, un premier travail dans la conception des VER est nécessaire. Il s'agit d'opérer un découpage de chaque VER en des

sous-domaines eux-mêmes de formes géométriques simples, comme par exemple des carrés en 2D et des cubes en 3D. Chaque sous domaine est à son tour généré par une approximation géométrique d'ordre n décrit dans le chapitre 3. Ensuite, chaque sous domaine est maillé de manière indépendante. La figure 5.1 illustre un exemple de partitionnement en 4 sous-domaines dans le cas bidimensionnel. Il est à noter qu'un soin particulier a été apporté au traitement dans la continuité du milieu aux interfaces internes Γ^i entre les sous-domaines d'une part, et d'autre part afin de pouvoir utiliser la méthode d'homogénéisation double-échelle avec conditions aux limites périodiques, la périodicité aux frontières extérieures Γ^0 au domaine complet Ω est assurée mais pas pour les sous-domaines Ω_i.

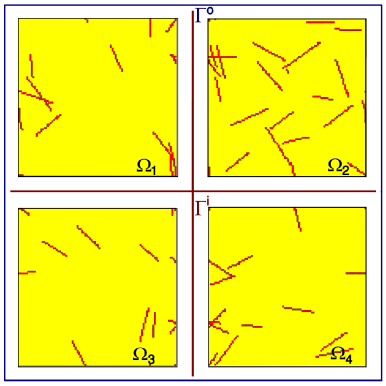

FIGURE 5.1 – Partitionnement en 4 sous-domaines d'un VER : approximation non-conforme correspondant à l'approche géométrique d'ordre 0

Ne perdons pas de vue que l'objectif est d'évaluer les propriétés mécaniques d'un composite par la méthode d'homogénéisation double-échelle précédemment décrite dans la section 4 du chapitre 3. Dans la section suivante, une approche combinant la méthode du complément de Schur [1] et FETI-1 [14,15] est présentée pour contourner la difficulté de la prise en compte des conditions aux limites périodiques.

2 Méthode mixte et homogénéisation double-échelle

2.1 La méthode du complément de Schur

La méthode du complément de Schur [1] conduit après discrétisation du problème à la matrice K qui s'écrit encore sous la forme suivante,

$$K = \begin{array}{c} \\ 1 \\ \vdots \\ i \\ \vdots \\ N \\ \Gamma \end{array} \begin{array}{c} \begin{array}{cccccc} 1 & \dots & i & \dots & N & \Gamma \end{array} \\ \begin{pmatrix} K_1 & 0 & \dots & \dots & 0 & K_{\Gamma 1}^t \\ 0 & \ddots & \ddots & & \vdots & \vdots \\ \vdots & \ddots & K_i & \ddots & \vdots & K_{\Gamma i}^t \\ \vdots & & \ddots & \ddots & 0 & \vdots \\ 0 & \dots & \dots & 0 & K_N & K_{\Gamma N}^t \\ K_{\Gamma 1} & \dots & K_{\Gamma i} & \dots & K_{\Gamma N} & K_{\Gamma\Gamma} \end{pmatrix} \end{array} \tag{5.1}$$

La matrice K est subdivisée en blocs diagonaux de matrice K_i correspondant à la matrice de rigidité de chaque sous-domaine i. Il est à noter que les contributions

relatives aux interfaces Γ^i sont quant à elles rassemblées dans les matrices K_{Γ_i}. Pour chaque sous-domaine, l'introduction du nœud fictif par Debordes [10] conduit à la prise en compte de la moyenne du tenseur de rigidité constituant le milieu par l'intermédiaire de la matrice E d'une part, et d'autre part la matrice KE ainsi que sa transposée KE^t lesquelles renvoient aux formes linéaires de la dérivée aux sens des distributions du tenseur de rigidité du milieu, conséquence de l'introduction du nœud fictif. Aussi, les expressions de KE, $\boldsymbol{\omega}^{kl}$ et $\mathbf{0}^{kl}$ pour l'ensemble des sous-domaines deviennent,

$$KE^t = \begin{bmatrix} KE_1^t \\ \vdots \\ KE_i^t \\ \vdots \\ KE_N^t \\ KE_\Gamma^t \end{bmatrix} \qquad \boldsymbol{\omega}^{kl} = \begin{bmatrix} \boldsymbol{\omega}_1^{kl} \\ \vdots \\ \boldsymbol{\omega}_i^{kl} \\ \vdots \\ \boldsymbol{\omega}_N^{kl} \\ \boldsymbol{\omega}_\Gamma^{kl} \end{bmatrix} \qquad \mathbf{0}^{kl} = \begin{bmatrix} \mathbf{0}_1^{kl} \\ \vdots \\ \mathbf{0}_i^{kl} \\ \vdots \\ \mathbf{0}_N^{kl} \\ \mathbf{0}_\Gamma^{kl} \end{bmatrix} \tag{5.2}$$

où $\boldsymbol{\omega}_i^{kl}$ est la solution locale liée au sous-domaine i, et $\boldsymbol{\omega}_\Gamma^{kl}$ celle liée aux noeuds de la frontière. P_{ij}^{kl} représente la matrice que par abus de langage je dénommerai matrice de souplesse homogénéisée effective. Ainsi, dans l'exemple d'un domaine subdivisé en 4 sous-domaines, le système matriciel pour calculer les coefficients homogénéisés s'écrit encore,

$$\begin{bmatrix} K_1 & 0 & 0 & 0 & K_{\Gamma 1}^t & KE_1^t \\ 0 & K_2 & 0 & 0 & K_{\Gamma 2}^t & KE_2^t \\ 0 & 0 & K_3 & 0 & K_{\Gamma 3}^t & KE_3^t \\ 0 & 0 & 0 & K_4 & K_{\Gamma 4}^t & KE_4^t \\ K_{\Gamma 1} & K_{\Gamma 2} & K_{\Gamma 3} & K_{\Gamma 4} & K_\Gamma & KE_\Gamma^t \\ KE_1 & KE_2 & KE_3 & KE_4 & KE_\Gamma & E \end{bmatrix} \begin{bmatrix} \boldsymbol{\omega}_1^{kl} \\ \boldsymbol{\omega}_2^{kl} \\ \boldsymbol{\omega}_3^{kl} \\ \boldsymbol{\omega}_4^{kl} \\ \boldsymbol{\omega}_\Gamma^{kl} \\ P_{ij}^{kl} \end{bmatrix} = \begin{bmatrix} \mathbf{0}_1^{kl} \\ \mathbf{0}_2^{kl} \\ \mathbf{0}_3^{kl} \\ \mathbf{0}_4^{kl} \\ \mathbf{0}_\Gamma^{kl} \\ \delta_i^k \delta_j^l \end{bmatrix} \tag{5.3}$$

Il est à noter que la moyenne du tenseur de rigidité constituant le milieu tout entier E est la somme des moyennes du tenseur de rigidité pour chaque sous-domaine.

$$E_i = \frac{1}{|\Omega_i|} \int_{\Omega_i} C \mathrm{d}Y \tag{5.4}$$

et donc,

$$E = \sum_i \frac{1}{|\Omega_i|} \int_{\Omega_i} C \mathrm{d}Y = \frac{1}{|\Omega|} \sum_i |\Omega_i| E_i \tag{5.5}$$

avec la matrice du complément de Schur $\mathcal{S}$ définie par,

$$\begin{cases} S\mathbf{u}_\Gamma^{kl} &= \tilde{\mathbf{f}}_\Gamma^{kl} \\ S &= \tilde{K}_\Gamma - \sum_i \tilde{K}_{\Gamma i} K_i^{-1} \tilde{K}_{\Gamma i}^t \end{cases} \tag{5.6}$$

où les expressions de $\tilde{K}_{\Gamma i}$, $\tilde{K}_{\Gamma}$, $\tilde{\mathbf{f}}_{\Gamma}^{kl}$ and $\mathbf{u}_{\Gamma}$ sont les suivantes,

$$\begin{aligned} \tilde{K}_{\Gamma i} &= \begin{bmatrix} K_{\Gamma i} \\ KE_i \end{bmatrix} & \tilde{K}_{\Gamma} &= \begin{bmatrix} K_{\Gamma} & KE_{\Gamma}^t \\ KE_{\Gamma} & E \end{bmatrix} \\ \tilde{\mathbf{f}}_{\Gamma}^{kl} &= \begin{bmatrix} \mathbf{0}^{kl} \\ \delta_i^k \delta_j^l \end{bmatrix} & \mathbf{u}_{\Gamma} &= \begin{bmatrix} \boldsymbol{\omega}_{\Gamma}^{kl} \\ P_{ij}^{kl} \end{bmatrix} \end{aligned} \tag{5.7}$$

De par, le caractère symétrique défini positif de la matrice du complément de Schur, une méthode de descente type gradient conjugué avec préconditionneur peut être utilisée en vue de la résolution du problème d'interface (5.6).

2.2 La méthode mixte à proprement parler

Dans cette méthode l'idée consiste à utiliser les avantages de la méthode FETI-1 [13, 14, 55] et celle du complément de Schur pour l'appliquer au cadre de la méthode d'homogénéisation double-échelle. Ici, il faut abandonner l'idée de la prise en compte des conditions de périodicités des frontières extérieures sous forme de contraintes sous peine de rendre la structure globalement flottante ce qui rend de facto le problème non résoluble. Dans un premier temps, nous distinguons la frontière intérieure Γ^i de celle extérieure Γ^e de manière à pouvoir prendre en compte les conditions de périodicité comme nous l'avons fait dans la méthode du complément de Schur. Ceci revient à assurer la continuité au niveau de l'interface intérieure par l'intermédiaire des multiplicateurs de Lagrange. Dans une seconde étape nous introduisons deux termes additionnels notés respectivement KE et E qui traduisent les propriétés élastiques du milieu hétérogène. Nous procédons alors comme dans le cas de la méthode du complément de Schur et nous les ajoutons à la matrice décrivant les connexions avec les frontières extérieures Γ^e. Ce qui au final conduit à écrire :

$$\begin{bmatrix} K_1 & 0 & 0 & 0 & K_{\Gamma^e 1}^t & KE_1^t & C_1^t \\ 0 & K_2 & 0 & 0 & K_{\Gamma^e 2}^t & KE_2^t & C_2^t \\ 0 & 0 & K_3 & 0 & K_{\Gamma^e 3}^t & KE_3^t & C_3^t \\ 0 & 0 & 0 & K_4 & K_{\Gamma^e 4}^t & KE_4^t & C_4^t \\ K_{\Gamma^e 1} & K_{\Gamma^e 2} & K_{\Gamma^e 3} & K_{\Gamma^e 4} & K_{\Gamma^e} & KE_{\Gamma^e}^t & \mathbb{O}_{\Gamma^i \Gamma^o}^t \\ KE_1 & KE_2 & KE_3 & KE_4 & KE_{\Gamma^e} & E & \mathbb{O}_{\Gamma^i E}^t \\ C_1 & C_2 & C_3 & C_4 & \mathbb{O}_{\Gamma^i \Gamma^o} & \mathbb{O}_{\Gamma^i E} & \mathbb{O}_{\Gamma^i} \end{bmatrix} \begin{bmatrix} \boldsymbol{\omega}_1^{kl} \\ \boldsymbol{\omega}_2^{kl} \\ \boldsymbol{\omega}_3^{kl} \\ \boldsymbol{\omega}_4^{kl} \\ \boldsymbol{\omega}_{\Gamma^e}^{kl} \\ P_{ij}^{kl} \\ \boldsymbol{\lambda}^{kl} \end{bmatrix} = \begin{bmatrix} \mathbf{0}_1^{kl} \\ \mathbf{0}_2^{kl} \\ \mathbf{0}_3^{kl} \\ \mathbf{0}_4^{kl} \\ \mathbf{0}_{\Gamma^o}^{kl} \\ \delta_i^k \delta_j^l \\ \mathbf{0}_{\Gamma^i}^{kl} \end{bmatrix} \tag{5.8}$$

Nous voyons que la matrice de rigidité est subdivisée en blocs de K_i de la même manière que dans la méthode du complément de Schur. Chaque K_i représente la

contribution strictement intérieure au sous-domaine i. En ce qui concerne les nœuds localisés sur l'interface $\Gamma = \Gamma^i \cup \Gamma^e$, leur contribution est soit dans la matrice $K_{\Gamma_i^e}$ liés au bord extérieur, soit dans les matrices C_i engendré par des 1 et des -1 pour décrire les relations linéaires sur l'interface Γ^i. Enfin, KE_i est une matrice de couplage entre K_i et E_i laquelle est identique à celle vue dans la méthode du complément de Schur. Les ω_i^{kl} sont les solutions locales liées aux sous-domaine i et $\omega_{\Gamma^e}^{kl}$ celles liées à la frontière Γ^e. Enfin λ^{kl} désigne le vecteur des multiplicateurs de Lagrange traduisant les contraintes au niveau de Γ^i. Nous remarquons que le système précédent peut encore se mettre sous la forme suivante :

$$\begin{bmatrix} K_1 & 0 & 0 & 0 & R_1^t \\ 0 & K_2 & 0 & 0 & R_2^t \\ 0 & 0 & K_3 & 0 & R_3^t \\ 0 & 0 & 0 & K_4 & R_4^t \\ R_1 & R_2 & R_3 & R_4 & K_R \end{bmatrix} \begin{bmatrix} \boldsymbol{\omega}_1^{kl} \\ \boldsymbol{\omega}_2^{kl} \\ \boldsymbol{\omega}_3^{kl} \\ \boldsymbol{\omega}_4^{kl} \\ \boldsymbol{\Lambda}^{kl} \end{bmatrix} = \begin{bmatrix} \mathbf{0}_1^{kl} \\ \mathbf{0}_2^{kl} \\ \mathbf{0}_3^{kl} \\ \mathbf{0}_4^{kl} \\ \mathbf{f}_R^{kl} \end{bmatrix} \tag{5.9}$$

où les expressions R_i, K_R, $\mathbf{f}_R^{kl}$ et $\boldsymbol{\Lambda}^{kl}$ sont les suivantes,

$$\begin{aligned} R_i &= \begin{bmatrix} K_{\Gamma^e i} \\ KE_i \\ C_i \end{bmatrix} & K_R &= \begin{bmatrix} K_{\Gamma^e} & KE_{\Gamma^e}^t & \mathbb{O}_{\Gamma^i\Gamma^e}^t \\ KE_{\Gamma^e} & E & \mathbb{O}_{\Gamma^i E}^t \\ \mathbb{O}_{\Gamma^i\Gamma^e} & \mathbb{O}_{\Gamma^i E} & \mathbb{O}_{\Gamma^i} \end{bmatrix} \\ \mathbf{f}_R^{kl} &= \begin{bmatrix} \mathbf{0}_{\Gamma^e}^{kl} \\ \delta_i^k \delta_j^l \\ \mathbf{0}_{\Gamma^i}^{kl} \end{bmatrix} & \boldsymbol{\Lambda}^{kl} &= \begin{bmatrix} \boldsymbol{\omega}_{\Gamma^e}^{kl} \\ P_{ij}^{kl} \\ \boldsymbol{\lambda}^{kl} \end{bmatrix} \end{aligned} \tag{5.10}$$

Chaque système linéaire de l'équation 5.10, n'est pas résoluble du fait de la singularité des matrices K_i et l'existence des sous-domaines flottants. Pour cela nous devons faire appel à des relations supplémentaires lesquelles doivent êtres vues comme des contraintes appliquées aux modes rigides. Nous utilisons donc les mêmes techniques exploitées dans la méthode FETI-1 classique et nous réécrivons le problème 5.10 sous la forme d'un problème d'interface FETI lequel s'écrit encore :

$$\begin{bmatrix} F_I & G_I \\ G_I^t & \mathbb{O} \end{bmatrix} \begin{bmatrix} \boldsymbol{\Lambda}^{kl} \\ \boldsymbol{\alpha}^{kl} \end{bmatrix} = \begin{bmatrix} \mathbf{f}_R^{kl} \\ \mathbf{0}^{kl} \end{bmatrix} \tag{5.11}$$

Pour résoudre ce système linéaire, nous utilisons la méthode du gradient conjugué projeté préconditionné. Ainsi la résolution de ce système conduit à déterminer la matrice de souplesse homogénéisée et donc donne accès aux coefficients homogénéisés.

3 Résultats numériques

3.1 Fiabilité

Différents tests sont effectués pour vérifier la fiabilité de la méthode mixte versus la méthode du complément de Schur dans le contexte du calcul d'homogénéisation double-échelle et d'un milieu composite hétérogène. Les graphes de la figure 5.2 sont une parfaite illustration de l'évolution du module de Young normalisé dans le cas d'un calcul fait avec et sans partitionnement du domaine. Les courbes continues représentent les valeurs estimées dans le cadre de la méthode du complément de Schur ; les symboles décrivent celles évaluées à l'aide de la méthode mixte.

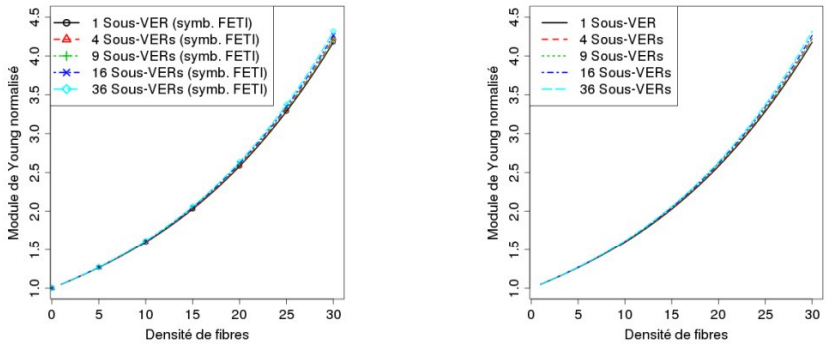

FIGURE 5.2 – Graphe de l'évolution du module de Young en fonction de la densité des hétérogénéités. De gauche à droite calcul en décomposition de domaine et calcul direct.

De ces graphiques, il ressort une très grande qualité et fiabilité des résultats. Il est à noter qu'un certain écart est observable à forte densité de fibres. La conjecture la plus probable pour expliquer cet écart est la suivante. L'écart peut en partie s'expliquer par un traitement spécial lié à la continuité sur l'interface Γ^i voir figure 5.3. Pour assurer la continuité des hétérogénéités, il faut générer des pixels supplémentaires et par ricochet des éléments finis supplémentaires entraînant un biais qui se traduit par une augmentation artificielle des valeurs numériques dès lors que le nombre de sous-domaines croît.

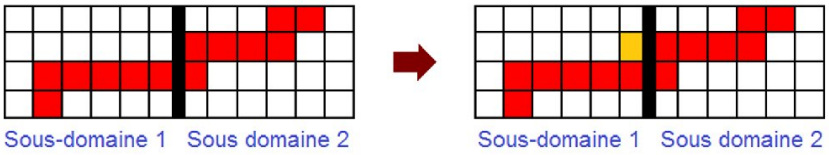

FIGURE 5.3 – Traitement spécifique de la continuité des hétérogénéités lors de la traversée d'une frontière interne d'un sous-domaine à l'autre

3.2 Gain en temps de calcul CPU

Pour tester l'efficacité de la méthode de décomposition de domaine, différentes situations ont été envisagées. Les comparaisons proposées sont les suivantes. Tout d'abord une méthode directe sans faire appel à la décomposition de domaine a été effectuée. Dans un second temps une décomposition de domaine mais dans un cadre séquentiel a été menée et dans un troisième temps, un calcul avec décomposition de domaine avec une architecture parallèle a été mis en place. Dans le dernier cas, la démarche pour effectuer les simulations est la suivante. Chaque sous domaine est traité par un processeur de sorte que le nombre de sous-domaines soit égal au nombre de processeurs. Les graphiques de la figure 5.4 parlent d'eux-mêmes. Ces graphiques mettent en avant l'intérêt d'exploiter l'architecture parallèle plus encore que les méthodes de décomposition de domaine et ce d'autant plus que le taux de charge est élevé.

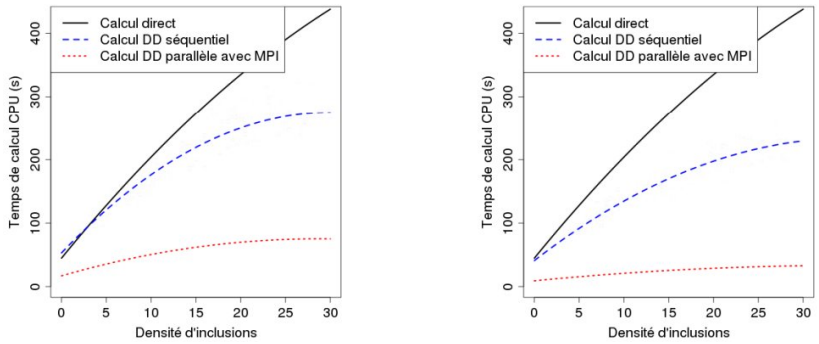

FIGURE 5.4 – De gauche à droite. Influence pour 4 et 9 sous-domaines sur le temps de calcul CPU

Cependant une réserve doit être apporté suite à l'enthousiasme produit par les simulations numériques et les courbes précédentes. Ces observations sur le gain de temps de calcul CPU en fonction du nombre de sous-domaines posent la question de l'efficacité du calcul parallèle au fur et à mesure que le nombre et la taille des sous-domaines croissent. Les graphiques de la figure 5.5 décrivent l'évolution de l'efficacité parallèle en fonction du nombre de sous-domaine. Sur le graphique de droite, la ligne continue en noir idéalise l'efficacité parallèle laquelle est identique au nombre de sous-domaine. Il est alors facile de constater que les simulations numériques, courbes discontinues bleues et rouges, sont très largement en deçà de la courbe théorique dès lors que le nombre de sous-domaines dépasse les 8 sous-domaines. Ce qui a priori découragerait l'usage des techniques de calcul parallèle. Je ferai donc trois remarques : premièrement nous ne sommes pas des spécialistes de la programmation sous MPI. Le code conçu est loin d'être parfait, il a été conçu pour disposer d'un moyen de calcul au sein du laboratoire afin de gagner du temps dans les tests et la vérification de certaines idées. Deuxièmement, le temps de communication entre processeurs est un facteur clé pour optimiser les gains de temps CPU. En conséquence il faut être équipé ou avoir accès à un centre de calcul puissant sur ce point. Troisièmement, il vaut mieux faire appel à des architectures parallèles dès lors que la taille des sous-domaines devient conséquente comme le suggère la courbe

discontinue en rouge.

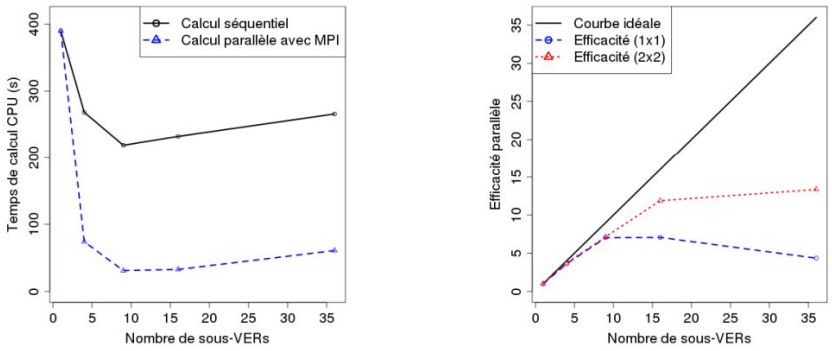

FIGURE 5.5 – De gauche à droite. Influence du nombre de sous-domaines sur le temps de calcul CPU. Influence du nombre et de la taille des sous-domaines sur l'efficacité parallèle

Dans l'approche 3D les mêmes remarques que dans la cas 2D sont obsérvées. Plus qu'un long discours les graphiques de la figue 5.6 illustre bien à eux-seuls ce qui a été dit pour le cas 2D.

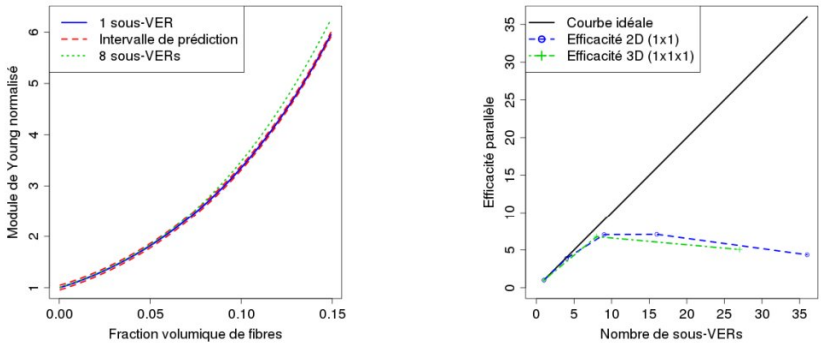

FIGURE 5.6 – De gauche à droite. Calcul par décomposition de domaine pour le Module de Young en fonction de la fraction volumique. Comparatif des résultats 2D versus 3D.

4 Bilan

Deux méthodes de décomposition de domaine sans recouvrement ont été exploitées pour élaborer une troisième méthode. La troisième méthode est qualifiée de méthode mixte laquelle s'appuie sur les méthodes du complément de Schur et de FETI. Il faut retenir que la méthode FETI est plus complexe à gérer. En effet, la plus grande difficulté réside dans la prise en charge des éléments flottants du domaine associé au VER en présence des conditions aux limites périodiques. Pour l'évaluation des propriétés mécaniques, un algorithme et un code parallélisés sous MPI de la méthode d'homogénéisation double-échelle ont été conçus et mis en place pour le cas bidimensionnel et tridimensionnel.

La méthode mixte, alternative proposée pour contourner la difficulté dans la gestion des éléments flottants avec conditions aux limites périodiques, se heurte cependant au délicat problème de la recherche d'un bon préconditionneur. En effet, pour inverser le problème à l'interface par la technique du gradient conjugué, celui-ci, pour être efficace et optimal, nécessite notamment la connaissance au préalable d'un préconditionneur puissant.

Pour l'heure, il s'agit d'une question ouverte. Les gains de temps de calcul ont été à la hauteur du travail fourni bien que pour un très grand nombre de sous domaines il y a une perte dans l'efficacité de la méthode mixte. Ces observations s'expliquent par une dégradation des communications entre processeurs lorsque le nombre des subdivisions du domaine est très important. Cette conjecture est la plus plausible qui puisse être avancée !

Troisième partie

Conclusion générale et perspectives

Chapitre 6

Conclusions et perspectives

1 Bilan et contributions

Dans ce mémoire d'habilitation à diriger des recherches le lecteur aura sans doute perçu que mes activités de recherche gravitent autour de deux thématiques lesquelles sont la théorie des coques élastiques minces avec toutes les difficultés que cela implique d'une part, et d'autre part une approche numérique des matériaux à microstructures complexes. Bien qu'en apparence mes deux thématiques de recherche peuvent sembler très éloignées l'une de l'autre, il y a cependant deux points sur lesquels elles se rejoignent. Le premier concerne l'aspect asymptotique des deux thématiques. Il s'agit de l'impact de l'épaisseur de la coque, qui en dépit de sa petitesse engendre bien des difficultés à la fois d'ordre théorique que numérique d'une part, et d'autre part par la taille et la morphologie des microstructures lesquelles nécessitent à leur tour des développements asymptotiques en double-échelle pour pouvoir calculer correctement les tenseurs de rigidité homogénéisés des composites. Le second point concerne la modélisation et l'usage des méthodes numériques basées sur les éléments finis aussi bien pour les coques minces que pour calculer de manière fiable les coefficients homogénéisés des composites. Tout ceci nous a conduit à concevoir deux codes de calcul, l'un dédié aux coques minces et le second au calcul des coefficients homogénéisées sous architecture parallèle en faisant appel à la technique de décomposition de domaine.

La première partie, dont les travaux sont d'ordre théorique et numérique, est une contribution pour mieux appréhender la simulation numérique des structures minces telles que les coques et le rôle joué par le petit paramètre ε, épaisseur de la coque, et ce d'autant plus que celle-ci devient très petite. Les points fondamentaux de mes travaux sont respectivement la notion de couches limites et couches internes qui apparaissent aussi bien pour les coques dont les surfaces moyennes sont parabolique ou hyperbolique. Un autre aspect fondamental de mon travail concerne la notion de propagation des singularités dans les coques hyperboliques ainsi que la notion de pseudo-réflexion ce qui a permis de comprendre les différents mécanismes mis en jeu lors des réflexions dans les coques minces hyperboliques. Parallèlement, nous avons montré qu'un raffinement de maillage dans les directions asymptotiques permet de gagner du temps de calcul tout en maîtrisant les erreurs de manière satisfaisante et ainsi optimiser les calculs pour les coques minces.

La seconde partie, dont les travaux sont éminemment numériques et en dépit d'une simplification des différents niveaux de difficultés du modèle, il en découle une contribution en terme de méthode numérique pour aborder les composites à microstructures complexes. Bien que l'étude se soit focalisée sur le cas des matériaux renforcés en fibres courtes pour lesquels l'orientation, l'entrelacement conduisent à des microstructures complexes la démarche intellectuelle s'applique à d'autres cas de figure comme nous le verrons dans les perspectives mais nécessitent de developper d'autres outils plus puissants et plus adaptés aux situations envisagées.

Un point fondamental a été la conception des VER contenant des fibres courtes lesquelles sont engendrées par un ensemble de paramètres morphologiques et ce dans un cadre stochastique. Un autre aspect tout aussi important pour la suite a été d'approcher la géométrie des fibres courtes à l'aide d'une grille d'éléments quadrangulaires en 2D ou hexaédriques en 3D. Afin d'éviter les effets de pixelisation en 2D ou voxelisation en 3D des stratégies de raffinements efficaces ont été développées, c'est ce que l'on désigne sous le terme d'approximation géométrique d'ordre n. Puis, les maillages ont été générés par triangulation en 2D ou tétraédrisation de Delaunay en 3D sous CAST3M à partir des contours de la géométrie approximée. Enfin, dans l'optique d'optimiser le temps de calcul des coefficients homogénéisés par la méthode double-échelle périodique en utilisant la technique du nœud fictif, une adaptation de la technique dans le cadre de la méthode de décomposition de domaine sous architecture parallèle a été réalisée. L'algorithme a été codé sous c++ avec les bibliothèques MPI et OpenMP.

2 Perspectives

Dans ce mémoire, je présente en ce qui concerne la théorie des coques et les matériaux composites, les orientations que je souhaite prendre et pour certaines d'entre elles que j'ai déjà commencées et qui sont dans la prolongation naturelle de mes travaux et résultats ainsi que mes différentes collaborations.

1. Dans la continuité du problème des pseudo-réflexions, je poursuis mes travaux de recherche sur la notion de réfraction des singularités dans les coques élastiques minces. En effet, étant donné deux coques dont les surfaces moyennes sont parabolique, hyperbolique ou tout autre combinaison de ce genre, lesquelles sont reliées entre elles par une arête rigide et supposons donné un chargement singulier dont le support est caractéristique. D'après ce qui précède, nous savons que la singularité va se propager le long de la caractéristique. La question sous-jacente est que devient cette singularité lorsqu'elle intercepte le pli rigide. La singularité va-t-elle traverser le pli ou s'y arrêter ? Dans l'éventualité où celle-ci traverse le pli, quel est le degré de la singularité, quelle est son amplitude ? Gagne-t-elle en régularité comme les pseudo-réflexions, reste-t-elle inchangée ou pire devient-elle plus singulière ? En ce qui concerne les coques paraboliques j'ai déjà quelques éléments de réponse et cela a fait

l'objet d'une soumission dans Journal of Mechanics A/solids.

2. Un autre aspect qui m'intéresse est l'utilisation des éléments isogéométriques dans la théorie des coques minces. L'idée de base repose sur le développement de nouveaux éléments finis pour les coques minces à partir des fonctions de base utilisées par les modèles de CAO servant à définir de manière exacte la géométrie des coques. Pour l'heure, la majorité des outils de modélisation utilise les fonctions NURBS (Non Uniform Rational Bsplines) pour ce qui concerne la description de la géométrie. Celles-ci ont des propriétés intéressantes et nécessitent des algorithmes stables permettant de les construire et de les exploiter de manière efficace. La possibilité de décrire de manière exacte la géométrie laisse entrevoir une approche intéressante dans les problèmes de verrouillages et de propagation des singularités et dans le traitement des plis des coques élastiques minces lors des simulations numériques de ces dernières.

Parallèlement, le projet ACCEA (Amélioration des Conductivités des Composites pour Equipements Aéronautiques), a débuté depuis le troisième trimestre 2013 pour une durée prévisionnelle de 36 mois. Le projet ACCEA a pour objectif d'améliorer les conductivités thermique et électrique des matériaux composites à matrices thermoplastiques mis en forme par injection et par thermo-compression, dans des applications destinées au secteur aéronautique. À l'issue du projet, les performances obtenues par ces matériaux permettront de procéder à des allégements significatifs. Les premières applications industrielles verront le jour dès 2016 dans le domaine des boitiers pour calculateurs embarqués, puis à l'horizon 2020 pour plusieurs composants non structuraux des futures gammes d'aéronefs. Il s'agit d'un travail en collaboration avec différents partenaires industriels tels que Aérospace, Safran, Aérazur, Aircelle, Arkema, Liefco etc ... et universitaires comme le laboratoire thermocinétique de Nantes et l'institut de recherche en énergie électrique de Nantes atlantique dans lequel le LMNO apportera ses compétences dans la modélisation des hétérogénéités par une approche probabiliste dans le cadre d'un calcul par homogénéisation multi-échelle pour déterminer des critères objectifs pour atteindre les caractéristiques du cahier des charges et pour la mise au point d'un matériau composite. Actuellement, en tant que responsable de ce projet au sein du laboratoire mathématique Nicolas Oresme dont je suis membre, j'encadre une thèse de doctorat et un post doctorant.

1. Dans ce contexte, j'ai imaginé avec mon équipe une nouvelle approche pour la conception des VER à microstructures complexes en 3D. En effet, à la vue des images acquises en tomographie par rayons X, j'ai tout de suite compris qu'il y avait un réel besoin de concevoir des microstructures ayant des formes et des tailles très diverses. À ma connaissance, la communauté scientifique ne dispose pas d'un tel outil. Alors avec mon équipe nous avons décidé d'entreprendre la conception d'un logiciel pour générer des microstructures à morphologies très variées et qui pourra servir la communauté. Nous n'en sommes qu'au début d'un vaste et ambitieux chantier mais un certain nombre de verrous ont été levés et je reste optimiste pour la suite.

2. Je souhaite mener une investigation plus complète sur l'influence des caractéristiques morphologiques et de la percolation en 3D car je reste convaincu que cela serait intéressant et important à réaliser. Notamment il faut travailler sur la dispersion spatiale inhomogène des inclusions avec des facteurs d'échelle plus élevés
3. Je souhaite également mettre en place une technique d'homogénéisation à l'aide de l'analyse multi-résolution. Je suis persuadé que l'analyse multi-résolution au sens des ondelettes permettra de détenir une méthode de résolution plus rapide et plus efficace que celle que nous utilisons à l'heure actuelle comme la méthode des éléments finis ou la méthode basée sur la transformée de Fourier rapide initiée et développée par M. Moulinec et P. Suquet.

4. La parallélisation des codes sous OpenMP et MPI ou en faisant appel à des processeurs GPU via le langage CUDA est aussi une voie à explorer pour gagner en performance de calcul.

5. En complément de ce travail, j'aimerais aussi m'intéresser au comportement non-linéaire de la matrice qui n'est généralement pas élastique mais plutôt plastique ou viscoplastique.

Je suis conscient que les différents points que je souhaite développer sont ambitieux et que j'aurai certainement du mal à les mener jusqu'au bout, néanmoins, les idées de recherche naissent et disparaissent au gré des rencontres, des échanges et des erreurs et sont en perpétuelle évolution.

Bibliographie

[1] Agoshkov V.I. and Lebedev V.I.. The Poincaré-Steklov's operators and the domain decomposition methods in variational problems. *Computational Processes and Systems*, Nauka, 173 – 227, 1985.

[2] Balberg I. , Anderson C.H., Alexander S. and Wagner N. Excluded volume and its relation to the onset of percolation. *Physical Review B*, 30(7), 1984.

[3] Balberg I. "Universal" percolation-threshold limits in the continuum. *Physical Review B*, 31(6), 1985.

[4] Bensoussan A., Lions J.L. and Papanicolaou G.C. *Asymptotic analysis for periodic structures.* Springer, North Holland, Amsterdam edition, 1978.

[5] Berger, M. J., Colella, P., 1989. Local adaptive mesh refinement for shock hydrodynamics. J. Comput. Phys. 82, 64-84.

[6] M. Bernadou M., Ciarlet, P.G., 1976. Sur l'ellipticité du modèle linéaire des coques de W.T. Koiter, in : Glowinski, R., Lions, J.L. *Computing Methods in Sciences and Engineering, Lecture Notes in Economics and Math. Systems /*, Vol. 134.

[7] Boyd S. and Müller R. Smooth surface meshing for automated finite element model generation from 3D image data. *Journal of Biomechanics*, 39(7) :1287 – 95, 2006.

[8] Cast3M software http ://www-cast3m.cea.fr/.

[9] Fundamental considerations for the finite element analysis of shell structures, *Computers and Structures* 66 (1998) 19-36.

[10] Débordes O. Homogenization computations in the elastic or plastic collapse range. Applications to unidirectional composites and perforated sheets. In : 4th. Int. Symp. Inn. Meth. in Eng.. Springer-Verlag, Atlanta, pp. 453–458.

[11] Drugan W.J. and Willis J.R. A micromechanics-based nonlocal constitutive equation and estimates of representative volume element size for elastic composites. *Journal of the Mechanics and Physics of Solids*, 44(4) :497 – 524, 1996.

[12] Egorov YuV and Shubin MA. Linear partial differential equations. Foundations of the classical theory. *Encyclop Math Sci (Part Diff Eqs I)*, Springer 1992 ;30 : 345–75.

[13] C. Fahrat and F.X. Roux. A method of finite element tearing and interconnecting and its parallel solution algorithm. *International Journal of Numerical Methods in Engineering*, 32 :1205 – 1227, 1991.

[14] C. Fahrat and F.X. Roux. *Implicit parallel processing in structural mechanics.* Computational Mechanics Advances, North Holland, 2(1) :1 – 124, 1994.

[15] C. Fahrat, C. Mandel and F.X. Roux. Optimal convergence properties of the FETI domain decomposition method. *Computer Methods in Applied Mechanics and Engineering*, 115 :365 – 385, 1994.

[16] Feyel F. *Multiscale fe2 elastoviscoplastic analysis of composite structures*. Computational Materials Science, p. 344–354.

[17] B. Fralick, E. Gatzke and S. Baxter. Three-dimensional evolution of mechanical percolation in nanocomposites with random microstructures. *Probabilistic Engineering Mechanics*, 602 :1 – 8, 2012.

[18] Gerard, P. Sanchez-Palencia, E. *Sensitivity phenomena for certain thin elastic shells with edges*. Math. Meth. Appl. Sci. 23, 379-399 2000

[19] A.L. Goldenveizer, Theory of elastic thin shells. *Pergamon* , New York (1962).

[20] X. Gong, J. Liu, S. Baskaran, R.D. Voise and J.S. Young Surface-assisted processing of carbon nanotube/polymer composites. *Chemistry of Materials* 12 :1049 – 1052, 2000.

[21] Halpin J.C., and Kardos. J.L. The Halpin-Tsai Equations : a review. *Polymer Engineering and Science*, 16(5) :344–352, 1976.

[22] Hashin Z. and Shtrikman S. A variational approach to the theory of the elastic behaviour of multiphase materials. *Journal of the Mechanics and Physics of Solids*, 11(2) :127–140, 1963.

[23] Jeulin D. and Moreaud M., Multi-scale simulation of random sphere aggregates - application to nanocomposites. 2005. 9th European Congress on Stereology and Image Analysis, Zakopane, Poland, 2005.

[24] D. Jeulin and M. Moreaud. Percolation of multi-scale fiber aggregates. 2006. S4G 6th international Conference, Prague, (2006).

[25] D. Jeulin and M. Moreaud. Percolation d'agrégats multi-échelles de sphères et de fibres - application aux nanocomposites. 2006. Congrès matériaux, Dijon, (2006).

[26] D. Jeulin and M. Moreaud. Percolation of random cylinder aggregates 2007. Image Analysis and Stereology, vol. 26, p. 121–127.

[27] Kanit T., Forest S., Galliet I., Mounoury V., Jeulin D., Determination of the size of the RVE for random composites : statistical and numerical approach, *International Journal of Solids and Structures* 40(13-14) (2003) 3647-3679

[28] Karamian-Surville P., 1998 Réflexion des singularités dans les coques hyperboliques inhibées Comptes Rendus de l'Académie des Sciences - Series IIB - Mechanics-Physics-Astronomy, Volume 326, Issue 10, October 1998, Pages 609-614

[29] P. Karamian , Nouveaux résultats numériques concernant les coques minces hyperboliques inhibées : cas du paraboloïde hyperbolique. *C. R. Acad. Sci. Paris Sér. IIb 326* (1998) 755-760.

[30] P. Karamian, Coques élastiques minces hyperboliques inhibées : calcul du problème limite par éléments finis et non reflexion des singularités. *Thèse de l'Universté de Caen* (1999).

[31] Karamian-Surville P., Sanchez-Hubert J., Sanchez Palencia É., 2000. A model problem for boundary layers of thin elastic shells. Math. Modell. Num. Anal. 34, N^0 1, 2000, 1-30.

[32] Karamian-Surville P., Sanchez-Hubert J., 2002 Boundary layers in thin elastic shells with developable middle surface. European Journal of Mechanics - A/Solids, Volume 21, Issue 1, 2002, 13-47.

[33] Karamian-Surville P., Sanchez-Hubert J., Sanchez Palencia É., 2002. Propagation of singularities and structure of layers in shells : Hyperbolic case. Computers & Structures, Volume 80, Issues 9–10, 2002, 747-768.

[34] Karamian-Surville P., Sanchez-Hubert J., Sanchez Palencia É., 2002. Nonsmothness in the asymptotics thin shells and propagation of singularities. Hyperbolic case. International Journal of Applied Mathematics and Computer Sciences, vol.12, $N^0$1, 2002, 81-90.

[35] Karamian-Surville P., Sanchez-Hubert J., Sanchez Palencia É., 2003. Pseudo-reflection phenomena for singularities in thin elastic shells. Mathematical Models and Methods in Applied Sciences,Vol. 26, 17, 2003, 1451-1485.

[36] Leclerc W., Karamian, P., Vivet, A., Campbell, A., 2012. Numerical evaluation of the effective elastic properties of 2D overlapping random fibre composites. Tech. Mech. 32, 2012, 358-368.

[37] Leclerc W., Karamian-Surville, P., Vivet, 2013. An efficient stochastic and double-scale model to evaluate the effective elastic properties of 2D overlapping random fibre composites. Comput. Mater. Sci. 69, 2013, 481-493.

[38] Leclerc W., Karamian-Surville, P. 2013. Domain decomposition methods to evaluate effective elastic properties of random fibre composites in the framework of the double-scale homogenization. Int. J. Solids Struct. 50(18), 2013, 2808-2816.

[39] Leclerc W., Karamian-Surville, P. 2013 Effects of fibre dispersion on the effective elastic properties of 2D overlapping random fibre composites. Computational Materials Science,79, 2013, 674-683

[40] Leclerc W., Karamian-Surville, P., Vivet, 2013 Influence of morphological parameters of a 2D random short fibre composite on its effective elastic properties Mechanics & Industry, Volume 14, Issue 05, 2013, 361-365

[41] Leclerc W., une approche numérique fiable et automatisée de l'estimation des propriétés élastiques des microstructures complexes thèse de doctorat, Université de Caen Basse-Normandie.

[42] Leclerc W., Karamian-Surville, P., Vivet, 2014 An efficient and automated 3D FE approach to evaluate effective elastic properties of overlapping random fibre composites préprint soumis à Computational Materials Science

[43] D. Leguillon , J. Sanchez-Hubert and É. Sanchez Palencia , Model problem of singular perturbation without limit in the space of finite energy and its computation.*C.R. Acad. Sci. Paris Sér. IIb 327* (1999) 485-492.

[44] Lions, J. L. *Perturbations singulières dans les problèmes aux limites* . Lecture Notes in mathematics vol. 323, Springer-Verlag, Berlin 1973

[45] Liu L.Q., Wagner H.D. Rubbery and glassy epoxy resins reinforced with carbon nanotubes. *Composites Science and Technology*, 65 :1861 – 1868, 2005.

[46] Moreaud, M. Propriétés morphologiques multi-échelles et prévision du comportement diélectrique de nanocomposites, thèse de doctorat, Ecole des Mines de Paris.

[47] Mori, T., Tanaka, K., 1973. Average stress in matrix and average elastic energy of materials with misfitting inclusions. Acta Metall. 21, 571-574.

[48] Mishnaevsky Jr., L. , Derrien, K., Baptiste, D., 2004. Effect of microstructure of particle reinforced composites on the damage evolution : probabilistic and numerical analysis. Compos. Sci. Technol. 64(12), 1805-1818.

[49] Mishnaevsky Jr, L., 2004. Three-dimensional numerical testing of microstructures of particle reinforced composites. Acta Mater. 52(14), 4177-4188.

[50] Mishnaevsky Jr, L. , 2005. Automatic voxel-based generation of 3D microstructural FE models and its application to the damage analysis of composites. Mater. Sci. Eng. A 407(1-2), 11-23.

[51] Moulinec H., Suquet P. A fast numerical method for computing the linear and nonlinear mechanical properties of composites. C. R. Acad. Sci. 1994, vol. 318 (11), pp. 1417-1423.

[52] Mori T., Tanaka K., Average stress in matrix and average elastic energy of materials with misfitting inclusions, *Acta Metallurgica* 21 (1973) 571-574

[53] Mishnaevsky L. Jr. Automatic voxel-based generation of 3D microstructural FE models and its application to the damage analysis of composites. *Material Science and Engineering A*, 407(1-2) :11 – 23, 2005.

[54] J. Pitkaranta and É. Sanchez Palencia , On the asymptotic behavior of sensitive shells with small thickness.*C.R. Acad. Sci. Paris Sér. IIb 325* , (1997) 127-134.

[55] Roux, François-Xavier Méthode de décomposition de domaine a l'aide de multiplicateurs de Lagrange et application a la résolution en parallèle des équations de l'élasticité linéaire. thèse de doctorat, Parix VI

[56] H.S. Rutten, Theory and design of shells on the basis of asymptotic analysis. *Rutten and Kruisman* , Voorburg (1973).em[H.S. Rutten (1973)]Rutten :1973 H.S. Rutten, Theory and design of shells on the basis of asymptotic analysis. *Rutten and Kruisman* , Voorburg (1973).

[57] J. Segurado, J. Llorca, A numerical approximation to the elastic properties of sphere-reinforced composites, *Journal of the Mechanics and Physics of Solids* 50(10) (2002) 2107-2121

[58] E. Sanchez-Palencia. *Non-homogeneous media and vibration theory.* Springer, Berlin, 127, 1980.

[59] Sanchez-Palencia E. *Statique et dynamique de l'élasticité tridimensionnelle à la théorie asymptotique des coques minces.* C. R. Acad. Sci. Paris, série I 309, 411-417, 531-537 1989

[60] Sanchez-Palencia E. *Passage à la limite de l'élasticité tridimensionnelle à la théorie asymptotique des coques minces.* C. R. Acad. Sci. Paris, série II 311, 909-916 1990

[61] Sanchez-Hubert J., Sanchez-Palencia E. *Introduction aux méthodes asymptotiques et à l'homogénéisation.* Masson, Paris, 1992.

[62] Sanchez-Hubert J., Sanchez-Palencia E. *Coques élastiques minces - Propriétés asymptotiques*. Masson, Paris, 1997.

[63] Sanchez-Hubert J., Sanchez-Palencia E. *Pathological phenomena in computation of thin elastic shells*. Soc. Mech. Engin. 22 435–446, 1998.

[64] Sanchez-Palencia, E. *New cases of propagation of singularities along characteristic boundaries for model problems of shell theory.* Compt Rend Acad Sci, Paris, série IIb 2001 ;329 :315–21.

[65] Sanchez-Palencia, E., Millet, O., Bechet, F. *Coques élastiques minces - Propriétés asymptotiques*. Lecture Notes in Applied and Computational Mechanics, Vol. 54

[66] G. D. Seidel and D. C. Lagoudas. Micromechanical analysis of the effective elastic properties of carbon nanotube reinforced composites. *Mechanics of Materials*, 38(8-10) :884 – 907, 2006. Advances in Disordered Materials.

[67] Wall P. A comparison of homogenization, Hashin-Shtrikman bounds and the Halpin-Tsai equations. *Application of Mathematics*, 42(4) :245–257, 1997.

Quatrième partie

Annexes

Mathematical Modelling and Numerical Analysis M2AN, Vol. 34, N° 1, 2000, pp. 1–30
Modélisation Mathématique et Analyse Numérique

A MODEL PROBLEM FOR BOUNDARY LAYERS OF THIN ELASTIC SHELLS

Philippe Karamian[1], Jacqueline Sanchez-Hubert[1, 2]
and Évarisite Sanchez Palencia[2]

Abstract. We consider a model problem (with constant coefficients and simplified geometry) for the boundary layer phenomena which appear in thin shell theory as the relative thickness ε of the shell tends to zero. For $\varepsilon = 0$ our problem is parabolic, then it is a model of developpable surfaces. Boundary layers along and across the characteristic have very different structure. It also appears internal layers associated with propagations of singularities along the characteristics. The special structure of the limit problem often implies solutions which exhibit distributional singularities along the characteristics. The corresponding layers for small ε have a very large intensity. Layers along the characteristics have a special structure involving subspaces; the corresponding Lagrange multipliers are exhibited. Numerical experiments show the advantage of adaptive meshes in these problems.

Résumé. Nous considérons un problème modèle (avec coefficients constants et géométrie simplifiée) pour l'étude des couches limites qui apparaissent en théorie des coques élastiques minces lorsque l'épaisseur relative ε tend vers zéro. Pour $\varepsilon = 0$, notre problème est parabolique, c'est donc un problème modèle pour les surfaces développables. Les couches limites le long et transversalement aux caractéristiques ont des structures très différentes. Il apparaît aussi des couches internes associées à la propagation des singularités le long des caractéristiques. Dans certains cas, à cause de sa structure particulière, le problème limite a des solutions qui présentent des singularités faisant intervenir des distributions le long des caractéristiques. Pour ε petit, les couches correspondantes sont de très grande intensité. Les couches le long des caractéristiques ont une structure particulière incluant des sous-espaces ; les multiplicateurs de Lagrange correspondants sont mis en évidence. Les calculs numériques montrent l'avantage de l'utilisation de maillages adaptés dans ce type de problèmes.

Mathematics Subject Classification. 73K15, 35B25.

Received: April 30, 1999.

1. Introduction

This paper is devoted to a model problem for the boundary and internal layers in shells so we first recall some features of thin shell theory. For generalities on shells the reader may refer to [1, 4, 7, 18]. Roughly speaking, a shell is described by a thin body, of thickness 2ε, close to a surface S the boundary of which is submitted to some kinematic conditions. The mechanical behavior is described by two bilinear forms $a(u, v)$ and $\varepsilon^2 b(u, v)$, associated with the deformations of the intrinsic metrics and the variations of curvature, which are called the

Keywords and phrases. Shells, boundary layers, singular perturbation.

[1] Laboratoire de Mécanique, Université de Caen, Boulevard Maréchal Juin, 14032 Caen Cedex, France.

[2] Laboratoire de Modélisation en Mécanique, Université Paris VI, 4 place Jussieu, 75252 Paris Cedex 05, France.
e-mail: sanchez@lmm.jussieu.fr

membrane form and the flexion form respectively. Note that the second one involves a factor ε^2, accounting for the small rigidity of a thin body to flexion. This fact entails very specific asymptotic properties for small ε, a part of them will be described hereafter, we refer mainly to [5, 7, 19] for more details.

In the sequel, we only consider the so called "inhibited shells", *i.e.* such that the surface S along with the kinematic boundary conditions is geometrically rigid. The corresponding system is of the form $A + \varepsilon^2 B$, where B is elliptic but A is of the same type as the points of the surface S, *i.e.* elliptic, parabolic or hyperbolic at elliptic, parabolic or hyperbolic points of the surface. In addition the order of derivation in B is higher than in A so that as ε tends to zero there is a singular perturbation phenomenon. In the sequel, we shall focus on the case when A is *uniformly parabolic* which corresponds to *developpable surfaces*. The limit process $\varepsilon \searrow 0$ is very singular, as it goes from a higher order elliptic system to a parabolic system. For $\varepsilon > 0$, the energy space V is chosen so that $a + \varepsilon^2 b$ be continuous and coercive on it, whereas the limit problem involves a new energy space V_a such that the form a is continuous and coercive on it. In fact, V_a is the completion of V with the norm $\sqrt{a(\cdot,\cdot)}$ (note that, it is a norm as a consequence of the hypothesis of inhibition).

Obviously, the space V_a contains functions which are less smooth than the functions of V. Consequently, the solutions u^ε belong to V but the limit as ε tends to zero is a less smooth function. As a consequence, u^ε for small ε exhibits "boundary layers" *i.e.* narrow regions where the gradient grows very quickly. In fact, there is another, even more important reason for the presence of boundary layers. Of course, as $V \subset V_a$, the dual spaces verify $V_a' \subset V'$ so that the admissible forces which are in V' for $\varepsilon > 0$ may not be admissible for the limit problem. In this case, the energy of u^ε tends to infinity, as we prove in Section 2.1. The corresponding solution of the limit problem is out of V_a and exhibits distributional singularities so that u^ε involves boundary layers of large intensity (see also [11] in this context). It is to be mentioned that this situation is very common in shell theory where the space V_a, which depends on the geometry, is often very large and consequently V_a' is a very small space. The most typical example of such a situation is given by the so called "sensitive shells" for which the space V_a' is so small that is does not contain the space $\mathcal{D}$ of test functions of distributions [12, 13]. Obviously, for sensitive shells almost any loading f is out of V_a' but, even for non-sensitive shells "very usual" loadings may be out of V_a'. For instance, in ruled surfaces with a free boundary along a generator, any loading not vanishing on that generator is out of V_a' (see [18], Sects. VII.2.4 and VII.4.2 as well as Sect. 2.2 of this paper for the model problem).

It should be emphasized that the non-smoothness of solutions of the limit problem has important consequences on the finite element computations of u^ε for small ε. It is not hard to prove (see [6] for instance) that when $f \notin V_a'$ the convergence of the finite element approximations u_k^ε to u^ε cannot be uniform with respect to $\varepsilon \in (0, \varepsilon_0)$ with values in V_a (and then also in any "smaller" space!). In other words, the smaller ε is the smaller h must be chosen in order to get a good approximation. We may refer to [8,10] for these features. As a result, the situation in the present case, of inhibited shells, is analogous to that of non-inhibited ones where the non-uniformity of the convergence is a consequence of the phenomenon of locking which appears for any conformal approximation with piecewise polynomial finite elements [3].

Up to our knowledge, very little is known about boundary layers of shells. They are called "edge effects" in [7, 14] which are mainly concerned with layers transversal to the characteristics. Specific solutions may perhaps be found in the impressive catalogue of analytical solutions of Rutten [16] but their utilisation in specific problems is not evident. So, in this paper, we consider a model problem for the above mentioned shell problems in the case when the limit operator A is parabolic. The model has constant coefficients and involves two unknowns u_1 and u_2; the first one plays the role of the two tangential components of the displacement vector in shells and the second is analogous to the normal component.

The paper is organized as follows: the model problem $P(\varepsilon)$ is presented hereafter at the end of this introduction (see (1.1)–(1.5)). The limit problem $P(0)$ is addressed in Section 2 which includes properties of the asymptotic process $\varepsilon \searrow 0$ (see Sect. 2.1) and a criterion for $f \in V_a'$ which is an adaptation of a criterion of sensitivity [13] (see Sect. 2.2). The scaling for the layers, either along or across the characteristics is obtained in Section 3 by a method based on asymptotic trends of exponential solutions. We point out that this method was used in another context in [15]. Boundary layer along a clamped characteristic is considered in Section 4.

The specific equations and boundary conditions are obtained by formal asymptotic expansions directly from the variational formulation. The analogous problem for a free boundary is handled in Section 5, two cases appear according to the loading vanishes or not on the boundary. In the second case, the intensity of the layer is very much larger because $f \notin V_a'$. Section 6 is devoted to the case of internal layers along the characteristics, the limit of which is the phenomenon of propagation of singularities. The structure of the characteristic layers involves a special structure involving subspaces. The corresponding Lagrange multiplier is considered in Section 7. The more classical case of layers transversal to the characteristics is addressed in Section 8. In Section 9, we prove that the limit as $\varepsilon \searrow 0$ of the internal layers are the solutions in the distributions sense of the limit problem which were given in Section 2.4 for $f \notin V_a'$. Section 10 contains numerical experiments with finite element approximations, mainly for $\varepsilon = 10^{-3}$. The advantage of using meshes adapted to the specific features of the layers is shown. The principal results, thicknesses and intensities of the layers in different cases are summed up in a table in Section 11.

The model problem $P(\varepsilon)$ is defined as follows. Let us consider the domain $\Omega = (0,\pi) \times (0,\pi)$ of the plane $x = (x_1, x_2)$. The boundary $\partial\Omega$ is composed of two parts Γ_0 and Γ_1 which are respectively the "clamped " part and the "free" part, they will be precisely defined later. Several choices will be done but, in any case, Γ_0 is made of whole sides and always contains two adjacent sides.

The configuration space V is a space of elements $v = (v_1, v_2)$ satisfying the boundary conditions:

$$v_1 = v_2 = \partial_n v_2 = 0 \text{ on } \Gamma_0 \tag{1.1}$$

where ∂_n denotes the normal derivative to the boundary, more precisely

$$V = \left\{ v \in H^1(\Omega) \times H^2(\Omega); v \text{ satisfies (1.1)} \right\}. \tag{1.2}$$

We consider the two bilinear forms

$$a(u,v) = \int_\Omega \left[(\partial_1 u_1)(\partial_1 v_1) + (\partial_2 u_1 - u_2)(\partial_2 v_1 - v_2) \right] \mathrm{d}x \tag{1.3}$$

$$b(u,v) = \int_\Omega \sum_{|\alpha| \le 2} \partial_\alpha u_2 \partial_\alpha v_2 \mathrm{d}x \equiv (u_2, v_2)_2 . \tag{1.4}$$

Let us denote by f a given element of V' (the dual of V), the problem $P(\varepsilon)$ writes:

$$\left\{ \begin{array}{l} \text{Find } u^\varepsilon \text{ such that } \forall v \in V \\ a(u^\varepsilon, v) + \varepsilon^2 b(u^\varepsilon, v) = \langle f, v \rangle_{V'V} . \end{array} \right. \tag{1.5}$$

From the previous hypotheses, it immediately follows that the problem $P(\varepsilon)$ with fixed $\varepsilon > 0$ is continuous and coercive on V, so that the existence and uniqueness of the solution is ensured by the Lax Milgram theorem. Clearly the coerciveness constant is of order ε^2 so that it vanishes as $\varepsilon \searrow 0$.

This problem is somewhat classical. It is equivalent to the system of equations

$$\left\{ \begin{array}{l} -\Delta u_1^\varepsilon + \partial_2 u_2^\varepsilon = f_1 \\ -\partial_2 u_1^\varepsilon + u_2^\varepsilon + \varepsilon^2 \left(\Delta^2 u_2^\varepsilon - \Delta u_2^\varepsilon + u_2^\varepsilon \right) = f_2 \end{array} \right. \tag{1.6}$$

with the principal boundary conditions (1.1) on Γ_0 and the natural boundary conditions on Γ_1:

$$\left\{ \begin{array}{l} \partial_n u_1^\varepsilon - n_2 u_2^\varepsilon = F_1 \\ \varepsilon^2 \left[\partial_n u_2^\varepsilon - \partial_n \Delta u_2^\varepsilon - \partial_t \left(\partial_{nt} u_2^\varepsilon \right) \right] = F_2 \\ \varepsilon^2 \partial_{nn} u_2^\varepsilon = \mathcal{C} \end{array} \right. \tag{1.7}$$

where n (resp. t) is the unit outer normal (resp. the unit tangent) to Γ_1 and where

$$\langle f, v\rangle_{V'V} = \int_\Omega f_i v_i \mathrm{d}x + \int_{\Gamma_1} \left(F_1 v_1 + F_2 v_2 + \mathcal{C}\frac{\partial v_2}{\partial n} \right) \mathrm{d}s \tag{1.8}$$

in the sequel, we always take $F_1 = F_2 = \mathcal{C} = 0$ unless the opposite is explicitly said.

Moreover,

$$v \in V,\ a(v,v) = 0 \Rightarrow v = 0 \tag{1.9}$$

so that

$$\|v\|_{V_a} = (a(v,v))^{\frac{1}{2}} \tag{1.10}$$

is a norm on V. We denote by V_a the completion of V with this norm. We note that (1.9) is analogous to the hypothesis of inhibition in shell theory.

Also we define the limit problem $P(0)$ in variational form:

$$\begin{cases} \text{Find } u^0 \in V_a \text{ such that } \forall v \in V_a \\ a(u^0, v) = \langle f, v\rangle_{V_a' V_a} \text{ for a given } f \in V_a' \end{cases} \tag{1.11}$$

which is obviously continuous and coercive on V_a. It should be noticed that the hypothesis $f \in V_a'$ is somewhat restrictive as we shall see later. When this hypothesis is satisfied the existence and uniqueness of u^0 in V_a are ensured.

2. The problem $P(0)$

2.1. **First considerations on the converge process**

In order to write down the equations and boundary conditions associated with classical integrations by parts, the space $L^2(\Omega)$ is identified with its dual; this will be used in the explicit description of dual spaces.

As follows from the completion process, V is densely contained in V_a so that

$$V_a' \subset V'. \tag{2.1}$$

Classical theory (Theorem 2.1) of convergence only holds for $f \in V_a'$. In the case when $f \in V$, but $f \notin V_a'$ general results of convergence are not available. The solution u^0 of the limit problem may or not exist but likely not in the finite energy space V_a. We recall that the energy of the solutions is defined by

$$E\left(u^\varepsilon\right) = \frac{1}{2}\left[a\left(u^\varepsilon, u^\varepsilon\right) + \varepsilon^2 b\left(u^\varepsilon, u^\varepsilon\right)\right] \tag{2.2}$$

$$E\left(u^0\right) = \frac{1}{2} a\left(u^0, u^0\right). \tag{2.3}$$

The classical result is:

Theorem 2.1. *Let $f \in V_a'$ be fixed independently of ε. Let u^ε and u^0 be the solutions of (1.5) and (1.11) respectively. Then*

$$u^\varepsilon \to u^0 \text{ in } V \text{ strongly} \tag{2.4}$$

and there exists a constant C such that

$$E\left(u^\varepsilon\right) \leq C. \tag{2.5}$$

The proof is classical, see for instance Section VI.1.3 in [18]. Let us recall that (2.5) follows from (1.5) with $v = u^\varepsilon$. Moreover, we have:

Theorem 2.2. *Let $f \in V'$ be fixed independently of ε. Let u^ε the solution of (1.5), then*

1. *The necessary and sufficient condition for $E(u^\varepsilon)$ to remain bounded for $\varepsilon \searrow 0$ is that $f \in V_a'$.*
2. *If $f \notin V_a'$, then $E(u^\varepsilon)$ tends to infinity as $\varepsilon \searrow 0$.*

Proof. In order to prove the first assertion, from Theorem 2.1, it is sufficient to prove that (2.5) implies $f \in V_a'$. To this end, (2.5) implies that for a subsequence

$$b(u^\varepsilon, u^\varepsilon) \leq \frac{C}{\varepsilon^2} \tag{2.6}$$

and

$$u^\varepsilon \to u^* \text{ weakly in } V_a$$

for some $u^* \in V_a$. Let us fix $v \in V$ in (1.5), then

$$a(u^\varepsilon, v) \to a(u^*, v)$$

$$\varepsilon^2 b(u^\varepsilon, v) \leq \varepsilon^2 b(u^\varepsilon, u^\varepsilon)^{\frac{1}{2}} b(v, v)^{\frac{1}{2}} \leq \varepsilon C \to 0$$

so that

$$a(u^*, v) = \langle f, v \rangle \ \forall v \in V. \tag{2.7}$$

The left-hand side is a functional of the variable v defined on V, continuous on V_a, so that the right-hand side is also, and this implies that $f \in V_a'$.

To prove the second assertion, let us suppose that it is false. Then for a subsequence we should have (2.5) and in this case the proof of the first assertion shows that $f \in V_a'$ what is a contradiction: Theorem 2.2 is proved. □

Remark 1. We shall see that the space V_a is somewhat "large" so that V_a' is "small" and $f \in V_a'$ implies strong restrictions which are not satisfied by "usual" loadings f. Consequently, we are often in the situation of the second assertion of Theorem 2.2. This situation is in some sense "pathological". As we noted above, when $f \notin V_a'$ the limit problem $P(0)$ may or not have a solution u^0 but if it does, it is not in the finite energy space V_a. This is the reason why we shall consider in the sequel solutions of the limit problem which are not variational solutions in V_a. An example of this situation is shown in [11] where it is seen that the energy confined in boundary and internal layers is not bounded (for $\varepsilon \searrow 0$) whereas the energy in outer regions does. Later on we shall search for the asymptotic behavior of u^ε using the method of matched asymptotic expansions [20] which shall exhibit such kind of layers. □

2.2. A criterion for $f \in V_a'$ and examples

In this section, we shall consider functionals f defined in (1.8) by functions f_i (on Ω) with $F_i = \mathcal{C} = 0$. The form a defined in (1.3) is associated with the two quantities

$$\begin{cases} \gamma_1(u) \equiv \partial_1 u_1 \\ \gamma_2(u) \equiv \partial_2 u_1 - u_2. \end{cases} \tag{2.8}$$

Let us define the injective application γ by (2.8)

$$V \overset{\gamma}{\to} \left(L^2\right)^2$$

this application may be continued by continuity to V_a to an isomorphism from V_a onto its range X which is clearly a closed subspace of $\left(L^2\right)^2$.

Let us now consider the functional

$$l_f(v) = \int_\Omega \left(f_1 v_1 + f_2 v_2\right) \mathrm{d}x \tag{2.9}$$

defined on V. Then we have:

Theorem 2.3. *The functional defined by (2.9) may be extended by continuity to V_a (that is equivalent to $f \in V_a'$) if, and only if, there exists $T = (T^1, T^2) \in \left(L^2\right)^2$ such that*

$$\int_\Omega \left(f_1 v_1 + f_2 v_2\right) \mathrm{d}x = \left(T^1, \gamma_1(v)\right)_{L^2} + \left(T^2, \gamma_2(v)\right)_{L^2} \ \forall v \in V. \tag{2.10}$$

Proof. Let us suppose that there exists $T \in \left(L^2\right)^2$ which satisfies to (2.10), then the right-hand side in (2.10) is continuous on V for the topology of V_a and consequently the left hand side also does: this proves that the condition is sufficient. If (2.9) may be extended by continuity to V_a, then let us denote by

$$\langle f, v \rangle_{V_a' V_a} \tag{2.11}$$

the functional so extended. Let F be its image by the isomorphism γ, it is continuous on X and defined by

$$F(\xi) = \left\langle f, \gamma^{-1}(\xi) \right\rangle \ \forall \xi \in X. \tag{2.12}$$

From the Hahn-Banach theorem, we know that it may be extended to a functional $\tilde{F}(\xi)$ continuous on $\left(L^2\right)^2$ and, by the Riesz theorem, it may be expressed as the scalar product

$$\tilde{F}(\xi) = \langle T, \xi \rangle_{(L^2)^2} \ \forall \xi \in \left(L^2\right)^2 \tag{2.13}$$

where T is some element of $\left(L^2\right)^2$. In particular (2.13) holds for any $\xi \in X$ and even for any ξ of the form $\xi = \gamma(v)$ with $v \in V$ (not necessarily to V_a). Then, from (2.13), we get

$$\langle f, v \rangle \equiv \int_\Omega \left(f_1 v_1 + f_2 v_2\right) \mathrm{d}x = \left(T, \gamma(v)\right)_{(L^2(\Omega))^2} \quad \forall v \in V$$

the necessity of the condition is then proved. □

Example 2.1. Let us consider the case when the whole boundary is clamped and let f_1, f_2 be smooth functions. We shall see that $f \in V_a'$. Indeed, (2.10) explicitly writes

$$\int_\Omega \left(f_1 v_1 + f_2 v_2\right) \mathrm{d}x = \int_\Omega \left[T_1 \partial_1 v_1 + T_2 \left(\partial_2 v_1 - v_2\right)\right] \mathrm{d}x \quad \forall v \in V. \tag{2.14}$$

Taking $v \in [\mathcal{D}(\Omega)]^2$ we obtain

$$\begin{cases} f_1 = -\partial_1 T_1 - \partial_2 T_2 \\ f_2 = -T_2. \end{cases} \tag{2.15}$$

As the two components f_1 and f_2 are smooth it is possible to construct smooth T^1 and T^2, in particular $\left(T^1, T^2\right) \in \left(L^2\right)^2$, satisfying (2.15). Then we have

$$\int_\Omega (f_1 v_1 + f_2 v_2)\,\mathrm{d}x = \int_\Omega \left[(-\partial_1 T_1 - \partial_2 T_2)\, v_1 + (-T_2)\, v_2\right]\mathrm{d}x \quad \forall v \in V. \tag{2.16}$$

In the considered case of a clamped boundary we have $V = H_0^1 \times H_0^2$ so that an obvious integration by parts in (2.16) gives (2.14). It then follows from Theorem 2.3 that

$$f \in V_a'. \tag{2.17}$$

Consequently, from Theorem 2.2 we see that the solution u^ε of (2.12) is such that the energy $E(u^\varepsilon)$ of u^ε remains bounded as $\varepsilon \searrow 0$.

Example 2.2. We consider again a totaly clamped boundary but f_i are no more smooth functions. We shall take

$$\begin{cases} f_1 \equiv 0 \\ f_2 = \begin{cases} 0 \text{ if } x_2 < \pi/2 \\ 1 \text{ if } x_2 > \pi/2 \end{cases} \end{cases} \tag{2.18}$$

the given forces defined on the domain Ω. We emphasize that the discontinuity of f is along a curve $x_2 = \text{const}$. We shall see later that these curves are the characteristics of the problem $P(0)$. Let us prove that $f \notin V_a'$.

Indeed, we are showing that $T_1, T_2 \in L^2$ and satisfying (2.14) cannot exist. If this was the case then taking $v \in [\mathcal{D}(\Omega)]^2$ we should have (2.15). In addition, as f_1, f_2 are piecewise smooth the corresponding traces of $T_1 n_1 + T_2 n_2$ make sense, allowing classical integration by parts. Then, from (2.14) with arbitrary v we get

$$[|T_2|] = 0 \text{ on } x_2 = \frac{\pi}{2} \tag{2.19}$$

where the brackets denote the jump across the discontinuity. We then see that (2.19) with (2.15) and (2.18) are not compatible. So that T_1, T_2 cannot exist. According to Theorem 2.3 the given force f does not belong to V_a'. Consequently, from Theorem 2.2 we see that the solution u^ε of (2.12) is such that the energy $E(u^\varepsilon)$ tends to infinity as $\varepsilon \searrow 0$.

Example 2.3. Now we consider a smooth given force f but the boundary is constituted of two parts Γ_0 and Γ_1. We recall that Γ_0 is clamped while Γ_1 is free. We shall take as Γ_1 the part $x_2 = 0$ of the boundary. We emphasize that, as in the previous example, this free boundary is along a characteristic of the problem $P(0)$. The space V is then defined as

$$V = \left\{v_1 \in H^1(\Omega)\,;\, v|_{\Gamma_0 = 0}\right\} \times \left\{v_2 \in H^2(\Omega)\,;\, v|_{\Gamma_0} = \left.\frac{\partial v}{\partial n}\right|_{\Gamma_0} = 0\right\}. \tag{2.20}$$

Exactly as in the previous example if T_1, T_2 exist, then they satisfy

$$\left\{ \begin{array}{l} \left\{ \begin{array}{l} -\partial_1 T_1 - \partial_2 T_2 = f_1 \\ T_2 = f_2 \end{array} \right. \text{ on } \Omega \\ T_2 = 0 \text{ on } \Gamma_1. \end{array} \right. \tag{2.21}$$

It is clear that $(2.21)_2$ and $(2.21)_3$ are compatible if and only if $f_2|_{\Gamma_1} = 0$. Oppositely, when this condition is satisfied we may construct smooth functions T_1, T_2 satisfying (2.21) and classical integration by parts show that T_1, T_2 satisfy (2.10). Then $f_2 = 0$ on Γ_1 is the necessary and sufficient condition for $f \in V_a'$. Obviously it is also the necessary and sufficient condition for $E(u^\varepsilon)$ to remain bounded as $\varepsilon \searrow 0$.

2.3. **Equations and boundary conditions of** $P(0)$

The variational formulation (1.11) of the limit problem is somewhat abstract as V_a was only defined by completion. We have not a precise description of V_a which depends on the disposition of Γ_0 and Γ_1. But in any case it follows from (1.10) and (1.3) that $v \in V_a \Rightarrow \partial_1 v_1 \in L^2(\Omega)$. Moreover, from the fact that Γ_0 contains at least one of the vertical segments of the boundary and Poincaré inequality for $x_2 = \text{const.}$, it follows that $v_1 \in L^2(\Omega)$. Consequently, the principal boundary condition $v_1 = 0$ is inherited by V_a on the parts of Γ_0 which are tranversal to $x_2 = \text{const.}$

As for v_2, if $v \in V_a$, it follows from (1.10) and (1.3) that v_2 is the sum of an element of $L^2(\Omega)$ and $\partial_2 v_1$ so that the principal boundary conditions of v_1 on $x_2 = \text{const.}$ and of v_2 everywhere are lost in the completion process. This allows us to write down the equations and boundary conditions of $P(0)$ (without a precise description of V_a):

$$\left\{ \begin{array}{l} -\Delta u_1 + \partial_2 u_2 = f_1 \\ -\partial_2 u_1 + u_2 = f_2 \end{array} \right. \tag{2.22}$$

$$\left\{ \begin{array}{l} u_1 = 0 \text{ on the parts of } \Gamma_0 \text{ transversal to } x_2 = \text{const.} \\ \partial_1 u_1 = 0 \text{ on the parts of } \Gamma_1 \text{ transversal to } x_2 = \text{const.} \end{array} \right. \tag{2.23}$$

obviously, the first of these boundary conditions is a principal one on V_a as we said above, whereas the second one is a natural condition coming from integration by parts.

Clearly (2.22) is equivalent to

$$-\partial_1^2 u_1 = f_1 - \partial_2 f_2 \tag{2.24}$$

$$u_2 = f_2 + \partial_2 u_1. \tag{2.25}$$

Under this form it is obvious that the limit problem is essentially equivalent to (2.24) for u_1. This equation is an elliptic one with respect to x_1 with parameter x_2. In Ω it is parabolic with double characteristics $x_2 = \text{const.}$ As x_2 appears as a parameter, f_1 and f_2 may be chosen to be distributions of x_2 with values in an appropriated space for the variable x_1. Consequently, when f_2 is not sufficiently smooth with respect to x_2, the equations (2.22) and the boundary conditions (2.23) keep a sense in a more general framework which is not that of the variational problem (1.11).

Let us define the operator A by

$$Au = -\partial_1^2 u_1 \tag{2.26}$$

for functions depending on the variable x_1 and the evident boundary conditions coming from (2.23). We note that according to the hypothesis that Γ_0 and Γ_1 are made of whole sides of the boundary of Ω, this operator is

independent of x_2 so that it commutes with differentiations with respect this parameter. Obviously, the solution of (2.24), (2.25) then writes

$$\left\{\begin{array}{l} u_1(\bullet,x_2) = A^{-1}\left[f_1(\bullet,x_2) - \partial_2 f_2(\bullet,x_2)\right] \\ u_2(\bullet,x_2) = f_2(\bullet,x_2) + A^{-1}\left[\partial_2 f_1(\bullet,x_2) - \partial_2^2 f_2(\bullet,x_2)\right]. \end{array}\right. \tag{2.27}$$

2.4. **Solutions in the sense of distributions**

According to the previous considerations, we now consider the system (2.22) or (2.24) and (2.25) as well as the solution (2.27) in the sense of distributions of x_2 with values in a space (for instance $L^2(0,\pi)$) of the variable x_1. In order to exhibit the singular terms, we consider the case when $f_1 = 0$ and f_2 is a piecewise smooth function of the variable x_2 with values in $L^2(0,\pi)$ with a discontinuity at a point γ of $(0,\pi)$. Let φ and $\psi \in L^2(0,\pi)$ be the jumps of the function and the first derivative at $x_2 = \gamma$. The solution (2.27) takes the form

$$\left\{\begin{array}{l} u_1(\bullet,x_2) = -A^{-1}\left(\partial_2^f f_2\right) - \left(A^{-1}\varphi(\bullet)\right)\delta_\gamma \\ u_2(\bullet,x_2) = f_2(\bullet,x_2) - A^{-1}\left(\partial_2^{f2} f_2(\bullet,x_2)\right) - \left(A^{-1}\psi(\bullet)\right)\delta_\gamma - \left(A^{-1}\varphi(\bullet)\right)\delta'_\gamma \end{array}\right. \tag{2.28}$$

where ∂_2^f denotes the derivative in the sense of functions. To fix ideas, let us take

$$\left\{\begin{array}{l} f_1 = 0 \\ f_2(\bullet,x_2) = \left\{\begin{array}{ll} 0 & \text{for } x_2 < \gamma \\ \varphi(\bullet) & \text{for } x_2 > \gamma \end{array}\right. \end{array}\right. \tag{2.29}$$

in this case the solution is

$$\left\{\begin{array}{l} u_1(\bullet,x_2) = -\left(A^{-1}\varphi(\bullet)\right)\delta_\gamma \\ u_2(\bullet,x_2) = f_2(\bullet,x_2) - \left(A^{-1}\varphi(\bullet)\right)\delta'_\gamma. \end{array}\right. \tag{2.30}$$

We shall see later that these solutions of problem $P(0)$ are the limits of the corresponding solutions of problem $P(\varepsilon)$ as $\varepsilon \searrow 0$. Clearly this implies that the solutions of $P(\varepsilon)$ involve boundary (in fact internal) layers terms which converge to the singular terms of (2.30).

2.5. **Localization of the boundary and internal layers**

As a consequence of Section 2.4 it appears that the problem $P(\varepsilon)$ exhibits internal layers terms along the segments $x_2 = \text{const.}$ where f is not smooth as function of x_2 with values in $L^2(0,\pi)$ for instance. The structure of the internal layer depends highly on the degree of non-smoothness of f. We emphazise that $x_2 = \text{const.}$ are the characteristics of the limit problem (2.24).

The explicit solution (2.30) exhibits an example of propagation of singularities along the characteristics. As the operator A^{-1} of the variable x_1 is non-local, we may have φ with compact support in $(0,\pi)$ whereas the solution u is singular along the whole segment of characteristic $x_2 = \text{const.}, x_1 \in (0,\pi)$.

Oppositely, let us consider the case when $f_1 = 0$ and f_2 is piecewise constant with a discontinuity along a curve $\mathcal{C}$ which is transversal to the characteristics. The method of solution with parameter x_2 shows that u is smooth unless on $\mathcal{C}$ where the function u_2 and the first derivative of u_1 have jumps. Clearly, in this case, u^ε exhibits an internal layer along the curve $\mathcal{C}$. In addition, if one of the extremities of $\mathcal{C}$ is a point interior to Ω, the solution is singular at this point and propagates from it along $x_2 = \text{const.}$

On the other hand, as x_2 is a parameter, the limit problem $P(0)$ has no boundary condition on $x_2 = 0$ and $x_2 = 1$ so that u^ε exhibits boundary layers along these (characteristic) boundaries.

Also boundary layers appear along the parts of Γ_0 transversal to the characteristics (vertical parts of Γ_0) as the boundary conditions (1.1) involving u_2 disappear in the limit (compare with (2.23)). We shall call them non-characteristic boundary layers.

3. Scaling in the layers. Method of exponential solutions

Classically [20], in order to describe the structure of a layer we must perform a change of variables including a dilatation of the variable normal to the layer. Moreover, in order to obtain a consistent system, a rescaling of the unknowns is usually needed. The deduction by a classical procedure of the appropriate scalings is possible but we use here a method issued from the analysis of the structure of the exponential solutions of the homogeneous system [15]. It should be pointed out that this method presents analogies with the study of asymptotic solutions of systems using the eikonal equation ([18], Sect. III.4).

3.1. **Characteristic layers**

We first consider the case of the layers along $x_2 = \text{const}$. As the characteristics of the limit problem are normal to the vector $(0,1)$ there exist solutions of the form

$$u(x_1, x_2) = ve^{i(\xi_1 x_1 + \xi_2 x_2)}$$

with $\xi_1 = 0, \xi_2 \neq 0$. Let us search, for $\varepsilon > 0$, solutions of the form

$$u^\varepsilon(x_1, x_2) = v^\varepsilon e^{i\xi_1 + \mu x_2} \tag{3.1}$$

with $|\mu| \to +\infty$ (*i.e.* such that $(\xi_1\,(real), \xi_2 \equiv -i\mu)$ tends to be proportional to $(0,1)$). The solutions (3.1) are sinusoidal in x_1 with wave length of order $\mathcal{O}(1)$ and very fast variations in x_2. By substitution of (3.1) in the homogeneous system associated with (1.6) we obtain

$$\begin{cases} \left(\xi_1^2 - \mu^2\right) v_1^\varepsilon + \mu v_2^\varepsilon = 0 \\ -\mu v_1^\varepsilon + v_2^\varepsilon + \varepsilon^2 \left[\left(\xi_1^2 - \mu^2\right)^2 v_2^\varepsilon + \left(\xi_1^2 - \mu^2\right) v_2^\varepsilon + v_2^\varepsilon\right] = 0. \end{cases} \tag{3.2}$$

The vanishing of the determinant of system (3.2) gives

$$\xi_1^2 + \varepsilon^2 \left(\xi_1^2 - \mu^2\right) \left[\left(\xi_1^2 - \mu^2\right)^2 + \xi_1^2 - \mu^2 + 1\right] = 0$$

which for finite ξ_1 and $\mu \to +\infty$ gives the behavior of μ:

$$\mu \cong e^{\frac{ik\pi}{3}} \xi_1^{\frac{1}{3}} \varepsilon^{-\frac{1}{3}}. \tag{3.3}$$

Then, from the first equation (3.2) we see that

$$\frac{v_2^\varepsilon}{v_1^\varepsilon} = \mathcal{O}\left(\varepsilon^{-\frac{1}{3}}\right). \tag{3.4}$$

It then appears that the just obtained solutions with $\xi_1 = \mathcal{O}(1)$, $\mu = \mathcal{O}\left(\varepsilon^{-\frac{1}{3}}\right)$ have a characteristic length of variation in the x_2 direction of order $\mathcal{O}\left(\varepsilon^{\frac{1}{3}}\right)$; this corresponds to a layer of thickness $\mathcal{O}(\eta)$,

$$\eta = \varepsilon^{\frac{1}{3}}. \tag{3.5}$$

Moreover, the corresponding scaling of u is

$$\frac{u_2^\varepsilon}{u_1^\varepsilon} = \mathcal{O}\left(\eta^{-1}\right). \tag{3.6}$$

3.2. **Non-characteristic layers**

Analogously, in the case of layers parallel to $x_1 = \text{const.}$ we search solutions of the form

$$u^\varepsilon(x_1, x_2) = v^\varepsilon e^{\mu x_1 + i\xi_2 x_2}$$

from which it follows that

$$\mu \cong (-1)^{\frac{1}{4}} \varepsilon^{-\frac{1}{2}} \tag{3.7}$$

so that the thickness of the layer is of order

$$\eta = \varepsilon^{\frac{1}{2}}. \tag{3.8}$$

and the scaling of u is

$$\frac{u_2^\varepsilon}{u_1^\varepsilon} = \mathcal{O}\left(\eta^{-1}\right) = \mathcal{O}\left(\varepsilon^{-\frac{1}{2}}\right). \tag{3.9}$$

4. Boundary layer along a characteristic part of Γ_0

As announced at the end of Section 2.5, there exists a boundary layers along the boundaries $x_2 = 0$ and $x_2 = \pi$. Their structure is different according to the boundary belongs to Γ_0 or to Γ_1. In this section we are concerned by the first case and we suppose that the boundary is $x_2 = 0$. We also suppose, to fix ideas that Γ_0 contains the vertical segments $x_1 = 0$ and $x_1 = \pi$. According to Section 3.1, the appropriate scaling is then (3.5) and (3.6) so we define the dilatation by

$$y_2 = \frac{x_2}{\eta} \tag{4.1}$$

and we search for asymptotic expansions of the form

$$\begin{cases} u_1^\varepsilon(x_1, x_2) = U_1^\eta(x_1, y_2) = U_1^0(x_1, y_2) + \cdots \\ u_2^\varepsilon = \eta^{-1} U_2^\eta(x_1, y_2) = \eta^{-1} U_2^0(x_1, y_2) + \cdots \end{cases} \tag{4.2}$$

Tentatively, we took the component u_1 of order $\mathcal{O}(1)$ in order to match it with the outer expansion (we recall that only the ratio u_2/u_1 was defined by (3.6)). In the sequel, we shall denote by D_2 the derivative with respect to y_2:

$$D_2 = \eta \partial_2. \tag{4.3}$$

According to the boundary layer theory [20], the expansions (4.2) holds true in the domain D defined by $x_1 \in (0, \pi)$, $y_2 \in (0, +\infty)$. The solution U^η must satisfy the boundary conditions

$$\begin{cases} U_1^\eta(x_1, 0) = U_2^\eta(x_1, 0) = D_2 U_2^\eta(x_1, 0) = 0 \\ U_1^\eta(0, y_2) = U_1^\eta(\pi, y_2) = 0 \end{cases} \tag{4.4}$$

and the matching conditions for $y_2 \to +\infty$ which shall consider later.

The variational formulation of (1.5) must hold true in the domain D at least for test functions with bounded support in y_2, we shall take them depending on η in a form analogous to (4.2). Consequently we have

$$\int_D \left\{ \partial_1 U_1^\eta \partial_1 V_1^\eta + \frac{1}{\eta^2} \left(D_2 U_1^\eta - U_2^\eta \right) \left(D_2 V_1^\eta - V_2^\eta \right) + \frac{\varepsilon^2}{\eta^6} \left[D_2^2 U_2^\eta D_2^2 V_2^\eta + \cdots \right] \right\} \mathrm{d}x_1 \mathrm{d}y_2 \tag{4.5}$$

$$= \int_D \left\{ \left[f_1 \left(x_1, 0 \right) + \cdots \right] V_1^\eta + \frac{1}{\eta} \left[f_2 \left(x_1, 0 \right) + \eta y_2 \partial_2 f_2 \left(x_1, 0 \right) + \cdots \right] V_2^\eta \right\} \mathrm{d}x_1 \mathrm{d}y_2$$

where f is supposed to be regular and was represented by its Taylor expansion in the vicinity of $x_2 = 0$. We note that, according to (3.5), $\varepsilon^2/\eta^6 = 1$ in formula (4.5). Taking $V_1^0 = 0$ and $V_2^0 \in \mathcal{D}\left(D\right)$, the leading term (of order η^{-2}) gives

$$D_2 U_1^0 - U_2^0 = 0 \tag{4.6}$$

which implies a constraint for the unknown U^0. In the sequel, we shall take test functions satisfying this constraint, thus the test functions will satisfy

$$V_2^0 = D_2 V_1^0. \tag{4.7}$$

Consequently, the term of order $1/\eta$ in (4.5) vanishes, indeed it is

$$\int_D f_2(x_1, 0) V_2^0(x_1, y2) d\mathrm{x}_1 \mathrm{d}y_2 = \int_0^\pi f_2(x_1, 0) \left(\int_0^{+\infty} D_2 V_1^0(x_1, y_2) \mathrm{d}y_2 \right) \mathrm{d}x_1 = 0$$

as V_1^0 vanishes for $y_2 = 0$ and y_2 sufficiently large.

Presently the leading term of (4.5) is of order $\mathcal{O}(1)$ and must vanish so that we have

$$\int_D \left[\partial_1 U_1^0 \partial_1 V_1^0 + D_2^2 U_2^0 D_2^2 V_2^0 \right] \mathrm{d}x_1 \mathrm{d}y_2 = \int_D \left[f_1 \left(x_1, 0 \right) V_1^0 + y_2 \partial_2 f_2 \left(x_1, 0 \right) V_2^0 \right] \mathrm{d}x_1 \mathrm{d}y_2.$$

Taking account of (4.6) and (4.7), the problem reduces to another one for the only unknown U_1^0 (with the only test function V_1^0) which, after an integration by parts in the right-hand side, writes

$$\int_D \left[\partial_1 U_1^0 \partial_1 V_1^0 + D_2^3 U_1^0 D_2^3 V_1^0 \right] \mathrm{d}x_1 \mathrm{d}y_2 = \int_D \left[f_1 \left(x_1, 0 \right) - \partial_2 f_2 \left(x_1, 0 \right) \right] V_1^0 \mathrm{d}x_1 \mathrm{d}y_2 \tag{4.8}$$

from which, taking $V_1^0 \in \mathcal{D}\left(\Omega\right)$, we obtain the equation satisfied by U_1^0:

$$-\partial_1^2 U_1^0 - D_2^6 U_1^0 = f_1 \left(x_1, 0 \right) - \partial_2 f_2 \left(x_1, 0 \right). \tag{4.9}$$

According to (4.4) and taking account of (4.6), the component U_1^0 must satisfy the boundary conditions

$$U_1^0 \left(x_1, 0 \right) = D_2 U_1^0 \left(x_1, 0 \right) = D_2^2 U_1^0 (x_1, 0) = 0 \tag{4.10}$$

and

$$U_1^0 (0, y_2) = U_1^0 \left(\pi, y_2 \right) = 0. \tag{4.11}$$

The solution of (4.9) may be written under the form

$$U_1^0(x_1, y_2) = \hat{U}_1^0(x_1) + \tilde{U}_1^0(x_1, y_2) \tag{4.12}$$

where $\hat{U}_1^0(x_1, 0)$ is the solution of

$$-\hat{U}_1^{0"}(x_1) = f_1(x_1, 0) - \partial_2 f_2(x_1, 0) \equiv F(x_1) \tag{4.13}$$

with the boundary conditions

$$\hat{U}_1^0(0) = \hat{U}_1^0(\pi) = 0. \tag{4.14}$$

i.e. of equation (2.24) and the boundary conditions (2.23) so that $\hat{U}_1^0$ is nothing but $u_1(x_1, 0)$ in Section 2.3.

As for the new unknown $\tilde{U}_1^0(x_1, y_2)$ it is solution of the homogeneous equation

$$-\partial_1^2 \tilde{U}_1^0 - D_2^6 \tilde{U}_1^0 = 0. \tag{4.15}$$

Let us search a solution of (4.15) under the form

$$\tilde{U}_1^0(x_1, y_2) = \sum_{n=1}^{+\infty} a_n(y_2) \sin n x_1 \tag{4.16}$$

we have

$$\tilde{U}_1^0(x_1, y_2) = \sum_{n=1}^{+\infty} a_n(y_2) \sin n x_1 = U_1^0(x_1, y_2) - \hat{U}_1^0(x_1).$$

Now, let us write the Fourier expansion of $F(x_1)$ under the form

$$F(x_1) = \sum_{n=1}^{+\infty} F_n \sin n x_1$$

then, from the conditions (4.10), the coefficients a_n must satisfy

$$a_n(0) = -\frac{F_n}{n^2} \tag{4.17}$$

$$a_n'(0) = a_n''(0) = 0 \tag{4.18}$$

and, from (4.15),

$$n^2 a_n(y_2) - \frac{\mathrm{d}^6}{\mathrm{d}y_2^6} a_n(y_2) = 0. \tag{4.19}$$

The bounded solution of (4.19) is of the form

$$a_n(y_2) = \sum_{k=2}^{4} b_k \exp\left\{ n^{\frac{1}{3}} \exp\left(\frac{ik\pi}{3} \right) y_2 \right\} \tag{4.20}$$

where the coefficients are uniquely determined on account of (4.17) and (4.18). Moreover, as $y_2 \to +\infty$, $U_1^0(x_1, y_2)$ tends to $\hat{U}_1^0(x_1)$ solution of the limit problem $P(0)$ that insures the matching with the solution of the limit problem $P(0)$ of Section 2.3.

As for the component U_2^0, as we saw it is given by

$$U_2{}^0(x_1, y_2) = D_2 U_1{}^0(x_1, y_2) = D_2 \tilde{U}_1^0(x_1, y_2)$$

and is such that

$$U_2{}^0(x_1, y_2) \xrightarrow[y_2 \to +\infty]{} 0$$

that constitutes the matching condition as u_2^ε is of order $\varepsilon^{-\frac{1}{3}}$ in the layer and $\mathcal{O}(1)$ out of it.

5. Boundary layer along a characteristic part of Γ_1

In this section we consider the case when Γ_1 contains the boundary $x_2 = 0$ and Γ_0 contains $x_1 = 0$ and $x_1 = \pi$. We consider the layer along $x_2 = 0$. As in the previous section, the scaling of the x_2 is defined by (4.1) but the asymptotic expansions are searched under the form

$$\left\{ \begin{array}{l} u_1^\varepsilon(x_1, x_2) = \theta(\eta) U_1^\eta(x_1, y_2) = \theta(\eta) U_1^0(x_1, y_2) + \cdots \\ u_2^\varepsilon = \eta^{-1}\theta(\eta) U_2^\eta(x_1, y_2) = \eta^{-1}\theta(\eta) U_2^0(x_1, y_2) + \cdots \end{array} \right. \tag{5.1}$$

where $\theta(\eta)$ is to be determined later. Indeed, the method introduced in Section 3 only gives the ratio $\frac{u_2}{u_1}$ (*c.f.* (3.6)) that is satisfied by (5.1); we shall see later that different functions $\theta(\eta)$ should be chosen according to the behavior of f_2 on the free boundary. We shall again denote by D_2 the derivative with respect to y_2 which, of course, satisfies (4.3).

As before, the variational formulation (1.5) must hold true in the domain D for test functions with compact support in y_2 and we shall choose them depending on η in a form analogous to (5.1) then, we have

$$\theta(\eta) \int_D \left\{ \partial_1 U_1^\eta \partial_1 V_1^\eta + \frac{1}{\eta^2} (D_2 U_1^\eta - U_2^\eta)(D_2 V_1^\eta - V_2^\eta) + \left[D_2^2 U_2^\eta D_2^2 V_2^\eta + \cdots \right] \right\} \mathrm{d}x_1 \mathrm{d}y_2 =$$
$$\int_D \left\{ \left[f_1(x_1, 0) + \cdots \right] V_1^\eta + \frac{1}{\eta} \left[f_2(x_1, 0) + \eta y_2 \partial_2 f_2(x_1, 0) + \cdots \right] V_2^\eta \right\} \mathrm{d}x_1 \mathrm{d}y_2 \tag{5.2}$$

Taking $V_1^0 = 0$ and arbitrary V_2^0, the leading term in the left-hand side is

$$\frac{\theta(\eta)}{\eta^2} \int_D \left(D_2 U_1^0 - U_2^0 \right) V_2^0 \mathrm{d}x_1 \mathrm{d}y_2$$

and in the right-hand side is

$$\frac{1}{\eta} \int_D f_2(x_1, 0) V_2^0 \mathrm{d}x_1 \mathrm{d}y_2$$

consequently, it immediately appears, taking account of the matching condition, that we have only two possibilities: $\theta(\eta) >> 1$ or $\theta(\eta) = 1$. Then, as we shall see Sections 5.1 and 5.2, in order to obtain problems consistent with the data, the function $\theta(\eta)$ must be chosen as follows, according to the value of the component f_2 at

the boundary $x_2 = 0$

$f_2(x_1,0) \neq 0$	$\theta(\eta) = \eta^{-1}$
$f_2(x_1,0) = 0$	$\theta(\eta) = 1$

(5.3)

with in any case $D_2U_1^0 - U_2^0 = 0$ *i.e.* (4.6).

5.1. Case when $f_2(x_1,0) \neq 0$

In this case, taking test functions such that $V_2^0 = D_2V_1^0$ in the variational formulation (5.2), its leading term is

$$\frac{1}{\eta}\int_D \left\{\partial_1^2 U_1^0 V_1^0 + D_2^3 U_1^0 D_2^3 V_1^0\right\} \mathrm{d}x_1\mathrm{d}y_2 = \int_D \frac{1}{\eta} f_2(x_1,0)\, D_2V_1^0 \mathrm{d}x_1\mathrm{d}y_2 \tag{5.4}$$

which, after evident integrations by parts, becomes

$$\begin{aligned}\int_D \left[-\partial_1^2 U_1^0 - D_2^6 U_1^0\right] V_1^0 \mathrm{d}x_1\mathrm{d}y_2 + \int_{\partial D} \Big\{ &\left[\partial_1 U_1^0 V_1^0\right] n_1 \\ &+ \left[D_2^3 U_1^0 D_2^2 V_1^0 - D_2^4 U_1^0 D_2 V_1^0 + D_2^5 U_1^0 V_1^0\right] n_2 \Big\} \mathrm{d}s \\ &= \int_{\Gamma_1} f_2(x_1,0)\, V_1^0 n_2 \mathrm{d}x_1.\end{aligned} \tag{5.5}$$

Then, taking $V_1^0 \in \mathcal{D}(D)$, we obtain the equation

$$-\partial_1^2 U_1^0 - D_2^6 U_1^0 = 0 \tag{5.6}$$

and, from the integrals along the boundary (as $D_2^2V_1^0$, $D_2V_1^0$ and V_1^0 are arbitrary on the part $x_2 = 0$ of ∂D), we have

$$\begin{cases} D_2^3 U_1^0(x_1,0) = 0 \\ D_2^4 U_1^0(x_1,0) = 0 \\ D_2^5 U_1^0(x_1,0) = f_2(x_1,0). \end{cases} \tag{5.7}$$

As in Section 4, we now search for a solution of the form

$$U_1^0(x_1,y_2) = \sum_{n=1}^{+\infty} a_n(y_2) \sin nx_1 \tag{5.8}$$

then the coefficients $a_n(y_2)$ are the bounded solution of the equation

$$-a_n^{(6)}(y_2) + n^2 a_n(y_2) = 0 \tag{5.9}$$

i.e. of the form

$$a_n(y_2) = \sum_{k=2}^{4} c_k \exp\left[n^{\frac{1}{3}} \exp\left(\frac{ik\pi}{3}\right) y_2\right] \tag{5.10}$$

where the coefficients c_k are determined by the boundary conditions

$$\begin{cases} a_n^{(3)}(0) = a_n^{(4)}(0) = 0 \\ a_n^{(5)}(0) = F_n \end{cases} \tag{5.11}$$

where F_n is the coefficient of $\sin nx_1$ in the Fourier expansion of $f_2(x_1, 0)$.

Of course, $U_2^0(x_1, y_2)$ is then given by (4.6).

5.2. **Case when** $f_2(x_1, 0) = 0$

This case, for which $\theta(\eta) = 1$, is worked out exactly as the previous one the only modifications concern the equation which becomes

$$-\partial_1^2 U_1^0 - D_2^{(6)} U_2^0 = f_1(x_1, 0) \tag{5.12}$$

and the last boundary condition in (5.7) which is now

$$D_2^{(5)} U_1^0(x_1, 0) = 0. \tag{5.13}$$

Consequently, the analogous of the coefficients $a_n(y_2)$ are solutions of

$$-a_n^{(6)}(y_2) + n^2 a_n(y_2) = f_1(x_1, 0) \tag{5.14}$$

with the boundary conditions

$$a_n^{(3)}(0) = a_n^{(4)}(0) = a_n^{(5)}(0) = 0. \tag{5.15}$$

It should be easily seen that the solution is unique and satisfy the matching conditions.

6. Internal characteristic layers

Let us consider the data (2.29) of Section 2.4. To fix ideas we shall suppose that Γ_0 contains the boundaries $x_1 = 0$ and $x_1 = \pi$. It appears, according to (2.30), that the solution of the limit problem exhibits a discontinuity along $x_2 = \gamma$. Moreover, we saw in example 2.2 that $f \notin V_a'$.

By comparison with example 2.3 the problem addressed in the present section is thus analogous to that of the Section 5.1 but in a layer near $x_2 = \gamma$. Instead of (4.1), the inner variable is now

$$y_2 = \frac{x_2 - \gamma}{\eta}\,. \tag{6.1}$$

The domain D is presently $D = (0, \pi) \times (-\infty, +\infty)$, consequently we shall have two matchings for $y_2 \to \pm\infty$.

As in Section 5.1, the inner expansion is (5.1) with $\theta(\eta) = \eta^{-1}$. The analogue of equation (5.4) is

$$\int_D \left\{\partial_1^2 U_1^0 V_1^0 + D_2^3 U_1^0 D_2^3 V_1^0\right\} \mathrm{d}x_1 \mathrm{d}y_2 = \int_{D^+} \varphi(x_1) D_2 V_1^0 \mathrm{d}x_1 \mathrm{d}y_2$$

where $D^+ = (0, \pi) \times (0, +\infty)$ (analogously $D^- = (0, \pi) \times (-\infty, 0)$).

In each region D^+ and D^- we again obtain equation (5.6) and the boundary conditions (taking on $x_2 = \gamma$ the quantities V_1^0, $D_2 V_1^0$ and $D_2^2 V_1^0$ are continuous) become the interface conditions

$$\left\{ \left[\left| \begin{array}{c} D_2^3 U_1^0 (x_1, 0) = 0 \\ D_2^4 U_1^0 (x_1, 0) = 0 \\ D_2^5 U_1^0 (x_1, 0) = \varphi(x_1) \end{array} \right| \right] \right. \tag{6.2}$$

where $[|\bullet|]$ denotes the jump across the interface. Obviously, we shall also prescribe

$$\left[\left| U_1^0 \right| \right] = \left[\left| D_2 U_1^0 \right| \right] = \left[\left| D_2^2 U_1^0 \right| \right] = 0. \tag{6.3}$$

Moreover, the function U_1^0 satisfies the boundary conditions

$$U_1^0 (0, y_2) = U_1^0 (\pi, y_2) = 0, \tag{6.4}$$

and the matching conditions

$$U_1^0 (x_1, y_2) \xrightarrow[y_2 \to \pm\infty]{} 0. \tag{6.5}$$

As in Section 5.1, we search in each region D^+ and D^- a solution of the form (5.8) with coefficients a_n^+ and a_n^- respectively which satisfy

$$-a_n^{\pm(6)} (y_2) + n^2 a_n^{\pm} (y_2) = 0 \tag{6.6}$$

and are bounded in their corresponding domain of definition, so that

$$\left\{ \begin{array}{l} a_n^+ (y_2) = \sum\limits_{k=2}^{4} c_k^+ \exp \left[n^{\frac{1}{3}} \exp \left(\frac{ik\pi}{3} \right) y_2 \right] \\ a_n^- (y_2) = \sum\limits_{k=0}^{3} c_k^- \exp \left[n^{\frac{1}{3}} \exp \left(\frac{i(2k+1)\pi}{3} \right) y_2 \right]. \end{array} \right. \tag{6.7}$$

Moreover, they satisfy the interface conditions

$$\left\{ \begin{array}{l} [|a_n|] = \left[\left| a_n^1 \right| \right] = \cdots = \left[\left| a_n^{(4)} \right| \right] = 0 \\ \left[\left| a_n^{(5)} \right| \right] = \Phi_n \end{array} \right. \tag{6.8}$$

where Φ_n is the coefficient of $\sin nx_1$ in the Fourier expansion of the function $\varphi(x_1)$.

7. The characteristic boundary layer revisited. Lagrange multiplier and boundary conditions

We saw in Sections 4, 5 and 6 that the leading terms of the solutions in the layers satisfy the constraint (4.6), and accordingly the corresponding equations must involve a Lagrange multiplier. This was avoided in the previous study by taking test functions satisfying themselves the constraint (4.6) so that, taking into account this constraint, we obtained the equation satisfied by $U_1^0(x_1, y_2)$ and the corresponding boundary conditions. Clearly this amounts to eliminate $U_2^0(x_1, y_2)$ and the Lagrange multiplier. In order to exhibit the role of the multiplier in the equations and the boundary conditions we now consider again the case of Section 5.1 which is a characteristic layer along the free boundary $x_2 = 0$. So that we consider expansions (5.1)

$$\left\{ \begin{array}{l} u_1^\varepsilon (x_1, x_2) = \eta^{-1} U_1^\eta (x_1, y_2) = \eta^{-1} U_1^0 + U_1^1 + \cdots \\ u_2^\varepsilon = \eta^{-2} U_2^\eta (x_1, y_2) = \eta^{-2} U_2^0 + \eta^{-1} U_2^1 + U_2^2 + \cdots \end{array} \right. \tag{7.1}$$

which gives the new form of (5.2):

$$\int_D \left\{ \partial_1 U_1^\eta \partial_1 V_1^\eta + \frac{1}{\eta^2} \left(D_2 U_1^\eta - U_2^\eta \right) \left(D_2 V_1^\eta - V_2^\eta \right) + D_2^2 U_2^\eta D_2^2 V_2^\eta + \cdots \right\} \mathrm{d}x_1 \mathrm{d}y_2$$
$$= \int_D \left[f_2 \left(x_1, 0 \right) + \cdots \right] V_2^\eta \mathrm{d}x_1 \mathrm{d}y_2. \quad (7.2)$$

Taking as test functions $V_1^\eta \equiv 0$, V_2 independent of η and by identifying to zero the terms of order η^{-2} and η^{-1} we obtain

$$D_2 {U_1}^0 - {U_2}^0 = 0 \quad (7.3)$$

$$D_2 {U_1}^1 - {U_2}^1 = 0. \quad (7.4)$$

In the sequel, it will prove useful to define the new unknown $p(x_1, y_2)$ by

$$D_2 U_1^2 - U_2^2 = p. \quad (7.5)$$

Now, taking V_1 V_2 arbitrary and independent of η in (7.2), on account of (7.3) and (7.4) at the leading order we have

$$\int_D \left\{ \partial_1 U_1^0 \partial_1 V_1 + p \left(D_2 V_1 - V_2 \right) + D_2^2 U_2 D_2^2 V_2 \right\} \mathrm{d}x_1 \mathrm{d}y_2 = \int_D f_2 \left(x_1, 0 \right) V_2 \mathrm{d}x_1 \mathrm{d}y_2.$$

Taking V_1 and V_2 vanishing in neighbourhoods of $x_1 = 0$ and $x_1 = \pi$, integration by parts give

$$\int_D \left\{ \left(-\partial_1^2 U_1^0 - D_2 p \right) V_1 + \left(D_2^4 U_2^0 - p \right) V_2 \right\} \mathrm{d}x_1 \mathrm{d}y_2$$

$$+ \int_{\Gamma_1} \left\{ -p V_1 + D_2^3 U_2^0 V_2 - D_2^2 U_2^0 D_2 V_2 \right\} (x_1, 0) dx_1 = \int_D f_2 \left(x_1, 0 \right) V_2 \mathrm{d}x_1 \mathrm{d}y_2$$

from which we obtain the system of equations

$$\begin{cases} -\partial_1^2 U_1^0 - D_2 p = 0 \\ D_2^4 U_2^0 - p = f_2(x_1, 0) \end{cases} \quad (7.6)$$

and, as V_1, V_2 and $D_2 V_2$ are arbitrary on Γ_1, we have the natural boundary conditions

$$\begin{cases} -p(x_1, 0) = 0 \\ D_2^3 U_2^0(x_1, 0) = 0 \\ -D_2^2 U_2^0(x_1, 0) = 0. \end{cases} \quad (7.7)$$

Moreover, U_1^0 satisfies the principal boundary conditions

$$U_1^0(0, y_2) = U_1^0(\pi, y_2) = 0 \quad (7.8)$$

and the matching conditions

$$\begin{cases} U_1^0(x_1, y_2) \xrightarrow[y_1 \to +\infty]{} 0 \\ U_2^0(x_1, y_2) \xrightarrow[y_1 \to +\infty]{} 0. \end{cases} \quad (7.9)$$

Problem (7.5)–(7.9) determines the unknowns U_1^0, U_2^0 and p, it constitutes the boundary layer problem with Lagrange multiplier. We should immediately verify that by eliminating p and U_2^0 we obtain the equation (5.6) and the boundary conditions (5.7).

Remark 2. It should be easily seen that, on account of expansions (7.1), of (7.3) and (7.4) and of the definition (7.5) of p, the equations (7.6) and the boundary conditions (7.7) are respectively the leading order terms of (1.6) and (1.7) with $F_1 = F_2 = \mathcal{C} = 0$. □

Remark 3. The solution $\left(U_1^0, U_2^0\right)$ was obtained using two different methods. In the first one, the test functions were taken satisfying the constraint and the equation was obtained with V_1 arbitrary (but not V_2). On the other hand, in the second method, we took V_1 and V_2 arbitrary so that the corresponding problem involved a new unknown p which is the Lagrange multiplier of the problem. Indeed, denoting by B the operator defined by

$$(u_1, u_2) \overset{B}{\longmapsto} D_2 u_1 - u_2$$

which defines the constraint (7.3), the corresponding adjoint B^* is defined by

$$B^* p = (-D_2 p, -p)^t$$

which are precisely the terms in p in system (7.6). Then we have the classical structure of a constrained problem with Lagrange multiplier [2]. Moreover, it is known that in penalty problems of the form (7.2) the Lagrange multiplier p of the limit problem is

$$p = \lim_{\eta \to 0} \frac{1}{\eta^2} (D_2 U_1^\eta - U_2^\eta)$$

that agrees with our results (see (7.1), (7.3), (7.4) and (7.5)).

8. Boundary layer along a non-characteristic part of Γ_0

We saw in Section 3.2 that the thickness of a non-characteristic layer is of order

$$\eta = \varepsilon^{\frac{1}{2}} \tag{8.1}$$

and the scaling of u^ε is such that $u_2^\varepsilon / u_1^\varepsilon = \mathcal{O}\left(\eta^{-1}\right) = \mathcal{O}\left(\varepsilon^{-\frac{1}{2}}\right)$. To fix ideas, let us consider the non-characteristic layer along $x_1 = 0$ which is supposed to belong to Γ_0. Then we tentatively search for asymptotic expansions of the form

$$\left\{ \begin{array}{l} u_1^\varepsilon(x_1, x_2) = \eta U_1^\eta(y_1, x_2) = \eta \left[U_1^0 + \eta U_1^1 + \cdots \right] \\ u_2^\varepsilon = U_2^\eta(y_1, x_2) = U_2^0 + \eta U_2^1 + \cdots \end{array} \right. \tag{8.2}$$

where

$$y_1 = \frac{x_1}{\eta} \cdot \tag{8.3}$$

In the sequel, we shall denote by D_1 the derivative with respect to y_1:

$$D_1 = \eta \partial_1. \tag{8.4}$$

The expansions (8.2) hold true in the domain D defined by $y_1 \in (0, +\infty)$, $x_2 \in (0, \pi)$.

The solution U^η must satisfy the boundary conditions

$$U_1^\eta(0,x_2) = U_2^\eta(0,x_2) = D_1U_2^\eta(0,x_2) = 0 \tag{8.5}$$

and the matching conditions for $y_1 \to +\infty$, which we shall consider later.

The variational formulation hold true in the domain D, at least for test functions with compact support in y_1, we shall take them depending on η in a form analogous to (8.2). Consequently, we have

$$\int_D \left\{ D_1U_1^\eta D_1V_1^\eta + (\eta\partial_2U_1^\eta - U_2^\eta)(\eta\partial_2V_1^\eta - V_2^\eta) + \frac{\varepsilon^2}{\eta^4}\left[D_1^2U_2^\eta D_1^2V_2^\eta + \cdots\right] \right\} \mathrm{d}x_1\mathrm{d}y_2 \tag{8.6}$$

$$= \int_D \left\{ \left[f_1(0,x_2) + \cdots\right]\eta V_1^\eta + \left[f_2(0,x_2) + \eta y_1\partial_1 f_2(0,x_2) + \cdots\right]V_2^\eta \right\} \mathrm{d}y_1\mathrm{d}x_2$$

where f is supposed to be smooth and was represented by its Taylor expansion in the vicinity of $x_1 = 0$. We note that, according to (8.1), $\varepsilon^2/\eta^4 = 1$ in (8.6).

Taking $V_1^\eta \in \mathcal{D}(D)$ and $V_2^\eta \equiv 0$ in (8.6), the leading term (of order $\mathcal{O}(1)$) gives

$$D_1^2U_1^0 = 0 \tag{8.7}$$

so that

$$U_1^0(y_1,x_2) = A(x_2)y_1 + B(x_2). \tag{8.8}$$

Conditions (8.5) give $B(x_2) = 0$ and the matching condition writes

$$A(x_2) = \partial_1 u_1^0(0,x_2) \tag{8.9}$$

where $u_1^0(x_1,x_2)$ is the corresponding solution of the limit problem $P(0)$.

On other hand, if we take $V_1^\eta \equiv 0$ and $V_2^\eta \in \mathcal{D}(D)$, then the leading term (of order $\mathcal{O}(1)$) gives

$$D_1^4U_2^0 + U_2^0 = f_2(0,x_2). \tag{8.10}$$

The solution of (8.10) may be written under the form

$$U_2^0 = \tilde{U}_2^0 + \hat{U}_2^0(x_2) \tag{8.11}$$

where

$$\hat{U}_2^0(x_2) = f_2(0,x_2) \tag{8.12}$$

then $\tilde{U}_2^0$ is the bounded solution of

$$D_1^4\tilde{U}_2^0 + \tilde{U}_2^0 = 0 \tag{8.13}$$

which is a differential equation in y_1 with parameter x_2, the bounded solution of which is

$$\tilde{U}_2^0(y_1,x_2) = \sum_{k=1}^{2} c_k(x_2)\exp\left(e^{\frac{(2k+1)i\pi}{4}}y_1\right). \tag{8.14}$$

It satisfies the conditions:

$$\lim_{y_1 \to +\infty} \tilde{U}_2^0(y_1, x_2) = f_2(0, x_2) \tag{8.15}$$

which is the matching condition with the corresponding solution of the limit problem $P(0)$ of Section 2.

Otherwise this solution must satisfy the boundary conditions (8.5) which gives

$$\begin{cases} c_1(x_2) + c_2(x_2) = f_2(0, x_2) \\ c_1(x_2) e^{\frac{3i\pi}{4}} + c_2(x_2) e^{-\frac{3i\pi}{4}} = 0 \end{cases} \tag{8.16}$$

which determine the functions $c_k(x_2)$.

9. The distributional solutions of $P(0)$ as limits of internal layers

We saw in Section 2.4 that the solutions of the limit problem $P(0)$ exhibit singular terms when the datum f is not smooth with respect to x_2. In the particular case when f is defined by (2.29) we considered in Section 6 the corresponding internal layer. We admit that Γ_0 contains the two vertical boundary layers. In this section we are showing that the singular terms (containing δ_γ and δ'_γ) in (2.30) are limits of the corresponding terms in the layers. In the sequel, we only consider the component u_1 as the study of u_2 is analogous and even follows from that of u_1.

In order to write explicitly $(2.30)_1$, let us consider the Fourier sinus expansion of φ:

$$\varphi(x_1) = \sum_{n=1}^{+\infty} A_n \sin n x_1. \tag{9.1}$$

As in the present case A is the Laplace operator on $(0, \pi)$ with Dirichlet boundary conditions, we have

$$\left(A^{-1}\varphi\right)(x_1) = -\sum_{n=1}^{+\infty} \frac{A_n}{n^2} \sin n x_1 \tag{9.2}$$

so that $(2.30)_1$ takes the form

$$u_1(x_1, x_2) = \left(-\sum_{n=1}^{+\infty} \frac{A_n}{n^2} \sin n x_1 \right) \delta(x_2 - \gamma). \tag{9.3}$$

It follows from Section 6 that the inner expansion of u_1^ε in the internal layer is

$$u_1^\varepsilon(x_1, x_2) \cong \frac{1}{\eta} U_1^0\left(x_1, \frac{x_2 - \gamma}{\eta}\right) + \cdots \tag{9.4}$$

The aim of this section is to prove that

$$u_1(x_1, x_2) = \lim_{\eta \to 0} \frac{1}{\eta} U_1^0\left(x_1, \frac{x_2 - \gamma}{\eta}\right). \tag{9.5}$$

From elementary distribution theory it follows that the right-hand side of (9.5) is

$$\left(\int_{-\infty}^{+\infty} U_1^0(x_1, y_2)\, \mathrm{d}y_2 \right) \delta(x_2 - \gamma)$$

where x_1 is a parameter. Consequently (9.5) amounts to prove that

$$\int_{-\infty}^{+\infty} U_1^0(x_1, y_2)\,\mathrm{d}y_2 = -\sum_{n=1}^{+\infty} \frac{A_n}{n^2} \sin nx_1. \tag{9.6}$$

The function U_1^0 is the unique solution of (5.6) in each region D^+ and D^- with the boundary and transmission conditions (6.3)–(6.5). It appears that U_1^0 is even with respect to y_2 as it coincides with the function obtained by changing y_2 into $-y_2$. Consequently, we may only consider the solution in the region D^+ where $y_2 > 0$ which satisfies (5.6) and the boundary conditions

$$\begin{cases} D_2 U_1^0(x_1, 0) = 0 \\ D_2^{(3)} U_1^0(x_1, 0) = 0 \\ D_2^{(5)} U_1^0(x_1, 0) = \dfrac{\varphi(x_1)}{2} \end{cases} \tag{9.7}$$

and (6.4) as well as the matching conditions

$$U_1^0(x_1, y_2) \xrightarrow[y_2 \to +\infty]{} 0.$$

It follows from $(6.7)_1$ that U_1^0 writes

$$U_1^0(x_1, y_2) = \sum_{n=1}^{+\infty} \sum_{k=2}^{4} C_{nk} \sin nx_1 \exp\left[n^{\frac{1}{3}} e^{\frac{ik\pi}{3}} y_2\right]. \tag{9.8}$$

The boundary conditions (9.7) give

$$\begin{cases} -e^{-\frac{i\pi}{3}} C_{n2} - C_{n3} - e^{\frac{i\pi}{3}} C_{n4} = 0 \\ C_{n2} - C_{n3} + C_{n4} = 0 \\ -e^{\frac{i\pi}{3}} C_{n2} - C_{n3} - e^{-\frac{i\pi}{3}} = \dfrac{A_n}{2n^{\frac{5}{3}}}. \end{cases} \tag{9.9}$$

As U_1^0 is even, the left-hand side of (9.6) is

$$\begin{aligned} 2\int_0^{+\infty} U_1^0(x_1, y_2)\,\mathrm{d}y_2 &= 2\sum_{n=1}^{+\infty} \sum_{k=2}^{4} C_{nk} \sin nx_1 \int_0^{+\infty} \exp\left[n^{\frac{1}{3}} e^{\frac{ik\pi}{3}} y_2\right] \mathrm{d}y_2 \\ &= -2\sum_{n=1}^{+\infty} \sum_{k=2}^{4} C_{nk} \sin nx_1 \frac{1}{n^{\frac{1}{3}}} e^{-\frac{ik\pi}{3}} = 2\sum_{n=1}^{+\infty} \frac{\sin nx_1}{n^{\frac{1}{3}}} \left(C_{n2} e^{\frac{i\pi}{3}} + C_{n3} + C_{n4} e^{-\frac{i\pi}{3}}\right) \\ &= -\sum_{n=1}^{+} \frac{A_n}{n^2} \sin nx_1 \end{aligned}$$

(where relation $(9.9)_3$ was used) which proves (9.6).

10. Numerical experiments

In this section we present numerical experiments concerning the problem $P(\varepsilon)$ in several cases of boundary conditions and loading. The numerical computations are implemented with reduced Hermite finite elements. An exact numerical integration of the rigidity matrices needs twelve Gauss points.

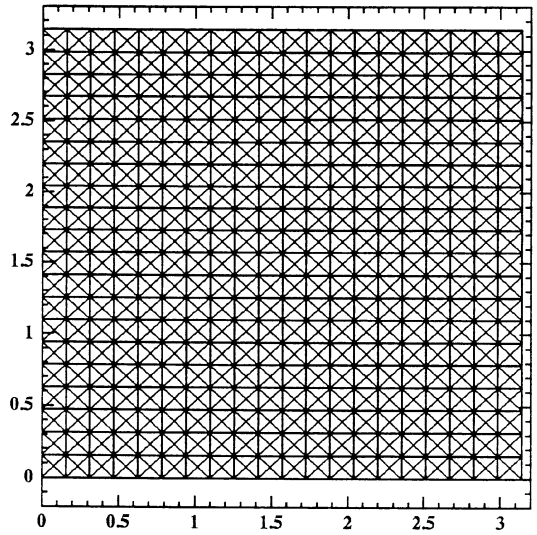

FIGURE 1. Uniform mesh.

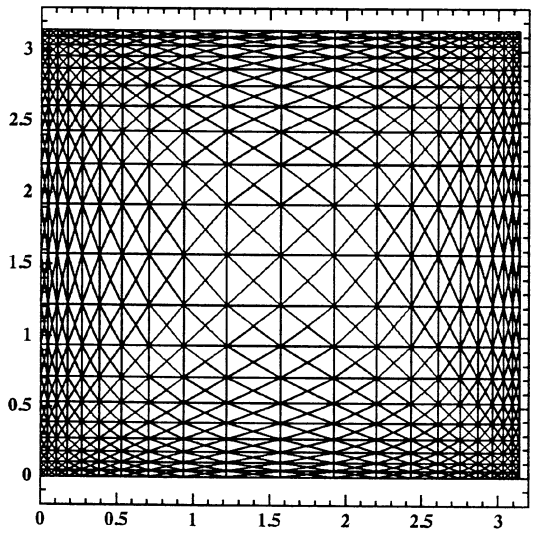

FIGURE 2. Adapted mesh for characteristic boundary layers.

The meshes for the domain $\Omega = [0, \pi] \times [0, \pi]$ are generated using the Modulef code. The mesh is obtained by symmetry from the basic square $[0, \pi/2] \times [0, \pi/2]$, a first time around $x_1 = \pi/2$ and then around $x_2 = \pi/2$. This device allows us to perform easily the refinement of the mesh in the vicinity of the boundary layers. In the sequel we shall compare the results obtained with an uniform mesh and a non uniform one refined in the vicinity of the boundary layers. In the uniform mesh, the basic square is divided in $N \times M$ rectangles where the parameters N and M correspond to the number of divisions along the axes x_1 and x_2 respectively. Each rectangle is then divided in four triangles. Figure 1, shows the uniform mesh generated in this way. The non uniform mesh (see Fig. 2) is generated in the same way but using a function of distribution of the points according to a geometric progression with ratio q.

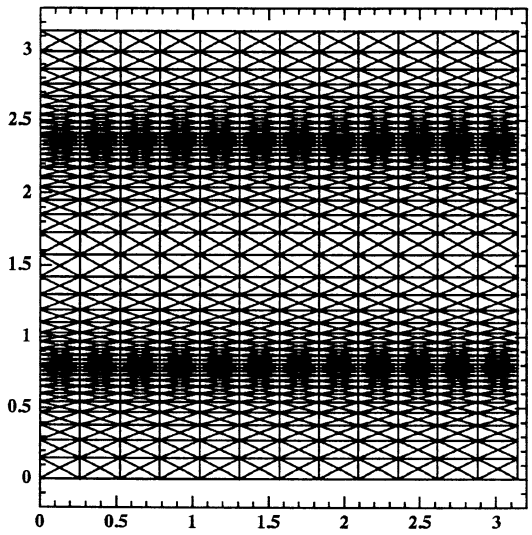

FIGURE 3. Adapted mesh for internal layers.

In the case of internal layers we analogously get the mesh shown in Figure 3.

10.1. **Totally clamped boundary**

We consider the problem $P(\varepsilon)$ for $\varepsilon = 0.001$ and $\overrightarrow{f} = (f_1, f_2) = (0, x_2 - 1)$. We shall focus our attention on the characteristic boundary layers along $x_2 = 0$ and $x_2 = \pi$ (see Sect. 4). These layers are more important than the non characteristic ones along $x_1 = 0$ and $x_1 = \pi$, compare (4.2) with $\eta = \varepsilon^{\frac{1}{3}}$ and (8.2) with $\eta = \varepsilon^{\frac{1}{2}}$.

In the characteristic layers the order of the thickness is $\eta = 0.1$. Computations with the uniform mesh (Fig. 1) give nearly good results with $N = M = 11$, *i.e.* with mesh step $h = \pi/21$ in both directions; the values of u_2^ε are shown in Figure 4. With the non uniform mesh (Fig. 2), we observe that the mesh may be coarse provided that the layer region is sufficiently covered, we took $N = 7$, $M = 11$, $q = 1.4$ so that the first four steps are contained in the length η; the values of u_2^ε are shown in Figure 5. The first and the second meshes contain 1600 and 960 triangular elements respectively. In the present case the advantage of the adapted mesh is not very significant.

10.2. **Case of a characteristic free boundary with $f_2 \neq 0$**

The problem $P(\varepsilon)$ is again considered with the previous data ε and $\overrightarrow{f}$. The boundary $x_2 = 0$ is free and the rest of the boundary is clamped. We observe that f_2 does not vanish on the free boundary so that in this case the corresponding boundary layer is (5.1) with $\theta(\eta) = \eta^{-1} = \varepsilon^{-\frac{1}{3}}$ (see (5.3)). We observe that u_2^ε is of order $\eta^{-2} = \varepsilon^{-\frac{2}{3}}$ whereas in the previous case it was of order $\varepsilon^{-\frac{1}{3}}$. The magnitude of the boundary layer in the present case leads to a significant advantage of the adapted mesh.

Taking the uniform mesh, the mesh step must be chosen sufficiently small to get a satisfactory result. In fact we must take at least $N = M = 31$ so that the mesh step is $h = \pi/61$ which corresponds to 14400 triangular elements.

When using a non uniform mesh, satisfactory results are obtained with the same mesh as in the previous subsection which correspond to 960 triangular elements.

The numerical results for u_2^ε in both cases are shown in Figures 6 and 7, they are obtained in 15 minutes with the uniform mesh and only 2 minutes with the adapted mesh.

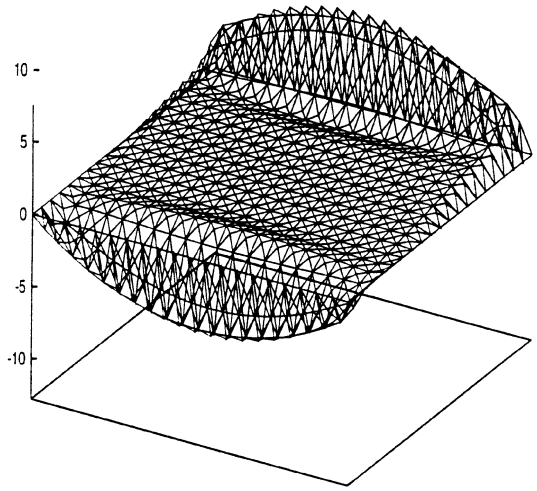

FIGURE 4. Three dimensional plot of U_2 (uniform mesh).

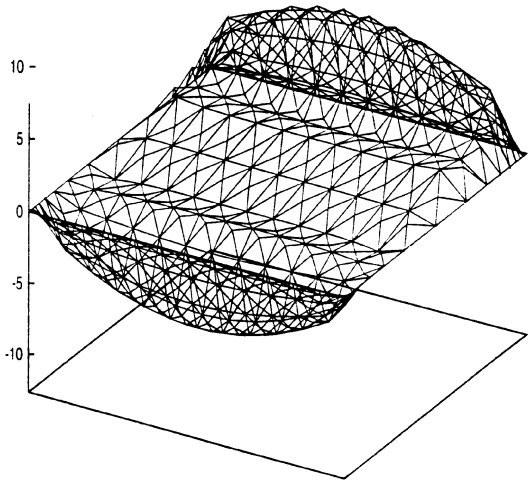

FIGURE 5. Three dimensional plot of U_2 (adapted mesh).

10.3. **Internal layers**

We now consider the problem $P(\varepsilon)$ with the whole boundary clamped, $\varepsilon = 0.001$ and

$$\overrightarrow{f} = \begin{cases} f_1 = 0 \\ f_2 = \begin{cases} 1 \text{ for } x_2 > \pi/2 \\ 0 \text{ for } x_2 < \pi/2 \end{cases} \end{cases} \tag{10.1}$$

so that the loading has a discontinuity along the characteristic $x_2 = \frac{\pi}{2}$. According to the results of Section 6, the scaling is the same as in the previous subsection. We present in Figure 8 the numerical results obtained with the same uniform mesh as before. Obviously, we observe the presence of an internal layer along the characteristic $x_2 = \pi/2$.

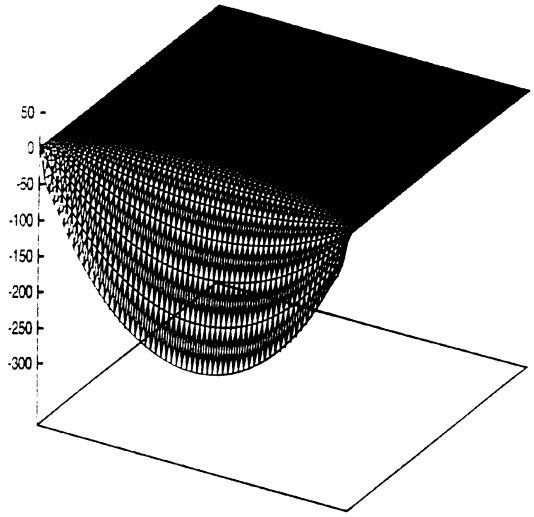

FIGURE 6. Three dimensional plot of U_2 (uniform mesh).

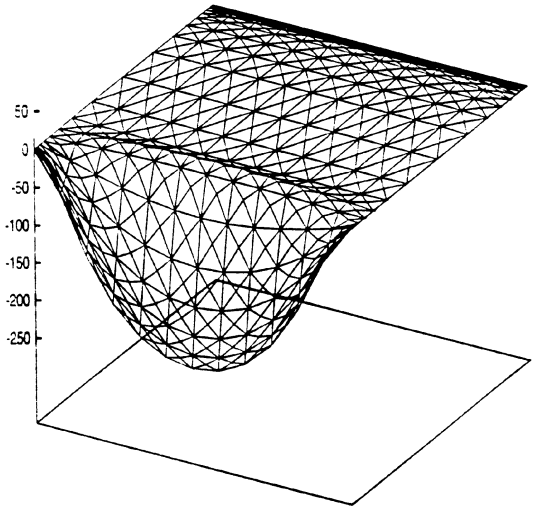

FIGURE 7. Three dimensional plot of U_2 (adapted mesh).

In order to exhibit the propagation of the singularities along the characteristics evoked in Section 2.5 we consider instead of (10.1) the loading

$$\overrightarrow{f} = \begin{cases} f_1 = 0 \\ f_2 = \begin{cases} 1 \text{ on } \left[0, \frac{\pi}{2}\right] \times \left[\frac{\pi}{2}, \pi\right] \\ 0 \text{ elsewhere.} \end{cases} \end{cases} \tag{10.2}$$

The numerical results for u_2^ε obtained with the non uniform mesh $N = 7$, $M = 11$, $q = 0.7$ are shown in Figure 9. We observe an internal layer along the whole characteristic $x_2 = \pi/2$ whereas the discontinuity of the data are

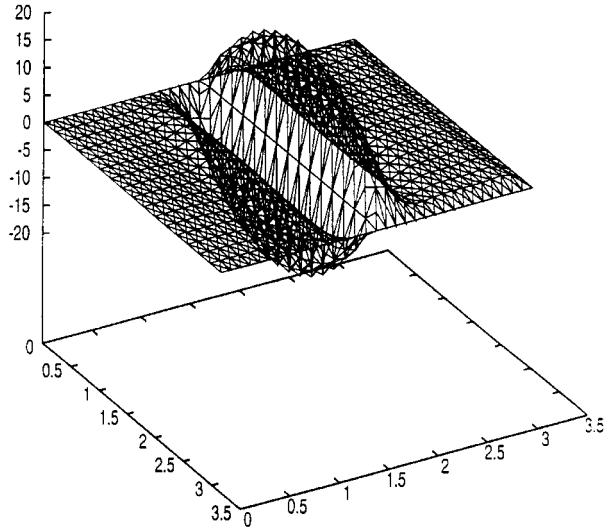

FIGURE 8. Three dimensional plot of U_2 for uniform unit upper rectangle loading (uniform mesh).

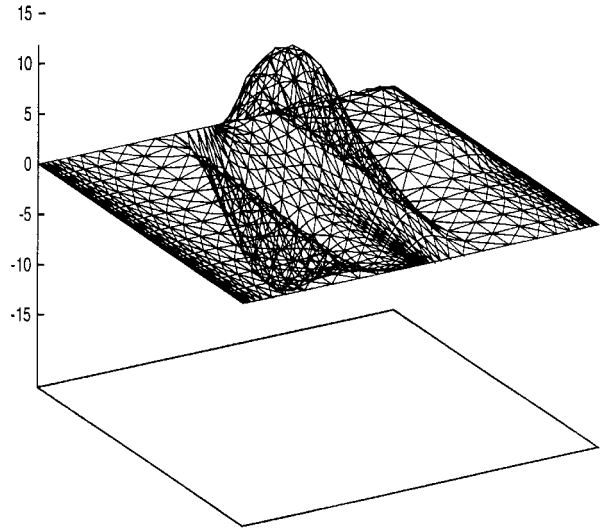

FIGURE 9. Three dimensional plot of U_2 for uniform unit square loading (adapted mesh).

confined in the interval $0 < x_1 < \pi/2$. This fact is even more explicit in Figure 10 which represents u_2^ε along the section $x_1 = 3\pi/4$.

Another interesting example of propagation of the singularities is given Figure 11 where the loading is chosen as follows

$$\overrightarrow{f} = \begin{cases} f_1 = 0 \\ f_2 = \begin{cases} 1 \text{ on } \Delta = \left\{ x_1 \in \left[\frac{\pi}{4}, \frac{3\pi}{4}\right], |x_2 + x_1 - \pi| \leq 0.1 \right\} \\ 0 \text{ elsewhere.} \end{cases} \end{cases} \tag{10.3}$$

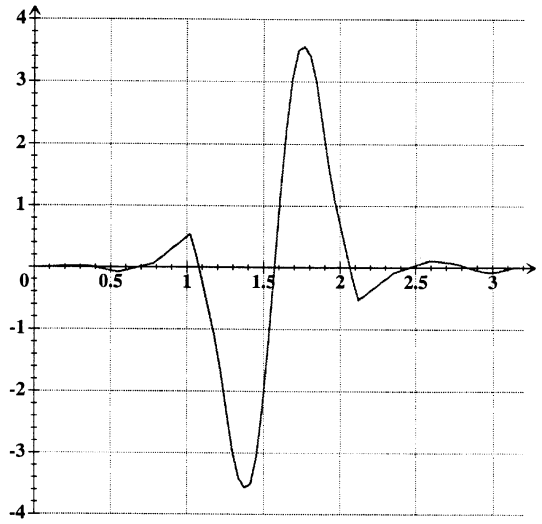

FIGURE 10. Graph of U_2 along the cross section $x = 3\pi/4$ for unif.

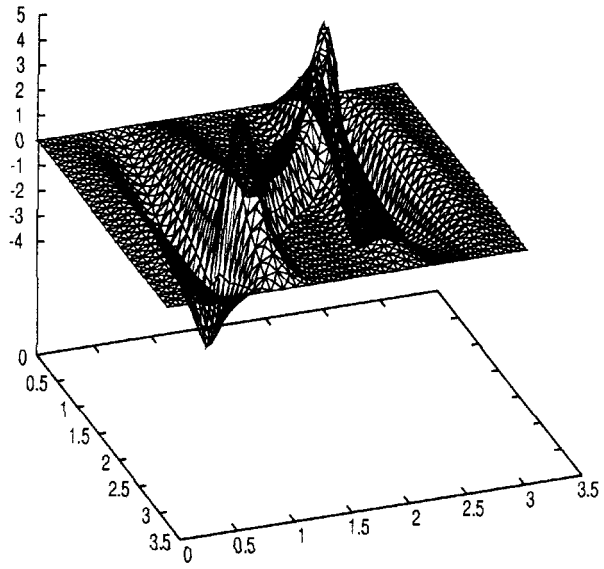

FIGURE 11. Three dimensional plot of U_2 for internal layer with propagation (adapted mesh).

We observe the presence of internal layers along the characteristics $x_2 = \pi/4$ and $x_2 = 3\pi/4$ which correspond to the extremities of the thin region Δ, the cross-section $x_1 = 3\pi/4$ is represented in Figure 12.

The numerical results for u_2^ε are obtained using the adapted mesh with parameters $q = 1$, $N = 7$ and $M = 11$ (which correspond to the mesh steps $h_{x_1} = \pi/13$ and $h_{x_2} = \pi/21$ in the directions x_1 and x_2) respectively.

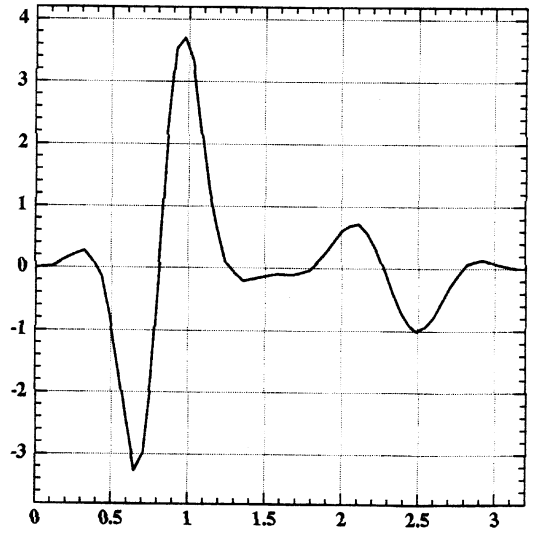

FIGURE 12. Graph of U_2 along the cross section $x = 3\pi/4$.

TABLE 1

Layer	**Behavior**	**Energy**
Characteristic thickness: $\eta(\varepsilon) = \varepsilon^{\frac{1}{3}}$	$\frac{v_2^\varepsilon}{v_1^\varepsilon} = \mathcal{O}\left(\eta^{-1}\right)$	
clamped	$\begin{cases} v_1^\varepsilon \cong U_1^0(x_1, y_2) \\ v_2^\varepsilon \cong \eta^{-1} U_2^0(x_1, y_2) \end{cases}$	$E_C = \mathcal{O}(\eta)$
free $f_2(x_1, 0) = 0$	$\begin{cases} v_1^\varepsilon \cong U_1^0(x_1, y_2) \\ v_2^\varepsilon \cong \eta^{-1} U_2^0(x_1, y_2) \end{cases}$	$E_C = \mathcal{O}(\eta)$
free $f_2(x_1, 0) \neq 0$	$\begin{cases} v_1^\varepsilon \cong \eta^{-1} U_1^0(x_1, y_2) \\ v_2^\varepsilon \cong \eta^{-2} U_2^0(x_1, y_2) \end{cases}$	$E_C = \mathcal{O}\left(\eta^{-1}\right)$
Non-characteristic thickness: $\eta(\varepsilon) = \varepsilon^{\frac{1}{2}}$	$\frac{v_2^\varepsilon}{v_1^\varepsilon} = \mathcal{O}\left(\eta^{-1}\right)$ $\begin{cases} v_1^\varepsilon \cong \eta U_1^0(x_1, y_2) \\ v_2^\varepsilon \cong U_2^0(x_1, y_2) \end{cases}$	$E = \mathcal{O}(\eta)$
Internal Characteristic thickness: $\eta(\varepsilon) = \varepsilon^{\frac{1}{3}}$ with discontinuity of f_2 on $x_2 = 0$	$\frac{v_2^\varepsilon}{v_1^\varepsilon} = \mathcal{O}\left(\eta^{-1}\right)$ $\begin{cases} v_1^\varepsilon \cong \eta^{-1} U_1^0(x_1, y_2) \\ v_2^\varepsilon \cong \eta^{-2} U_2^0(x_1, y_2) \end{cases}$	$E_C = \mathcal{O}\left(\eta^{-1}\right)$

11. CONCLUSIONS

The main results of this paper are summed up in Table 1 which gives the order of the thickness η and of the two components of u. The energy in the layer is also reported in Table 1.

It appears that the energy tends to infinity in two cases: free characteristic boundary with $f_2 \neq 0$ on it and internal layer bearing a discontinuity of f_2 on a characteristic. The energy in the layer tends to infinity as ε tends to zero. Obviously, the energy in a region out of the layers is of order unity so that the above mentioned result agrees with Theorem 2.2. But the asymptotic structure also shows that the energy is asymptotically concentrated in the layers (but this is probably associated with the very definition of layers!). Finally, it should be pointed out that layers cutting the characteristics $x_2 = \text{const.}$ at angle $\neq \pi/2$ are analogous to the layers along $x_1 = \text{const.}$ considered above. This is the reason why all these layers are called "non characteristic".

References

[1] M. Bernadou, *Méthodes d'éléments finis pour les problèmes de coques minces*. Masson, Paris (1994).

[2] F. Brezzi and F. M. Fortin, *Mixed and hybrid finite elements methods*. Springer (1991).

[3] D. Choï, F.J. Palma, É. Sanchez Palencia and M.A. Vilariño, Remarks on membrane locking in the finite element computation of very thin elastic shells. *Math. Modell. Num. Anal.* **32** (1998) 131–152.

[4] P.G. Ciarlet, *Mathematical elasticity, Vol. III, Theory of shells*. North Holland, Amsterdam (to appear).

[5] D. Chapelle and K.J. Bathe, *Fundamental considerations for the finite element analysis of shell structures, Computers and Structures* **66** (1998) 19–36.

[6] P. Gérard and É. Sanchez Palencia, Sensitivity phenomena for certain thin elastic shells with edges. *Math. Meth. Appl. Sci.* (to appear).

[7] A.L. Goldenveizer, *Theory of elastic thin shells*. Pergamon, New York (1962).

[8] P. Karamian, Nouveaux résultats numériques concernant les coques minces hyperboliques inhibées: cas du paraboloïde hyperbolique. *C. R. Acad. Sci. Paris Sér. IIb* **326** (1998) 755-760.

[9] P. Karamian, Réflexion des singularités dans les coques hyperboliques inhibées. *C.R. Acad. Sci. Paris Sér. IIb* **326** (1998) 609–614.

[10] P. Karamian, *Coques élastiques minces hyperboliques inhibées : calcul du problème limite par éléments finis et non reflexion des singularités*. Thèse de l'Universté de Caen (1999).

[11] D. Leguillon, J. Sanchez-Hubert and É. Sanchez Palencia, Model problem of singular perturbation without limit in the space of finite energy and its computation. *C.R. Acad. Sci. Paris Sér. IIb* **327** (1999) 485–492.

[12] J.L. Lions and É. Sanchez Palencia, Problèmes sensitifs et coques élastiques minces. in *Partial Differential Equations and Functional Analysis*, in memory of P. Grisvard (J. Céa, D. Chesnais, G. Geymonat, J.L. Lions Eds.), Birkhauser, Boston (1996) 207–220.

[13] J.L. Lions and É. Sanchez Palencia, Sur quelques espaces de la théorie des coques et la sensitivité, in *Homogenization and applications to material sciences*, Cioranescu, Damlamian, Doneto Eds., Gakkotosho, Tokyo (1995) 271–278.

[14] A.E.H Love, *A treatrise on the mathematical theory of elasticity*, Reprinted by Dover, New-York (1944).

[15] J. Pitkaranta and É. Sanchez Palencia, On the asymptotic behavior of sensitive shells with small thickness. *C.R. Acad. Sci. Paris Sér. IIb* **325** (1997) 127–134.

[16] H.S. Rutten, *Theory and design of shells on the basis of asymptotic analysis*. Rutten and Kruisman, Voorburg (1973).

[17] J. Sanchez-Hubert and É. Sanchez Palencia, *Introduction aux méthodes asymptotiques et à l'homogénéisation*, Masson, Paris (1992).

[18] J. Sanchez-Hubert and É. Sanchez Palencia, *Coques élastiques minces. Propriétés asymptotiques*. Masson, Paris (1997).

[19] J. Sanchez-Hubert and É. Sanchez Palencia, Pathological phenomena in computation of thin elastic shells. *Transactions Can. Soc. Mech. Engin.* **22** (1998) 435–446.

[20] M. Van Dyke, *Perturbation methods in fluid mechanics*. Academic Press, New-York (1964).

ELSEVIER

European Journal of Mechanics A/Solids 21 (2002) 13–47

Boundary layers in thin elastic shells with developable middle surface

P. Karamian, J. Sanchez-Hubert *

Laboratoire de Mécanique, Université de Caen Basse-Normandie, Boulevard Maréchal Juin, 14032 Caen, France

Received 28 April 2000; revised and accepted 10 September 2001

Abstract

We consider the boundary layer phenomena which appear in thin shell theory as the relative thickness ε tends to zero. We deal with a developable middle surface. Boundary layers along and across the generators (which are the characteristics of the underlying system) have very different structure. It also appear internal layers associated with propagation of singularities along the characteristics. The special structure of the limit problem often implies solutions which exhibit distributional singularities along the characteristics. The corresponding layers for small ε have a very large intensity. Layers along the characteristics have a special structure involving subspaces, the corresponding Lagrange multipliers are exhibited. Numerical experiments show the advantage of adaptive anisotropic meshes in these problems.

Keywords: Shells; Boundary layers; Anisotropic meshes

1. Introduction

In recent times a number of new results were obtained concerning the behavior of shells for very small values of the relative thickness 2ε. This behavior is highly dependent of the geometrical properties of the middle surface and of the loadings. The corresponding solutions exhibit peculiarities concerning the deformations of the shell, so that accurate numerical computations must be adapted to such peculiarities. In particular, the solutions develop boundary and internal layers, i.e. narrow regions where the displacement changes drastically. Moreover, in certain cases (which, as we shall see in the sequel, are often encountered in applications) the deformation energy concentrates in the layers. As a consequence, the knowledge of the layers determines almost completely the deformation field. It is then evident that an accurate numerical computation of the layers is a necessary, and often sufficient, condition to get a suited description of the behavior of the shell. The asymptotic curves (see hereafter) of the middle surface are the characteristic curves of the membrane system of shells (i.e. shell theory without flexion effects) they play a central role in the structure of the layers. Layers along the asymptotic curves (characteristic layers) exhibit classical properties of propagation of singularities along the characteristics.

In this paper, we address such problems for shells in the framework of Kirchhoff–Love theory, but this point is not essential. The mechanical behavior is described by two energy forms $a_m(u, v)$ and $\varepsilon^2 a_f(u, v)$, associated with the deformations of the intrinsic metrics and the variation of the curvature, they are called the membrane and the flexion forms respectively. On account of the small rigidity of a thin body to the flexion, the second form involves the factor ε^2 and the above evoked specific properties for small ε follow.

* Correspondence and reprints.
E-mail address: sanchez@meca.unicaen.fr (J. Sanchez-Hubert).

0997-7538/02/$ – see front matter
PII: S0997-7538(01)01182-2

In the sequel, we only consider "inhibited" shells, i.e. such that the middle surface $\mathcal{S}$ with the kinematic boundary conditions is geometrically rigid. This means that the boundary conditions are such that $\mathcal{S}$ does not admit "pure bendings" i.e. displacements keeping invariant the length on $\mathcal{S}$.

This paper is only concerned with the case when the middle surface $\mathcal{S}$ is developable. Let us recall that a ruled surface is generated by the displacement of a straight line so called generator. If we denote by $\mathbf{e}(y^2)$ the unit vector along the generator containing a given point $M(y^2)$, where $M(y^2)$ is a point on a curve $\mathcal{C}$ defined by $\overrightarrow{OM} = \boldsymbol{\rho}(y^2)$, then a point $P \in \mathcal{S}$ belonging to the generator issued from M is given by $\overrightarrow{OP} = \boldsymbol{\rho}(y^2) + y^1\mathbf{e}(y^2)$ which is the equation of the surface $\mathcal{S}$. A developable surface is a particular case of ruled surface: a ruled surface is said developable when its tangent plane is the same along each generator. A necessary and sufficient condition for a ruled surface to be developable is that $(\boldsymbol{\rho}, \mathbf{e}, \mathrm{d}\mathbf{e}/\mathrm{d}y^2) = 0$.

Let us recall some elements of general surface theory. At each point $P \in \mathcal{S}$ there are two directions (called asymptotic directions) tangent to $\mathcal{S}$ where the normal curvature vanishes. The point P is said to be elliptic, hyperbolic or parabolic when its asymptotic directions are imaginary, real and distinct and real coincident respectively. The two families of curves which are tangent at each point to the asymptotic directions are called asymptotic curves. It is classical that a surface is developable when all its points are parabolic. It is also well known that the generators of a ruled surface are asymptotic curves. As a consequence, all along this paper the asymptotic curves are double and coincide with the generators of the surface $\mathcal{S}$. Moreover, they coincide with the double characteristics of the membrane system.

Let us denote by $A_m + \varepsilon^2 A_f$ the operator associated with the two bilinear forms a_m and a_f. Classically, A_f is elliptic and A_m is of the same type as the points of the surface $\mathcal{S}$ and its characteristics are the asymptotic curves of $\mathcal{S}$. In this paper A_m is then parabolic. Moreover, because the order of differentiation in A_f is higher than in A_m, as $\varepsilon \searrow 0$ a singular perturbation phenomenon appears. Moreover, as the limit process $\varepsilon \searrow 0$ goes from a higher-order elliptic system to a lower-order parabolic one, it is clear that the limit process $\varepsilon \searrow 0$ is rather non-standard.

For $\varepsilon > 0$, the energy space V is such that $a_m + \varepsilon^2 a_f$ is continuous and coercive on it whereas the limit problem involves a new energy space V_m (membrane energy space) for which the bilinear form a_m is continuous and coercive. In fact, V_m is the completion of V with the norm $\sqrt{a_m(\cdot,\cdot)}$ (which is a norm as a consequence of the hypothesis of inhibition).

Obviously, V_m contains functions less smooth than those of V. As a consequence, the solutions u^ε belong to V but their limit as $\varepsilon \searrow 0$ is a less smooth function so that u^ε for small ε exhibits boundary layers. In fact, there is another important reason for the presence of boundary layers. Indeed, as $V \subset V_m$, the dual spaces satisfy $V'_m \subset V'$ consequently, the usual forces $\mathbf{f}$ which are in V' are admissible for the variational problem with $\varepsilon > 0$ but it may happen, and often happens, that $\mathbf{f} \notin V'_m$. As a consequence, in this case, the limit problem does not make sense as a variational one in V_m. The corresponding solution of the limit problem is out of V_m and exhibits distributional singularities so that u^ε involves boundary layers of large intensity (see (Leguillon et al., 1999) and (Karamian et al., 2000) for a model problem, as well as the forecoming papers (Karamian et al., 2001-a) and (Karamian et al., 2001-b) for the case of a hyperbolic middle surface). In this case, the energy of u^ε tends to infinity as the solution goes out of the space of membrane energy. Such a situation is often encountered in thin shell theory. The extreme case is the so called "sensitive shells" for which the space V'_m is so small that it does not contain the space $\mathcal{D}$ of the test functions of the distributions (see (Lions and Sanchez Palencia, 1995, 1996, 1998)), consequently in sensitive shells almost any loading $\mathbf{f}$ is not contained in V'_m. Moreover, for non-sensitive shells, very usual loadings may be out of V'_m. For instance, as we shall see in the sequel, in developable surfaces with a free boundary along a generator, any normal loading not vanishing on that generator does not belong to V'_m (see (Sanchez-Hubert and Sanchez Palencia, 1997, Sect. VII.4.2) and (Karamian et al., 2000, Sect. 2.2)).

It should be emphasized that the non-smoothness of the solutions of the limit problem has important consequences on the finite element computations of u^ε for small ε. It is easy to prove (see (Gérard and Sanchez Palencia, 2000) for instance) that when $f \notin V'_m$ the convergence of the finite element approximations u^ε_h to u^ε cannot be uniform with respect to $\varepsilon \in (0, \varepsilon_0)$ with values in V_m (and then also in any "smaller" space!). In other words, the smaller ε is the smaller h must be chosen in order to get a good approximation. We may refer to (Karamian, 1998, 1999) for these features. It then appears a somewhat paradoxical situation: shell theory is concerned with $\varepsilon \ll 1$ but as $\varepsilon \searrow 0$ the solutions are more and more distorted and difficult to compute. We shall note that the situation, in the present case of inhibited shells, is in this concern analogous to that of non-inhibited ones. We may recall that in non-inhibited shells there are pure bendings and the limit behavior of u^ε is one of them. The phenomenon of locking is due to an incompatibility between the approximating spaces V_h and the subspace of pure bendings. This phenomenon appears for any conformal approximation with piecewise polynomial finite elements ((Choï et al., 1998) and (Sanchez-Hubert and Sanchez Palencia, 1997, Sect. XI.1)) and leads again to non-uniformity of the convergence of the approximation u^ε_h to u^ε. Obviously, as a consequence of the presence of layers, an accurate numerical computation implies refinement of the mesh in the vicinity of the layers.

Up to our knowledge, very little is known about boundary layers of shells. They are called "edge effects" in (Goldenveizer, 1962) and (Love, 1944) which are mainly concerned with layers transversal to the characteristics. In this paper we mainly consider the layers along the characteristics (i.e. along the generators of the developable surface $\mathcal{S}$) the structure of which is very different of the previous ones. It should be noticed that all kinds of layers enter in the framework of (Pitkaranta et al., 2001)

but, in the present paper, we take into account the boundary conditions which allow us to obtain a precise description of the boundary layer problem including the orders of magnitude. The impressive catalogue of analytical solutions of Rutten (1973) perhaps contains boundary solutions but their utilization in specific problems is not evident.

The problem $P(\varepsilon)$ is defined as follows. We denote by Ω the domain $(0, l_1) \times (0, l_2)$ of the plane (y^1, y^2). Obviously, according to the above description of the surface, the parameter y^1 runs along the generators and y^2 is transversal to them. As the study of the layers is mainly local along the generators the fact that Ω is a rectangle is not essential, but just convenient to perform easily dilatation with respect the transversal variable. The boundary $\partial\Omega$ of Ω is composed of two parts Γ_0 (clamped part) and Γ_1 (free part), they will be defined later but, in any case, Γ_0 is such that the shell is inhibited.

The configuration space V is a space of functions $v = (v_1, v_2, v_3)$ which satisfy the kinematic boundary conditions

$$v_1 = v_2 = v_3 = \frac{\partial v_3}{\partial n} = 0 \quad \text{on } \Gamma_0, \tag{1.1}$$

more precisely,

$$V = \big\{v;\, v_1, v_2 \in H^1(\Omega),\, v_3 \in H^2(\Omega),\ v \text{ satisfies (1.1)}\big\}, \tag{1.2}$$

where H^1 and H^2 denote the standard Sobolev spaces (see, for instance (Bernadou, 1994)).

The two energy forms are:

$$a_m(u, v) = \int_\Omega A_{11}^{\alpha\beta\lambda\mu} \gamma_{\lambda\mu}(u)\gamma_{\alpha\beta}(v)\sqrt{a}\,\mathrm{d}y, \tag{1.3}$$

$$a_f(u, v) = \int_\Omega A_{22}^{\alpha\beta\lambda\mu} \rho_{\lambda\mu}(u)\rho_{\alpha\beta}(v)\sqrt{a}\,\mathrm{d}y, \tag{1.4}$$

where the coefficients $A_{\rho\rho}^{\alpha\beta\lambda\mu}$ are the elasticity coefficients which depend on the parameters y^1 and y^2 and satisfy the properties of symmetry and positivity. The covariant components $\gamma_{\alpha\beta}$ of the deformation tensor are defined by

$$\gamma_{\alpha\beta}(u) = \frac{1}{2}(D_\alpha u_\beta + D_\beta u_\alpha) - b_{\alpha\beta}u_3 \tag{1.5}$$

and the covariant components of the tensor of variation of curvature are

$$\rho_{\alpha\beta}(u) = \partial_\alpha\partial_\beta u_3 - \Gamma_{\alpha\ \beta}^{\ \lambda}\partial_\gamma u_3 - b_\alpha^\lambda b_{\lambda\beta}u_3 + D_\alpha\big(b_\beta^\lambda u_\lambda\big) + b_\alpha^\lambda D_\beta u_\lambda, \tag{1.6}$$

where $D_\alpha u_\beta$ is the covariant derivative

$$D_\alpha u_\beta = \partial_\alpha u_\beta - \Gamma_{\alpha\ \beta}^{\ \lambda} u_\lambda. \tag{1.7}$$

The coefficients $b_{\alpha\beta}$ are the coefficients of the second fundamental form, $b_\alpha^\beta \equiv \Gamma_{\alpha 3}^\beta$ at least, the coefficients $\Gamma_{\alpha\ \beta}^{\ \lambda}$ are the Christoffel symbols. Then, the problem $P(\varepsilon)$ writes

$$\text{For given } f \in V' \text{ (dual of } V), \text{ find } u^\varepsilon \text{ such that } a_m\big(u^\varepsilon, v\big) + \varepsilon^2 a_f\big(u^\varepsilon, v\big) = \langle f, v\rangle \quad \forall v \in V \tag{1.8}$$

and from the previous hypotheses, for fixed ε, existence and uniqueness of the solution follow by the Lax–Milgram theorem (Bernadou and Ciarlet, 1976).

Moreover, the hypothesis of inhibition amounts to

$$a_m(v, v) = 0,\ v \in V \Rightarrow v = 0 \tag{1.9}$$

so that

$$\|v\|_{V_m} = \big[a(v, v)\big]^{1/2} \tag{1.10}$$

is a norm on V, V_m denotes the completion of V with this norm.

Classically (see, for instance, (Sanchez-Hubert and Sanchez Palencia, 1997)), this problem is equivalent to the system of equations

$$\begin{aligned} &-D_\alpha T^{\alpha\beta} - \varepsilon^2\big[b_\gamma^\beta D_\alpha M^{\alpha\gamma} + D_\gamma\big(b_\alpha^\gamma M^{\alpha\beta}\big)\big] = f^\beta, \\ &-b_{\alpha\beta}T^{\alpha\beta} + \varepsilon^2\big[D_\alpha D_\beta M^{\alpha\beta} - b_\alpha^\delta b_{\beta\delta} M^{\alpha\beta}\big] = f^3 \end{aligned} \tag{1.11}$$

(where $T^{\alpha\beta} = A^{\alpha\beta\lambda\mu}\gamma_{\lambda\mu}(u)$ and $M^{\alpha\beta\lambda\mu}\rho_{\lambda\mu}(u)$) with the kinematic boundary conditions

$$\begin{aligned} &u^{\varepsilon} = 0, \\ &\partial_n u_3^{\varepsilon} = 0, \end{aligned} \quad \text{on the part } \Gamma_0 \text{ of the boundary,} \tag{1.12}$$

and the boundary conditions on the free part Γ_1:

$$\begin{aligned} &T^{11}n_1 + T^{12}n_2 = 0, \\ &T^{12}n_1 + T^{22}n_2 + 2\varepsilon^2\big(M^{12}n_1 + M^{22}n_2\big) = 0, \\ &\varepsilon^2\big\{-n_1\partial_1 M^{11} - 2n_2\partial_1 M^{12} - n_2\partial_2 M^{22} - \partial_t\big(n_1 t_1 M^{11} + 2n_1 t_2 M^{12} + n_2 t_2 M^{22}\big)\big\} = f_3, \\ &\varepsilon^2\big[M^{11}n_1 n_1 + 2M^{12}n_1 n_2 + M^{22}n_2 n_2\big] = 0 \end{aligned} \tag{1.13}$$

where $\mathbf{n}$ is the outer normal and $\mathbf{t}$ the unit tangent to Γ_1 in the plane tangent to $\mathcal{S}$.

Also, we define the variational form of the limit problem $P(0)$:

$$\text{For given } f \in V_m', \text{ find } u^0 \in V_m \text{ such that } a_m\big(u^0, v\big) = \langle f, v\rangle_{V_m', V_m} \quad \forall v \in V_m, \tag{1.14}$$

where obviously a_m is continuous and coercive. As we shall see later the hypothesis $f \in V_m'$ is somewhat restrictive, when it is satisfied the existence and uniqueness of the solution $u^0 \in V_m$ is insured.

The paper is organized as follows: Taking account of the complexity of the computations in the general case of developable surfaces, in a first part, Sections 2–4, we study in details the case of a cylinder for which the coefficients are constants and all the Christoffel symbols vanish. We focus our attention on the case of a characteristic boundary layer. The Lagrange multipliers are exhibited in Section 4.6. The case of internal layers (which appear when the normal component f_3 of the loading is discontinuous along a generator or a part of it) is not fundamentally different and was studied in details for a model problem in (Karamian et al., 2000).

In Section 3.2 we give a criterion for $\mathbf{f} \in V_m'$ which is not satisfied for loadings such that their normal component are piecewise constant bearing discontinuities along a characteristic $y^2 = \text{Const.}$ (generator) or for loadings such that their normal component do not vanish on a characteristic free boundary. It appears that the energy concentrates in layers of thickness $\mathcal{O}(\varepsilon^{1/4})$ so that the layers are described in terms of an inner variable $z^2 = \varepsilon^{-1/4}y^2$. In the sequel we shall define $\delta = \varepsilon^{1/4}$. The asymptotic behavior of $\mathbf{u}^{\varepsilon}$ is such that out of the layers it is of order $\mathcal{O}(1)$ while inside the components u_i^{ε} tends to infinity as δ^{-2}, δ^{-3} and δ^{-4} respectively:

$$\begin{aligned} u_1^{\varepsilon} &= \delta^{-2}U_1^{\delta}, \\ u_2^{\varepsilon} &= \delta^{-3}U_2^{\delta}, \\ u_1^{\varepsilon} &= \delta^{-4}U_3^{\delta}, \end{aligned} \tag{1.15}$$

where U_i^{δ} are finite limits as $\delta \searrow 0$. The exact variational formulation of the problem $P(\varepsilon)$ after the scaling is thus

$$\begin{aligned} &\frac{1}{\delta^4}\int_{\mathcal{B}_\delta} A_{11}^{2222}\big(D_2U_2^{\delta} - b_{22}U_3^{\delta}\big)\big(D_2V_2^{\delta} - b_{22}V_3^{\delta}\big)\,\mathrm{d}y^1\,\mathrm{d}z^2 \\ &\quad + \frac{1}{\delta^2}\int_{\mathcal{B}_\delta}\big[A_{11}^{1212}\big(\partial_1U_2^{\delta} + D_2U_1^{\delta} - 2\Gamma_{12}^2U_2^{\delta}\big)\big(\partial_1V_2^{\delta} + D_2V_1^{\delta} - 2\Gamma_{12}^2V_2^{\delta}\big) \\ &\quad + A_{11}^{1122}\big(D_2U_2^{\delta} - b_{22}U_3^{\delta}\big)\partial_1V_1^{\delta} + A_{11}^{2211}\partial_1U_1^{\delta}\big(D_2V_2^{\delta} - b_{22}V_3^{\delta}\big)\big]\,\mathrm{d}y^1\,\mathrm{d}z^2 \\ &\quad + \frac{1}{\delta}\int_{\mathcal{B}_\delta}\big[A_{11}^{1211}\partial_1U_1^{\delta}\big(\partial_1V_2^{\delta} + D_2V_1^{\delta} - 2\Gamma_{12}^2V_2^{\delta}\big) \\ &\quad + A_{11}^{1112}\big(\partial_1U_2^{\delta} + D_2U_1^{\delta} - 2\Gamma_{12}^2U_2^{\delta}\big)\partial_1V_1^{\delta}\big]\,\mathrm{d}y^1\,\mathrm{d}z^2 \\ &\quad + \int_{\mathcal{B}_\delta}\big[A_{11}^{1111}\partial_1U_1^{\delta}\partial_1V_1^{\delta} + A_{2222}^{2222}D_2^2U_3^{\delta}D_2^2V_3^{\delta}\big]\,\mathrm{d}y^1\,\mathrm{d}z^2 \\ &= \int_{\mathcal{B}_\delta} f_3\big(y^1, 0\big)V_3^{\delta}\,\mathrm{d}y^1\,\mathrm{d}z^2, \end{aligned} \tag{1.16}$$

where

$$\mathcal{B}_\delta = (0, l_1) \times \left(0, \frac{l_2}{\delta}\right). \tag{1.17}$$

We see that, after the scaling, the layer problem looks as a penalty one for $\delta \searrow 0$. Indeed, the vanishing of the terms with negative powers of δ does not imply the vanishing of the solution but only constitutes two constraints to be prescribed to the solution. As a consequence, the corresponding equations at the leading orders involve two Lagrange multipliers. This penalty problem implies classical locking phenomena in the finite element approximation. Coming back to the original problem $P(\varepsilon)$ in the variables $y^1,\ y^2$, it appears a non-uniformity of the convergence as it was foreseen for $\mathbf{f} \notin V'_m$. We then see that the non-uniformity may be explained in terms of a special kind of locking inside the layers (local locking). As a consequence of such a local structure, for the numerical computation, in addition to the obvious refinement of the mesh in the vicinity of the layer, we may take advantage of using anisotropic meshes (i.e. with triangles elongated in the tangential direction). Precise finite element estimates in this context were given in (Sanchez-Hubert and Sanchez Palencia, 2001-a) for a model problem and in (Sanchez-Hubert and Sanchez Palencia, 2001-b) for the developable surfaces.

In Section 5 we only consider the case of a cone for which the coefficients are functions of only one parameter y^1 and where two of the Christoffel symbols are different from zero. We show that the layer has the same structure as for the cylinder but now the coefficients are no more constant and, consequently, the precise description of the local constraints is more involved.

In Section 6, the previous results allow us to consider the general case of a developable surface for a general anisotropic material. Of course, in this case the coefficients depend on the two parameters y^1 and y^2 but, at the leading order they are only functions of y^1 and the numerical difficulties are not more important than for the cone.

Section 7 is devoted to numerical experiences in the case of a cone for several loadings normal to the surface. The first one $\mathbf{f}_1$ is a uniform loading then non-vanishing at the free characteristic boundary $y^2 = 0$ and $y^2 = 1/2$ which illustrates the theory of Section 5.3. The second loading $\mathbf{f}_2$ is concerned with the case of an internal layer along the characteristic $y^2 = 1/4$. The third loading $\mathbf{f}_3$ has discontinuities along pieces of the characteristic $y^2 = 1/4$ and of the non-characteristic curve $y^1 = 1/2$. The solution u_3 exhibits an important singularity propagated along the whole characteristic $y^2 = 1/4$ whereas the singularity along the non-characteristic curve $y^1 = 1/2$ is less relevant and undetectable on the numerical plot. The fourth loading $\mathbf{f}_4$ is similar to the previous one with discontinuities along pieces of the characteristics $y^2 = 3/16$ and $y^2 = 5/16$ as well as of the non-characteristics $y^1 = 1/4$ and $y^1 = 3/4$. The comments are analogous to those of the previous case.

2. Setting of the problem for a cylinder

2.1. General equations for a circular cylinder

As we saw, in terms of the constraints the shell equations are (1.11) where the linear constitutive laws write

$$\begin{aligned} T^{\alpha\beta} &= A_{1\,1}^{\alpha\beta\lambda\mu}\gamma_{\lambda\mu}, \\ M^{\alpha\beta} &= A_{2\,2}^{\alpha\beta\lambda\mu}\rho_{\lambda\mu}. \end{aligned} \tag{2.1}$$

For an isotropic and homogeneous material, the elasticity coefficients are given by Bernadou (1994):

$$A_{1\,1}^{\alpha\beta\lambda\mu} = \frac{E}{2(1+\nu)}\left[a^{\alpha\lambda}a^{\beta\mu} + a^{\alpha\mu}a^{\beta\lambda} + \frac{2\nu}{1-\nu}a^{\alpha\beta}a^{\lambda\mu}\right], \qquad A_{2\,2}^{\alpha\beta\lambda\mu} = \frac{1}{12}A_{1\,1}^{\alpha\beta\lambda\mu}. \tag{2.2}$$

To fix ideas, let us consider a circular cylinder of radius unity with generators perpendicular to the plane of the circle, then we have $a^{\alpha\beta} = \delta^{\alpha\beta}$ and consequently the elasticity coefficients are the following constants:

$$\begin{aligned} &A_{1\,1}^{1111} = A_{1\,1}^{2222} = \frac{E}{1-\nu^2}, \\ &A_{1\,1}^{1112} = A_{1\,1}^{1211} = A_{1\,1}^{1222} = A_{1\,1}^{2212} = 0, \\ &A_{1\,1}^{1122} = A_{1\,1}^{2211} = \frac{E\nu}{1-\nu^2}, \\ &A_{1\,1}^{1212} = \frac{E}{1+\nu}. \end{aligned} \tag{2.3}$$

As for the components $\gamma_{\alpha\beta}$ (strain components) and $\rho_{\alpha\beta}$ (variation of curvature components), as all the Christoffel symbols $\Gamma_{\alpha\beta}^{\delta}$ vanish and $b_{11} = b_{12} = 0$, taking $b_{22} = 1$ (i.e. the radius equal to 1) they are given by

$$\begin{aligned}\gamma_{11} &= \partial_1 u_1,\\ \gamma_{12} &= \frac{1}{2}(\partial_1 u_2 + \partial_2 u_1),\\ \gamma_{22} &= \partial_2 u_2 - u_3\end{aligned} \tag{2.4}$$

and

$$\begin{aligned}\rho_{11} &= \partial_1^2 u_3,\\ \rho_{12} &= \partial_1(u_2 + \partial_2 u_3),\\ \rho_{22} &= \partial_2(u_2 + \partial_2 u_3) + \partial_2 u_2 - u_3,\end{aligned} \tag{2.5}$$

respectively.

Then, in terms of the components of the displacement u the linear shell equations write

$$\begin{aligned}&-\partial_1\big[\partial_1 u_1 + \nu(\partial_2 u_2 - u_3)\big] - (1-\nu)\partial_2(\partial_1 u_2 + \partial_2 u_1) - \frac{\varepsilon^2}{6}(1-\nu)\partial_2\partial_1(u_2 + \partial_2 u_3) = F^1,\\ &-(1-\nu)\partial_1(\partial_1 u_2 + \partial_2 u_1) - \partial_2[\nu\partial_1 u_1 + \partial_2 u_2 - u_3]\\ &\quad - \frac{\varepsilon^2}{6}\big\{(1-\nu)\partial_1^2(u_2 + \partial_2 u_3) + \partial_2\big[\nu\partial_1^2 u_3 + \partial_2(u_2 + \partial_2 u_3) + \partial_2 u_2 - u_3\big]\big\} = F^2,\\ &-\big[\nu\partial_1 u_1 + (\partial_2 u_2 - u_3)\big] + \frac{\varepsilon^2}{12}\big\{\partial_1^2\big[\partial_1^2 u_3 + \nu\big(\partial_2(u_2 + \partial_2 u_3) + \partial_2 u_2 - u_3\big)\big]\\ &\quad + 4(1-\nu)\partial_2\partial_1^2(u_2 + \partial_2 u_3) + \partial_2^2\big[\nu\partial_1^2 u_3 + \partial_2(u_2 + \partial_2 u_3) + \partial_2 u_2 - u_3\big]\\ &\quad - \nu\partial_1^2 u_3 - \partial_2(u_2 + \partial_2 u_3) - \partial_2 u_2 + u_3\big\} = F_3,\end{aligned} \tag{2.6}$$

where

$$F^k = \frac{1-\nu^2}{E} f^k, \quad k = 1, 2, 3. \tag{2.7}$$

3. The limit problem

3.1. Considerations about the convergence process

As it is usual, in the sequel we shall identify L^2 with its dual. From the completion process, it follows that V is densely contained in V_m so that

$$V_m' \subset V'. \tag{3.1}$$

In the classical theory of singular perturbations for variational problems (Lions, 1973), convergence only holds for $f \in V_m'$ and we have the theorem 3.1 hereafter. In the case when $f \in V'$ but $f \notin V_m'$, general results of convergence are not available. The solution u^0 may or not exist but certainly it does not belong to the finite energy space V_m.

Theorem 3.1. *Let $f \in V_m'$ be fixed independently of ε. Let us denote by u^ε and u^0 the solutions of* (1.8) *and of the limit problem* (1.14) *respectively then*

$$u^\varepsilon \underset{\varepsilon\to 0}{\to} u^0 \quad \text{in } V_m \text{ strongly} \tag{3.2}$$

and there exists a constant C such that the energy

$$E\big(u^\varepsilon\big) = \frac{1}{2}\big[a_m\big(u^\varepsilon, u^\varepsilon\big) + \varepsilon^2 a_f\big(u^\varepsilon, u^\varepsilon\big)\big] < C. \tag{3.3}$$

The proof is classical, see for instance (Sanchez-Hubert and Sanchez Palencia, 1997), Sect. VI.1.4. Moreover, we have

Theorem 3.2. *Let $f \in V'$ be fixed independently of ε and u^ε be the solution of* (1.8)*, then*

(1) *The necessary and sufficient condition for $E(u^\varepsilon)$ to remain bounded for $\varepsilon \searrow 0$ is that $f \in V_m'$.*
(2) *If $f \notin V_m'$, then $E(u^\varepsilon)$ tends to infinity as $\varepsilon \searrow 0$.*

Proof. In order to prove the first assertion, from theorem 3.1, it is sufficient to prove that (3.3) implies $f \in V'_m$. To this end, (3.3) implies that for a subsequence

$$a_f\big(u^\varepsilon, u^\varepsilon\big) \leqslant \frac{C}{\varepsilon^2} \tag{3.4}$$

and

$$u^\varepsilon \to u^* \quad \text{weakly in } V_m$$

for some $u^* \in V_m$. Let us fix $v \in V$ in (1.8), then

$$a_m\big(u^\varepsilon, v\big) \to a_m\big(u^*, v\big),$$
$$\varepsilon^2 a_f\big(u^\varepsilon, v\big) \leqslant \varepsilon^2 a_f\big(u^\varepsilon, u^\varepsilon\big)^{1/2} a_f(v, v)^{1/2} \leqslant \varepsilon C \to 0$$

so that

$$a_m\big(u^*, v\big) = \langle f, v\rangle \quad \forall v \in V. \tag{3.5}$$

The left-hand side is a functional of the variable v defined on V, continuous on V_m, so that the right-hand side is also, and this implies that $f \in V'_m$.

To prove the second assertion, let us suppose that it is false. Then for a certain subsequence we should have (3.3) and in this case the proof of the first assertion shows that $f \in V'_m$ what is a contradiction and theorem 3.2 is proved. □

Remark 3.1. We shall see that the space V_m is somewhat "large" so that V'_m is "small" and $f \in V'_m$ implies strong restrictions which are not satisfied by "usual" loadings f. Consequently, we are often in the situation of the second assertion of theorem 3.2. This situation is very different of the case $f \in V'_m$ for given forces quantitatively analogous. As we noted above, when $f \notin V'_m$ the limit problem $P(0)$ may, or not, have a solution u^0 but if it does, such a solution is not in the finite energy space V_m. This is the reason why we shall consider in the sequel solutions of the limit problem which are not variational solutions in V_m. An example of this situation is shown in (Leguillon et al., 1999) where it is shown that the energy confined in boundary and internal layers is not bounded (for $\varepsilon \searrow 0$) whereas the energy in outer regions does. Later on we shall search for the asymptotic behavior of u^ε using the method of matched asymptotic expansions (see for instance (Van Dyke, 1964)) which shall exhibit such kind of layers.

3.2. A criterion for $f \in V'_m$

The form a_m defined in (1.3) is associated with the quantities

$$\begin{aligned} \gamma_{11} &= \partial_1 u_1, \\ \gamma_{12} &= \frac{1}{2}(\partial_1 u_2 + \partial_2 u_1), \\ \gamma_{22} &= \partial_2 u_2 - u_3. \end{aligned} \tag{3.6}$$

Let us define by (3.6) the application $\gamma : V \xrightarrow{\gamma} (L^2)^3$. As a consequence of inhibition $\gamma(u) = 0 \Rightarrow u = 0$, γ is thus an injective application. This application may be continued by continuity to V_m to an isomorphism from V_m onto its range R which is clearly a closed subspace of $(L^2)^3$. Now, we consider the functional

$$l_f(v) = \int_\Omega (f_1 v_1 + f_2 v_2 + f_3 v_3)\,\mathrm{d}y \quad \forall v \in V, \tag{3.7}$$

then we have:

Theorem 3.3. *The functional defined by* (3.7) *on V may be extended by continuity to V_m (that it is equivalent to $f \in V'_m$) if and only if there exists $T = (T^{11}, T^{12}, T^{22}) \in (L^2)^3$ such that*

$$\int_\Omega (f_1 v_1 + f_2 v_2 + f_3 v_3)\,\mathrm{d}y = \big(T^{11}, \gamma_{11}(v)\big) + 2\big(T^{12}, \gamma_{12}(v)\big) + \big(T^{22}, \gamma_{22}(v)\big) \quad \forall v \in V. \tag{3.8}$$

Proof. Let us suppose that there exists $T \in (L^2)^3$ which satisfies to (3.8), then the right-hand side in (3.8) is continuous on V for the topology of V_m and consequently the left-hand side also does: this proves that the condition is sufficient.

If (3.7) may be extended by continuity to V_m, then let us denote by

$$\langle f, v\rangle_{V_m' V_m} \tag{3.9}$$

the functional so extended. Let F be its image by the isomorphism γ, it is continuous on R and defined by

$$F(\xi) = \left\langle f, \gamma^{-1}(\xi)\right\rangle \quad \forall \xi \in R. \tag{3.10}$$

From the Hahn–Banach theorem, we know that it may be extended to a functional $\tilde{F}(\xi)$ continuous on $(L^2)^3$ and, by the Riesz theorem, it may be expressed as the scalar product

$$\tilde{F}(\xi) = \langle T, \xi\rangle_{(L^2)^3} \quad \forall \xi \in \left(L^2\right)^3, \tag{3.11}$$

where T is some element of $(L^2)^3$. In particular (3.11) holds for any $\xi \in R$ and then for any ξ of the form $\xi = \gamma(v)$ with $v \in V$ (not necessarily to V_m). Then, from (3.11), we get

$$\langle f, v\rangle \equiv \int_\Omega (f_1 v_1 + f_2 v_2 + f_3 v_3)\,\mathrm{d}y = \left(T, \gamma(v)\right)_{(L^2(\Omega))^3} \quad \forall v \in V, \tag{3.12}$$

the necessity of the condition is then proved. □

3.3. Examples

3.3.1. First example: case when $f_3 \neq 0$ on a characteristic boundary layer

Let us consider a smooth given force **f**. The free part Γ_1 of the boundary is the part $y^2 = 0$. We emphasize that this free boundary is along a characteristic of the problem $P(0)$. The space V is then defined by (1.2) with (1.1). The components $T^{\alpha\beta}$ then satisfy

$$\begin{aligned} &-\partial_1 T^{11} - \partial_2 T^{12} = f^1, \\ &-\partial_1 T^{12} - \partial_2 T^{22} = f^2 \quad \text{in } \Omega, \\ &T^{22} = -f_3, \\ &T^{\alpha\beta} n_\beta = 0 \quad \text{on } \Gamma_1. \end{aligned} \tag{3.13}$$

It is clear that $(3.13)_3$ and $(3.13)_4$ are compatible if and only if $f_3 = 0$ on Γ_1. Oppositely, when this condition is satisfied we may construct smooth functions $T^{\alpha\beta}$ satisfying (3.13). Then integration by parts show that the components $T^{\alpha\beta}$ satisfy (3.12). The necessary and sufficient condition for $\mathbf{f} \in V_m'$ is thus that $f_3 = 0$ on Γ_1.

3.3.2. Second example: case when f_3 is discontinuous along a generator

Let us denote by Γ_1 the free part of the boundary. Then the boundary condition

$$T^{\alpha\beta} n_\beta = 0 \quad \text{on } \Gamma_1$$

gives

$$\begin{aligned} &T^{11}\left(l_1, y^2\right) = 0, \\ &T^{12}\left(y^1, 0\right) = T^{12}\left(y^1, l_2\right) = T^{12}\left(l_1, y^2\right) = 0, \\ &T^{22}\left(y^1, 0\right) = T^{22}\left(y^1, l_2\right) = 0. \end{aligned} \tag{3.14}$$

We consider the case when the loading $f = (0, 0, f_3)$ with the component f_3 of the form

$$f_3\left(y^1, y^2\right) = \begin{cases} C = \text{Const.} & \text{for } y^2 > \gamma, \\ 0 & \text{for } y^2 < \gamma, \end{cases} \tag{3.15}$$

where γ is a constant, to fix ideas, we shall assume that it is positive. Let us now apply the theorem 3.3, the equations (1.11) give

$$\begin{aligned} -\partial_1 T^{11} - \partial_2 T^{12} &= 0, \\ -\partial_1 T^{12} - \partial_2 T^{22} &= 0 \end{aligned} \tag{3.16}$$

and

$$T^{22} = -f_3\big(y^1, y^2\big) = -CY\big(y^2 - \gamma\big), \tag{3.17}$$

where Y denotes the Heaviside function

$$Y(\eta) = \begin{cases} 0 & \text{for } \eta < 0, \\ 1 & \text{for } \eta > 0. \end{cases}$$

By substituting the expression of T^{22} in the second equation (3.16), taking account of the boundary conditions on $y^1 = l_1$, we obtain

$$T^{12} = C\big(y^1 - l_1\big)\delta_\gamma, \tag{3.18}$$

where δ_γ denotes the Dirac distribution at $y^2 = \gamma$. Then, from the first equation, we get

$$T^{11} = -C\frac{(y^1 - l_1)^2}{2}\delta'_\gamma. \tag{3.19}$$

We see that the components $T^{\alpha\beta}$ do not belong to L^2 and consequently $f_3 \notin V'_m$.

3.3.3. Third example: case when f_3 is not zero on a rectangular domain contained in $]0, l_1[\times]0, l_2[$

Let f_3 be of the form

$$f_3\big(y^1, y^2\big) = CY\left(y^1 - \frac{l_1}{2}\right)Y\left(y^2 - \frac{l_2}{2}\right)$$

we then have

$$T^{22} = -CY\left(y^1 - \frac{l_1}{2}\right)Y\left(y^2 - \frac{l_2}{2}\right) \tag{3.20}$$

from which

$$T^{12} = Cy^1 Y\left(y^1 - \frac{l_1}{2}\right)\delta\left(y^2 - \frac{l_2}{2}\right) + \tau\big(y^2\big),$$

where

$$T^{12}\big(l_1, z^2\big) = 0 \Rightarrow \tau\big(z^2\big) = -Cl_1\delta\left(y^2 - \frac{l_2}{2}\right)$$

from which

$$T^{12} = C\left[y^1 Y\left(y^1 - \frac{l_1}{2}\right) - l_1\right]\delta\left(y^2 - \frac{l_2}{2}\right). \tag{3.21}$$

At least, taking account of the boundary condition $T^{11}(l_1, y^2) = 0$, we get

$$T^{11} = -C\left[\frac{(y^1)^2}{2}Y\left(y^1 - \frac{l_1}{2}\right) - l_1 y^1 + \frac{l_1^2}{2}\right]\delta'\left(y^2 - \frac{l_2}{2}\right). \tag{3.22}$$

We again see that the components $T^{\alpha\beta} \notin L^2$ and consequently that the given loading $f \notin V'_a$. Moreover, for $y^1 < l_1/2$ we have $T^{12} = -Cl_1\delta(y^2 - l_2/2)$ and $T^{11} = C\frac{l_1^2}{2}\delta(y^2 - l_2/2)$ and we observe *the "propagation" of the singularity* of T^{12}, as well as the one of T^{11}, along the characteristic $y^2 = l_2/2$.

3.4. Equations and boundary conditions of $P(0)$

Let us suppose $\Gamma_0 = \{(y^1, y^2),\ y^1 = 0\}$, then the characteristic boundaries $y_2 = 0$ and $y_2 = l_2$ are free and they constitute with $y_1 = l_1$ the part Γ_1 of the boundary.

As V_m was only defined by completion, the variational formulation (1.14) of the limit problem is somewhat abstract. But, in any case, from (1.14), (1.3) and $(3.6)_1$ it follows that $v \in V_m \Rightarrow \partial_1 v_1 \in L^2(\Omega)$. Moreover, as Γ_0 contains one of the vertical segments of the boundary and from the Poincaré inequality for $y^2 = \text{Const.}$ it follows that $v_1 \in L^2(\Omega)$. Consequently, the principal boundary condition $v_1 = 0$ is inherited by V_m on Γ_0. In fact,

$$v_1 \in L^2\big(0, l_2; H^1(0, l_1)\big) \quad \Rightarrow \quad \partial_2 v_1 \in H^1\big(0, l_1; H^{-1}(0, l_2)\big) \equiv H^{-1}\big(0, l_2; H^1(0, l_1)\big)$$

then, from $(3.6)_2$ we get

$$\partial_1 v_2 \in H^{-1}\big(0, l_2; L^2(0, l_1)\big)$$

and, as $u_2 = 0$ for $y_2 = 0$, from the Poincaré inequality

$$v_2 \in H^{-1}\big(0, l_2; H^1(0, l_1)\big)$$

and the trace of v_2 takes sense on $y_2 = \text{Const.}$ in $H^{-1}(0, l_2)$.

As for v_3, if $v \in V_m$, it follows from (1.10), (1.3) and (3.6) that v_3 is the sum of an element of $L^2(\Omega)$ and $\partial_2 v_2$ so that in the completion process the kinematic boundary conditions are lost everywhere for v_3. For v_1 and v_2 they are lost on $y^2 = \text{const.}$ This allows us to write down the equations in the general sense of distributions and boundary conditions of $P(0)$ (without a precise description of V_m):

$$\begin{aligned}
&-\partial_1\big[\partial_1 u_1 + \nu(\partial_2 u_2 - u_3)\big] - (1-\nu)\partial_2(\partial_1 u_2 + \partial_2 u_1) = F^1,\\
&-(1-\nu)\partial_1(\partial_1 u_2 + \partial_2 u_1) - \partial_2[\nu\partial_1 u_1 + \partial_2 u_2 - u_3] = F^2,\\
&-\big[\nu\partial_1 u_1 + (\partial_2 u_2 - u_3)\big] = F_3
\end{aligned} \tag{3.23}$$

with the kinematics boundary conditions

$$u_1 = u_2 = 0 \quad \text{on } \Gamma_0. \tag{3.24}$$

Clearly, the system (3.23) is equivalent to the following system for $\partial_1 u_1$ and u_2:

$$\begin{aligned}
&-\big(1-\nu^2\big)\partial_1^2(\partial_1 u_1) = \partial_1(F_1 - \nu\partial_1 F_3) - \partial_2\big(-\partial_2 F_3 + F^2\big) \underset{\text{def}}{=} \Phi_1,\\
&-(1-\nu)\partial_1^2 u_2 = -\partial_2 F_3 + F^2 + (1-\nu)\partial_2(\partial_1 u_1) \underset{\text{def}}{=} \Phi_2
\end{aligned} \tag{3.25}$$

with

$$u_3 = F_3 + \nu\partial_1 u_1 + \partial_2 u_2 \tag{3.26}$$

which is an elliptic system with respect to the y^1 with parameter y^2. In Ω (3.25) is parabolic with double characteristic $y^2 = \text{Const.}$ As y^2 appears as a parameter the loading F may be chosen to be a distribution of y^2 with values in an appropriate space for the variable y^1. Consequently, when F is not sufficiently smooth with respect to y^2 the equations (3.23) and the boundary conditions (3.24) have a sense in a more general framework which is not that of the variational problems (1.14).

3.5. Solutions in the sense of distributions

According to the previous considerations, we now consider the system (3.23) or (3.25) in the sense of distributions of y^2 with values in a space (for instance $L^2(0, l_1)$) of the variable y^1. In order to exhibit the singular terms, let us consider the case when $F_1 = F_2 = 0$ and F_3 defined as in (3.15), then the system takes the form:

$$\begin{aligned}
&\partial_1^2\big(\partial_1 u_1(\bullet, y^2)\big) = \frac{\nu}{1-\nu^2}\partial_1^2 F_3 Y\big(y^2 - \gamma\big) - \frac{C}{1-\nu^2}\delta'_\gamma,\\
&\partial_1^2\big(u_2(\bullet, y^2)\big) = \frac{1}{1-\nu} C\delta_\gamma - \partial_2(\partial_1 u_1),\\
&u_3\big(\bullet, y^2\big) = CY\big(y^2 - \gamma\big) + \nu\partial_1 u_1 + \partial_2 u_2
\end{aligned} \tag{3.27}$$

of which the solution writes, taking account of the boundary condition $u_1(0, y^2) = u_2(0, y^2) = 0$,

$$\begin{aligned}
u_1\big(\bullet, y^2\big) &= \frac{\nu C}{1-\nu^2} y^1 Y\big(y^2 - \gamma\big) - \frac{C}{6(1-\nu^2)}\big(y^1\big)^3\delta'_\gamma + \frac{A_2(y^2)}{2}\big(y^1\big)^2 + A_1\big(y^2\big)y^1,\\
u_2\big(\bullet, y^2\big) &= \frac{C}{2(1-\nu^2)}\big(y^1\big)^2\delta_\gamma + \frac{C}{24(1-\nu^2)}\big(y^1\big)^4\delta''_\gamma + B_1 y^1 + B_0 - \partial_2\left[\frac{A_2(y^2)}{2}\big(y^1\big)^2 + A_1\big(y^2\big)y^1\right],\\
u_3\big(\bullet, y^2\big) &= \frac{1}{1-\nu^2} C(\bullet, x_2) Y\big(y^2 - \gamma\big) + \nu\left[\frac{\nu C}{1-\nu^2} Y\big(y^2 - \gamma\big) - \frac{C}{2(1-\nu^2)}\big(y^1\big)^2\delta'_\gamma + A_2 y^1 + A_1\right]\\
&\quad + \frac{C}{2(1-\nu^2)}\big(y^1\big)^2\delta'_\gamma + \frac{C}{24(1-\nu^2)}\big(y^1\big)^4\delta'''_\gamma\\
&\quad + \partial_2\left\{B_1 y^1 + B_0 - \partial_2\left[\frac{A_2(y^2)}{2}\big(y^1\big)^2 + A_1\big(y^2\big)y^1\right]\right\},
\end{aligned} \tag{3.28}$$

where $A_1(y^2)$ and $A_2(y^2)$ are functions which may be defined using the boundary conditions at $y^2 = l_2$. But, in any case, it follows from (3.28) that u_1, u_2 and u_3 involve singular (distributional) terms in δ'_γ, δ''_γ and δ'''_γ respectively. Clearly this implies that the solutions of $P(\varepsilon)$ involve boundary (in fact internal) layers terms which converge to the singular terms of (3.27).

3.6. Localization of the boundary and internal layers

As a consequence of Subsection 3.5 it appears that the problem $P(\varepsilon)$ exhibits internal layers terms along the segments $y^2 = \text{const.}$ where f is not smooth as a function of y^2 (with values in $L^2(0, l_2)$ for instance). The structure of the internal layer depends highly on the degree of non-smoothness of f. We emphasize that $y^2 = \text{const.}$ are the characteristics of the limit problem (3.25).

The explicit solution (3.27) exhibits an example of propagation of singularities along the characteristics.

Oppositely, let us consider the case when $f_1 = f_2 = 0$ and f_3 is piecewise constant with a discontinuity along a curve $\mathcal{C}$ which is transversal to the characteristics. The method of solution with parameter y^2 shows that u is smooth unless on $\mathcal{C}$ where the function u_3 and the first derivatives of u_1 and u_2 have jumps. Clearly, in this case, u^ε exhibits an internal layer along the curve $\mathcal{C}$. In addition, if one of the extremities of $\mathcal{C}$ is a point interior to Ω, the solution is singular at this point and propagates from it along $y^2 = \text{const.}$

On the other hand, as y^2 is a parameter, the limit problem $P(0)$ has no boundary condition on $y^2 = 0$ and $y^2 = l_2$ so that u^ε exhibits boundary layers along these (characteristic) boundaries. Let us note that the intensity of a characteristic layer is highly dependent of the boundary conditions. In particular, it is more important for a free boundary than for a clamped one.

Also boundary layers appear along the parts of Γ_0 transversal to the characteristics (vertical parts of Γ_0) as the boundary conditions (1.1) involving u_3 disappear in the limit (compare with (3.24)). We shall call them non-characteristic boundary layers.

We shall see later that the intensity of the characteristic layers with free boundary conditions is more important than the intensity of the non-characteristic ones. Moreover, the intensities of a non-characteristic layer and of the layer for a clamped characteristic boundary are of the same order.

4. Boundary and internal layers

4.1. Scaling in the layers. Method of exponential solutions

Classically (Van Dyke, 1964), in order to describe the structure of a layer we must perform a change of variables including a dilatation of the variable normal to the layer. Moreover, in order to obtain a consistent system, a rescaling of the unknowns is usually needed. The deduction by a classical procedure of the appropriate scalings is possible but we use here a method issued from the analysis of the structure of the exponential solutions of the homogeneous system. It should be pointed out that this method presents analogies with the study of asymptotic solutions of systems using the eikonal equation (Sanchez-Hubert and Sanchez Palencia, 1997), Section III.4.

4.1.1. Characteristic layers

We first consider the case of the layers along $y^2 = \text{const.}$ As the characteristics of the limit problem are normal to the vector $(0, 1)$ there exist solutions of the form

$$u\big(y^1, y^2\big) = v\mathrm{e}^{-i(\xi_1 y^1 + \xi_2 y^2)}$$

with $\xi_1 = 0, \xi_2 \neq 0$. Let us search, for $\varepsilon > 0$, solutions of the form

$$u^\varepsilon\big(y^1, y^2\big) = v^\varepsilon \mathrm{e}^{i\xi_1 y^1 + \mu y^2} \tag{4.1}$$

with ξ_1 real of order unity and $|\mu| \to +\infty$ (i.e. such that $(\xi_1(\text{real}), \xi_2 \equiv -i\mu)$ tends to be proportional to $(0, 1)$). The solutions (4.1) are sinusoidal in y^1 with wave length of order $\mathcal{O}(1)$ and very fast variations in y^2. By substitution of (4.1) in the homogeneous system associated with (2.6) we obtain

$$\begin{aligned}
&\big[\xi_1^2 - (1-\nu)\mu^2\big]v_1^\varepsilon + i\xi_1\mu v_2^\varepsilon - i\xi_1\nu v_3^\varepsilon = 0,\\
&i\xi_1\mu v_1^\varepsilon + \big[(1-\nu)\xi_1^2 - \mu^2 + \mathcal{O}\big(\varepsilon^2\lambda^2\big)\big]v_2^\varepsilon + \big[\mu + \mathcal{O}\big(\varepsilon^2\mu^3\big)\big]v_3^\varepsilon = 0,\\
&i\xi_1\nu v_1^\varepsilon + \big[-\mu + \mathcal{O}\big(\varepsilon^2\mu^3\big)\big]v_2^\varepsilon + \left[1 + \frac{1}{12}\varepsilon^2\mu^4 + \cdots\right]v_3^\varepsilon = 0.
\end{aligned} \tag{4.2}$$

The vanishing of the determinant of this system gives

$$D(\varepsilon,\mu)=D(0,\mu)+\frac{1}{12}\varepsilon^2\mu^4\begin{vmatrix}-(1-\nu)\mu^2 & i\xi_1\mu\\ i\xi_1\mu & -\mu^2\end{vmatrix}+\cdots=0,$$

where

$$D(0,\mu)=(1-\nu)\big(1-\nu^2\big)\xi_1^4$$

and, at the leading order, we have

$$(1-\nu)\left[\big(1-\nu^2\big)\xi_1^4+\frac{1}{12}\varepsilon^2\mu^8\right]=0\quad\Longrightarrow\quad\mu^8=-12\big(1-\nu^2\big)\varepsilon^{-2}\xi_1^4$$

which for finite ξ_1 and $\mu\to+\infty$ gives

$$\mu=\mathcal{O}\big(\varepsilon^{-1/4}\big). \tag{4.3}$$

It then appears that the just obtained solutions with $\xi_1=\mathcal{O}(1)$, $\mu=\mathcal{O}(\varepsilon^{-1/4})$ have a characteristic length of variation in the y^2 direction of order $\mathcal{O}(\varepsilon^{1/4})$; this corresponds to a layer of thickness $\mathcal{O}(\varepsilon^{1/4})$, in the sequel we shall write

$$\delta=\varepsilon^{1/4}. \tag{4.4}$$

Then, from (4.2) the corresponding scaling of v is

$$\frac{v_2^\varepsilon}{v_1^\varepsilon}=\mathcal{O}\big(\delta^{-1}\big),\qquad\frac{v_3^\varepsilon}{v_1^\varepsilon}=\mathcal{O}\big(\delta^{-2}\big). \tag{4.5}$$

4.1.2. Non-characteristic layers

Analogously, in the case of layers parallel to $y^1=\text{const.}$ we search solutions of the form

$$u^\varepsilon\big(y^1,y^2\big)=v^\varepsilon\mathrm{e}^{\mu y^1+i\xi_2 y^2}$$

from which it follows that

$$\mu\cong(-1)^{1/4}\varepsilon^{-1/2} \tag{4.6}$$

so that the thickness of the layer is of order

$$\delta=\varepsilon^{1/2} \tag{4.7}$$

and the scaling of v is

$$\frac{v_2^\varepsilon}{v_1^\varepsilon}=\mathcal{O}\big(\delta^{-1}\big),\qquad\frac{v_3^\varepsilon}{v_1^\varepsilon}=\mathcal{O}\big(\delta^{-2}\big). \tag{4.8}$$

4.2. Boundary layer along a free characteristic part of the boundary

As we saw in Section 3.6, there exist boundary layers along the free characteristic boundaries $y^2=0$ and $y^2=l_2$. As they belong to $\Gamma_1$their structures are analogous and more important than those of the non-characteristic layers. Consequently, we shall only consider an example of characteristic layer, namely the layer in the vicinity of $y^2=0$. The loading $f=(0,0,f_3)$ is such that $f_3\neq0$ on $y^2=0$. According to the Section 4.1, the appropriate scaling is then (4.3) and (4.5) so we define the dilatation by

$$z^2=\frac{y^2}{\delta},\quad\delta=\varepsilon^{1/4}, \tag{4.9}$$

and we search for asymptotic expansions of the form

$$\begin{aligned}u_1^\varepsilon\big(y^1,y^2\big)&=\delta^\eta U_1^\delta,\\ u_2^\varepsilon\big(y^1,y^2\big)&=\delta^{\eta-1}U_2^\delta,\\ u_3^\varepsilon\big(y^1,y^2\big)&=\delta^{\eta-2}U_3^\delta,\end{aligned} \tag{4.10}$$

where η is undetermined for the time being and U^δ tends to a finite limit as $\eta\searrow0$. In the sequel we shall denote by D_2 the derivative with respect to z^2:

$$D_2=\delta\partial_2. \tag{4.11}$$

According to boundary layer theory (Van Dyke, 1964), the expansions (4.10) hold true in the domain $\mathcal{B}$ defined by $y^1 \in (0, l_1)$, $z^2 \in (0, +\infty)$. The solution U^δ must satisfy the kinematic boundary conditions

$$\begin{aligned} &U_1^\delta(0, z^2) = U_2^\delta(0, z^2) = U_3^\delta(0, z^2) = 0, \\ &D_1 U_3^\delta(0, z^2) = 0 \end{aligned} \tag{4.12}$$

and the matching conditions for $z^2 \to +\infty$ which we shall consider later as well as the "natural" boundary conditions on $z^2 = 0$ and $y^1 = l_1$.

Taking account of the data, we verify that the appropriate expansions for the components of the displacement are

$$\begin{aligned} u_1^\varepsilon &= \delta^{-2} U_1^1 + \delta^{-1} U_1^2 + U_1^3 + \delta U_1^4 + \cdots, \\ u_2^\varepsilon &= \delta^{-3} U_2^1 + \delta^{-2} U_2^2 + \delta^{-1} U_2^3 + U_2^4 + \delta U_2^5 + \cdots, \\ u_3^\varepsilon &= \delta^{-4} U_3^1 + \delta^{-3} U_3^2 + \delta^{-2} U_3^3 + \delta^{-1} U_3^4 + U_3^5 + \cdots. \end{aligned} \tag{4.13}$$

The variational formulation (1.8) becomes an equivalent one in $(0, l_1) \times (0, l_2/\delta)$ with the change of variables (4.9) and the change of variables and of test functions (4.10). In particular, taking the test functions with compact support in z^2 we may consider the domain

$$\mathcal{B} = (0, l)_{y^1} \times (0, +\infty)_{z^2}, \tag{4.14}$$

the expansions (4.13) then give

$$\begin{aligned} &\int_{\mathcal{B}} \Bigg\{ \frac{E}{1-\nu^2} \big[\nu\delta^{-4}\big(D_2 U_2^1 - U_3^1\big) + \nu\delta^{-3}\big(D_2 U_2^2 - U_3^2\big) + \nu\delta^{-2}\big(D_2 U_2^3 - U_3^3\big) + \cdots + \delta^{-2}\partial_1 U_1^1 + \cdots\big]\big(\delta^{-2}\partial_1 V_1^1 + \cdots\big) \\ &\quad + \frac{E}{1+\nu}\big[\delta^{-3}\big(\partial_1 U_2^1 + D_2 U_1^1\big) + \delta^{-2}\big(\partial_1 U_2^2 + D_2 U_1^2\big) + \cdots\big] \\ &\quad \times \big[\delta^{-3}\big(\partial_1 V_2^1 + D_2 V_1^1\big) + \delta^{-2}\big(\partial_1 V_2^2 + D_2 V_1^2\big) + \cdots\big] \\ &\quad + \frac{E}{1-\nu^2}\big[\delta^{-4}\big(D_2 U_2^1 - U_3^1\big) + \delta^{-3}\big(D_2 U_2^2 - U_3^2\big) + \delta^{-2}\big(D_2 U_2^3 - U_3^3\big) + \cdots \\ &\qquad\quad + \nu\delta^{-2}\partial_1 U_1^1 + \nu\delta^{-1}\partial_1 U_1^2 + \cdots\big] \\ &\quad \times \big[\delta^{-4}\big(D_2 V_2^1 - V_3^1\big) + \delta^{-3}\big(D_2 V_2^2 - V_3^2\big) + \delta^{-2}\big(D_2 V_2^3 - V_3^3\big) + \cdots\Bigg\} \mathrm{d}y^1 \delta\, \mathrm{d}z^2 \\ &\quad + \frac{\varepsilon^2}{12}\int_{\mathcal{B}} \frac{E}{1-\nu^2}\big(\delta^{-12} D_2^2 U_3^1 D_2^2 V_3^1 + \cdots\big)\, \mathrm{d}y^1 \delta\, \mathrm{d}z^2 \\ &= \int_{\mathcal{B}} \big[\delta^{-4} f_3\big(y^1, 0\big) V_3^1 + \cdots\big]\, \mathrm{d}y^1 \delta\, \mathrm{d}z^2. \end{aligned} \tag{4.15}$$

At the leading order (δ^{-7}) we have

$$\frac{E}{1-\nu^2}\int_{\mathcal{B}} \big(D_2 U_2^1 - U_3^1\big)\big(D_2 V_2^1 - V_3^1\big)\, \mathrm{d}y^1\, \mathrm{d}z^2 = 0$$

then, as $D_2 V_2^1 - V_3^1$ is arbitrary, we immediately obtain

$$D_2 U_2^1 - U_3^1 = 0 \tag{4.16}$$

then, by taking test functions which satisfy (4.16), we obtain at the next order (δ^{-5})

$$\int_{\mathcal{B}} \Bigg\{ \frac{E}{1+\nu}\big(\partial_1 U_2^1 + D_2 U_1^1\big)\big(\partial_1 V_2^1 + D_2 V_1^1\big) + \frac{E}{1-\nu^2}\big(D_2 U_2^2 - U_3^2\big)\big(D_2 V_2^2 - V_3^2\big)\Bigg\}\, \mathrm{d}y^1\, \mathrm{d}z^2 = 0$$

which gives, by taking $V_1^1 = V_2^1 = V_2^2 = 0$ and V_3^2 arbitrary,

$$D_2 U_2^2 - U_3^2 = 0 \tag{4.17}$$

and, as $\partial_1 V_2^1 + D_2 V_1^1$ is arbitrary,

$$\partial_1 U_2^1 + D_2 U_1^1 = 0. \tag{4.18}$$

With test functions satisfying the constraints (4.16)–(4.18) we get at order δ^{-3}

$$\begin{aligned}
&\frac{E}{1-\nu^2}\delta^{-3}\int_{\mathcal{B}}\Big\{\big[\nu\big(D_2U_2^3-U_3^3\big)+\partial_1U_1^1\big]\partial_1V_1^1+\big(D_2U_2^3-U_3^3+\nu\partial_1U_1^1\big)\big(D_2V_2^3-V_3^3\big)\\
&\qquad\times\frac{E}{1+\nu}\big(\partial_1U_2^2+D_2U_1^2\big)\big(\partial_1V_2^2+D_2V_1^2\big)\Big\}\,\mathrm{d}y^1\,\mathrm{d}z^2\\
&\qquad+\frac{\varepsilon^2}{12}\int_{\mathcal{B}}\frac{E}{1-\nu^2}\big(\delta^{-12}D_2^2U_3^1D_2^2V_3^1+\cdots\big)\,\mathrm{d}y^1\delta\,\mathrm{d}z^2\\
&=\int_{\mathcal{B}}\big[\delta^{-4}f_3\big(y^1,0\big)V_3^1+\cdots\big]\,\mathrm{d}y^1\delta\,\mathrm{d}z^2.
\end{aligned}$$

In fact, taking account of

$$\varepsilon^2=\delta^8 \quad\Rightarrow\quad \varepsilon^2\delta^{-12}=\delta^{-4}$$

we have

$$\begin{aligned}
&\frac{E}{1-\nu^2}\int_{\mathcal{B}}\Big\{\big[\nu\big(D_2U_2^3-U_3^3\big)+\partial_1U_1^1\big]\partial_1V_1^1+\big(D_2U_2^3-U_3^3+\nu\partial_1U_1^1\big)\big(D_2V_2^3-V_3^3\big)\\
&\qquad+(1-\nu)\big(\partial_1U_2^2+D_2U_1^2\big)\big(\partial_1V_2^2+D_2V_1^2\big)+\frac{1}{12}D_2^2U_3^1D_y^2V_3^1\Big\}\,\mathrm{d}y^1\delta\,\mathrm{d}z^2+\cdots\\
&=\int_{\mathcal{B}}\big[f_3\big(y^1,0\big)V_3^1+\cdots\big]\,\mathrm{d}y^1\,\mathrm{d}z^2.
\end{aligned}\tag{4.19}$$

Now, by taking $V_1^1=V_3^1=V_2^3=V_3^3=0$, arbitrary V_1^2 and V_2^2, we obtain

$$\partial_1U_2^2+D_2U_1^2=0. \tag{4.20}$$

At least, with $V_1^1=V_3^1=V_2^3=0$ and V_3^3 arbitrary we get

$$D_2U_2^3-U_3^3+\nu\partial_1U_1^1=0.$$

Finally, we have

$$\frac{E}{1-\nu^2}\int_{\mathcal{B}}\Big\{\big(1-\nu^2\big)\partial_1U_1^1\partial_1V_1^1+\frac{1}{12}D_2^2U_3^1D_2^2V_3^1\Big\}\,\mathrm{d}y^1\,\mathrm{d}z^2=\int_{\mathcal{B}}\big[f_3\big(y^1,0\big)V_3^1+\cdots\big]\,\mathrm{d}y^1\,\mathrm{d}z^2+\cdots. \tag{4.21}$$

4.3. Boundary layer along a clamped characteristic part

As we saw in Section 3.6, there exist boundary layers along the clamped characteristic boundaries. Let us suppose Γ_0 constituted by $y^2=0$ (characteristic part) and to fix ideas $y^1=0$ and $y^1=l_1$. According to Section 4.1.1, the appropriate scaling is then (4.4) and (4.5) so we define the dilatation by (4.9) and we search for asymptotic expansions of the form

$$\begin{aligned}
u_1^\varepsilon\big(y^1,y^2\big)&=\delta^\eta U_1^\delta,\\
u_2^\varepsilon\big(y^1,y^2\big)&=\delta^{\eta-1}U_2^\delta,\\
u_3^\varepsilon\big(y^1,y^2\big)&=\delta^{\eta-2}U_3^\delta,
\end{aligned}\tag{4.22}$$

where η is undetermined for the time being and U^δ tends to a finite limit as $\delta\searrow 0$.

The solution U^δ must satisfy the kinematic boundary conditions

$$\begin{aligned} &U_1^\delta\big(y^1,0\big)=U_2^\delta\big(y^1,0\big)=U_3^\delta\big(y^1,0\big)=0,\\ &D_2U_3^\delta\big(y^1,0\big)=0, \end{aligned} \tag{4.23}$$

$$\begin{aligned} &U_1^\delta\big(y^1,z^2\big)=U_2^\delta\big(y^1,z^2\big)=U_3^\delta\big(y^1,z^2\big)=0,\\ &\partial_1U_3^\delta\big(y^1,z^2\big)=0 \end{aligned} \tag{4.24}$$

on $y^1=0$ and $y^1=l_1$ and the matching conditions for $z^2\to+\infty$ which we shall consider later.

Tentatively, we look for the component u_1 of order $\mathcal{O}(1)$, i.e. $\eta=0$, in order to match it with the outer expansion (we recall that only the ratio $v_{\acute{e}}^\varepsilon/v_1^\varepsilon$ and $v_3^\varepsilon/v_1^\varepsilon$ are defined in (4.5)).

As in the previous section, the variational formulation (1.8) becomes an equivalent one in $(0,l_1)\times(0,l_2/\delta)$ with the change of variables (4.9) and the change of test functions analogous to (4.10). In particular, taking the test functions with compact support in z^2 we may consider the domain

$$\mathcal{B}=(0,l)_{y^1}\times(0,+\infty)_{z^2}. \tag{4.25}$$

The expansions (4.22) then give

$$\begin{aligned} &\int_{\mathcal{B}}\bigg\{\frac{E}{1-\nu^2}\big[\delta^{-2}\nu\big(D_2U_2^\delta-U_3^\delta\big)+\partial_1U_1^\delta\big]\partial_1V_1^\delta+\frac{E}{1+\nu}\delta^{-2}\big(\partial_1U_2^\delta+D_2U_1^\delta\big)\times\big(\partial_1V_2^\delta+D_2V_1^\delta\big)\\ &\qquad+\frac{E}{1-\nu^2}\big[\delta^{-2}\big(D_2U_2^\delta-U_3^\delta\big)+\nu\partial_1U_1^\delta\big]\times\delta^{-2}\big(D_2V_2^\delta-V_3^\delta\big)\bigg\}\,\mathrm{d}y^1\delta\,\mathrm{d}z^2\\ &\qquad+\frac{\varepsilon^2}{12}\int_{\mathcal{B}}\frac{E}{1-\nu^2}\delta^{-7}D_2^2U_3^\delta D_2^2V_3^\delta\,\mathrm{d}y^1\,\mathrm{d}z^2\\ &\quad=\int_{\mathcal{B}}\big[\delta^{-2}\big[f_3\big(y^1,0\big)+\delta z^2\partial_2f_3\big(y^1,0\big)\big]V_3^\delta+\cdots\big]\,\mathrm{d}y^1\delta\,\mathrm{d}z^2, \end{aligned} \tag{4.26}$$

where f_3 is assumed regular and was represented by its Taylor expansion in the vicinity of $z^2=0$. From (4.26), we obtain at the leading order δ^{-3}:

$$\frac{E}{1-\nu^2}\int_{\mathcal{B}}\big(D_2U_2^1-U_3^1\big)\big(D_2V_2^1-V_3^1\big)\,\mathrm{d}y^1\,\mathrm{d}z^2=0$$

and, as $D_2V_2^1-V_3^1$ is arbitrary, we immediately get

$$D_2U_2^1-U_3^1=0 \tag{4.27}$$

then, by taking test functions which satisfy (4.27), we obtain at the next order δ^{-1}

$$\begin{aligned} &\frac{E}{1-\nu^2}\int_{\mathcal{B}}\big[(1-\nu)\big(\partial_1U_2^1+D_2U_1^1\big)\big(\partial_1V_2^1+D_2V_1^1\big)+\big(D_2U_2^2-U_3^2\big)\big(D_2V_2^2-V_3^2\big)\big]\,\mathrm{d}y^1\,\mathrm{d}z^2\\ &\quad=\int_{\mathcal{B}}f_3\big(y^1,0\big)V_3^1\,\mathrm{d}y^1\,\mathrm{d}z^2, \end{aligned} \tag{4.28}$$

where

$$\int_{\mathcal{B}}f_3\big(y^1,0\big)V_3^1\,\mathrm{d}y^1\,\mathrm{d}z^2=\int_0^{l_1}f_3\big(y^1,0\big)\bigg(\int_0^{+\infty}D_2V_3^1\big(x_1,z^2\big)\,\mathrm{d}y^2\bigg)\,\mathrm{d}y^1=0$$

as V_3^1 vanishes for $z^2=0$ and z^2 sufficiently large. Then, taking $V_2^1=V_1^1=V_2^2=0$, as V_3^2 is arbitrary, we obtain

$$D_2U_2^2-U_3^2=0.$$

Now, as $\partial_1V_2^1+D_2V_1^1$ is arbitrary, we have

$$\partial_1U_2^1+D_2U_1^1=0. \tag{4.29}$$

At the present step the leading term in (4.26) is

$$\begin{aligned}
&\frac{E}{1-\nu^2}\int_{\mathcal{B}}\{\nu(D_2U_2^3-U_3^3)+\partial_1U_1^1\}\partial_1V_1^1\,\mathrm{d}y^1\,\mathrm{d}z^2\\
&\quad+\frac{E}{1-\nu^2}\int_{\mathcal{B}}(D_2U_2^3-U_3^3+\nu\partial_1U_1^1)(D_2V_2^3-V_3^3)\,\mathrm{d}y^1\,\mathrm{d}z^2\\
&\quad+\frac{E}{1+\nu}\int_{\mathcal{B}}(\partial_1U_2^2+D_2U_1^2)(\partial_1V_2^2+D_2V_1^2)+\frac{1}{12}\frac{E}{1-\nu^2}\int_{\mathcal{B}}D_2^2U_3^1D_2^2V_3^1\,\mathrm{d}y^1\,\mathrm{d}z^2\\
&=\int_{\mathcal{B}}z^2\partial_2f_3(y^1,0)V_3^1\,\mathrm{d}y^1\,\mathrm{d}z^2=-\int_{\mathcal{B}}\partial_2f_3(y^1,0)V_2^1\,\mathrm{d}y^1\,\mathrm{d}z^2
\end{aligned}\tag{4.30}$$

then, taking $V_1^1=V_3^1=V_2^3=V_3^3=0$, arbitrary V_1^2 and V_2^2, we obtain

$$\partial_1U_2^2+D_2U_1^2=0.$$

At least, with $V_1^1=V_3^1=V_2^3=0$ and arbitrary V_3^3 we get

$$D_2U_2^3-U_3^3+\nu\partial_1U_1^1=0$$

and, finally,

$$\int_{\mathcal{B}}\left[(1-\nu^2)\partial_1U_1^1\partial_1V_1^1+\frac{1}{12}D_2^2U_3^1D_2^2V_3^1\right]\mathrm{d}y^1\,\mathrm{d}z^2=-\int_{\mathcal{B}}\partial_2F_3(y^1,0)V_2^1\,\mathrm{d}y^1\,\mathrm{d}z^2\in\overline{\mathcal{V}}\tag{4.31}$$

which has the same structure as (4.21) but $u_1=\mathcal{O}(1)$, $u_2=\mathcal{O}(\delta^{-2})$ and $u_3=\mathcal{O}(\delta^{-2})$.

4.4. Existence and uniqueness of the solution of the limit problem

Let us consider the problem (4.21) as a problem for U^1 satisfying the constraints (4.16) and (4.18). The test functions V^1 will be taken satisfying them. We note that

$$\begin{aligned}
&\partial_1V_2+D_2V_1=0\quad\Longrightarrow\quad\exists\psi(y^1,z^2)\colon\begin{cases}V_1=\partial_1\psi,\\ V_2=-D_2\psi,\end{cases}\\
&D_2V_2-V_3=0\quad\Longrightarrow\quad V_3=-D_2^2\psi
\end{aligned}\tag{4.32}$$

so that the variational formulation (4.21) takes the form

$$\int_{\mathcal{B}}\left[(1-\nu^2)\partial_1^2\varphi\partial_1^2\psi+\frac{1}{12}D_2^4\varphi D_2^4\psi\right]\mathrm{d}y^1\,\mathrm{d}z^2=-\int_{\mathcal{B}}F_3(y^1)D_2^2\psi\,\mathrm{d}y^1\,\mathrm{d}z^2\quad\forall\psi\in\overline{\mathcal{V}},\tag{4.33}$$

where, as before (see (2.7)),

$$F_3(y^1)=\frac{1-\nu^2}{E}f_3(y^1,0).$$

We then may use (4.33) as the variational formulation of the limit problem in a space $\overline{\mathcal{V}}$ which is the completion of the space $\mathcal{V}$ of the smooth functions, vanishing in a vicinity of $y=+\infty$ (or quickly decreasing at infinity) which satisfy the boundary kinematic conditions (in terms of φ) with the norm

$$\|\psi\|^2=\int_{\mathcal{B}}\left[(\partial_1^2\psi)^2+\frac{1}{12}(D_2^4\psi)^2\right]\mathrm{d}y^1\,\mathrm{d}z^2.\tag{4.34}$$

The solution U must satisfy all the boundary conditions, namely the kinematic conditions on Γ_0:

$$\begin{aligned}
&V_1^1(0,z^2)=V_2^1(0,z^2)=V_3^1(0,z^2)=0,\\
&\partial_1V_3^1(0,z^2)=0
\end{aligned}$$

and the dynamic conditions on Γ_1:

$$
\begin{aligned}
&T^{11}n_1 + T^{12}n_2 = 0,\\
&T^{12}n_1 + T^{22}n_2 + 2\varepsilon^2\big(M^{12}n_1 + M^{22}n_2\big) = 0,\\
&\varepsilon^2\big\{-n_1\partial_1 M^{11} - 2n_2\partial_1 M^{12} - n_2\partial_2 M^{22} - \partial_t\big(n_1 t_1 M^{11} + 2n_1 t_2 M^{12} + n_2 t_2 M^{22}\big)\big\} = 0,\\
&\varepsilon^2\big[M^{11}n_1 n_1 + 2M^{12}n_1 n_2 + M^{22}n_2 n_2\big] = 0
\end{aligned}
$$

which become, in the case considered here:

$$
\left.
\begin{aligned}
&-T^{12} = 0,\\
&-\big(T^{22} + 2\varepsilon^2 M^{22}\big) = 0,\\
&\varepsilon^2\big(-2\partial_1 M^{12} - \delta^{-1} D_2 M^{22}\big) = 0,\\
&\varepsilon^2 M^{22} = 0,
\end{aligned}
\right\}
\quad \text{on } z^2 = 0,
$$

and

$$
\left.
\begin{aligned}
&T^{11} = 0,\\
&T^{12} + 2\varepsilon^2 M^{12} = 0,\\
&\varepsilon^2\big[-\partial_1 M^{11} - 2\delta^{-1} D_2 M^{12}\big] = 0,\\
&\varepsilon^2 M^{11} = 0,
\end{aligned}
\right\}
\quad \text{on } y^1 = l_1
$$

where

$$
\begin{aligned}
T^{11} &= \frac{E}{1-\nu^2}\big(\delta^{-2}\partial_1 U_1^1 + \cdots\big),\\
T^{12} &= \mathcal{O}\big(\delta^{-1}\big),\\
T^{22} &= \frac{E}{12(1-\nu^2)}\big(D_2^4 U_3^1 + \cdots\big),\\
M^{11} &= \frac{\nu E}{12(1-\nu^2)}\big(\delta^{-6} D_2^2 U_3^1 + \cdots\big),\\
M^{12} &= \frac{E}{12(1+\nu)}\big(\delta^{-5}\partial_1 D_2 U_3^1 + \cdots\big),\\
M^{22} &= \frac{E}{12(1-\nu^2)}\big(\delta_1^{-6} D_2^2 U_3^1 + \cdots\big).
\end{aligned}
$$

We then have the kinematic boundary conditions satisfied by φ and ψ:

$$
\begin{aligned}
&\partial_1\psi\big(0, z^2\big) = D_2\psi\big(0, z^2\big) = 0,\\
&D_2^2\psi\big(0, z^2\big) = \partial_1 D_2\psi\big(0, z^2\big) = 0.
\end{aligned}
\tag{4.35}
$$

As ψ is, according to (4.32), a potential defined up to an additive constant, we may fix the constant and write

$$
\psi\big(0, z^2\big) = 0 \tag{4.36}
$$

which will be considered in the sequel. At least, the boundary conditions satisfied only by the solution φ are

$$
\begin{aligned}
&\partial_1^2\varphi\big(l_1, z^2\big) = 0 \quad \Leftrightarrow \quad T^{11}\big(l_1, z^2\big) = 0,\\
&\partial_1^3\varphi\big(l_1, z^2\big) = 0 \quad \Leftrightarrow \quad M^{11}\big(l_1, z^2\big) = 0,
\end{aligned}
\tag{4.37}
$$

$$
\begin{aligned}
&D_2^{(4)}\varphi\big(y^1, 0\big) = 0 \quad \Leftrightarrow \quad M^{22}\big(y^1, 0\big) = 0,\\
&D_2^{(5)}\varphi\big(y^1, 0\big) = 0 \quad \Leftrightarrow \quad D_2 M^{22}\big(y^1, 0\big) = 0,\\
&D_2^{(6)}\varphi\big(y^1, 0\big) - 12F_3\big(y^1\big) = 0 \quad \Leftrightarrow \quad T^{22}\big(y^1, 0\big) = 0,
\end{aligned}
\tag{4.38}
$$

$$
D_2^{(7)}\varphi\big(y^1, 0\big) = 0. \tag{4.39}
$$

The solution, if it exists, must satisfy the conditions (4.35)–(4.39).

To prove existence in the framework of the Lax–Milgram theorem, it is sufficient to show that the right-hand side is a linear and continuous functional on $\overline{\mathcal{V}}$

Let us define the space

$$W(0,\infty)=\left\{u;\, u\in L^2(0,\infty),\, D_2^4u\in L^2(0,\infty)\right\}$$

equipped with the norm

$$\|u\|_W^2=\int_0^\infty\left[|u|^2+\left|D_2^4u\right|^2\right]\mathrm{d}z^2 \tag{4.40}$$

then (Lions and Magenes, 1968, Vol. 1, p. 19, théorème 2.3) the functions $u',u'',u^{(3)}$ belong to $L^2(0,\infty)$ and we have the evident inclusions so that $W\equiv H^4(0,\infty)$ in which the traces exist and we have

$$\left|D_2u(0)\right|\leqslant C\|u\|_W\quad\forall u\in W. \tag{4.41}$$

The completion $\overline{\mathcal{V}}$ of $\mathcal{V}$ with the norm (4.34) gives, using the boundary conditions (4.41)

$$u\in H^2_{y^1}\left((0,l_1);L^2_{z^2}(0,\infty)\right)\Longrightarrow u\in L^2_{y^1}\left((0,l_1);L^2_{z^2}(0,\infty)\right),$$
$$D_2^4u\in L^2_{y^1}\left((0,l_1);L^2_{z^2}(0,\infty)\right)$$

from which we deduce

$$u\in L^2_{y^1}\left((0,l_1);W(0,\infty)\right)$$

and consequently

$$V\subset L^2_{y^1}\left((0,l_1);W(0,\infty)\right)$$

so that

$$\|u\|_V\geqslant C\|u\|_{L^2_{y^1}((0,l_1);W(0,\infty))}\quad\forall u\in\mathcal{V}. \tag{4.42}$$

Then, let us consider the functional $\tilde{f_3}\int_{\mathcal{B}}V_3\,\mathrm{d}y^1\,\mathrm{d}z^2$, using (4.41) we get

$$\begin{aligned}\left|\tilde{f_3}\int_{\mathcal{B}}V_3\,\mathrm{d}y^1\,\mathrm{d}z^2\right| &= \left|\tilde{f_3}\int_{\mathcal{B}}D_2^2\psi\,\mathrm{d}y^1\,\mathrm{d}z^2\right|=\left|\tilde{f_3}\int_0^{l_1}-D_2\psi\left(y^1,0\right)\mathrm{d}y^1\right|\\ &\leqslant C_1\left(\int_0^{l_1}\left|D_2\psi\left(y^1,0\right)\right|^2\mathrm{d}y^1\right)^{1/2}\underset{(4.41)}{\leqslant}C_2\left(\int_0^{l_1}\|\psi\|_W^2\,\mathrm{d}y^1\right)^{1/2}\\ &= C_3\|\psi\|_{L^2_{y^1}((0,l_1);W(0,\infty))}\underset{(4.42)}{\leqslant}C\|\psi\|_{\mathcal{V}}\end{aligned}$$

which insures the existence and uniqueness of the solution by the Lax–Milgram theorem in $\overline{\mathcal{V}}$. □

We note that existence and uniqueness are proved in the space $\overline{\mathcal{V}}$. This implies in a generalized sense that φ tends to zero as $z^2\to+\infty$ (as, for fixed y^1, the functions are in W). This constitutes the matching with the region out of the layer.

4.5. Explicit solution in the boundary layer

The function $\varphi(y^1,z^2)$ is the unique solution of the equation

$$\left(1-\nu^2\right)\partial_1^4\varphi+\frac{1}{12}D_2^8\varphi=0 \tag{4.43}$$

with the boundary conditions (4.35)–(4.39). Let us search for a solution of the form

$$\varphi\left(y^1,z^2\right)=\sum_{k=1}^{\infty}\Psi_k\left(z^2\right)\Phi_k\left(y^1\right),$$

where the functions $\Phi_k(y^1)$ are the eigenfunctions which are solutions of

$$\left(1-\nu^2\right)\frac{\mathrm{d}^4\Phi_k}{(\mathrm{d}y^1)^4}=\lambda_k\Phi_k$$

with the boundary conditions on $y^1=0$ and $y^1=l_1$ so that the solution is of the form

$$\varphi\left(y^1,z^2\right)=\sum_{k=1}A_k\left(z^2\right)\cos\omega_k y^1+B_k\left(z^2\right)\cosh\omega_k y^1+C_k\left(z^2\right)\sin\omega_k y^1+D_k\sinh\omega_k y^1.$$

With the first boundary condition in (4.35) we have

$$\partial_1\varphi\left(0,z^2\right)=0\quad\Rightarrow\quad C_k\left(z^2\right)+D_k\left(z^2\right)=0$$

and from (4.36)

$$A_k\left(z^2\right)+B_k\left(z^2\right)=0.$$

Now, from the two conditions (4.37) we get the system

$$\begin{aligned}&\partial_1^2\varphi\left(l_1,z^2\right)=0\quad\Rightarrow\quad -A_k(\cos\omega_k l_1+\cosh\omega_k l_1)-C_k(\sin\omega_k l_1+\sinh\omega_k l_1)=0,\\&\partial_1^3\varphi\left(l_1,z^2\right)=0\quad\Rightarrow\quad A_k(\sin\omega_k l_1-\sinh\omega_k l_1)-C_k(\cos\omega_k l_1+\cosh\omega_k l_1)=0\end{aligned}$$

which has a non-trivial solution only if the ω_k satisfy the relation

$$\cos\omega_k l_1=\frac{-1}{\cosh\omega_k l_1}. \tag{4.44}$$

There exists a double infinity $\pm\omega_k$ of such values. One of the corresponding functions $A_k(z^2)$ or $C_k(z^2)$ is then arbitrary, for example $A_k(z^2)$, the other one is then

$$C_k\left(z^2\right)=-\frac{\cos\omega_k l_1+\cosh\omega_k l_1}{\sin\omega_k l_1+\sinh\omega_k l_1}A_k\left(z^2\right)\underset{\text{def}}{=}\Omega(\omega_k)A_k\left(z^2\right). \tag{4.45}$$

Consequently, the solution $\varphi(y^1,z^2)$ is of the form

$$\varphi\left(y^1,z^2\right)=\sum_{k=0}^{+\infty}A_k\left(z^2\right)\left[\cos\omega_k y^1-\cosh\omega_k y^1+\Omega(\omega_k)\left(\sin\omega_k y^1-\sinh\omega_k y^1\right)\right], \tag{4.46}$$

where the coefficients $A_k(z^2)$ are the solutions of the equations

$$\left(1-\nu^2\right)\omega_k^4A_k+\frac{1}{12}\frac{\mathrm{d}^8A_k}{(\mathrm{d}z^2)^8}=0. \tag{4.47}$$

As we search for solutions which tend to zero as $z^2\to+\infty$, they are given by

$$A_k\left(z^2\right)=\sum_{p=2}^{5}B_{kp}\exp\left(\mathrm{e}^{\frac{(2p+1)i\pi}{8}}\Theta_k z^2\right),\quad\Theta_k=\left[12\left(1-\nu^2\right)\omega_k^4\right]^{1/8}, \tag{4.48}$$

where

$$\Theta_k=\left[12\left(1-\nu^2\right)\omega_k^4\right]^{1/8}. \tag{4.49}$$

At least, the solution φ is

$$\varphi\left(y^1,z^2\right)=\sum_{k=0}^{+\infty}\sum_{p=2}^{5}B_{kp}\exp\left(\mathrm{e}^{\frac{(2p+1)i\pi}{8}}\Theta_k z^2\right)\Psi_k\left(y^1\right),$$

where

$$\Psi_k\left(y^1\right)=\cos\omega_k y^1-\cosh\omega_k y^1+\Omega(\omega_k)\left(\sin\omega_k y^1-\sinh\omega_k y^1\right).$$

The boundary conditions

$$D_2^4\varphi\big(y^1,0\big)=0,$$
$$D_2^5\varphi\big(y^1,0\big)=0,$$
$$D_2^6\varphi\big(y^1,0\big)=12\alpha_k,$$
$$D_2^7\varphi\big(y^1,0\big)=0$$

allow us to determine for every k the four constants B_{kp}.

4.6. The characteristic boundary layer revisited. Lagrange multiplier and boundary conditions

We saw in Sections 4.2 and 4.3 that the leading terms of the solutions in the layers satisfy the constraints (4.16) and (4.18), accordingly the corresponding equations must involve two Lagrange multipliers. This was avoid in the previous sections by taking test functions satisfying themselves the constraints so that, taking account this constraints we obtained (4.31) and the equation (4.43) satisfied by the potential $\varphi(y^1,z^2)$ as well as the boundary conditions. We now consider again the case of the cylinder with a characteristic layer along the free boundary $y^2=0$. So that we consider the expansions (4.13) which give the new form of (4.15):

$$\begin{aligned}
&\int_{\mathcal{B}}\frac{E}{1-\nu^2}\big[\delta^{-4}\big(D_2U_2^1-U_3^1\big)+\delta^{-3}\big(D_2U_2^2-U_3^2\big)\big](D_2V_2-V_3)\\
&\quad+\int_{\mathcal{B}}\delta^{-2}\left\{\frac{E}{1-\nu^2}\big[D_2U_2^3-U_3^3+\nu\partial_1U_1^1\big](D_2V_2-V_3)+\frac{E}{1+\nu}\big(\partial_1U_2^1+D_2U_1^1\big)(\partial_1V_2+D_2V_1)\right\}\mathrm{d}y^1\,\mathrm{d}z^2\\
&\quad+\int_{\mathcal{B}}\delta^{-1}\left\{\frac{E}{1-\nu^2}\big(D_2U_2^4-U_3^4+\nu\partial_1U_1^2\big)(D_2V_2-V_3)+\frac{E}{1+\nu}\big(\partial_1U_2^2+D_2U_1^2\big)(\partial_1V_2+D_2V_1)\right\}\mathrm{d}y^1\,\mathrm{d}z^2\\
&\quad+\int_{\mathcal{B}}\left\{\frac{E}{1-\nu^2}\big(D_2U_2^5-U_3^5+\nu\partial_1U_1^3\big)(D_2V_2-V_3)+\frac{E}{1+\nu}\big(\partial_1U_2^3+D_2U_1^3\big)(\partial_1V_2+D_2V_1)\right.\\
&\quad\left.+\frac{\nu E}{1-\nu^2}\big(D_2U_2^3-U_3^3\big)\partial_1V_1+\frac{E}{1-\nu^2}\partial_1U_1^1\partial_1V_1\right\}\mathrm{d}y^1\,\mathrm{d}z^2+\int_{\mathcal{B}}\frac{1}{12}\frac{E}{1-\nu^2}D_2^2U_3^1D_2^2V_3\\
&=\int_{\mathcal{B}}f_3\big(y^1,0\big)V_3\,\mathrm{d}y^1\,\mathrm{d}z^2,
\end{aligned}$$

where the test functions are taken independent of η. We then immediately obtain at the leading orders δ^{-4} and δ^{-3}:

$$D_2U_2^1-U_3^1=0 \tag{4.50}$$

and

$$D_2U_2^2-U_3^2=0. \tag{4.51}$$

At order δ^{-2} we then obtain, taking $V_1=V_2=0$, V_3 arbitrary:

$$D_2U_2^3-U_3^3+\nu\partial_1U_1^1=0 \tag{4.52}$$

and, as $\partial_1V_2+D_2V_1$ is arbitrary,

$$\partial_1U_2^1+D_2U_1^1=0. \tag{4.53}$$

Then the terms of order δ^{-1} give, taking $V_1=V_2=0$, V_3 arbitrary

$$D_2U_2^4-U_3^4+\nu\partial_1U_1^2=0 \tag{4.54}$$

and, as $\partial_1V_2+D_2V_1$ is arbitrary,

$$\partial_1U_2^2+D_2U_1^2=0. \tag{4.55}$$

Now the terms of order $\mathcal{O}(1)$ are

$$\int_{\mathcal{B}} \left\{ \frac{E}{1-\nu^2}\left(D_2U_2^5 - U_3^5 + \nu\partial_1 U_1^3\right)(D_2V_2 - V_3) + \frac{E}{1+\nu}\left(\partial_1 U_2^3 + D_2U_1^3\right)(\partial_1 V_2 + D_2V_1) \right.$$
$$\left. + \frac{\nu E}{1-\nu^2}\left(D_2U_2^3 - U_3^3\right)\partial_1 V_1 + \frac{E}{1-\nu^2}\partial_1 U_1^1 \partial_1 V_1 \right\} \mathrm{d}y^1\,\mathrm{d}z^2 + \int_{\mathcal{B}} \frac{1}{12}\frac{E}{1-\nu^2} D_2^2U_3^1 D_2^2V_3\,\mathrm{d}y^1\,\mathrm{d}z^2$$
$$= \int_{\mathcal{B}} f_3\left(y^1, 0\right)V_3\,\mathrm{d}y^1\,\mathrm{d}z^2.$$

In the sequel it will prove useful to define the new unknowns $p(y^1, z^2)$ and $q(y^1, z^2)$ by

$$D_2U_2^5 - U_3^5 = p\left(y^1, z^2\right) \tag{4.56}$$

and

$$\partial_1 U_2^3 + D_2U_1^3 = q\left(y^1, z^2\right). \tag{4.57}$$

Then, taking V vanishing in neighborhoods of $y^1 = 0$ and $y^1 = l_1$, integrations by parts give

$$-(1-\nu)D_2q - (1+\nu)\partial_1^2 U_1^1 = 0, \tag{4.58}$$
$$-D_2p - (1-\nu)\partial_1 q - \nu\partial_1 D_2U_1^3 = 0, \tag{4.59}$$
$$-p - \nu\partial_1 U_1^3 + \frac{1}{12}D_2^4U_3^1 = F_3\left(y^1, 0\right). \tag{4.60}$$

Now, as V and D_2V_3 are arbitrary on Γ_1, we have the natural boundary conditions

$$\begin{aligned} &qn_2 + (1+\nu)\partial_1 U_1^1 n_1 = 0 \Rightarrow q = 0 \quad \text{on } y^2 = 0,\\ &pn_2 + (1-\nu)qn_1 + \nu\partial_1^3 U_1^3 n_2 = 0 \Rightarrow p + \nu\partial_1^3 U_1^3 = 0 \quad \text{on } y^2 = 0,\\ &D_2^2U_1^3 = 0 \quad \text{on } y^2 = 0,\\ &D_2^3U_1^3 = 0 \quad \text{on } y^2 = 0. \end{aligned} \tag{4.61}$$

Moreover, U^η satisfies the principal boundary conditions

$$\begin{aligned} &U^k\left(0, y^2\right) = 0,\\ &\partial_1 U_3^k\left(0, y^2\right) = 0 \end{aligned} \tag{4.62}$$

and the matching conditions

$$U^k\left(y^1, z^2\right) \underset{z^2\to+\infty}{\longrightarrow} 0. \tag{4.63}$$

Differentiating (4.60) with respect to z^2, we get

$$-D_2p - \nu D_2\partial_1 U_1^3 + \frac{1}{12}D_2^5U_3^1 = 0 \tag{4.64}$$

then, eliminating p between (4.59) and (4.64), we obtain

$$\sqrt{1-\nu}\partial_1 q + \frac{1}{12}D_2^5U_3^1 = 0 \tag{4.65}$$

now, taking account of (4.58), after differentiation with respect to z^2, (4.65) writes

$$-\frac{1}{12}D_2\left(D_2^5U_3^1\right) = \sqrt{1-\nu}D_2\partial_1 q = -\left(1-\nu^2\right)\partial_1^3 U_1^1 \tag{4.66}$$

and, from (4.50) and (4.53),

$$\frac{1}{12}D_2^2\left(-D_2^6U_3^1\right) = \left(1-\nu^2\right)\partial_1^3 D_2^2U_1^1 = \left(1-\nu^2\right)\partial_1^4 U_3^1$$

that is to say

$$\left(1-\nu^2\right)\partial_1^4 U_3^1 + \frac{1}{12}D_2^8U_3^1 = 0. \tag{4.67}$$

Equation (4.67) with the boundary conditions (4.62) and the matching condition (4.63) determines the component U_3^1 using calculations analogous to that of Section 4.5.

Once U_3^1 is known, we may determine q with (4.65), U_1^1 with (4.66) and U_1^3 with (4.64) and the appropriate boundary conditions.

The system (4.56)–(4.60) with the boundary conditions (4.62) and (4.63) constitutes the boundary layer problem with Lagrange multipliers. The solution (U_1^1, U_2^1, U_3^1) is obtained taking (V_1^1, V_2^1, V_3^1) arbitrarily so that the corresponding problem involves two new unknowns p and q which are the Lagrange multipliers of the problem. Indeed, let us denote by $\mathcal{L}$ the operator

$$\big(U_1^1, U_2^1, U_3^1\big) \overset{\mathcal{L}}{\to} \big(D_2U_2^1 - U_3^1, \partial_1 U_2^1 + D_2U_1^1\big) \tag{4.68}$$

which defines the constraints (4.50) and (4.53), the corresponding adjoint $\mathcal{L}^*$ is defined by

$$\mathcal{L}^*(p,q) = \big(-\sqrt{1-\nu}D_2q, -D_2p - \sqrt{1-\nu}\partial_1 q, -p\big) \tag{4.69}$$

which are precisely the terms in (p,q) in the system (4.56)–(4.60). We have the classical structure of a constrained problem with Lagrange multipliers (Brezzi and Fortin, 1991).

5. Case when the middle surface is a part of a circular cone

5.1. Setting of the problem

In the sequel we shall consider the cone $\mathcal{S}$ parametrized by the mapping Ψ:

$$\begin{aligned} &\Psi : \Omega \to \mathcal{S}, \\ &\big(y^1, y^2\big) \overset{\Psi}{\to} \big(y^1, \big(y^1-\alpha\big)\sin\big(2\pi y^2\big), \big(y^1-\alpha\big)\cos\big(2\pi y^2\big)\big), \quad \alpha > l_1. \end{aligned} \tag{5.1}$$

As before, we consider the domain $\Omega = (0,l_1)\times(0,l_2)$.

Of course, most of the previous reasoning are valid, but the elasticity coefficients as well as the geometric ones are no more constants, they are functions of the parameters y^1 and y^2. We give hereafter the main relationships:

5.1.1. Geometric quantities

$$\begin{aligned} &a^1 = \left(\frac{1}{2}, \frac{\sin(2\pi y^2)}{2}, \frac{\cos(2\pi y^2)}{2}\right), \\ &a^2 = \left(0, \frac{\cos(2\pi y^2)}{2\pi(y^1-\alpha)}, -\frac{\sin(2\pi y^2)}{2\pi(y^1-\alpha)}\right), \\ &a^3 = a_3 = \frac{1}{\sqrt{2}}\big(-1, \sin\big(2\pi y^2\big), \cos\big(2\pi y^2\big)\big), \\ &\det(a_{\alpha\beta}) = 8\pi^2\big(y^1-\alpha\big)^2, \\ &a^{11} = \frac{1}{2}, \qquad a^{12} = 0, \qquad a^{22} = \frac{1}{4\pi^2(y^1-\alpha)^2}, \\ &b_{11} = b_{12} = 0, \qquad b_{22} = \frac{-4\pi^2(y^1-\alpha)}{\sqrt{2}}, \\ &\Gamma_{22}^1 = -2\pi^2\big(y^1-\alpha\big), \qquad \Gamma_{12}^2 = \frac{1}{y^1-\alpha}, \qquad \Gamma_{11}^\alpha = \Gamma_{12}^1 = \Gamma_{22}^2 = 0, \\ &b_1^2 = b_2^1 = b_1^1 = 0, \qquad b_2^2 = \frac{-1}{\sqrt{2}(y^1-\alpha)}. \end{aligned} \tag{5.2}$$

For an isotropic and homogeneous material, according to (2.2), the elasticity coefficients $A_{\gamma\ \delta}^{\alpha\beta\lambda\mu}$ are the following expressions:

$$\begin{aligned} &A_{1\,1}^{1\,1\,1\,1} = 4\pi^4 Q, \qquad A_{1\,1}^{1\,2\,\alpha\alpha} = A_{1\,1}^{\alpha\alpha\,1\,2} = 0, \qquad A_{1\,1}^{2\,2\,2\,2} = \frac{Q}{(y^1-\alpha)^4}, \\ &A_{1\,1}^{1\,2\,1\,2} = \frac{(1-\nu)\pi^2 Q}{(y^1-\alpha)^2}, \qquad A_{1\,1}^{1\,1\,2\,2} = A_{1\,1}^{2\,2\,1\,1} = \frac{2\pi^2\nu Q}{(y^1-\alpha)^2}, \qquad A_{2\,2}^{\alpha\beta\lambda\mu} = \frac{1}{12}A_{1\,1}^{\alpha\beta\lambda\mu}, \end{aligned} \tag{5.3}$$

where

$$Q = \frac{E}{16\pi^4(1-\nu^2)}. \tag{5.4}$$

5.1.2. Equations of shells

From the previous section, the components of the strain tensor are:

$$\gamma_{11} = \partial_1 u_1, \tag{5.5}$$
$$\gamma_{12} = \frac{1}{2}(\partial_1 u_2 + \partial_2 u_1) - \Gamma_{12}^2 u_2, \tag{5.6}$$
$$\gamma_{22} = \partial_2 u_2 - \Gamma_{22}^1 u_1 - b_{22} u_3. \tag{5.7}$$

As for the components of the tensor of variation of curvature, they have the expressions

$$\rho_{11} = \partial_1^2 u_3, \tag{5.8}$$
$$\rho_{12} = \partial_1\partial_2 u_3 - \Gamma_{12}^2 \partial_2 u_3 + \partial_1\big(b_2^2 u_2\big) - \Gamma_{12}^2 b_2^2 u_2, \tag{5.9}$$
$$\rho_{22} = \partial_2^2 u_3 - \Gamma_{22}^1 \partial_1 u_3 - 2\pi^2 u_3 + \partial_2\big(b_2^2 u_2\big) + b_2^2 \partial_2 u_2. \tag{5.10}$$

In the present problem the equations (1.11) take the form:

$$\begin{aligned}
&-\big(\partial_\alpha T^{\alpha 1} + \Gamma_{12}^2 T^{11} + \Gamma_{22}^1 T^{22}\big) - \varepsilon^2 \Gamma_{22}^1 b_2^2 M^{22} = f^1 = 0,\\
&-\big(\partial_\alpha T^{\alpha 2} + 3\Gamma_{12}^2 T^{12}\big) - \varepsilon^2\big[\partial_\lambda\big(b_2^2 M^{2\lambda}\big) + b_2^2 \partial_\lambda M^{\lambda 2} + 5\Gamma_{12}^2 b_2^2 M^{12}\big] = f^2 = 0,\\
&-b_{22} T^{22} + \varepsilon^2\big[\partial_\alpha\partial_\beta M^{\alpha\beta} + 2\Gamma_{12}^2 \partial_2 M^{12} - 4\pi^2 M^{22} + \Gamma_{22}^1 \partial_1 M^{22}\big] = f_3,
\end{aligned} \tag{5.11}$$

where f_3 does not vanish on $y^2 = 0$ and where

$$\begin{aligned}
T^{11} &= A^{1111}\partial_1 u_1 + A^{1122}\big(\partial_2 u_2 - \Gamma_{22}^1 u_1 - b_{22} u_3\big),\\
T^{12} &= 2A^{1212}\left[\frac{1}{2}(\partial_1 u_2 + \partial_2 u_1) - \Gamma_{12}^2 u_2\right],\\
T^{22} &= A^{2211}\partial_1 u_1 + A^{2222}\big(\partial_2 u_2 - \Gamma_{22}^1 u_1 - b_{22} u_3\big),
\end{aligned} \tag{5.12}$$

$$\begin{aligned}
M^{11} &= \frac{1}{12}\big[A^{1111}\partial_1^2 u_3 + A^{1122}\big(\partial_2^2 u_3 - \Gamma_{22}^1 \partial_1 u_3 - 2\pi^2 u_3 + \partial_2\big(b_2^2 u_2\big) + b_2^2 \partial_2 u_2\big)\big]\\
M^{12} &= \frac{A^{1212}}{6}\big[\partial_1\partial_2 u_3 - \Gamma_{12}^2 \partial_2 u_3 + \partial_1\big(b_2^2 u_2\big) - \Gamma_{12}^2 b_2^2 u_2\big]\\
M^{22} &= \frac{1}{12}\big[A^{2211}\partial_1^2 u_3 + A^{2222}\big(\partial_2^2 u_3 - \Gamma_{22}^1 \partial_1 u_3 - 2\pi^2 u_3 + \partial_2\big(b_2^2 u_2\big) + b_2^2 \partial_2 u_2\big)\big].
\end{aligned} \tag{5.13}$$

5.1.3. Boundary conditions

On a clamped part Γ_0 of the boundary, the boundary conditions are:

$$\begin{aligned}
&u_1 = u_2 = u_3 = 0,\\
&\frac{\partial u_3}{\partial n} = 0
\end{aligned} \tag{5.14}$$

and on a free part Γ_1:

$$\begin{aligned}
&T^{1\alpha} n_\alpha = 0,\\
&T^{2\alpha} n_\alpha + 2\varepsilon^2 b_2^2 M^{2\beta} n_\beta = 0,\\
&\varepsilon^2\big[-\partial_t\big(M^{\alpha\beta} t_\alpha n_\beta\big) - \Gamma_{\alpha\beta}^{\lambda} M^{\alpha\beta} n_\lambda - \big(\partial_\beta M^{\alpha\beta}\big) n_\alpha\big] = 0,\\
&\varepsilon^2 M^{\alpha\beta} n_\alpha n_\beta = 0.
\end{aligned} \tag{5.15}$$

In the problem considered here we take $\Gamma_0 = \{y^1 = 0\}$, the part Γ_1 is then constituted by $y^1 = l_1$ on which $(n_1, n_2) = (1/|\mathbf{a}^1|, 0)$, $y^2 = 0$ with $(n_1, n_2) = (0, -1/|\mathbf{a}^2|)$ and $y^2 = l_2$ the normal of which is $(n_1, n_2) = (0, 1/|\mathbf{a}^2|)$.

5.2. Scaling in the layers. Method of exponential solutions

As an example, we only consider the characteristic layers when the characteristic is a part of Γ_1 on which $f_3 \neq 0$:

As in the Section 4, to describe the characteristic boundary layer along $y^2 = 0$, we determine the scaling by searching for solutions of the form

$$u^\varepsilon\big(y^1, y^2\big) = v^\varepsilon \mathrm{e}^{-i\xi_1 y^1 + \mu y^2} \tag{5.16}$$

with ξ_1 real of order unity and $|\mu| \to +\infty$. By substituting (5.16) in the homogeneous system associated with (5.11) with (5.12) and (5.13) we obtain a homogeneous system the determinant of which must vanish in order to have non-trivial solutions. The vanishing of the determinant

$$\begin{aligned}\Delta(\varepsilon) &= \begin{vmatrix} A^{1111}\xi_1^2 - A^{1212}\mu^2 & i\mu\xi_1(A^{1212} + A^{1122}) & -i\xi_1 b_{22}A^{1122} \\ i\xi_1\mu(A^{1212} + A^{1122}) & A^{1212}\xi_1^2 - \mu^2 A^{2222} & b_{22}A^{2222}\mu \\ i\xi_1 b_{22}A^{1122} & -b_{22}A^{2222}\mu & A^{2222}(b_{22})^2 + \frac{\varepsilon^2}{12}\mu^4 A^{2222} \end{vmatrix} \\ &= \Delta(0) + \frac{\varepsilon^2}{12}\mu^4 A^{2222} \begin{vmatrix} A^{1111}\xi_1^2 - A^{1212}\mu^2 & i\mu\xi_1(A^{1212} + A^{1122}) \\ i\mu\xi_1(A^{1212} + A^{1122}) & A^{1212}\xi_1^2 - A^{2222}\mu^2 \end{vmatrix}\end{aligned}$$

gives at the leading order

$$(b_{22})^2\big(A^{1111}A^{2222} - \big(A^{1122}\big)^2\big)\xi_1^2 + \frac{\varepsilon^2}{12}\big(A^{2222}\big)^2\mu^8 = 0$$

from which, as in Section 4, we see that $\mu = \mathcal{O}(\varepsilon^{-1/4})$ and consequently that the thickness of the boundary layer is of order $\varepsilon^{1/4}$. We obtain, as before the scaling (4.5) (with (4.4)) for the components of $\mathbf{u}^\varepsilon$.

5.3. Boundary layer along the characteristic $y^2 = 0$

As in the Section 4.2, we search for an asymptotic expansion of the form

$$\begin{aligned} u_1^\varepsilon &\cong \delta^{-2}U_1^1 + \delta^{-1}U_1^2 + \cdots, \\ u_2^\varepsilon &\cong \delta^{-3}U_2^1 + \delta^{-2}U_2^2 + \cdots, \\ u_3^\varepsilon &\cong \delta^{-4}U_3^1 + \delta^{-3}U_3^2 + \cdots. \end{aligned} \tag{5.17}$$

Then, from the formulas:

$$\begin{aligned} \gamma_{11} &= \delta^{-2}\partial_1 U_1^1 + \delta^{-1}\partial_1 U_1^2 + \cdots, \\ \gamma_{12} &= \sum_{k=0}^{\infty} \delta^{-3+k}\left[\frac{1}{2}\big(\partial_1 U_2^{k+1} + D_2 U_1^{k+1}\big) - \Gamma_{12}^2 U_2^{k+1}\right], \\ \gamma_{22} &= \sum_{k=0}^{\infty} \delta^{-4+k}\big[D_2 U_2^{k+1} - b_{22}U_3^{k+1} - \Gamma_{22}^1 U_1^{k-1}\big], \\ \rho_{22} &= \delta^{-6} D_2^2 U_3^1 + \cdots, \end{aligned}$$

where ρ_{11} and ρ_{12} were disregarded because do not appear at the retained orders and ρ_{22} is given by (1.6) in which the only significative term is $\rho_{22} = A_{22}^{2222}\partial_2^2 U_3^1$. After the scaling, we have for the variational formulation (1.8)

$$\begin{aligned} \int_{\mathcal{B}} \big\{ & A^{1111}\big(\delta^{-2}\partial_1 U_1^1 + \delta^{-1}\partial_1 U_1^2 + \cdots\big)\big(\delta^{-2}\partial_1 V_1^1 + \delta^{-1}\partial_1 V_1^2 + \cdots\big) \\ & + A^{1122}\big[\partial^{-4}\big(D_2 U_2^1 - b_{22}U_3^1\big) + \delta^{-3}\big(D_2 U_2^2 - b_{22}U_2^2\big) \\ & + \delta^{-2}\big(D_2 U_2^3 - b_{22}U_3^3 - \Gamma_{22}^1 U_1^1\big) + \cdots\big] \times \big(\delta^{-2}\partial_1 V_1^1 + \delta^{-1}\partial_1 V_1^2 + \cdots\big) \\ & + A^{2211}\big(\delta^{-2}\partial_1 U_1^1 + \delta^{-1}\partial_1 U_1^2 + \cdots\big) \times \big[\partial^{-4}\big(D_2 V_2^1 - b_{22}V_3^1\big) + \delta^{-3}\big(D_2 V_2^2 - b_{22}V_2^2\big) \\ & + \delta^{-2}\big(D_2 V_2^3 - b_{22}V_3^3 - \Gamma_{22}^1 V_1^1\big) + \cdots\big] \\ & + A^{1212}\big[\delta^{-3}\big(\partial_1 U_2^1 + D_2 U_1^1 - 2\Gamma_{12}^2 U_2^1\big) + \delta^{-2}\big(\partial_1 U_2^2 + D_2 U_1^2 - 2\Gamma_{12}^2 U_2^2\big) + \cdots\big] \end{aligned}$$

$$\times\left[\delta^{-3}\left(\partial_1 V_2^1 + D_2 V_1^1 - 2\Gamma_{12}^2 V_2^1\right) + \delta^{-2}\left(\partial_1 V_2^2 + D_2 V_1^2 - 2\Gamma_{12}^2 V_2^2\right)\right]$$
$$+ A^{2222}\left[\delta^{-4}\left(D_2 U_2^1 - b_{22} U_3^1\right) + \delta^{-3}\left(D_2 U_2^2 - b_{22} U_3^2\right)\right.$$
$$\left.+ \delta^{-2}\left(D_2 U_2^3 - b_{22} U_3^3 - \Gamma_{22}^1 U_1^1\right) + \cdots\right] \times \left[\delta^{-4}\left(D_2 V_2^1 - b_{22} V_3^1\right) + \delta^{-3}\left(D_2 V_2^2 - b_{22} V_3^2\right)\right.$$
$$\left.+ \delta^{-2}\left(D_2 V_2^3 - b_{22} V_3^3 - \Gamma_{22}^1 V_1^1\right) + \cdots\right]\Big\}\,\mathrm{d}y^1\delta\,\mathrm{d}z^2$$
$$+ \varepsilon^2 \int_{\mathcal{B}} \frac{A^{2222}}{12}\delta^{-12} D_2^2 U_3^1 D_2^2 V_3^1\,\mathrm{d}y^1\delta\,\mathrm{d}z^2 = \int_{\mathcal{B}} f_3\left(y^1, 0\right)\delta^{-4} V_3^1\,\mathrm{d}y^1\delta\,\mathrm{d}z^2.$$

As in Section 4.2 at the leading order δ^{-7} we have

$$\int_{\mathcal{B}} A^{2222}\left(D_2 U_2^1 - b_{22} U_3^1\right)\left(D_2 V_2^1 - b_{22} V_3^1\right)\mathrm{d}y^1\,\mathrm{d}z^2 = 0$$

from which we obtain as in Section 4.3

$$D_2 U_2^1 - b_{22}\left(y^1\right) U_3^1 = 0. \tag{5.18}$$

At the next order δ^{-5} taking V satisfying (5.18) we have

$$\int_{\mathcal{B}}\left[A^{1212}\left(\partial_1 U_2^1 + D_2 U_1^1 - 2\Gamma_{12}^2 U_2^1\right)\left(\partial_1 V_2^1 + D_2 V_1^1 - 2\Gamma_{12}^2 V_2^1\right)\right.$$
$$\left.+ A^{2222}\left(D_2 U_2^2 - b_{22} U_3^2\right)\left(D_2 V_2^2 - b_{22} V_3^2\right)\right]\mathrm{d}y^1\,\mathrm{d}z^2 = 0$$

which, as in Section 4.3, gives

$$D_2 U_2^2 - b_{22} U_3^2 = 0 \tag{5.19}$$

and, by taking V satisfying (5.19):

$$\partial_1 U_2^1 + D_2 U_1^1 - 2\Gamma_{12}^2 U_2^1 = 0. \tag{5.20}$$

Now, taking V satisfying (5.20) and taking account of $\varepsilon^2 = \delta^8$, at the next order δ^{-3} we get

$$\int_{\mathcal{B}}\left\{A^{1111}\partial_1 U_1^1\partial_1 V_1^1 + A^{1122}\left(D_2 U_2^3 - b_{22} U_3^3 - \Gamma_{22}^1 U_1^1\right)\partial_1 V_1^1\right.$$
$$+ A^{2211}\partial_1 U_1^1\left(D_2 V_2^3 - b_{22} V_3^3 - \Gamma_{22}^1 V_1^1\right)$$
$$+ A^{1212}\left(\partial_1 U_2^2 + D_2 U_1^2 - 2\Gamma_{12}^2 U_2^2\right)\left(\partial_1 V_2^2 + D_2 V_1^2 - 2\Gamma_{12}^2 V_2^2\right)$$
$$\left.+ A^{2222}\left(D_2 U_2^3 - b_{22} U_3^3 - \Gamma_{22}^1 U_1^1\right)\left(D_2 V_2^3 - b_{22} V_3^3 - \Gamma_{22}^1 V_1^1\right) + \frac{A^{2222}}{12} D_2^2 U_3^1 D_2^2 V_3^1\right\}$$
$$= \int_{\mathcal{B}} f_3\left(y^1, 0\right) V_3^1\,\mathrm{d}y^1\,\mathrm{d}z^2.$$

If we take $V^1 = V_2^3 = V_3^3 = 0$ and arbitrary V_1^2 and V_2^2 then we obtain

$$\partial_1 U_2^2 + D_2 U_1^2 - 2\Gamma_{12}^2 U_2^2 = 0. \tag{5.21}$$

Now, with V satisfying (5.21), $V_1^1 = V_3^1 = V_2^3 = 0$ and arbitrary V_3^3, we get

$$A^{2222}\left(D_2 U_2^3 - b_{22} U_3^3 - \Gamma_{22}^1 U_1^1\right) + A^{2211}\partial_1 U_1^1 = 0. \tag{5.22}$$

Finally, with V satisfying (5.22), the variational formulation of the problem in the boundary layer takes the form

$$\int_{\mathcal{B}}\left[\frac{A^{1111}A^{2222} - (A^{1122})^2}{A^{2222}}\partial_1 U_1^1\partial_1 V_1^1 + \frac{A^{2222}}{12} D_2^2 U_3^1 D_2^2 V_3^1\right]\mathrm{d}y^1\,\mathrm{d}z^2 = \int_{\mathcal{B}} f_3\left(y^1, 0\right) V_3^1\,\mathrm{d}y^1\,\mathrm{d}z^2. \tag{5.23}$$

The structure is exactly the same as in (4.34) but now the coefficients depend on y^1. The solution should be obtained as in Sections 4.4 and 4.5. To obtain the equation analogous to (4.43), we need other relations, they are obtained by considering the system (5.11). The last equation

$$-b_{22}T^{22}+\varepsilon^2\big[\partial_\alpha\partial_\beta M^{\alpha\beta}+2\Gamma_{12}^2\partial_2 M^{12}-4\pi^2M^{22}+\Gamma_{22}^1\partial_1 M^{22}\big]=f_3$$

writes

$$-b_{22}\big[A^{2211}\partial_1u_1+A^{2222}\big(\partial_2u_2-\Gamma_{22}^1u_1-b_{22}u_3\big)\big]+\varepsilon^2\frac{A^{2222}}{12}\partial_2^2u_2+\cdots=f_3. \tag{5.24}$$

The asymptotic expansion of (5.24), taking account of (5.18)–(5.22), gives

$$D_2U_2^4-b_{22}U_3^4-\Gamma_{22}^1U_1^2=-\frac{A^{2211}}{A^{2222}}\partial_1U_1^2, \tag{5.25}$$

$$D_2U_2^5-b_{22}U_3^5-\Gamma_{22}^1U_1^3=-\frac{A^{2211}}{A^{2222}}\partial_1U_1^3+\frac{1}{12b_{22}}D_2^4U_3^1-\frac{f_3(y^1,0)}{b_{22}A^{2222}}. \tag{5.26}$$

The two first equations (5.11) write

$$\begin{aligned}&\partial_1T^{11}+\partial_2T^{12}+\Gamma_{12}^2T^{11}+\Gamma_{22}^1T^{22}=0,\\&\partial_1T^{12}+3\Gamma_{12}^2T^{12}+\partial_2T^{22}=0\end{aligned} \tag{5.27}$$

and their asymptotic expansions give

$$\begin{aligned}&\partial_1\big\{A^{1111}\big(\delta^{-2}\partial_1U_1^1+\delta^{-1}\partial_1U_1^2+\delta^0\partial_1U_1^3+\cdots\big)\\&\quad+A^{1122}\big[\delta^{-2}\big(D_2U_2^3-b_{22}U_3^3-\Gamma_{22}^1U_1^1\big)\big\}+\delta^{-1}\big(D_2U_2^4-b_{22}U_3^4-\Gamma_{22}^1U_1^2\big)+\cdots\big]\\&\quad+\delta^{-1}A^{1212}D_2\big[\delta^{-1}\big(\partial_1U_2^3+D_2U_1^3-2\Gamma_{12}^2U_2^3\big)\\&\quad+\Gamma_{12}^2A^{1111}\big(\delta^{-2}\partial_1U_1^1+\delta^{-1}\partial_1U_1^2+\delta^0\partial_1U_1^3+\cdots\big)\\&\quad+A^{1122}\big[\delta^{-2}\big(D_2U_2^3-b_{22}U_3^3-\Gamma_{22}^1U_1^1\big)+\delta^{-1}\big(D_2U_2^4-b_{22}U_3^4-\Gamma_{22}^1U_1^2\big)+\cdots\big]\\&\quad+\Gamma_{22}^1\big\{A^{2211}\big(\delta^{-2}\partial_1U_1^1+\delta^{-1}\partial_1U_1^2+\delta^0\partial_1U_1^3+\cdots\big)\\&\quad+A^{2222}\big[\delta^{-2}\big(D_2U_2^3-b_{22}U_3^3-\Gamma_{22}^1U_1^1\big)\big\}+\delta^{-1}\big(D_2U_2^4-b_{22}U_3^4-\Gamma_{22}^1U_1^2\big)+\cdots\big]=0,\\&\partial_1A^{1212}\big[\delta^{-1}\big(\partial_1U_2^3+D_2U_1^3-2\Gamma_{12}^2U_2^3\big)+\cdots\big]\\&\quad+3\Gamma_{12}^2A^{1212}\big[\delta^{-3}\big(\partial_1U_2^3+D_2U_1^3-2\Gamma_{12}^2U_2^3\big)+\delta^{-2}\big(\partial_1U_2^4+D_2U_1^4-2\Gamma_{12}^2U_2^4\big)+\cdots\big]\\&\quad+\delta^{-1}D_2\big\{A^{2211}\big(\delta^{-2}\partial_1U_1^1+\delta^{-1}\partial_1U_1^2+\cdots\big)+A^{2222}\big[\delta^{-2}\big(D_2U_2^3-b_{22}U_3^3-\Gamma_{22}^1U_1^1\big)\\&\quad+\delta^{-1}\big(D_2U_2^4-b_{22}U_3^4-\Gamma_{22}^1U_1^2\big)\big]\big\}+\varepsilon^2\delta^{-8}\frac{A^{2222}}{12}D_2^4U_3^1=f_3\big(y^1,0\big).\end{aligned}$$

In the first equation, the successive terms are:

$$D_2\big(\partial_1U_2^3+D_2U_1^3-2\Gamma_{12}^2U_2^3\big)=-\frac{C^{1111}}{A^{1212}}\big(\partial_1^2U_1^1+\Gamma_{12}^2\partial_1U_1^1\big) \tag{5.28}$$

in δ^{-2} where

$$C^{1111}=A^{1111}-\frac{(A^{1122})^2}{A^{2222}}=\text{Const.} \tag{5.29}$$

and

$$D_2\big(\partial_1U_2^4+D_2U_1^4-2\Gamma_{12}^2U_2^4\big)=-\frac{C^{1111}}{A^{1212}}\big(\partial_1^2U_1^2+\Gamma_{12}^2\partial_1U_1^2\big) \tag{5.30}$$

in δ^{-1}.

In the second equation we have:

$$D_2\big[A^{1122}\partial_1U_1^2+A^{2222}\big(D_2U_2^4-b_{22}U_3^4-\Gamma_{22}^1U_1^2\big)\big]=0 \tag{5.31}$$

in δ^{-2} and

$$\partial_1\big[A^{1212}\big(\partial_1 U_2^3 + D_2 U_1^3 - 2\Gamma_{12}^2 U_2^3\big) + 3\Gamma_{12}^2 A^{1212}\big(\partial_1 U_2^3 + D_2 U_1^3 - 2\Gamma_{12}^2 U_2^3\big)\big] = -\frac{A^{2222}}{12b_{22}} D_2^6 U_3^1 \tag{5.32}$$

in δ^{-1}.

Then, by differentiating (5.32) with respect to z^2 we obtain, taking account of (5.28)

$$-C^{1111}\partial_1\big(\partial_1^2 U_1^1 + \Gamma_{12}^2 \partial_1 U_1^1\big) - 3\Gamma_{12}^2 C^{1111}\big(\partial_1^2 U_1^1 + \Gamma_{12}^2 \partial_1 U_1^1\big) = -\frac{A^{2222}}{12b_{22}} D_2^8 U_3^1.$$

At least, differentiating twice with respect to z^2, we get the equation in the boundary layer

$$C^{1111}\big(\partial_1 + 3\Gamma_{12}^2\big)\big(\partial_1^2 + \Gamma_{12}^2\partial_1\big)(\partial_1 - 2\Gamma_{12}^2)U_3^1 + \frac{A^{2222}}{12b_{22}} D_2^8 U_3^1 = 0. \tag{5.33}$$

6. Case when $\mathcal{S}$ is a general developable surface

6.1. Asymptotic expansions

For a general developable surface, the equation of which is of the form $\mathbf{r}(y^1, y^2) = \boldsymbol{\rho}(y^2) + y^1\mathbf{e}(y^2)$ where $\mathbf{e}$ is a unit vector and with $b_{12} = 0$, we have

$$\Gamma_{11}^{\alpha} = 0, \qquad b_{22} \neq 0, \qquad \text{the other } b_{\alpha\beta} = 0. \tag{6.1}$$

Consequently

$$\begin{aligned}
\gamma_{11} &= \partial_1 u_1,\\
\gamma_{12} &= \frac{1}{2}(\partial_1 u_2 + \partial_2 u_1) - \Gamma_{12}^1 u_1 - \Gamma_{12}^2 u_2,\\
\gamma_{22} &= \partial_2 u_2 - \Gamma_{22}^1 u_1 - \Gamma_{22}^2 u_2 - b_{22} u_3
\end{aligned} \tag{6.2}$$

with ρ_{22} given by (1.6) but in the layer the only significative term is $\rho_{22} = A_{2\,2}^{2222}\partial_2^2 u_3$.

Moreover, for a general geometry, the coefficients of elasticity A^{1211} and A^{1222} do not vanish and the variational formulation of the shell problem writes

$$\begin{aligned}
&\int_\Omega \big\{A_{1\,1}^{1111}\partial_1 u_1 \partial_1 v_1 + A_{1\,1}^{1211}\partial_1 u_1\big(\partial_1 v_2 + \partial_2 v_1 - 2\Gamma_{12}^1 v_1 - 2\Gamma_{12}^2 v_2\big)\\
&\quad + A_{1\,1}^{2211}\partial_1 u_1\big(\partial_2 v_2 - \Gamma_{22}^1 v_1 - \Gamma_{22}^2 v_2 - b_{22} v_3\big)\\
&\quad + A_{1\,1}^{1112}\big(\partial_1 u_2 + \partial_2 u_1 - 2\Gamma_{12}^1 u_1 - 2\Gamma_{12}^2 u_2\big)\partial_1 v_1\\
&\quad + A_{1\,1}^{1212}\big(\partial_1 u_2 + \partial_2 u_1 - 2\Gamma_{12}^1 u_1 - 2\Gamma_{12}^2 u_2\big)\big(\partial_1 v_2 + \partial_2 v_1 - 2\Gamma_{12}^1 v_1 - 2\Gamma_{12}^2 v_2\big)\\
&\quad + A_{1\,1}^{2212}\big(\partial_1 u_2 + \partial_2 u_1 - 2\Gamma_{12}^1 u_1 - 2\Gamma_{12}^2 u_2\big)\big(\partial_2 v_2 - \Gamma_{22}^1 v_1 - \Gamma_{22}^2 v_2 - b_{22} v_3\big)\\
&\quad + A^{1222}\big(\partial_2 u_2 - \Gamma_{22}^1 u_1 - \Gamma_{22}^2 u_2 - b_{22} u_3\big)\big(\partial_1 v_2 + \partial_2 v_1 - 2\Gamma_{12}^1 v_1 - 2\Gamma_{12}^2 v_2\big)\\
&\quad + A_{1\,1}^{1122}\big(\partial_2 u_2 - \Gamma_{22}^1 u_1 - \Gamma_{22}^2 u_2 - b_{22} u_3\big)\partial_1 v_1\\
&\quad + A_{1\,1}^{2222}\big(\partial_2 u_2 - \Gamma_{22}^1 u_1 - \Gamma_{22}^2 u_2 - b_{22} u_3\big)\big(\partial_2 v_2 - \Gamma_{22}^1 v_1 - \Gamma_{22}^2 v_2 - b_{22} v_3\big)\big\}\,\mathrm{d}y^1\,\mathrm{d}y^2\\
&\quad + \varepsilon^2 \int_\Omega A_{2\,2}^{2222}\partial_2^2 u_3 \partial_2^2 v_3\,\mathrm{d}y^1\,\mathrm{d}y^2 = \int_\Omega f_3 v_3\,\mathrm{d}y^1\,\mathrm{d}y^2.
\end{aligned} \tag{6.3}$$

By substituting the asymptotic expansions (5.17) and the Taylor expansions of the coefficients, we obtain, at the successive orders, as in the previous sections, the constraints

$$D_2 U_2^1 - \tilde{b}_{22} U_3^1 = 0, \tag{6.4}$$

$$D_2 U_2^2 - \tilde{\Gamma}_{22}^2 U_2^1 - \tilde{b}_{22} U_3^2 - z^2 \tilde{b}_{22,2} U_3^1 = 0, \tag{6.5}$$

$$\partial_1 U_2^1 + D_2 U_1^1 - 2\tilde{\Gamma}_{12}^2 U_2^1 = 0, \tag{6.6}$$

where $\tilde{b}$ and $\tilde{\Gamma}$ are $b(y^1,0)$ and $\Gamma(y^1,0)$ respectively, then taking account of (6.4)–(6.6) we obtain

$$\tilde{A}^{1212}\big(\partial_1 U_2^2 + D_2 U_1^2 - 2\tilde{\Gamma}_{12}^1 U_1^1 - 2\tilde{\Gamma}_{12}^2 U_2^2 - z^2\tilde{\Gamma}_{12,2}^2 U_2^1\big) = -2\tilde{A}^{1211}\partial_1 U_1^1, \tag{6.7}$$

$$\tilde{A}^{2222}\big(D_2 U_2^3 - \tilde{\Gamma}_{22}^1 U_1^1 - \tilde{b}_{22} U_3^3 - \tilde{\Gamma}_{22}^2 U_2^2\big) = \frac{-\tilde{A}^{1122}\tilde{A}^{1212} + \tilde{A}^{1112}\tilde{A}^{1222}}{\tilde{A}^{1212}}\partial_1 U_1^1 \tag{6.8}$$

from which the variational formulation follows:

$$\int_{\mathcal{B}} \big[\tilde{B}^{1111}\partial_1 U_1^1 \partial_1 V_1^1 + \tilde{A}_{22}^{2222} D_2^2 U_3^1 D_2^2 V_3^1\big]\,\mathrm{d}y^1\,\mathrm{d}z^2 = \int_{\mathcal{B}} f_3\big(y^1,0\big)V_3^1\,\mathrm{d}y^1\,\mathrm{d}z^2, \tag{6.9}$$

where the coefficient B^{2222} has the complicated expression

$$\begin{aligned}\tilde{B}^{1111} = {} & \frac{\tilde{A}^{1111}\tilde{A}^{2222} - (\tilde{A}^{1122})^2}{\tilde{A}^{2222}} - \frac{(\tilde{A}^{1122})^2}{\tilde{A}^{1212}} + \frac{\tilde{A}^{1122}\tilde{A}^{1112}\tilde{A}^{1222}}{\tilde{A}^{1212}\tilde{A}^{2222}} \\ & - \frac{\tilde{A}^{1222}\tilde{A}^{1112}}{(\tilde{A}^{1212})^2\tilde{A}^{2222}}\big(-\tilde{A}^{1122}\tilde{A}^{1212} + \tilde{A}^{1112}\tilde{A}^{1222}\big).\end{aligned} \tag{6.10}$$

Again the equation (6.9) as the same structure as in the previous sections. The advantage of the last expressions is that they apply for any material not necessarily isotropic and for any middle surface which is developable.

6.2. Application of the criterion of the Section 3.3 for a shell with middle surface which is developable

We now use a criterion analogous to theorem 3.3. The integrations are performed on the surface $\mathcal{S}$ using covariant derivatives (we may refer to (Lions and Sanchez Palencia, 1998))

Theorem 6.1. *Let us consider a shell the middle surface of which is developable and such that $b_{22} \neq 0$. If the loading* **f** *is such that $f_1 = f_2 = 0$, $f_3 \neq 0$ piecewise smooth with a discontinuity along a part of a generator then* $\mathbf{f} \notin V_m'$.

Proof. The shell equations in term of the strain components write

$$-D_{\alpha\beta}T^{\alpha\beta} = 0,$$
$$-b_{22}T^{22} = f_3,$$

where, as the surface is developable, $\tilde{\Gamma}_{11}^{\alpha} = 0$. The last equation immediately gives

$$T^{22} = -\frac{f_3}{b_{22}}$$

then, if we suppose $y^2 \in [-l_2, +l_2]$, $y^1 \in [0, l_1]$ and $f_3(y^1, y^2) = F(y^1)Y(y^2)$ where $Y(y^2)$ is the Heaviside function, we have

$$T^{22} = -\frac{F(y^1)Y(y^2)}{b_{22}},$$
$$-D_1 T^{11} - D_2 T^{12} = 0,$$
$$\partial_1 T^{12} - 3\Gamma_{12}^2 T^{12} = \frac{F(y^1)}{b_{22}}\delta\big(y^2\big) + \big(\Gamma_{12}^1 + 2\Gamma_{22}^2\big)\frac{F(y^1)Y(y^2)}{b_{22}}.$$

The second equation is a differential equation with respect to y^1 with parameter y^2 the solution of which is classically

$$T^{12} = \delta\big(y^2\big)\Phi\big(y^1, y^2\big) + \Psi\big(y^1, y^2\big) + K\big(y^2\big),$$

where

$$\Phi(y^1, y^2) \underset{\text{definition}}{\equiv} \int_0^{y^1} \exp\left(-\int_0^{\eta} 3\Gamma_{12}^2\big(\xi, y^2\big)\,\mathrm{d}\xi\right)\frac{F(\eta)}{b_{22}}\,\mathrm{d}\eta$$

and

$$\Psi\left(y^1, y^2\right) \underset{\text{definition}}{\equiv} Y\left(y^2\right) \int_0^{y^1} \exp\left(- \int_0^{\eta} 3\Gamma_{12}^2\left(\xi, y^2\right) \mathrm{d}\xi \right) \left(\Gamma_{12}^1 + 2\Gamma_{22}^2\right) \frac{F(\eta)}{b_{22}} \, \mathrm{d}\eta.$$

Clearly, $\Psi \in L^2((0, l_1) \times (-l_2, l_2))$, $\Phi \in L^2((0, l_1), H^{-1}(-l_2, l_2))$ and $K \in H^{-1}(-l_2, l_2)$. As the function Φ depends on y^1 and K is only a function of y^2, the solution T^{12} cannot belong to $L^2(\Omega)$ and the theorem is proved.

7. Numerical simulations

In this section, we present some numerical simulations concerning the case considered in Sections 5 (where the middle surface is a part of a cone) for various boundary conditions and loadings. The numerical computations are implemented with Hermite finite elements. The exact numerical integration of the rigidity matrices needs six Gauss points. In this case, the error estimate is of order $\mathcal{O}(h^3)$ see (Bernadou, 1994). The developable surface $\mathcal{S}$ is the cone parametrized by (5.1) where $\Omega = (0, 1) \times (0, 1/2)$, the image of the mapping is shown in Fig. 1. We recall that the generators are $y^2 = \text{Const}$.

The meshes for the domain Ω are generated using the Modulef code. The mesh is obtained by symmetry from the basic rectangular domain $(0, 1) \times (0, 1/4)$ around $y^2 = 1/4$, this will allow us to perform the refinement of the mesh in the vicinity of the layers.

In the sequel, we shall compare the results obtained with a uniform mesh and a non uniform one. For the uniform mesh (Fig. 2), the basic rectangle is divided in $N \times M$ rectangles where N and M are the number of divisions along the axes y^1 and y^2 respectively, each rectangle is divided in in four triangles. For the non-uniform mesh, we use a function of distribution of the points according to a geometric progression with ratio q (see Fig. 3: refined mesh in the vicinity of the boundary and internal layers which will be considered in the sequel).

The value of the small parameter ε is taken equal to 10^{-3} and the external forces are successively

$$Y\left(y^\alpha\right) = \begin{cases} 1 & \text{if } y^\alpha > 0, \\ 0 & \text{if } y^\alpha < 0. \end{cases}$$

We shall focus our attention on the characteristic boundary and internal layers which are more significative than the non-characteristic ones.

7.1. Characteristic boundary layers

Let us consider the loading $\mathbf{f}_1$ (see Table 1). The boundary is clamped along $y^1 = l_1 = 1$ and the rest of the boundary is free. As a consequence, the normal component f_3 does not vanish on the characteristic free boundaries $y^2 = 0$ and $y^2 = l_2 = 1/2$. Consequently, taking an uniform mesh, we must refine it sufficiently in order to obtain a good approximation of the boundary layers in the vicinity of $y^1 = 1$ and $y^2 = 1/2$. In fact, we have to take at least $N = 11$ and $M = 21$ (i.e. $h_{y^2} = 1/40$, that is

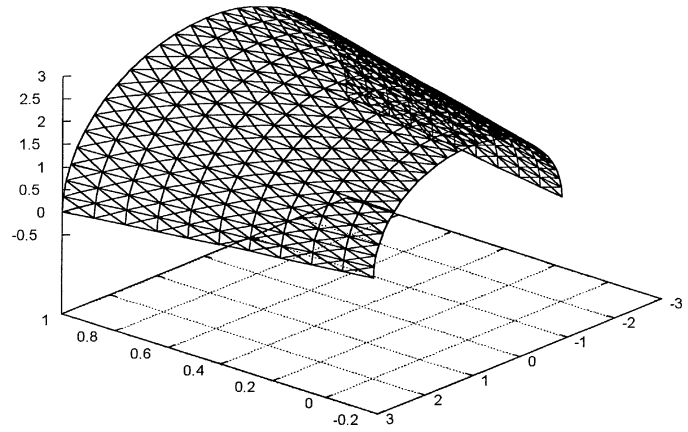

Fig. 1. Mapping of the cone of Section 5.1: $\Omega = (0, 1) \times (0, 0.5)$, $x = y^1$, $y = (y^1 + 2)\sin 2\pi y^2$, $z = (y^1 + 2)\cos 2\pi y^2$.

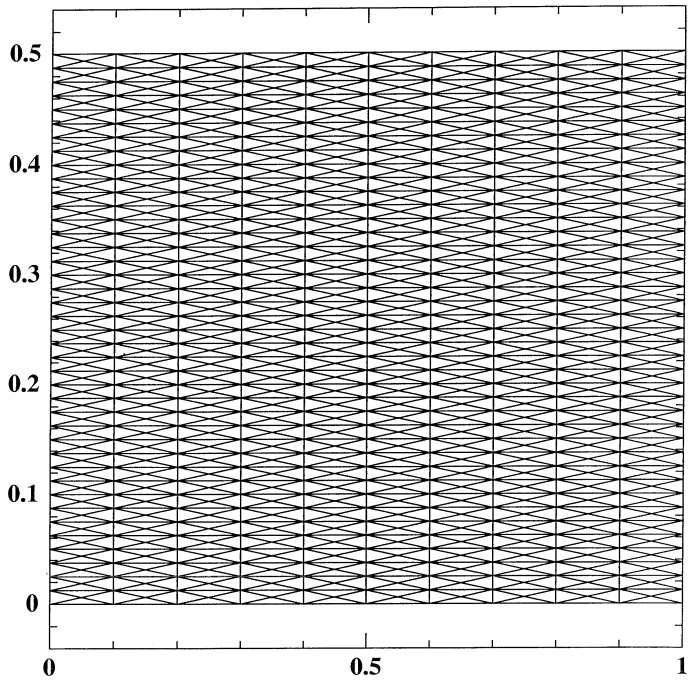

Fig. 2. Uniform mesh.

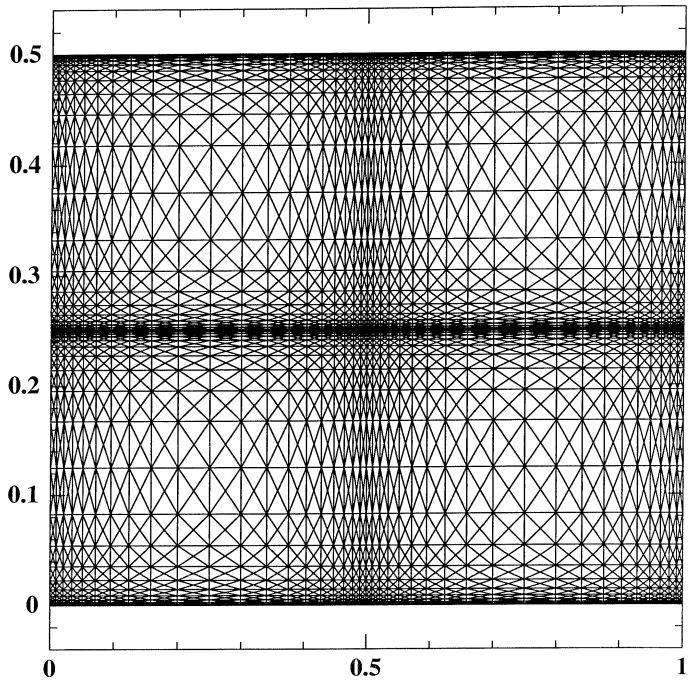

Fig. 3. Non-uniform anisotropic mesh.

to say 7659 degrees of freedom). Whereas, using a non uniform mesh (refined in the vicinity of the boundaries with elongated mesh), satisfactory results are obtained with only $N = 11$, $M = 15$ and $q = 1.15$. We have gained 30% of degrees of freedom for the same accuracy. The numerical results for u_3^{ε} are shown on Fig. 4. We also may observe the results in a cross section on Fig. 5.

Table 1

$\mathbf{f} = (f_1, f_2, f_3)$	f_1	f_2	f_3
$\mathbf{f}_1$	0	0	-1.0
$\mathbf{f}_2$	0	0	$-Y(y^2 - \frac{1}{4})$
$\mathbf{f}_3$	0	0	$-Y(y^1 - \frac{1}{2})Y(y^2 - \frac{1}{4})$
$\mathbf{f}_4$	0	0	$\begin{cases} 1 & \text{on } (\frac{1}{4}, \frac{3}{4}) \times (\frac{3}{16}, \frac{5}{16}) \\ 0 & \text{elsewhere} \end{cases}$

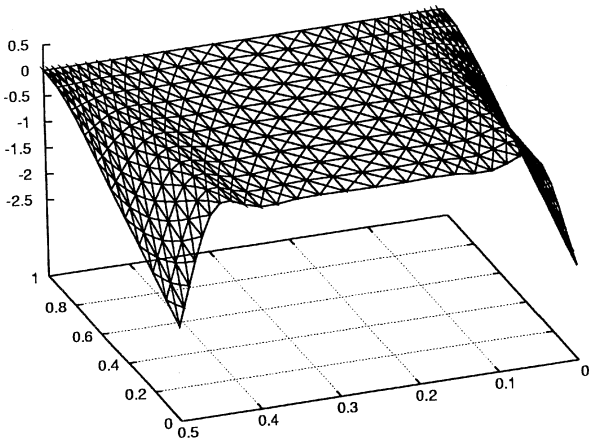

Fig. 4. Case of a characteristic boundary layer for the loading $\mathbf{f}_1$ (Table 1). Plot of u_3^ε in the whole domain Ω.

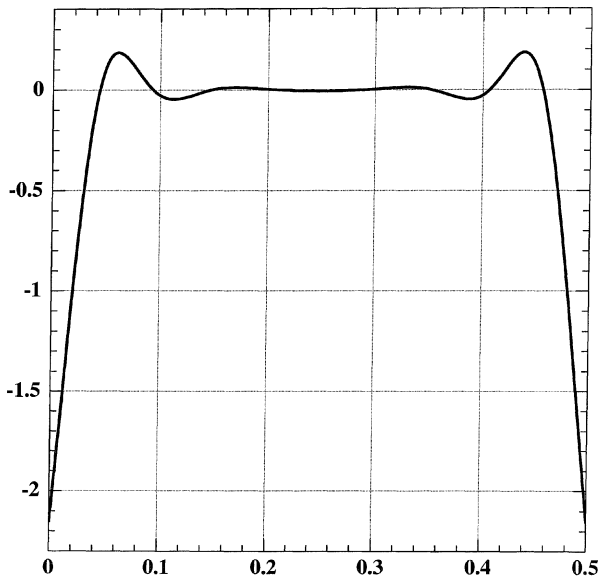

Fig. 5. Case of a characteristic boundary layer for the loading $\mathbf{f}_1$ (Table 1). Plot of u_3^ε in the cross section $y^2 = 0$.

7.2. Internal characteristic layers and propagation of the singularities

Now the clamped part Γ_0 is constituted by $y^1 = 0$, $y^1 = 1$ and $y^2 = 1$, and the loading is $\mathbf{f}_2$ (see Table 1). As the loading has a discontinuity along the characteristic $y^2 = 1/4$, we observe an internal layer along this characteristic. The results with the

uniform mesh and the non-uniform one are given on Figs. 6–8. For the uniform mesh we have good results for $N = 11$, $M = 21$ whereas for the non-uniform mesh, Fig. 6, satisfactory results are obtained for $N = 11$, $M = 15$ and $q = 0.85$. The comparison of the Figs. 7 and 8 shows some differences. In the case of the uniform mesh, Fig. 7, we observe some oscillations (right part of the curve) whereas with the non-uniform mesh (Fig. 8) we have a better approximation of the influence of the internal layer. In other words, in the case of a uniform mesh there are "numerical pollution" of the computation out of the layer due to the layer and this pollution disappear when using an adapted mesh.

In order to exhibit the propagation of the singularities along the characteristics, we now consider the loading $\mathbf{f}_3$ (see Table 1). The numerical results with a non-uniform mesh $N = 11$, $M = 15$ and $q = 0.85$ are shown on Fig. 9. We observe an internal layer along the whole characteristic $y^2 = 1/4$ while the discontinuity of the data is only along the interval $1/2 < y^1 < 1$. As in the previous case, we observe that by using the non uniform mesh the oscillations of the graph are less than for the uniform mesh.

Another interesting example with propagation of singularities is given in Figs. 10–12. The loading is defined by $\mathbf{f}_4$ (see Table 1). We observe internal layers along the whole characteristics $y^2 = 3/16$ and $y^2 = 5/16$ while the discontinuity of the loading lies only on $1/4 < y^1 < 3/4$.

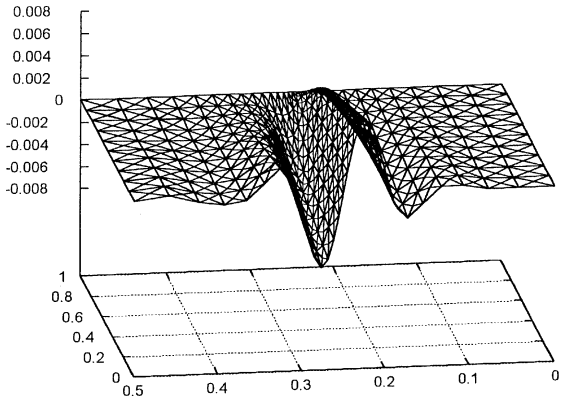

Fig. 6. Case of a characteristic internal layer, propagation of the singularity for the loading $\mathbf{f}_2$ (Table 1). Plot of u_3^ε in the whole domain.

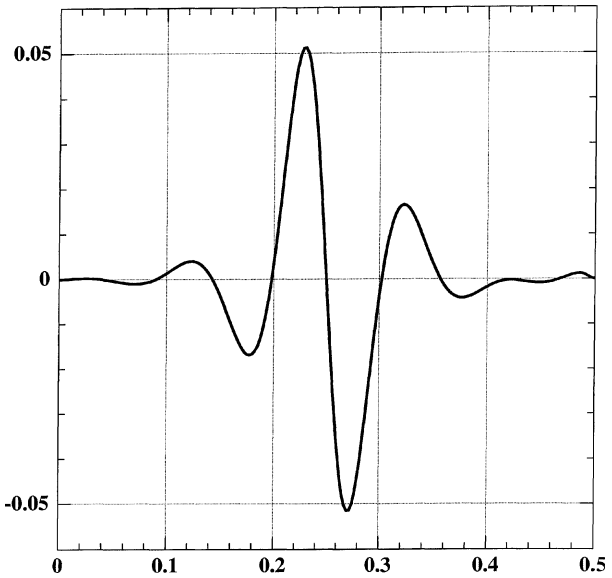

Fig. 7. Case of a characteristic internal layer, propagation of the singularity for the loading $\mathbf{f}_2$ (Table 1). Plot of u_3^ε at the cross section $y^2 = 0$ (uniform mesh).

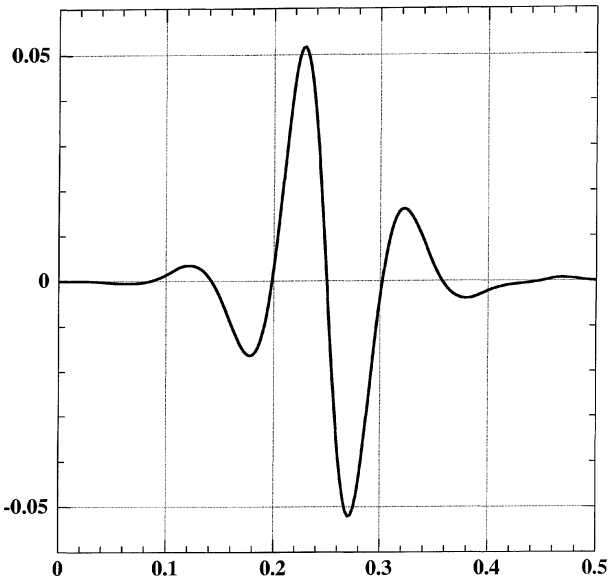

Fig. 8. Case of a characteristic internal layer, propagation of the singularity for the loading $\mathbf{f}_2$ (Table 1). Plot of u_3^ε at the cross section $y^2 = 0$ (non-uniform anisotropic mesh).

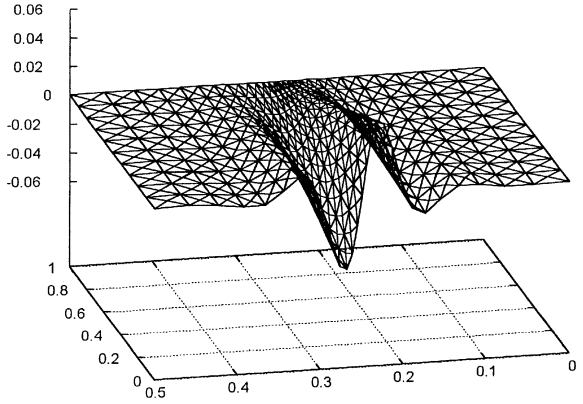

Fig. 9. Case of a characteristic internal layer, propagation of the singularity for the loading $\mathbf{f}_3$ (Table 1). Plot of u_3^ε in the whole domain.

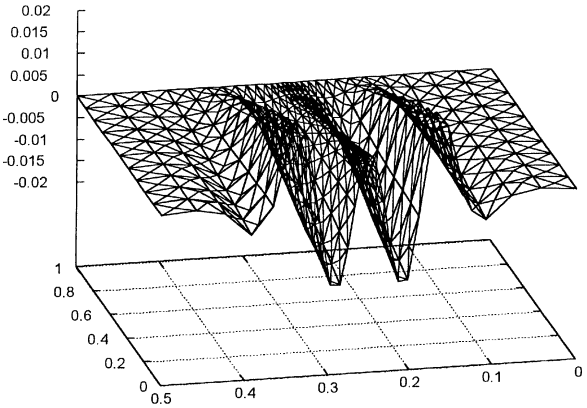

Fig. 10. Case of a characteristic internal layer, propagation of the singularity for the loading $\mathbf{f}_4$ (Table 1). Plot of u_3^ε in the whole domain.

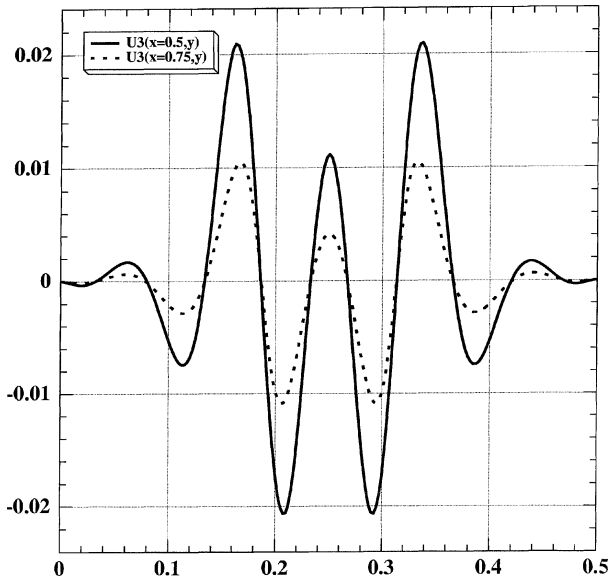

Fig. 11. Case of a characteristic internal layer, propagation of the singularities for the loading $\mathbf{f}_4$ (Table 1). Plot of u_3^ε at the cross section $y^2 = 0$ (uniform mesh).

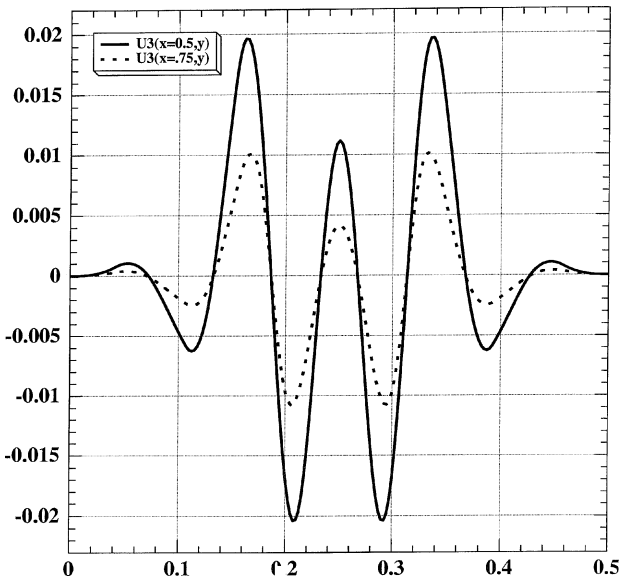

Fig. 12. Case of a characteristic internal layer, propagation of the singularities for the loading $\mathbf{f}_4$ (Table 1). Plot of u_3^ε at the cross section $y^2 = 0$ (non-uniform anisotropic mesh).

Remark 7.1. The small oscillations which appear at the end of the curves may be explained by the fact that we have not refined the mesh in the vicinity of the boundary layer corresponding to a clamped characteristic, which are less important than the characteristic ones as seen in Sections 4.2 and 4.3. We observe that they are less important when the layers are better approximated.

References

Bernadou, M., 1994. Méthodes d'Éléments Finis pour les Problèmes de Coques Minces. Masson, Paris.

Bernadou, M., Ciarlet, P.G., 1976. Sur l'ellipticité du modèle linéaire des coques de W.T. Koiter, in: Glowinski, R., Lions, J.L. (Eds.), Computing Methods in Sciences and Engineering, Lecture Notes in Economics and Math. Systems, Vol. 134. Springer, pp. 89–136.

Brezzi, F., Fortin, M., 1991. Mixed and Hybrid Finitelement Methods. Springer, Heidelberg.
Choï, D., Palma, F.J., Sanchez Palencia, É., Vilariño, M.A., 1998. Remarks on the membrane locking in the finite element computation of very thin elastic shells. Math. Modell. Num. Anal. 32, 131–152.
Gérard, P., Sanchez Palencia, É., 2000. Sensitivity phenomena for certain thin elastic shells with edges. Math. Meth. Appl. Sci. 23, 379–399.
Goldenveizer, A.L., 1962. Theory of Thin Elastic Shells. Pergamon, New York.
Karamian, P., 1998. Nouveaux résultats numériques concernant les coques minces hyperboliques inhibées: cas du paraboloïde hyperbolique. C. R. Acad. Sci. Paris, Sér. IIb 326, 755–760.
Karamian, P., 1999. Coques élastiques minces hyperboliques inhibées: calcul du problème limite par éléments finis et non reflexion des singularités, thèse de l'Université de Caen.
Karamian, P., Sanchez-Hubert, J., Sanchez Palencia, É., 2000. A model problem for boundary layers of thin elastic shells. Math. Modell. Num. Anal. 34, 1–30.
Karamian, P., Sanchez-Hubert, J., Sanchez Palencia, É., 2001-a. Propagation of singularities and structure of layers in shells. Hyperbolic case. Computers and Structures, in press.
Karamian, P., Sanchez-Hubert, J., Sanchez Palencia, É., 2001-b. Non-smoothness in the asymptotics of thin shells and propagation of the singularities. Hyperbolic case. Int. J. Appl. Math. and Comp. Sci., to appear.
Leguillon, D., Sanchez-Hubert, J., Sanchez Palencia, É., 1999. Model problem of singular perturbation without limit in the space of finite energy and its computation. C. R. Acad. Sci. Paris Sér. IIb 327, 485–492.
Lions, J.L., 1973. Perturbations Singulières dans les Problèmes aux Limites et en Contrôle Optimal, Lecture Notes in Math., Vol. 323. Springer-Verlag, Berlin.
Lions, J.L., Magenes, 1968. Problèmes aux Limites Non Homogènes et Applications. Vols. I and II. Dunod, Paris.
Lions, J.L., Sanchez Palencia, É., 1995. Sur quelques espaces de la théorie des coques et la sensitivité, in: Cioranescu, Damlamian, Donato, Gakkotosho (Eds.), Homogenization and Applications to Material Sciences, Tokyo, pp. 271–278.
Lions, J.L., Sanchez Palencia, É., 1996. Problèmes sensitifs et coques élastiques minces, in: Céa, J., Chesnais, D., Geymonat, G., Lions, J.L. (Eds.), Partial Differential Equations and Functional Analysis in memory of P. Grisvard. Birkhäuser, Boston, pp. 207–220.
Lions, J.L., Sanchez Palencia, É., 1998. Instabilities produced by edges in thin shells, in: Argoul, P., Frémond, M., Nguyen, Q.S. (Eds.), Variation of Domains and Free Boundary Problems. Kluwer, pp. 277–284.
Love, A.E.H., 1944. A Treatrise on the Mathematical Theory of Elasticity. Reprinted by Dover, New York.
Pitkaranta, J., Matache, A.M., Schwab, C., 2001. Fourier mode analysis of layers in shallow shell deformation. Computational Methods in Applied Mechanics and Engineering 190, 2943–2975.
Rutten, H.S., 1973. Theory and Design of Shells on the Basis of Asymptotic Analysis. Rutten & Kruisman, Voorburg.
Sanchez-Hubert, J., Sanchez Palencia, É., 1997. Coques Élastiques Minces. Propriétés Asymptotiques. Masson, Paris.
Sanchez-Hubert, J., Sanchez Palencia, É., 2001-a. Singular perturbations with non-smooth limit and finite element approximation of layers for model problems of shells, in: Ali Mehmeti, F., von Below, J., Nicaise, S. (Eds.), Partial Differential Equations in Multistructures. Dekker, New York, pp. 207–226.
Sanchez-Hubert, J., Sanchez Palencia, É., 2001-b. Anisotropic finite element estimates and local locking for shells: parabolic case. C. R. Acad. Sci. Paris, Sér. IIb 329, 153–159.
Van Dyke, M.. Perturbation Methods in Fluid Mechanics. Academic Press, New York.

Int. J. Appl. Math. Comput. Sci., 2002, Vol.12, No.1, 81–90

NON-SMOOTHNESS IN THE ASYMPTOTICS OF THIN SHELLS AND PROPAGATION OF SINGULARITIES. HYPERBOLIC CASE

PHILIPPE KARAMIAN*, JACQUELINE SANCHEZ-HUBERT*, ÉVARISTE SANCHEZ PALENCIA**

* Laboratoire de Mécanique, Université de Caen,
boulevard Maréchal Juin, 14032 Caen, France,
e-mail: {karen,sanchez}@meca.unicaen.fr

** Laboratoire de Modélisation en Mécanique, Université Paris VI,
8 rue du capitaine Scott, 75015 Paris, France,
e-mail: sanchez@lmm.jussieu.fr

We consider the limit behaviour of elastic shells when the relative thickness tends to zero. We address the case when the middle surface has principal curvatures of opposite signs and the boundary conditions ensure the geometrical rigidity. The limit problem is hyperbolic, but enjoys peculiarities which imply singularities of unusual intensity. We study these singularities and their propagation for several cases of loading, giving a somewhat complete description of the solution.

Keywords: hyperbolic systems, propagation of singularities, shells

1. Introduction

In this paper we study the propagation of singularities for the membrane system of shells in the hyperbolic case, i.e. when the middle surface has principal curvatures of opposite signs. The structure of the system is essentially hyperbolic, but presents certain peculiarities which imply singularities stronger than in ordinary hyperbolic systems. For instance, discontinuities of the first kind (i.e. Heaviside singularities) of the normal loading may imply δ'-like singularities of the normal displacement. As a consequence, the knowledge of the singularity gives most of the structure of the solutions, and often furnishes their good description, both from the qualitative and quantitative viewpoints. The motivation to study this problem is as follows: We are interested in a singular perturbation of the variational problems of the form

$$\text{For given } f \in V', \text{ find } u^\varepsilon \in V \text{ satisfying}$$

$$a_m(u^\varepsilon, v) + \varepsilon^2 a_f(u^\varepsilon, v) = (f, v), \quad \forall\, v \in V \qquad (1)$$

involving two positive and symmetric energy forms $a_m(u,v)$ and $\varepsilon^2 a_f(u,v)$, which are called the membrane and the flexion forms, respectively, because of the mechanical application to shell theory, as we shall see in Section 2. The factor ε^2 in the second form is a small parameter. For $\varepsilon > 0$, the energy space V is such that $a_m + \varepsilon^2 a_f$ is continuous and coercive on it, whereas the limit problem for $\varepsilon = 0$ involves a new energy space V_m (membrane energy space) for which the bilinear form a_m is continuous and coercive. In fact, V_m is the completion of V equipped with the norm $\sqrt{a_m(\cdot,\cdot)}$. Clearly, the above considerations only make sense in the case when a_m is the square of a norm, i.e. under the hypothesis that

$$v \in V \text{ and } a_m(v,v) = 0 \Rightarrow v = 0. \qquad (2)$$

The order of differentiation in a_f is higher than in a_m, so that as $\varepsilon \searrow 0$, a singular perturbation phenomenon appears.

Obviously, V_m contains functions less smooth than those of V. As a consequence, the solutions u^ε of the variational problem belong to V but their limit as $\varepsilon \searrow 0$ is a less smooth function (i.e. containing some kind of singularities). In fact, there is another important reason for the presence of singularities. Indeed, as $V \subset V_m$, the dual spaces satisfy $V_m' \subset V'$, so that the data f which are in V' are admissible for the variational problem with $\varepsilon > 0$, but it may happen, and often does happen in applications (see Section 2), that $f \notin V_m'$. As a consequence, the limit problem does not make sense as a variational one in V_m. The corresponding solution of the limit problem, if it exists, is out of V_m. In the sequel, we shall consider the case when the limit problem is hyperbolic and such that there is a unique solution satisfying the boundary conditions even when $f \notin V_m'$.

The case of $f \in V_m'$ will be called classical. In that situation, a well-known theorem, see, e.g., (Lions, 1973), asserts that u^ε converges to u^0 in the strong topology of

V_m, where u^ε and u^0 are the solutions of the variational problems for $\varepsilon > 0$ and $\varepsilon = 0$, respectively.

In the case of $f \notin V_m'$, even if the solution u^0 of the limit problem exists out of V_m, to our knowledge there is no theorem regarding the convergence of u^ε to u^0. Assuming that this convergence holds true, the corresponding topology is weaker than the one of V_m. Moreover, for the energy of the solution u^ε, we have

$$a_m\left(u^\varepsilon, u^\varepsilon\right) + \varepsilon^2 a_f\left(u^\varepsilon, u^\varepsilon\right) \to +\infty \text{ as } \varepsilon \searrow 0 \qquad (3)$$

(see, e.g., (Gérard and Sanchez Palencia, 2000)). There is some evidence that such a convergence actually holds at least for certain examples. This evidence follows from formal asymptotic expansions and numerical experiments. The formal asymptotic expansions are concerned with boundary layer theory for either thin shell problems or their simplified models (Karamian *et al.*, 2000; Karamian and Sanchez-Hubert, 2002; Leguillon *et al.*, 1999). Moreover, the convergence for the model problem addressed in (Karamian *et al.*, 2000) was proven in (Sanchez Palencia, 2000). The numerical computations for small ε are not very reliable because of the clearly non-smooth character of the solutions; nevertheless, they seem to confirm the above-mentioned convergence.

The context of this paper (which will be more explicitly explained in Section 2) is the following. We consider problems for thin elastic shells the middle surface of which is hyperbolic (i.e. the principal curvatures are everywhere different from zero and of opposite sign). Taking a special parametrization (y^1, y^2), where the coordinate lines are the asymptotic curves of the middle surface, the limit problem for $\varepsilon = 0$ (the so-called membrane problem) may be written as

$$\begin{cases} -D_1 T^{11} - D_2 T^{12} = f^1, \\ -D_1 T^{12} - D_2 T^{22} = f^2, \\ -2b_{12} T^{12} = f_3, \end{cases} \qquad (4)$$

$$\begin{cases} D_1 u_1 = C_{11\alpha\beta} T^{\alpha\beta}, \\ D_2 u_2 = C_{22\alpha\beta} T^{\alpha\beta}, \\ \dfrac{1}{2}\left(D_2 u_1 + D_1 u_2\right) - b_{12} u_3 = C_{12\alpha\beta} T^{\alpha\beta} \end{cases} \qquad (5)$$

in a domain Ω of the plane (y^1, y^2). The unknowns are the symmetric membrane stresses $T^{\alpha\beta}$ $(\alpha, \beta = 1, 2)$ and the displacements u_i $(i = 1, 2, 3)$. The symbols D_α are the covariant derivatives with respect to the variables y^1, y^2. The coefficients $C_{\alpha\beta\lambda\mu}$ are the compliance ones, given smooth functions. The coefficient b_{12} (coefficient of the second fundamental form) is a given smooth function everywhere different from zero. Finally, $f = (f^1, f^2, f_3)$ is a datum such that in general $f \notin V_m'$.

Obviously, the system (4)–(5) has six equations and six unknowns. Nevertheless, T^{12} is immediately given by $(4)_3$ and u_3 only appears in the last equation (5), which can be considered as a definition of u_3. Then the unknowns are essentially T^{11}, T^{22}, u_1, u_2; the first two equations of (4) only involve T^{11} and T^{22} and constitute a first-order hyperbolic system for them with the simple characteristics $y^1 = \text{Const}$ and $y^2 = \text{Const}$. Assuming that the boundary conditions allow us to determine T^{11} and T^{22}, the right-hand side of (5) is known and the first two equations of (5) form again a first-order hyperbolic system for u_1 and u_2 with the same simple characteristics. At this point, the high order of singularity of the solutions is easy to understand. We see that the first two equations of (4) for T^{11} and T^{22} involve as 'data' the first-order derivatives of f_3. Moreover, the unknown u_3 in the third equation of (5) inherits singularities from the first-order derivatives of u_1 and u_2. If, as usual, we focus our attention on normal forces f_3 and the normal displacement u_3, we see that the singularities are by two orders stronger than in the genuine hyperbolic system.

We are mainly concerned with the propagation of the singularities of this system. We consider the classical sequence of distributions on $\mathbb{R}$ with increasing singularities

$$\ldots xY(x), Y(x), \delta(x), \delta'(x), \ldots, \qquad (6)$$

where Y and δ denote the Heaviside function and the Dirac mass, respectively. More precisely, these distributions are considered as singularities at $x = 0$ whereas their values for $x \neq 0$ are discarded; for instance, $Y(x)$ is considered merely as the unit jump at $x = 0$. In order to describe the singularity, for example, along $y^2 = 0$, we consider expansions of the form (for instance)

$$w \simeq \delta'\left(y^2\right) W^0\left(y^1\right) + \delta\left(y^2\right) W^1\left(y^1\right) + \cdots, \qquad (7)$$

where it is understood that the terms denoted by dots are less singular than the previous ones at $y^2 = 0$. Such a kind of expansion is in the framework of discontinuous solutions, see, e.g., (Egorov and Shubin, 1992, Sec. 4.11; Gérard, 1988; Sanchez Palencia, 2001). We always assume that the geometric data and the coefficients are smooth, so that the sequence (7) is consistent with the singularities of the solutions provided that the singularities of the loadings are in that sequence, which covers most of the usual examples.

The very description of the singularities is given in Section 3. Precisions on the mechanical problem and the specific data will be given in Section 2. Numerical experiments exhibiting such a kind of behaviour are given in Section 4.

2. Description of the Mechanical Problem

We give here the elements of shell theory which are necessary for understanding the sequel of the paper. More explicit descriptions of shells can be found in shell treatises (Bernadou, 1994; Ciarlet ,2000; Goldenveizer, 1962; Sanchez-Hubert and Sanchez Palencia, 1997).

Let us denote by Ω a bounded and connected domain of the (y^1, y^2)-plane (the parameter plane). The middle surface $\mathcal{S}$ of the shell is defined by a smooth function $\vec{r}$, i.e.

$$\Omega \ni \left(y^1, y^2\right) \longmapsto \vec{r}\left(y^1, y^2\right) \in \mathbb{R}^3. \tag{8}$$

At any point of $\mathcal{S}$ we define the tangent vectors

$$\vec{a}_\alpha = \partial_\alpha \vec{r}, \tag{9}$$

$(\vec{a}_1, \vec{a}_2)$ being the local covariant basis of the tangent plane.

The first fundamental form which defines the distances on the surface is given by

$$\mathrm{d}s^2 = a_{\alpha\beta}\,\mathrm{d}y^\alpha\,\mathrm{d}y^\beta, \tag{10}$$

where $a_{\alpha\beta} = \vec{a}_\alpha \cdot \vec{a}_\beta$. The corresponding contravariant basis $\vec{a}^\alpha$ is defined by $\vec{a}^\alpha \cdot \vec{a}_\beta = \delta^\alpha_\beta$. We also consider the unit normal vector $\vec{a}^3 = \vec{a}_3$. We note that, when changing the parametrization, $\vec{a}_3$ is invariant up to the orientation, so that normal components behave essentially as scalars.

We recall that the Christoffel symbols are

$$\Gamma^\lambda_{\alpha\beta} = \partial_\beta \vec{a}_\alpha \cdot \vec{a}^\lambda$$

and that the coefficients of the second fundamental form describing the curvatures are

$$b_{\alpha\beta} = b_{\beta\alpha} = -\partial_\beta \vec{a}_3 \cdot \vec{a}_\alpha.$$

We also recall that a point of $\mathcal{S}$ is said to be elliptic, hyperbolic or parabolic when the second fundamental form is definite, indefinite or degenerate, respectively. This is equivalent to saying that the product of the principal curvatures is more than, equal to, or less than zero, respectively.

In contrast to ordinary differentiation ∂_α, the covariant differentiation is denoted by D_α. Its action on vectors and tensors is

$$\begin{cases} D_\alpha u_\beta = \partial_\alpha u_\beta - \Gamma^\lambda_{\alpha\beta} u_\lambda, \\ D_\lambda T^{\alpha\beta} = \partial_\lambda T^{\alpha\beta} + \Gamma^\alpha_{\lambda\mu} T^{\mu\beta} + \Gamma^\beta_{\lambda\mu} T^{\alpha\mu}. \end{cases} \tag{11}$$

Let $\vec{u}$ be the displacement of $\mathcal{S}$ for its deformation. Specifically, we consider that $\vec{r}$ changes into $\vec{r} + \vec{u}$ and we linearize for small $\vec{u}$. Then the strain tensor is given by the components

$$\gamma_{\alpha\beta} = \frac{1}{2}\left(D_\alpha u_\beta + D_\beta u_\alpha\right).$$

It describes the variation produced by $\vec{u}$ on the coefficients of the first fundamental form.

Analogously, the components of the second fundamental form vary along

$$\rho_{\alpha\beta} = \partial_\alpha \partial_\beta u_3 - \Gamma^\lambda_{\alpha\beta}\partial_\lambda u_3 - b^\lambda_\alpha b_{\lambda\beta} u_3 + D_\alpha\left(b^\lambda_\beta u_\lambda\right) + b^\lambda_\alpha D_\beta u_\lambda.$$

Then the classical (Love Kirchhoff or Koiter) theory of thin shells is described in terms of the two bilinear forms a_m and $\varepsilon^2 a_f$ of membrane and flexion energies which are given by

$$a_m\left(\vec{u}^\varepsilon, \vec{v}\right) = \int_{\mathcal{S}} A^{\alpha\beta\lambda\mu}\gamma_{\lambda\mu}\left(\vec{u}^\varepsilon\right)\gamma_{\alpha\beta}\left(\vec{v}\right)\mathrm{d}S, \tag{12}$$

$$a_f\left(\vec{u}^\varepsilon, \vec{v}\right) = \int_{\mathcal{S}} B^{\alpha\beta\lambda\mu}\rho_{\lambda\mu}\left(\vec{u}^\varepsilon\right)\rho_{\alpha\beta}\left(\vec{v}\right)\mathrm{d}S, \tag{13}$$

respectively, where $A^{\alpha\beta\lambda\mu}$ and $B^{\alpha\beta\lambda\mu}$ are the coefficients of membrane and flexion rigidities which satisfy usual conditions of symmetry and positivity.

Here 2ε denotes the relative thickness of the shell (equal to the ratio of the thickness to any other characteristic length of the shell). Obviously, the factor ε^2 in front of the form a_f accounts for the fact that the flexion rigidity is asymptotically small with respect to the membrane rigidity. Obviously, as the form a_f contains derivatives of higher orders than a_m, the asymptotic process $\varepsilon \searrow 0$ is a singular perturbation.

The stress membrane components $T^{\alpha\beta}$ are related to the strains by

$$T^{\alpha\beta}\left(\vec{u}^\varepsilon\right) = A^{\alpha\beta\lambda\mu}\gamma_{\lambda\mu}\left(\vec{u}^\varepsilon\right). \tag{14}$$

Conversely, the strains can be expressed in terms of the stresses as

$$\gamma_{\lambda\mu}\left(\vec{u}^\varepsilon\right) = C_{\lambda\mu\alpha\beta}T^{\alpha\beta}\left(\vec{u}^\varepsilon\right), \tag{15}$$

where the $C_{\lambda\mu\alpha\beta}$'s are the compliance coefficients.

The energy space V of vectors $\vec{v}$ satisfying the kinematic boundary conditions (bound. cond. for brevity) is

$$V = \left\{\vec{v} = (v_1, v_2, v_3) \in H^1(\Omega) \times H^1(\Omega) \times H^2(\Omega);\ \text{bound. cond.}\right\}. \tag{16}$$

Typical kinematic boundary conditions are either fixed conditions:

$$\vec{v} = 0,$$

or clamped conditions:

$$\begin{cases} \vec{v} = 0, \\ \dfrac{\partial v_3}{\partial n} = 0 \end{cases} \tag{17}$$

on a part Γ_0 of the boundary.

Under the hypothesis that the surface is geometrically rigid or inhibited in the terminology of (Sanchez-Hubert and Sanchez Palencia, 1997), i.e. that (2) holds true, and thus has to be checked in each case, $a_m(\vec{v},\vec{v})$ is the square of a norm on V and we may construct the space V_m as the completion of V with this norm. Obviously, because of the positivity of the coefficients $A^{\alpha\beta\lambda\mu}$, this norm is equivalent to

$$\|\vec{v}\|_{V_m} = \left(\sum_{\alpha,\beta} \|\gamma_{\alpha\beta}(\vec{v})\|_0^2 \right)^{\frac{1}{2}}. \tag{18}$$

From now on we make the hypothesis that the surface $\mathcal{S}$ is everywhere hyperbolic. Moreover, it is described with the special parametrization where the coordinate lines are the asymptotic curves so that $b_{11} = b_{22} = 0$, $b_{12} \neq 0$. In this context, the left-hand sides in (5) are γ_{11}, γ_{22} and γ_{12}.

The limit problem for $\varepsilon = 0$ is as follows: For given $\vec{f} \in V_m'$, find $\vec{u}^0 \in V_m$ satisfying

$$\begin{aligned} a_m\left(\vec{u}^0,\vec{v}\right) &\equiv \int_{\mathcal{S}} T^{\alpha\beta}\left(\vec{u}^0\right)\gamma_{\alpha\beta}\left(\vec{v}\right)\mathrm{d}S \\ &= \left(\vec{f},\vec{v}\right), \quad \forall\, \vec{v} \in V_m. \end{aligned} \tag{19}$$

Classical integration by parts shows that the problem (19) is equivalent to the system (4), (5) with the boundary conditions

$$u_1 = u_2 = 0 \text{ on } \Gamma_0 \tag{20}$$

and

$$T^{\alpha\beta} n_\beta = 0 \text{ on } \Gamma_1, \tag{21}$$

where $\Gamma_1 = \partial\Omega\backslash\Gamma_0$ is the free part of the boundary and $\vec{n}$ denotes the unit vector tangent to $\mathcal{S}$ and normal to the boundary. Kinematic boundary conditions (20) amount to (17) for the tangent components but the conditions for u_3 disappear because they obviously do not make sense in V_m, cf. (18). Moreover, (20) holds true under the hypothesis that Γ_0 is nowhere parallel to the characteristic curves, i.e. nowhere parallel to axes $y^1 = 0$, $y^2 = 0$. For all these questions, see (Sanchez-Hubert and Sanchez Palencia, 1997, Sec. VII.2).

Obviously, the problem for $\varepsilon > 0$ makes sense for any $\vec{f} \in V'$ which is a product of duals of standard Sobolev spaces. In contrast, the space V_m is not classical. Let us say that V_m is "large" so that its dual is "small". As a result, quite "usual" loadings do not belong to V_m' and will be in the non classical case mentioned in the Introduction. Let us state this in a more precise form as follows:

Theorem 1. *A necessary and sufficient condition for $\vec{f}$ to be in V_m' is that there exist $T^{\alpha\beta} = T^{\beta\alpha}$ in $L^2(\Omega)$ satisfying*

$$\begin{cases} -D_\beta T^{\alpha\beta} = f^\alpha, \\ -2b_{12}T^{12} = f_3 \end{cases} \tag{22}$$

in Ω and

$$T^{\alpha\beta} n_\beta = 0 \tag{23}$$

on the free part Γ_1 of the boundary.

The proof is analogous to that of Theorem 2.3 in (Karamian *et al.*, 2000). In fact, the property that if there is no $T \in L^2(\Omega)$ satisfying (22) and (23) then $\vec{f} \notin V_m'$ follows directly from the previous considerations. Indeed, if $\vec{f} \in V_m'$, then the solution to the limit problem exists so that the corresponding $T^{\alpha\beta}(\vec{u}^0)$ exist and belong to $L^2(\Omega)$ and, by virtue of (4) and (21), may be taken as $T^{\alpha\beta}$.

Example 1. Let us take $f^\alpha = 0$ and $f_3 = Y(y^2 - c)f(y^1)$, where f is a smooth function and Y denotes the Heaviside function. System (22) gives

$$\begin{cases} -\partial_1 T^{11} = \delta\left(y^2 - c\right)\Phi\left(y^1\right) + \text{element} \in L^2\left(\Omega\right), \\ -\partial_2 T^{22} = \text{element} \in L^2\left(\Omega\right), \end{cases}$$

which is impossible with $T^{11} \in L^2(\Omega)$. Consequently, $\vec{f} \notin V_m'$. ♦

Example 2. It is even easier to prove that $f^\alpha = 0$ and $f_3 = \delta(\mathcal{C})$, where $\mathcal{C}$ denotes a curve of the surface, does not belong to V_m'. Indeed, this follows immediately from the fact that the trace of v_3 is not defined for $\vec{v} \in V_m$, cf. (18). ♦

In the two previous examples, obviously $\vec{f} \in V'$.

3. Propagation of the Singularities

For the sake of conciseness, let us consider a specific example of geometry, as well as boundary conditions. Let Ω be the domain shown in Figs. 1 or 2. The surface $\mathcal{S}$ is assumed to be smooth and uniformly hyperbolic. The parametrization is chosen such that the asymptotic curves coincide with the coordinate ones $y^1\mathrm{const}$ and $y^1\mathrm{const}$, so that

$$b_{11} = b_{22} = 0, \quad b_{12} \neq 0. \tag{24}$$

The boundary is fixed along $\Gamma_0 \equiv AB$, which is not a characteristic curve, so that the boundary conditions are (20). The rest of the boundary $\partial\Omega\backslash\Gamma_0$ is free. Two cases of loading will be considered, and a wide variety of examples may be handled in an analogous way.

3.1. First Example of Loading

In this subsection, the loading is defined as follows:

$$\vec{f} = \left(0, 0, \delta\left(y^2 - c^2\right)\theta_{[a^1,b^1]}\left(y^1\right)\right) F\left(y^1\right), \tag{25}$$

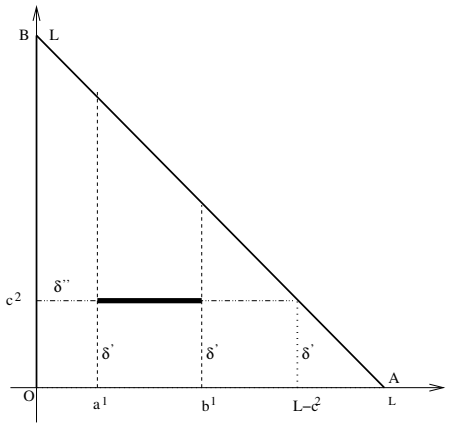

Fig. 1. Domain Ω in the first case of loading (25) (δ' and δ'' indicate the type of the singularity of u_3).

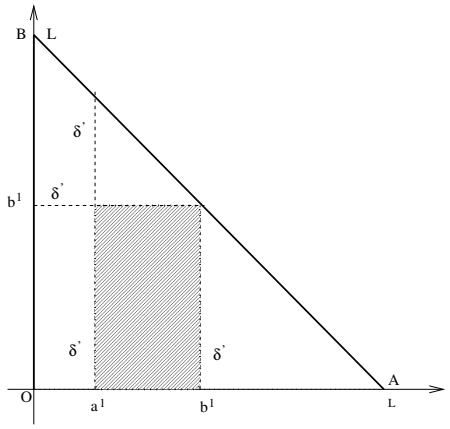

Fig. 2. Domain Ω in the second case of loading (49) (δ' indicates the type of the singularity along the characteristics).

where $\theta_{[a^1,b^1]}$ is the characteristic function of the interval $[a^1, b^1]$ and F is assumed to be a smooth function.

Let us now address the propagation of the singularities along the characteristic curve which supports the loading.

3.1.1. Propagation of the Singularities Along $y^2 = c^2$

We first study the singularities of the components $T^{\alpha\beta}$ in the system (4), which is of the form

$$\begin{cases} -\partial_1 T^{11} - \left(2\Gamma^1_{11} + \Gamma^2_{12}\right) T^{11} - \Gamma^1_{22} T^{22} \\ \qquad = \partial_2 T^{12} + \left(3\Gamma^1_{12} + \Gamma^2_{22}\right) T^{12}, \\ -\partial_2 T^{22} - \left(2\Gamma^2_{22} + \Gamma^1_{12}\right) T^{22} - \Gamma^2_{11} T^{11} \\ \qquad = \partial_1 T^{12} + \left(3\Gamma^2_{12} + \Gamma^1_{11}\right) T^{12}, \\ -2b_{12} T^{12} = \delta\left(y^2 - c^2\right) \theta_{[a^1,b^1]}\left(y^1\right) f\left(y^1\right). \end{cases} \tag{26}$$

By substituting the expression for T^{12} in $(26)_3$ into $(26)_1$ and $(26)_2$, we obtain for the leading order of singularity

$$\begin{cases} -\partial_1 T^{11} - \left(2\Gamma^1_{11} + \Gamma^2_{12}\right) T^{11} - \Gamma^1_{22} T^{22} \\ \qquad \simeq -\delta'\left(y^2 - c^2\right) \Phi_1\left(y^1\right) + \cdots, \\ -\partial_2 T^{22} - \left(2\Gamma^2_{22} + \Gamma^1_{22}\right) T^{22} - \Gamma^2_{11} T^{11} \\ \qquad \simeq -\delta\left(y^2 - c^2\right) \Phi_2\left(y^1\right) + \cdots, \\ T^{12} = -\delta\left(y^2 - c^2\right) \Phi_1\left(y^1\right), \end{cases} \tag{27}$$

where

$$\Phi_1\left(y^1\right) = \frac{\theta_{[a^1,b^1]}\left(y^1\right) f\left(y^1\right)}{2b_{12}\left(y^1, c^2\right)} \tag{28}$$

and

$$\Phi_2\left(y^1\right) = \partial_1 \Phi_1\left(y^1\right). \tag{29}$$

We note that Φ_2 contains terms in $\delta(y^1 - a^1)$ and $\delta(y^1 - b^1)$.

We see that the appropriate singularity expansions for $T^{\alpha\beta}$ in the framework of (7) are

$$\begin{cases} T^{11} \simeq \delta'\left(y^2 - c^2\right) \mathcal{T}^{11}\left(y^1\right) + \cdots, \\ T^{22} \simeq \delta\left(y^2 - c^2\right) \mathcal{T}^{22}\left(y^1\right) + \cdots, \\ T^{12} = -\delta\left(y^2 - c^2\right) \Phi_1\left(y^1\right). \end{cases} \tag{30}$$

The system (27) then gives the system satisfied by $\mathcal{T}^{11}$ and $\mathcal{T}^{22}$:

$$\begin{cases} \dfrac{\mathrm{d}\mathcal{T}^{11}}{\mathrm{d}y^1} + \left(2\Gamma^1_{11} + \Gamma^2_{12}\right) \mathcal{T}^{11} = \Phi_1\left(y^1\right), \\ \mathcal{T}^{22} + \Gamma^2_{11} \mathcal{T}^{11} = 0. \end{cases} \tag{31}$$

This system is of total order one. Let us look for the corresponding boundary condition. At the leading order (23) gives $\mathcal{T}^{11} n_1 = 0$, where $n_1 \neq 0$. Indeed, we have $\vec{n} = n_1 \vec{a}^1 + n_2 \vec{a}^2$, where $\vec{n}$ is normal to $\vec{a}_2$, i.e. parallel to $\vec{a}^1$. The boundary condition for $\mathcal{T}^{11}$ is then

$$\mathcal{T}^{11}(0) = 0. \tag{32}$$

We then have

$$\begin{cases} \mathcal{T}^{11}\left(y^1\right) = \displaystyle\int_{a^1}^{y^1} \Phi_1(\eta) \exp\left[\int_{y^1}^{\eta} \left(2\Gamma^1_{11}\left(\xi, c^2\right) \right.\right. \\ \qquad\qquad \left.\left. + \Gamma^2_{12}\left(\xi, c^2\right)\right) \mathrm{d}\xi\right] \mathrm{d}\eta, \\ \mathcal{T}^{22} = -\Gamma^2_{11}\left(y^1, c^2\right) \mathcal{T}^{11}\left(y^1\right), \end{cases} \tag{33}$$

and the leading order of the singularity is completely determined.

Remark 1. For $0 < y^1 < a^1$, $\mathcal{T}^{11}(y^1) = 0$ but for $b^1 < y^1 < L - c^2$, in general, $\mathcal{T}^{11}(y^1) \neq 0$ though $\theta_{[a^1,b^1]}(y^1) \equiv 0$: this manifests the *phenomenon of propagation of singularities*.

Remark 2. According to the previous results, at the leading order both boundary conditions (21) are automatically satisfied.

Let us now examine the singularities of the displacement components u_i. The system (5) gives at the leading orders

$$\begin{cases} \partial_1 u_1 - \Gamma^1_{11} u_1 - \Gamma^2_{11} u_2 \\ \qquad \simeq C_{1111}\delta'\left(y^2 - c^2\right)\mathcal{T}^{11}\left(y^1\right) + \cdots, \\ \partial_2 u_2 - \Gamma^1_{22} u_1 - \Gamma^2_{22} u_2 \\ \qquad \simeq C_{2211}\delta'\left(y^2 - c^2\right)\mathcal{T}^{11}\left(y^1\right) + \cdots, \\ \dfrac{1}{2}\left(\partial_1 u_2 + \partial_2 u_1\right) - \Gamma^1_{12} u_1 - \Gamma^2_{12} u_2 - b_{12} u_3 \\ \qquad \simeq C_{1211}\delta'\left(y^2 - c^2\right)\mathcal{T}^{11}\left(y^1\right) + \cdots. \end{cases} \tag{34}$$

Then the appropriate expansions of the components u_i are

$$\begin{cases} u_1 \simeq \delta'\left(y^2 - c^2\right) U_1\left(y^1\right) + \cdots, \\ u_2 \simeq \delta\left(y^2 - c^2\right) U_2\left(y^1\right) + \cdots, \\ u_3 \simeq \delta''\left(y^2 - c^2\right) U_3\left(y^1\right) + \cdots. \end{cases} \tag{35}$$

Substitution of (35) into (34) leads to

$$\begin{cases} \dfrac{\mathrm{d}U_1}{\mathrm{d}y^1} - \Gamma^1_{11} U_1 = C_{1111}\left(y^1, c^2\right)\mathcal{T}^{11}\left(y^1\right) \\ \qquad\qquad \equiv \Psi_1\left(y^1\right), \\ U_2 - \Gamma^1_{22} U_1 = C_{2211}\left(y^1, c^2\right)\mathcal{T}^{11}\left(y^1\right) \\ \qquad\qquad \equiv \Psi_2\left(y^1\right), \\ \dfrac{1}{2} U_1 - b_{12} U_3 = 0. \end{cases} \tag{36}$$

The components U_1 and U_2 satisfy a system of total order one with the boundary condition

$$U_1\left(L - c^2\right) = 0 \tag{37}$$

and we obtain

$$\begin{cases} U_1\left(y^1\right) = \left(\displaystyle\int_{L-c^2}^{y^1} \Psi_1(\eta)\right)\left[\exp\left(\int_{L-c^2}^{\eta} \Gamma^1_{11}\left(\xi, c^2\right)\mathrm{d}\xi\right)\right]\mathrm{d}\eta, \\ U_2\left(y^1\right) = \Gamma^1_{22} U_1 + \Psi_2\left(y^1\right), \\ U_3\left(y^1\right) = \dfrac{1}{2b_{12}\left(y^1, c^2\right)} U_1\left(y^1\right). \end{cases} \tag{38}$$

The leading orders of the singularities of the components u_i are completely known.

Remark 3. We observe that $U_2(L - c^2) \neq 0$. The boundary condition (20) for u_2 (which is of an order of singularity lower than u_1, see (35)) is not satisfied. This provokes a new (reflected) singularity of lower order along $y^1 = c^2$. This kind of phenomenon was considered in (Karamian, 1998b). See also Remark 6 here after.

Remark 4. The components U_1 and U_3 are different from zero on the whole interval $0 < y^1 < L - c^2$ (propagation of the singularities).

3.1.2. Propagation of the Singularities along the Characteristic $y^1 = a^1$

In the sequel, we shall study the propagation along the characteristic $y^1 = a^1$. Propagation along $y^1 = b^1$ is analogous. We now have

$$T^{12} = -Y\left(y^1 - a^1\right)\frac{f\left(a^1\right)\delta\left(y^2 - c^2\right)}{2b_{12}\left(a^1, y^2\right)}. \tag{39}$$

We note that (39) is merely the singularity of $(26)_3$ at $y^1 = a^1$. Nevertheless, the roles of $Y(y^1 - a^1)$ and $\delta(y^2 - c^2)$ are "reversed" in the study of the propagation along $y^2 = c^2$ (Subsection 3.1.1) and along $y^1 = a^1$ (now). Indeed, along $y^2 = c^2$, the "singularity" in the sense of (6) or (7) was $\delta(y^2 - c^2)$ and the "coefficient", Φ_1, was given by (28), which contains Y terms in the tangential variable y^1. Consequently, for studying the propagation along $y^1 = a^1$, the "singularity " is $Y(y^1 - a^1)$ and the "coefficient" is $\delta(y^2 - c^2)$; it is "more singular", but in the tangential variable. Consequently,

$$\begin{cases} \partial_1 T^{12} = -\delta\left(y^1 - a^1\right)\dfrac{f\left(a^1\right)\delta\left(y^2 - c^2\right)}{2b_{12}\left(a^1, c^2\right)}, \\ \partial_2 T^{12} = -Y\left(y^1 - a^1\right)\dfrac{f\left(a^1\right)\delta'\left(y^2 - c^2\right)}{2b_{12}\left(a^1, c^2\right)}, \end{cases}$$

and the system (5) reduces to

$$\begin{cases} -\partial_1 T^{11} - \left(2\Gamma^1_{11} + \Gamma^2_{12}\right) T^{11} - \Gamma^1_{22} T^{22} \\ \qquad = -Y\left(y^1 - a^1\right)\dfrac{f\left(a^1\right)\delta'\left(y^2 - c^2\right)}{2b_{12}\left(a^1, c^2\right)}, \\ -\partial_2 T^{22} - \left(2\Gamma^2_{22} + \Gamma^1_{12}\right) T^{22} - \Gamma^2_{11} T^{11} \\ \qquad = \delta\left(y^1 - a^1\right)\dfrac{f\left(a^1\right)\delta\left(y^2 - c^2\right)}{2b_{12}\left(a^1, c^2\right)} \end{cases} \tag{40}$$

with (39). The appropriate expansion is then

$$\begin{cases} T^{11} \simeq Y\left(y^1 - a^1\right)\Upsilon^{11}\left(y^2\right) + \cdots, \\ T^{22} \simeq \delta\left(y^1 - a^1\right)\Upsilon^{22}\left(y^2\right) + \cdots, \end{cases} \tag{41}$$

where Υ^{11} and Υ^{22} satisfy

$$\begin{cases} -\Upsilon^{11} - \Gamma^1_{22}\Upsilon^{22} = 0, \\ -\dfrac{\mathrm{d}\Upsilon^{22}}{\mathrm{d}y^2} - \left(2\Gamma^1_{11} + \Gamma^2_{12}\right)\Upsilon^{22} \\ \qquad = \dfrac{f\left(a^1\right)}{2b_{12}\left(a^1, c^2\right)}\delta\left(y^2 - c^2\right). \end{cases} \tag{42}$$

The explicit solution is

$$\Upsilon^{22}\left(y^2\right) = \frac{f\left(a^1\right)}{2b_{12}\left(a^1, c^2\right)} Y\left(y^2 - c^2\right) \times \exp\left(-\int_{c^2}^{y^2}\left(2\Gamma^1_{11}\left(a^1, \eta\right) + \Gamma^2_{12}\left(a^1, \eta\right)\right)\mathrm{d}\eta\right). \tag{43}$$

The corresponding system satisfied by the displacement components is

$$\begin{cases} \partial_1 u_1 - \Gamma^1_{11}u_1 - \Gamma^2_{11}u_2 \\ \quad = C_{1122}\left(a^1, y^2\right)\delta\left(y^1 - a^1\right)\Upsilon^{22}\left(y^2\right) + \cdots, \\ \partial_2 u_2 - \Gamma^1_{22}u_1 - \Gamma^2_{22}u_2 \\ \quad = C_{2222}\left(a^1, y^2\right)\delta\left(y^1 - a^1\right)\Upsilon^{22}\left(y^2\right) + \cdots, \\ \dfrac{1}{2}\left(\partial_2 u_1 + \partial_1 u_2\right) - \Gamma^1_{12}u_1 - \Gamma^2_{12}u_2 - b_{12}u_3 \\ \quad = C_{1222}\left(a^1, y^2\right)\delta\left(y^1 - a^1\right)\Upsilon^{22}\left(y^2\right) + \cdots, \end{cases} \tag{44}$$

and their expansions are of the form

$$\begin{cases} u_1 \simeq Y\left(y^1 - a^1\right)V_1\left(y^2\right) + \cdots, \\ u_2 \simeq \delta\left(y^1 - a^1\right)V_2\left(y^2\right) + \cdots, \\ u_3 \simeq \delta'\left(y^1 - a^1\right)V_3\left(y^2\right) + \cdots, \end{cases} \tag{45}$$

where the functions V_i satisfy

$$\begin{cases} V_1 - \Gamma^2_{11}V_2 = C_{1122}\Upsilon^{22}\left(y^2\right), \\ \dfrac{\mathrm{d}V_2}{\mathrm{d}y^2} - \Gamma^2_{22}V_2 = C_{2222}\Upsilon^{22}\left(y^2\right), \\ \dfrac{1}{2}V_2 - b_{12}V_3 = 0. \end{cases} \tag{46}$$

Taking account of the boundary condition $V_2(L - c^2) = 0$, we obtain the solution

$$V_2\left(y^2\right) = \left[-\int_{y^2}^{L-a^1}\exp\left(-\int_0^{\eta}\Gamma^2_{22}\left(a^1, \xi\right)\mathrm{d}\xi\right)F\left(\eta\right)\mathrm{d}\eta\right] \times \exp\left(\int_0^{y^2}\Gamma^2_{22}\left(a^1, \eta\right)\mathrm{d}\eta\right), \tag{47}$$

where

$$F\left(\eta\right) = C_{2222}\left(a^1, \eta\right)\Upsilon^{22}\left(\eta\right). \tag{48}$$

Then V_1 is given by $(46)_1$ and V_3 by $(46)_3$, so that the propagation of the singularity along the characteristic $y^1 = a^1$ is completely determined at the leading order.

3.2. Second Example of Loading

We now consider another loading which is less singular than the previous one. In order to make comparisons with Section 3.1, we keep the same surface $\mathcal{S}$ and domain Ω. The loading is

$$\vec{f} = \Big(0, 0, Y\left(y^2 - b^1\right)Y\left(y^1 - a^1\right) \times Y\left(b^1 - y^1\right)F\left(y^1, y^2\right)\Big), \tag{49}$$

where F is a smooth function. Clearly, we have discontinuities of f_3 along the characteristics $y^1 = a^1$, $y^1 = b^1$ and $y^2 = b^1$ (see Fig. 2).

As regards the singularities along $y^2 = b^1$, the loading f_3 is singular in $Y(y^2 - b^1)$ instead of $\delta(y^2 - c^2)$ as in Section 3.1, so that the singularities of the unknowns are studied exactly in the same manner as in Section 3.1, but their order is lower by one. As a result, instead of (30) and (35), we have

$$\begin{cases} T^{11} \simeq \delta\left(y^2 - b^1\right)\mathcal{T}^{11}\left(y^1\right) + \cdots, \\ T^{22} \simeq Y\left(y^2 - b^1\right)\mathcal{T}^{22}\left(y^1\right) + \cdots, \\ T^{12} = -Y\left(y^2 - b^1\right)\Phi_1\left(y^1\right) \end{cases} \tag{50}$$

and

$$\begin{cases} u_1 \simeq \delta\left(y^2 - b^1\right)U_1\left(y^1\right) + \cdots, \\ u_2 \simeq Y\left(y^2 - b^1\right)U_2\left(y^1\right) + \cdots, \\ u_3 \simeq \delta'\left(y^2 - b^1\right)U_3\left(y^1\right) + \cdots, \end{cases} \tag{51}$$

respectively, where the functions $\mathcal{T}^{11}, \ldots, U_3$ can be determined in much the same way as in Section 3.1.

As for the singularities along $y^1 = a^1$ (resp. $y^1 = b^1$), the loading is singular in $Y(y^1 - a^1)$ (resp. $Y(b^1 - y^1)$), i.e. of the same order as in Section 3.1.2, so that nothing is changed in formulae (41) and (45), where $\Upsilon^{11}, \ldots, V_3$ can be determined as in that section.

Fig. 2 shows the order of the singularity of u_3 along the above-mentioned characteristics.

Remark 5. For the present loading, where f_3 is distributed and does not vanish on a part of the characteristic boundary $y^2 = 0$, in addition to the previous singularities, there is a strong boundary layer along $y^2 = 0$ enjoying propagation properties (Sanchez Palencia, 2001) (see also an analogous situation for a model problem in (Karamian *et al.*, 2000)).

4. Numerical Experiments

Numerical experiments are concerned with u^ε for $\varepsilon > 0$. As we mentioned in Section 1, when $\vec{f} \notin V'_m$, to our knowledge there is no proof of the convergence of u^ε as $\varepsilon \searrow 0$ in the general case. Nevertheless, a proof in appropriate topologies after a re-scaling was given for a model problem in (Sanchez Palencia, 2000). Of course, as we shall see in the sequel, there is "numerical evidence" of such convergence. Clearly, for $\varepsilon > 0$ the singularities become internal layers with thickness $\eta(\varepsilon) \searrow 0$. We must emphasize that such numerical computations are very tricky since the finite element approximation $u_h^\varepsilon \to u^\varepsilon$ is not uniform with respect to ε with values in V_m or in any smaller space (Gérard and Sanchez Palencia, 2000, Prop. 4.1). Consequently, the smaller ε is, the smaller h must be taken to have a good approximation. This peculiarity generates a variety of difficulties when computing thin shells (Chapelle and Bathe, 1998; Karamian, 1998b; 1999; Sanchez-Hubert and Sanchez Palencia, 1998). Some of these difficulties are linked to the presence of boundary layers and the corresponding local locking phenomena (Pitkaranta *et al.* (to appear); Sanchez-Hubert and Sanchez Palencia, 2001a; 2001b).

Let us recall some elementary properties of distributions of $\mathcal{D}'(\mathbb{R})$, which will be useful for understanding the numerical experiments and, more precisely, the sections on the internal layers. It is classical that the Dirac mass is the limit of a sequence of functions

$$\frac{1}{\eta}\varphi\left(\frac{x}{\eta}\right) \to \delta(x) \quad \text{as} \quad \eta \to 0$$

provided that

$$\int_{\text{support}} \varphi(x)\,\mathrm{d}x = 1.$$

More generally (Sanchez-Hubert and Sanchez Palencia, 1989, Sec. VI.14), a sequence of functions $\varphi^\eta(x) = \varphi(x/\eta)$ can be expanded in the form

$$\varphi^\eta(x) \simeq \eta m^0(\varphi)\,\delta(x) - \frac{\eta^2}{2!} m^1(\varphi)\,\delta'(x)$$

$$+ \frac{\eta^3}{3!} m^2(\varphi)\,\delta''(x) + \cdots,$$

where the coefficients are the moments of φ:

$$m^k(\varphi) = \int_{\text{support}} x^k \varphi(x)\,\mathrm{d}x.$$

Consequently, if φ is such that

$$m^k(\varphi) = 0 \ \text{ for } k = 0, \ldots, p, \tag{52}$$

then

$$\frac{(-1)^p\, p!}{\eta^{p+1} m^p(\varphi)} \varphi^\eta(x) \to \delta^{(p)}(x). \tag{53}$$

In this section, we present some numerical experiments concerning the cases considered in Section 3 for two different cases of loading. The numerical computations are implemented with reduced Hermite finite elements that are used for the normal displacement u_3, as well as for the tangential displacement (u_1, u_2). The numerical integration of the rigidity matrices needs six Gauss points.

The meshes for the domain Ω are generated by using the Modulef code. The domain is covered with right-angled triangles such that the sides opposite the hypotenuse of each triangle are parallel to the y^1 and y^2 coordinates. This allows us to perform uniformly the mesh refinement by respecting the asymptotic curves.

The surface is defined by the mapping (8) with

$$\vec{r}\,(y^1, y^2) = \left(y^1, y^2, y^1 y^2\right),$$

so that the surface is a hyperbolic paraboloid satisfying all the required hypotheses.

The material is isotropic and homogeneous, with Young's modulus 28500 Nm^{-2} and Poisson's ratio 0.4. The thickness is equal to 10^{-4}.

In both cases, the numerical experiment involves 14400 triangles, 7381 nodes and 66429 degrees of freedom.

4.1. First Example of Loading

In the case of Section 3.1, we take $L = 4,\ a^1 = c^2 = 1$ and $b^2 = 2$ (Fig. 1) and $F(y^1) = 1$. Below we give and explain the behavior of u_3^ε in different sections.

Figure 3 shows u_3^ε in the section $y^1 = 0.5$, i.e. in the region $(0 < y^1 < a^1 = 1)$ on the left of the loading. We observe that this function is nearly vanishing except

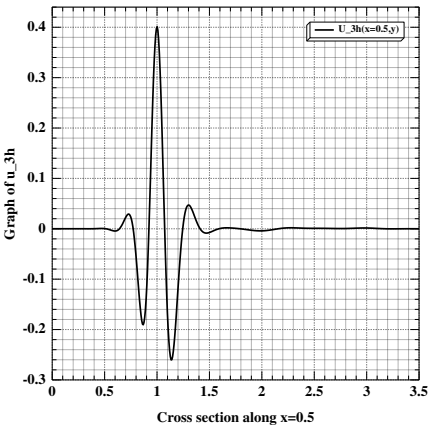

Fig. 3. The first example of loading, Sec. 3.1. The graph of u_3 for $y^1 = 1.5$ manifesting a propagated δ''-like singularity at $y^2 = 1$.

in the neighbourhood of $y^2 = c^2 = 1$, where it manifests a behaviour analogous to (53) with $p = 2$. Indeed, the moments m^0 and m^1 with respect to $x = y^2 - 1$ are clearly small and $m_2 \neq 0$. This perfectly agrees with the structure of the singularity in δ'' of u_3 in (35). Of course, as the section is on the left of the loading, the singularity is propagated in the sense of Remark 4.

Figure 4 shows u_3^ε in the section $y^1 = 1.5$, which cuts the support of the loading. The behaviour is exactly the same as in Fig. 3 but quantitatively larger.

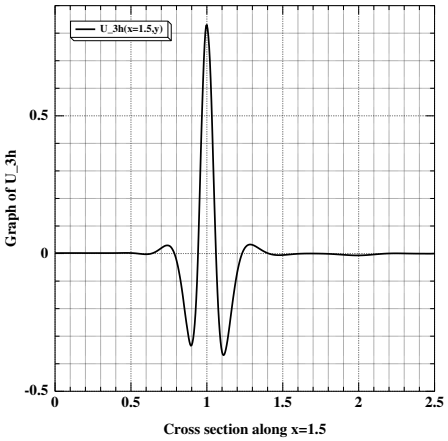

Fig. 4. The first example of loading, Sec. 3.1. The graph of u_3 for $y^1 = 1.5$ manifesting a non-propagated singularity at $y^2 = 1$.

Figure 5 shows u_3^ε in the section $y^2 = 0.5$, which cuts the characteristics $y^1 = a^1 = 1$ and $y^1 = b^1 = 2$ bearing the propagated singularities in δ', cf. (45). We observe that the function manifests in the neighbourhoods of $y^1 = 1$ and $y^1 = 2$ a behaviour analogous to (53) with $p = 1$. Indeed, the moment m^0 is clearly small and $m^1 \neq 0$.

Remark 6. Figure 5 also shows a δ' singularity in the vicinity of $y^1 = 3$. According to Fig. 1, with $c^2 = 1$, this corresponds to the section of the characteristic $y^1 = 3$, which bears the "pseudo-reflected" singularity of that along $y^2 = 1$ (Karamian, 1998b). Indeed, the δ''-singularity along $y^2 = 1$ intersects the non-characteristic boundary AB at the point $(3, 1)$ so that a singularity of the order lower by one, i.e. in δ', appears along $y^1 = 3$.

4.2. Second Example of Loading

In the case of Section 3.2, we take $l = 4,\ a^1 = 1$ and $b^2 = 2$ (Fig. 2) and $F(y^1, y^2) = 1$.

Figure 6 shows u_3^ε in the section $y^1 = 0.5$, i.e. in the region $\left(0 < y^1 < a^1 = 1\right)$ on the left of the loading.

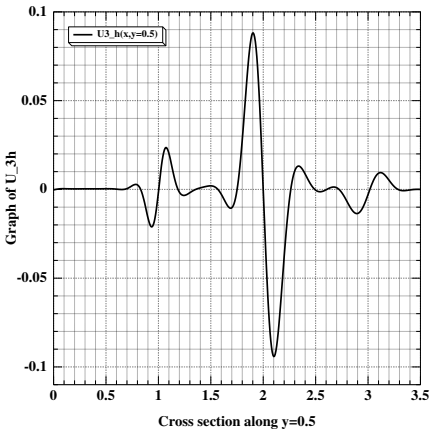

Fig. 5. The first example of loading, Sec. 3.1. The graph of u_3 for $y^2 = 0.5$ manifesting propagated δ'-like singularities at $y^1 = 1$ nad $y^1 = 2$.

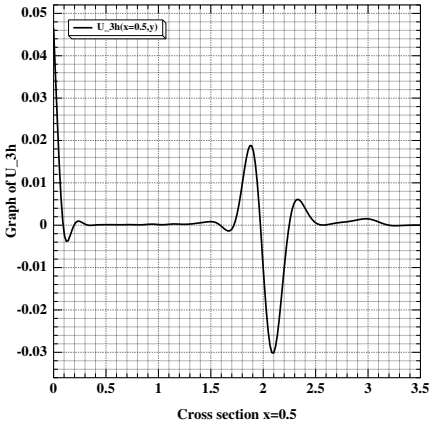

Fig. 6. The second example of loading, Sec. 3.2. The graph u_3 for $y^1 = 0.5$ manifesting a propagated δ'-like singularity at $y^2 = 2$ and a propagated boundary layer at $y^2 = 0$.

As has been explained in Section 3.2, the singularity along $y^2 = 2$ is in δ' for u_3. Its section by $y^1 = 0.5$ clearly appears in the figure, which also shows in the vicinity of $y^1 = 0$ the boundary layer mentioned in Remark 5. Both singularities are propagated from the support of $\vec{f}$.

Figure 7 shows the section $y^2 = 0.5$ and manifests δ' singularities at $y^1 = 1$ and $y^1 = 2$. This perfectly agrees with the description given in Section 3.2. The graph is analogous to that of Fig. 5 except for the pseudo-reflected singularities along $y^1 = 3$, which do not exist in the present case (cf. Remark 5). It should be noticed that the singularities in Fig. 5 are propagated, whereas those in Fig. 7 are not. Nevertheless, the shapes are closely similar. The fact that there is a loading between $y^1 = 1$ and $y^1 = 2$ in Fig. 7 is not relevant. Only the discontinuities at the extremities of its support yield significant singularities.

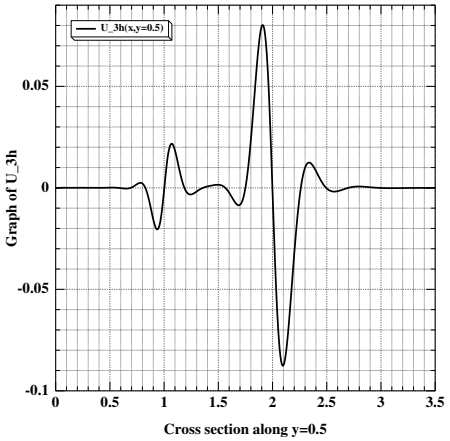

Fig. 7. The second example of loading, Sec. 3.2. The graph of u_3 for $y^2 = 0.5$ manifesting two propagated δ'-like singularities at $y^1 = 1$ and $y^1 = 2$.

References

Bernadou M. (1994): *Méthodes d'Éléments Finis pour les Problèmes de Coques Minces*. — Paris: Masson.

Chapelle D. and Bathe K.J. (1998): *Fundamental considerations for the finite element analysis of shell structures*. — Comp. Struct., Vol. 66, No. 1, pp. 19–36.

Ciarlet P.G. (2000): *Mathematical Elasticity, Vol. III, Theory of Shells*. — Amsterdam: North Holland.

Egorov Yu.V. and Shubin M.A. (1992): *Linear partial differential equations. Foundations of the classical theory*, In: Encyclopaedia of Mathematical Sciences, Vol. 30 (Part. Diff. Eqs. I). – New York: Springer, pp. 345–375.

Gérard P. (1988): *Solutions conormales analytiques d'équations hyperboliques non linéaires*. — Comm. Part. Diff. Eqns., Vol. 13, No. 3, pp. 345–375.

Gérard P. and Sanchez Palencia É. (2000): *Sensitivity phenomena for certain thin elastic shells with edges*. — Math. Meth. Appl. Sci., Vol.23, No. 4, pp. 379–399.

Goldenveizer A. L. (1962): *Theory of Thin Elastic Shells*. — New York: Pergamon.

Karamian P., Sanchez-Hubert J. and Sanchez Palencia É. (2000): *A model problem for boundary layers of thin elastic shells*. — Math. Modell. Num. Anal., Vol. 34, No. 1, pp. 1–30.

Karamian P. (1998a): *Nouveaux résultats numériques concernant les coques minces hyperboliques inhibées: Cas du paraboloïde hyperbolique*. — Compt. Rend. Acad. Sci., Paris, Série IIb, Vol. 326, No. 11, pp. 755–760.

Karamian P. (1998b): *Réflexion des singularités dans les coques hyperboliques inhibées*. — Compt. Rend. Acad. Sci., Paris, Série IIb, Vol. 326, No. 1, pp. 609–614.

Karamian P. (1999) *Coques élastiques minces hyperboliques inhibées: calcul du problème limite par éléments finis et non reflexion des singularités*. — Ph. D. thesis, Université de Caen.

Karamian P. and Sanchez-Hubert J. (2002): *Boundary layers in thin elastic shells with developable middle surface*. — Euro. J. Mech. /A solids, Vol. 21, No. 1, pp. 13–47.

Leguillon D., Sanchez-Hubert J. and Sanchez Palencia É. (1999): *Model problem of singular perturbation without limit in the space of finite energy and its computation*. — C. R. Acad. Sci. Paris, Série IIb, Vol. 327, No. 5, pp. 485–492.

Lions J.L. (1973): *Perturbations Singulières dans les Problèmes aux Limites et en Contrôle Optimal*. — Berlin: Springer.

Pitkaranta J., Matache A.M. and Schwab C. (1998): *Fourier mode analysis of layers in shallow shell deformation*. — Res. rep., No. 98–18, seminar für Angewandte Mathematik, Technische Hochschule Zürich.

Sanchez-Hubert J. and Sanchez Palencia É. (1989), *Vibration and Coupling of Continuous Systems. Asymptotic Methods*. — Berlin: Springer.

Sanchez-Hubert J. and Sanchez Palencia É. (1998): *Pathological phenomena in computation of thin elastic shells*. — Trans. Can. Mech. Eng., Vol. 22, No. 4B, pp. 435–446.

Sanchez-Hubert J. and Sanchez Palencia É. (2001a): *Singular perturbations with non-smooth limit and finite element approximation of layers for model problems of shells*, In: Partial Differential Equations in Multistructures (F. Ali Mehmeti, J. von Below and S. Nicaise, Eds.). — New York: Dekker.

Sanchez-Hubert J. and Sanchez Palencia É. (2001b): *Anisotropic finite element estimates and local locking for shells: parabolic case*. — Compt. Rend. Acad. Sci., Paris, Série IIb, Vol. 329, No. 2, pp.153–159.

Sanchez-Hubert J. and Sanchez Palencia É (1997): *Coques Élastiques Minces. Propriétés Asymptotiques*. — Paris: Masson.

Sanchez Palencia É. (2000): *On a singular perturbation going out of the energy space*. — J. Math. Pures Appl., Vol. 79, No. 8, pp. 591–602.

Sanchez Palencia É. (2001) *New cases of propagation of singularities along characteristic boundaries for model problems of shell theory*. — Compt. Rend. Acad. Sci., Paris, Série IIb, Vol. 329, No. 5, pp. 315–321.

PERGAMON

Computers and Structures 80 (2002) 747–768

Computers & Structures

www.elsevier.com/locate/compstruc

Propagation of singularities and structure of layers in shells Hyperbolic case

P. Karamian-Surville [a], J. Sanchez-Hubert [b,*], É. Sanchez Palencia [b]

[a] *Université de Caen, Laboratoire de Mécanique, Département de Mathématiques et Mécanique, Boulevard Maréchal Juin, 14032 Caen, France*

[b] *Laboratoire de Modélisation en Mécanique, Université Paris VI, 8 rue du Capitaine Scott, 75015 Paris, France*

Accepted 1 February 2002

Abstract

We consider the boundary layer phenomena which appear in thin shell theory as the relative thickness ε tends to zero. We consider here the hyperbolic case. We focus our attention on the internal layers associated with propagation of singularities along the characteristics. The special structure of the limit problem often implies solutions which exhibit distributional singularities along the characteristics. The corresponding layers for small ε have a very large intensity. Layers along the characteristics have a special structure implying local locking. Numerical experiments using adaptive meshes exhibit the behavior foreseen by using asymptotic methods.

Keywords: Thin shells; Propagation of singularities; Asymptotics; Local locking; Anisotropic meshes

1. Introduction

The behavior of shells for very small values of the relative thickness 2ε is strongly dependent of the geometry of the middle surface $\mathscr{S}$ and of the loading. In particular, for certain loadings it may appear boundary and internal layers, i.e. narrow regions where the displacement is submitted to fast variations. Moreover, it may happen that the energy concentrates in the layers. Consequently, the knowledge of the behavior in the layers determines almost completely the deformation field. It is then evident that an accurate numerical computation of the layers is necessary to obtain a good description of the behavior of the deformation field of the shell.

As we shall see, the asymptotic curves (see hereafter) of the middle surface which are the characteristic curves of the membrane system of shells (i.e. the system without bending effects) play an essential role in the structure of the layers. The layers along the asymptotic curves (characteristic layers) have intensity stronger than the non-characteristic ones; moreover they exhibit classical properties of propagation of the singularities along the characteristics.

In this paper, we consider such problems, for shells whose middle surface is hyperbolic (see hereafter), in the framework of the Kirchhoff–Love theory but, this point is not essential. Analogous results may be obtained from the Mindlin model, as the corresponding asymptotic behavior for small thickness is the same (see, for instance, [6] in this respect).

Let us recall that the mechanical behavior of a shell is described by two energy forms $a_{\mathrm{m}}(u,v)$ and $\varepsilon^2 a_{\mathrm{f}}(u,v)$, associated with the deformations of the intrinsic metrics and the variation of the curvature, called membrane and flexion forms respectively, see [2,8,25,28]. The presence of the factor ε^2 in front of the second form accounts for the small rigidity of a thin body due to the flexion, it induces the above evoked specific properties for small ε.

In the sequel, we only consider "inhibited" shells, i.e. such that the middle surface $\mathscr{S}$ with the kinematic

* Corresponding author. Fax: +33-1-44-27-52-59.

E-mail addresses: jsanchez@lmm.jussieu.fr (J. Sanchez-Hubert), sanchez@lmm.jussieu.fr (É. Sanchez Palencia).

0045-7949/02/$ - see front matter
PII: S0045-7949(02)00045-7

boundary conditions is geometrically rigid. This means that the boundary conditions are such that $\mathscr{S}$ does not admit "pure bendings" i.e. displacements keeping the length on $\mathscr{S}$ invariant.

Let us now recall that at each point P of a surface $\mathscr{S}$ there exists two directions (called asymptotic directions) tangent to $\mathscr{S}$ where the normal curvature vanishes. The point P is said elliptic, hyperbolic or parabolic according to its asymptotic directions are imaginary, real and distinct or real coincident respectively. The two families of curves tangent at each point to the asymptotic directions are called asymptotic curves. In this paper, we only consider the hyperbolic case (for the case of developable surfaces see [17]).

If we denote by A_{m} and A_{f} the operators associated with the two bilinear forms a_{m} and a_{f} respectively, then classically $A_{\mathrm{m}} + \varepsilon^2 A_{\mathrm{f}}$ is elliptic for $\varepsilon > 0$ and A_{m} is of the same type as the points of the surface $\mathscr{S}$ and its characteristics are the asymptotic curves of $\mathscr{S}$. In this paper A_{m} is then a hyperbolic operator.

On the other hand, as the order of differentiation in A_{f} is higher than in A_{m}, as $\varepsilon \searrow 0$ a singular perturbation phenomenon [20] appears. Moreover, as the limit process $\varepsilon \searrow 0$ goes from a higher order elliptic system to a lower order hyperbolic one, it is clear that the limit process $\varepsilon \searrow 0$ is non-standard.

For $\varepsilon > 0$, the energy space V is such that $a_{\mathrm{m}} + \varepsilon^2 a_{\mathrm{f}}$ is continuous and coercive on it whereas the limit problem involves a new energy space V_{m} (membrane energy space) for which the bilinear form a_{m} is continuous and coercive. In fact, V_{m} is the completion of V with the norm $(a_{\mathrm{m}}(.,.))^{1/2}$ (which is a norm as a consequence of the hypothesis of inhibition).

Obviously, V_{m} contains functions less smooth than those of V. As a consequence, the solutions u^ε for $\varepsilon > 0$ belong to V but their limit as $\varepsilon \searrow 0$ is a less smooth function so that u^ε for small ε exhibits internal or boundary layers. Another important reason for the presence of layers follows from the fact that, as $V \subset V_{\mathrm{m}}$, the dual spaces are such that $V'_{\mathrm{m}} \subset V'$ and consequently, the usual forces $\vec{f}$ which belong to V' are admissible for the variational problem with $\varepsilon > 0$, but it may happen, and often it does, that $\vec{f} \notin V'_{\mathrm{m}}$. As a consequence, the limit problem does not make sense as a variational one in V_{m}. The corresponding solution of the limit problem does not belong to V_{m} and exhibits distributional singularities so that u^ε involves layers of large intensity (see [17–19] in this context). In this case, the energy of u^ε tends to infinity as the solution goes out of the space of membrane energy. In this paper, we only consider loadings f not belonging to V'_{m}. There is a criterion for $f \in V'_{\mathrm{m}}$ in terms of existence of solutions of the membrane problem (see [22] for shells and [18] for a version adapted to a model problem). Nevertheless, we shall not use this criterion here: in fact it is apparent from the structure of the solutions of the limit problem (see (2.10), (2.19) and (2.23)) that strains $\gamma_{\alpha\beta}$ do not belong to L^2 and are then out of V_{m}. Moreover, in the case $\vec{f} \notin V'_{\mathrm{m}}$ there is no general proof of the convergence of the solution u^ε for $\varepsilon \searrow 0$ to the corresponding solution of the limit problem. Up to our knowledge, this property was only proved in [30] for the model problem [18] using the structure of the boundary layer and estimates for the corresponding scaled unknowns.

It is then obvious that the non-smoothness of the solution of the limit problem has important consequences on the finite element computation of u^ε for small ε [26]. It is easy to prove (see [12] for instance) that when $f \notin V'_{\mathrm{m}}$ the convergence of the finite element approximations u_h^ε to u^ε cannot be uniform with respect to $\varepsilon \in (0, \varepsilon_0)$ with values in V_{m} (as well as in any "smaller" space!). In other words, the smaller ε is the smaller h must be chosen in order to get a good approximation. We may refer to [15,16] for these features. We shall note that the situation, in the present case of inhibited shells, is in this concern analogous to that of non-inhibited ones. We recall that in non-inhibited shells there are pure bendings and the limit behavior of u^ε is one of them. The phenomenon of locking is due to an incompatibility between the approximating spaces V_h and the subspace of pure bendings. This phenomenon appears for any conformal approximation with piecewise polynomial finite elements ([7,28]; Section XI.1) and leads again to non-uniformity of the convergence of the approximation u_h^ε to u^ε.

Let us remark that the boundary layers are usually called "edge effects" in shell theory. The existing literature (see, for instance, [13,14,23]) is mainly concerned with layers transversal to the characteristics which are non-propagating and of lower intensity than layers along the characteristics. Oppositely, most of this paper deals with characteristic layers and the associated propagation phenomena. It should be noticed that all kinds of layers enter in the framework of [24] but, in the present paper, we take into account boundary conditions which allow us to obtain a precise description of the boundary layer problem including the orders of magnitude.

For $\varepsilon > 0$, we define the problem $P(\varepsilon)$ as follows. We shall denote by Ω the domain $(0, \pi) \times (0, \pi)$ of the plane (y^1, y^2), the boundary $\partial\Omega$ of which is composed of two parts Γ_0 (clamped part) and Γ_1 (free part), they will be defined later but, in any case, Γ_0 is such that the shell is inhibited.

The configuration space V is a space of functions $v = (v_1, v_2, v_3)$ which satisfy the kinematic boundary conditions

$$v_1 = v_2 = v_3 = \frac{\partial v_3}{\partial n} = 0 \quad \text{on } \Gamma_0 \tag{1.1}$$

more precisely,

$$V = \{v; v_1, v_2 \in H^1(\Omega), v_3 \in H^2(\Omega), v \text{ satisfies } (1.1)\} \tag{1.2}$$

The two energy forms are:

$$a_{\mathrm{m}}(u,v) = \int_{\Omega} A_{11}^{\alpha\beta\lambda\mu}\gamma_{\lambda\mu}(u)\gamma_{\alpha\beta}(v)\,\mathrm{d}y \tag{1.3}$$

$$a_{\mathrm{f}}(u,v) = \int_{\Omega} A_{22}^{\alpha\beta\lambda\mu}\rho_{\lambda\mu}(u)\rho_{\alpha\beta}(v)\,\mathrm{d}y \tag{1.4}$$

where the coefficients $A_{\rho\rho}^{\alpha\beta\lambda\mu}$ are the elasticity coefficients which depend on the parameters y^1 and y^2 and satisfy the properties of symmetry and positivity. The covariant components $\gamma_{\alpha\beta}$ of the strain tensor are defined by

$$\gamma_{\alpha\beta}(u) = \tfrac{1}{2}\big(D_\alpha u_\beta + D_\beta u_\alpha\big) - b_{\alpha\beta}u_3 \tag{1.5}$$

and the covariant components of the tensor of variation of curvature are

$$\rho_{\alpha\beta}(u) = \partial_\alpha\partial_\beta u_3 - \Gamma_{\alpha\beta}^{\lambda}\partial_\gamma u_3 - b_\alpha^\lambda b_{\lambda\beta}u_3 + D_\alpha\Big(b_\beta^\lambda u_\lambda\Big) + b_\alpha^\lambda D_\beta u_\lambda \tag{1.6}$$

where D_α is the covariant derivative which acts on vectors and tensors by:

$$\begin{cases} D_\alpha u_\beta = \partial_\alpha u_\beta - \Gamma_{\alpha\beta}^{\lambda}u_\lambda \\ D_\alpha T^{\alpha\beta} = \partial_\alpha T^{\alpha\beta} + \Gamma_{\alpha\lambda}^{\beta}T^{\alpha\lambda} + \Gamma_{\alpha\lambda}^{\alpha}T^{\beta\lambda} \end{cases} \tag{1.7}$$

The coefficients $b_{\alpha\beta}$ are the coefficients of the second fundamental form of the surface $\mathscr{S}$ and b_α^β denote the corresponding covariant–contravariant components. At least, the coefficients $\Gamma_{\alpha\beta}^{\lambda}$ are the Christoffel symbols. Then, the problem $P(\varepsilon)$ is written

$$\begin{cases} \text{For given } f \in V', \text{ find } u^\varepsilon \text{ such that} \\ a_{\mathrm{m}}(u^\varepsilon, v) + \varepsilon^2 a_{\mathrm{f}}(u^\varepsilon, v) = \langle f, v\rangle \quad \forall v \in V \end{cases} \tag{1.8}$$

and from the previous hypotheses, for fixed ε, existence and uniqueness of the solution follow by the Lax–Milgram theorem [3].

Moreover, by definition of inhibited shell,

$$a_{\mathrm{m}}(v,v) = 0, \quad v \in V \Rightarrow v = 0 \tag{1.9}$$

so that

$$\|v\|_{V_{\mathrm{m}}} = [a(v,v)]^{1/2} \tag{1.10}$$

is a norm on V, V_{m} denotes the completion of V with this norm.

Classically (see, for instance, [28], Section VIII.3.1), this problem is equivalent to the system of equations

$$\begin{cases} -D_\alpha T^{\alpha\beta} - \varepsilon^2\Big[b_\gamma^\beta D_\alpha M^{\alpha\gamma} + D_\gamma\big(b_\alpha^\gamma M^{\alpha\beta}\big)\Big] = f^\beta \\ -b_{\alpha\beta}T^{\alpha\beta} + \varepsilon^2\big[D_\alpha D_\beta M^{\alpha\beta} - b_\alpha^\delta b_{\beta\delta}M^{\alpha\beta}\big] = f^3 \end{cases} \tag{1.11}$$

(where $T^{\alpha\beta} = A_{11}^{\alpha\beta\lambda\mu}\gamma_{\lambda\mu}(u^\varepsilon)$ and $M^{\alpha\beta} = A^{\alpha\beta\lambda\mu}\rho_{\lambda\mu}(u^\varepsilon)$ are the membrane stresses and flexion moments respectively) with the kinematic boundary conditions

$$\begin{cases} u^\varepsilon = 0 \\ \partial_n u_3^\varepsilon = 0 \end{cases} \quad \text{on the part } \Gamma_0 \text{ of the boundary} \tag{1.12}$$

and the natural boundary conditions on the complementary part Γ_1:

$$\begin{cases} T^{11}n_1 + T^{12}n_2 = 0 \\ T^{12}n_1 + T^{22}n_2 + 2\varepsilon^2(M^{12}n_1 + M^{22}n_2) = 0 \\ \varepsilon^2\{-n_1\partial_1 M^{11} - 2n_2\partial_1 M^{12} - n_2\partial_2 M^{22} \\ \quad -\partial_t(n_1 t_1 M^{11} + 2n_1 t_2 M^{12} + n_2 t_2 M^{22})\} = f_3 \\ \varepsilon^2[M^{11}n_1 n_1 + 2M^{12}n_1 n_2 + M^{22}n_2 n_2] = 0 \end{cases} \tag{1.13}$$

where $\vec{n}$ is the outer normal and $\vec{t}$ the unit tangent to Γ_1 in the plane tangent to $\mathscr{S}$.

We also define the variational form of the limit problem $P(0)$:

$$\begin{cases} \text{For given } f \in V'_{\mathrm{m}}, \text{ find } u^0 \in V_{\mathrm{m}} \text{ such that} \\ a_{\mathrm{m}}(u^0, v) = \langle f, v\rangle_{V'_{\mathrm{m}}, V_{\mathrm{m}}} \quad \forall v \in V_{\mathrm{m}} \end{cases} \tag{1.14}$$

where obviously a_{m} is continuous and coercive. As we shall see later the hypothesis $f \in V'_{\mathrm{m}}$ is a very restrictive condition; when it is satisfied, the existence and uniqueness of the solution $u^0 \in V_{\mathrm{m}}$ are insured.

The paper is organized as follows. In Section 2 we consider the limit problem $P(0)$ for different loadings $f \notin V'_{\mathrm{m}}$. Taking as coordinates curves $y^1 = \text{Const.}$, $y^2 = \text{Const.}$ the characteristic curves (which also are the asymptotic curves of the surface), we show, by examples, the phenomenon of propagation of the singularities along the characteristics, and we verify that the singularities of the displacement are more important, for a given loading, according to the loading lies on a characteristic or not.

In Section 3, we deduce from the previous results the scaling for the asymptotic expansions in the corresponding layers. For a normal loading $\vec{f}$ with a jump along $y^2 = \text{Const.}$ we obtain for the components of the displacement

$$\begin{cases} u_1^\varepsilon = \eta^{-1}U_1^\eta \\ u_2^\varepsilon = U_2^\eta \\ u_1^\varepsilon = \eta^{-2}U_3^\eta \end{cases}$$

where $\eta = \varepsilon^{1/3}$ (order of the thickness of the layer), and U_i^η have finite limits as $\eta \searrow 0$.

Section 4 is devoted to obtain the asymptotic behavior in a characteristic layer. We search for the components U_i^η an asymptotic expansion of the form

$$U_i^\eta \simeq U_i^0 + \eta U_i^1 + \cdots$$

where $U_i^k = U_i^k(z^1, z^2)$ with $z^1 = y^1$ and $z^2 = y^2/\eta$, the last variable being the inner one. Then the exact variational

formulation of the problem $P(\varepsilon)$ after the scaling takes the form

$$\frac{1}{\eta^2}a_2(U^0,V)+\frac{1}{\eta}a_1(U^0,V)+a_0(U^0,V)=\int_{\mathscr{B}_\eta} f_3(y^1,0)V_3^\eta\,\mathrm{d}y^1\,\mathrm{d}z^2$$

where

$$\mathscr{B}_\eta=(0,\pi)\times\left(0,\frac{\pi}{\eta}\right)$$

and the bilinear form $a_2(U^0,V)$ is such that its kernel is infinite dimensional. Consequently, the structure of the perturbation problem is that one of a penalty problem in addition to the perturbation of the domain $\mathscr{B}_\eta$ which converges to a strip. As a result, the leading order terms in the layer satisfy a constraint accounting of the vanishing of the leading term $a_2(U^0,V)$. As a consequence, the corresponding equations at the leading orders involve a Lagrange multiplier. This penalty problem implies classical locking phenomena in the finite element approximation. Coming back to the original problem $P(\varepsilon)$ in the variables y^1, y^2, it appears a non-uniformity of the convergence as it was foreseen for $\vec{f}\notin V'_{\mathrm{m}}$. We then see that the non-uniformity may be explained in terms of a special kind of locking (see [4]) inside the layers (local locking). As a consequence of such a local structure, we may take advantage of using anisotropic meshes (i.e. with triangles elongated in the tangential direction see [1]) for the numerical computations (see examples of the numerical experiments in Section 7). The precise finite element estimates of these phenomena were considered in [27] for a model parabolic problem and in [17] and [29] for developable shells. The present paper extends them to hyperbolic shells (Section 6).

Section 5 is concerned by the asymptotic behavior of a non-characteristic layer. As in Section 4, we exhibit the exponential decreasing of the solution as z^2 tends to infinity.

2. Singularities for the limit problem and their propagation

2.1. Singularity along a characteristic due to a discontinuity of the loading f_3

We consider a shell with hyperbolic middle surface. The domain Ω of the parameters (y^1,y^2) which define the middle surface $\mathscr{S}$ is $\Omega=(0,\pi)\times(0,\pi)$. The coordinates curves $y^1=\text{Const.}$, $y^2=\text{Const.}$ are the asymptotic curves so that the coefficients $b_{\alpha\beta}$ of the second fundamental form are $b_{11}=b_{22}=0$, $b_{12}\neq 0$. It should be noticed that the considered portion of surface is limited by asymptotic curves. This fact is not essential and only used to facilitate ulterior changes of variables. The shell is clamped along $\Gamma_0=\{y^1=\pi\}\cup\{y^2=\pi\}$.

Let us consider the limit problem $P(0)$. The equations satisfied by the components of the constraints are

$$\begin{cases}-D_\alpha T^{\alpha\beta}=f^\beta\\ -2b_{12}T^{12}=f_3\end{cases}\tag{2.1}$$

and the components of the displacement are solutions of the system

$$\gamma_{\alpha\beta}(u)=\tfrac{1}{2}(D_\alpha u_\beta+D_\beta u_\alpha)-b_{\alpha\beta}u_3=B_{\alpha\beta\lambda\mu}T^{\lambda\mu}\tag{2.2}$$

where the coefficients $B_{\alpha\beta\lambda\mu}$ denote the compliances which constitute the inverse matrix of that of the $A^{\alpha\beta\lambda\mu}$ and where D_α are the covariant derivatives.

We note that the classical description of the limit problem is (2.1) with $T^{\alpha\beta}$ expressed in terms of u as in (1.11). Nevertheless, in order to study the singularities we shall consider the unknowns $T^{\alpha\beta}$ and u_i satisfying (2.1) and (2.2). The system (2.1) only involves the unknowns $T^{\alpha\beta}$; and (2.2) is then a system for the unknowns u_i. Both systems are essentially hyperbolic ones with the characteristics $y^1=\text{Const.}$, $y^2=\text{Const.}$

The boundary conditions are chosen such that the shell is inhibited: in the sequel, the boundary will be fixed along the two characteristics $y^1=\pi$ and $y^2=\pi$.

We take as loading $\vec{f}$

$$\begin{cases}f^\beta=0\\ f_3=\widetilde{F}(y^1,y^2)\theta_{[a^1,b^1]}(y^1)Y\left(y^2-\frac{\pi}{2}\right)\end{cases}\tag{2.3}$$

where $\theta_{[a^1,b^1]}$ is the characteristic function of an interval $[a^1,b^1]\subset[0,\pi]$ and $\widetilde{F}$ is a smooth function on $[0,\pi]\times[\pi/2,\pi]$; Y is the Heaviside function (i.e. the step function), see Fig. 9.

On the free part of the boundary we have the natural boundary condition $T^{\alpha\beta}n_\beta=0$ where $\vec{n}$ is, in the tangent plane, the unit normal to the boundary $\Gamma_1=\{y^1=0\}\cup\{y^2=0\}$. Let us denote by $\vec{a}_1$ and $\vec{a}_2$ the covariant tangent vectors at the current point of the surface and by $\vec{a}^\alpha$ $(\vec{a}^\alpha\vec{a}_\beta=\delta^\alpha_\beta)$ the corresponding contravariant vectors. As the boundary $y^1=0$ is tangent to $\vec{a}_2$ we have $\vec{n}\|\vec{a}^1$ and consequently $n_1\neq 0$ and $n_2=0$. As a consequence, the boundary conditions write

$$\begin{cases}T^{11}(0,y^2)=0\\ T^{12}(0,y^2)=0\end{cases}\tag{2.4}$$

Analogously, on the boundary $y^2=0$ we have $\vec{n}\|\vec{a}^2$ and then $n_2\neq 0$ and $n_1=0$ consequently

$$\begin{cases}T^{22}(y^1,0)=0\\ T^{12}(0,y^2)=0\end{cases}\tag{2.5}$$

The problem (2.1) is a hyperbolic one for T^{11} and T^{22} and

$$T^{12} = -\frac{\widetilde{F}(y^1,y^2)\theta_{[a^1,b^1]}(y^1)Y\left(y^2-\frac{\pi}{2}\right)}{2b_{12}(y^1,y^2)}$$

is well determined.

On Γ_1 the boundary conditions (2.4) and (2.5) classically insure existence and uniqueness for the hyperbolic problem.

Now, let us consider the system (2.1) and write it under the form

$$\begin{cases} -\partial_1 T^{11} - \left(2\Gamma^1_{11}+\Gamma^2_{12}\right)T^{11} - \Gamma^1_{22}T^{22} = \partial_2 T^{12} + \left(3\Gamma^1_{12}+\Gamma^2_{22}\right)T^{12} \\ -\partial_2 T^{22} - \left(2\Gamma^2_{22}+\Gamma^1_{12}\right)T^{22} - \Gamma^2_{11}T^{11} = \partial_1 T^{12} + \left(3\Gamma^2_{12}+\Gamma^1_{11}\right)T^{12} \\ -2b_{12}T^{12} = \widetilde{F}(y^1,y^2)\theta_{[a^1,b^1]}(y^1)Y\left(y^2-\frac{\pi}{2}\right) \end{cases} \tag{2.6}$$

Taking account of the singularity of the right-hand side of (2.6), we are concerned with the propagation of the singularities of this system. Let us consider the classical sequence of distributions on $\mathbb{R}$ with increasing singularities

$$\ldots, xY(x), Y(x), \delta(x), \delta'(x), \ldots$$

where Y and δ denote the Heaviside function and the Dirac mass respectively. More precisely, this distributions will be considered as singularities at $x=0$ whereas their values for $x\neq 0$ are discarded; for instance $Y(x)$ is considered merely as the unit jump at $x=0$. In order to describe the singularity, for example along $y^2=\pi/2$, we consider expansions of the form (for instance)

$$w \simeq \delta'\left(y^2-\frac{\pi}{2}\right)W^0\left(y^1\right) + \delta\left(y^2-\frac{\pi}{2}\right)W^1\left(y^1\right) + \cdots$$

where it is understood that the terms $\cdots$ are less singular than the previous ones at $y^2=\pi/2$. Such kind of expansion is in the framework of discontinuous solutions (see for instance [11], Section 4.11 and also [18,31]). In this context, we search for the unknowns T^{11} and T^{22} expansions of the form

$$\begin{cases} T^{11} \cong A^{11}(y^1)\delta\left(y^2-\frac{\pi}{2}\right)+\cdots \\ T^{22} \cong A^{22}(y^1)Y\left(y^2-\frac{\pi}{2}\right)+\cdots \end{cases} \tag{2.7}$$

By substituting (2.7) into (2.6) we obtain for the coefficient of the main singularity of T^{11}:

$$\begin{aligned} &-\frac{\mathrm{d}A^{11}}{\mathrm{d}y^1} - \left(2\Gamma^1_{11}+\Gamma^2_{12}\right)A^{11} \\ &\quad = -\frac{F(y^1)\theta_{[a^1,b^1]}(y^1)}{2b_{12}\left(y^1,\frac{\pi}{2}\right)} \underset{\text{déf}}{\equiv} -\Phi_1\left(y^1\right)\theta_{[a^1,b^1]}\left(y^1\right) \end{aligned} \tag{2.8}$$

where $F(y^1)=\widetilde{F}(y^1,\pi/2)$.

Then, the boundary condition $T^{11}(0,y^2)=0$ gives $A^{11}(0)=0$, consequently Eq. (2.8) completely determines the unknown A^{11}. More precisely, we have

$$\begin{cases} A^{11}(y^1)=0 \quad \text{for } 0<y^1<a^1 \\ A^{11}(y^1) = \left(\int_{a^1}^{y^1}\Phi_1(\eta)\exp\left[\int_{a^1}^{\eta}\Gamma(\xi)\,\mathrm{d}\xi\right]\mathrm{d}\eta\right) \\ \qquad\qquad \times\exp\left(-\int_{a^1}^{y^1}\Gamma(\xi)\,\mathrm{d}\xi\right) \quad \text{for } a^1<y^1<b^1 \\ A^{11}(y^1) = \lambda\exp\left[\int_{y^1}^{l}\Gamma(\xi)\,\mathrm{d}\xi\right] \quad \text{for } b^1<y^1<l \end{cases}$$

where

$$\Gamma(\xi) \equiv 2\Gamma^1_{11}\left(\xi,\frac{\pi}{2}\right) + \Gamma^2_{12}\left(\xi,\frac{\pi}{2}\right)$$

and λ is such that $A^{11}(y^1)$ is continuous at $y^1=\pi/2$. As for T^{22}, the coefficient of the main singularity, in $Y(y^2-(\pi/2))$, is

$$A^{22} = -\Gamma^2_{11}\left(y^1,\frac{\pi}{2}\right)A^{11}\left(y^1\right)$$

Remark 2.1. We observe that $A^{11}(y^1)=0$ for $0<y^1<a^1$ but for $a^1<y^1<l$, in general, $A^{11}(y^1)\neq 0$ though $\theta_{[a^1,b^1]}(y^1)\equiv 0$: this is the *phenomenon of propagation of the singularities*.

Now, from (2.2) we get the system, at the leading order, for the components of the displacement

$$\begin{cases} \partial_1 u_1 - \Gamma^1_{11}u_1 - \Gamma^2_{11}u_2 = \delta\left(y^2-\frac{\pi}{2}\right)C_{1111}\left(y^1,\frac{\pi}{2}\right)A^{11}(y^1) \\ \partial_2 u_2 - \Gamma^1_{22}u_1 - \Gamma^2_{22}u_2 = \delta\left(y^2-\frac{\pi}{2}\right)C_{2211}\left(y^1,\frac{\pi}{2}\right)A^{11}(y^1) \\ \frac{1}{2}(\partial_1 u_2+\partial_2 u_1) - \Gamma^1_{12}u_1 - \Gamma^2_{12}u_2 - b_{12}u_3 \\ \quad = \delta\left(y^2-\frac{\pi}{2}\right)C_{1211}\left(y^1,\frac{\pi}{2}\right)A^{11}(y^1) \end{cases} \tag{2.9}$$

which suggests to search for the main singularities of the components of the form

$$\begin{cases} u_1 \cong \delta\left(y^2-\frac{\pi}{2}\right)U_1(y^1) \\ u_2 \cong Y\left(y^2-\frac{\pi}{2}\right)U_2(y^1) \\ u_3 = \delta'\left(y^2-\frac{\pi}{2}\right)U_3(y^1) \end{cases} \tag{2.10}$$

Substituting (2.10) into (2.9) we get:

$$\begin{cases} \frac{\mathrm{d}U_1}{\mathrm{d}y^1} - \Gamma^1_{11}U_1 = C_{1111}\left(y^1,\frac{\pi}{2}\right)A^{11}(y^1) \underset{\text{déf}}{=} \Psi_1(y^1) \\ U_2(y^1) = \Gamma^1_{22}U_1(y^1) + C_{2211}\left(y^1,\frac{\pi}{2}\right)A^{11}(y^1) \underset{\text{déf}}{=} \Psi_2(y^1) \\ U_3(y^1) = \dfrac{U_1(y^1)}{2b_{12}\left(y^1,\frac{\pi}{2}\right)} \end{cases} \tag{2.11}$$

from which, by using the boundary condition

$$u_1\left(\pi,y^2\right)=0$$

we obtain

$$\begin{aligned} U_1\left(y^1\right) = &\left[\int_{y^1}^{\pi} -\Psi_1(\eta)\exp\left(-\int_0^{\eta}\Gamma^1_{11}\left(\eta,c^2\right)\mathrm{d}\eta\right)\right] \\ &\times\exp\left(\int_0^{y^1}\Gamma^1_{11}\left(\xi,c^2\right)\mathrm{d}\xi\right) \end{aligned} \tag{2.12}$$

which completely determines the unknown $U_1(y^1)$ and consequently $U_2(y^1)$ and $U_3(y^1)$.

2.2. Complements and comments to the previous case

In the same configuration as in the previous section, we consider the boundary $y^2 = 0$ and the datum

$$\begin{cases} f^\beta = 0 \\ f_3 = f(y^1, y^2) \end{cases} \quad \text{with } f(y^1, 0) \neq 0 \tag{2.13}$$

By extending the datum f_3 by $f_3(y^1, y^2) \equiv 0$ for $y^2 < 0$ and considering the problem in the corresponding extended domain $\widetilde{\Omega}$, we have in $\widetilde{\Omega}$ a datum $\widetilde{f}_3$ of the form (2.3) (for details see [31], Section 3). Then, the singularities of the components $T^{\alpha\beta}$ and u_i are analogous to these obtained in the previous section. In particular, the singularities of the components of the displacement are again of the form (2.10).

2.3. Loading with a δ-like singularity along a non-characteristic segment

We now consider the loading (see Fig. 10)

$$\begin{cases} f^\beta = 0 \\ f_3 = Y\left(\frac{\pi}{2} - y^2\right)\delta(y^1 - y^2) \end{cases} \tag{2.14}$$

which is merely a δ-like loading of intensity 1 along the non-characteristic segment $y^2 = y^1$, $y^2 < \pi/2$ and the solution will be singular along it but it does not exhibit propagation properties. Moreover, when considering f_3 as a function of y^2 with values in a space of distributions of the variable y^1, it clearly has a jump at $y^2 = \pi/2$. This implies a singularity of the solution there which propagates along the whole characteristic $y^2 = \pi/2$. Obviously the same property holds along $y^1 = \pi/2$ (note that $Y((\pi/2) - y^2)$ may be replaced in (2.14) by $Y((\pi/2) - y^1)$). So the solution will be singular along the segment $y^2 = y^1$, $y^2 < \pi/2$ and along the whole characteristics $y^1 = \pi/2$ and $y^2 = \pi/2$. We shall see later that the former singularity is weaker than the others due to the fact that the later lies along characteristics.

We always have exactly

$$T^{12} = -\frac{Y\left(\frac{\pi}{2} - y^2\right)\delta(y^1 - y^2)}{2b_{12}}$$

2.3.1. Singularities along the characteristic $y^2 = \pi/2$

2.3.1.1. Behavior of the components $T^{\alpha\beta}$. In order to describe the behavior of T^{12} at $y^2 = \pi/2$, let us take a test function $\varphi(y^1)$ of $\mathscr{D}(\mathbb{R})$, then we have

$$\begin{aligned} &\left\langle Y\left(\frac{\pi}{2} - y^2\right)\delta(y^1 - y^2), \varphi(y^1)\right\rangle \\ &= Y\left(\frac{\pi}{2} - y^2\right)\left\langle \delta(y^1 - y^2), \varphi(y^1)\right\rangle = Y\left(\frac{\pi}{2} - y^2\right)\varphi(y^2) \\ &= Y\left(\frac{\pi}{2} - y^2\right)\left[\varphi\left(\frac{\pi}{2}\right) + y^2\varphi'\left(\frac{\pi}{2}\right) + \cdots\right] \\ &= \left\langle Y\left(\frac{\pi}{2} - y^2\right)\left[\delta\left(y^1 - \frac{\pi}{2}\right) - y^1\delta'\left(y^1 - \frac{\pi}{2}\right)\right.\right. \\ &\quad \left.\left. + \cdots\right], \varphi(y^1)\right\rangle \end{aligned}$$

Consequently, the main singularity of T^{12} in the vicinity of $y^2 = \pi/2$ is

$$T^{12} \simeq -\frac{Y\left(\frac{\pi}{2} - y^2\right)\delta\left(y^1 - \frac{\pi}{2}\right)}{2b_{12}\left(y^1, \frac{\pi}{2}\right)} \tag{2.15}$$

Then the system (2.6) gives, as in the Section 2.3.1, for T^{11} and T^{22}:

$$\begin{cases} T^{11} \simeq \delta\left(y^2 - \frac{\pi}{2}\right)\widetilde{A}^{11}(y^1) \\ T^{22} \simeq Y\left(\frac{\pi}{2} - y^2\right)A^{22}(y^1) \end{cases} \tag{2.16}$$

where

$$\begin{cases} -\dfrac{\mathrm{d}\widetilde{A}^{11}}{dy^1} - \left(2\Gamma^1_{11} + \Gamma^2_{12}\right)\widetilde{A}^{11} = \dfrac{\delta\left(y^1 - \frac{\pi}{2}\right)}{2b_{12}\left(y^1, \frac{\pi}{2}\right)} \\ A^{22}(y^1) = -\Gamma^2_{11}\widetilde{A}^{11}(y^1) \end{cases} \tag{2.17}$$

The solution of the differential Eq. (2.17) is

$$\begin{aligned} \widetilde{A}^{11}(y^1) = \frac{-1}{2b_{12}\left(\frac{\pi}{2}, \frac{\pi}{2}\right)} Y\left(y^1 - \frac{\pi}{2}\right) \exp\left(- \int_{\pi/2}^{y^1} \left(2\Gamma^1_{11}\left(\eta, \frac{\pi}{2}\right)\right.\right. \\ \left.\left. + \Gamma^2_{12}\left(\eta, \frac{\pi}{2}\right)\right) \mathrm{d}\eta\right) \end{aligned} \tag{2.18}$$

Remark 2.2. We observe that $\widetilde{A}^{11}(y^1)$ is identically zero for $y^1 < \pi/2$ but does not vanish in general for $y^1 > \pi/2$: propagation of the singularity along the characteristic $y^2 = \pi/2$ from the extremity of the segment where lies the singularity of the loading to its extremity $y^1 = \pi$.

2.3.1.2. Singularities of the components of the displacement. Now, we consider the singularities of the components of the displacement. From the system (2.9) we see that the main singularities are respectively

$$\begin{cases} u_1 \simeq \delta\left(y^2 - \frac{\pi}{2}\right)U_1(y^1) \\ u_2 \simeq Y\left(\frac{\pi}{2} - y^2\right)U_2(y^1) \\ u_3 \simeq \delta'\left(y^2 - \frac{\pi}{2}\right)U_1(y^1) \end{cases} \tag{2.19}$$

where the functions U_i satisfy the system

$$\begin{cases} \dfrac{\mathrm{d}U_1}{\mathrm{d}y^1} - \Gamma^1_{11}U_1 = C_{1111}\left(y^1, \dfrac{\pi}{2}\right)\widetilde{A}^{11}(y^1) \underset{\text{déf}}{=} \widetilde{\Psi}_1(y^1) \\ -U_2(y^1) = \Gamma^1_{22}U_1(y^1) + C_{2211}\left(y^1, \frac{\pi}{2}\right)\widetilde{A}^{11}(y^1) \underset{\text{déf}}{=} \widetilde{\Psi}_2(y^1) \\ U_3(y^1) = \dfrac{U_1(y^1)}{2b_{12}\left(y^1, \frac{\pi}{2}\right)} \end{cases} \tag{2.20}$$

which are exactly the same as in the previous example, but with $\widetilde{A}^{11}(y^1)$ and $\widetilde{\Psi}_\alpha(y^1)$ instead of $A^{11}(y^1)$ and $\Psi_\alpha(y^1)$ respectively. The expression of the component $U_1(y^1)$ is (2.12) with $\widetilde{\Psi}_1(y^1)$ instead of $\Psi_1(y^1)$.

2.3.2. Singularities along the non-characteristic segment Σ

To study the singularities generated by $\delta(y^1 - y^2)$ we take as new curvilinear coordinates ξ^1 curvilinear abscise along Σ and ξ^2 in the direct normal direction. Then, for these new coordinates $\xi^2 = \text{Const.}$ is not a characteristic and consequently $b_{11} \neq 0$; of course, we also have $b_{22} \neq 0$. Consequently, in (2.6) the third equation becomes

$$T^{12} = -\frac{Y\left(\frac{\pi}{2} - \xi^1\right)\delta(\xi^2)}{2b_{12}(\xi^1, 0)} + \frac{b_{11}(\xi^1, 0)}{2b_{12}(\xi^1, 0)}T^{11} + \frac{b_{22}(\xi^1, 0)}{2b_{12}(\xi^1, 0)}T^{22} \tag{2.21}$$

and in the two first equations T^{12} must be replaced by (2.21).

Using the same technique as before, we search for the singularities of the components $T^{\alpha\beta}$ of the form

$$T^{\alpha\beta} \simeq \delta(\xi^2)A^{\alpha\beta}(\xi^1) + \cdots \tag{2.22}$$

The components of the displacement are then solutions of the system

$$\partial_1 u_1 - \Gamma^1_{11}u_1 - \Gamma^2_{11}u_2 - b_{11}u_3 = \delta(\xi^2)C_{11\lambda\mu}A^{\lambda\mu}(\xi^1) + \cdots$$

$$\partial_2 u_2 - \Gamma^1_{22}u_1 - \Gamma^2_{22}u_2 - b_{22}u_3 = \delta(\xi^2)C_{22\lambda\mu}A^{\lambda\mu}(\xi^1) + \cdots$$

$$\tfrac{1}{2}(\partial_1 u_2 + \partial_2 u_1) - \Gamma^1_{12}u_1 - \Gamma^2_{12}u_2 - b_{12}u_3 = \delta(\xi^2)C_{12\lambda\mu}A^{\lambda\mu}(\xi^1) + \cdots$$

We then see that the singularities of components u_i are of the form

$$\begin{cases} u_1 \simeq Y(\xi^2)U_1(\xi^1) + \cdots \\ u_2 \simeq Y(\xi^2)U_2(\xi^1) + \cdots \\ u_3 \simeq \delta(\xi^2)U_3(\xi^1) + \cdots \end{cases} \tag{2.23}$$

As announced, we see that "the singularities due to the Dirac along the non-characteristic segment Σ are lower than those due to the Y singularity along the characteristic $y^2 = \pi/2$. On the other hand, as the equations are not differential, the singularities do not propagate, they are confined on Σ.

3. Singularities and asymptotics: scaling for the internal layers

The examples of the previous section where chosen such that they give for the components of the displacement the main singularities described in (2.10) or (2.19). Our aim is now to describe the internal layers which develop in the vicinity of the characteristic $y^2 = \pi/2$ and of the non-characteristic segment Σ respectively. Classically [10], the asymptotic expansions in a layer are obtained by introducing an internal variable

$$z^2 = \frac{y^2 - \frac{\pi}{2}}{\eta(\varepsilon)}, \quad \text{resp. } \frac{\xi^2}{\eta(\varepsilon)},\ \eta(\varepsilon) \searrow 0 \text{ as } \varepsilon \searrow 0 \tag{3.1}$$

where $\eta(\varepsilon)$ is of order of the thickness of the layer. Then, the asymptotic expansions of the components of the displacement $\vec{u}^\varepsilon$ are of the form

$$u_i^\varepsilon = \sum_k \eta^k u_i^k\left(y^1, \frac{y^2 - \frac{\pi}{2}}{\eta}\right), \quad \text{resp. } \sum_k \eta^k u_i^k\left(\xi^1, \frac{\xi^2}{\eta}\right) \tag{3.2}$$

Let us show that the singularities exhibited in Section 2 are the limits as $\eta \searrow 0$ of the asymptotic expansions of the form (3.2).

Lemma 3.1. *Let $\Phi(\xi)$ be a function* satisfying

$$\begin{aligned} &\int_{\mathbb{R}} \xi^n \Phi(\xi)\,\mathrm{d}\xi = 0 \quad \textit{for } n = 0, \ldots, k-2, \\ &\int_{\mathbb{R}} \xi^{k-1}\Phi(\xi)\,\mathrm{d}\xi = C \end{aligned} \tag{3.3}$$

with $C \neq 0$. Then we have in the distribution sense

$$\frac{1}{\eta^k}\Phi\left(\frac{x}{\eta}\right) \underset{\eta\to 0}{\to} (-1)^{k-1}C\delta^{(k-1)} \tag{3.4}$$

Proof. Let $\varphi(x) \in \mathscr{D}(\mathbb{R})$, we have

$$\begin{aligned} &\int_{\mathbb{R}} \frac{1}{\eta^k}\Phi\left(\frac{x}{\eta}\right)\varphi(x)\,\mathrm{d}x \\ &\quad = \int_{\mathbb{R}} \frac{1}{\eta^k}\Phi\left(\frac{x}{\eta}\right)\left[\varphi(0) + \cdots + x^k\varphi^{(k)}(0) + \cdots\right]\mathrm{d}x \\ &\quad = \frac{1}{\eta^{k-1}}\varphi(0)\int_{\mathbb{R}} \Phi(u)\,\mathrm{d}u + \cdots + \frac{1}{\eta}\varphi^{(k-1)}(0) \\ &\qquad \times \int_{\mathbb{R}} \left[\left(\eta u\right)^{k-1}\Phi(u)\right]\mathrm{d}\eta u + \mathscr{O}(\eta) \end{aligned}$$

where the $k-1$ first integrals vanish and the kth one is, taking account of (3.3), equal to

$$C\varphi^{(k-1)}(0)$$

As $\eta \to 0$ we then have

$$\lim_{\eta\to 0}\int_{\mathbb{R}} \frac{1}{\eta^k}\Phi\left(\frac{x}{\eta}\right)\varphi(x)\,\mathrm{d}x = C\varphi^{(k-1)}(0) = \left\langle (-1)^{k-1}C\delta^{(k-1)}, \varphi\right\rangle$$

i.e. (3.4). □

Consequently, as the behavior of the components of the displacement solution of the limit problem are

$$\begin{cases} u_1 \simeq \delta\left(y^2-\frac{\pi}{2}\right)U_1(y^1)\\ u_2 \simeq Y\left(y^2-\frac{\pi}{2}\right)U_2(y^1)\\ u_3 \simeq \delta'\left(y^2-\frac{\pi}{2}\right)U_3(y^1)\end{cases}$$

in the internal layer in the vicinity of $y^2=\pi/2$, we shall search for the asymptotic behavior of u_i^ε as $\varepsilon \searrow 0$ under the form

$$\begin{cases} u_1^\varepsilon \simeq \eta^{-1}U_1^\eta\left(y^1,\dfrac{y^2-\frac{\pi}{2}}{\eta}\right)\\ u_2^\varepsilon \simeq \eta^{0}U_2^\eta\left(y^1,\dfrac{y^2-\frac{\pi}{2}}{\eta}\right)\\ u_3^\varepsilon \simeq \eta^{-2}U_3^\eta\left(y^1,\dfrac{y^2-\frac{\pi}{2}}{\eta}\right)\end{cases} \tag{3.5}$$

In the same way, we obtain in the vicinity of the internal non-characteristic layer Σ, according to (2.23),

$$\begin{cases} u_1^\varepsilon \simeq U_1^\eta\left(\xi^1,\frac{\xi^2}{\eta}\right)\\ u_2^\varepsilon \simeq U_2^\eta\left(\xi^1,\frac{\xi^2}{\eta}\right)\\ u_3^\varepsilon \simeq \eta^{-1}U_3^\eta\left(\xi^1,\frac{\xi^2}{\eta}\right)\end{cases} \tag{3.6}$$

where $\eta(\varepsilon)$ is a small parameter undetermined for the time being.

4. Structure of the characteristic internal layer in the vicinity of $y^2=\pi/2$

4.1. Preliminaries

Let us recall that the domain is $\Omega=(0,\pi)\times(0,\pi)$ of the (y^1,y^2) plane, the fixed part Γ_0 of the boundary is $y^1=\pi$, $y^2=\pi$ the rest of the boundary being assumed to be free. At last, we consider the loading defined by (2.3).

The shell problem is: find u^ε satisfying

$$\begin{aligned}&\int_\Omega \{A^{1111}\gamma_{11}(u^\varepsilon)\gamma_{11}(v) + 2A^{1112}[\gamma_{12}(u^\varepsilon)\gamma_{11}(v)\\ &+\gamma_{11}(u^\varepsilon)\gamma_{12}(v)]\,\mathrm{d}y^1\,\mathrm{d}y^2 + A^{1122}[\gamma_{22}(u^\varepsilon)\gamma_{11}(v)\\ &+\gamma_{11}(u^\varepsilon)\gamma_{22}(v)] + 4A^{1212}\gamma_{12}(u^\varepsilon)\gamma_{12}(v)\\ &+2A^{2212}[\gamma_{12}(u^\varepsilon)\gamma_{22}(v)+\gamma_{22}(u^\varepsilon)\gamma_{12}(v)]\\ &+A^{2222}\gamma_{22}(u^\varepsilon)\gamma_{22}(v)\}\,\mathrm{d}y^1\,\mathrm{d}y^2+\varepsilon^2\\ &\times\int_\Omega B^{\alpha\beta\lambda\mu}\rho_{\lambda\mu}\rho_{\alpha\beta}\,\mathrm{d}y^1\,\mathrm{d}y^2\\ &=\int_\Omega f(y^1,y^2)v_3(y^1,y^2)\,\mathrm{d}y^1\,\mathrm{d}y^2\end{aligned} \tag{4.1}$$

where

$$\begin{cases}\gamma_{11}(v)=\partial_1 v_1-\Gamma_{11}^1 v_1-\Gamma_{11}^2 v_2\\ \gamma_{12}(v)=\frac{1}{2}(\partial_1 v_2+\partial_2 v_1)-\Gamma_{12}^1 v_1-\Gamma_{12}^2 v_2-b_{12}v_3\\ \gamma_{22}(v)=\partial_2 v_2-\Gamma_{22}^1 v_1-\Gamma_{22}^2 v_2\end{cases}$$

in the space

$$\mathscr{V}=\left\{v=(v_1,v_2,v_3)\in H^1\times H^1\times H^2;\ v=\frac{\partial v_3}{\partial n}=0 \text{ on } \Gamma_0\right\} \tag{4.2}$$

The internal variable is defined by (3.1) then, taking account of the results of Section 3, the scaling for the components of the displacement is

$$\begin{cases} u_1^\varepsilon=\eta^{-1}U_1^\eta(y^1,z^2)\\ u_2^\varepsilon=\eta^{0}U_2^\eta(y^1,z^2)\\ u_3^\varepsilon=\eta^{-2}U_3^\eta(y^1,z^2)\end{cases} \tag{4.3}$$

where $z^2=(y^2-(\pi/2))\eta$, in the sequel we shall denote by D_2 the derivative

$$D_2=\frac{\partial}{\partial z^2}=\eta\frac{\partial}{\partial y^2}.$$

(to be not taken as the covariant differentiation which will be developed to avoid confusion).

Substituting (4.3) into (4.1) and taking the test functions depending on η as in (4.3), we obtain at the successive orders, after multiplying by η,

$$
\begin{aligned}
&\eta^{-2}\int_{B^\eta} 4A^{1212}\left(\frac{1}{2}D_2U_1^\eta - b_{12}U_3^\eta\right)\left(\frac{1}{2}D_2V_1^\eta - b_{12}V_3^\eta\right)\mathrm{d}y^1\,\mathrm{d}z^2\\
&\quad+\eta^{-1}\Bigg\{\int_{B^\eta}\Bigg\langle 2A^{1112}\Bigg[\left(\partial_1U_1^\eta-\Gamma_{11}^1U_1^\eta\right)\left(\frac{1}{2}D_2V_1^\eta-b_{12}V_3^\eta\right)\\
&\quad+\left(\frac{1}{2}D_2U_1^\eta-b_{12}U_3^\eta\right)\left(\partial_1V_1^\eta-\Gamma_{11}^1V_1^\eta\right)\Bigg]\\
&\quad-4A^{1212}\Bigg[\left(\frac{1}{2}D_2U_1^\eta-b_{12}U_3^\eta\right)\Gamma_{12}^1V_1^\eta\\
&\quad+\Gamma_{12}^1U_1^\eta\left(\frac{1}{2}D_2V_1^\eta-b_{12}V_3^\eta\right)\Bigg]\\
&\quad+2A^{2212}\Bigg\langle\left(\frac{1}{2}D_2U_1^\eta-b_{12}U_3^\eta\right)\left(D_2V_2^\eta-\Gamma_{22}^1V_1^\eta\right)\\
&\quad+\left(D_2U_2^\eta-\Gamma_{22}^1U_1^\eta\right)\left(\frac{1}{2}D_2V_1^\eta-b_{12}V_3^\eta\right)\Bigg\rangle\mathrm{d}y^1\,\mathrm{d}z^2\Bigg\}\\
&\quad+\eta^0\Bigg\{\int_{B^\eta}\Bigg\langle A^{1111}\left(\partial_1U_1^\eta-\Gamma_{11}^1U_1^\eta\right)\left(\partial_1V_1^\eta-\Gamma_{11}^1V_1^\eta\right)\\
&\quad-2A^{1112}\left[\left(\partial_1U_1^\eta-\Gamma_{11}^1U_1^\eta\right)\Gamma_{12}^1V_1^\eta\right.\\
&\quad\left.+\left(\partial_1V_1^\eta-\Gamma_{11}^1V_1^\eta\right)\Gamma_{12}^1U_1^\eta\right]\\
&\quad+A^{1122}\left[\left(\partial_1U_1^\eta-\Gamma_{11}^1U_1^\eta\right)\left(D_2V_2^\eta-\Gamma_{22}^1V_1^\eta\right)\right.\\
&\quad\left.+\left(D_2U_2^\eta-\Gamma_{22}^1U_1^\eta\right)\left(\partial_1V_1^\eta-\Gamma_{11}^1V_1^\eta\right)\right]4A^{1212}\\
&\quad\times\Bigg[\left(\partial_1U_2^\eta-\Gamma_{12}^2U_2^\eta\right)\left(\frac{1}{2}D_2V_1^\eta-b_{12}V_3^\eta\right)\\
&\quad+\left(\frac{1}{2}D_2U_1^\eta-b_{12}U_3^\eta\right)\left(\partial_1V_2^\eta-\Gamma_{12}^2V_2^\eta\right)\\
&\quad+\left(\Gamma_{12}^1\right)^2V_1^\eta U_1^\eta\Bigg]-2A^{2212}\Bigg[\left(\frac{1}{2}D_2U_1^\eta-b_{12}U_3^\eta\right)\Gamma_{22}^2V_2^\eta\\
&\quad+\Gamma_{12}^1U_1^\eta\left(D_2V_2^\eta-\Gamma_{22}^1V_1^\eta\right)\Bigg]\\
&\quad+A^{2222}\left(D_2U_2^\eta-\Gamma_{22}^1U_1^\eta\right)\left(D_2V_2^\eta-\Gamma_{22}^1V_1^\eta\right)\Bigg\rangle\mathrm{d}y^1\,\mathrm{d}z^2\Bigg\}\\
&\quad+\varepsilon^2\left[\eta^{-6}\int_{B^\eta}B^{2222}\left(D_2^2U_3^\eta\right)\left(D_2^2V_3^\eta\right)\mathrm{d}y^1\,\mathrm{d}z^2+\cdots\right]\\
&\quad=\int_{B^\eta}f\left(y^1,\eta z^2\right)V_3^\eta\left(y^1,z^2\right)\mathrm{d}y^1\,\mathrm{d}z^2 \qquad (4.4)
\end{aligned}
$$

where B_η is the dilated domain $(0,\pi)\times(-(\pi/2\eta),+(\pi/2\eta))$. The elasticity coefficients $A^{\alpha\beta\lambda\mu}$ and the Christoffel symbols are taken at $(y^1,\pi/2)$. At last, in the expression of the components $\rho_{\alpha\beta}(U^\eta)$ and $\rho_{\alpha\beta}(V^\eta)$ of order less than η^{-6} were represented by $\cdots$ and will be discarded in the sequel.

We choose η such way that the leading term of flexion is of order η^0 in order to appear in the limit problem. Then we have $\eta=\mathcal{O}\left(\varepsilon^{1/3}\right)$, we shall take

$$\eta(\varepsilon)=\varepsilon^{1/3} \qquad (4.5)$$

Roughly speaking, this is a penalty problem for $\eta\searrow 0$. Indeed, we observe that the vanishing of the terms of higher order (in η^{-2} defines a subspace $G\neq\{0\}$ where the limit lives. Moreover, this penalty problem is not classical because there are terms of intermediate order η^{-1}. Formally, we are in the framework of [5] but there are significant differences

1. The specific hypotheses of [5] leading to a rigorous proof of the limit process are not necessarily satisfied.
2. The domain B_η depends on the parameter and tends to an unbounded domain as $\eta\searrow 0$.
3. There are perturbation terms, denoted by $\cdots$ in (4.4).

In order to simplify the expressions, as in [5], let us define

$$
\begin{cases}
l_{12}(V)=\frac{1}{2}D_2V_1-b_{12}V_3\\
l_2(V)=\left\{l_{11}(V),l_{22}(V),l_2^3(V),l_2^4\right\}\\
\quad=\left\{\partial_1V_1-\Gamma_{11}^1V_1,D_2V_2-\Gamma_{22}^1V_1,D_2^2V_3,\Gamma_{12}^1V_1\right\}\\
l_3(V)=\frac{1}{2}\partial_1V_2-\Gamma_{12}^2V_2
\end{cases} \qquad (4.6)
$$

and the bilinear forms

$$a_{11}(U,V)=\int_B 4A^{1212}l_{12}(U)l_{12}(V)\,\mathrm{d}y^1\,\mathrm{d}z^2 \qquad (4.7)$$

$$
\begin{aligned}
a_{22}(U,V)=\int_B&\left\{A^{1111}l_{11}(U)l_{11}(V)+4A^{1212}l_2^4(U)l_2^4(V)\right.\\
&+A^{2222}l_{22}(U)l_{22}(V) \qquad (4.8)\\
&\left.+B^{2222}l_2^3(U)l_2^3(V)+A^{1122}[l_{11}(U)l_{22}(V)\right.\\
&\left.\quad+l_{22}(U)l_{11}(V)]\right\}\mathrm{d}y^1\,\mathrm{d}z^2 \qquad (4.9)
\end{aligned}
$$

$$
\begin{aligned}
a_{12}(U,V)=\int_B&\left\{2A^{1112}l_{12}(U)l_{11}(V)\right.\\
&\left.+2A^{2212}l_{12}(U)l_{22}(V)\right\}\mathrm{d}y^1\,\mathrm{d}z^2 \qquad (4.10)
\end{aligned}
$$

$$
\begin{aligned}
a_{21}(U,V)=\int_B&\left\{2A^{1112}l_{11}(U)l_{12}(V)\right.\\
&\left.+2A^{2212}l_{22}(U)l_{12}(V)\right\}\mathrm{d}y^1\,\mathrm{d}z^2 \qquad (4.11)
\end{aligned}
$$

$$a_{31}(U,V)=\int_B 2A^{1212}l_3(U)l_{12}(V)\,\mathrm{d}y^1\,\mathrm{d}z^2 \qquad (4.12)$$

$$a_{13}(U,V)=\int_B 2A^{1212}l_{12}(U)l_3(V)\,\mathrm{d}y^1\,\mathrm{d}z^2 \qquad (4.13)$$

where $B=(0,\pi)\times(0,+\infty)$.

The problem (4.4) then takes the form

$$
\begin{aligned}
&\eta^{-2}a_{11}(U^\eta,V)+\eta^{-1}[a_{12}(U^\eta,V)+a_{21}(U^\eta,V)]\\
&\quad+\eta^0[a_{22}(U,V)+a_{31}(U,V)+a_{13}(U,V)]+\cdots\\
&\quad=\int_B f\left(y^1,\frac{\pi}{2}+\eta z^2\right)V_3\left(y^1,z^2\right)\mathrm{d}y^1\,\mathrm{d}z^2 \qquad (4.14)
\end{aligned}
$$

where

$$f\left(y^1,\frac{\pi}{2}+\eta z^2\right)=\widetilde{F}\left(y^1,\frac{\pi}{2}+\eta z^2\right)\theta_{[a^1,b^1]}\left(y^1\right)$$

4.2. Asymptotic process

In the framework of Section 3, let us search for an asymptotic expansion of U^η of the form

$$U^\eta=U^0+\eta U^1+\cdots \tag{4.15}$$

and let us take test functions depending on η of the form (4.15), substituting these expansions into (4.14) we obtain

$$\begin{aligned}
&\eta^{-2}a_{11}\left(U^0+\eta U^1+\cdots,V^0+\eta V^1+\cdots\right)\\
&\quad+\eta^{-1}\left[a_{12}\left(U^0+\eta U^1+\cdots,V^0+\eta V^1+\cdots\right)\right.\\
&\quad\left.+a_{21}\left(U^0+\eta U^1+\cdots,V^0+\eta V^1+\cdots\right)\right]\\
&\quad+\eta^0\left[a_{22}\left(U^0+\eta U^1+\cdots,V^0+\eta V^1+\cdots\right)\right.\\
&\quad+a_{31}\left(U^0+\eta U^1+\cdots,V^0+\eta V^1+\cdots\right)\\
&\quad\left.+a_{13}\left(U^0+\eta U^1+\cdots,V^0+\eta V^1+\cdots\right)\right]+\cdots\\
&\quad=\int_B f\left(y^1,\frac{\pi}{2}+\eta z^2\right)V_3^0\left(y^1,z^2\right)\mathrm{d}y^1\,\mathrm{d}z^2
\end{aligned}\tag{4.16}$$

Taking $V^\eta=U^\eta$, we see that the leading term, of order η^{-2}, is

$$a_{11}\left(U^0,V^0\right)=0$$

from which we deduce

$$l_{12}\left(U^0\right)=0\Longleftrightarrow\tfrac{1}{2}D_2U_1^0-b_{12}U_3^0=0 \tag{4.17}$$

so that the limit U^0, which is not determined at the present state, is submitted to the constraint (4.17). In the sequel we shall take V^0 satisfying the same constraint. Then the next leading term, in η^{-1}, vanishes identically.

Let us consider explicitly the case of the loading (2.3). Expanding the right-hand side of (4.16) in Taylor series, taking account of (4.17), we obtain, taking test functions vanishing at infinity,

$$\begin{aligned}
&\int_B f_3\left(y^1,\frac{\pi}{2}+\eta z^2\right)V_3\left(y^1,z^2\right)\mathrm{d}y^1\,\mathrm{d}z^2\\
&\quad=\frac{1}{2}\int_{B^+}\left[\frac{\widetilde{F}\left(y^1,\frac{\pi}{2}\right)\theta_{[a^1,b^1]}\left(y^1\right)}{b_{12}\left(y^1,\frac{\pi}{2}\right)}\right.\\
&\qquad\left.+\mathcal{O}(\eta)\right]D_2V_1\left(y^1,z^2\right)\mathrm{d}y^1\,\mathrm{d}z^2\\
&\quad=\int_0^\pi\tilde{f}\left(y^1\right)V_1\left(y^1,0\right)\mathrm{d}y^1+\mathcal{O}(\eta)
\end{aligned}$$

where $B^+=(0,\pi)\times(0,+\infty)$ and

$$\tilde{f}\left(y^1\right)=-\frac{\tilde{F}\left(y^1,\frac{\pi}{2}\right)\theta_{[a^1,b^1]}\left(y^1\right)}{2b_{12}\left(y^1,\frac{\pi}{2}\right)}$$

The next term, of order unity, then gives

$$\begin{aligned}
&a_{11}\left(U^1,V^1\right)+a_{12}\left(U^1,V^0\right)+a_{21}\left(U^0,V^1\right)+a_{22}\left(U^0,V^0\right)\\
&\quad=\int_0^\pi\tilde{f}\left(y^1\right)V_1\left(y^1,0\right)\mathrm{d}y^1
\end{aligned}\tag{4.18}$$

Let $\mathscr{W}$ be the space of the smooth vectors $V=(V_1,V_2,V_3)$ vanishing at infinity and satisfying

$$\begin{aligned}
&l_{12}(V)\in L^2(B),\quad l_2(V)\in\left[L^2(B)\right]^4,\quad l_3(V)\in L^2(B);\\
&\text{B.C. at } y^1=\pi
\end{aligned}\tag{4.19}$$

Lemma 4.1. *Let us give the six coefficients $A^{\alpha\beta\lambda\mu}$ satisfying the positivity property. Then*

$$\begin{aligned}
[a(V,V)]^{1/2}=&[a_{11}(V,V)+a_{12}(V,V)+a_{21}(V,V)\\
&+a_{22}(V,V)]^{1/2}
\end{aligned}$$

defines a norm on $\mathscr{W}$.

Proof. We have

$$\begin{aligned}
&A^{1111}\|l_{11}(V)\|_0^2+4A^{1112}(l_{12}(V),l_{11}(V))_0\\
&\quad+2A^{1122}(l_{11}(V),l_{22}(V))_0+4A^{1212}\|l_{12}(V)\|_0^2\\
&\quad+4A^{1222}(l_{12}(V),l_{22}(V))_0+A^{2222}\|l_{22}(V)\|_0^2\\
&\quad+4A^{1212}\left\|l_2^4(V)\right\|_0^2+B^{2222}\left\|l_2^3(V)\right\|_0^2\\
&\quad\geqslant C\left[\|l_{11}(V)\|_0^2+\|l_{12}(V)\|_0^2+\|l_{22}(V)\|_0^2\right]\\
&\quad+B^{2222}\left\|l_2^3(V)\right\|_0^2+4A^{1212}\left\|l_2^4(V)\right\|_0^2\\
&\quad\geqslant C'\left[\|l_{11}(V)\|_0^2+\|l_{12}(V)\|_0^2+\|l_{22}(V)\|_0^2\right.\\
&\quad\left.+\left\|l_2^3(V)\right\|_0^2+\left\|l_2^4(V)\right\|_0^2\right]
\end{aligned}\tag{4.20}$$

Consequently, if the left-hand side vanishes then we have

$$\begin{cases}
l_{11}(V)=0\Rightarrow\partial_1V=0\Rightarrow V_1\equiv0\\
l_{12}(V)=0\Rightarrow\frac{1}{2}D_2V_1-b_{12}V_3=0\Rightarrow V_3\equiv0\\
l_{22}(V)=0\Rightarrow D_2V=0\Rightarrow V_2\equiv0
\end{cases}\tag{4.21}$$

and the lemma is proved. □

Let denote by $\widetilde{\mathscr{W}}$ the completion of $\mathscr{W}$ for this norm. We then define the subspace

$$G=\left\{V\in\mathscr{V};\ l_{12}(V)=\tfrac{1}{2}D_2V_1^0-b_{12}V_3^0=0\right\},$$

which is clearly a closed subspace of $\widetilde{\mathscr{W}}$, and let us consider $\widetilde{\mathscr{W}}$ as $G\times G^\perp$.

We know that $U^0\in G$. Writing the two terms U^1 and V^1under the form $U_G^1+U_\perp^1$ and $V_G^1+V_\perp^1$ respectively, we see that only the components in the orthogonal space play a part in (4.18) which then takes the form

$$a_{11}(U_\perp^1, V_\perp^1) + a_{12}(U_\perp^1, V^0) + a_{21}(U^0, V_\perp^1) + a_{22}(U^0, V^0) = \int_0^\pi \tilde{f}(y^1) V_1^0(y^1, 0)\, \mathrm{d}y^1 \tag{4.22}$$

It is evident that

Lemma 4.2. *The left-hand side in* (4.22) *defines a norm on* $G \times G^\perp$.

We also have

Lemma 4.3. *The right-hand side in* (4.22) *is a linear continuous form on* G.

Proof. The proof is a simplified version of Lemma 4.1 in [30]. We have

$$I_2^3(V) \in L^2(B) \Rightarrow D_2^2 V_3 \in L^2(B)$$

then

$$V \in G \Rightarrow V_3 = \frac{1}{2b_{12}} D_2 V_1 \Rightarrow D_2^3 V_1 \in L^2\Big((0, +\infty)_{y^2}; L^2(0, \pi)_{y^1}\Big)$$

On the other hand,

$$I_{11}(V) \in L^2(B) \Rightarrow \partial_1 V_1 \in L^2\Big((0, +\infty)_{y^2}; L^2(0, \pi)_{y^1}\Big)$$

with the boundary condition $V_1(\pi, y^2) = 0$. Consequently, by applying the Poincaré lemma in $(0, \pi)$,

$$V_1 \in L^2\Big((0, +\infty)_{y^2}; H^1(0, \pi)_{y^1}\Big)$$

A fortiori,

$$\begin{cases} D_2^3 V_1 \in L^2\Big((0, \pi)_{y^1}; L^2(0, +\infty)_{y^2}\Big) \\ V_1 \in L^2\Big((0, \pi)_{y^1}; L^2(0, +\infty)_{y^2}\Big) \end{cases}$$

But in $H^2(0, +\infty)$ the standard norm is equivalent to $(\|\cdot\|^2_{L^2(0,+\infty)} + \|D_2 \cdot\|^2_{L^2(0,+\infty)})^{1/2}$ (see [21]; Vol. 1, Chapter 1, Theorem 2.3) and we have

$$V_1 \in L^2\Big((0, \pi)_{y^1}; H^3(0, +\infty)_{y^2}\Big) \Rightarrow \|V_1\|_{L^2} \leqslant C \|V_1\|_{\widetilde{\mathscr{W}}}$$

with continuity of the norms. Taking the trace on $z^2 = 0$, we obtain

$$\|V_1(0, \pi)\|_{L^2} \leqslant C \|V_1\|_{\widetilde{\mathscr{W}}}$$

from which the lemma follows. □

As a consequence, (4.22) is the variational formulation in $G \times G^\perp$, for which we have existence and uniqueness, the unknown being $(U^0, U_\perp^1)$.

Proposition 4.1. *The asymptotic process* (4.15) *allows us to determine uniquely the limit* $U^0 \in G$ *as well as the component in* $G^\perp$ *of the next term* U^1 *of the asymptotic expansion.*

The property of describing the limit U^0 and a part $U^{1\perp}$ of the next term at the same time in the expansion is classical in this kind of problem [5].

4.3. Explicit description of the limit problem

In this section, we eliminate $U_\perp^1$ and obtain a reduced problem for U^0 (which is the limit of U^η).

Taking $V^0 = 0$ in (4.22), we obtain

$$\int_B \left[4A^{1212}\left(\frac{1}{2} D_2 U_1^{1\perp} - b_{12} U_3^{1\perp}\right) + 2A^{1112}\left(\partial_1 U_1^0 - \Gamma_{11}^1 U_1^0\right) + 2A^{2212}\left(D_2 U_2^0 - \Gamma_{22}^1 U_1^0\right)\right]\left(\frac{1}{2} D_2 V_1^\perp - b_{12} V_3^\perp\right) \mathrm{d}y^1\, \mathrm{d}z^2 = 0 \tag{4.23}$$

taking arbitrary $V^\perp \in G^\perp$ (but, of course, we may take $V \in \widetilde{\mathscr{W}}$ instead of $V^\perp \in G^\perp$), as the quantity $\frac{1}{2} D_2 V_1^\perp - b_{12} V_3^\perp$ is arbitrary we obtain

$$\frac{1}{2} D_2 U_1^{1\perp} - b_{12} U_3^{1\perp} = \frac{-A^{1112}\left(\partial_1 U_1^0 - \Gamma_{11}^1 U_1^0\right) - A^{2212}\left(D_2 U_2^0 - \Gamma_{22}^1 U_1^0\right)}{2A^{1212}} \tag{4.24}$$

Now, with $V^\perp = 0$ in (4.22) we get

$$a_{12}(U_1^\perp, V^0) + a_{22}(U^0, V^0) = -\int_0^\pi \tilde{f}(y^1, 0) V_1^0(y^1, 0)\, \mathrm{d}y^1$$

i.e.

$$\begin{aligned} &\int_B \Big\{ A^{1111}\left(\partial_1 U_1^0 - \Gamma_{11}^1 U_1^0\right)\left(\partial_1 V_1^0 - \Gamma_{11}^1 V_1^0\right) \\ &+ 2A^{1112}\left(\frac{1}{2} D_2 U_1^\perp - b_{12} U_3^\perp\right)\left(\partial_1 V_1^0 - \Gamma_{11}^1 V_1^0\right) \\ &+ A^{1122}\left[\left(\partial_1 U_1^0 - \Gamma_{11}^1 U_1^0\right)\left(D_2 V_2^0 - \Gamma_{22}^1 V_1^0\right) + \left(D_2 U_2^0 - \Gamma_{22}^1 U_1^0\right)\left(\partial_1 V_1^0 - \Gamma_{11}^1 V_1^0\right)\right] \\ &+ 2A^{1222} \frac{-A^{1112}\left(\partial_1 U_1^0 - \Gamma_{11}^1 U_1^0\right) - A^{2212}\left(D_2 U_2^0 - \Gamma_{22}^1 U_1^0\right)}{2A^{1212}} \times \left(D_2 V_2^0 - \Gamma_{22}^1 V_1^0\right) + 2A^{1222}\left(\frac{1}{2} D_2 U_1^\perp - b_{12} U_3^\perp\right) \\ &\times \left(D_2 V_2^0 - \Gamma_{22}^1 V_1^0\right) + A^{2222}\left(D_2 U_2^0 - \Gamma_{22}^1 U_2^0\right) \\ &\times \left(D_2 V_2^0 - \Gamma_{22}^1 V_1^0\right) + B^{2222} D_2^2 U_3^0 D_2^2 V_3^0 \Big\} \mathrm{d}y^1\, \mathrm{d}z^2 \\ &= \int_0^\pi \tilde{f}(y^1) V_1^0(y^1, 0)\, \mathrm{d}y^1 \end{aligned} \tag{4.25}$$

Taking account of (4.24), (4.25) becomes

$$\int_B \left\{ \frac{\left(-\left(A^{1112}\right)^2 + A^{1111}A^{1212}\right)}{A^{1212}} \right.$$
$$\times \left(\partial_1 U_1^0 - \Gamma_{11}^1 U_1^0\right)\left(\partial_1 V_1^0 - \Gamma_{11}^1 V_1^0\right)$$
$$+ \frac{A^{1122}A^{1212} - A^{2212}A^{1112}}{A^{1212}}$$
$$\times \left[\left(\partial_1 U_1^0 - \Gamma_{11}^1 U_1^0\right)\left(D_2 V_2^0 - \Gamma_{22}^1 V_1^0\right)\right.$$
$$\left. + \left(D_2 U_2^0 - \Gamma_{22}^1 U_1^0\right)\left(\partial_1 V_1^0 - \Gamma_{11}^1 V_1^0\right)\right]$$
$$+ \frac{A^{2222}A^{1212} - \left(A^{2212}\right)^2}{A^{1212}}\left(D_2 U_2^0 - \Gamma_{22}^1 U_1^0\right)\left(D_2 V_2^0 - \Gamma_{22}^1 V_1^0\right)$$
$$\left. + 4A^{1212}\left(\Gamma_{12}^1\right)^2 U_1^0 V_1^0 + \frac{B^{2222}}{4\left(b_{12}\right)^2} D_2^3 U_1^0 D_2^3 V_1^0 + \right\} \mathrm{d}y^1\,\mathrm{d}z^2$$
$$= \int_0^\pi \tilde{f}\left(y^1\right) V_1^0\left(y^1, 0\right)\mathrm{d}y^1 \tag{4.26}$$

Let us define

$$C_{11} = \frac{-\left(A^{1112}\right)^2 + A^{1111}A^{1212}}{A^{1212}} \tag{4.27}$$

$$C_{12} = \frac{A^{1122}A^{1212} - A^{2212}A^{1112}}{A^{1212}} \tag{4.28}$$

$$C_{22} = \frac{A^{2222}A^{1212} - \left(A^{2212}\right)^2}{A^{1212}} \tag{4.29}$$

$$K_{22} = \frac{B^{2222}}{4\left(b_{12}\right)^2} \tag{4.30}$$

$$K_{11} = 4A^{1212}\left(\Gamma_{12}^1\right)^2 \tag{4.31}$$

then, 4.26 writes

$$\int_B \left\{C_{11}\left(\partial_1 U_1^0 - \Gamma_{11}^1 U_1^0\right)\left(\partial_1 V_1^0 - \Gamma_{11}^1 V_1^0\right)\right.$$
$$+ C_{12}\left[\left(\partial_1 U_1^0 - \Gamma_{11}^1 U_1^0\right)\left(D_2 V_2^0 - \Gamma_{22}^1 V_1^0\right)\right.$$
$$\left. + \left(D_2 U_2^0 - \Gamma_{22}^1 U_1^0\right)\left(\partial_1 V_1^0 - \Gamma_{11}^1 V_1^0\right)\right]$$
$$+ K_{11} U_1^0 V_1^0 + C_{22}\left(D_2 U_2^0 - \Gamma_{22}^1 U_1^0\right)\left(D_2 V_2^0 - \Gamma_{22}^1 V_1^0\right)$$
$$\left. + K_{22} D_2^3 U_1^0 D_2^3 V_1^0\right\}\mathrm{d}y^1\,\mathrm{d}z^2 = \int_0^\pi \tilde{f}\left(y^1\right) V_1^0\left(y^1, 0\right)\mathrm{d}y^1 \tag{4.32}$$

Lemma 4.4. *It is possible to choose a parametrization for which the symbol $\Gamma_{11}^1(y^1, \pi/2)$ is equal to zero.*

Proof. The system of curvilinear coordinates (y^1, y^2) was chosen such that

$$b_{11} = b_{22} = 0,\ b_{12} \neq 0 \tag{4.33}$$

so that the characteristics (asymptotic curves) are $y^1 = \text{Const.}$, $y^2 = \text{Const.}$ This property is not lost by passing to a new parametrization such that each new parameter is a function of only one of the previous ones. So we may only assume that, in the initial description, one of the parameters is the arc s of a given characteristic $\mathscr{C}$, here $y^2 = \pi/2$. In order to have

$$\Gamma_{11}^1\left(y^1, y^2\right) = 0 \quad \text{on } \mathscr{C} \tag{4.34}$$

we take as parameters

$$\left(y^1, y^2\right) = \left(y^1(s), y^2\right) \tag{4.35}$$

and we have

$$\vec{a}_1 = \frac{\partial \vec{r}}{\partial y^1} = \frac{\partial \vec{r}}{\partial s}\frac{ds}{dy^1} \underset{\text{déf}}{=} \frac{1}{\varphi(s)}\vec{e}_1(s), \quad \vec{a}_2 = \frac{\partial \vec{r}}{\partial y^2} \text{ unchanged}$$

Let $\vec{e}_2$ be the unit vector normal to $\vec{e}_1$ in the tangent plane and $\theta(s) = (\vec{a}_1, \vec{a}_2)$, then

$$\vec{a}^1 = \varphi(s)\left[\vec{e}_1 - \cot\theta(s)\vec{e}_2\right]$$

With such a parametrization we have

$$\Gamma_{11}^1\left(y^1, y^2\right) = \vec{a}_{1,1}\cdot\vec{a}^1 = \frac{d\left[\frac{1}{\varphi(s)}\vec{e}_1(s)\right]}{\mathrm{d}s}\varphi(s)\left[\vec{e}_1 - \cot\theta(s)\vec{e}_2\right]$$
$$= \frac{\varphi'(s)}{\varphi(s)} - \frac{\cot\theta(s)}{R(s)}$$

where $1/R$ is the curvature of $\mathscr{C}$. Consequently, if φ is solution of

$$\frac{\varphi'(s)}{\varphi(s)} - \frac{\cot\theta(s)}{R(s)} \Rightarrow \varphi(s) = \varphi(0)\exp\left[\int_0^s \frac{\cot\theta(\xi)}{R(\xi)}\,\mathrm{d}\xi\right]$$

then (4.34) will be satisfied. □

The variational formulation (4.32) then writes: find $U^0 \in G$ satisfying

$$\int_B \left\{C_{11}\partial_1 U_1^0 \partial_1 V_1^0 + C_{12}\left[\partial_1 U_1^0\left(D_2 V_2^0 - \Gamma_{22}^1 V_1^0\right)\right.\right.$$
$$\left. + \left(D_2 U_2^0 - \Gamma_{22}^1 U_1^0\right)\partial_1 V_1^0\right] + K_{11} U_1^0 V_1^0$$
$$+ C_{22}\left(D_2 U_2^0 - \Gamma_{22}^1 U_1^0\right)\left(D_2 V_2^0 - \Gamma_{22}^1 V_1^0\right)$$
$$\left. + K_{22} D_2^3 U_1^0 D_2^3 V_1^0\right\}\mathrm{d}y^1\,\mathrm{d}z^2$$
$$= \int_0^\pi \tilde{f}\left(y^1\right) V_1^0\left(y^1, 0\right)\mathrm{d}y^1 \quad \forall V^0 \in G \tag{4.36}$$

4.4. Solution of the limit problem

In this section, we eliminate the components U_2^0 and U_3^0 and obtain a boundary valued problem for U_1^0 which we solve by separation of the variables.

Let us take $V_1^0 = 0$ and arbitrary $V_2^0 \in \mathscr{D}(B)$ in (4.36), we obtain

$$\int_B -\left[C_{12}\partial_1 D_2 U_1^0 + C_{22} D_2\left(D_2 U_2^0 - \Gamma_{22}^1 U_1^0\right)\right] V_2^0 \,\mathrm{d}y^1\,\mathrm{d}z^2$$

and consequently

$$C_{12}\partial_1 U_1^0 + C_{22}\left(D_2 U_2^0 - \Gamma_{22}^1 U_1^0\right) = C\left(y^1\right) \equiv 0 \tag{4.37}$$

Indeed, this follows from the proof of Lemma 4.4 which shows that the expression in (4.37) belongs to $L^2(B)$ and from the fact that it only depends on y^1.

Now, taking $V_2^0 = 0$ and arbitrary V_1^0, we get on account of (4.37)

$$\int_B \left\{ \frac{C_{11}C_{22} - \left(C_{12}\right)^2}{C_{22}} \partial_1 U_1^0 \partial_1 V_1^0 + K_{11} U_1^0 V_1^0 + K_{22} D_2^3 U_1^0 D_2^3 V_1^0 \right\} \mathrm{d}y^1\,\mathrm{d}z^2 = \int_0^\pi \tilde{f}\left(y^1\right) V_1^0\left(y^1, 0\right) \mathrm{d}y^1$$

which may also be written

$$\begin{aligned} &\int_B \left[-\partial_1\left(C\left(y^1\right)\partial_1 U_1^0\right) + K_{11} U_1^0 - K_{22} D_2^6 U_1^0\right] V_1^0\left(y^1, z^2\right) \\ &- \int_0^\infty C(0)\partial_1 U_1^0\left(0, z^2\right) V_1^0\left(0, z^2\right) \mathrm{d}z^2 \\ &- \int_0^\pi K_{22}\left[\left|D_2^3 U_1^0\right|\right] D_2^2 V_1^0\left(y^1, 0\right) \mathrm{d}y^1 \\ &+ \int_0^\pi K_{22}\left[\left|D_2^4 U_1^0\right|\right] D_2 V_1^0\left(y^1, 0\right) \mathrm{d}y^1 \\ &- \int_0^\pi K_{22}\left[\left|D_2^5 U_1^0\right|\right] V_1^0\left(y^1, 0\right) \mathrm{d}y^1 \\ &= \int_0^\pi \tilde{f}\left(y^1\right) V_1^0\left(y^1, 0\right) \mathrm{d}y^1 \end{aligned} \tag{4.38}$$

where

$$C\left(y^1\right) = \frac{C_{11}C_{22} - \left(C_{12}\right)^2}{C_{22}}\left(y^1, \frac{\pi}{2}\right)$$

and

$$[|W|] = W\left(y^1, 0^+\right) - W\left(y^1, 0^-\right)$$

As V_1^0 is arbitrary, from (4.38) we get the equation satisfied by U_1^0:

$$-\partial_1\left(C\partial_1 U_1^0\right) + K_{11} U_1^0 - K_{22} D_2^6 U_1^0 = 0 \tag{4.39}$$

and the natural boundary condition

$$\begin{cases} \left[\left|D_2^3 U_1^0\left(y^1, 0\right)\right|\right] = 0 \\ \left[\left|D_2^4 U_1^0\left(y^1, 0\right)\right|\right] = 0 \\ \left[\left|D_2^5 U_1^0\left(y^1, 0\right)\right|\right] = -\dfrac{\tilde{f}\left(y^1\right)}{K_{22}} \\ \partial_1 U_1^0\left(0, z^2\right) = 0 \end{cases} \tag{4.40}$$

in addition to the kinematic boundary condition

$$U_1^0\left(\pi, z^2\right) = 0$$

and to

$$U_1^0\left(y^1, z^2\right) \to 0 \quad \text{as } z^2 \to \pm\infty$$

Let us search for a solution of the form

$$U_1^0\left(y^1, z^2\right) = \sum_k \Phi_k\left(y^1\right) \Psi_k\left(z^2\right) \tag{4.41}$$

then, Φ_k and Ψ_k satisfy

$$\left[-\partial_1\left(C\partial_1 \Phi_k\right) + K_{11}\Phi_k\left(y^1\right)\right] \Psi_k\left(z^2\right) - K_{22}\Phi_k\left(y^1\right)\Psi_k^{(6)}\left(z^2\right) = 0$$

i.e.

$$\frac{\left[C\Phi_k'\left(y^1\right)\right]'}{\Phi_k\left(y^1\right)} - K_{11}\left(y^1\right) = -\frac{\Psi_k^{(6)}\left(z^2\right)}{\Psi_k} = \text{Const.} = \lambda_k \tag{4.42}$$

The equation satisfied by Φ_k writes

$$\left[C\Phi_k'\left(y^1\right)\right]' - K_{11}\left(y^1\right)\Phi_k\left(y^1\right) = \lambda_k K_{22}\left(y^1\right)\Phi_k\left(y^1\right) \tag{4.43}$$

and the boundary conditions are

$$\Phi_k(\pi) = \Phi_k'(0) = 0 \tag{4.44}$$

Eq. (4.43) is associated with the bilinear form

$$\int_0^\pi -C\Phi_k'\left(y^1\right)\widetilde{\Phi}'\left(y^1\right)\mathrm{d}y^1 - \int_0^\pi K_{11}\left(y^1\right)\Phi_k\left(y^1\right)\widetilde{\Phi}\left(y^1\right)\mathrm{d}y^1 = \int_0^\pi \lambda_k K_{22}\left(y^1\right)\Phi_k\left(y^1\right)\widetilde{\Phi}\left(y^1\right)\mathrm{d}y^1$$

This problem is a standard spectral self-adjoint problem with the space H with weight $K_{22}(y^1)$ and the space V with weights C and $K_{11}(y^1)$, consequently the eigenvalues λ_k have real values. Because of the complexity of the expression of the coefficients, in general it is impossible to know the sign of the eigenvalues. But, we may easily verify that in the homogeneous isotropic case when $a^{\alpha\beta} = \delta^{\alpha\beta}$ they are positive. Several numerical tests including anisotropic cases give also positive values for the eigenvalues. We shall admit that hypothesis.

The eigenfunctions $\Phi_k(y^1)$ and eigenvalues λ_k being known (positive), the functions Ψ_k are solutions of

$$-\Psi_k^{(6)}\left(z^2\right) - \lambda_k \Psi_k\left(z^2\right) = 0 \tag{4.45}$$

of which we search for solutions vanishing to infinity.

Finally, the solution is of the form

$$U_1^0\left(y^1, z^2\right) = \sum_{k=2}^4 \Phi_k\left(y^1\right) \exp\left[\mathrm{e}^{2k\mathrm{i}\pi/6}\left(\lambda_k\right)^{1/6} z^2\right] \tag{4.46}$$

of which the decreasing at infinity is exponential.

Remark 4.1. The asymptotic behavior (3.5) was constructed on the basis of Lemma 3.1. Let us check that the components of U^0 satisfy (3.3). Only the third component is concerned by this condition. We must verify that

$$\int_{-\infty}^{+\infty} U_3^0\left(y^1,z^2\right)\mathrm{d}z^2 = 0$$

Indeed, we have

$$\int_{-\infty}^{+\infty} U_3^0\left(y^1,z^2\right)\mathrm{d}z^2 = \frac{\int_{-\infty}^{+\infty} D_2U_1^0(y^1,z^2)\,\mathrm{d}z^2}{2b_{12}\left(y^1,\frac{\pi}{2}\right)} = \frac{\left[U_1^0(y^1,z^2)\right]_{z^2=-\infty}^{z^2=+\infty}}{2b_{12}\left(y^1,\frac{\pi}{2}\right)} = 0$$

from the exponential decreasing at infinity.

5. Structure of the non-characteristic internal layer in the vicinity of $= \{y^1 = y^2, y^1 > \pi/2\}$ in the case of the loading (2.14)

According the results obtained in Sections 3 and 2.3.2, we search for asymptotic expansions of the form

$$\begin{cases} u_1^\varepsilon \simeq U_1^\eta\left(\xi^1,\zeta^2\right) \\ u_2^\varepsilon \simeq U_2^\eta\left(\xi^1,\zeta^2\right) \\ u_3^\varepsilon \simeq \eta^{-1}U_3^\eta\left(\xi^1,\zeta^2\right) \end{cases} \quad \text{where } \zeta^2 = \frac{\xi^2}{\eta} \tag{5.1}$$

where $\eta(\varepsilon)$ will be determined later.

Substituting (5.1) to (4.1) where

$$\begin{cases} \gamma_{11}(v) = \partial_1 v_1 - \Gamma_{11}^1 v_1 - \Gamma_{11}^2 v_2 - b_{11}v_3 \\ \gamma_{12}(v) = \frac{1}{2}(\partial_1 v_2 + \partial_2 v_1) - \Gamma_{12}^1 v_1 - \Gamma_{12}^2 v_2 - b_{12}v_3 \\ \gamma_{22}(v) = \partial_2 v_2 - \Gamma_{22}^1 v_1 - \Gamma_{22}^2 v_2 - b_{22}v_3 \end{cases}$$

and multiplying by η, we obtain at the leading orders:

$$\begin{aligned} \int_{B^\eta} \Big\{ & A^{1111}(b_{11})^2 U_3^0 V_3 - 2A^{1112}b_{11}\left[U_3^0\left(\frac{1}{2}D_2V_1 - b_{12}V_3\right)\right. \\ & \left. + \left(\frac{1}{2}D_2U_1^0 - b_{12}U_3^0\right)V_3\right] - A^{1122}b_{11}\left[U_3^0(D_2V_2 - b_{22}V_3)\right. \\ & \left. + \left(D_2U_2^0 - b_{22}U_3^0\right)V_3\right] \\ & + 4A^{1212}\left(\frac{1}{2}D_2U_1^0 - b_{12}U_3^0\right)\left(\frac{1}{2}D_2V_1 - b_{12}V_3\right) \\ & + 2A^{2212}\left[\left(\frac{1}{2}D_2U_1^0 - b_{12}U_3^0\right)(D_2V_2 - b_{22}V_3)\right. \\ & \left. + \left(D_2U_2^0 - b_{22}U_3^0\right)\left(\frac{1}{2}D_2V_1 - b_{12}V_3\right)\right] \\ & + A^{2222}\left(D_2U_2^0 - b_{22}U_3^0\right)(D_2V_2 - b_{22}V_3) \\ & + \varepsilon^2\eta^{-4}B^{2222}D_2^2U_3^0D_2^2V_3\Big\}\,\mathrm{d}\xi^1\,\mathrm{d}\zeta^2 = \int_0^{\sqrt{2}\pi} f_3\left(\xi^1,0\right)V_3\,\mathrm{d}\xi^1 \end{aligned} \tag{5.2}$$

where $B^\eta = \left(0,\sqrt{2}\pi\right)\times\left(-(\xi_2/\eta),+(\xi_2/\eta)\right)$.

We impose that η is such that the leading term of flexion is of order η^0 then we have $\eta = \mathcal{O}\left(\varepsilon^{1/2}\right)$, we shall take

$$\eta = \varepsilon^{1/2} \tag{5.3}$$

Let $\mathscr{W}$ be the space of the smooth functions vanishing in a vicinity of infinity and satisfying

$$\begin{aligned} & U_3^0 \in L^2\left(B\right), \quad D_2U_1^0 - 2b_{12}U_3^0 \in L^2(B), \\ & D_2U_2^0 - b_{22}U_3^0 \in L^2(B), \quad D_2^2U_3^0 \in L^2(B) \end{aligned} \tag{5.4}$$

Lemma 5.1. *The left-hand side $a(U^0,V)$ of* (5.2) *defines a scalar product on $\mathscr{W}$.*

The positivity immediately follows from the property of positivity of the elasticity coefficients. Moreover,

$$a\left(U^0,U^0\right) = 0 \Rightarrow \begin{cases} U_3^0 = 0 \\ D_2U_1^0 - 2b_{12}U_3^0 = 0 \Rightarrow D_2U_1^0 = 0 \\ D_2U_2^0 - b_{22}U_3^0 = 0 \Rightarrow D_2U_2^0 = 0 \\ D_2^2U_3^0 = 0 \end{cases} \tag{5.5}$$

then, U_1^0 and U_2^0 are only functions of y^1 but, as the both functions tend to zero at infinity, we have $U_1^0 = U_2^0$.

Taking $V_1 = V_3 = 0$ in (5.2) and arbitrary V_2, we obtain:

$$T^{22}\left(U^0\right) = A^{2211}\gamma_{11}^0 + 2A^{2212}\gamma_{12}^0 + A^{2222}\gamma_{22}^0 = 0$$

or

$$2A^{2212}\gamma_{12}^0 + A^{2222}\gamma_{22}^0 = -A^{2211}\gamma_{11}^0 \tag{5.6}$$

where

$$\begin{cases} \gamma_{11}^0 = (b_{11})^2U_3^0 \\ \gamma_{12}^0 = \frac{1}{2}\left(D_2U_1^0 - b_{12}U_3^0\right) \\ \gamma_{22}^0 = D_2U_2^0 - b_{22}U_3^0 \end{cases} \tag{5.7}$$

Now, with $V_2 = V_3 = 0$ and arbitrary V_1 we get

$$T^{12}\left(U^0\right) = A^{1211}\gamma_{11}^0 + 2A^{1212}\gamma_{12}^0 + A^{1222}\gamma_{22}^0 = 0.$$

or

$$2A^{1212}\gamma_{12}^0 + A^{1222}\gamma_{22}^0 = -A^{1211}\gamma_{11}^0 \tag{5.8}$$

Lemma 5.2. *The system* (5.6) *and* (5.8) *determines* γ_{12}^0 and γ_{22}^0 *as functions of* γ_{11}^0.

Proof. By contradiction: if the determinant of the system does not vanish the associated homogeneous system has a solution $\left(\widetilde{\gamma}_{12}^0,\widetilde{\gamma}_{22}^0\right) \neq 0$, then the corresponding $\widetilde{\gamma}_{11}^0 = 0$ and we may define $\widetilde{T}^{\alpha\beta} = A^{\alpha\beta\lambda\mu}\widetilde{\gamma}_{\lambda\mu}^0$ and $A^{\alpha\beta\lambda\mu}\widetilde{\gamma}_{\lambda\mu}^0\widetilde{\gamma}_{\alpha\beta}^0$. By

virtue of the property of positivity of the coefficients of elasticity $A^{\alpha\beta\lambda\mu}$ we have $C\widetilde{\gamma}^0_{\alpha\beta}\widetilde{\gamma}^0_{\alpha\beta} \leqslant A^{\alpha\beta\lambda\mu}\widetilde{\gamma}^0_{\lambda\mu}\widetilde{\gamma}^0_{\alpha\beta} =$ (by definition of the components $\widetilde{\gamma}^0_{\alpha\beta}$) $= A^{11\lambda\mu}\widetilde{\gamma}^0_{\lambda\mu}\widetilde{\gamma}^0_{11} = 0$ that is impossible and the lemma is proved. We then have

$$\gamma_{\alpha\beta}\big(U^0\big) = \mathscr{R}_{\alpha\beta}\gamma^{11} \quad \square$$

The formulation (5.2) then becomes: find $U^0_3 \in L^2((0,\sqrt{2}\pi)_{\xi_1}; H^2(\mathbb{R})_{\zeta_2})$ such that

$$\int_B \left\{A^{11\alpha\beta}\mathscr{R}_{\alpha\beta}\gamma_{11}\big(U^0_3\big)\gamma_{11}(V) + B^{2222}D^2_2U^0_3D^2_2V_3\right\}\mathrm{d}\xi^1\,\mathrm{d}\zeta^2 = \int_0^{\sqrt{2}\pi} f_3\big(\xi^1\big)V_3\big(\xi^1,0\big)\,\mathrm{d}\xi^1 \tag{5.9}$$

Lemma 5.3. *The solution* $U^0_3 \in L^2(\big(0,\sqrt{2}\pi\big)_{\xi_1}; H^2(\mathbb{R})_{\zeta_2})$ *of the problem* (5.9) *exists and is unique.*

Proof. We immediately verify the coerciveness of the bilinear form in the left-hand side of (5.9). Indeed, we have

$$\begin{aligned} A^{11\alpha\beta}\mathscr{R}_{\alpha\beta}\gamma_{11}\big(U^0\big)\gamma_{11}\big(U^0\big) &\equiv A^{11\alpha\beta}\gamma_{\alpha\beta}\big(U^0\big)\gamma_{11}\big(U^0\big) \\ &= (\text{as } T^{12} = T^{22} = 0) \\ &= A^{\lambda\mu\alpha\beta}\gamma_{\alpha\beta}\big(U^0\big)\gamma_{\lambda\mu}\big(U^0\big) \end{aligned}$$

which insures the positivity.

As the traces exit in $H^2(\mathbb{R})$, the continuity of the traces gives

$$\big|V_3\big(\xi^1,0\big)\big|^2 \leqslant C\|V_3\|^2_{H^2(\mathbb{R})} \Rightarrow \int_0^{\sqrt{2}\pi}\big|V_3\big(\xi^1,0\big)\big|^2\,\mathrm{d}\xi^1 \leqslant C\|V_3\|^2_{L^2\left((0,\pi)\xi^1;H^2(\mathbb{R})\right)}$$

and consequently

$$\left|\int_0^{\sqrt{2}\pi} f_3\big(\xi^1\big)V_3\big(\xi^1,0\big)\,\mathrm{d}\xi^1\right| \leqslant \|f_3\|_{L^2\left(0,\sqrt{2}\pi\right)}\|V_3\|_{L^2\left((0,\pi)\xi^1;H^2(\mathbb{R})\right)}$$

from the Lax–Milgram theorem we get the result which was to be proved. $\square$

From (5.9) we get the differential equation with constant coefficients (depending on ξ^1) satisfied by U^0_3:

$$A^{11\alpha\beta}\mathscr{R}_{\alpha\beta}(b_{11})^2U^0_3 + B^{2222}D^4_2U^0_3 = 0 \tag{5.10}$$

The boundary conditions to be satisfied by U^0_3 are

$$\begin{cases} \left[\left|D^2_2U^0_3\big(\xi^1,0\big)\right|\right] = 0 \\ \left[\left|D^3_2U^0_3\big(\xi^1,0\big)\right|\right] = f_3\big(\xi^1\big) \end{cases} \tag{5.11}$$

moreover,

$$U^0_3\big(\xi^1,\zeta^2\big) \underset{\zeta^2\to\pm\infty}{\to} 0 \tag{5.12}$$

As the solution is symmetric with respect to $\zeta^2 = 0$, we may only search for the solution for $\zeta^2 > 0$.

Lemma 5.4. *The quantity* $A^{11\alpha\beta}\mathscr{R}_{\alpha\beta}$ *is positive.*

Proof. As $\mathscr{R}_{11} = 1$, we have

$$A^{11\alpha\beta}\mathscr{R}_{\alpha\beta} = A^{11\alpha\beta}\mathscr{R}_{\alpha\beta}\mathscr{R}_{11}$$

then, as $A^{12\alpha\beta}\mathscr{R}_{\alpha\beta}\mathscr{R}_{12} = A^{22\alpha\beta}\mathscr{R}_{\alpha\beta}\mathscr{R}_{22} = 0$ we see that $A^{11\alpha\beta}\mathscr{R}_{\alpha\beta} \equiv A^{\lambda\mu\alpha\beta}\mathscr{R}_{\alpha\beta}\mathscr{R}_{\lambda\mu} \geqslant 0$ by positivity of the coefficients $A^{\lambda\mu\alpha\beta}$ and the lemma follows.

Consequently, $U^0_3\big(\xi^1,\zeta^2\big)$ is for $\zeta^2 > 0$ of the form

$$U^0_3 = \sum_{k=1}^{2} A_k \exp\left(\exp\left(\frac{(2k+1)\mathrm{i}\pi}{4}\sqrt[4]{\frac{A^{1111}(b_{11})^2}{B^{2222}}}\zeta^2\right)\right) \tag{5.13}$$

The two constants A_k are determined by the boundary conditions (5.11). $\square$

6. Anisotropic finite element estimates and local locking

In this section, we take advantage of the peculiarities of the asymptotic structure of the solution to write the corresponding error estimates for finite element approximation. Our aim is to exhibit the essential properties issued from the asymptotic behavior, so that we shall take into account the properties of the leading term, disregarding the other terms.

First, as the energy is concentrated in the layers let us consider the layer of Section 4, i.e. a region $y^1 \in (0,\pi)$, $y^2 \in ((\pi/2) - \eta L, (\pi/2) + \eta L)$ for some large L (note that because of the exponential decay this is the significant region). Clearly a fitted mesh should be constructed in the vicinity of each layer according to the present study.

Next, the essential features are given by the leading term of the asymptotic expansion so that we shall replace $U^\eta(y^1,z^2)$ by $U^0(y^1,z^2)$.

In order to clarify the reasoning of the next subsection, we have to keep in mind the following features:

1. Our objective is to estimate the errors of the expressions which play a dominant role in the variational formulation of the limit problem.
2. As we know, the variational formulation of the problem for U^η involves a penalty problem. The bilinear form (associated with the corresponding energy form) contains the parameter η^{-2}. As the finite element approximation is the element which minimizes the error in energy norm, it appears the factor η^{-1} in the error estimate of the Galerkin solution. This is the classical locking phenomenon for penalty problems.
3. As the energy of the solution tends to infinity only the relative errors are significant.
4. As the leading term of the asymptotic expansion is $U^0(y^1,z^2)$, which does not involves η, we shall consider estimates for isotropic finite elements in y^1 and

z^2 (i.e. with mesh step $\mathcal{O}(H)$ in both variables). We then deduce the corresponding estimates for finite elements in y^1 and y^2, which will be anisotropic (i.e. with mesh $\mathcal{O}(H)$ and $\mathcal{O}(\eta H)$ in y^1 and y^2 respectively).

6.1. Galerkin approximation error for anisotropic finite element in the layer

For the sake of simplicity but without loss of generality, we shall consider in the sequel the case of the shallow shells, i.e. we take the Christoffel coefficients equal to zero. Then, the energy form in Ω writes

$$a(u^\varepsilon,u^\varepsilon)=\int_\Omega \left[A^{\alpha\beta\lambda\mu}\gamma_{\lambda\mu}(u^\varepsilon)\gamma_{\alpha\beta}(u^\varepsilon)+\varepsilon^2 B^{\alpha\beta\lambda\mu}\rho_{\lambda\mu}(u^\varepsilon)\rho_{\alpha\beta}(u^\varepsilon)\right]\mathrm{d}y^1\,\mathrm{d}y^2$$

and, from the property of positivity of the elasticity coefficients, we have

$$a(u^\varepsilon,u^\varepsilon)\geqslant C\int_\Omega\left[\gamma_{\alpha\beta}(u^\varepsilon)\gamma_{\alpha\beta}(u^\varepsilon)+\varepsilon^2\rho_{\alpha\beta}(u^\varepsilon)\rho_{\alpha\beta}(u^\varepsilon)\right]\mathrm{d}y^1\,\mathrm{d}y^2$$

After the scaling, we have

$$\tilde{a}(U^\eta,U^\eta)\geqslant C\int_{B^L}\left\{\eta^{-1}(\partial_1U_1^\eta)^2+\eta\left[\frac{1}{2}\partial_1U_2^\eta+\eta^{-2}\left(\frac{1}{2}D_2U_1^\eta-b_{12}U_3^\eta\right)\right]^2+\eta^{-1}(D_2U_2^\eta)^2+\eta^{-1}\left(D_2^2U_2^\eta\right)^2\right\}\mathrm{d}y^1\,\mathrm{d}z^2 \tag{6.1}$$

where, as in the previous sections we disregard the terms of higher order in $\rho_{\alpha\beta}$. For technical reasons, the integration domain is B^L (i.e. B^η truncated at $z^2>L$, for sufficiently large L).

Then, let us consider the functions $U_1^\eta\in H^1(B^L)$, $U_2^\eta\in H^1(B^L)$ and $U_3^\eta\in H^2(B^L)$. Let U_{1H}^η, U_{2H}^η and U_{3H}^η be their finite element approximations obtained with polynomials of degree k_1 for the two first components and of degree k_2 for the third one and for an isotropic mesh of step $\mathcal{O}(H)$ under the standard hypotheses. At last, let δ_H be the interpolation error. From the classical formula [9]

$$\|\delta_H(U_i^\eta)\|_m\simeq\left\|\delta_H\left(U_i^0\right)\right\|_m\leqslant CH^{k_j+1-m}\left\|U_i^0\right\|_{k_j+1}$$

where C denotes a constant independent of η. As U_i^0 is independent of η, we have

$$\|\delta_H(U_1^\eta)\|_1\leqslant CH^{k_1},\quad \|\delta_H(U_2^\eta)\|_1\leqslant CH^{k_i},\quad \left\|\delta_H(U_3^\eta)\right\|_2\leqslant CH^{k_2-1} \tag{6.2}$$

We know (Galerkin property) that,

$$\tilde{a}(\delta_{HG}(U^\eta),\delta_{HG}(U^\eta))\leqslant\tilde{a}(\delta_H(U^\eta),\delta_H(U^\eta))$$

where δ_{HG} denotes the error of the Galerkin approximation. Then, from the inequalities

$$\begin{aligned}
&C_1\left[\eta^{-1}\left\|\delta_{HG}\left(\partial_1U_1^0\right)\right\|_0^2+\eta^{-1}\left\|\delta_{HG}\left(D_2U_2^0\right)\right\|_0^2\right.\\
&\left.+\eta^{-1}\left\|\delta_{HG}\left(D_2^2U_3^0\right)\right\|_0^2\right]\\
&\leqslant\tilde{a}\left(\delta_{HG}\left(U^0\right),\delta_{HG}\left(U^0\right)\right)\leqslant\tilde{a}\left(\delta_H\left(U^0\right),\delta_H\left(U^0\right)\right)\\
&\leqslant C_2\left[\eta^{-1}\left\|\delta_H\left(\partial_1U_1^0\right)\right\|_0^2+\eta^{-1}\left\|\delta_H\left(D_2U_2^0\right)\right\|_0^2\right.\\
&+\eta^{-1}\left\|\delta_H\left(D_2^2U_3^0\right)\right\|_0^2+\eta\left\|\tfrac{1}{2}\delta_H\left(\partial_1U_2^0\right)\right.\\
&+\eta^{-2}\left\|\left(\tfrac{1}{2}\left(\delta_H\left(D_2U_1^0\right)-b_{12}\delta_H\left(U_3^0\right)\right)\right)\right\|_0^2\\
&\left.+\eta^{-1}\left\|\delta_{HG}\left(D_2^2U_3^0\right)\right\|_0^2\right]\\
&\leqslant C_3\left[\eta^{-1}H^{2k_1}+H^{2k_1}+\eta^{-3}H^{2\inf(k_1,k_2-1)}+\eta^{-1}H^{2(k_2-1)}\right]\\
&\leqslant C_4\eta^{-3}H^{2\inf(k_1,k_2-1)}
\end{aligned}$$

we get the relevant estimates

$$\begin{cases}\left\|\delta_{HG}\left(\partial_1U_1^0\right)\right\|_0\leqslant C\eta^{-1}H^{\inf(k_1,k_2-1)}\\ \left\|\delta_{HG}\left(D_2U_2^0\right)\right\|_0^2\leqslant C\eta^{-1}H^{\inf(k_1,k_2-1)}\\ \left\|\delta_{HG}\left(D_2^2U_3^0\right)\right\|_0^2\leqslant C\eta^{-1}H^{\inf(k_1,k_2-1)}\end{cases} \tag{6.3}$$

Taking account of (4.3), we then obtain the estimates for the components u_i^ε:

$$\begin{aligned}
\left\|\delta_{HG}\left(\partial_1u_1^\varepsilon\right)\right\|_0&\leqslant\left(\int_\Omega\delta_{HG}\left(\partial_1u_1^\varepsilon\right)^2\mathrm{d}y^1\,\mathrm{d}y^2\right)^{1/2}\\
&=\eta^{-(1/2)}\left\|\delta_{HG}\left(\partial_1U_1^0\right)\right\|_0\\
\left\|\delta_{HG}\left(\partial_2u_2^\varepsilon\right)\right\|_0&\leqslant\left(\int_\Omega\delta_{HG}\left(\partial_2u_2^\varepsilon\right)^2\mathrm{d}y^1\,\mathrm{d}y^2\right)^{1/2}\\
&=\eta^{-(1/2)}\left\|\delta_{HG}\left(D_2U_2^0\right)\right\|_0\\
\left\|\delta_{HG}\left(\partial_2^2u_3^\varepsilon\right)\right\|_0&\leqslant\left(\int_\Omega\delta_{HG}\left(\partial_2^2u_3^\varepsilon\right)^2\mathrm{d}y^1\,\mathrm{d}y^2\right)^{1/2}\\
&=\eta^{-(7/2)}\left\|\delta_{HG}\left(\partial_1U_1^0\right)\right\|_0
\end{aligned} \tag{6.4}$$

which correspond to an anisotropic mesh with step $\mathcal{O}(H)$ in y^1 and $\mathcal{O}(\eta H)$ in y^2. We note that the errors tend to infinity as $\eta\searrow 0$ but, the functions themselves satisfy

$$\left\|\partial_1u_1^\varepsilon\right\|_0=\mathcal{O}\left(\eta^{-(1/2)}\right),\quad \left\|\partial_2u_2^\varepsilon\right\|_0=\mathcal{O}\left(\eta^{-(1/2)}\right),\quad \left\|\partial_2^2u_3^\varepsilon\right\|_0=\mathcal{O}\left(\eta^{-(7/2)}\right)$$

consequently,

$$\begin{cases}\dfrac{\left\|\delta_{HG}\left(\partial_1u_1^\varepsilon\right)\right\|_0}{\left\|\partial_1u_1^\varepsilon\right\|_0}\leqslant C\eta^{-1}H^{\inf(k_1,k_2-1)}\\ \dfrac{\left\|\delta_{HG}\left(\partial_2u_2^\varepsilon\right)\right\|_0}{\left\|\partial_2u_2^\varepsilon\right\|_0}\leqslant C\eta^{-1}H^{\inf(k_1,k_2-1)}\\ \dfrac{\left\|\delta_{HG}\left(\partial_2^2u_3^\varepsilon\right)\right\|_0}{\left\|\partial_2^2u_3^\varepsilon\right\|_0}\leqslant C\eta^{-1}H^{\inf(k_1,k_2-1)}\end{cases} \tag{6.5}$$

Proposition 6.1. *The estimates for the relative errors* (6.5) *for u^ε with an anisotropic mesh of step H and ηH in y^1* and *y^2 respectively are the same order as the estimates* (6.3) *for U^0 with an isotropic mesh of step H in y^1 and z^2. Moreover, because of the locking, they are η^{-1} times the corresponding ones for an analogous problem without small parameter.*

6.2. Comparison with estimates for an isotropic mesh

Let us consider in Ω the region $y^1 \in (0,\pi)$, $y^2 = (0,\mathcal{O}(\eta))$ and an isotropic mesh of step (h,h). Denoting by $\delta_h(u^\varepsilon)$ and $\delta_{h\mathrm{G}}(u^\varepsilon)$ the interpolation and Galerkin approximation errors of u^ε respectively. Reasoning as in the previous subsection, we have:

$$\begin{aligned}
&C_1\left[\left\|\delta_{h\mathrm{G}}\left(\partial_1 u_1^\varepsilon\right)\right\|_0^2 + \left\|\delta_{h\mathrm{G}}\left(\partial_2 u_2^\varepsilon\right)\right\|_0^2 + \varepsilon^2\left\|\delta_{h\mathrm{G}}\left(\partial_2^2 u_3^\varepsilon\right)\right\|_0^2\right]\\
&\quad\leqslant a(\delta_{h\mathrm{G}}(u^\varepsilon),\delta_{h\mathrm{G}}(u^\varepsilon))a(\delta_h(u^\varepsilon),\delta_h(u^\varepsilon))\\
&\quad\leqslant C_2\left[\left(\left\|\delta_h\left(\partial_1 u_1^\varepsilon\right)\right\|_0^2\right) + \left(\left\|\delta_h\left(\partial_2 u_2^\varepsilon\right)\right\|\right)_0^2\right.\\
&\qquad + \left\|\tfrac{1}{2}\left(\delta_h\left(\partial_1 u_2^\varepsilon\right) + \delta_h\left(\partial_2 u_1^\varepsilon\right)\right)\right.\\
&\qquad \left.\left. - \delta_h\left(b_{12}u_3^\varepsilon\right)\right\|_0^2 + \varepsilon^2\left\|\delta_h\left(\partial_2^2 u_3^\varepsilon\right)\right\|_0^2\right] \qquad (6.6)
\end{aligned}$$

From the classical estimate of the interpolation error

$$\|\delta_h(v)\|_{\mathrm{m}} \leqslant Ch^{k+1-m}|v|_{k+1}$$

where

$$|v|_{k+1} = \left[\int_{(0,\pi)\times(0,\mathcal{O}(\eta))}\sum_{i=0}^{k+1}\left(\frac{\partial^i v}{(\partial y^2)^i}\right)^2 \mathrm{d}y^1\,\mathrm{d}y^2\right]^{1/2}$$

As in the previous subsection, replacing u^ε by the leading term of asymptotic expansion, we obtain:

$$\begin{cases}
\left\|\delta_h\left(\partial_1 u_1^\varepsilon\right)\right\|_0 \leqslant C\left(\frac{h}{\eta}\right)^{k_1}\eta^{-3/2}\\
\left\|\delta_h\left(\partial_2 u_2^\varepsilon\right)\right\|_0 \leqslant C\left(\frac{h}{\eta}\right)^{k_1}\eta^{-1/2}\\
\varepsilon\left\|\delta_h\left(\partial_2^2 u_3^\varepsilon\right)\right\|_0 \leqslant C\left(\frac{h}{\eta}\right)^{k_2-1}\eta^{-1/2}
\end{cases} \qquad (6.7)$$

Analogously,

$$\begin{aligned}
&\left\|\tfrac{1}{2}\left(\delta_h\left(\partial_1 u_2^\varepsilon\right) + \delta_h\left(\partial_2 u_1^\varepsilon\right)\right) - \delta_h\left(b_{12}u_3^\varepsilon\right)\right\|_0^2\\
&\quad\leqslant C\left[\left\|\delta_h\left(\partial_1 u_2^\varepsilon\right)\right\|_0^2 + \left\|\delta_h\left(\partial_2 u_1^\varepsilon\right)\right\|_0^2 + \left\|\delta_h\left(u_3^\varepsilon\right)\right\|_0^2\right]\\
&\quad\leqslant C\left(\frac{h}{\eta}\right)^{\inf(k_1,k_2-1)}\eta^{-3/2}
\end{aligned}$$

Consequently, from (6.6),

$$\begin{cases}
\left\|\delta_{h\mathrm{G}}\left(\partial_1 u_1^\varepsilon\right)\right\|_0 \leqslant C\left(\frac{h}{\eta}\right)^{\inf(k_1,k_2-1)}\eta^{-3/2}\\
\left\|\delta_{h\mathrm{G}}\left(\partial_2 u_2^\varepsilon\right)\right\|_0 \leqslant C\left(\frac{h}{\eta}\right)^{\inf(k_1,k_2-1)}\eta^{-3/2}\\
\left\|\delta_{h\mathrm{G}}\left(\partial_2^2 u_3^\varepsilon\right)\right\|_0 \leqslant C\varepsilon^{-1}\left(\frac{h}{\eta}\right)^{\inf(k_1,k_2-1)}\eta^{-(3/2)}\\
\qquad\qquad \leqslant C\left(\frac{h}{\eta}\right)^{\inf(k_1,k_2-1)}\eta^{-9/2}
\end{cases} \qquad (6.8)$$

we observe that taking

$$h = \eta H \qquad (6.9)$$

estimates (6.8) coincide with (6.5). Moreover, in that case, the areas of the triangles are in the ratio

$$\frac{\text{Area of a triangle in the isotropic case}}{\text{Area of a triangle in the anisotropic case}} = \frac{\mathcal{O}(h^2)}{\mathcal{O}(\eta H^2)} = \mathcal{O}(\eta)$$

Proposition 6.2. *The estimate of the error for the Galerkin approximation is given by* (6.7) *for an isotropic mesh (h,h) and by* (6.5) *for an anisotropic one $(H,\eta H)$. By taking H and h as in* (6.9), *the number of triangles for the anisotropic mesh is $\eta = \varepsilon^{1/3}$ times the one for the isotropic mesh whereas the error estimates are the same in both cases.*

7. Numerical experiments

In this section, we give numerical experiments concerning the examples of Sections 2.1 and 2.3.

The numerical computations are implemented with two kinds of finite elements which are used for the normal displacement u_3 as well as for the tangential displacement (u_1,u_2).

For the numerical simulations we used Bell and reduced Hermite finite elements.

The numerical integration of the rigidity matrix needs 12 and 6 G points for Bell and reduced Hermite finite elements respectively.

The meshes for the domain $\Omega = [0,\pi]\times[0,\pi]$ are generated by using the Modulef code. The domain is covered with meshes the sides of which are parallel to the y^1 and y^2 axes. This allows us to generate meshes along the asymptotic curves. Two kinds of meshes are used in this section.

The first mesh for the domain Ω is obtained by dividing Ω into 12 rectangles as seen in Fig. 1. In each one of these triangles an anisotropic mesh is generated by using a function of distribution of the points according to a geometric progression with ratio q_1 less than one in such a way that the mesh is refined in the neighborhood of the searched internal layers. Obviously, the nodes of adjacent regions are chosen to agree.

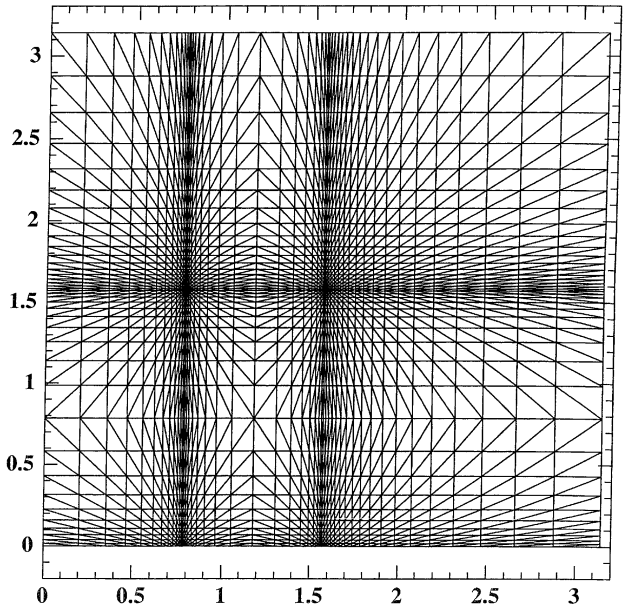

Fig. 1. Anisotropic mesh for the first case of loading (113).

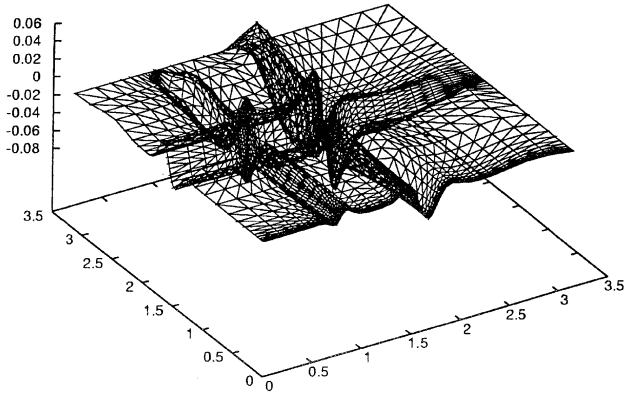

Fig. 2. First case of loading (113). Plot of u_3 in the whole domain.

The second non-uniform mesh for the domain Ω is obtained by symmetry from the basic square $[0,\pi/2]\times[0,\pi/2]$, around $y^1=\pi/2$ and $y^2=\pi/2$ (see Fig. 5). Here again a function of distribution of the points is used according to geometric progression with ratio q_2 (such that the mesh is refined for y^1 and y^2 tending to $\pi/2$).

The surface $\mathscr{S}$ is parameterized with the mapping $\mathbf{\Psi}$:

$$\begin{aligned}&\mathbf{\Psi}:\Omega\to S\subset\mathscr{E}\\&(y^1,y^2)\mapsto\mathbf{\Psi}(y^1,y^2)=(y^1,y^2,y^1y^2)\end{aligned}\tag{7.1}$$

The material is isotropic and homogeneous, with Young modulus 28500 $\mathrm{N\,m^{-2}}$ and Poisson ratio 0.4. The thickness ε is equal to 10^{-4}. The shell is clamped along the boundaries $y^1=y^2=\pi$.

The loadings are

$$\vec{f}_1=\begin{cases}f^\beta=0\\ f^3=\begin{cases}1 & \text{on } [\frac{\pi}{4},\frac{\pi}{2}]\times[\frac{\pi}{2},\pi]\\ 0 & \text{elsewhere}\end{cases}\end{cases}\tag{7.2}$$

and

$$\vec{f}_2=\begin{cases}f^\beta=0\\ f^3=\begin{cases}50 & \text{on } \{y^1\in[0,\frac{\pi}{2}],\ |y^1-y^2|\leqslant 2\times10^{-2}\}\\ 0 & \text{elsewhere}\end{cases}\end{cases}\tag{7.3}$$

respectively. Clearly, the loading $\vec{f}_2$ is a numerical approximation of the δ function of (2.14).

7.1. First example of loading (7.2)

Fig. 1 shows the non-uniform mesh used for the numerical experiment.

The numerical experiments involves 8468 triangles, 4368 nodes and 39,294 degrees of freedom.

Fig. 2 is a plot of u_3^ε on the whole domain.

Fig. 3 is a plot of u_3^ε on the section $y^2=3\pi/8$. As foreseen from Section 2.1 this function exhibits two (propagated) singularities in the neighborhoods of $y^1=\pi/4$ and $y^1=\pi/2$. They look like the structure of the distribution δ'.

Fig. 4 is a plot of u_3^ε on the section $y^1=3\pi/8$. This function exhibits two singularities in the neighborhoods

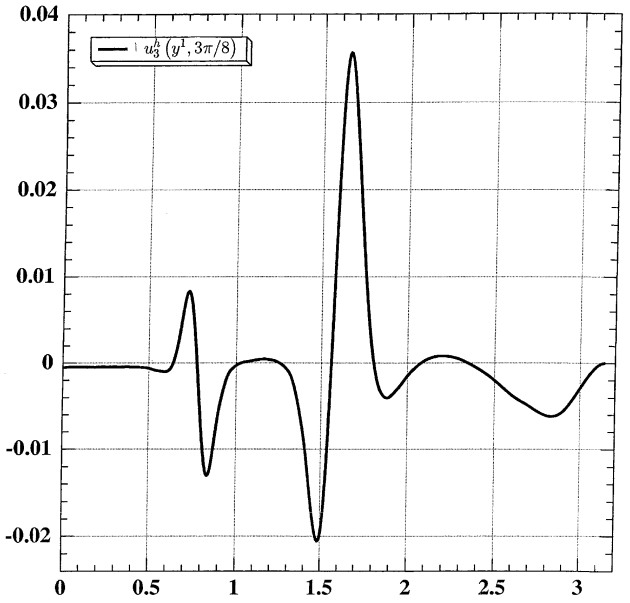

Fig. 3. First case of loading (113). Plot of u_3 for $y^2=3\pi/8$ exhibiting two propagated δ'-like singularities at $y^1=\pi/4$ and $y^1=\pi/2$.

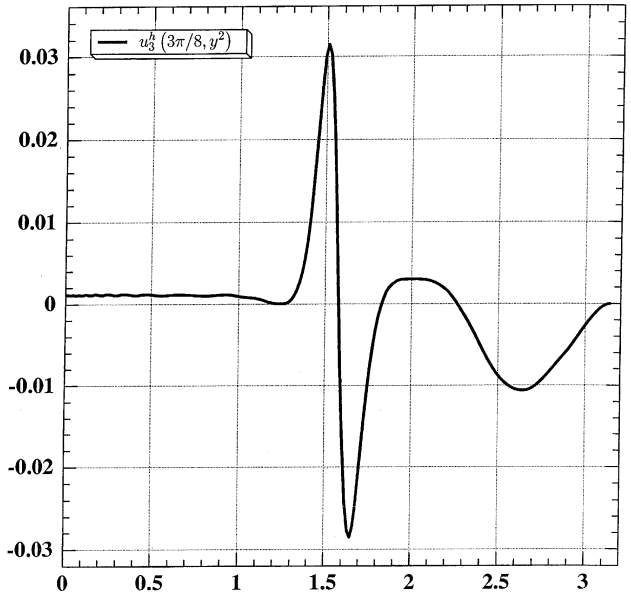

Fig. 4. First case of loading (113). Plot of u_3 for $y^1 = 3\pi/8$ exhibiting a δ'-like propagated singularity at $y^2 = \pi/2$.

of $y^2 = \pi/2$ and $y^2 = \pi$. The first one as foreseen looks like the structure of the distribution δ'. The second one is a genuine boundary layer in δ (which is not considered in this paper).

7.2. Second example of loading

Fig. 5 shows the second non-uniform mesh domain.

The numerical experiments involves 14,400 triangles, 7381 nodes and 60,000 degrees of freedom.

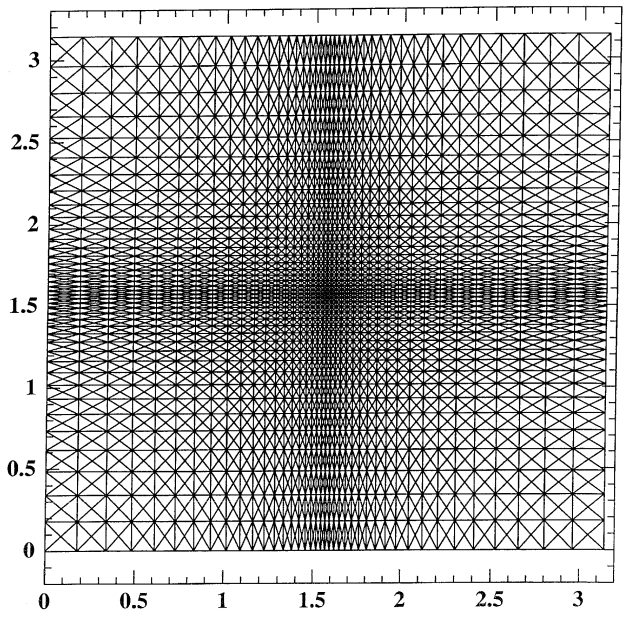

Fig. 5. Anisotropic mesh for the second case of loading (114).

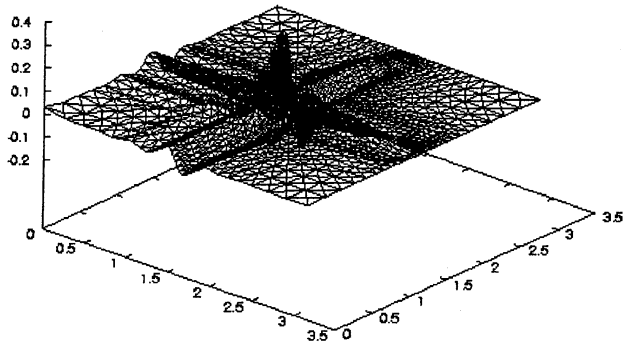

Fig. 6. Second case of loading (114). Plot of u_3 in the whole domain.

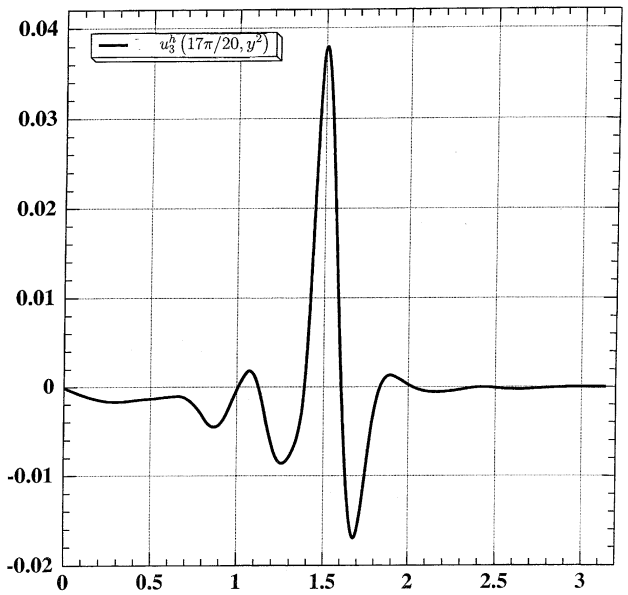

Fig. 7. Second case of loading (114). Plot of u_3 for $y^1 = 17\pi/20$ exhibiting a propagated δ'-like singularities at $y^2 = \pi/2$.

Fig. 6 is a plot of u_3^ε on the whole domain.

Fig. 7 is a plot of u_3^ε on the section $y^1 = 17\pi/20$. As foreseen this function exhibits a (propagated) singularity in the neighborhood of $y^2 = \pi/2$. It looks like the structure of the distribution δ'.

Fig. 8 is a plot of u_3^ε on the section $y^1 = 3\pi/20$. We observe that this function exhibits two singularities. The first one in the neighborhood of $y^2 = \pi/2$ is propagated and looks as δ'. The second one at $y^2 = 11\pi/5$ is the δ-like singularity on the support Σ of the loading considered in Section 2.3.2.

8. Conclusion

In this paper, we dealt with the system of equations describing very thin shells of hyperbolic type i.e. such

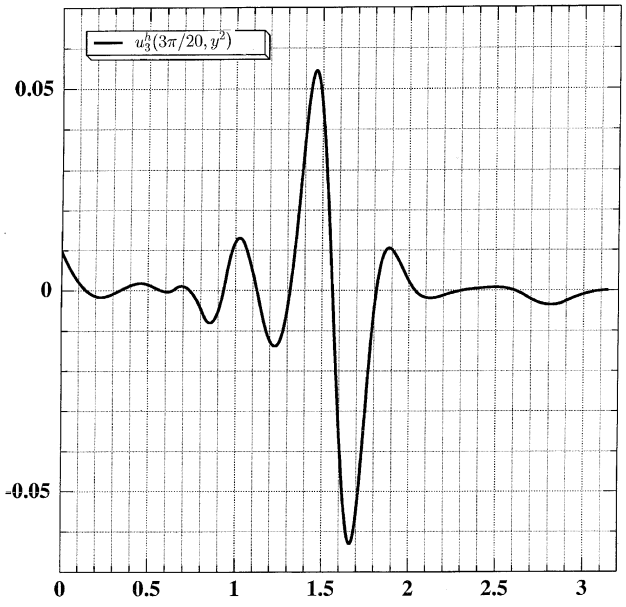

Fig. 8. Second case of loading (114). Plot of u_3 for $y^1 = 3\pi/20$ exhibiting a propagated δ'-like singularities at $y^2 = \pi/2$ and a non-propagated one at $y^2 = 11\pi/5$.

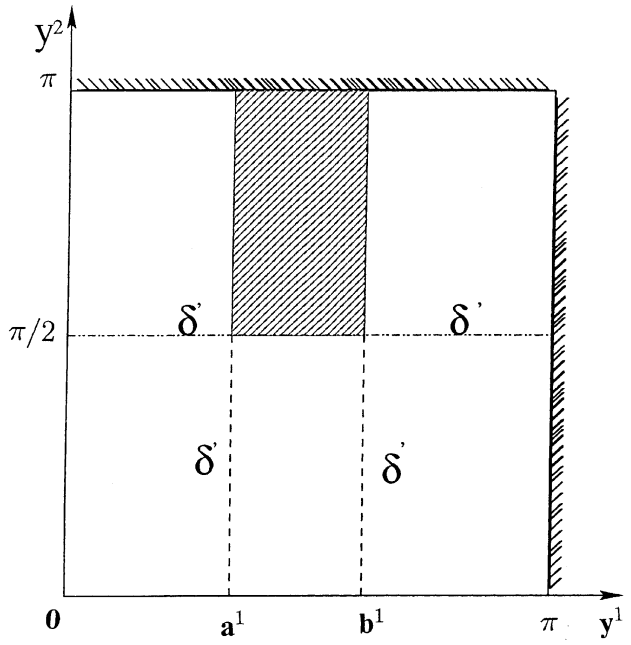

Fig. 9. Domain Ω in the first case of loading (17) δ' indicates the type of propagated singularities of u_3.

that the principal curvatures of the middle surface $\mathscr{S}$ have opposite signs. In this case, the type of the limit system as the relative thickness tends to zero is also hyperbolic. Consequently, the limit solutions exhibit the classical phenomenon of propagation of singularities along the characteristics (which coincide with the asymptotic curves of $\mathscr{S}$. Obviously, for small values of ε these singularities are replaced by narrow layers. Analogy with supersonic aerodynamics is evident. Indeed, in that case it is classical that the limit behavior as the dissipation tends to zero is hyperbolic exhibiting propagation of singularities along the characteristics (which are the Mach lines) which become shock layers for small values of the dissipation. Nevertheless, the specific structure of the limit system of hyperbolic shells it such that the degree of singularity of the solutions is larger than that of the data. Singularities are very strong and most of the energy often concentrates in the layers.

Typical examples are concerned with ruled non-developable surfaces which are hyperbolic and the generators are one of the families of characteristics. Numerical examples are given for a hyperbolic paraboloid so that the two systems of characteristics coincide with the two families of generators. Of course qualitative properties hold true in the general case of curvilinear characteristics.

To fix ideas, let us consider Figs. 9 and 10. The loading is normal, equal to a constant different from zero in the shadowed region (which is limited by segments of characteristics) and vanishes elsewhere. This

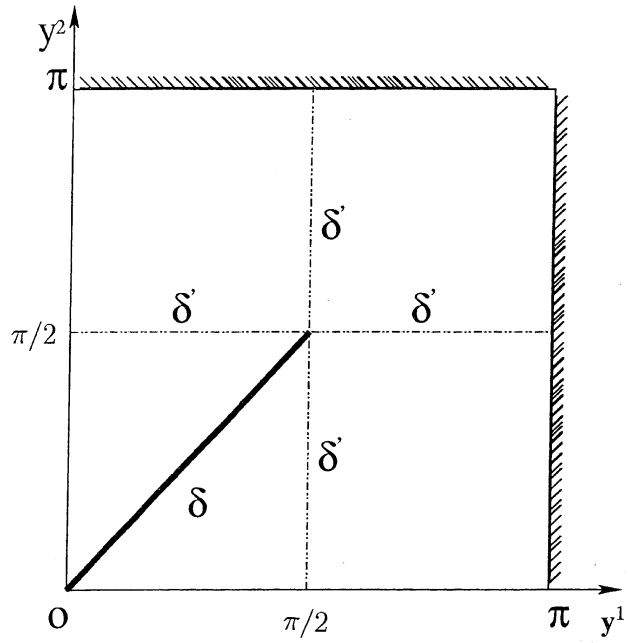

Fig. 10. Domain Ω in the second case of loading (28) δ' indicates the type of propagated singularities of u_3, δ is the non-propagated singularity on $y^1 \in [0, \pi]$, $|y^1 - y^2| \leqslant 2 \times 10^{-2}$.

loading implies a limit solution for which the normal component u_3 of the displacement exhibits δ'-like propagated singularities along the whole characteristic i.e. doublet-like singularities transversal to them.

Singularities of the same type (i.e. δ'-like of u_3) along characteristics may also be obtained with a singularity of

the normal loading f^3 along a segment of a non-characteristic curve, but we need a δ-like singularity there. In addition we have a δ-like non-propagating singularity of u_3 along the support of the singularity of the loading.

We also considered the internal structure of the solution in the layers for small values of ε. The corresponding thickness is $\mathcal{O}(\varepsilon^{1/3})$ for characteristic layers and $\mathcal{O}(\varepsilon^{1/2})$ for non characteristic ones. The knowledge of the structure of the layers allows us to define suited meshes for computing efficiently the solutions in the layers (where the highest values of stresses appear). Moreover, the structure of the solutions in the layers is highly anisotropic as the gradients are mainly normal to the layers. The corresponding estimates for anisotropic (elongated) finite element approximation were given. The superiority with respect to isotropic meshes is shown.

Moreover, the structure of the layers involves subspaces so that the study and computation in the layers are in the framework where classically the phenomenon of locking appears. The above mentioned estimates are poorer than the analogous ones for constraint-free problems (local locking).

It appears, in the specific problem considered here, the explicit reason of a known property in computation of shells: the finite element approximation cannot be uniform with respect to ε, the smaller ε is taken, the finer the mesh must be, but we can optimize its geometry.

References

[1] Apel T, Lube G. Anisotropic mesh refinement in stabilized Galerkin method. Numer Math 1996;74:261–82.

[2] Bernadou M. Méthodes d'éléments finis pour les problèmes de coques minces. Masson: Paris; 1994.

[3] Bernadou M, Ciarlet PG. Sur l'ellipticité du modèle linéaire des coques de W.T. Koiter. In: Glowinski R, Lions JL, editors. Computing methods in sciences and engineering. Lecture notes in economics and mathematical systems, vol. 134. Springer; 1976. p. 89–136.

[4] Brezzi F, Fortin M. Mixed and hybrid finite element methods. Heidelberg: Springer; 1991.

[5] Caillerie D, Sanchez Palencia É. A new kind of singular stiff problems and application to thin elastic shells. Math Models Meth Appl Sci 1995;5:47–66.

[6] Chapelle D, Bathe KJ. Fundamental considerations for the finite element analysis of shell structures. Comput Struct 1998;66:19–36.

[7] Choï D, Palma FJ, Sanchez Palencia É, Vilariño MA. Remarks on the membrane locking in the finite element computation of very thin elastic shells. Math Modell Numer Anal 1998;32:131–52.

[8] Ciarlet PG. Mathematical elasticity. In: Theory of shells, vol. III. Amsterdam: North Holland; 2000.

[9] Ciarlet PG, Raviart PA. General Lagrange and Hermite interpolation in $\mathbb{R}^n$ with applications to finite element method. Arch Rational Mech Anal 1972;46:177–99.

[10] Eckhaus W. Asymptotic analysis of singular perturbations. Amsterdam: North Holland; 1979.

[11] Egorov YuV, Shubin MA. Linear partial differential equations. Foundations of the classical theory. Encyclop Math Sci (Part Diff Eqs I), Springer 1992;30: 345–75.

[12] Gérard P, Sanchez Palencia É. Sensitivity phenomena for certain thin elastic shells with edges. Math Meth Appl Sci 2000;23:379–99.

[13] Goldenveizer AL. Theory of thin elastic shells. New York: Pergamon; 1962.

[14] Green AE, Zerna W. Theoritical elasticity. Oxford: Clarendon Press; 1954.

[15] Karamian P. Nouveaux résultats numériques concernant les coques minces hyperboliques inhibées: cas du paraboloïde hyperbolique. Compt Red Acad Sci, Paris, série IIb 1998;326:755–60.

[16] Karamian P. Coques élastiques minces hyperboliques inhibées: calcul du problème limite par éléments finis et non reflexion des singularités thèse de l'Université de Caen, 1999.

[17] Karamian P, Sanchez-Hubert J. Boundary layers in thin elastic shells with developable middle surface. Eur J Mech A/Solids 2002;21:13–47.

[18] Karamian P, Sanchez-Hubert J, Sanchez Palencia É. A model problem for boundary layers of thin elastic shells. Math Modell Numer Anal 2000;34:1–30.

[19] Leguillon D, Sanchez-Hubert J, Sanchez Palencia É. Model problem of singular perturbation without limit in the space of finite energy and its computation. CR Acad Sci Paris, série IIb 1999;327:485–92.

[20] Lions JL. Perturbations singulières dans les problèmes aux limites et en contrôle optimal. In: Lectures notes in mathematics, vol. 323. Berlin: Springer; 1973.

[21] Lions JL, Magenes. Problèmes aux limites non homogènes et applications. Dunod, Paris 1968;I&II.

[22] Lions JL, Sanchez Palencia É. Instabilities produced by edges in thin shells. In: Argoul P, Frémond M, Nguyen QS, editors. Variation of domains and free boundary problems. Kluwer; 1998. p. 277–84.

[23] Love AEH. A treatrise on the mathematical theory of elasticity. New York: Dover; 1944.

[24] Pitkaranta J, Matache AM, Schwab C. Fourier mode analysis of layers in shallow shell deformation. Research report 98-18, seminar für Angewandte Mathematik, Technische Hochschule Zürich, Comput Meth Appl Mech Eng, in press.

[25] Rutten HS. Theory and design of shells on the basis of asymptotic analysis. Voorburg: Rutten & Kruisman; 1973.

[26] Sanchez-Hubert J, Sanchez Palencia É. Pathological phenomena in computation of thin elastic shells. Trans Can Mech Eng 1998;22(4B):435–46.

[27] Sanchez-Hubert J, Sanchez Palencia É. Singular perturbations with non-smooth limit and finite element approximation of layers for model problems of shells. In: Ali Mehmeti F, von Below J, Nicaise S, editors. Partial differential equations in multistructures. New York: Dekker; 2001. p. 207–26.

[28] Sanchez-Hubert J, Sanchez Palencia É. Coques élastiques minces. Propriétés asymptotiques. Paris: Masson; 1997.
[29] Sanchez-Hubert J, Sanchez Palencia É. Anisotropic finite element estimates and local locking for shells: parabolic case. Compt Red Acad Sci, Paris, série IIb 2001;329: 153–9.
[30] Sanchez Palencia É. On a singular perturbation going out of the energy space. J Math Pures Appl 2000;79:591–602.
[31] Sanchez Palencia É. New cases of propagation of singularities along characteristic boundaries for model problems of shell theory. Compt Red Acad Sci, Paris, série IIb 2001;329:315–21.

MATHEMATICAL METHODS IN THE APPLIED SCIENCES
Math. Meth. Appl. Sci. 2003; **26**:1451–1485 (DOI: 10.1002/mma.421)
MOS subject classification: 74 K 25; 35 A 21; 35 Q 72

Pseudo-reflection phenomena for singularities in thin elastic shells

P. Karamian-Surville[1], J. Sanchez-Hubert[2] and E. Sanchez Palencia[2,*,†]

[1] *Laboratoire de Mécanique, Modélisation Mathématique et Numérique, Université de Caen, BP 5186, 14032 Caen, France*
[2] *Laboratoire de Modélisation en Mécanique, Université Paris VI, 4 place Jussieu, 75252 Paris, France*

Communicated by W. Sprößig

SUMMARY

We consider problems of statics of thin elastic shells with hyperbolic middle surface subjected to boundary conditions ensuring the geometric rigidity of the surface. The asymptotic behaviour of the solutions when the relative thickness tends to zero is then given by the membrane approximation. It is a hyperbolic problem propagating singularities along the characteristics. We address here the reflection phenomena when the propagated singularities arrive to a boundary. As the boundary conditions are not the classical ones for a hyperbolic system, there are various cases of reflection. Roughly speaking, singularities provoked elsewhere are not reflected at all at a free boundary, whereas at a fixed (or clamped) boundary the reflected singularity is less singular than the incident one. Reflection of singularities provoked along a non-characteristic curve $\mathscr{C}$ are also considered. Copyright © 2003 John Wiley & Sons, Ltd.

1. INTRODUCTION AND GENERALITIES

In this paper, we consider problems of statics of thin elastic shells with hyperbolic middle surface $\mathscr{S}$ (i.e. with non-zero principal curvatures of opposite signs). It is known that in this case, under appropriate hypotheses the problem leads to a hyperbolic system that may be written under different forms. Without going into details, which may be found in Reference [1, Section VII.2]; [2], we may quote that we deal with the asymptotic behaviour of shells such that the middle surface $\mathscr{S}$ with the corresponding boundary conditions is geometrically rigid (i.e. no deformation of the surface is possible without modifying the intrinsic metrics of $\mathscr{S}$). Moreover, the whole context of our problem is linear (in particular, geometric rigidity is understood in the linear sense of small deformation). The description of the problem is then based on the surface $\mathscr{S}$ itself (so that 'shell' or 'surface' will be equivalent); the thickness of the shell only appears when taking into account the flexion terms (see Section 9) which do not appear in the asymptotic behaviour for small thickness.

* Correspondence to: E. Sanchez Palencia, Laboratoire de Modélisation en Mécanique, Université Paris VI, 4 place Jussieu, 75252 Paris, France.
† E-mail: sanchez@lmm.jussieu.fr

Received 8 July 2002

It will prove useful to take a parametrization of the surface $\mathscr{S}$ where the parametric curves are the asymptotic ones so that the coefficients of the second fundamental form are such that: $b_{11} = b_{22} = 0$; $b_{12} \neq 0$. Then, the stresses $T^{\alpha\beta} = T^{\beta\alpha} \alpha, \beta = 1, 2$, satisfy the following system:

$$\begin{cases} -D_1 T^{11} - D_2 T^{12} = f^1 \\ -D_1 T^{12} - D_2 T^{22} = f^2 \\ -2b_{12} T^{12} = f_3 \end{cases} \tag{1}$$

where D_α denote the covariant differentiation which will be defined hereafter. For the time being, it is sufficient to know that it amounts to ordinary differentiation which will be denoted by ∂_α plus certain terms not containing derivatives which do not modify the general structure of the system nor its characteristics. The f^i, $i = 1, 2, 3$, are the three components of the applied forces (after appropriate normalization); f^α, $\alpha = 1, 2$, are the tangential components and f^3 the normal one. Here and in the sequel, latin or greek indices are assumed to run in (1,2,3) and (1,2), respectively, and the convention of summation of the repeated indices is used.

This system has three equations, one of which does not contain differentiation, and three unknowns. Its total order is 2, it reduces to a hyperbolic system of order one for T^{11} and T^{22}.

As for the displacements u_i, where u_α are the tangential components and u_3 is the normal one, they are solutions of the system:

$$\begin{cases} D_1 u_1 = C_{11\lambda\mu} T^{\lambda\mu} \\ D_2 u_2 = C_{22\lambda\mu} T^{\lambda\mu} \\ \dfrac{1}{2}(D_1 u_2 + D_2 u_1) - C_{12} u_3 = C_{12\lambda\mu} T^{\lambda\mu} \end{cases} \tag{2}$$

where the $C_{\alpha\beta\lambda\mu}$ are the coefficients of membrane compliance of the shell. When the $T^{\alpha\beta}$ are assumed to be known, this system has three equations and three unknowns and its total order is 2. The two first equations form a hyperbolic system for u_1 and u_2. The unknown u_3 is then obtained from the third equation which may be considered as a definition of it.

We observe that the complete system (1) and (2) is of total order 4. Disregarding the boundary conditions which will be considered later, the partial system (1) has two families of simple characteristic which are parallel to the axes. In the same way, system (2), with the $T^{\alpha\beta}$ assumed to be known, has two families of simple characteristics which are parallel to the axes too. Consequently, the total system has the double characteristics $y^1 = const$ and $y^2 = const$.

More precisely, let us denote by Ω a bounded and connected domain of the (y^1, y^2)-plane (the parameter plane). The middle surface $\mathscr{S}$ of the shell is defined by a smooth function $\vec{\mathbf{r}}$

$$\Omega \ni (y^1, y^2) \mapsto \vec{\mathbf{r}}(y^1, y^2) \in \mathbb{R}^3 \tag{3}$$

At any point of $\mathscr{S}$ we define the tangent vectors

$$\vec{\mathbf{a}}_\alpha = \partial_\alpha \vec{\mathbf{r}} \tag{4}$$

$(\vec{\mathbf{a}}_1, \vec{\mathbf{a}}_2)$ is the local covariant basis of the tangent plane.

The first fundamental form which defines the distances on the surface is given by

$$ds^2 = a_{\alpha\beta}\, dy^\alpha\, dy^\beta \quad \text{where } a_{\alpha\beta} = \vec{\mathbf{a}}_\alpha \cdot \vec{\mathbf{a}}_\beta \tag{5}$$

The corresponding contravariant basis $\vec{\mathbf{a}}^\alpha$ is defined by $\vec{\mathbf{a}}^\alpha \cdot \vec{\mathbf{a}}_\beta = \delta^\alpha_\beta$. We also consider the unit normal vector $\vec{\mathbf{a}}^3 = \vec{\mathbf{a}}_3$. We note that when changing the parametrization $\vec{\mathbf{a}}_3$ is invariant up to the orientation so that normal components behave essentially as scalars.

We recall that the Christoffel symbols are

$$\Gamma^\lambda_{\alpha\beta} = \partial_\beta \vec{\mathbf{a}}_a \cdot \vec{\mathbf{a}}^\lambda \tag{6}$$

they account for the non-constant character of the local basis. The covariant differentiation of vectors and tensors are then given by

$$D_\alpha u_\beta = \partial_\alpha u_\beta - \Gamma^r_{\alpha\beta} u_r \tag{7}$$

$$D_\lambda T^{\alpha\beta} = \partial_\lambda T^{\alpha\beta} + \Gamma^\alpha_{\lambda\mu} T^{\mu\beta} + \Gamma^\beta_{\lambda\mu} T^{\alpha\mu} \tag{8}$$

The coefficients of the second fundamental form describing the curvatures are

$$b_{\alpha\beta} = b_{\beta\alpha} = -\partial_\beta \vec{\mathbf{a}}_3 \cdot \vec{\mathbf{a}}_\alpha \tag{9}$$

Let Γ be the boundary of Ω which we always consider to be non-tangent to the characteristics. It is the union of a fixed (or clamped) part Γ_0 and of a free part Γ_1. The boundary conditions are

$$T^{\alpha\beta} v_\beta = 0 \quad \text{on } \Gamma_1 \tag{10}$$

and

$$u_1 = u_2 = 0 \quad \text{on } \Gamma_0 \tag{11}$$

where we note that (11) are Cauchy conditions for system (2) when the $T^{\alpha\beta}$ are supposed known.

The v_α are the covariant components of the vector $\vec{\mathbf{v}}$ which is the outer unit normal to the boundary Γ in the tangent plane to the surface.

As Γ_1 is not a characteristic, its normal $\vec{\mathbf{v}}$ it is not normal to the vectors $\vec{\mathbf{a}}_\alpha$, then from

$$\vec{\mathbf{v}} = v_1 \vec{\mathbf{a}}^1 + v_2 \vec{\mathbf{a}}_2 \quad \text{with } \vec{\mathbf{v}} \cdot \vec{\mathbf{a}}_\alpha \neq 0$$

we see that

$$v_1 \quad \text{and} \quad v_2 \neq 0$$

so that the boundary conditions (10) become

$$\begin{cases} T^{11} = -\dfrac{v_2}{v_1} T^{12} \\ T^{22} = -\dfrac{v_1}{v_2} T^{12} \end{cases} \quad \text{on } \Gamma_1 \tag{12}$$

which are Cauchy conditions for hyperbolic system (1).

We emphasize that the previous description is only concerned with the membrane equations, without flexion terms. As a consequence, as derivatives of u_3 does not appear, the trace of u_3 does not make sense. In this context there is no difference between fixed and clamped boundaries, and the corresponding boundary conditions are merely (11). The difference between clamped and fixed boundaries only appears in the internal structure of the layer which replaces a singularity when the flexion terms are taken into account (see Section 9).

In the sequel, we shall assume that there is no segment of characteristic with both extremities in a free boundary Γ_1 (likely, the case of two free extremities should correspond to a non-geometrically rigid surface and then out of our framework).

Obviously, hyperbolic systems enjoy properties of propagation of singularities along the characteristics. The peculiar structure of system (1) and (2) implies that the singularities of the data f_i induce very high order singularities of the unknowns $T^{\alpha\beta}$ and u_i. Indeed, T^{12} is explicitly given by the third equation (1) so that the hyperbolic system for T^{11} and T^{22} has as effective data the first-order derivatives of f_3. After considering the classical system formed by these equations and the two first (2), the unknown u_3 is in its turn defined by the first derivative of u_α. So that the 'order of singularity' (defined hereafter) of u_3 implied by the singularity of f_3 is two units larger than for a classical hyperbolic system. For this reason, singularities are very important in this kind of problems. We shall see in Section 9 that a good description of the singularities gives most of the shape of the solution, see References [3,4] for various aspects of propagation of singularities and the corresponding boundary layers. The methods used here for studying the singularities, which are recalled in Sections 2 and 4 hereafter, are variants of the classical theory (see [5, Section V.1.3]; [6, Section 4.11]).

The objective of this paper is to study the *reflection properties of these singularities when they intersect a (nowhere characteristic) boundary*. It is easily seen that the boundary conditions prescribed either on Γ_0 or Γ_1 are not the standard ones leading to classical reflection properties. As we shall recall hereafter, classical reflection for a first-order hyperbolic system with two unknowns are obtained when prescribing one boundary condition. This is not the case in the present problem. Indeed, in each one of the two cases of free or fixed boundary (see (11) and (12)) we have two conditions for one of the partial systems ((1) and (2)) and no condition for the other. We shall consider the various possible cases and we shall see that in most of them the reflected singularity has one order of singularity lower than the incident one and even disappears in certain cases. A first announcement of this property was given in Reference [7], but we shall deal here with more general situations. It should be noticed that the concepts of incident and reflected are not obvious as the time is not involved in our problem. We must go on to causality of the phenomenon for having a proper description of it.

In order to emphasize the differences with the *classical reflections* let us recall them in the following elementary examples: let us consider the first-order hyperbolic system (equivalent to the *wave equation*):

$$\partial_t \begin{pmatrix} u_1 \\ u_2 \end{pmatrix} - \begin{pmatrix} 0 & 1 \\ 1 & 0 \end{pmatrix} \partial_x \begin{pmatrix} u_1 \\ u_2 \end{pmatrix} = \begin{pmatrix} 0 \\ 0 \end{pmatrix}$$

in the quadrant $t>0$, $x>0$ with the two Cauchy conditions at $t=0$

$$\begin{cases} u_1(0,x) = a_1(x) \\ u_2(0,x) = a_2(x) \end{cases}$$

and the unique boundary condition on $x=0$

$$u_1(t,0)=0$$

The general solution of the system takes the form

$$\begin{cases} u_1(t,x)=F(t+x)+G(t-x) \\ u_2(t,x)=F(t+x)-G(t-x) \end{cases}$$

where F and G are arbitrary functions of one variable. The boundary condition implies

$$F(t)+G(t)=0 \tag{13}$$

that is to say, when the function $F(s)$ has a singularity at $s=c$ (i.e. $F(t+x)$ propagates such a singularity along $x=-t+c$) then $G(s)=-F(s)$ has the same singularity up to the sign at $s=c$ (i.e. $G(t-x)$ propagates the same singularity up to the sign along $x=t+c$). Consequently, any singularity arriving to the origin $x=0$ at the time $t=c$ along $x=-t+c$ from $t<c$ starts again up to the sign along $x=t+c$ for $t>c$.

Oppositely, when considering a vicinity of $t=0$, where the Cauchy conditions are prescribed, we have

$$F(s)+G(-s)=a_1(s)$$

$$F(s)-G(-s)=a_2(s)$$

then $F(s)$ and $G(-s)$ do not satisfy a universal condition (i.e. independent of a_1 and a_2) such that (13).

It should be noticed that in more general systems (i.e. with variable coefficients and lower-order terms) the above properties of propagation of singularities and reflections hold true even if there is no exact solutions.

As we mentioned above, boundary conditions in shell theory are not standard so that reflections have very different properties than in the classical case. We shall see later that in most cases the reflected singularity is one order more smooth than the incident one. Such a situation will be generically called *pseudo-reflection*.

The paper is organized as follows. Section 2 contains definitions of the orders of singularity (or smoothness) as well as elementary tools for handling their propagation. Section 3 has an auxiliary character. It contains some properties concerning the effects of change of variables on singularities. General properties on singularities along characteristic or no characteristic curves are given in Section 4. A classification of the different cases of reflection problems is given in Section 5. The phenomena of pseudo-reflection are addressed in Sections 6 and 7. Section 6 is concerned with a rather general example where a singularity is prescribed along a characteristic. Section 7 deals with the case when a singularity is prescribed along a non-characteristic curve. The general properties of reflection are then stated in Section 8. At last, numerical experiments are shown in Section 9.

2. SOME AUXILIARY PROPERTIES ON SINGULARITIES AND VECTOR VALUED FUNCTIONS

In this section, we give some definitions and properties of functions or distributions in two variables x, y. It appears that the most appropriate way to study propagation of singularities is to consider functions or distributions in x, y as functions or distributions of the unique variable y with values in a space of functions or distributions of the other variable x. As a consequence, the most general framework in this concern is that of distributions of the variable y with values distributions of x so that we shall work in the space

$$\mathscr{D}'(\mathbb{R}_y, \mathscr{D}'(\mathbb{R}_x)) \tag{14}$$

We shall only study in the sequel local properties of such distributions, for instance singularities in the vicinity of a segment of the axis x so that we shall refer to (14) for functions or distributions on a domain Ω of the (x, y)-plane.

Let us first consider distributions of y with numerical values. In order to define some classes of singularities at $y=0$, we may think about the chain of distributions

$$\dots yY(y), Y(y), \delta(y), \delta'(y), \dots \tag{15}$$

where Y and δ denote the Heaviside (step) function and the Dirac mass respectively. Obviously, the first explicit distribution in (15) has a jump of its first derivative at $y=0$, the second one has a jump of the function itself, the others are classical distributions with support at $y=0$. Of course, the chain is considered unlimited in both senses. In the sequel we shall consider that distributions as singularities at $y=0$ whereas their values for $y\neq 0$ will be discarded; for instance $Y(y)$ will be considered merely as the unit jump at $y=0$. This amounts to saying that the elements of the chain (15) are only considered up to a smooth additive function. We then observe that the singular support of any one of them is $y=0$, and we are not interested in the support itself. In fact (15) is considered as a chain of singularities. Clearly, this chain is stable by differentiation. More generally, we may consider analogous chains of the form

$$\dots Y(y)\frac{y^{\alpha-1}}{\alpha-1}, Y(y)y^{\alpha}, \frac{\mathrm{d}}{\mathrm{d}y}(Y(y)y^{\alpha}), \frac{\mathrm{d}^2}{\mathrm{d}y^2}(Y(y)y^{\alpha}), \dots \tag{16}$$

for a given $\alpha\in(0,1)$. Obviously, the derivatives in (16) are considered in the distribution sense and involve the finite parts of the corresponding integrals, see for instance [8]. This chain enjoys the above mentioned stability property; we also note that for integer α this chain becomes (15).

Any one of the previous chains will generically be noted

$$\dots \varphi^{(-2)}, \varphi^{(-1)}, \varphi, \varphi', \varphi'', \varphi^{(3)}, \dots \tag{17}$$

It will prove useful considering *formal series* involving a certain singularity $\varphi^{(k)}$ and the less singular ones of the corresponding chain i.e. expression of the form

$$\sum_{n\leqslant k} a_n \varphi^{(n)}(y) \tag{18}$$

where the a_k are numerical coefficients. Formal algebraic operations involving differentiations and multiplication by a smooth function are obviously allowed in such formal series according to the classical rules of distribution theory.

When considering distributions of form (14) we may define new formal series of form (18) where the coefficients a_n are distributions of x. In that case, the allowed formal algebraic operations involve differentiation either with respect to y or x and multiplication by smooth functions of y and x. In practice we shall be concerned with a few terms and the formal series will take the form

$$a_k(x)\varphi^{(k)}(y) + a_{k-1}(x)\varphi^{(k-1)}(y) + \cdots \tag{19}$$

where $\cdots$ denote less singular terms with respect to y. Obviously in such kind of expression, the coefficients $a_n(x)$ may be singular in x, not necessarily ordered.

Example 2.1
We consider the function $f(x, y)$ defined by

$$f(x, y) = \begin{cases} 1 & \text{for } y > 0, 0 < x < cy \\ 0 & \text{elsewhere} \end{cases} \tag{20}$$

where $c > 0$ is a given constant.

Let us write the function $f(x, y)$ under the form

$$f(x, y) = Y(x)[1 - Y(x - cy)]$$

it is easily seen that for $y \neq 0$ it is a smooth function of y with values in $\mathscr{D}'(\mathbb{R}_x)$ indeed, for $y > 0$ we have

$$\partial_y^p f(\cdot, y) = (-1)^{p+1} c^p \delta_{cy}^{(p-1)}(\cdot), \quad p = 1, 2, \ldots$$

which is obviously continuous in $\mathscr{D}'(\mathbb{R}_x)$ as is immediately seen by taking the duality product with $\theta \in \mathscr{D}(\mathbb{R}_x)$.

Moreover, around $y = 0$ we have

$$f(x, y) = c\delta(x)Y(y)y + \cdots \tag{21}$$

where $\cdots$ denote terms less singular than $Y(y)y$. Indeed, by expanding the test function by the Taylor formula at $y = 0$ we have

$$\langle f(\cdot, y), \theta(\cdot) \rangle = \int_0^{cy} \theta(x)\,\mathrm{d}x = cy\langle \delta, \theta \rangle + \cdots$$

for $y > 0$. As this expression vanishes for $y < 0$, we obtain (21).

Example 2.2
Let us now consider the function $f(x, y)$ defined by

$$f(x, y) = \begin{cases} \varphi(x, y) & \text{for } y > \psi(x) \\ 0 & \text{elsewhere} \end{cases}$$

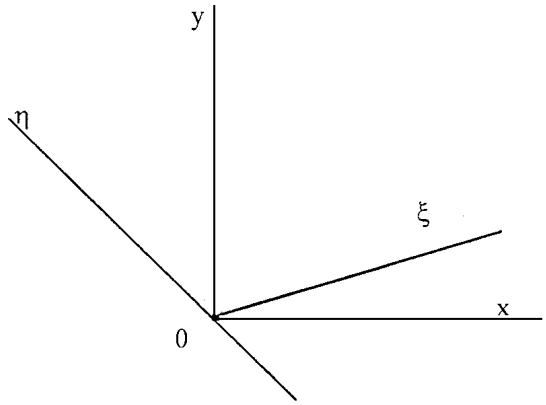

Figure 1. Change of variables in Example 3.1.

where φ is a smooth function and ψ is smooth and satisfies

$$\psi(0)=\psi'(0)=0,\ \ \psi''(0)>0.$$

Exactly in the same way as in the previous example we show that f is smooth with values in $\mathscr{D}'(\mathbb{R}_x)$ for $y\neq 0$ and that for $y=0$ it is

$$f(x,y)=2^{3/2}[\psi''(0)]^{-1/2}\varphi(0,0)\delta(x)Y(y)y^{1/2}+\cdots$$

We observe that this example generates naturally a singularity in chain (16) with $\alpha=\frac{1}{2}$.

3. CHANGE OF VARIABLES FOR SOME DISTRIBUTIONS WITH SINGULAR SUPPORT ALONG A SEGMENT

The objective in this paper is to study the propagation of singularities of the solutions along the characteristics. But, as the data are often singular along other curves we shall need to perform appropriate changes of variables. This involves a change in framework (14) which has non-evident consequences. In this section, we give two examples which will be used in the sequel with eventual slight modifications.

Example 3.1
Let us consider (see Figure 1) the two frames (x,y) (orthogonal) and (ξ,η) (oblique in general). We then consider the distribution

$$f(\xi,\eta)=Y(\xi)\delta^{(p)}(\eta),\ \ p \text{ given integer } \geqslant 0 \tag{22}$$

This is a p-upple in the direction η along the half axis $\xi>0$, we shall show hereafter that in the framework of (14) it has an expansion of form (18) beginning by $\delta^{(p-1)}(y)$ with as coefficient $c\delta(x)$. Let

$$\begin{aligned} x&=a_{11}\xi+a_{12}\eta\\ y&=a_{21}\xi+a_{22}\eta \end{aligned} \tag{23}$$

be the change of coordinates. The action of (22) on a test function $\theta \in \mathscr{D}(\mathbb{R}_\xi \times \mathbb{R}_\eta)$ is

$$\langle f, \theta \rangle = (-1)^p \int_0^{+\infty} \frac{\partial^p \theta}{\partial \eta^p}(\xi, 0)\, \mathrm{d}\xi \tag{24}$$

Let us choose $\theta(\xi, \eta) = \theta_1(x)\theta_2(y)$ where x and y are expressed in ξ, η by (23), then we have

$$\begin{aligned}\langle f, \theta_1\theta_2 \rangle &= (-1)^p \int_0^{+\infty} \frac{\partial^p(\theta_1\theta_2)}{\partial \eta^p}(\xi, 0)\, \mathrm{d}\xi = (-1)^p \sum_{k=0}^{p} C_k^{p-k} \int_0^{+\infty} \frac{\partial^k \theta_1}{\partial \eta^k} \frac{\partial^{p-k}\theta_2}{\partial \eta^{p-k}}\, \mathrm{d}\xi \\ &= (-1)^p \sum_{k=0}^{p} C_k^{p-k} (a_{12})^k (a_{22})^{p-k} \int_0^{+\infty} \theta_1^{(k)}(a_{11}\xi)\theta_2^{(p-k)}(a_{21}\xi)\, \mathrm{d}\xi \end{aligned} \tag{25}$$

In order to exhibit a distribution of $\mathscr{D}'(\mathbb{R}_y, \mathscr{D}'(\mathbb{R}_x))$ we integrate by parts for eliminating the derivatives of θ_2. The generic term of (25) gives

$$\begin{aligned}&\int_0^{+\infty} \theta_1^{(k)}(a_{11}\xi)\theta_2^{(p-k)}(a_{21}\xi)\, \mathrm{d}\xi \\ &= \sum_{m=1}^{p-k} \left[(-1)^{p+m} \left(\frac{a_{21}}{a_{11}} \right)^m \langle \delta^{(k+m-1)}(x), \theta_1(x) \rangle \langle \delta^{(p-k-m)}(y), \theta_2(y) \rangle \right] \\ &\quad + \left(-\frac{a_{11}}{a_{21}} \right)^{p-k} \int_0^{+\infty} \theta_1^{(p)}(a_{11}\xi)\theta_2(a_{21}\xi)\, \mathrm{d}\xi \end{aligned} \tag{26}$$

Clearly the right-hand side of (26), concerning dependence with respect to y, is a sum of singularities of the kind $\delta(y)$, $\delta'(y), \ldots, \delta^{(p-k-1)}(y)$, plus the integral term. Let us show that this term is only singular as $Y(y)$. We have

$$\begin{aligned}\int_0^{+\infty} \theta_1^{(p)}(a_{11}\xi)\theta_2(a_{21}\xi)\, \mathrm{d}\xi &= \frac{1}{a_{21}} \int_0^{+\infty} \theta_1^{(p)}\left(\frac{a_{11}}{a_{21}}\zeta \right) \theta_2(\zeta)\, \mathrm{d}\zeta \\ &= \frac{(-1)^p}{a_{21}} \int_0^{+\infty} \left\langle \delta^{(p)}\left(x - \frac{a_{11}}{a_{21}}\zeta \right), \theta_1(x) \right\rangle \theta_2(\zeta)\, \mathrm{d}\zeta \\ &= \frac{(-1)^p}{a_{21}} \left\langle Y(y) \left\langle \delta^{(p)}\left(x - \frac{a_{11}}{a_{21}} y \right), \theta_1(x) \right\rangle, \theta_2(y) \right\rangle \end{aligned}$$

which is $Y(y)$ multiplied by a function of $\mathscr{C}^\infty(y, \mathscr{D}'(\mathbb{R}_x))$ acting on $\theta_1(x)\theta_2(y)$ as we announced above.

Coming back to (25), we see that the singularity of higher order with respect to y follows from $m=1$ in (26) for $k=0$, as a result we have

$$Y(\xi)\delta^{(p)}(\eta) = -(a_{22})^p \frac{a_{21}}{a_{11}}\,\delta(x)\delta^{(p-1)}(y) + \cdots \tag{27}$$

where $\cdots$ are for less singular terms at $y=0$.

Remark 3.1
This formula may be obtained easily in a heuristic way. Indeed, let us first consider the case $p=0$ for which $f = Y(\xi)\delta(\eta)$ then (27) takes the form

$$Y(\xi)\delta(\eta) = -\frac{a_{21}}{a_{11}}\,\delta(x)Y(y) + \cdots \tag{28}$$

This formula follows easily from the fact that $\delta(\eta)$ is a smooth function with respect to y with values in $\mathscr{D}'(\mathbb{R}_x)$ in the region $y>0$; then multiplication by $Y(\xi)$ implies a jump at $y=0$ from the value 0 for $y<0$ to $\delta(\eta)$ for $y=0$, i.e. $c\delta(x)$ where the constant c comes from the change of the measure.

In the case $p>0$ using the formula of differentiation with respect to η:

$$\frac{\partial^{(p)}}{\partial\eta^p} = \sum_{k=0}^{p} C^p_{p-k}(a_{12})^k(a_{22})^{p-k}\frac{\partial^k}{\partial x^k}\,\frac{\partial^{p-k}}{\partial y^{p-k}} = (a_{22})^p\frac{\partial^p}{\partial y^p} + \cdots$$

formula (27) follows from (28).

Example 3.2
We have analogous properties for

$$f(\xi,\eta) = Y(\xi)Y(\eta)\eta^q,\ q \text{ given integer } \geqslant 0 \tag{29}$$

By inversion of (23) we obtain

$$\xi = b_{11}x + b_{12}y$$
$$\eta = b_{21}x + b_{22}y$$

where the coefficients, in the specific disposition of Figure 1, satisfy $b_{11}>0$, $b_{12}>0$, $b_{21}<0$, $b_{22}>0$. In the present case we shall only deal with functions of y with values in $\mathscr{D}'(\mathbb{R}_x)$ so that we shall only take test functions $\theta(x)$. Let

$$\tilde{f}(x,y) = f(b_{11}x + b_{12}y, b_{21}x + b_{22}y)$$

we then have

$$\langle \tilde{f}(\cdot,y),\theta(\cdot)\rangle = \sum_{k=0}^{q} C^{q-k}_k (b_{21})^{q-k}(b_{22})^k y^{q-k}\int_{-(b_{12}/b_{11})y}^{-(b_{22}/b_{21})y} x^k\theta(x)\,\mathrm{d}x$$

We note that for $q=0$ we are in a case analogous to Example 2.1. The general case is handled in a similar way expanding θ by the Taylor formula at $y=0$:

$$\int_{-(b_{12}/b_{11})y}^{-(b_{22}/b_{21})y} x^k\theta(x)\,\mathrm{d}x = \frac{1}{k+1}\left[\left(\frac{b_{22}}{b_{21}}\right)^k - \left(\frac{b_{12}}{b_{11}}\right)^k\right] y^{k+1}\theta(0) + o(y^{k+1})$$

we obtain

$$\langle \tilde{f}(\cdot, y), \theta(\cdot)\rangle = Cy^{q+1}\langle \delta(x), \theta(x)\rangle + o(y^{k+1})$$

where

$$C = \left\{\sum_{k=0}^{q} C_k^{q-k}(b_{21})^{q-k}(b_{22})^k \frac{1}{k+1}\left[\left(\frac{b_{22}}{b_{21}}\right)^k - \left(\frac{b_{12}}{b_{11}}\right)^k\right]\right\}$$

so that we finally have

$$\tilde{f}(x, y) = C\delta(x)Y(y)y^{q+1} + \cdots.$$

Remark 3.2
We may sum up Examples 3.1 and 3.2 by saying that if we have a singularity of the form $Y(\xi)\varphi(\eta)$ (see Figure 1) with φ in chain (15) then, considering it as a function of y with values in $\mathscr{D}'(\mathbb{R}_x)$ it has at $y=0$ a singularity of the form $c\delta(x)\varphi^{(-1)}(y)$.

Remark 3.3
There are very many variants of the above examples. For instance, f may be multiplied by a smooth function not vanishing at the origin. Otherwise, the singularity may be beard by a smooth curve instead of by the half-axis $\xi>0$. In any case, the above results hold true at the leading order with obvious modifications.

4. FIRST CONSIDERATIONS ON SINGULARITIES ALONG A CURVE FOR THE SHELL SYSTEM

In this section, we shall consider the shell system (1) and (2) with right-hand sides f^i having a singularity of form (18) along a curve $\mathscr{C}$. We search for the corresponding expansions of the unknowns $T^{\alpha\beta}$ and u_i. The two cases of $\mathscr{C}$ non-characteristic and characteristic will be considered in Sections 4.1 and 4.2, respectively.

4.1. Case of a non-characteristic curve

We recall that system (1) and (2) is written in the special parameterization where the asymptotic curves are $y^1 = Const$, $y^2 = Const$. Let $\mathscr{C}$ be a curve which is nowhere (in the region under consideration) parallel to the axes. We define locally (in a neighborhood of $\mathscr{C}$) curvilinear co-ordinates ξ and η which are tangent and transversal (not necessarily normal) to $\mathscr{C}$, respectively. We shall take the loading

$$\begin{cases} f^\alpha = F^\alpha(\xi)\varphi'(\eta) + \cdots \\ f^3 = F^3(\xi)\varphi(\eta) + \cdots \end{cases} \tag{30}$$

for any given singularity level φ. We shall see later that these three data lead to the same order of singularity for all the unknowns. Obviously,

$$D_\alpha = (\partial_\alpha \xi)\frac{\partial}{\partial \xi} + (\partial_\alpha \eta)\frac{\partial}{\partial \eta} + \cdots = (\partial_\alpha \eta)\frac{\partial}{\partial \eta} + \cdots \tag{31}$$

as we are considering singularities with respect to η. The consistent expansions for the unknowns $T^{\alpha\beta}$ is

$$T^{\alpha\beta} = \mathscr{T}^{\alpha\beta}(\xi)\varphi(\eta) + \cdots \tag{32}$$

By substituting (30) and (32) into (1) we obtain at the leading order of singularity (which is φ' for the two first equations and φ for the third one)

$$\begin{cases} -\partial_1\eta\mathscr{T}^{11}(\xi) - \partial_2\eta\mathscr{T}^{12}(\xi) = F^1(\xi) \\ -\partial_1\eta\mathscr{T}^{12}(\xi) - \partial_2\eta\mathscr{T}^{22}(\xi) = F^2(\xi) \\ -2b_{12}\mathscr{T}^{12}(\xi) = F^3(\xi) \end{cases} \tag{33}$$

Taking as unknowns the $\mathscr{T}^{\alpha\beta}$, the determinant $-2b_{12}\partial_1\eta\partial_2\eta$ of the system is different from zero as $\mathscr{C}$ is not parallel to the axes. Consequently the $\mathscr{T}^{\alpha\beta}$ are well determined. Obviously, the process may be pursued at any order.

We now consider system (2) where the right-hand sides according to (32) are singular at level of singularity $\varphi(\eta)$. The consistent expansions for the unknowns u_i are:

$$\begin{cases} u_\alpha = U_\alpha(\xi)\varphi^{(-1)}(\eta) + \cdots \\ u_3 = U_3(\xi)\varphi(\eta) + \cdots \end{cases} \tag{34}$$

By substituting (34) and (32) into (2) we obtain at the leading order of singularity (which is φ for all the three equations)

$$\begin{cases} \partial_1\eta U_1(\xi) = B_{11\lambda\mu}\mathscr{T}^{\lambda\mu} \\ \partial_2\eta U_2(\xi) = B_{22\lambda\mu}\mathscr{T}^{\lambda\mu} \\ \frac{1}{2}(\partial_1\eta U_2(\xi) + \partial_2\eta U_1(\xi)) - b_{12}U_3 = B_{12\lambda\mu}\mathscr{T}^{\lambda\mu} \end{cases}$$

where the right-hand sides are known at the present state. The determinant of the system is again $-2b_{12}\partial_1\eta\partial_2\eta \neq 0$ so that the U_i are well determined. As before, the process may be pursued at any order.

Obviously the equations involved in the above process are algebraic and the unknowns depend locally on the data in particular, if at a point ξ the three functions F^i vanish, then the $\mathscr{T}^{\lambda\mu}$ and U_i vanish there too.

4.2. Case of a characteristic curve

We now assume that the curve $\mathscr{C}$ is the characteristic $y^2 = 0$ so that obviously $\xi = y^1$, $\eta = y^2$. The third equation of system (1) immediately gives $T^{12} = -f^3/(2b_{12})$ that we replace into

the two first ones. Then system (1) is equivalent to

$$\begin{cases} -\partial_1 T^{11} - (2\Gamma^1_{11} + \Gamma^2_{12})T^{11} - \Gamma^1_{22}T^{22} \\ = \partial_2 T^{12} + (2\Gamma^1_{12} + \Gamma^2_{12} + \Gamma^2_{22})T^{12} + f^1 \underset{\text{def}}{=} \tilde{f}^1 \\ -\partial_2 T^{22} - (2\Gamma^2_{22} + \Gamma^1_{12})T^{22} - \Gamma^2_{11}T^{11} \\ = \partial_1 T^{12} + (2\Gamma^2_{12} + \Gamma^1_{11} + \Gamma^1_{12})T^{12} + f^2 \underset{\text{def}}{=} \tilde{f}^2 \end{cases} \tag{35}$$

where the effective right-hand sides are $\tilde{f}^\alpha$ defined in (35). Let us search for the unknowns T^{11} and T^{22} expansions of form (18). It is easily seen that consistent expansions will take the form

$$\begin{cases} T^{11} \simeq \psi(y^2)\mathscr{T}^{11}_{(0)}(y^1) + \psi^{(-1)}(y^2)\mathscr{T}^{11}_{(-1)}(y^1) + \cdots \\ T^{22} \simeq \psi^{(-1)}(y^2)\mathscr{T}^{22}_{(-1)}(y^1) + \psi^{(-2)}(y^2)\mathscr{T}^{22}_{(-2)}(y^1) + \cdots \end{cases} \tag{36}$$

Let us first consider the homogeneous system associated with (35). Substituting (36) into this last system we obtain at the leading order (which is equal to $\psi(y^2)$ for both equations, arbitrary for the time being)

$$\begin{cases} -\dfrac{\mathrm{d}\mathscr{T}^{11}_{(0)}}{\mathrm{d}y^1} - (2\Gamma^1_{11} + \Gamma^2_{12})\mathscr{T}^{11}_{(0)} = 0 \\ -\mathscr{T}^{22}_{(-1)} - \Gamma^2_{11}\mathscr{T}^{11}_{(0)} = 0 \end{cases} \tag{37}$$

which is a differential system of total order one for the unknowns $\mathscr{T}^{11}_{(0)}$, $\mathscr{T}^{22}_{(-1)}$ which may be integrated with an arbitrary constant. The successive terms of the expansions may be obtained analogously, they satisfy the same system but with known non-vanishing right-hand side.

Let us now give the $\tilde{f}^\alpha$ of the form

$$\tilde{f}^\alpha = \tilde{F}^\alpha(y^1)\varphi'(y^2) + \cdots$$

The expansion is again (36) but ψ is at least of the same order of singularity of the right-hand side of (35). The minimal singularity is obtained by choosing $\psi = \varphi'$, then $\mathscr{T}^{11}$ and $\mathscr{T}^{22}$ are solutions of system (37) with right-hand sides $\tilde{F}^\alpha(y^1)$. Here, minimal is understood in the sense that singularities of higher order (and then satisfying the homogeneous equation relative to the leading order) may occur when they are provoked by causes localized elsewhere and propagating in the considered region. Of course, the problems are linear and solutions may be added. We consider here solutions provoked by the right-hand sides in the part of characteristic under consideration. Moreover, it should be noted that expansion (36) is *generic*, but in certain cases, for instance if Γ^2_{11} vanishes, T^{22} may be less singular (see the second equation (37)).

Let us go on with system (2) for the unknowns u_i. On account of (36) it takes the form

$$\begin{cases} \partial_1 u_1 - \Gamma^1_{11}u_1 - \Gamma^2_{11}u_2 \simeq C_{1111}\varphi'(y^2)\mathscr{T}^{11}_{(0)}(y^1) + \cdots \\ \partial_2 u_2 - \Gamma^1_{22}u_1 - \Gamma^2_{22}u_2 \simeq C_{2211}\varphi'(y^2)\mathscr{T}^{11}_{(0)}(y^1) + \cdots \\ \frac{1}{2}(\partial_1 u_2 + \partial_2 u_1) - \Gamma^1_{12}u_1 - \Gamma^2_{12}u_2 - b_{12}u_3 \\ \simeq C_{1211}\varphi'(y^2)\mathscr{T}^{11}_{(0)}(y^1) + \cdots \end{cases} \tag{38}$$

We first focus on the two first equations for u_1 et u_2, then u_3 will be determined by the third equation. As above, we consider the homogeneous system. The consistent expansions for u_α are

$$\begin{cases} u_1 \simeq U_1^{(0)}(y^1)\zeta(y^2) + \cdots \\ u_2 \simeq U_2^{(-1)}(y^1)\zeta^{(-1)}(y^2) + \cdots \end{cases} \tag{39}$$

Let us first consider the homogeneous system associated with (38). Substituting (39) into this last system we obtain at the leading order (which is equal to $\zeta(y^2)$ for both equations, arbitrary for the time being)

$$\begin{cases} \dfrac{\mathrm{d}U_1^{(0)}}{\mathrm{d}y^1} - \Gamma_{11}^1 U_1^{(0)} = 0 \\ U_2^{(-1)} - \Gamma_{22}^1 U_1^{(0)} = 0 \end{cases} \tag{40}$$

which is a differential system of total order one for the unknowns $U_1^{(0)}$, $U_2^{(-1)}$ which may be integrated with an arbitrary constant. The successive terms of the expansions may be obtained analogously, they satisfy the same system but with known non-vanishing right-hand side.

Now we consider system (38) where the right-hand side is in φ'. The minimal singularity is obtained by choosing $\zeta = \varphi'$, then $U_1^{(0)}$ and $U_2^{(-1)}$ are solutions of system (40) with right-hand sides $C_{1111}\mathscr{T}_{(0)}^{11}(y^1)$ and $C_{2211}\mathscr{T}_{(0)}^{11}(y^1)$, respectively.

The component u_3 is then given by

$$\frac{1}{2}\varphi'' U_1^{(0)} - b_{12}u_3 = 0 + \cdots \Rightarrow u_3 \simeq U_3^{(-2)}(y^1)\varphi''(y^2), U_3^{(-2)}(y^1) = \frac{1}{2b_{12}} U_1^{(0)} \tag{41}$$

Summing up we have for any arbitrary level of singularity φ:

$$\begin{cases} f^1 \simeq F_{(1)}^1 \varphi'(y^2) + \cdots \\ f^2 \simeq F_{(1)}^2 \varphi'(y^2) + \cdots \\ f^3 \simeq F_{(0)}^3 \varphi(y^2) + \cdots \end{cases} \Rightarrow \begin{cases} T^{11} \simeq \mathscr{T}_{(1)}^{11}(y^1)\varphi'(y^2) + \cdots \\ T^{12} \simeq \mathscr{T}_{(0)}^{12}(y^1)\varphi(y^2) + \cdots \\ T^{22} \simeq \mathscr{T}_{(0)}^{22}(y^1)\varphi(y^2) + \cdots \\ u_1 \simeq U_1^{(1)}(y^1)\varphi'(y^2) + \cdots \\ u_2 \simeq U_2^{(0)}(y^1)\varphi(y^2) + \cdots \\ u_3 \simeq U_3^{(2)}(y^1)\varphi''(y^2) + \cdots \end{cases} \tag{42}$$

We note that the process $\Rightarrow$ in (42) implies integration of a system of total order 2 implying two arbitrary constants which may be generically determined by two boundary conditions.

Remark 4.1

It is easily seen that the two arbitrary constants may be determined by imposing conditions to $\mathscr{T}_{(1)}^{11}$ and $U_1^{(1)}$ (which are the components bearing the leading order singularities of the $T^{\alpha\beta}$ and u_i, respectively) at certain points of the characteristic. For instance, we may prescribe the values of $\mathscr{T}_{(1)}^{11}$ at a point P and of $U_1^{(1)}$ at another point Q. Another useful choice are the values of $U_1^{(1)}$ at two different points P and Q. Oppositely it is obvious that we cannot

prescribe the values of $\mathscr{T}^{11}_{(1)}$ at two different points P and Q. We shall come again on this determination in the sequel, and we shall see that the case of impossibility appears when both extremities of the considered characteristics are free, but that case was excluded from our study because it likely correspond to a non geometrically rigid surface.

Remark 4.2
It is worthwhile to consider the structure of the singularity on a segment where the data $F^{\alpha}_{(1)}(y^1)$ and $F^{3}_{(0)}(y^1)$ vanish. We then have the solutions of the homogeneous system depending on two arbitrary constants which may be determined as in the previous remark. We may consider the case when $\mathscr{T}^{11}_{(1)}$ vanishes at a point P of the segment: then $\mathscr{T}^{11}_{(1)}$ vanishes all along the segment but $U^{(1)}_1$ does not vanish necessarily on it. Then there is a family of such solutions with one arbitrary parameter. They are merely singularities (at the considered orders) of the displacements, not of the stresses.

5. CLASSIFICATION OF THE DIFFERENT CASES OF REFLECTION PROBLEMS

Classical reflection theory which was recalled at the end of Section 1 is concerned with singularities 'arriving' to a boundary produced by singularities of the data elsewhere. The term 'arriving' is usually associated with 'causality' of the Cauchy problem for hyperbolic systems involving time. In the present context which involves systems (1) and (2) with various boundary conditions, the concept 'arriving' is not clear. We shall often need to define precise problems in order to exhibit the causality of the phenomena so that our study will not be exhaustive. Nevertheless, rather general laws will be given in Section 8.

As we said we only consider reflection phenomena on boundaries Γ which are not parallel to the characteristics. They may be either fixed (denoted by Γ_0) or free (denoted by Γ_1). The main problems are concerned with the case when $\vec{\mathbf{f}}$ is smooth in a neighborhood of the boundary:

(a) free boundary Γ_1 with $\vec{\mathbf{f}}$ smooth in a vicinity of a point $A \in \Gamma_1$,
(b) fixed boundary Γ_0 with $\vec{\mathbf{f}}$ smooth in a vicinity of a point $A \in \Gamma_0$.
Moreover, there are cases when $\vec{\mathbf{f}}$ is singular in any neighbourhood of the point A of the boundary. In the context of the singularities of Section 2 we may consider singularities of the data along a characteristic or along a non-characteristic curve:
(c) free boundary Γ_1 with $\vec{\mathbf{f}}$ singular along a characteristic at any neighbourhood of $A \in \Gamma_1$,
(d) fixed boundary Γ_0 with $\vec{\mathbf{f}}$ singular along a characteristic at any neighbourhood of $A \in \Gamma_0$,
(e) free boundary Γ_1 with $\vec{\mathbf{f}}$ singular along a non-characteristic curve at any neighbourhood of $A \in \Gamma_1$,
(f) fixed boundary Γ_0 with $\vec{\mathbf{f}}$ singular along a non-characteristic curve at any neighbourhood of $A \in \Gamma_0$.

It is easily seen that there is no reflection phenomena in case (a). Indeed, as the boundary Γ_1 is free and $\vec{\mathbf{f}}$ is assumed to be smooth in the considered region, T^{12} given by the third equation (1) is smooth then (1) and (12) constitute a Cauchy problem with a smooth data for T^{11} and T^{22} so that all the components $T^{\alpha\beta}$ are smooth in the considered neighbourhood of A.

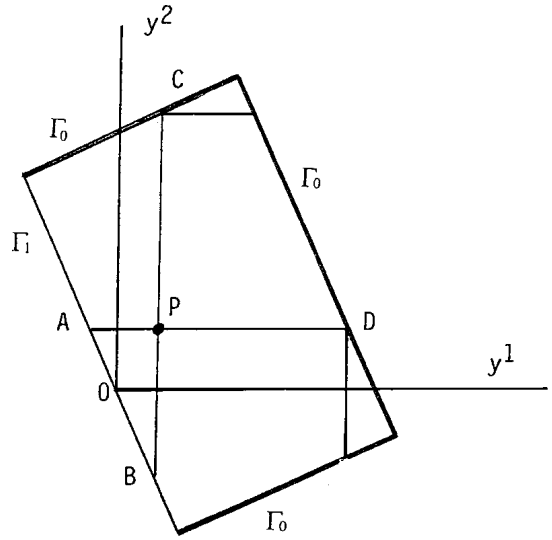

Figure 2. Loading at P. There are reflections at C and D, not A and B.

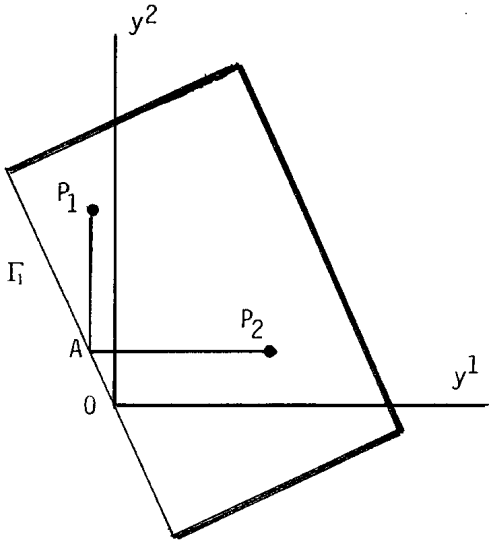

Figure 3. Two singularities issued from P_1 and P_2 arrive to A.

Then in system (2) the right-hand sides are smooth. As there are no boundary condition for $\vec{\mathbf{u}}$ on Γ_1 the components u_i may carry singularities provoked out of the considered neighbourhood of A. There are no constraints to it implying reflection.

As an example, let us imagine the situation pictured in Figure 2 where a point loading is applied at a point P.

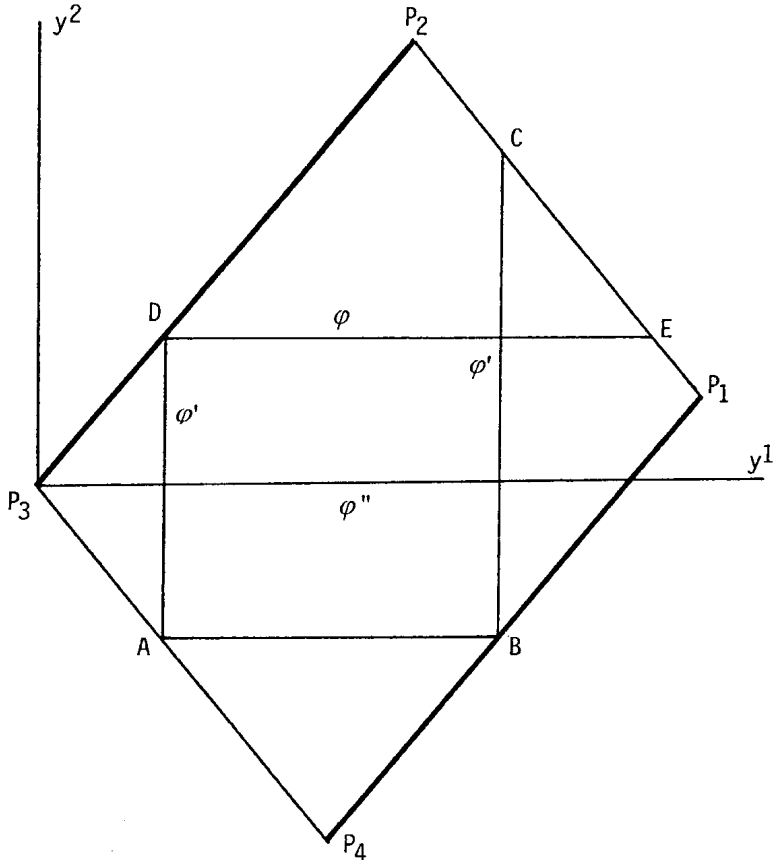

Figure 4. Domain for the example of Section. The symbols $\varphi'', \varphi', \varphi$ denote the levels of singularity of u_3 for data (43).

The singularities issued from P and arriving at A and B on the free boundary Γ_1 does not imply reflection phenomena. Oppositely, those arriving at C and D where the boundary is fixed provoke a phenomenon of 'pseudo-reflection' which will be considered later.

Obviously, it is not impossible that for certain data two singularities of the same level coming from different origins arrive to the same point A of the boundary, but they are independent (see Figure 3).

In order to study the above mentioned cases of reflection phenomena, we must specify a precise boundary value problem as we said at the beginning of the present section.

We shall consider the situation of Figure 4. The domain Ω of the plane of the special parameters y^1, y^2 is the rectangle $P_1P_2P_3P_4$ with non-characteristic sides. The two opposite sides P_2P_3 and P_1P_4 are fixed whereas the others two are free.

In the next section the singular loading will be given along the characteristic AB. The support of this loading is assumed to start from the point A. The case when the support does not arrive at A was considered above (case a) and we saw that it does not imply propagation phenomena.

Consequently, the considered example will furnish the following situations:

case(b) at point B when the support of the singular loading is off B;
case(c) at point A;
case(d) at point B when the support of the singular loading arrives up to B.

6. AN EXAMPLE CONCERNING CASES (b)–(d)

As we just announced, let us consider in the (y^1, y^2)-*plane* the domain Ω of Figure 4. The loading $\vec{\mathbf{f}}$ is given by

$$\begin{cases} f^1 \simeq F^1_{(1)}(y^1)\varphi'(y^2 - y^2_A) + \cdots \\ f^2 \simeq F^2_{(1)}(y^1)\varphi'(y^2 - y^2_A) + \cdots \\ f^3 \simeq F^3_{(0)}(y^1)\varphi(y^2 - y^2_A) + \cdots \end{cases} \tag{43}$$

for any fixed level of singularity φ, i.e. of form (30) along AB. The given functions $F^\alpha_{(1)}(y^1)$ and $F^3_{(0)}(y^1)$ are smooth with $F^3_{(0)}(y^1_A) \neq 0$.

According to the study of Section 4.2 the minimal singularities along the characteristic AB will take the form

$$\begin{cases} T^{11} \simeq \mathscr{T}^{11}_{(1)}(y^1)\varphi'(y^2 - y^2_A) + \cdots, & u_1 \simeq U^{(1)}_1(y^1)\varphi'(y^2 - y^2_A) + \cdots \\ T^{12} \simeq \mathscr{T}^{12}_{(0)}(y^1)\varphi(y^2 - y^2_A) + \cdots, & u_2 \simeq U^{(0)}_2(y^1)\varphi(y^2 - y^2_A) + \cdots \\ T^{22} \simeq \mathscr{T}^{22}_{(0)}(y^1)\varphi(y^2 - y^2_A) + \cdots, & u_3 \simeq U^{(2)}_3(y^1)\varphi''(y^2 - y^2_A) + \cdots \end{cases} \tag{44}$$

where, as we know, the $\mathscr{T}$ and U are defined up to two constants of integration. As we shall see in details later, such a singularity cannot exist without the presence of others singularities in the vicinity of A and B. Indeed, there are four boundary conditions to be satisfied: the two conditions (12) on the free boundary P_3P_4 and the two conditions (11) on the fixed boundary P_4P_1. This implies four conditions (involving $\mathscr{T}^{11}_{(1)}$ and $\mathscr{T}^{22}_{(0)}$ at A, $U^{(1)}_1$ and $U^{(0)}_2$ at B) whereas we only have two parameters at our disposal. We only may satisfy the conditions on $\mathscr{T}^{11}_{(1)}$ at A and $U^{(1)}_1$ at B which are the terms of highest order of singularity (see (44)). As a consequence, the two other conditions imply existence of appropriate singularities of lower order along AD and BC which amounts to a reflection phenomenon.

6.1. Study of the components $T^{\alpha\beta}$ along AB

According to (35) and (36), the equations for T^{11} and T^{22} (with T^{12} given by the third equation (1) take the form

$$\begin{cases} -\partial_1 T^{11} - (2\Gamma^1_{11} + \Gamma^2_{12})T^{11} - \Gamma^1_{22}T^{22} \\ \qquad = \left[-\dfrac{F^3_{(0)}(y^1)}{2b_{12}} + F^1_{(1)}(y^1) \right] \varphi'(y^2 - y^2_A) + \cdots \\ -\partial_2 T^{22} - (2\Gamma^2_{22} + \Gamma^1_{12})T^{22} - \Gamma^2_{11}T^{11} = F^2_{(1)}(y^1)\varphi'(y^2 - y^2_A) + \cdots \end{cases} \tag{45}$$

and according to expansions (42), we have at the leading order

$$\begin{cases} -\dfrac{\mathrm{d}\mathscr{T}^{11}_{(1)}}{\mathrm{d}y^1} - (2\Gamma^1_{11} + \Gamma^2_{12})\mathscr{T}^{11}_{(1)} = -\dfrac{F^3_{(0)}(y^1)}{2b_{12}} + F^1_{(1)}(y^1) \\ -\mathscr{T}^{22}_{(0)} - \Gamma^2_{11}\mathscr{T}^{11}_{(1)} = F^2_{(1)}(y^1) \end{cases} \tag{46}$$

According to (12), the boundary conditions on P_3P_4 (and in particular at A) are

$$\begin{cases} T^{11} = -\dfrac{v_2}{v_1}\, T^{12} \\ T^{22} = -\dfrac{v_1}{v_2}\, T^{12} \end{cases} \text{ on } n_1(y^1 - y^1_A) + n_2(y^2 - y^2_A) = 0 \tag{47}$$

where $\vec{\mathbf{n}} = (n_1, n_2)$ is the unit normal to P_3P_4 in the (y^1, y^2)-*plane*, or equivalently

$$\begin{cases} T^{11} = \dfrac{v_2}{v_1}\, \varphi(y^2 - y^2_A) \dfrac{F^3_{(0)}(y^1_A)}{2b_{12}(y^1_A, y^2_A)} + \cdots \\ T^{22} = \dfrac{v_1}{v_2}\, \varphi\left[-\dfrac{n_1}{n_2}\,(y^1 - y^1_A)\right] \dfrac{F^3_{(0)}(y^1_A)}{2b_{12}(y^1_A, y^2_A)} + \cdots \end{cases} \tag{48}$$

Relations (48) are the explicit expressions of the singularities of the Cauchy data on P_3P_4 (see (12)) which are completely known. It should be noted that any function on P_3P_4 may be expressed in terms of y^1, y^2 or any variable describing this curve. For ulterior convenience, we used y^1 and y^2 in the first and second equations (48), respectively.

From (44) we see that T^{11} is singular in φ', namely $T^{11} \simeq \mathscr{T}^{11}_{(1)}(y^1)\varphi'(y^2 - y^2_A)$, the boundary conditions (48) give

$$\begin{aligned} T^{11} &\simeq \mathscr{T}^{11}_{(1)}(y^1_A)\varphi'(y^2 - y^2_A) + \cdots = \frac{v_2}{v_1}\, \varphi(y^2 - y^2_A) \frac{F^3_{(0)}(y^1_A)}{2b_{12}(y^1_A, y^2_A)} + \cdots \\ T^{22} &\simeq \mathscr{T}^{22}_{(0)}(y^1_A)\varphi(y^2 - y^2_A) + \cdots = \frac{v_1}{v_2}\, \varphi\left[-\frac{n_1}{n_2}\,(y^1 - y^1_A)\right] \frac{F^3_{(0)}(y^1_A)}{2b_{12}(y^1_A, y^2_A)} + \cdots \end{aligned} \tag{49}$$

the leading order for T^{11} must vanish at A, i.e.

$$\mathscr{T}^{11}_{(1)}(y^1_A) = 0 \tag{50}$$

which is the boundary condition for the differential system of total order one (46). Consequently the two functions $\mathscr{T}^{11}_{(1)}(y^1)$ and $\mathscr{T}^{22}_{(0)}(y^1)$ are completely defined. We observe, from $(46)_2$ that $\mathscr{T}^{22}_{(0)}(y^1_A) = 0$. From the hypothesis $F^3_{(0)}(y^1_A) \neq 0$ we see that *the boundary condition* $(49)_2$ *is certainly not satisfied at the leading order*.

6.2. Singularities of $T^{\alpha\beta}$ along AD

According to the previous section there exist singularities along AD. The second equation (49), where the right-hand side is known, show that the singularity for T^{22} may be in

$\varphi(-n_1/n_2(y^1 - y_A^1))$; then the structure of the system implies that the singularity of T^{11} must be in $\varphi^{(-1)}(-n_1/n_2(y^1 - y_A^1))$. In other words, let us define

$$\psi(y^1 - y_A^1) = \varphi^{(-1)}\left(-\frac{n_1}{n_2}(y^1 - y_A^1)\right) \tag{51}$$

then along AD we shall have singularities analogous to (44) exchanging the indices 1 and 2 and ψ instead of φ namely

$$\begin{cases} T^{22} \simeq \tilde{\mathscr{T}}_{(1)}^{22}(y^2)\psi'(y^1 - y_A^1) + \cdots, & u_2 \simeq \tilde{U}_2^{(1)}(y^2)\psi'(y^1 - y_A^1) + \cdots \\ T^{12} = 0, & u_1 \simeq \tilde{U}_1^{(0)}(y^2)\psi(y^1 - y_A^1) + \cdots \\ T^{11} \simeq \tilde{\mathscr{T}}_{(0)}^{11}(y^2)\psi(y^1 - y_A^1) + \cdots, & u_3 \simeq \tilde{U}_3^{(2)}(y^2)\psi''(y^1 - y_A^1) + \cdots \end{cases}$$

The corresponding transport equations are analogous to (46) with the obvious exchange of indices and vanishing right-hand side as the data $\vec{\mathbf{f}}$ are smooth on AD:

$$\begin{cases} -\tilde{\mathscr{T}}^{11}(y^2) - \Gamma_{22}^1(y_A^1, y^2)\tilde{\mathscr{T}}^{22}(y^2) = 0 \\ -\dfrac{\mathrm{d}}{\mathrm{d}y^2}\tilde{\mathscr{T}}^{22}(y^2) - (2\Gamma_{22}^2 + \Gamma_{12}^1)_{(y_A^1, y^2)}\tilde{\mathscr{T}}^{22}(y^2) = 0 \end{cases} \tag{52}$$

this a system of total order one. The boundary condition (49) for T^{22}, on account of the two singularities along AB and AD takes the form

$$T^{22} \simeq 0 + \tilde{\mathscr{T}}_{(1)}^{22}(y_A^2)\psi'(y^1 - y_A^1) + \cdots = \frac{v_1}{v_2}\varphi\left[-\frac{n_1}{n_2}(y^1 - y_A^1)\right]\frac{F_{(0)}^3(y_A^1)}{2b_{12}(y_A^1, y_A^2)} + \cdots$$

where

$$\psi'(y^1 - y_A^1) = -\frac{n_1}{n_2}\varphi\left(-\frac{n_1}{n_2}(y^1 - a^1)\right)$$

which gives at the leading order the condition:

$$\tilde{\mathscr{T}}_{(1)}^{22}(y_A^2) = -\frac{n_2}{n_1}\frac{v_1}{v_2}\frac{F_{(0)}^3(y_A^1)}{2b_{12}(y_A^1, y_A^2)} \tag{53}$$

then system (52) defines completely the functions $\tilde{\mathscr{T}}_{(1)}^{22}$ and $\tilde{\mathscr{T}}_{(0)}^{11}$ along AD.

It is obvious that the boundary condition for $\mathscr{T}_{(1)}^{11}$ is not modified by the presence of the new singularity of lower order along AD.

6.3. *Singularities of the displacement along AB et BC*

The $T^{\alpha\beta}$ being known along AB we have for the displacements, according to (2):

$$\begin{cases} \partial_1 u_1 - \Gamma_{11}^1 u_1 - \Gamma_{11}^2 u_2 \simeq \varphi'(y^2 - y_A^2)C_{1111}(y^1, y_A^2)\mathscr{T}_{(1)}^{11}(y^1) + \cdots \\ \partial_2 u_2 - \Gamma_{22}^1 u_1 - \Gamma_{22}^2 u_2 \simeq \varphi'(y^2 - y_A^2)C_{1211}(y^1, y_A^2)\mathscr{T}_{(1)}^{11}(y^1) + \cdots \\ \frac{1}{2}(\partial_1 u_2 + \partial_2 u_1) - \Gamma_{12}^1 u_1 - \Gamma_{12}^2 u_2 - b_{12}u_3 \\ \quad \simeq \varphi'(y^2 - y_A^2)C_{1211}(y^1, a^2)\mathscr{T}_{(1)}^{11}(y^1) + \cdots \end{cases} \tag{54}$$

so that the minimal singularities for the components u_i are those of (44) with the transport equations at the leading order

$$\begin{cases} \dfrac{\mathrm{d}U_1^{(1)}}{\mathrm{d}y^1} - \Gamma_{11}^1(y^1, y_A^2)U_1^{(1)}(y^1) = B_{1111}(y^1, y_A^2)\mathscr{T}_{(1)}^{11}(y^1) \\ U_2^{(0)}(y^1) - \Gamma_{22}^1(y^1, y_A^2)U_1^{(1)}(y^1) = B_{2211}(y^1, y_A^2)\mathscr{T}_{(1)}^{11}(y^1) \\ \frac{1}{2}U_1^{(1)}(y^1) - b_{12}(y^1, y_A^2)U_3^{(2)}(y^1) = 0 \end{cases} \tag{55}$$

which is a system of total order one. The boundary conditions on the fixed boundary P_4P_1:

$$u_1 = u_2 = 0 \quad \text{on } n_1(y^1 - y_B^1) + n_2(y^2 - y_B^2) = 0 \tag{56}$$

are equivalent to

$$\begin{cases} U_1^{(1)}(y_B^1)\varphi'(y^2 - y_B^2) + \cdots = 0 \\ U_2^{(0)}(y_B^1)\varphi\left(-\dfrac{n_1}{n_2}(y^1 - y_B^1)\right) + \cdots = 0 \end{cases} \tag{57}$$

which for ulterior convenience, were written taking, respectively, y^2 and y^1 as parameter of the boundary P_4P_1. As we only have one arbitrary constant at our disposal, we impose the boundary condition to the term of higher order:

$$U_1^{(1)}(y_B^1) = 0 \tag{58}$$

and this determines completely the unknowns at the leading order (see (55)).

Generically (up to exceptional cases), we shall have

$$U_2^{(0)}(y_B^1) \neq 0. \tag{59}$$

so that the second equation (57) will not be satisfied at the leading order. In that case, singularity (44) cannot be the only one in the vicinity of B. There also exists a singularity of $\vec{\mathbf{u}}$ along BC (see the analogy with Section 6.2).

Along BC we define

$$\psi(y^1 - y_B^1) = \varphi^{(-1)}\left(-\frac{n_1}{n_2}(y^1 - y_B^1)\right)$$

(where $\vec{\mathbf{n}}$ is the unit normal to P_4P_1 in the parameters plane) and we search for the components $T^{\alpha\beta}$ and u_i expansions of the form

$$\begin{cases} T^{22} \simeq \hat{\mathscr{T}}_{(1)}^{22}(y^2)\psi'(y^1 - y_B^1) + \cdots \\ T^{12} = 0 \\ T^{11} \simeq \hat{\mathscr{T}}_{(0)}^{11}(y^2)\psi(y^1 - y_B^1) + \cdots \end{cases}, \begin{cases} u_2 \cong \hat{U}_2^{(1)}(y^2)\psi'(y^1 - y_B^1) + \cdots \\ u_1 \cong \hat{U}_1^{(0)}(y^2)\psi(y^1 - y_B^1) + \cdots \\ u_3 \cong \hat{U}_3^{(2)}(y^2)\psi''(y^1 - y_B^1) + \cdots \end{cases} \tag{60}$$

which is exactly analogous to the singularities along AD which were considered in Section 6.2. The functions involved in (60) are determined up to two arbitrary constants. The boundary condition $(57)_2$ on account of the new singularity (60) becomes

$$0 = u_2 \simeq U_2^{(0)}(y_B^1)\varphi\left(-\frac{n_1}{n_2}(y^1 - y_B^1)\right) + \cdots - \frac{n_1}{n_2}\hat{U}_2^{(1)}(y^2)\varphi\left(-\frac{n_1}{n_2}(y^1 - y_B^1)\right) + \cdots \tag{61}$$

so that at the leading order we have

$$\hat{U}_2^{(1)}(y^2) = -\frac{n_2}{n_1} U_2^{(0)}(y_B^1) \text{ known } \neq 0. \tag{62}$$

The other boundary condition for the unknowns $\hat{\mathscr{T}}$ and $\hat{U}$ comes from the free boundary conditions on P_1P_2 at C. As $\vec{\mathbf{f}} = 0$ in a neighbourhood of C, conditions (12) become $T^{11} = T^{22} = 0$ which gives at the leading order

$$\hat{T}^{22}_{(1)}(y_C^2) = 0 \tag{63}$$

The two conditions (62) and (63) are sufficient for determining all the unknowns involved at the leading order in (60). Moreover from the transport equations

$$\begin{cases} -\hat{\mathscr{T}}^{11}(y^2) - \Gamma^1_{22}(y_B^1, y^2)\hat{\mathscr{T}}^{22}(y^2) = 0 \\ -\dfrac{\mathrm{d}}{\mathrm{d}y^2}\hat{\mathscr{T}}^{22}(y^2) - (2\Gamma^2_{22} + \Gamma^1_{12})_{(y_B^1, y^2)}\hat{\mathscr{T}}^{22}(y^2) = 0 \end{cases}$$

analogous to (52) we get

$$\hat{\mathscr{T}}^{11}_{(0)}(y_C^2) = 0 \tag{64}$$

so that all the boundary conditions for the components $\mathscr{T}$ are satisfied. Consequently in the present case there is not reflection phenomenon at point C along the characteristic $y^2 = y_C^2$. This agrees with the property mentioned in Section 5 that there are no reflection phenomena in case (a).

6.4. *Singularities along AD and DE and conclusions*

In the previous section, from the knowledge of $T^{\alpha\beta}$ along AB (Section 6.1) we obtained the singularities of $\vec{\mathbf{u}}$ along AB and of $\vec{\mathbf{u}}$ and T along BC. Exactly in the same way, from the knowledge of the singularities of T along AD (Section 6.2), the singularities of $\vec{\mathbf{u}}$ along AD and of $\vec{\mathbf{u}}$ and T along DE are determined. As the final points C and E are on a free boundary, there are no more reflection phenomena and the study of the example is achieved.

It should be noted that in the previous study the qualitative results are independent of the fact that the support of F reaches or not to the point B, consequently the point B may be considered either of type (b) or (d) (see Section 5).

As a result, the singularity along AB is minimal for the given forces in the sense of (42). Then, *at each intersection with the boundary the singularity has the same structure but, with order of singularity one unity lower*. This takes place *at each intersection of type* (*b*)–(*d*) *and stops at an intersection* (*a*) i.e. at points C and E.

7. SINGULARITIES IN CASES (e) AND (f)

We consider a curve $\mathscr{C}$ nowhere tangent to the characteristics $y^1 = Const.$, $y^2 = Const.$ and a singularity of the data of the form

$$\begin{cases} f^\alpha = F^\alpha(\xi)\varphi'(\eta) + \cdots \\ f^3 = F^3(\xi)\varphi(\eta) + \cdots \end{cases} \tag{65}$$

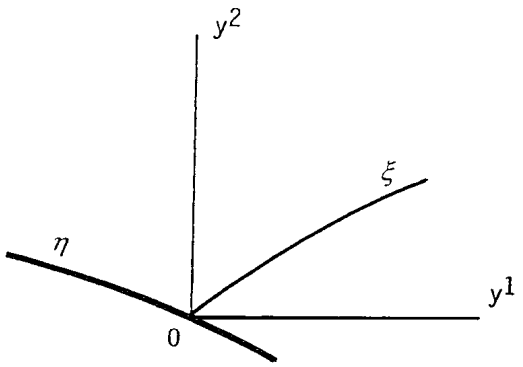

Figure 5. A singular loading is applied along a non-characteristic curve.

where ξ is the curvilinear co-ordinate along $\mathscr{C}$ and η is a transversal co-ordinate (not necessarily normal). The functions F^i are assumed to be smooth. The local singularities of the T and $\vec{\mathbf{u}}$ along $\mathscr{C}$ were considered in Section 4.1. Their structures have form (32) and (34) which are locally determined, i.e. they are non-propagative. The problem which arises now is: what happens when $\mathscr{C}$ intersects the boundary Γ (see Figure 5) i.e. are there singularities propagating along the characteristics issued from the intersection point (i.e. along $y^2 = 0$ and $y^1 = 0$ in Figure 5)? The two cases (e) and (f) of Section 5 correspond to the cases when the boundary Γ is free or fixed, respectively. The following study is done taking the transversal direction η tangent to the boundary Γ (see Figure 5).

7.1. Singularities of the components $T^{\alpha\beta}$ in case (e)

We are in the case of Figure 5 with the loading defined in (65) along $\mathscr{C}$. The boundary Γ is free. Let $T^{\alpha\beta}$ be a solution of system (1) with the boundary condition (10) on Γ. Classically, we may extend $T^{\alpha\beta}$ and f^i with value zero out of the domain Ω obtaining again a solution of the same system in a neighbourhood of O, i.e.

$$\begin{cases} -D_1\tilde{T}^{11} - D_2\tilde{T}^{12} = \tilde{f}^1 \\ -D_1\tilde{T}^{12} - D_2\tilde{T}^{22} = \tilde{f}^2 \\ -2b_{12}\tilde{T}^{12} = \tilde{f}_3 \end{cases} \tag{66}$$

This is easily seen, for instance, using the equivalence with a hyperbolic Cauchy problem with vanishing initial data when taking as parameters ξ (time-like) and η (space-like). In addition, this shows that $T^{\alpha\beta}$ as well as $\tilde{T}^{\alpha\beta}$ is completely determined in a neighbourhood of O. Obviously, $\tilde{f}^i$ writes:

$$\begin{aligned} \tilde{f}^\alpha &= Y(\xi)F^\alpha(\xi)\varphi'(\eta) + \cdots \\ \tilde{f}^3 &= Y(\xi)F^3(\xi)\varphi(\eta) + \cdots \end{aligned} \tag{67}$$

In order to study the singularities along $y_2 = 0$, we consider $T^{\alpha\beta}$ and f^i as distributions of y^2 with values in $\mathscr{D}'(\mathbb{R}_{y^1})$. In this context, according to Remark 3.2, $\tilde{f}^i$ have singularities

along $y_2 = 0$ of the form

$$\begin{aligned} \tilde{f}^{\alpha} &= C^{\alpha} F^{\alpha}(0)\delta(y^1)\varphi(y^2) + \cdots \\ \tilde{f}^{3} &= C^{3} F^{3}(0)\delta(y^1)\varphi^{(-1)}(y^2) + \cdots \end{aligned} \tag{68}$$

where the C^{i} are well determined constants. Obviously (68) holds for y^1 in a neighbourhood of the origin. We are in a situation analogous to that of Section 4.2 with singularities one unity lower and functions F replaced by δ distributions. Consequently, the minimal singularities are

$$\begin{aligned} \tilde{T}^{11} &\simeq \mathscr{T}^{11}_{(0)}(y^1)\varphi(y^2) + \cdots \\ \tilde{T}^{12} &\simeq \mathscr{T}^{12}_{(-1)}(y^1)\varphi^{(-1)}(y^2) + \cdots \\ \tilde{T}^{22} &\simeq \mathscr{T}^{22}_{(-1)}(y^1)\varphi^{(-1)}(y^2) + \cdots \end{aligned} \tag{69}$$

with the transport equations

$$\begin{cases} -\dfrac{\mathrm{d}\tilde{\mathscr{T}}^{11}_{(0)}}{\mathrm{d}y^1} - (2\Gamma^1_{11} + \Gamma^2_{12})\tilde{\mathscr{T}}^{11}_{(0)} = \left[-\dfrac{C^3F^3(0)}{2b_{12}} + C^1F^1(0)\right]\delta(y^1) \\ -\tilde{\mathscr{T}}^{22}_{(-1)} - \Gamma^2_{11}\tilde{\mathscr{T}}^{11}_{(0)} = C^2F^2(0)\delta(y^1) \end{cases} \tag{70}$$

which are easily integrated. The first equation gives with the condition $\tilde{\mathscr{T}}^{11}_{(0)} = 0$ for $y^1 < 0$:

$$\begin{cases} \tilde{\mathscr{T}}^{11}_{(0)} = \left[-\dfrac{C^3F^3(0)}{2b_{12}} + C^1F^1(0)\right] Y(y^1) \exp\left[-\displaystyle\int_0^{y^1} (2\Gamma^1_{11} + \Gamma^2_{12})\,\mathrm{d}t\right] \\ \tilde{\mathscr{T}}^{22}_{(-1)} = -\Gamma^2_{11}\tilde{\mathscr{T}}^{11}_{(0)} - C^2F^2(0)\delta(y^1) \\ \tilde{\mathscr{T}}^{12}_{(-1)} = -\dfrac{C^3F^3(0)\delta(y^1)}{2b_{12}} \end{cases} \tag{71}$$

We note that, when comparing the singularities (69) along $y^2 = 0$ with the ones along the curve $\mathscr{C}$ (see (32)), the most singular component (T^{11}) has the same order of singularity in both cases.

7.2. Singularities of the components u_i in case (e)

The components u_i satisfy system (2) where the right-hand side are known and extended with value zero out of Ω in the vicinity of O. Obviously, the u_i may also be extended as solutions of the corresponding Cauchy problem. Let $\tilde{u}_i$ be the extended functions. They satisfy

$$\begin{cases} \partial_1\tilde{u}_1 - \Gamma^1_{11}\tilde{u}_1 - \Gamma^2_{11}\tilde{u}_2 = C_{1111}\varphi(y^2)\tilde{\mathscr{T}}^{11}_{(0)}(y^1) \\ \partial_2\tilde{u}_2 - \Gamma^1_{22}\tilde{u}_1 - \Gamma^2_{22}\tilde{u}_2 \simeq C_{2211}\varphi(y^2)\tilde{\mathscr{T}}^{11}_{(0)}(y^1) \\ \frac{1}{2}(\partial_1\tilde{u}_2 + \partial_2\tilde{u}_1) - \Gamma^1_{12}\tilde{u}_1 - \Gamma^2_{12}\tilde{u}_2 - b_{12}\tilde{u}_3 \\ \quad \simeq C_{1211}\varphi(y^2)\tilde{\mathscr{T}}^{11}_{(0)}(y^1) \end{cases} \tag{72}$$

We are now in a situation analogous to that of Section 6.3 for the study of the displacement along AB. Indeed, in the present situation (Figure 5) along $y^2 = 0$ with increasing y^1, a point

B on a fixed boundary is necessarily reached. The minimal singularities of the components $\tilde{u}_i$ are the analogue of (44):

$$\begin{cases} \tilde{u}_1 \cong \tilde{U}_1^{(0)}(y^1)\varphi(y^2) + \cdots \\ \tilde{u}_2 \cong \tilde{U}_2^{(-1)}(y^1)\varphi^{(-1)}(y^2) + \cdots \\ \tilde{u}_3 \cong \tilde{U}_3^{(1)}(y^1)\varphi'(y^2) + \cdots \end{cases} \tag{73}$$

and the transport equations are

$$\begin{cases} \dfrac{\mathrm{d}\tilde{U}_1^{(0)}}{\mathrm{d}y^1} - \Gamma_{11}^1(y^1,0)\tilde{U}_1^{(0)}(y^1) = C_{1111}(y^1,0)\tilde{\mathscr{T}}_{(0)}^{11}(y^1) \\ \tilde{U}_2^{(-1)}(y^1) - \Gamma_{22}^1(y^1,0)\tilde{U}_1^{(0)}(y^1) = C_{2211}(y^1,0)\tilde{\mathscr{T}}_{(0)}^{11}(y^1) \\ \frac{1}{2}\,\tilde{U}_1^{(0)}(y^1) - b_{12}(y^1,0)\tilde{U}_3^{(1)}(y^1) = 0 \end{cases} \tag{74}$$

The integration is carried out as in Section 6.3 imposing $\tilde{U}_1^{(0)} = 0$ at the point B of the fixed boundary. Clearly $\tilde{U}_2^{(-1)}$ in general does vanish at point B, a pseudo-reflected singularity of lower order arises along $y^1 = y_B^1$.

Comparing again singularities (73) along $y^2 = 0$ with the ones in (34) along the curve $\mathscr{C}$, we see that the displacement along the characteristic is (with exception of u_2) one order more singular than along $\mathscr{C}$.

Moreover, comparing (69) and (73) with (42), we observe that the singularity along the characteristic $y^2 = 0$ is analogous to (42) but of level one unity lower.

7.3. Singularities in case (f)

We are again in the case of Figure 5 with the loading defined in (65) along $\mathscr{C}$. The boundary Γ is presently fixed. Let $T^{\alpha\beta}$ be a solution of system (1). Obviously, according to Section 4.1, they are singular along the curve $\mathscr{C}$ with singularity (32) and, as the $T^{\alpha\beta}$ are not submitted to any condition on the fixed boundary Γ, they have no more singularity. Of course, it may bear singularities produced by singular data elsewhere but, it is not the sake of our study (see Remark 7.1 hereafter).

The components u_i are obviously singular along $\mathscr{C}$ according to Section 4.1, in particular (34). Let us consider eventual singularities along the characteristic $y^2 = 0$. They are solution of (2) in Ω which according to the previous considerations are of the form

$$\begin{cases} \partial_1 u_1 - \Gamma_{11}^1 u_1 - \Gamma_{11}^2 u_2 \simeq \Phi_{11}(\xi)\varphi(\eta) + \cdots \\ \partial_2 u_2 - \Gamma_{22}^1 u_1 - \Gamma_{22}^2 u_2 \simeq \Phi_{22}(\xi)\varphi(\eta) + \cdots \\ \frac{1}{2}(\partial_1 u_2 + \partial_2 u_1) - \Gamma_{12}^1 u_1 - \Gamma_{12}^2 u_2 - b_{12}u_3 \simeq \Phi_{12}(\xi)\varphi(\eta) + \cdots \end{cases} \tag{75}$$

where the Φ are smooth know functions which, in general, does not vanish at O. The u_i satisfy the boundary conditions

$$u_1 = u_2 = 0 \quad \text{on } \Gamma \tag{76}$$

The first two equations (75) with the boundary conditions (76) constitute a Cauchy problem whereas u_3 is defined by the third equation. Classically, the u_i as well as the right-hand side may be extended with value zero out of Ω in the vicinity of O and the extended functions $\tilde{u}_i$ satisfy the same system i.e.

$$\begin{cases} \partial_1\tilde{u}_1 - \Gamma^1_{11}\tilde{u}_1 - \Gamma^2_{11}\tilde{u}_2 \simeq Y(\xi)\Phi_{11}(\xi)\varphi(\eta) + \cdots \\ \partial_2\tilde{u}_2 - \Gamma^1_{22}\tilde{u}_1 - \Gamma^2_{22}\tilde{u}_2 \simeq Y(\xi)\Phi_{22}(\xi)\varphi(\eta) + \cdots \\ \frac{1}{2}(\partial_1\tilde{u}_2 + \partial_2\tilde{u}_1) - \Gamma^1_{12}\tilde{u}_1 - \Gamma^2_{12}\tilde{u}_2 - b_{12}\tilde{u}_3 \simeq Y(\xi)\Phi_{12}(\xi)\varphi(\eta) + \cdots \end{cases} \tag{77}$$

In order to study singularities along $y^2 = 0$, we consider the unknowns and the right-hand side as functions of y^2 with values in $\mathscr{D}'(\mathbb{R}_{y^1})$. According to Remark 3.2, the right-hand sides are singular along $y^2 = 0$ and (77) becomes

$$\begin{cases} \partial_1\tilde{u}_1 - \Gamma^1_{11}\tilde{u}_1 - \Gamma^2_{11}\tilde{u}_2 \simeq C_1\delta(y^1)\varphi^{(-1)}(y^2) + \cdots \\ \partial_2\tilde{u}_2 - \Gamma^1_{22}\tilde{u}_1 - \Gamma^2_{22}\tilde{u}_2 \simeq C_2\delta(y^1)\varphi^{(-1)}(y^2) + \cdots \\ \frac{1}{2}(\partial_1\tilde{u}_2 + \partial_2\tilde{u}_1) - \Gamma^1_{12}\tilde{u}_1 - \Gamma^2_{12}\tilde{u}_2 - b_{12}\tilde{u}_3 \simeq C_3\delta(y^1)\varphi^{(-1)}(y^2) + \cdots \end{cases} \tag{78}$$

where the constants C_i are determined (see Example 3.2), and the minimal singularities for the u_i (which are effective because we have a Cauchy problem) are

$$\begin{aligned} \tilde{u}_1 &\simeq \tilde{U}_1^{(-1)}(y^1)\varphi^{(-1)}(y^2) + \cdots \\ \tilde{u}_2 &\simeq \tilde{U}_2^{(-2)}(y^1)\varphi^{(-2)}(y^2) + \cdots \\ \tilde{u}_3 &\simeq \tilde{U}_3^{(0)}(y^1)\varphi(y^2) + \cdots \end{aligned} \tag{79}$$

satisfying the transport equations

$$\begin{cases} \dfrac{\mathrm{d}\tilde{U}_1^{(-1)}}{\mathrm{d}y^1} - \Gamma^1_{11}\tilde{U}_1^{(-1)} = C_1\delta(y^1) \\ \tilde{U}_2^{(-2)} - \Gamma^1_{22}\tilde{U}_1^{(-1)} = C_2\delta(y^1) \\ \frac{1}{2}\tilde{U}_1^{(-1)} - b_{12}\tilde{U}_3^{(0)} = 0 \end{cases} \tag{80}$$

the first equation may be integrated, on account of $\tilde{U}_1^{(-1)} = 0$ for $y^1 < 0$ we obtain

$$\begin{cases} \tilde{U}_1^{(-1)}(y^1) = C_1 Y(y^1)\exp\left[-\displaystyle\int_0^{y^1} \Gamma^1_{11}(t)\,\mathrm{d}t\right] \\ \tilde{U}_2^{(-2)}(y^1) = \Gamma^1_{22}\tilde{U}_1^{(-1)} + C_2\delta(y^1) \\ \tilde{U}_3^{(0)}(y^1) = \dfrac{1}{2b_{12}}\,\tilde{U}_1^{(-1)}(y^1) \end{cases} \tag{81}$$

We note that the singularities of u_1 and u_3 are of the same order as in (34), whereas u_2 is one order more regular.

Remark 7.1

Moreover, we observe that (79) for $y^1 > 0$ is a singularity of the standard type (42) with order of singularity two unities lower and in the case (see Remark 4.2) when the corresponding stresses $\mathscr{T}$ vanish (note that the right-hand side of (78) vanishes for $y^1 > 0$). It is a singularity completely defined (i.e. not containing arbitrary constants) and involving only the displacements. This is perfectly consistent with the case when the other extremity of the characteristic $y^2 = 0$ (point B) is at a free boundary. Indeed, in that case the boundary condition only deals with the constraint $\mathscr{T}$ which vanishes at the considered order all along the segment OB so that the boundary condition is automatically satisfied.

Oppositely, in the case when the extremity B is on a fixed boundary, the solution (79) and (81) is impossible as we must prescribe $\tilde{U}_1^{(-1)}(y_B^1) = 0$ whereas it is completely determined. In that case, we must add along the segment of characteristic OB an additional solution of type (42) with order of singularities two units lower (i.e. with u_1 of level $\varphi^{(-1)}$) corresponding to vanishing forces (at the considered levels) and bearing two arbitrary constants. They are determined by imposing that the constraint T^{11} for the additional term vanishes at O and that the u_1 (total) vanishes at B. We note that the 'incompatibility' at B induces a singular constraint along the whole segment of characteristic $y^2 = 0$. The generic orders of the singularities are not changed by this modification.

8. GENERAL LAWS OF REFLECTION

In the previous sections, we considered examples more or less general exhibiting reflection phenomena (rather pseudo-reflection according to the definition given in Section 4). Nevertheless, it is easily seen that we have at our disposal all elements for general situations (in the considered framework of free and fixed or clamped boundaries nowhere parallel to a characteristic).

Let us consider singularities produced by a loading f^i as indicated in (42) where the F^i are assumed to vanish near extremities A and B of an arc of characteristic $y^2 = 0$. The extremities are either one fixed and the other free or both fixed. We prescribe that the components $T^{\alpha\beta}$ and u_α bearing the leading order of singularity (i.e. T^{11} and u_1) satisfy the corresponding boundary conditions at A and B. Then, according to Remark 4.1, the two arbitrary constants are determined so that the leading order is completely defined all along the segment AB. We observe that at a free extremity (A for instance) we imposed $T^{11}(A) = 0$ at the leading order then we have automatically $T^{22}(A) = 0$ at its leading order and no reflection phenomena occurs at A. Oppositely, at a fixed extremity (B for instance) we imposed $u_1(B) = 0$ at its leading order (φ' for instance) but $u_2(B)$ does not vanish, in general, at its leading order φ. In order to satisfy that boundary condition we must consider a new singularity along the other characteristic passing by B (i.e. $y^1 = y_B^1$) of kind (42) but with exchange of the indices 1 and 2 and order of singularity a unit lower. We then have a pseudo-reflection at B. Obviously the process may be continued at the successive intersections with the boundaries: there is a pseudo reflection at fixed boundaries and no reflection at free boundaries.

Let us now consider the more general case where the support of the F^i is allowed to contain A or B. We then proceed as in the previous case, with the only difference that the

conditions at a free boundary are

$$T^{11} = \frac{v_2}{v_1} \frac{f^3}{2b_{12}} \tag{82}$$

$$T^{22} = \frac{v_1}{v_2} \frac{f^3}{2b_{12}} \tag{83}$$

and, always in the context of (42), the leading order of T^{11} is φ' so that, at the leading order, (82) gives $\mathscr{T}^{11}_{(1)}(A) = 0$ as before. We then automatically get a certain value of $\mathscr{T}^{22}_{(0)}(A)$ whereas (83) gives

$$\mathscr{T}^{22}_{(0)}(A) = \frac{v_1}{v_2} \frac{F^3(A)}{2b_{12}}$$

As these two values are generically different, in order to satisfy this boundary condition we must consider a new singularity along the other characteristic passing by A and we have again a pseudo-reflection.

In the case of a singularity of f^i along a non-characteristic curve $\mathscr{C}$ we have a local (i.e. non-propagative) singularity of the solution along $\mathscr{C}$. The reflection problem only appears when $\mathscr{C}$ intersects a boundary Γ. The corresponding reflection phenomena were explicitly considered in Section 7.

All these results may be summarized in the following proposition where for the sake of conciseness we only give explicitly the singularities of the normal component u_3 of the displacement.

Proposition 8.1

(I) Let us give f^3 with order of singularity φ (or equivalently f^α with order φ') along a characteristic. Then, u_3 has a singularity of order φ'' along that characteristic. This singularity has a propagative character. When it arrives at a boundary, it propagates along the other characteristic lossing one order of singularity (i.e. u_3 is singular as φ'); There is an exceptional case when the boundary is free and the support of the singularity of f^3 does not reach the boundary. In that case, there is no reflection at all. The process is continued at successive intersections with boundaries, losing one order of singularity at each intersection (with the same exceptional case). Details may be seen in Sections 5 and 6.

(II) Let us give f^3 with order of singularity φ (or equivalently f^α with order φ') along a non-characteristic curve $\mathscr{C}$. Then, u_3 has a local singularity of order φ on $\mathscr{C}$. In the case when the support of the applied singularity contains the intersection of $\mathscr{C}$ with a free or fixed boundary Γ then u_3 is singular (with order of singularity φ' or φ, respectively) along the characteristics issued from the intersection of $\mathscr{C}$ and Γ. This singularities have a propagative character. At the other intersections of that characteristics with the boundaries pseudo-reflection phenomena occur according to the previous laws described in (I). Details may be seen in Sections 5 and 7.

As we said above, the previous description of propagation and reflection phenomena may be considered as general. Of course, as the problem is linear, the superposition principle holds true and several schemes as the above described ones may appear simultaneously. It will prove useful to point out that in the context of Sections 4.2 and 6, the functions F which

are the coefficients of the singularities may be singular in their turn, generating propagated singularities along the other characteristic. Let us explain this a little more in the context of Section 4.2 for normal applied forces. The loading is of the form

$$f^3 = F^3(y^1)\varphi(y^2) + \cdots \tag{84}$$

corresponding to a singularity along the axis $y^2 = 0$ with intensity level $\varphi(y^2)$ and coefficient $F^3(y^1)$. In the case when $F^3(y^1)$ is singular at a point $y^1 = c^1$, of the form

$$F^3(y^1) \simeq A\psi(y^1 - c^1) + \cdots \tag{85}$$

where A is a numerical coefficient, we have as a result

$$f^3 \simeq A\psi(y^1 - c^1)\varphi(y^2) + \cdots \tag{86}$$

along $y^1 = c^1$ (i.e. starting from the point $y^1 = c^1$, $y^2 = 0$ along the other characteristic $y^1 = c^1$) with order of singularity $\psi(y^1 - c^1)$ and 'coefficient' $\varphi(y^2)$. As an example of this situation, we may apply a point normal force f^3 at the origin, and consider the singularities of the corresponding 'fundamental solution'. In that case, we have

$$f^3 = A\delta(y^1)\delta(y^2)$$

which provokes along $y^2 = 0$ and $y^1 = 0$ singularities corresponding to the level of intensity $\delta(y^2)$ and $\delta(y^1)$ for f^3 which may be described according to the previous considerations (with 'coefficients' $\delta(y^1)$ and $\delta(y^2)$, respectively).

9. NUMERICAL EXPERIMENTS

As indicated in Section 1, the singularity problem addressed in this paper is concerned with the limit problem when the relative thickness ε of the shell tends to zero. For small $\varepsilon > 0$, the problem (for instance in the Kirchhoff–Love framework) is variational of the form

For given $f \in V'$ find $u^\varepsilon \in V$ such that

$$a_m(u^\varepsilon, v) + \varepsilon^2 a_f(u^\varepsilon, v) = (f, v) \quad \forall v \in V \tag{87}$$

where a_m and a_f are the bilinear forms corresponding to the membrane and the bending energies, respectively. The limit problem for $\varepsilon = 0$ is equivalent to the hyperbolic problem (1) and (2). For $\varepsilon > 0$, the bilinear form a_f involves derivatives of higher order than in a_m. Moreover, this problem is elliptic and the solutions enjoy usual elliptic regularity properties. Then the limit process $\varepsilon \searrow 0$ is a singular perturbation. The singularities of the solutions of the limit problem appear as limits of 'boundary' and 'internal' layers, i.e. regions of thickness $\eta(\varepsilon)$ tending to zero as ε tends to zero and where u^ε has important gradients (see, for instance, References [9,10]) for the general theory of these problems. In problems of hyperbolic shells, this thickness is $\eta(\varepsilon) = \mathcal{O}(\varepsilon^{\frac{1}{3}})$ [4].

Numerical computations are concerned with (87) for small ε. General considerations on finite element discretization of (87) may be found in Reference [11]. Nevertheless, for the

above reasons, the main difficulties appear for very small ε involving in particular locking phenomenon (see, for instance, References [12]–[15]). Moreover, as we said above, the gradients of the solutions are very large in the direction transversal to the layers whereas they are not along them. We may take advantage of this fact for using anisotropic meshes elongated in the direction of the layers (see References [16]–[18] in this respect).

In order to interpret the numerical results in terms of singularities across a curve, it should be useful to bear in mind that a δ singularity described by a layer of thickness $\eta(\varepsilon)$ is nearly a function with a small support $\mathcal{O}(\eta)$ and large values $\mathcal{O}(\eta^{-1})$. A δ' singularity is the derivative of the previous one, i.e. nearly a function with small support $\mathcal{O}(\eta)$ and very large oscillations (one positive and one negative parts) with values $\mathcal{O}(\eta^{-2})$. Analogously a δ'' singularity is the derivative of the previous one, it has values of order $\mathcal{O}(\eta^{-3})$ and two positive and one negative (or the opposite) regions. Obviously, the derivatives of higher-order admit analogous descriptions.

We performed numerical experiments with small ε, specifically $\varepsilon = 10^{-4}$. The variational formulation (see Reference [11] for instance) involves the space $H^1 \times H^1 \times H^2$ for the unknown vector (u_1, u_2, u_3). The corresponding discretization is done with reduced Hermite elements. The numerical integration of the rigidity matrix needs six Gauss points. The shell is made of an isotropic and homogeneous material with Young modulus $E = 28\,500\ \mathrm{Nm}^{-2}$ and Poisson ratio $v = 0.3$.

We basically did two numerical experiments. The first one is more or less in the framework of the theory in Section 6 (then associated with propagation and pseudo-reflection on characteristics) whereas the second one is concerned with singularities provoked along a non-characteristic curve $\mathscr{C}$ which reaches two (free and fixed) boundaries (Section 7).

9.1. *First experiment*

The domain Ω for the first experiment is the rectangle with vertices $(-4,0)$, $(0,-4)$, $(6,2)$, $(2,6)$, see Figure 6 and the surface is the hyperbolic paraboloid defined by

$$\vec{\mathbf{r}}(y^1, y^2) = (y^1, y^2, y^1 y^2) \tag{88}$$

The asymptotic curves are the straight lines $y^1 = Const.$, $y^2 = Const.$, so that the parametrization is the special one used in this paper. The shell is clamped by the boundaries $y^1 - y^2 = \pm 4$, and free by the two others. The loading is

$$\vec{\mathbf{f}} = (0, 0, f^3) \quad \text{with } f^3 = \delta(y^2 + 2) \tag{89}$$

this amounts to give a concentrated force along $y^2 = -2$ with unit density. This force is discretized by applying appropriate point forces on the nodes along $y^2 = -2$. According to Section 6, we observe singularities along the characteristics $y^2 = -2$, $y^1 = \pm 2$. In order to obtain a precise description of the layers, a mesh was first defined on the triangle $(-2,-2)$, $(0,0)$, $(2,-2)$ refined near $y^2 = -2$ in a neighbourhood of which the triangles are elongated in the y^1 direction. That mesh is then reproduced by symmetries around $y^2 = -2$, $y^1 + y^2 = 0$, $y^1 - y^2 = 0$ and $y^1 + y^2 - 4 = 0$. The whole mesh has 23 232 triangles, 11 837 nodes and 104 211 degrees of freedom.

The first example is (up to small geometric differences) in the context of Section 6, with $\varphi = \delta$. Global numerical results for u_3^ε are presented in Figure 7 where the *δ''-like* singularity along $y^2 = -2$ is apparent as well as the two (much less apparent) pseudo-reflected *δ'-like*

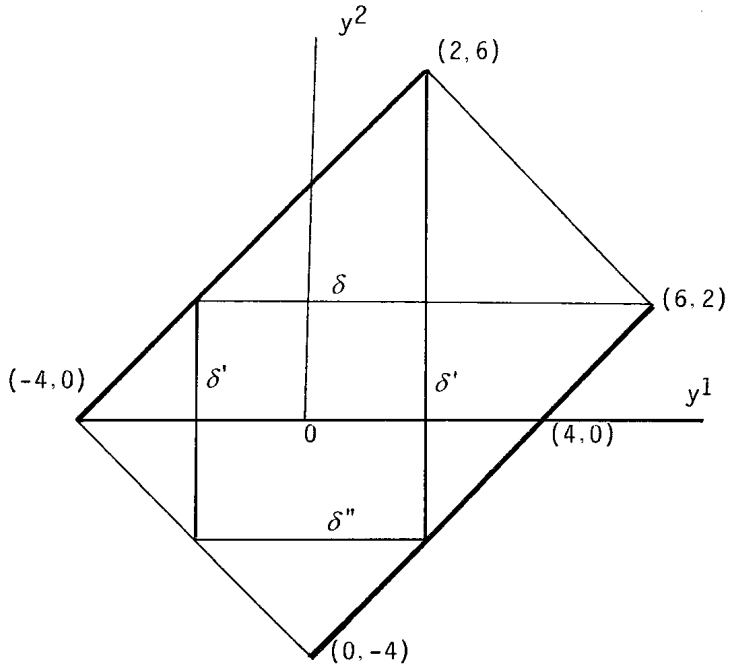

Figure 6. Domain for the first numerical experiment. The symbols $\delta'', \delta', \delta$ denote the levels of singularity of u_3 for data (89).

singularities. Sections by $y^1 = 0$ and $y^2 = 0$ are given in Figures 8 and 9, respectively, where the δ''-*like* and δ'-*like* structures of the singularities along $y^2 = -2$ and $y^1 = \pm 2$, respectively, are more apparent.

Obviously, the numerical values of u_3 at the pseudo-reflected singularities $y^1 = \pm 2$ are much lower that on the directly applied singularity $y^2 = -2$. This explains why the twice pseudo-reflected δ-singularity along $y^2 = 2$ (which appears according to Section 6) is not apparent in the numerical experiment.

9.2. *Second experiment*

The domain Ω for the second experiment is the rectangle with sides $y^1 = \pm 1$, $y^2 = \pm 0.5$ and the surface is given by

$$\vec{\mathbf{r}} = \left(y^1, y^2, \frac{1}{2\sqrt{2}} (y^1 - y^2)(y^1 + y^2) \right) \tag{90}$$

It is also a hyperbolic paraboloid, but the asymptotic curves are now $y^1 \pm y^2 = Const.$ The thickness and the material are the same as before and the shell is clamped by the boundary unless along the side $y^1 = -1$ which is free. The loading is normal, as in (89), and f^3 is a pseudo-delta function along the axis $y^2 = 0$. It means that its value is 50 on the narrow domain $|y^2| < 5.10^{-3}$ and vanishes elsewhere. Clearly, this amounts nearly to a $0.5\delta(y^2)$ normal force.

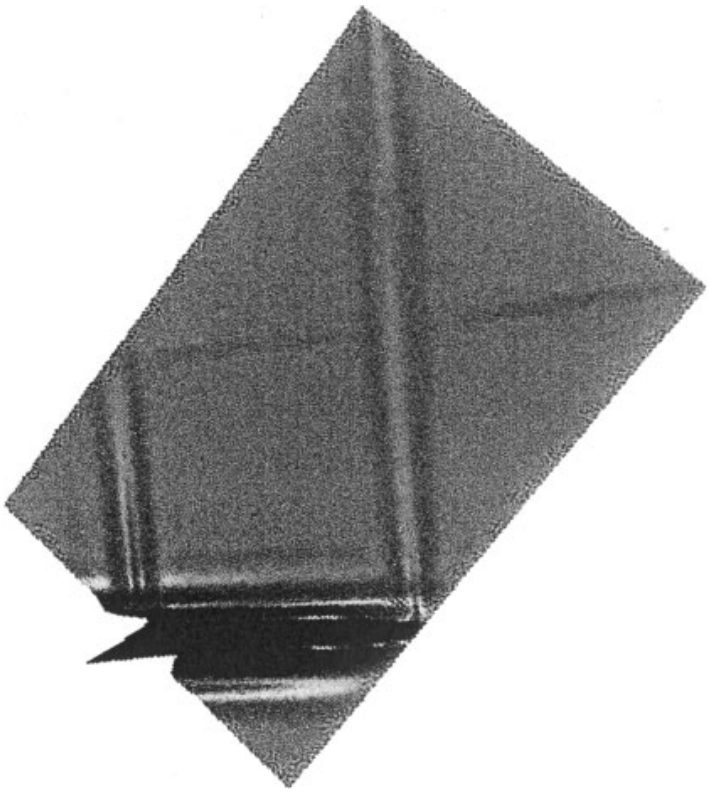

Figure 7. Plot of u_3 in the first experiment.

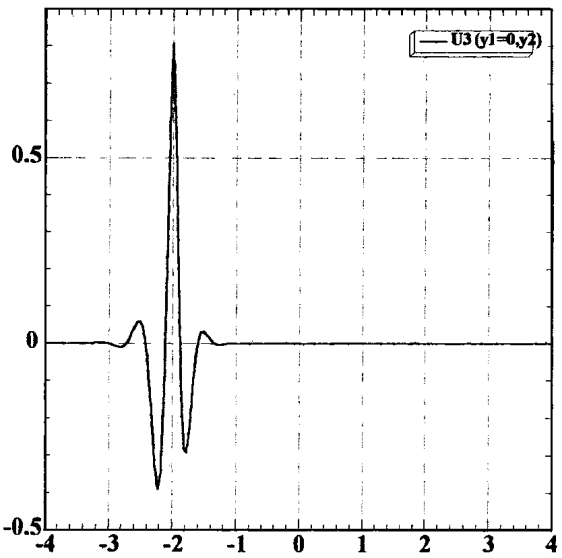

Figure 8. Cross section along $y1 = 0$.

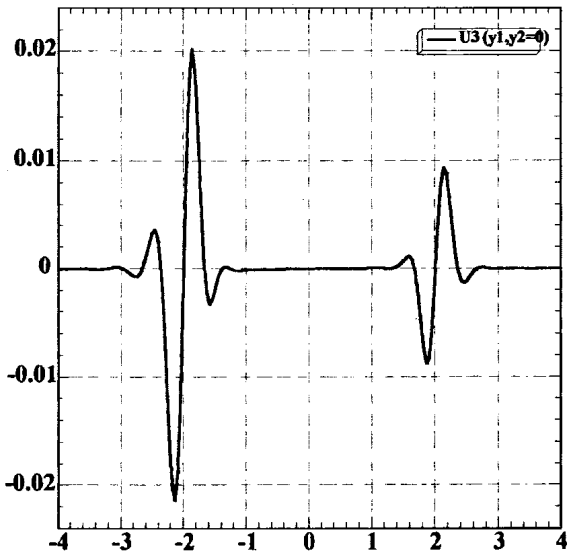

Figure 9. Cross section $y2 = 0$.

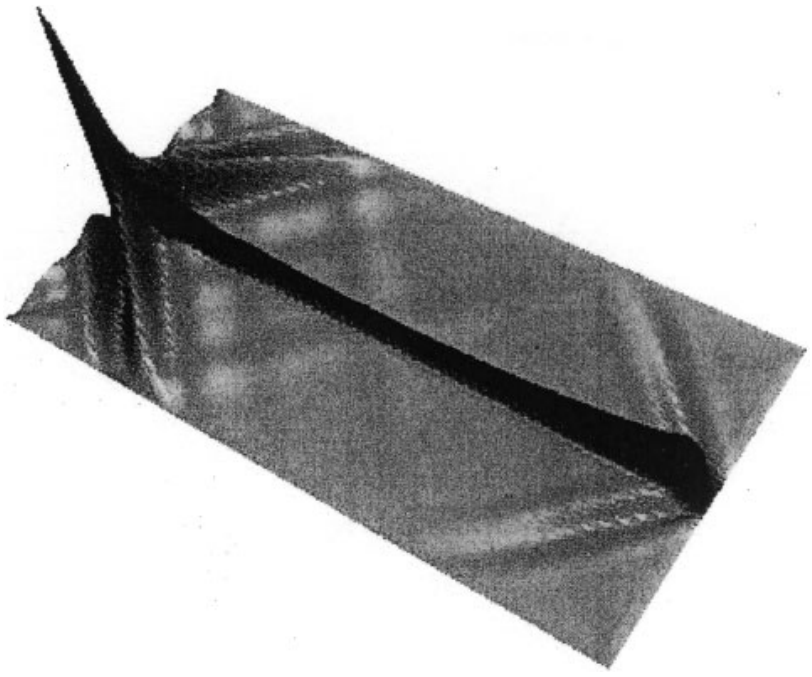

Figure 10. Plot of u_3 in the second experiment.

According to Section 7, the solution exhibits a singularity along the non-characteristic curve $y^2 = 0$ where the singular loading is applied and propagated singularities along the characteristics $y^2 = \pm (y^1 + 1)$ and $y^2 = \pm (y^1 - 1)$ issued from the intersection of the previous non-characteristic curve with the boundaries.

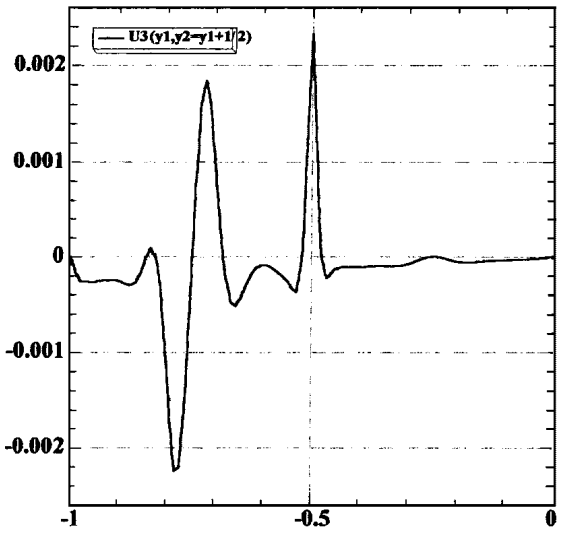

Figure 11. Cross section along $y2 = y1 + 1/2$.

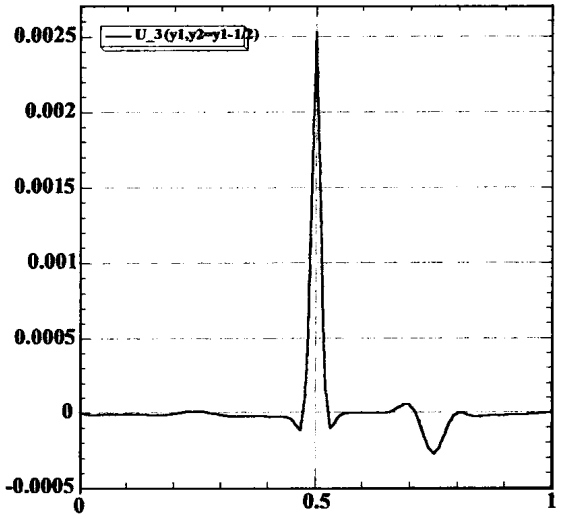

Figure 12. Cross section along $y2 = y1 - 1/2$.

The mesh is constructed with squares, each one divided by the diagonals into four triangles so that the mesh has alignments of nodes along the asymptotic curves. The effective used mesh has 16 384 triangles, 8321 nodes and 73 096 degrees of freedom.

This second example is in the framework of Section 7, with $\varphi = \delta$. The non-characteristic curve $\mathscr{C}$ is the axis $y^2 = 0$; it intersects a free and a fixed boundaries at the points $(-1, 0)$ and $(1,0)$, respectively. The pseudo-reflection phenomena are in the context of Sections 7.1 and 7.2

in the vicinity of $(-1,0)$ and of Section 7.3 in the vicinity of (1,0) (Figures 10–12). Global numerical results for u_3^ε are presented in Figure 10 where the *δ-like* singularity along $y^2=0$ is apparent as well as the two (less apparent) pseudo-reflected *δ′-like* singularities along the characteristics issued from $(-1,0)$ and the *δ-like* ones issued from (1,0). This appears more explicitly in Figures 11 and 12 corresponding to sections along $y^2=y^1+\frac{1}{2}$ and $y^2=y^1-\frac{1}{2}$, respectively, where we note that the abscissa in this figures is $1/\sqrt{2}$ times the arc.

REFERENCES

1. Sanchez-Hubert J, Sanchez Palencia É. *Coques élastiques minces. Propriétés asymptotiques*. Masson: Paris, 1997.
2. Flügge W. *Stresses in Shells* (2nd edn). Springer: Berlin, 1973.
3. Karamian P, Sanchez-Hubert J, Sanchez Palencia É. Non-smoothness in the asymptotics of thin shells and propagation of singularities. Hyperbolic case. *International Journal of Applied Mathematics and Computer Sciences* (special issue on Mathematical Modelling and Numerical Analysis in Solid Mechanics) 2002; **12**(1): 81–90.
4. Karamian-Surville P, Sanchez-Hubert J, Sanchez Palencia É. Propagation of singularities and structure of layers in shells. Hyperbolic case. *Computers and Structures* 2002; **80**:747–768.
5. Courant R, Hilbert D. *Methods of Mathematical Physics*, vol. 2. Inter Science: New York, 1962.
6. Egorov Yu V, Shubin MA. Linear partial differential equations. Foundations of the classical theory. In *Encyclopaedia of Mathematical Sciences*, vol. 30 (Partial Differential Equations 1). Springer: Berlin, 1992; 345–375.
7. Karamian P. Réflexion des singularités dans les coques hyperboliques inhibées. *Comptes Rendus Académie Sciences de Paris*, Série IIb 1998b; **326**:609–614.
8. Guelfand IM, Chilov GE. *Les distributions*. Dunod: Paris, 1969.
9. Lions J. *Perturbations Singulières dans les problèmes aux limites et en contrôle optimal*, Lectures Notes in Mathematics, vol. 323. Springer: Berlin, 1973.
10. Eckhaus W. *Asymptotic Analysis of Singular Perturbations*. North-Holland: Amsterdam, 1979.
11. Bernadou M. *Méthodes d'éléments finis pour les problèmes de coques minces*, Masson, Paris, 1994.
12. Pitkaranta J. The problem of membrane locking in finite element analysis of cylindrical shells. *Numerische Mathematik* 1992; **61**:523–542.
13. Sanchez-Hubert J, Sanchez Palencia É. Pathological phenomena in computation of thin elastic shells. *Transactions of the Canadian Mechanical Engineers* 1998; **22**(4B):435–446.
14. Chapelle D, Bathe KJ. Fundamental considerations for the finite element analysis of shell structures. *Computer and Structures* 1998; **66**(1):19–36.
15. Lee PS, Bathe KJ. On the asymptotic behavior of shell structures and the evaluation in finite element solutions. *Computer and Structures* 2002; **80**:235–255.
16. Apel T, Lube G. Anisotropic mesh refinement in stabilized Galerkin methods. *Numerische Mathematik* 1996; **74**:261–282.
17. Sanchez-Hubert J, Sanchez Palencia É. Singular perturbations with non-smooth limit and finite element approximation of layers for model problems of shells. In *Partial Differential Equations in Multistructures*, Ali Mehmeti F, von Below J, Nicaise S (eds). Dekker: New York, 2001; 207–226.
18. Sanchez-Hubert J, Sanchez Palencia É. Anisotropic finite element estimates and local locking for shells: parabolic case. *Comptes Rendus Académie Sciences de Paris*, Série IIb 2001b; **329**:153–159.

Computational Materials Science 69 (2013) 481–493

Contents lists available at SciVerse ScienceDirect

Computational Materials Science

journal homepage: www.elsevier.com/locate/commatsci

An efficient stochastic and double-scale model to evaluate the effective elastic properties of 2D overlapping random fibre composites

W. Leclerc [a,b], P. Karamian-Surville [a,b,*], A. Vivet [c,d,e,f]

[a] Université de Caen Basse-Normandie, UMR 6139, LMNO, F-14032 Caen, France
[b] CNRS, UMR 6139, LMNO, F-14032 Caen, France
[c] Université de Caen Basse-Normandie, UMR 6252, F-14032, France
[d] ENSICAEN, UMR 6252, CIMAP, F-14050, France
[e] CNRS, UMR 6252, F-14032, France
[f] CEA, UMR 6252, F-14032, France

ARTICLE INFO

Article history:
Received 28 February 2012
Received in revised form 29 August 2012
Accepted 30 October 2012
Available online 20 January 2013

Keywords:
Fibre composites
Stochastic modelling
Homogenisation
Finite element analysis (FEA)

ABSTRACT

This paper focuses on a stochastic and multi-scale finite element (FE) model to estimate the effective properties of 2D overlapping random fibre composites. We describe a new and efficient geometric approximation to solve different problems encountered when building the mesh in which the overlapping phenomenon between two or more fibres arises. The basic idea is to attain an approximation of the fibre geometry relative to quadrangular grid elements and an adaptive mesh refinement (AMR). Thus, the model allows one to obtain a fast, reliable and totally automated generation of a large number of representative volume elements (RVEs) of random fibre composites. Several numerical tests are performed to evaluate both the efficiency of the model and the reliability of the results. It can be noted that, here we only consider the mechanical response of the material in the framework of linear continuum mechanics.

1. Introduction

Intrinsic lightweight and high stiffness as well as, in some cases, a low cost of production have designated fibre composites as excellent candidates for industrial purposes in aerospace or automotive engineering. The use of analytical bounds such as Voigt and Reuss' and Hashin–Shtrikman's ones [1] as well as models such as Mori–Tanaka [2] and self-consistent estimates [3] turns out to be a convenient way to evaluate effective elastic properties of such a kind material. However, an entwined network of fibres has a complex microstructure which is difficult to consider in a micromechanics bound or model. Thus, the contact between two or more fibres leads to several questions which are not solved by the Eshelby tensor [4] for which each fibre is supposed as embedded in an infinite medium. FE analysis provides an interesting alternative framework to consider complex networks of fibres. The evaluation of effective elastic properties requires the setting up of an RVE which can be defined as a volume V large enough to take into account the microstructure of the medium and sufficiently small to limit the calculation cost and respect a minimum scale ratio with the macroscopic material [5]. The notion of RVE has a huge importance in the field of heterogeneous media and requires an accurate determination depending on the material configuration [6].

In the last decade, the stochastic generation of representative patterns has led to numerous investigations. Different techniques have been used which can be classified in three major domains, (1) the methods based on a random sequential adsorption (RSA) process [7–12], (2) the methods based on a Monte Carlo calculation [13,14], and (3) the image-based techniques [15]. An RSA approach exhibits several shortcomings. Indeed, the process is restricted by a jamming limit of the concentration of fibres within the matrix [16]. In addition, the non-overlapping assumption prevents the appearance of pathways of percolation which impacts the mechanical reinforcement of the composite material according to [17]. Thus, an unbiased stochastic generation of the microstructure, for which the overlap between two or more fibres is allowed, turns out to be necessary to avoid the previous drawbacks. However, such a kind concept requires the construction of a mesh that is difficult to design for a complex overlapping geometry. A possible alternative to get round the difficulty is to consider a voxel-based FE approach based on an approximation of the geometry [18–20]. This method enables the efficient setting up of representative patterns of complex composite materials in the framework of homogenisation. Its main shortcoming is related to the accuracy of the geometry which can be improved by smoothing algorithms [21], and the calculation cost to get it.

* Corresponding author at: Université de Caen Basse-Normandie, UMR 6139, LMNO, F-14032 Caen, France. Tel.: +33 2 31 56 74 61.
E-mail addresses: willy.leclerc@unicaen.fr (W. Leclerc), philippe.karamian@unicaen.fr (P. Karamian-Surville), alexandre.vivet@unicaen.fr (A. Vivet).

0927-0256/$ - see front matter © 2012 Elsevier B.V. All rights reserved.
http://dx.doi.org/10.1016/j.commatsci.2012.10.036

In this paper, an efficient stochastic and double-scale FE model to evaluate elastic properties of 2D overlapping random fibre composites is suggested. The latter consists of a fast, reliable and automated generation of a large number of representative patterns of the composite material for which overlaps between fibres are possible. The modelling is based on the voxel-based approach of the geometry combined with an AMR [22]. This concept greatly improves the computation time required to obtain both an accurate geometry and the effective properties, and can be used for any kind of inhomogeneities. Moreover, although the geometry remains approximate this kind of model respects all morphological parameters of the network of fibres. Here, the composite material is seen as a plate structure with a very small thickness in which each material phase is considered as an elastic one. That is why we set up an asymptotic evaluation of effective mechanical properties under the hypotheses of plane stress and perfect bondings at the interface fibre/matrix. Our choice is to build a large number of 2D small RVEs and estimate properties with the help of the double-scale homogenisation method described by Sanchez-Palencia [23] and Bensoussan et al. [24].

The generation of RVEs is carried out according to a Monte Carlo draw. Indeed, Monte Carlo simulations present an interesting benefit in comparison with other stochastic methods. They enable a direct use of deterministic FE problems such as the elasticity framework. Thus, in the field of carbon nanotube (CNT)-based polymer composites, the Monte Carlo stochastic approach has recently been introduced to predict effective properties by Spanos and Kontsos [25] and Shokrieh and Rafiee [26]. It turns out that such a kind of process is suitable to investigate effects of morphological parameters such as curvature, aspect ratio and alignment of fibres which impact the reinforcement of random fibre composites. Indeed, the morphology of fibres widely affects the effective properties of fibre composites. Thus, for example, Odegard et al. [27] exhibited that aligned CNT-based composites allow an interesting improvement according to the preferential direction, nevertheless they have a negative impact on the transverse properties. In addition, Seidel and Lagoudas [28] highlighted the critical impact of CNT distribution within the matrix. Here we consider a semi-deterministic process in such a way that each fibre morphological parameter is either introduced as a random variable according to a given distribution law or fixed. Thus, the morphology of the fibre network is only controlled by a limited number of parameters for which the investigation is more easily done. One must keep in mind that we do not perform a stochastic evaluation of the effective mechanical properties such as Young's and shear moduli but a deterministic homogenisation process for that purpose. Roughly speaking the stochastic aspect of the method only concerns the generation of the main fibres factors such as the orientation or the aspect ratio. However, great care must be taken in the Monte Carlo calculation to check out the final set of results well behaves in a probabilistic sense. Thus, the residuals, that are the estimates of the numerical error committed when predicting effective properties, must follow a Gaussian law to ensure an unbiased evaluation.

This paper is outlined as follows: first we describe the setting up of the modelling by two concepts (1) the smooth boundaries and (2) the *n*-order approximate geometry. Second, some comparisons in CPU time, reliability and effective mechanical properties are exhibited. Then the asymptotic homogenisation process is described in the framework of an isotropic medium and the 0-order model. Some comparisons with micromechanics bounds and model as well as numerical simulations of uniaxial tensile tests are provided. Finally, the reliability and accuracy of the *n*-order approximate geometry is discussed in the case of specific configurations, namely the alignment and aspect ratio of fibres.

2. Numerical modelling

We set up a model based on the construction of 2D representative volume elements of random fibre composites in which the overlap between two or more fibres is allowed. First, the size of RVE requires a specific study which will be studied in Section 4. The idea is that we have to consider a small enough template to perform a FE computation over a large sample of patterns and large enough to reduce the bias introduced by the boundary conditions [6]. Here RVEs are 2-dimensional and respect an assumption of periodicity which is not realistic but gives the best results to limit the bias in comparison with kinematic or static uniform boundary conditions. The mesh and the geometry of each representative pattern are created with the Cast3M software developed by the CEA [29]. The program gives the possibility to the users to vary a large number of morphological parameters. Thus, the parameters such as area fraction, length, width, orientation and in-plane curvature are implemented to follow a probability law which can be chosen by the user or merely be fixed. The overlap is allowed so that entanglement and contact effects are taken into account in our modelling [30]. It is well-known that an entwined network greatly influences the effective properties and consequently must be taken into account in the modelling. From now on, in the purpose of analysing the only effects of geometric representations, randomly oriented fibres and non-dimensional values for composite geometry are used. Thus, the size of RVE is set at 1, the mean length is set at 0.2 with a standard deviation of 0.04 and the fibre width is 0.01 so that the aspect ratio is set at 20. The effects of the last parameter will be studied in Section 5.

2.1. Construction of the geometry

We consider square-shaped RVEs in which the microstructure is stochastically introduced according to different morphological characteristics. The objective is to conceive a representative template for which each morphological parameter can be controlled as a random variable. Thus, each fibre is defined by a point identified as its centroid, a length, a width and an orientation. Fig. 1 shows an example of primitive RVE with 25 inhomogeneities. Two important observations have to be made: first some fibres overlap each other which can be observed in the network and second some fibres partially located outside the representative template exist. A special treatment of previous fibres is set up to respect the boundaries of the RVE. It deals with translating the pieces located outside of the RVE inside the domain. Fig. 1a and b show the representation of the RVE before and after the periodic treatment. In the perspective of the mesh design the main difficulty turns out to be the generation of overlaps between fibres. Indeed, it requires a complex reconstruction of boundaries of each cluster of fibres.

2.2. RVE model with smooth boundaries

In a first approach we consider a model called smooth boundaries in which borders of fibres are smooth. The model respects the geometry previously set up and uses a special treatment of the overlaps. This process consists of recreating the geometry of each intersected fibre according to the location of their neighbours (Fig. 2). An order of priority (1 or 2) is then randomly drawn to construct each intersected fibre as an independent element. The basic idea consists of building a sort of clustered chopped fibre geometry for which the chopped parts are out-of-plane. Thus, the process is adapted to the design of non-redundant meshes for the complete network of fibres, but leads to a loss of the independency of each fibre from a geometrical point of view. However, it is subsequently

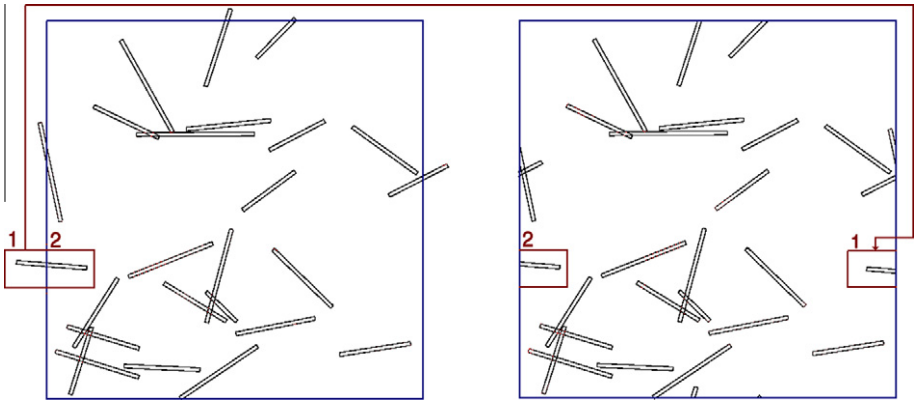

Fig. 1. Primitive RVE (a) before and (b) after periodic treatment.

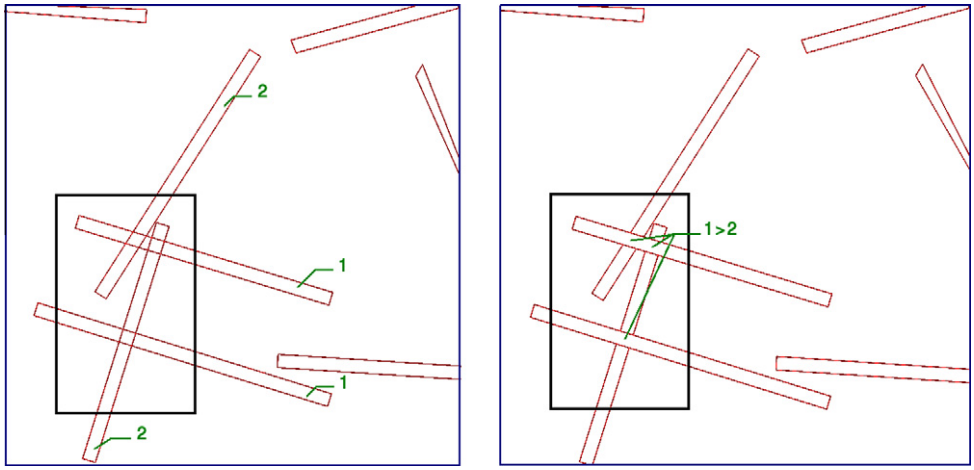

Fig. 2. Treatment of overlaps between fibres.

realised in the homogenisation calculation when we take into account the orientation of each inhomogeneity in their mechanical behaviour.

Fig. 3 illustrates an example of RVE with the exact geometry built from the program that we have coded with the Cast3M software. We can observe the matrix in yellow (1) and the inhomogeneities in red (2). The mesh is generated in two steps. First, we construct the mesh of each fibre according to a refinement parameter. Then, we set up the mesh of the matrix by an automatic triangulation around the boundaries of RVEs and fibres with 3-node triangular elements. This choice is motivated by the low execution time and reliability demonstrated by a preliminary study on different types of elements and a study of the refinement effect which allows us to choose coarse meshes for the matrix in the case of a high contrast of properties. In the case of the fibres, we consider elements of a size equal to fibre width. Indeed, other

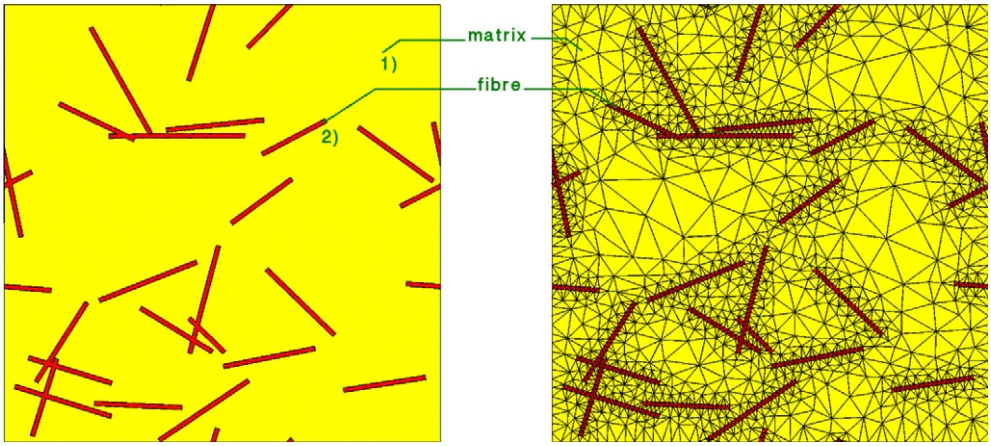

Fig. 3. RVE model with smooth boundaries (without and with mesh).

preliminary studies exhibited such a hypothesis yields an acceptable accuracy in a FE calculation. We will present the effects of mesh refinement on the effective mechanical properties in sub Section 3.3. However, the concept presents 2 main shortcomings. First, the execution time to treat each agglomerate is quite long and undermines the prospect of generating a large number of RVEs. Second, the process lacks reliability in the sense that the geometry of inhomogeneities can not be respected. Indeed, the greater the number of fibres is, the more complex and numerous the intersections are, the more the treatment fails. Thus, in the present context, the generation of RVEs turns out to be really difficult for more than seventy fibres. To end up, the process of triangulation induces the generation of elongated triangular elements. This kind of structural defects leads to ill-conditioned matrices in the calculation of homogenised properties and must be absolutely avoided. Thus, due to the above-mentioned issues, the RVE model with smooth boundaries is not suitable for a numerical study of overlapping random fibre composites. We have suggested and developed a new model to avoid the various shortcomings discussed here.

2.3. RVE model with an n-order approximate geometry

We propose a concept based on a structured grid of quadrangular elements for which each fibre is approximated by a set of 4-node elements located within its edges. A local adaptive mesh refinement (LAMR) around each fibre can then be done to improve the accuracy of boundaries. Thus, the geometry of the fibre is more irregular but respects the morphological parameters such as length, width and orientation. From now on, this paradigm is called RVE model with an approximate geometry and depends on an *n*-order describing the refinement by LAMR process. Let us consider a grid of elements the size of which is equal to the fibre width, the *n*-order is as follows,

$$n = \log_2\left(\frac{\text{Fibre width}}{\text{Size of the small elements}}\right) \quad (1)$$

Fig. 4 shows an example of LAMR process around a fibre for an initial grid of quadrangular elements of the size of the fibre width and a 1-order of subdivision. First a selection is made among the elements of the structured grid located close to each fibre 4a. In a second step the coarse elements are subdivided according to the chosen order and the method selects the small elements for which the centroid is located inside the boundaries of the fibre 4b and c. Finally the primitive smooth representation of each fibre is replaced by their approximated representative formed by the small elements 4d. Each quadrangular element is then subdivided in two 3-node triangular elements and the mesh of the matrix is constructed in the same way as the mesh for the model with an exact geometry. Thus, the model allows one to build each fibre with an approximate irregular boundary but preserves its main morphological parameters. This modelling presents different advantages compared to the modelling set up with smooth boundaries. Indeed the overlaps are easier and faster to take into account with the concept based on a LAMR process. Moreover, whatever the numbers of fibres and intersections inside the RVE are, the reliability of the treatment of overlaps by the model with an *n*-order approximate geometry is very satisfactory.

2.4. RVE model with a rough geometry

The lower the order of the model with an approximate geometry is the more the CPU time is reduced. However in the case of the 0-order the concept can be improved by considering a new approach to construct the RVEs: the RVE model with a rough geometry. The first improvement of this modelling is related to the initial grid for which the size does not equal to the fibre width but is several times larger so that the LAMR process can be fully used. The fibre and fibre-network morphological parameters are considered as random variables too but the primitive RVE is differently generated. The idea consists in considering the primitive fibres as one-dimensional straight elements rather than two-dimensional quadrangular forms. In this point of view the quadrangular elements of the coarse grid are selected when an intersection with a primitive fibre exists. To end up, the elements which are labelled as fibre elements are subdivided in two 3-node triangles. Fig. 5 shows the RVE corresponding to the pattern pictured on Fig. 3. We can observe some irregularities on the boundaries of each fibre but the morphological parameters are all respected. In addition, the complete fibre network obtained with the rough geometry is very close to the one modelled with smooth

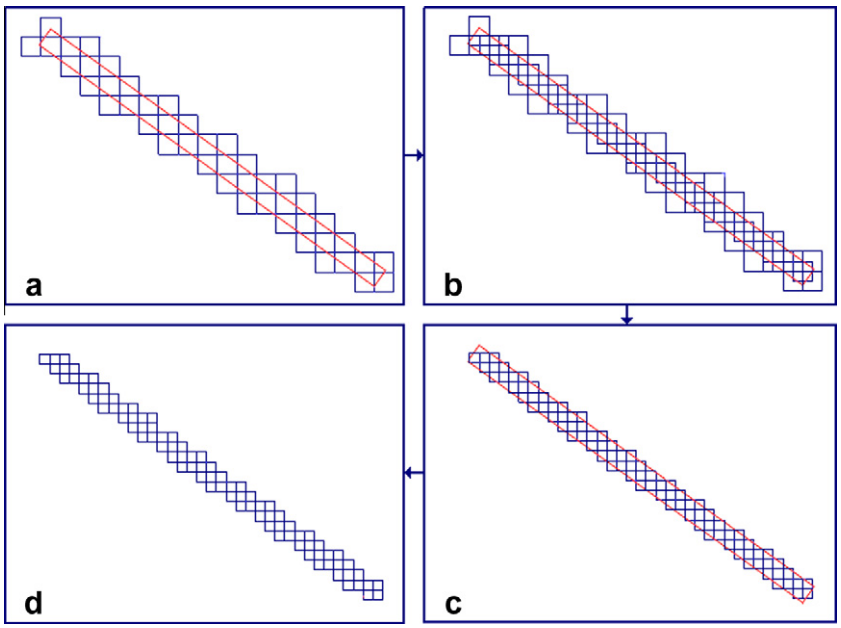

Fig. 4. LAMR process around a fibre for a subdivision parameter of 1.

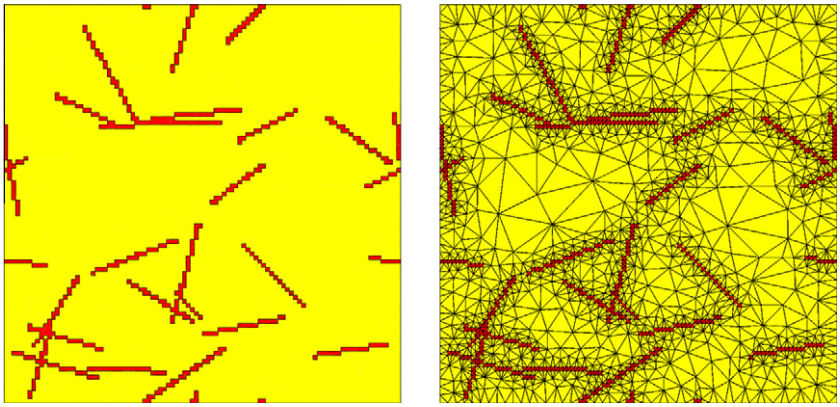

Fig. 5. RVE model with a rough geometry (without and with mesh).

boundaries. In the sequel, we consider the concept of the rough geometry to generate RVEs with a 0-order approximate geometry.

3. Comparative study of models

We search to assess the impact of the model of geometry on the process of calculation of effective properties of random fibre composites. The first step focuses on highlighting the advantages of the model with an approximate geometry, namely an excellent reliability combined with a reduced CPU time. However, the main issue is related to the accuracy in the calculation of effective mechanical properties such as the shear and Young's moduli. At that stage, this latter greatly depends on the n-order of the model which requires an in-depth investigation. So, a preliminary study of the geometric convergence of the model with an approximate geometry is provided as well as some elements of comparison in effective properties and calculation time.

3.1. Geometric convergence of the model with an n-order approximate geometry

Let n be the order of the model, W_C, N_C and S_R the fibre width, the number of inhomogeneities and the size of the RVE respectively. We can estimate the geometric error E_n of the model with an n-order approximate geometry as follows,

$$E_n = \frac{1}{S_R}\sum_{i=1}^{N_C}\sum_{j=1}^{N_i}\frac{d_{i,j}}{N_i} \tag{2}$$

for which $d_{i,j}$ represents the length between the vertice j of the approximate boundaries of the fibre i and its projection on the boundaries of the corresponding smooth fibre. N_i denotes the nodes number situated on the interface of each fibre i. We can estimate an upper bound of the error by using the hypothesis on the inner location of the centres of each element. We have,

$$E_n \leqslant \frac{1}{S_R}\sum_{i=1}^{N_C}\frac{\sqrt{2}}{2}S_E \tag{3}$$

for which S_E is the size of the small quadrangular elements. Thus we can link the previous relation to the order of the model as follows,

$$E_n \leqslant \frac{1}{S_R}\sum_{i=1}^{N_C}\frac{\sqrt{2}}{2^{n+1}}W_C \tag{4}$$

and finally get the following inequality,

$$E_n \leqslant \frac{\sqrt{2}}{2^{n+1}}\frac{W_C}{S_R}N_C \tag{5}$$

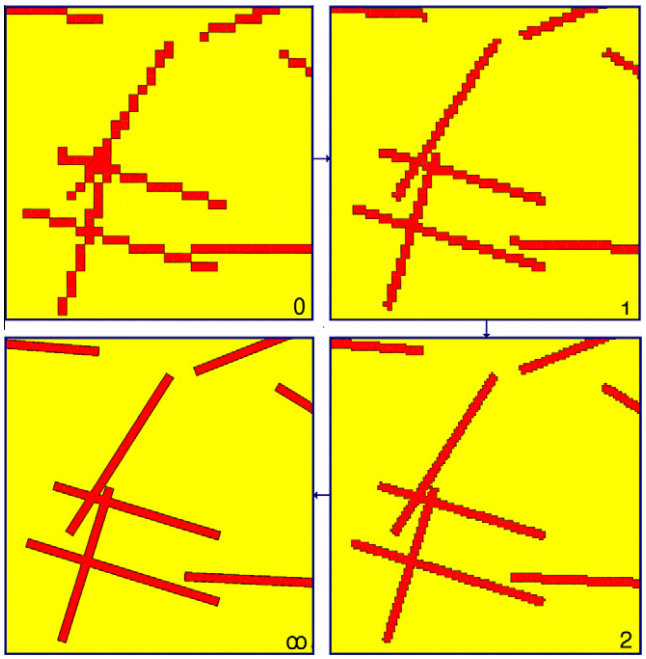

Fig. 6. Geometric convergence of the n-order approximate model (n = 0, 1, 2, ∞).

Let suppose that S_R and W_C are fixed then E_n tends to zero as n tends to infinity. In other words, the model with an n-order approximate geometry converges to the model with an exact geometry according to an exponential decay. Hence the model with smooth borders can be viewed as an ∞-order approximate geometry. Fig. 6 shows the geometric convergence of the n-order approximate model. The greater the order is the fewer irregularities are observed at the interface fibre/matrix. A good candidate for practical applications is an n value less than 3 which exhibits a good compromise between suitable approximation of the smooth geometry and reduced CPU time.

3.2. Comparison in reliability and CPU time

First, a sample of 442 RVEs with unit length is considered to study the model with smooth boundaries. In that case, the treatment of overlaps turns out to be unreliable for more than 25 fibres inside the RVE and practically unfeasable as soon as we have more than 70 fibres. Moreover the CPU time[1] to generate one RVE hugely

[1] Quadricore Intel (R) Xeon (R) W3670 @ 3.20 GHz.

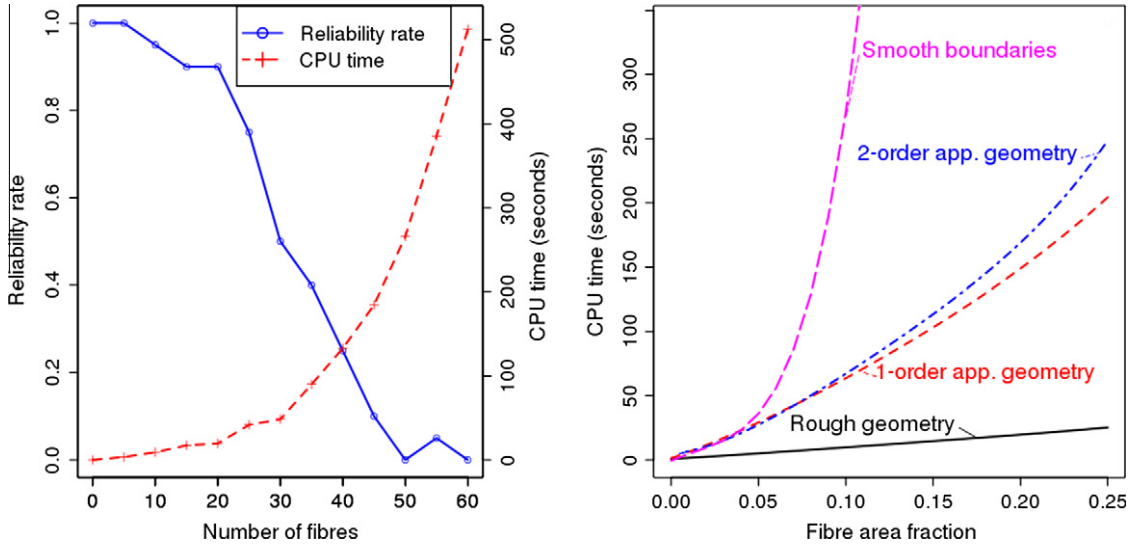

Fig. 7. (a) Simultaneous evolution of the reliability and the CPU time to generate an RVE with the model with smooth boundaries according to the number of fibres and, (b) CPU calculation time for different models according to the fibre area fraction.

increases depending on the number of fibres and intersections inside the RVE. Fig. 7a shows the parallel evolutions of the CPU time and the reliability of the generation of representative patterns. The loss of reliability according to the number of inhomogeneities is related to an important increase of the calculation time which is more than 8 min for 60 fibres. However the model presents some interesting results for fewer than 20 fibres with a low calculation time. Thus, for 10 fibres the reliability is 0.96 and the mean CPU calculation time equals to 9.2 s.

Second, we investigate the model with an *n*-order approximate geometry. We consider a sample of 1699 RVEs built under the same hypotheses as previously used. In this case the reliability is perfect and the CPU calculation time greatly depends on the *n*-order. Fig. 7b exhibits the CPU time according to the fibre area fraction for the 0, 1 and 2-order approximate geometries. The fibre area fraction is estimated by considering the intersected areas only one time. We observe that the greater the order is the longer the generation of an RVE becomes. Thus, constructing RVEs with 10% fibre area fraction with the help of 0, 1 and 2-orders requires 10, 63 and 67 s respectively. To make clear the results for the 0-order are obtained from considering the RVE model with a rough geometry which optimises the CPU time. The same figure shows the evolution of the CPU time for the model with smooth boundaries as well. Thus, one can observe that for a fibre area fraction less than 5%, the CPU time to generate one RVE is identical to the one for generating the same pattern with the rough geometry. However the treatment of the overlaps drastically affects the performances of this model when the concentration of fibres is more important. Thus, an RVE obtained by the model with smooth boundaries for a 10% fibre area fraction requires more than 4 min to be generated. So, the best efficiency is given by the model with an *n*-order approximate geometry for which the reliability in the calculation of effective properties requires an additional study.

3.3. Comparison in effective properties

We investigate the influence of the model on the effective mechanical properties of random fibre composites. The study focuses on the calculation of Young's and shear moduli according to an asymptotic method subsequently described. We suppose

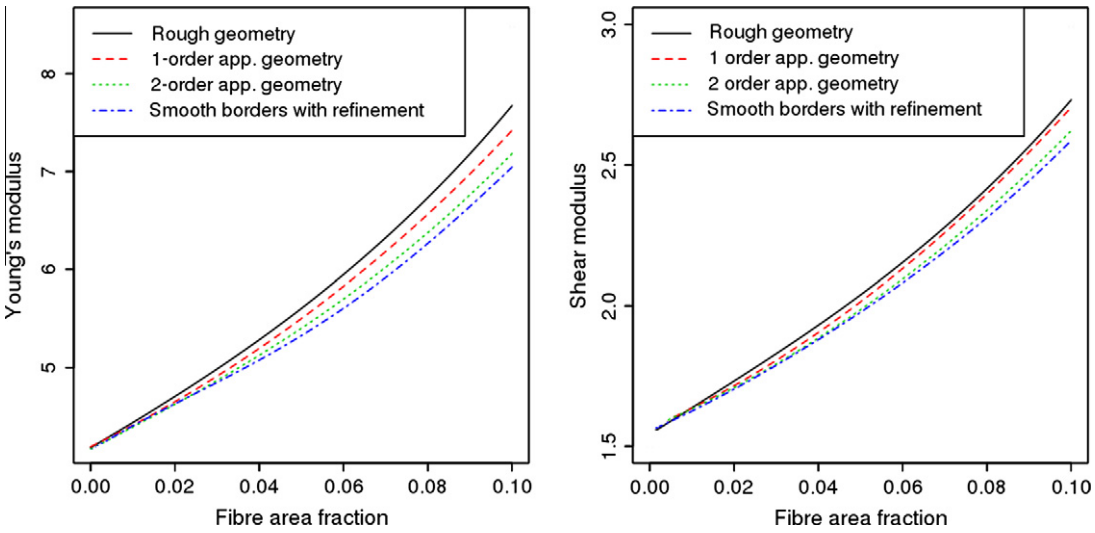

Fig. 8. Comparison of the (a) Young's and (b) shear moduli evolution according to the fibre area fraction for different orders of the approximate geometry.

Table 1
Relative scatter of the effective Young's modulus between the model with smooth boundaries, and the model with an *n*-order approximate geometry.

Fibre area fraction (%)	Rough (%)	1-order (%)	2-order (%)
0	0.785	0.212	0.029
2	1.62	0.456	0.109
4	4.07	2.33	0.962
6	6.11	3.98	1.67
8	7.45	4.75	1.76
10	8.91	5.34	1.97

the isotropy of the media that is checked out for randomly oriented fibres and a suitable size of RVE. The evaluation is performed on the two samples of RVEs previously presented according to morphological and behavioural parameters given in Section 4. In addition, we consider a maximum fibre area fraction of 10% as regards to the loss in reliability of the model with smooth boundaries. In this last case, the mesh around the edges of each fibre is enough refined to get the convergence in effective properties depending on the mesh refinement. The model with an *n*-order approximate geometry is investigated by considering the 0, 1 and 2-orders. Fig. 8 illustrates the convergence of the Young's and shear moduli depending on the order of the geometry. We observe the greater the order is the more the effective properties tend to the results obtained with a smooth representation of each fibre and a high degree of refinement.

Table 1 enables one to observe the relative dispersion of Young's modulus between the smooth modelling (or ∞-order) and the 0, 1 and 2-order approximate geometries. We notice a clear influence of the order on the convergence of the effective property. For instance, if we consider a fibre area fraction of 6% inside the matrix the relative dispersion decreases from 6.11% to 1.67% according to the order of the model. In addition, the relative scatter for the 2-order is relatively low and exhibits a good agreement with the ∞-order. The accuracy of the effective properties greatly depends on the fibre area fraction as well. For instance, the relative dispersion increases from 0.029% to 1.97% for the 2-order and a range of fibre area fraction of 10%. Therefore the choice of the order depends on the expected accuracy and CPU time. Thus, the rough geometry yields the best performances in calculation time but a sensitive loss in accuracy while the 2-order enables to get a much better accuracy combined with a greater CPU time. One must keep in mind the present conclusions are only valid for a concentration of fibres less than 10% for which the comparison of both models is possible. In the sequel, unless otherwise stated, we will only consider the calculation of effective properties according to the rough model.

4. Asymptotic evaluation of the effective properties of a fibre random composite

An asymptotic process is set up to evaluate the effective mechanical properties of random fibre composites with help of the model with a rough geometry. The basic idea deals with building a large number of RVEs for which a network of randomly oriented and distributed fibres is generated. First, in such a concept, we estimate effective properties for each pattern. Then the final properties are obtained from averaging the scope of results. The reliability greatly depends on the RVE size that must be large enough to avoid directional effects and the bias introduced by the boundary conditions [31,32]. Here, we consider a method based on the estimation of the variance to evaluate the sufficient number of realizations and the suitable RVE size [6]. From now on, we apply our model to the framework of CNT-based polymer composites that exhibit higher effective properties than usual composites due to exceptional properties and long aspect ratio of CNTs. CNT-based polymer composites arouse a great interest in research community and could lead to the design of high performance composites in several domains such as thermal, electrical and mechanical ones. We chose effective moduli of CNTs from [28,33,34]. Thus, the mechanical properties of fibres are as follows, the longitudinal Young's modulus is set at 1050 GPa, the transverse one is set at 600 GPa, the shear modulus is set at 450 GPa and the Poisson ratio is set at 0.25. The matrix medium has a Young's modulus of 4.2 GPa, a shear modulus of 1.55 GPa and a Poisson ratio of 0.35. Under the hypotheses of a homogeneous distribution of randomly oriented fibres inside the matrix we will consider the homogenised medium as isotropic.

4.1. Setting of the double-scale homogenisation method

We evaluate the homogenised properties of the material in two steps. First, mechanical properties are obtained on each RVE by performing a periodic homogenisation. We use the double-scale method described by Sanchez-Palencia [23] and Bensoussan, Lions and Papanicolaou [24]. It deals with setting a multi-scale problem via an asymptotic expansion of the equations describing the behaviour of the material. In our case we consider a double-scale problem in the framework of the elastic continuum mechanics. The first scale corresponding to the composite material is called macroscopic and the second scale corresponding to the RVE is called microscopic. The hypothesis of periodicity we suppose in the generation of each RVE and the evaluation of the homogenised properties is convenient in the setting up of the homogenisation method but is not realistic. That is why we qualify the homogenisation process as pseudo-periodic. In a second step, we consider a Monte Carlo draw of a large number of RVEs in the same way as Spanos and Kontsos [25] and Shokrieh and Rafiee [26]. The main idea consists in generating automatically each RVE according to different fibre network morphological parameters such as the length, the width and the curvature of each fibre that follow a distribution law (uniform, normal or logarithmic-normal). In such a concept each RVE is a possible representative of the composite material which leads to the evaluation of one possible set of effective properties. The final effective properties are then obtained by averaging the scope of results. An important issue is finally related to the estimation of the number of realizations and the suitable RVE size. The next section gives some elements to answer to this question.

4.2. Choice of RVE size

The crucial issue of the RVE size is investigated in this section. We use a statistical approach based on an important Monte Carlo draw and the study of the variance parameter in the same way as Kanit et al. [6] in the framework of Voronoï mosaics. The RVE size must respect several conditions to have a good representativeness of the composite material in a homogenisation process. First, a suitable RVE has to be large enough to take into account sufficient informations on the microstructure of the material and avoid directional effects. However a large RVE affects the calculation cost, especially in an asymptotic process, and consequently loses its elementary aspect. In addition, an important drawback is related to the boundary conditions that introduce a bias in the calculation of the effective properties [31,32]. The RVE area A can be linked to a given absolute error ε_{abs} and the standard deviation of the investigated effective property Y, $D_Y(A)$. Thus, for n independent realizations of area A, we have,

$$\varepsilon_{abs} = \frac{1.96 D_Y(A)}{\sqrt{n}} \tag{6}$$

$$\varepsilon_{rel} = \frac{1.96 D_Y(A)}{\sqrt{n} Y} \tag{7}$$

Thus, the calculation of the confidence interval for large samples of RVEs yields the suitable RVE size for a given number of realizations and absolute error ε_{abs}. Therefore, a critical point is related to the following question, do we have to consider a small number of realizations of large RVEs or a large number of realizations of small RVEs to obtain the expected error ε_{abs}? First, the Young's modulus and the variance parameter must be investigated to check out the level of reliability and accuracy of the asymptotic process according to the RVE size. Fig. 9a illustrates the evolution of the mean effective Young's modulus for different non-dimensional values of RVE size between 0.75 and 2. Here we consider the framework of CNT-based polymer composites for which properties are previously provided and we set the fibre area fraction at 5%. The number of realizations for each RVE size is obtained so that the relative error ε_{rel} is less than 0.002. We observe a near stabilisation of the effective property according to the RVE size around a mean value of 5.6. In addition, the standard deviation $D_Y(A)$ slightly decreases in the same time. Fig. 9b) exhibits the evolution of the number of realizations according to the RVE size for a fibre area fraction set at 5%. Here, the relative error ε_{rel} is 0.005. The CPU time to carry out the corresponding realizations is illustrated on the same figure. We observe the greater the RVE is, the lower the number of realizations is, the greater the CPU time becomes. Thus the investigation of the calculation cost does not exhibit an optimal value of RVE size but a steady evolution according to the same parameter. Such a kind observation is connected to the total area of RVEs and number of triangular elements used in the homogenisation process that is lower in the case of small RVEs. As a result, the suitable size has to be chosen by considering the convergence of the effective property Y to ensure reliable results. Here, the study has led us to choose an RVE size of 1 for which, on the one hand, the convergence in Y is observed and, on the other hand, the calculation cost stays reasonable.

4.3. Comparison with micromechanics bounds

We compare the numerical results obtained from the rough modelling with Hashin–Shtrikman's bounds [1,35] and Halpin-Tsai's self-consistent estimates [36,37]. Here, we consider a comparative study under the hypotheses previously presented and the assumption of an effective isotropic medium. First, the effective Young's modulus is investigated in comparison with Voigt and Reuss bounds and Halpin-Tsai's estimates (Fig. 10a) which are obtained by considering extreme cases of longitudinal and transversal orientations of the material [38]. We notice that the mean curve increases continuously according to the concentration of fibres inside the RVE. All data are localised between the bounds and the confidence interval is very narrow around the fitting curve obtained by a multiple linear regression. One must keep in mind that we estimate confidence intervals from performing predictions on the complete sample of data, which explains its constancy around the mean curve. Second, we consider a similar study for the effective bulk and shear moduli which are compared to Hashin–Shtrikman's bounds. Fig. 10a and b illustrate the evolutions of the Young's and shear moduli according to the area fraction of fibres. We observe our results are all localised between the bounds as well. Therefore, the comparisons allow us to state our results respect the bounds.

4.4. Comparison with Mori–Tanaka micromechanics model

We set up a comparative study of the effective mechanical properties obtained from the model with a rough geometry and the Mori–Tanaka micromechanics model [2]. In the framework of an isotropic medium with transversely isotropic fibres, the effective stiffness tensor given by the model [35] is as follows,

$$\mathbf{C} = \mathbf{C}^m + v_f \langle (\mathbf{C}^f - \mathbf{C}^m)\mathbf{A}^f \rangle (v_m \mathbf{I} + v_f \langle \mathbf{A}^f \rangle)^{-1} \tag{8}$$

where $\mathbf{C}^m$ is the stiffness tensor of the matrix, $\mathbf{C}^f$ is the stiffness tensor of the fibres, $\mathbf{I}$ is the identity tensor, v_m and v_f the fibre area fractions of the matrix and the fibres, $\mathbf{A}^f$ is the dilute mechanical strain concentration which depends on the Eshelby's tensor as follows,

$$\mathbf{A}^f = [\mathbf{I} + \mathbf{S}(\mathbf{C}^m)^{-1}(\mathbf{C}^f - \mathbf{C}^m)]^{-1} \tag{9}$$

Here, $\mathbf{S}$ designates the Eshelby's tensor [4] and comes from [39] in the case of 2D thin elliptical inclusions. The brackets $\langle . \rangle$ stand for a mean integral of the stiffness tensor depending on the orientation of the fibres. We invite the readers to refer to the paper of Odegard et al. [27] on this subject. In the framework of the Eshelby's hypotheses, each inclusion is embedded in an infinite medium and the contact between two or more fibres is not taken into account. Thus, as the fibre area fraction goes up, a FE approach is more needed as the Mori–Tanaka model can not account for direct interactions.

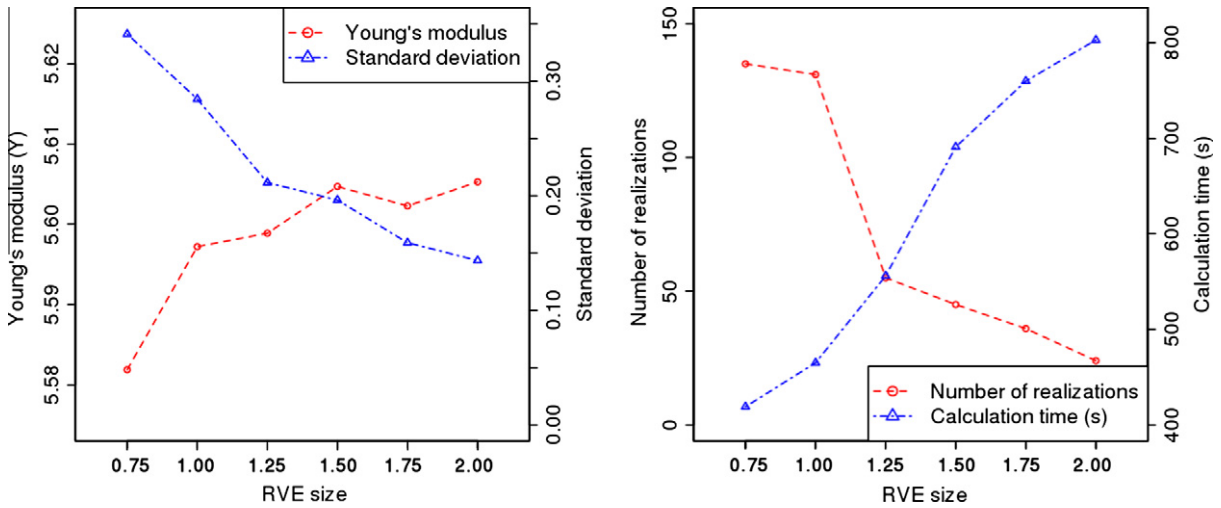

Fig. 9. Parallel evolutions of (a) the standard deviation and the Young's modulus and (b) the number of realizations and the corresponding calculation time according to the RVE size for a fibre area fraction set at 5%.

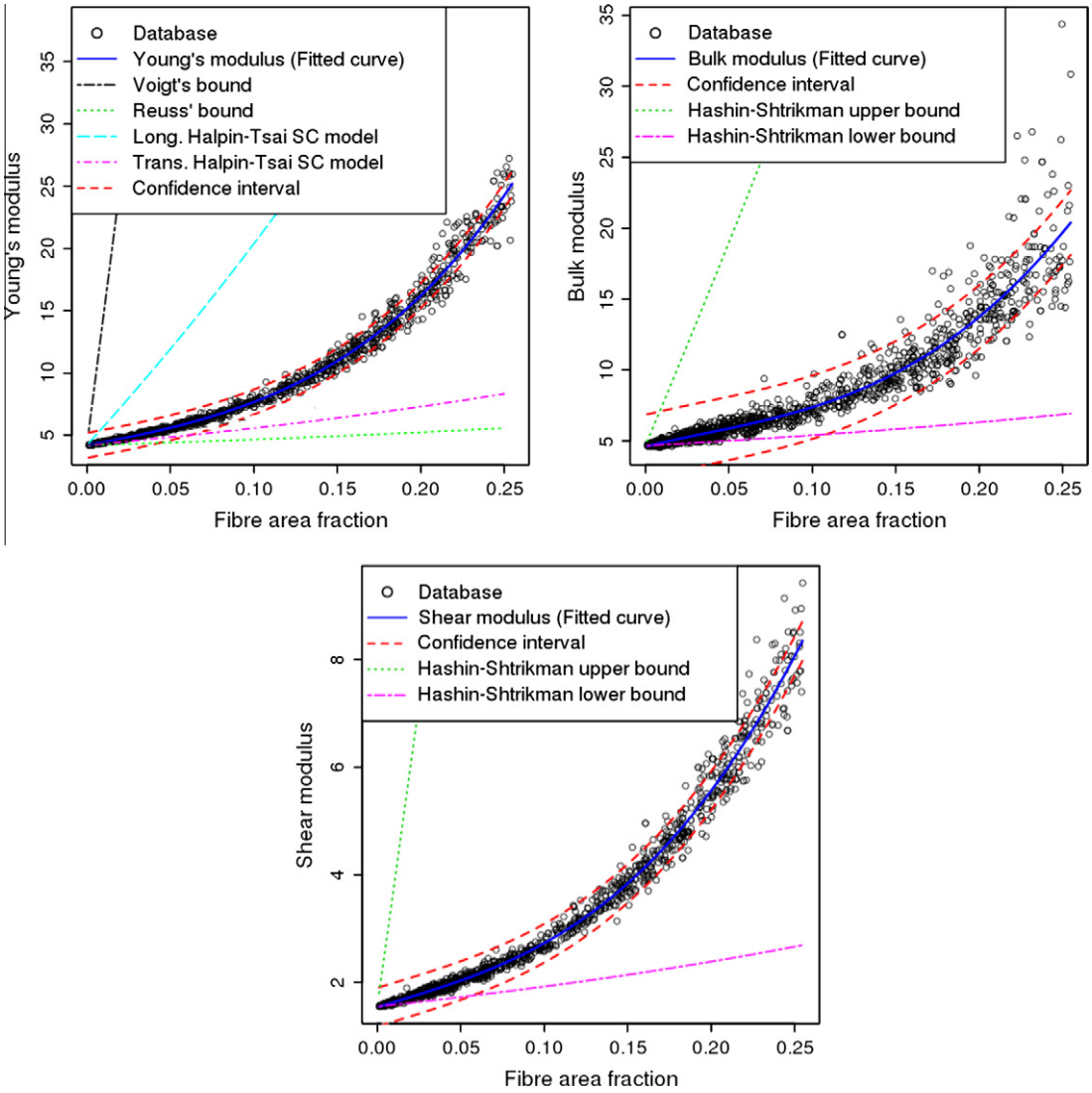

Fig. 10. Evolution of (a) the Young's modulus, (b) the bulk modulus and (c) the shear modulus according to the fibre area fraction and comparison with (a) Voigt and Reuss bounds and Halpin-Tsai estimates, (b) and (c) Hashin–Shtrikman bounds.

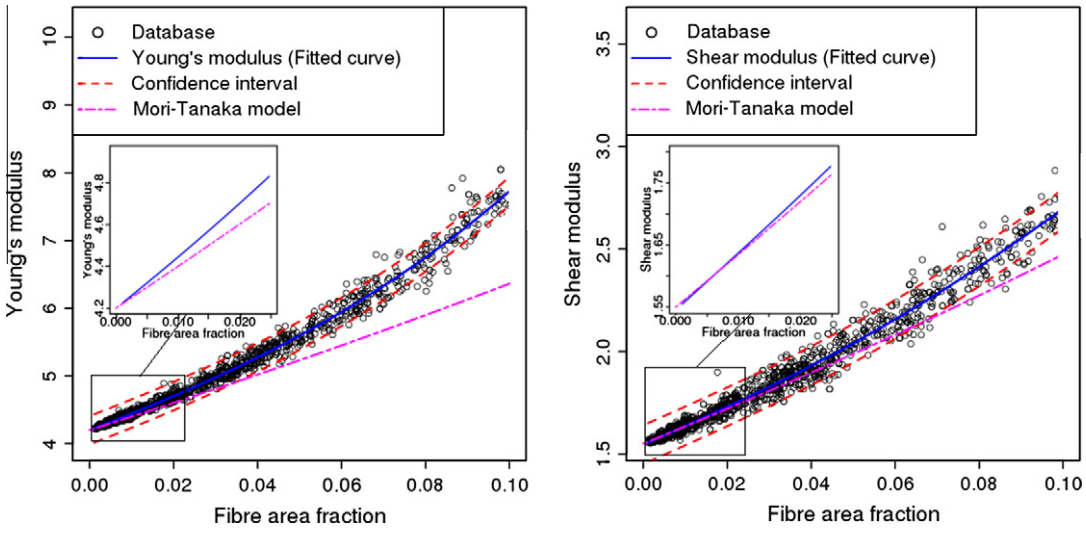

Fig. 11. Comparison of (a) the Young's modulus and (b) the shear modulus between the model with a rough geometry and the Mori–Tanaka model.

Fig. 11a and b exhibit the Young's and shear moduli according to the area fraction of fibres. We observe Mori–Tanaka micromechanics model yields results cleary less stiff than the model with a rough geometry and a double-scale homogenisation. However, as we can see on zoomed-in insets of the curves drawn in Fig. 11a and b the models fit together for a low area fraction less than 2%.

4.5. Comparison with numerical simulations of uniaxial tensile tests

A comparative study of the double-scale homogenisation method with a direct FE calculation is set up. It deals with simulating a uniaxial tensile test, in other words a traction applied on independent squared samples of the composite material. Effective Young's and shear moduli are then estimated by FE. However, the calculation is performed without taking into account the double-scale expansion of the constitutive equations. That is why we talk about a direct FE calculation. 459 RVEs with a rough geometry are used to represent the samples of the material in this purpose. We assume the same hypotheses on the morphological and behavioural characteristics of fibres as previously used in the framework of the double-scale homogenisation to perform a relevant comparative study. A uniaxial pressure is applied on the right edge of each squared RVE to simulate the traction. We impose specific periodic boundary conditions on the other edges to avoid boundary layer effects. Thus, we assume no horizontal displacements on the left edge, and no vertical displacements on the upper edge.

Fig. 12a and b enable one to visualise the evolution of the Young's and shear moduli according to the fibre area fraction. Each dot represents one single data obtained from one uniaxial tensile test. The provided confidence interval is calculated on the results of numerical tensile tests and stays practically steady for any fibre concentration. Important discrepancies are observed for a high concentration but the values are generally located in the confidence interval around the mean curve. In addition, one can notice that the fitting curves drawn are very close. Thus, the properties provided by the two methods fit together and consequently highlight the good agreement between the double-scale homogenisation and the numerical simulations of uniaxial tensile tests.

5. Effects of morphology

We intend to examine the influence of the model with an n-order approximate geometry on the expected morphological effects of alignment and aspect ratio. The aim is to check out that the approximate geometry does not affect the results in the case of specific configurations for which the effects are well-known and widely studied. We consider the model with an n-order approximate geometry for values of n-order less than 2. Unless otherwise stated, the basic assumptions on the construction of RVEs are identical to the isotropic case studied in Section 4. The RVE size is set at 1 according to the discussion done in sub Section 4.2.

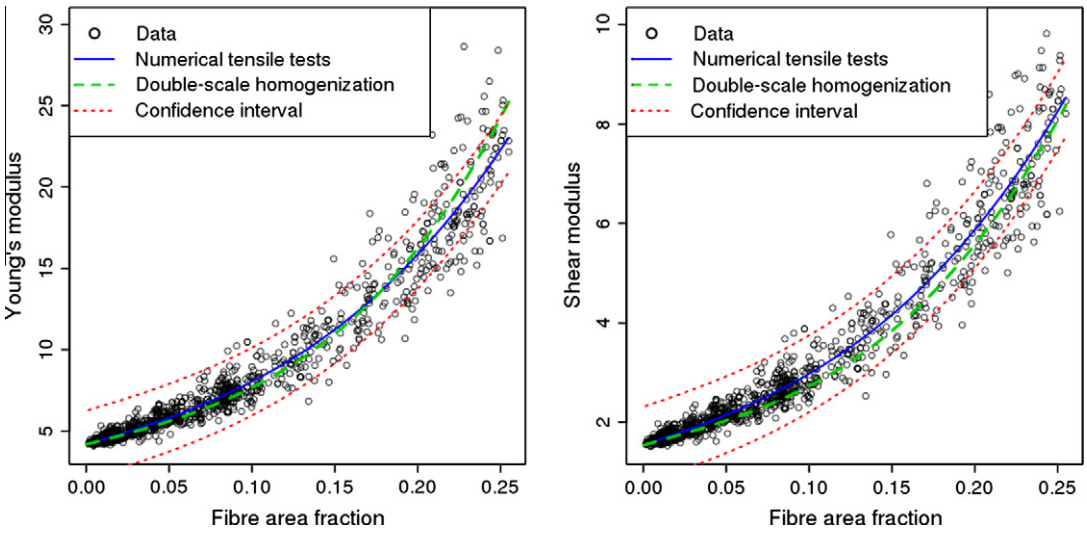

Fig. 12. Evolution of (a) the Young's and (b) the shear moduli according to the fibre area fraction for the double-scale homogenisation method and the numerical simulations of tensile tests.

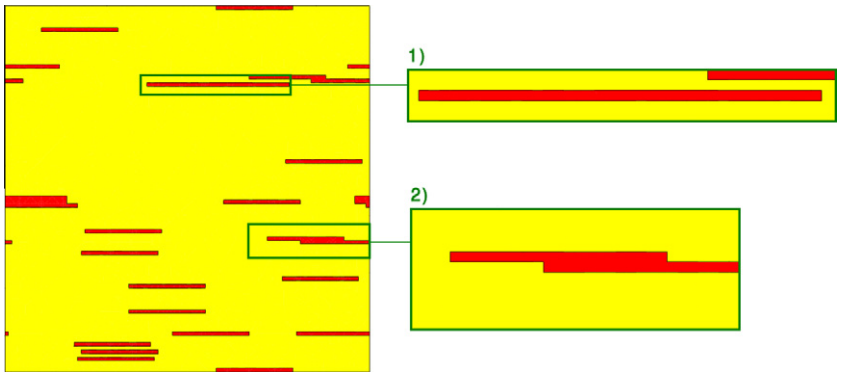

Fig. 13. RVE with 25 aligned fibres.

5.1. Fibre alignment

We study the effect of alignment on the effective mechanical properties of random fibre composites. In this configuration the orientation is fixed so that the fibres form a parallel network within the matrix. We allow both the overlap and the contact between fibres as previously seen in the isotropic case. Fig. 13 depicts an RVE composed of a network of 25 aligned fibres. We notice that the overlapping assumption leads to an issue about the independency of each inhomogeneity. Indeed, the constant orientation involves that two differents fibres are not distinguishable anymore. Thus, we observe two kinds of drawback, (1) two fibres connected at ends form a single long fibre, (2) two or more fibres connected at edges form other kinds of inhomogeneity. In the present work, we assume that the homogenised material follows a transversely isotropic behaviour. First, we search to estimate the order of the approximate geometry to evaluate effective properties in this framework.

Fig. 14a and b highlight the impact of the n-order on the effective Young's moduli in the case of aligned fibres. Results are very similar except for a high area fraction more than 15%. We observe parabolic curves that are more consistent with a network of non-continuous chopped fibres, for which end effects are paramount, than with a network of independent ones. In addition, Table 2 shows the estimations of Young's (E_t, E_l) and shear (G) moduli for the 0, 1 and 2-orders according to the fibre area fraction (a_f). We observe the greater the concentration is the greater the relative scatter between the different orders is. Thus, in the case of the longitudinal Young's modulus, the relative scatter between the 0 and 2-orders increases up to 16.5% for an area fraction of 25%. In the cases of the transversal Young's and shear moduli, the maximum value is only 2.34% and 4.27% but the matrix is so strongly dominant what explains the weak impact of the n-order. Therefore, the results lead us to choose the model with a rough geometry in the sequel of the present study.

In a second step, we set up a comparative study of the rough model with the Mori–Tanaka (MT) [2,27,35] and self-consistent (SC) [3] micromechanics models. Fig. 15a exhibits the effective longitudinal Young's modulus evaluated with help of the rough geometry and the both discussed micromechanics models. A comparison is also provided with the results obtained in Section 4 for which the mechanical response of the composite material is isotropic, and the inhomogeneities follow a transversely isotropic behaviour. In addition, a zoomed-in inset shows an acceptable adequacy for a fibre area fraction less than 2% as previously observed in sub Section 4.4. However the models diverge for a higher concentration of fibres for which the overlaps appear. The case of the SC model is more inquisitive since the divergence is then really important. However, the method is really sensitive to the Eshelby's tensor which was chosen strongly asymmetric to correspond with elongated ellipses. Hence, the micromechanics model yields a strongly parabolic curve instead of the near linear one given by the MT model. Fig. 15b shows the fitted curve drawn for the transversal Young's modulus. One can observe the same adequacy for a low concentration of fibres as previously observed but the fit is this time much better. Similar results have also been checked out for the shear modulus.

Table 2
Effective Young's and shear moduli for the 0, 1 and 2-orders and a fibre area fraction less than 25%.

a_f	E_l (0)	E_l (1)	E_l (2)	E_t (0)	E_t (1)	E_t (2)	G (0)	G (1)	G (2)
0	4.17	4.37	4.46	4.21	4.20	4.20	1.55	1.55	1.55
5	7.56	7.36	7.25	4.68	4.66	4.65	1.65	1.65	1.65
10	12.6	12.3	11.9	5.12	5.09	5.06	1.77	1.76	1.76
15	20.2	19.4	18.6	5.56	5.51	5.48	1.92	1.90	1.89
20	31.5	29.8	27.8	6.03	5.95	5.91	2.11	2.06	2.05
25	47.5	45.7	40.8	6.55	6.45	6.40	2.34	2.27	2.24

5.2. Fibre aspect ratio

We investigate the impact of the aspect ratio on the effective mechanical properties. This parameter is defined as the ratio between the length and the width of fibres. Let us consider an isotropic medium for which the fibres are randomly oriented and distributed. The RVE size is chosen to be more than 5 times the mean value of length of fibres. Indeed, under this assumptions, some preliminary studies exhibited no impact of the chosen length for a given fibre aspect ratio. First we investigate the validity of the model with an n-order approximate geometry under the assumptions of a fibre aspect ratio set at 20 and a fibre area fraction set at 5%. Fig. 16a shows the influence of the n-order on the evolution of the Young's modulus depending on the fibre area fraction for different aspect ratios. We observe small gaps between the 0, 1 and 2-orders but all exhibit a quasi-linear behaviour for a concentration of fibres higher than 10%. In addition, results for a minimum aspect ratio of 1 for which the fibres are equivalent to square inhomogeneities

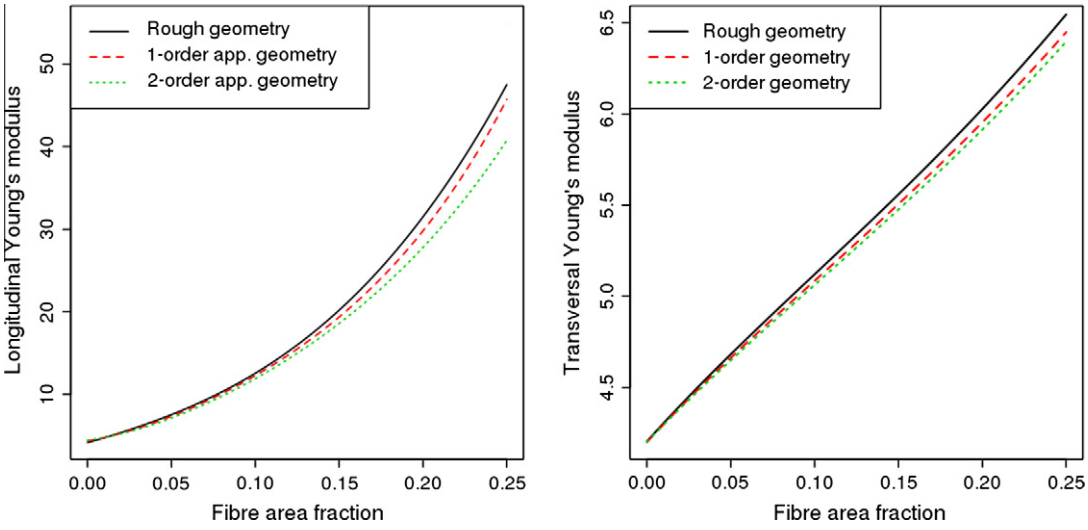

Fig. 14. Influence of the n-order on the (a) longitudinal and (b) transversal Young's moduli.

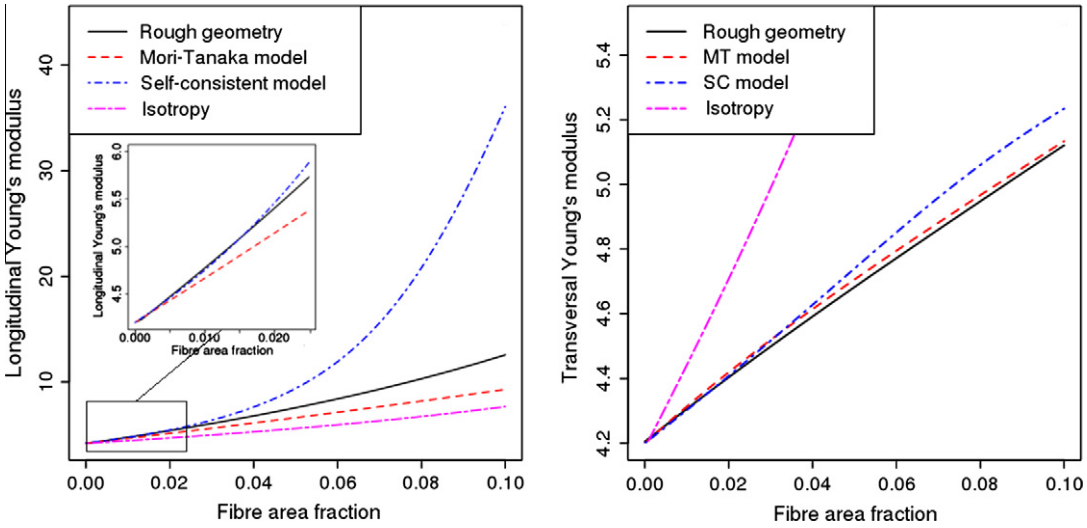

Fig. 15. Evolutions of (a) the longitudinal and (b) the transversal Young's moduli according to the fibre area fraction and comparison with the Mori–Tanaka and self-consistent micromechanics models.

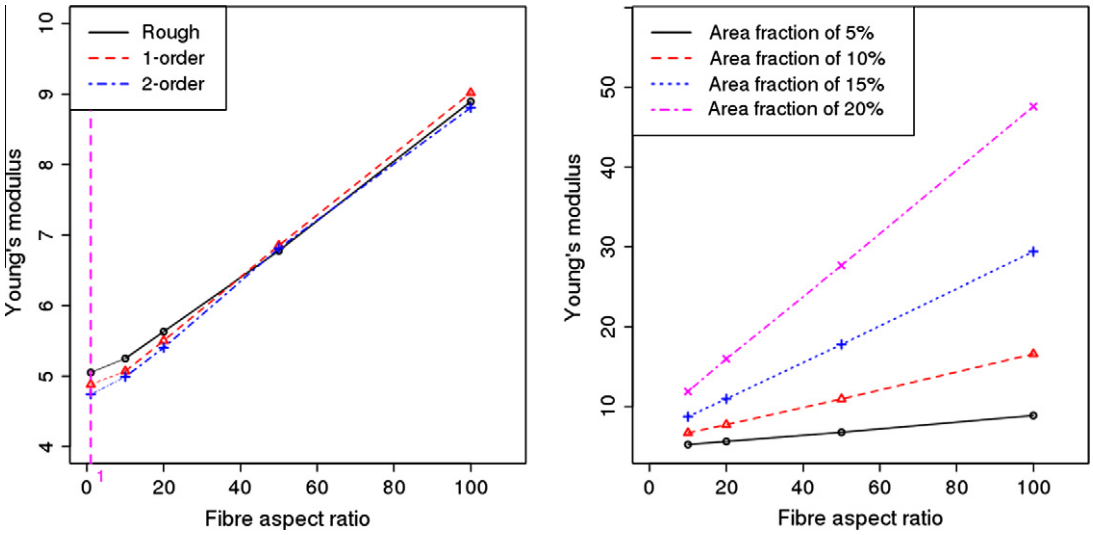

Fig. 16. (a) Influence of the n-order on the evolution of the Young's modulus according to the fibre aspect ratio for a fibre area fraction set at 5% and (b) Evolution of the Young's modulus according to the fibre aspect ratio for different fibre area fractions.

are provided. Here, we notice a greater impact of the n-order as well as a loss of linearity around this value. It could be related to the geometrical approximation but a more in-depth study is required to check out this point. In a second step we consider the impact of the parameter of fibre aspect ratio under the assumption of isotropy and rough modelling. Fig. 16b exhibits the influence of the fibre aspect ratio on the Young's modulus for different fibre area fractions. Results show an expected increase of the Young's modulus according to the aspect ratio and practically no saturation effects. Thus, the diminishing of end effects [40] is not reached for the studied range of aspect ratio. This observation is consistent with different authors [41] who have shown saturation effects only appear around an aspect ratio of 200.

6. Conclusion

We have developed a double-scale stochastic FE model adapted to efficiently estimate the effective properties of overlapping random fibre composites. The model is based on a geometric approximation of fibres avoiding the main drawbacks of a complex mesh building, namely a lack of reliability, a long CPU time and ill-structured meshes. Thus, the model enables us to set up an efficient Monte Carlo draw of large samples of RVEs for which fibre morphological parameters such as the orientation and the aspect ratio of fibres can be controlled. The consistency of the model has been checked out by different comparisons. First, a comparative study has been set up with a model with smooth boundaries. This has highlighted an important benefit in calculation time and reliability as well as a proper accuracy of estimated effective properties. In addition, results have been compared with classical micromechanics bounds and models. As expected, results only fit for a very small fibre concentration, for which the overlap does not affect the effective properties, and consequently diverge for a high fibre area fraction. At last the model has been validated by investigating some morphological parameters, namely the orientation and the aspect ratio. Results turned out being in good agreement with the theoretical expectations. The outlooks of the model are numerous. The model could in fact be easily modified and used to assess more deeply the effects of poorly known parameters such as the agglomeration,

the curvature of fibres or the phenomenon of decohesion at the interface fibre/matrix. In addition, the concept can be applied to other problems such as electrical or thermal ones for any kind of inhomogeneity and dimensional framework.

Acknowledgments

The authors thank the conseil régional de Basse-Normandie for its financial support to Willy Leclerc's Ph.D. thesis and the High-Performance Computing Centre of Haute-Normandie (CRIHAN) for the computing means put at their disposal. All the fitted curves, graphs and statistical analyses related to the results presented in this paper were conducted in R [42].

References

[1] Z. Hashin, S. Shtrikman, Journal of the Mechanics and Physics of Solids 11 (2) (1963) 127–140.
[2] T. Mori, K. Tanaka, Acta Metallurgica 21 (1973) 571–574.
[3] R. Hill, Physics of Solids 13 (1965) 213–222.
[4] J. Eshelby, Proceedings of the Royal Society of London A241 (1957) 376–396.
[5] W.J. Drugan, J.R. Willis, Journal of the Mechanics and Physics of Solids 44 (4) (1996) 497–524.
[6] T. Kanit, S. Forest, I. Galliet, V. Mounoury, D. Jeulin, International Journal of Solids and Structures 40 (13–14) (2003) 3647–3679.
[7] J. Segurado, J. Llorca, Journal of the Mechanics and Physics of Solids 50 (10) (2002) 2107–2121.
[8] H.J. Böhm, A. Eckschlager, W. Han, Computational Materials Science 25 (1–2) (2002) 42–53.
[9] S. Kari, H. Berger, R. Rodriguez-Ramos, U. Gabbert, Composite Structures 77 (2007) 223–231.
[10] S. Kari, H. Berger, U. Gabbert, Computational Materials Science 39 (1) (2007) 198–204.
[11] Y. Pan, L. Lorga, A.A. Pelegri, Computational Materials Science 43 (3) (2008) 450–461.
[12] Y. Pan, L. Lorga, A.A. Pelegri, Composites Science and Technology 68 (2008) 2792–2798.
[13] A.A. Gusev, P.J. Hine, I.M. Ward, Composites Science and Technology 60 (2000) 535–541.
[14] D. Duschlbauer, H.J. Böhm, H.E. Pettermann, Journal of Composite Materials 40 (2006) 2217–2234.
[15] C. Redenbach, I. Vecchio, Composites Science and Technology 71 (2) (2011) 107–112.
[16] P. Viot, G. Tarjus, S.M. Ricci, J. Talbot, Random sequential adsorption of anisotropic particles. I. Jamming limit and asymptotic behavior. Journal of Chemical Physics 97 (7) (1992) 5212–5218.
[17] D. Jeulin, M. Moreaud, Image Analysis and Stereology 6 (2007) 121–127.
[18] L. Mishnaevsky Jr., K. Derrien, D. Baptiste, Composites Science and Technology 64 (12) (2004) 1805–1818.
[19] L. Mishnaevsky Jr., Acta Materiala 52 (14) (2004) 4177–4188.
[20] L. Mishnaevsky Jr., Materials Science and Engineering A 407 (1-2) (2005) 11–23.
[21] S. Boyd, R. Müller, Journal of Biomechanics 39 (7) (2006) 1287–1295.
[22] M.J. Berger, P. Colella, Journal of Computational Physics 82 (1989) 64–84.
[23] E. Sanchez-Palencia, Non-homogeneous media and vibration theory, vol. 127, Berlin, 1980.
[24] A. Bensoussan, J.L. Lions, G.C. Papanicolaou, Asymptotic Analysis for Periodic Structures, Springer Verlag, North Holland, Amsterdam Edition, 1978.
[25] P.D. Spanos, A. Kontsos, Probabilistic Engineering Mechanics 23 (4) (2008) 456–470. Dedicated to Professor Ove Ditlevsen.
[26] M.M. Shokrieh, R. Rafiee, Computational Materials Science 50 (2) (2010) 437–446.
[27] G.M. Odegard, T.S. Gates, K.E. Wise, C. Park, E.J. Siochi, Composites Science and Technology 63 (11) (2003) 1671–1687. Modeling and Characterization of Nanostructured Materials.
[28] G.D. Seidel, D.C. Lagoudas, Mechanics of Materials 38 (8–10) (2006) 884–907. Advances in Disordered Materials.
[29] Cast3M Software <http://www-cast3m.cea.fr/>.
[30] R. Everaers, K. Kremer, G.S. Grest, Entanglement effects in model polymer networks, Macromolecular Symposia 93 (1) (1995).
[31] M. Ostoja-Starzewski, International Journal of Solids and Structures 35 (19) (1998) 2429–2455.
[32] K. Sab, European Journal of Mechanics 11 (5) (1992) 585–607.
[33] A.L. Kalamkarov, A.V. Georgiades, S.K. Rokkam, V.P. Veedu, M.N. Ghasemi-Nejhad, International Journal of Solids and Structures 43 (22–23) (2006) 6832–6854.
[34] C. Fan, Y. Liu, H. Chyanbin, Applied Physics A: Materials Science Processing 95 (2009) 819–831.
[35] Y. Benveniste, Mechanics of Materials 6 (2) (1987) 147–157.
[36] J.C. Halpin, J.L. Kardos, Polymer Engineering and Science 16 (5) (1976) 344–352.
[37] P. Wall, Application of Mathematics 42 (4) (1997) 245–257.
[38] R. Guzmán De Villoria, A. Miravete, Acta Materialia 55 (9) (2007) 3025–3031.
[39] M. Huang, W. Zou, Q.-. Zheng, International Journal of Engineering Science 47 (2009) 1240–1250.
[40] R.G.C. Arridge, P.J. Barham, C.J. Farrell, A. Keller, Journal of Materials Science 11 (1976) 788–790.
[41] R.L. McCullough, Delaware Composites Design Encyclopedia 2 (1990) 93–142.
[42] R: A language and Environment for Statistical Computing. Vienna, Austria: R Foundation for Statistical Computing R Software <http://www.R-project.org>.

Computational Materials Science 79 (2013) 674–683

Contents lists available at ScienceDirect

Computational Materials Science

journal homepage: www.elsevier.com/locate/commatsci

Effects of fibre dispersion on the effective elastic properties of 2D overlapping random fibre composites

W. Leclerc, P. Karamian-Surville *

Université de Caen Basse-Normandie, UMR 6139 LMNO, 14032 Caen, France
CNRS, UMR 6139 LMNO, 14032 Caen, France

ARTICLE INFO

Article history:
Received 13 April 2013
Received in revised form 29 May 2013
Accepted 1 July 2013
Available online 24 August 2013

Keywords:
Fibre composites
Finite element analysis (FEA)
Percolation
Representative volume elements (RVEs)

ABSTRACT

The present paper is dedicated to the numerical investigation of the effects of fibre dispersion on the effective elastic properties of 2D overlapping random fibre composites. The mechanical response of the composite material is related to the percolation phenomenon which occurs when the concentration of fibres is important. The main purpose of the present work is to investigate whether an inhomogeneous fibre dispersion can lead or not to a decrease in percolation threshold, and to a beneficial mechanical reinforcement. For that purpose, we consider a fast and relevant pixel-based FE simulation, the model with an *n*-order approximate geometry. Indeed, such a modelling turns out to be more convenient to easily set up large samples of RVEs, and estimates both the effective properties and the percolation threshold. The fibre distribution is generated according to a 2-scale Boolean scheme of circles which enables one to vary the state of dispersion. Numerical results are also provided which highlight the influence of the dispersion depending on different parameters of distribution such as the scale ratio, the density of fibres or the area fraction of circles. Other calculations extend the study to different morphological features of the fibre such as its orientation and its aspect ratio.

1. Introduction

The influence of the fibre dispersion on the effective elastic properties of random fibre composites is investigated. Different states of dispersion are discussed. On the one hand, a homogeneous one for which fibres are randomly distributed and the medium is statiscally isotropic. On the other hand, an inhomogeneous one for which heterogeneities are not well dispersed. In this case, one has to distinguish an agglomerated state with clusters from which we call a true inhomogeneous dispersion. In such a material configuration the composite is homogeneous at the microscopic scale and void areas and aggregates are only observable at the mesoscopic one. In the mechanical field, experimental results exhibit that a homogeneous dispersion of fibres provide a greater available area to bond with the surrounding matrix. In addition, the agglomerates act as stress concentrators which thwart the reinforcement of the composite material [1,2]. Therefore, a classical experimental assumption is that a homogeneous dispersion of fibres leads to optimized properties. The numerical results are less decisive. Thus, the dilute suspension of clusters micromechanics model introduced by Guzmãn De Villoria and Miravete [3] exhibits the same conclusion about the benefit of a homogeneous dispersion of fibres. However, the studies performed by Jeulin and Moreaud [4–6] highlight other findings. According to the authors, a suitable arrangement of fibres could lead to an improvement of the effective properties due to the percolation phenomenon. This latter is related to the appearance of pathways formed by fibres for a high concentration of inclusions. In the electrical field, this phenomenon is well-studied and indeed turns out to improve the electrical conductivity [7]. However, in the mechanical field, the benefit of the percolation phenomenon is much more discutable because of the non-diffusive behaviour of the constitutive equations. Recent works provide some responses in the context of a homogeneous state of dispersion. Thus, Niklaus and Shea [8] achieved a direct comparison between conductivity and Young's modulus knowing the volume fraction of metallic heterogeneities within a metal-elastomer nanocomposite. Their results exhibit a narrow link between percolation and enhancement of mechanical properties. Numerical studies realized by Fralick et al. [9] lead to similar conclusions in the context of 3D random cells for which heterogeneities are modelled by subcells. Their works highlight the key role of both the microstructure, and the interface between the matrix and the inclusions, on the percolation effects. However, in the context of an inhomogeneous dispersion, the improvement of the percolation phenomenon which was showed by Jeulin and Moreaud still remains inquisitive. This could be not necessarily connected to a beneficial reinforcement of the material.

* Corresponding author at: Université de Caen Basse-Normandie, UMR 6139 LMNO, 14032 Caen, France. Tel.: +33 2 31 56 74 61; fax: +33 2 31 56 73 20.
E-mail addresses: willy.leclerc@unicaen.fr (W. Leclerc), philippe.karamian@unicaen.fr (P. Karamian-Surville).

0927-0256/$ - see front matter © 2013 Elsevier B.V. All rights reserved.
http://dx.doi.org/10.1016/j.commatsci.2013.07.009

In this paper, the mechanical effects of the dispersion of fibres are numerically investigated by estimating both the effective Young's and shear moduli, and the percolation threshold for different spatial configurations of a 2-dimensional network of overlapping fibres. For this purpose, we use a finite element modelling based on the random generation of representative volume elements (RVEs). We consider a pixel-based finite element (FE) model [10–12] called model with an n-order approximate geometry [13] for which the microstructure is approximated but respects all morphological parameters of the network of fibres. Such a kind of simulation enables us to take into account the overlap between two or several fibres which is necessary to estimate the effects of the percolation. Here, the composite material is seen as an isotropic plate structure with a very small thickness in which each material phase is considered as an elastic one. That is why we evaluate the properties under the hypotheses of plane stress and perfect bondings at the interface fibre/matrix. Our choice is to build a large number of 2-dimensional small RVEs and to estimate properties in two steps. First, we perform a double-scale homogenization method as described by Sanchez-Palencia [14] and Bensoussan et al. [15] on each RVE. It deals with setting up a 2-scale expansion of the constitutive equations of linear elasticity the dominant term which leads to an expression of effective elastic properties. Such a process is based under a periodic assumption without taking into account any loadings see for instance [16]. Second, we evaluate the effective mechanical properties by averaging the scope of results obtained from a Monte-Carlo draw of a large sample of RVEs.

The inhomogeneous dispersion of fibres is simulated with the help of a 2-scale Boolean scheme of circles [17,18]. The principle is based on a 2-scale generation of the heterogeneities within an RVE. In a first step, circular inclusions are randomly distributed within the RVE. In a second step, the fibres are randomly dispersed within the circles so that we obtain an inhomogeneous network of fibres. The state of dispersion then depends on the ratio between the diameter of the circles and the length of the fibres. Moreover, the percolation phenomenon is studied by evaluating the percolation threshold for different configurations of the network of fibres. This latter corresponds to the minimum fibre area fraction for which the probability that the phenomenon of percolation appears is more than 50%. In the sequel, we assume the appearance of the phenomenon when two opposite edges of a given direction of an RVE are connected. The evaluation is then performed by directly testing the intersections between two or more fibres within each RVE of a large sample of representative patterns. The pixel-based FE model turns out to be more convenient for this purpose. Indeed, the generation of the representative patterns is performed according to a grid of quadrangular elements which enables one to easily test the contacts. In addition, we propose a partitioning method of RVEs based on a dichotomous and recursive concept. Such a kind of paradigm leads to a tremendous decreasing of calculation time to check out the intersections as well as an important gain in memory storage.

This paper is outlined as follows, the first part illustrates the numerical modelling of a random fibre composite by the pixel-based FE model. The setting up of the 2-scale Boolean scheme is explained as well. The second part is dedicated to the evaluation of the percolation threshold. Different results and comparisons with the analytical excluded volume method are provided in the framework of a homogeneous distribution of fibres. The following section exhibits some numerical results in effective mechanical properties and percolation threshold in the framework of an inhomogeneous dispersion of randomly oriented fibres. Different parameters, namely the fibre density, the area fraction of circular inclusions and the scale ratio between the diameter of the circles and the length of the fibres are also investigated. To end up, some results are provided in the framework of a twofold effect of the morphology of the fibres and their dispersion.

2. Numerical modelling

An RVE is a powerful tool to model a material with inhomogeneities. This consists of a representative pattern the size of which must respect several criterions. Thus, this latter must be large enough to provide accurate informations on the microstructure but small enough to remain elementary and limit the calculation cost in a FE process [19,20]. In the present paper, large samples of 2-dimensional RVEs are built to model a random fibre composite. The fibre network is generated according to different morphological features such as the orientation, the aspect ratio or the dispersion of fibres. Each parameter can be either fixed or randomly distributed according to a probability law. In the prospect of a large generation of RVEs we have chosen the RVE model with an n-order approximate geometry. The model is based on a coarse but fast generation of a pixel-based FE mesh which is relevant to design RVEs with complex microstructures as a network of overlapping fibres. In addition, a 2-scale Boolean scheme of circles is set up to model the inhomogeneous distribution of fibres within an RVE.

2.1. Model with an n-order approximate geometry

We consider a modelling of the fibre network based on a structured grid of quadrangular elements for which each fibre is approximated by 4-node elements located within its boundaries. Such a kind of concept is done in 3 steps. First, a primitive fibre network is built according to different fibre morphological features such as the diameter, the length or the orientation which can be fixed or randomly distributed. Fig. 1a depicts an example of primitive fibre network for which we suppose randomly oriented and distributed fibres. In addition, the overlap between two or more fibres is allowed so that the percolation phenomenon can be subsequently estimated.

Second, we build the mesh around the boundaries of the network. Here, one can consider a direct triangulation but the process turns out to be difficult and unreliable. That is why we have preferred the use of a geometric approximation of fibres [13]. The idea focuses on realizing a quadrangular tessellation of the RVE area and picking out the elements the centres of which are located within the boundaries of the inhomogeneities. Fig. 1b exhibits the pixel-based approximation of the geometry corresponding to the present primitive fibre network. One can notice that the boundaries of each heterogeneity are rough but the geometric approximation respects the morphology of the fibre network. Third, an adaptive mesh refinement (AMR) [21] can be performed around each fibre to improve the accuracy of the geometry. An order of subdivision describes the accuracy of the refinement in power of 2 hence the name of n-order approximate geometry. In the sequel, unless otherwise stated, we will only consider the 0-order which corresponds to a model with no refinement. We also talk about a model with a rough geometry.

2.2. 2-scale Boolean scheme of circles

The fibre dispersion is simulated by a 2-scale Boolean scheme of circles according to a Cox point process [17,18]. The concept focuses on a 2-scale modelling of composite materials for which the large scale corresponds to the scale of agglomerates and the small one corresponds to the scale of inhomogeneities. The agglomerates are simulated with the help of circular inclusions. The process is realized in two steps. First, the set of circles is randomly generated inside the RVE. Second, the geometric centres of

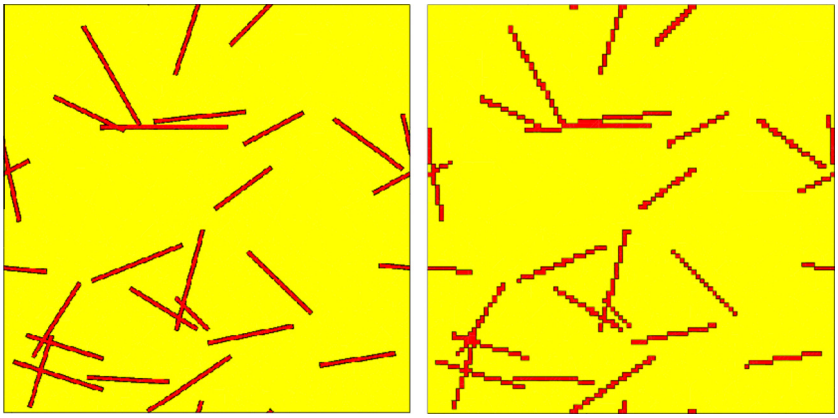

Fig. 1. (a) Geometric generation of the fibre network inside the RVE and (b) geometric approximation of the fibre network by a pixel-based FE approach.

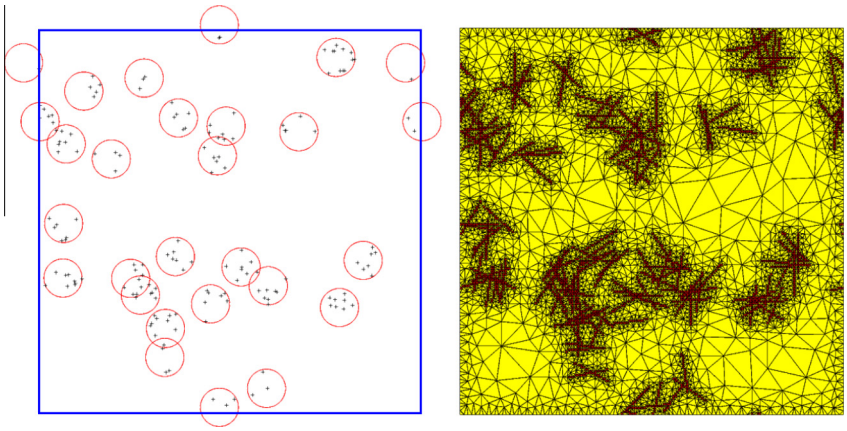

Fig. 2. (a) 2-scale Boolean scheme of circles with geometric centres of fibres and (b) final RVE with mesh.

fibres are randomly distributed inside the representative pattern so that the only fibres located within the circles are finally kept. Fig. 2a depicts an example of distribution of circles and fibres. One must keep in mind that the ratio between the size of RVE and the dimensions of the circles must be large enough to ensure a suitable representativeness of the microstructure. According to [22], the ratio between a one-dimensional characteristic length of the RVE (L) and the size of the heterogeneities (δ) must tend to infinity in order to ensure the validity of the RVE. However, in the context of a sampling of a large number of representative patterns as we consider here, dimensions of each RVE can be chosen largely smaller since the complete sample can be seen as one single large RVE. Nevertheless, two important points have to be respected [20]. First the number of realizations must be sufficiently important to ensure the convergence of properties when averaging the scope of results. Second, L must be greater than a critical length L_c in order to avoid the bias related to boundary conditions and take into account enough informations on the microstructure [23,24]. Consequently L_c must be evaluated for each material configuration and kind of modelling. In the present paper, the diameter of circles corresponds to δ and is chosen 5 times lower than the size of RVE according to a study realized in a previous work [13]. Moreover, we allow the overlap between two or more circles to avoid a bias on the dispersion. Other parameters play a key role in the setting up of a 2-scale Boolean scheme of circles. First, the scale ratio between the diameter of circles and the fibre dimensions directly impact on the morphology of the fibre network and consequently on the evaluated effective properties. Thus, a scale ratio of 1 tends to form agglomerates of fibres while a larger value leads to a true inhomogeneous dispersion of fibres in the same sense as it was discussed in introduction section. Second, the fibre density inside each circle characterizes the level of agglomeration within the composite material. Thus the greater the density is the more agglomerated the fibre network is. Finally, the area fraction of circles within the RVE provides another parameter describing the level of agglomeration.

We must make clear that the area fraction of circles must be greater than the percolation threshold of circular inclusions a_c to ensure the consistency of the investigation of percolation effects. Thus, a preliminary step was to evaluate the percolation threshold in the framework of a random distribution of overlapping circles. A value of $a_c = 0.62045$ was found which is largely higher than the one estimated in the case of spheres in 3D (0.2895 according to [25]). However the assessment is close to the percolation threshold estimated by Quintanilla and Ziff [26] in the case of 2D overlapping circles (0.67635). Fig. 2b shows a possible mesh generated from the 2-scale Boolean scheme of circles. In the present case, the scale ratio is set at 1 and the area fraction of circles is less than a_c. We observe some clusters of entangled fibres where the circles are located.

3. Evaluation method of the percolation phenomenon

We intend to assess percolation thresholds with the help of the previously quoted model with an n-order approximate geometry. It turns out that such a kind of modelling enables a fast and convenient evaluation of the percolation rate which is the probability

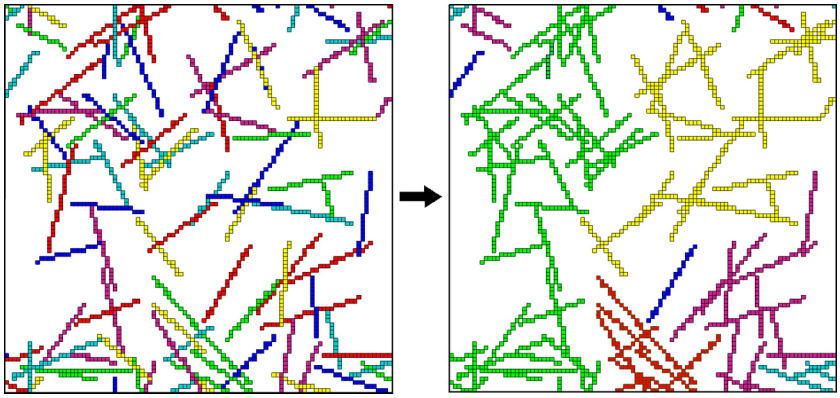

Fig. 3. Identification process of agglomerates within a network of random fibre composites.

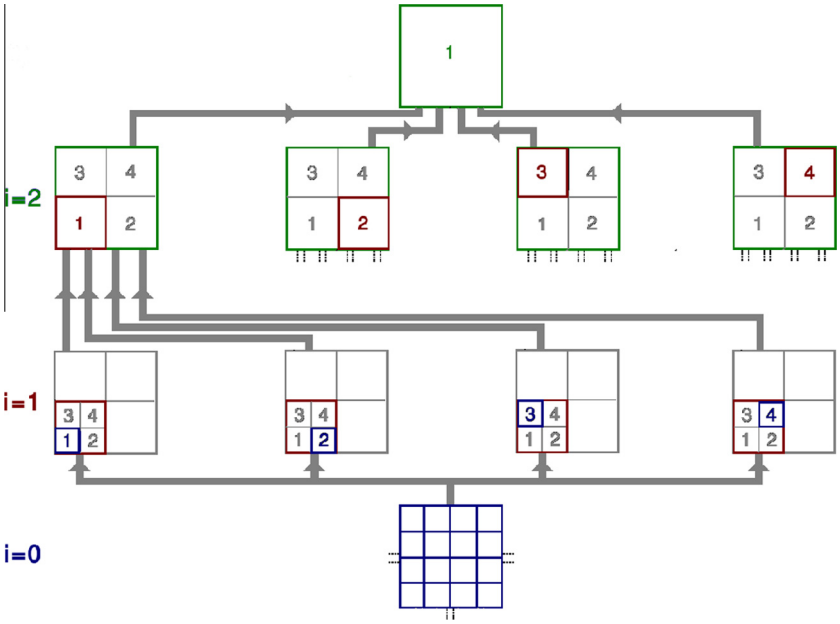

Fig. 4. Diagram of the dichotomous and recursive treatment of the connections between sub-domains with p chosen equal to 2.

that the percolation phenomenon appears for a given fibre area fraction. Indeed the quadrangular elements are easily checked out whether they belong to two or several fibre inclusions. Thus, a classical method based on simple tests of intersections is usable but remains long to compute. In the present paper, another approach is proposed which is based on a partitioning method depending on a dichotomous and recursive process that widely reduces both calculation cost and storage in memory. To end up, some tests are realized in the framework of a homogeneous distribution of randomly oriented fibres.

3.1. Basic evaluation method

The evaluation method is based on testing the crossing between two or several inclusions for the complete fibre network. The concept consists in first identifying the clusters of fibres within the RVE then checking out the contact of each agglomerate with two opposite edges of the representative pattern. However the identification step requires to test the crossing of each inclusion with all other inclusions and consequently proves to be long to process. Thus, the number of tests of intersections is $\mathcal{O}(n^2)$ where n is the number of inclusions. A first optimization can be realized by constructing step-by-step the agglomerates during the process instead of testing the complete network before the identification. In addition, the percolation can be easily checked out during the process so as to stop the program if the phenomenon is detected.

Fig. 3 exhibits an example of results obtained with the help of both the identification process and the modelling with an n-order approximate geometry. The network of fibres is composed of 85 randomly oriented fibres the aspect ratio of which is set at 20. The RVE size is chosen so that the ratio between the dimensions of the RVE and the length of the inclusions is 5. Before processing each inclusion is labelled by a specific colour[1] and the identification process is performed so that each agglomerate is labelled by a single colour at the end. The present example exhibits a percolation path between bottom and up edges, but not between left and right edges.

3.2. Partitioning method

The previous evaluation method is deterministic and perfectly reliable but requires a long calculation time to process. A natural

[1] For interpretation of color in Fig. 3, the reader is referred to the web version of this article.

Table 1
CPU time to perform the partitioning method on a single RVE.

Area fraction	5%	10%	15%	20%	25%
$p = 0$	0′16″70	0′48″04	1′30″30	2′09″23	2′50″36
$p = 1$	0′14″31	0′32″20	0′48″67	1′03″24	1′17″05
$p = 2$	0′18″02	0′31″03	0′41″53	0′50″46	0′57″28
$p = 3$	0′31″44	1′00″51	1′07″62	1′11″74	1′11″86

mean to solve the problem is first to partition the RVE area so that the method is independently performed on each sub-area. Then, a second step consists in connecting the sub-domains. The main issue is to define a relevant partitioning to minimize the cost of the step of connections. In the present paper, we propose a concept which consists of connecting the sub-domains according to a dichotomous and recursive partitioning of the RVE. The process is realized in p steps where p designates the order of partitioning in power of 4. Thus, for example, the order 2 leads to a subdivision in 16 sub-domains. In a preliminary step (or step 0), a dichotomous subdivision of the domain in 2^p parts in each main direction is realized so that the process starts with a grid of 4^p square-shaped domains. For each step i, with $i > 0$, the process consists first in building a new dichotomous subdivision in 4^q domains with $q = p - i$. We talk about domains of rank i while the domains obtained at the previous step are now designated as the sub-domains of the new domains, or the domains of rank $i - 1$. Then, the connections are identically and independently realized by group of 4 sub-domains within each domain. The process is repeated until $i = p$, in other words, till the RVE is subdivided in a sole domain and all the connections are realized. Fig. 4 illustrates a diagram of the dichotomous and recursive treatment with p chosen equal to 2. Each domain of rank i is labelled with a number corresponding to its position inside the domain of rank $i + 1$, and a specific colour corresponding to the value of i. Thus, the treatment of the connections between sub-domains is identically realized whatever is the step i of the process. Such a kind of process is totally automated and guarantees a fast and low-cost computational estimations of percolation thresholds. The number of tests of intersections is here equivalent to $n^2/2^{2p+1} + n_{con}$ where n_{con} is the number of connections and depends on the mean number of aggregates inside each sub-domain.

The order p must be chosen so that the reduction in CPU time is maximal and consequently requires a preliminary study. Table 1 exhibits the necessary CPU time[2] to perform the partitioning method on a single RVE for different values of p and fibre area fractions. In the present work, the aspect ratio of randomly oriented inclusions is set at 20 and the length of fibres (l) is set at 0.2. One can observe that the calculation time is widely reduced between the powers 0 and 2 for which $1/2^p > l$ while if p is equal to 3 the CPU time increases again. Thus, the optimal p can be chosen as the maximum integer v such as $v < log_2(l)$. However, in the case of a low area fraction, the number of connections becomes quickly predominant. Thus, a fibre area fraction of 5% exhibits a premature increase in calculation time for p equal to 2.

3.3. Results for a homogeneous distribution of random fibres

We set up the assessment of the percolation threshold in the framework of a homogeneous distribution of random fibres. A comparison is realized with the analytical values predicted by the excluded volume method [27,28]. The excluded area depends on the geometry of fibres. In the present work, we suppose that the inclusions are 2D thin rectangles. Thus, in the case of randomly oriented fibres, the average excluded area $\langle A_{ex} \rangle$, obtained after integration over all possible orientations, is as follows,

$$\langle A_{ex} \rangle = 2WL + \frac{L^2 + W^2}{2\pi}$$

where W is the width of rectangles and L the length of rectangles. The percolation threshold s of a 2D network of randomly oriented fibres is as follows,

$$s = \frac{\langle A \rangle}{\langle A_{ex} \rangle}$$

where $\langle A \rangle$ is the average area of a fibre. First, we consider a network of randomly oriented fibres and the aspect ratio is set at 20. In this case, the percolation threshold given by the excluded volume method is 0.1925. Fig. 5 depicts the influence of the fibre area fraction on the percolation rate for a sample of 13892 data under the same hypotheses and a ratio between the size of RVE and the length of inclusions set at 5. A fitted curve has been drawn according to a Gaussian law and the median straight line in red corresponds to a percolation of 50%. The percolation threshold is assessed to 0.1924 that is identical to the previous value.

Fig. 6 shows a comparison for different values of aspect ratios. We observe that the greater the aspect ratio is the lower the

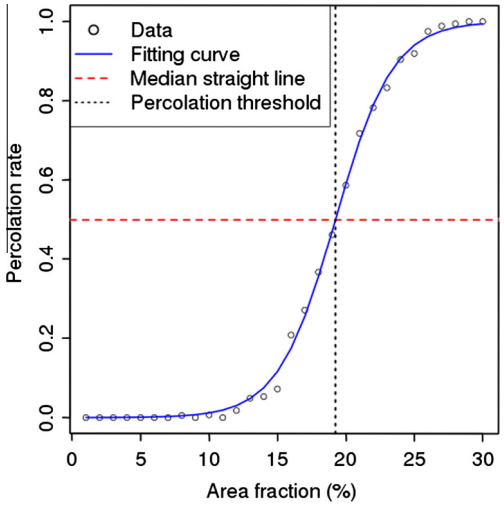

Fig. 5. Influence of the fibre area fraction on the percolation rate for an aspect ratio (AR) set at 20.

percolation threshold is, which is consistent with theoretical expectations. Table 2 exhibits a good agreement between numerically evaluated percolation thresholds and values given by the excluded volume method. Thus, for an aspect ratio of 100, the numerical study yields a percolation threshold of 0.0523 while the theoretical value is 0.0558. One can notice that the results are less accurate for a high aspect ratio while the excluded volume method is only exact for an infinite aspect ratio. We must make clear that the number of realizations of RVEs for high-aspect ratio fibres is widely less important than for low-aspect ratio fibres. Indeed, the numerical calculation time is longer because it requires larger RVEs to respect a ratio of 5 between the size of RVE and the length of inclusions. In addition, an estimation of the percolation threshold for aligned fibres of aspect ratio 20 is provided as well. One can notice that the value is widely greater than for randomly oriented fibres (0.3047 vs 0.1924) due to the loss of the rotation degree of freedom. Thus, the results check out the negative effect of an alignment of fibres on the percolation phenomenon [6].

[2] Quadricore Intel (R) Xeon (R) W3670 @ 3.20 GHz.

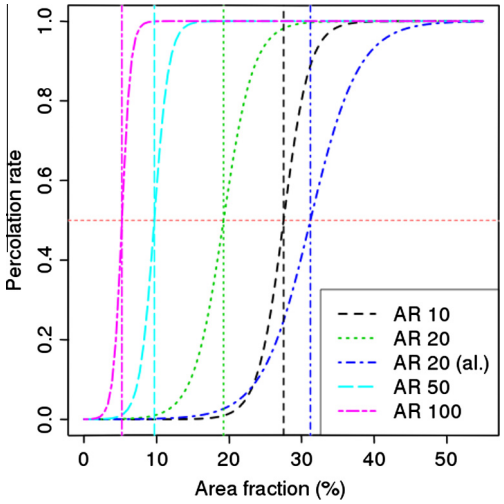

Fig. 6. Comparison of the influence of the fibre area fraction on the percolation rate for different values of ARs.

Table 2
Influence of the aspect ratio on the percolation threshold.

AR (aspect ratio)	10	20	20 (alig.)	50	100
Excluded volume method	0.2771	0.1925	0.3333	0.1004	0.0558
Numerical evaluation	0.2753	0.1924	0.3047	0.0970	0.0523
Number of realizations	4238	13892	6505	5344	2441
Standard deviation	0.0012	0.0005	0.0018	0.0004	0.0003

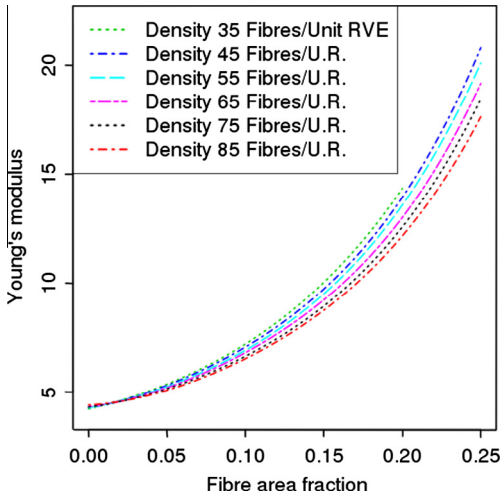

Fig. 7. Influence of the average fibre density on the effective Young's modulus for an inhomogeneous dispersion of fibres.

4. Effects of the dispersion of randomly oriented fibres

Effects of dispersion on the effective mechanical properties are studied in the framework of randomly oriented fibres. The agglomerates of fibres are simulated with the help of the 2-scale Boolean scheme of circles discussed in Section 2.2. We consider the model with an n-order approximate geometry to represent the fibres in the framework of a finite element calculation of effective properties. The ratio between the size of RVE and the diameter of circles is set at 5 to respect the representativeness of the pattern and avoid the bias introduced by the boundary conditions. The size of the RVE is set at 1 and the aspect ratio of fibres is set at 20. Different states of dispersion are also studied with the help of the parameter of scale ratio which is the ratio between the diameter of the circles and the length of the fibres. The evaluation of properties is done with the help of an asymptotic process based on a Monte Carlo draw of RVEs. In this concept, the properties are estimated for each pattern by the periodic double-scale homogenization described by Sanchez-Palencia [14] and Bensoussan et al. [15] then averaged on the complete sample of investigated RVEs. The mechanical properties of inclusions are chosen as follows, the longitudinal Young's modulus is set at 1050 GPa, the transverse one is set at 600 GPa, the shear modulus is set at 450 GPa and the Poisson ratio is set at 0.25. The matrix has a Young's modulus of 4.2 GPa, a shear modulus of 1.55 GPa and a Poisson ratio of 0.35. These values are related to carbon nanotube (CNT)-based polymer composites and come from articles [29–31]. This choice is motivated by their high contrast of properties what is suitable to relate the mechanical reinforcement to the percolation phenomenon.

4.1. Impact of the average fibre density

First, we investigate the effects of the average fibre density within the circular inclusions under the hypothesis of a scale ratio set at 1. In other words, the study consists in investigating the influence of the level of agglomeration on the effective mechanical properties. In addition, we randomly draw the area fraction of circular inclusions between 0% and 100% so that the average fibre density within the circles is a relevant criterion of the level of agglomeration. We perform some estimations in effective mechanical properties and percolation thresholds in the same way as seen in Section 3.3. Figs. 7 and 8 illustrate the influence of the fibre density on the effective Young's (E) and shear (G) moduli. The density is given for a unit RVE (U.R.) which is a RVE the size of which is set at 1. One can observe that the greater the density is the lower the effective properties are. In other words, the clustering phenomenon undermines the reinforcement of fibres. This observation is in agreement with experimental results. Indeed, in the field of nanocomposites, experimental results show that a good dispersion of fibres provide more available area to bond with the matrix. In addition, the clusters of fibres act as stress concentrators which thwart the performances of the composite material [1,2,32].

Table 3 exhibits the influence of the fibre density on both the effective mechanical properties and the percolation threshold of the composite material. Effective Young's and shear moduli are assessed for a fibre area fraction set at 25%. One can observe that a decrease in reinforcement of effective properties is combined with

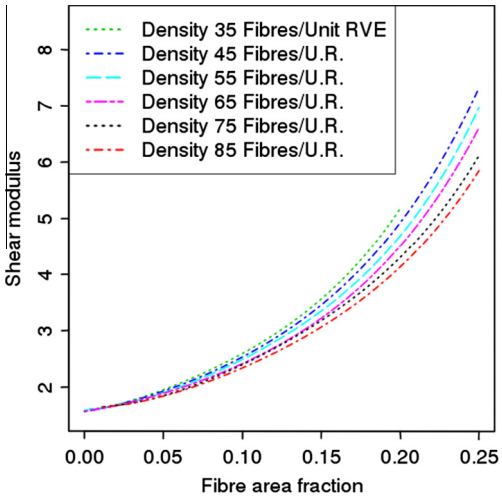

Fig. 8. Influence of the average fibre density on the effective shear modulus for an inhomogeneous dispersion of fibres.

Table 3
Influence of the fibre density on both the effective mechanical properties and the percolation threshold of the composite material.

Density (/U.R.)	35	45	55	65	75	85
E (25%, GPa)	20.81	20.80	20.11	19.17	18.44	17.63
G (25%, GPa)	8.02	7.32	6.97	6.61	6.12	5.85
Percolation threshold	0.1973	0.2081	0.2211	0.2370	0.2500	0.2609

Table 4
Influence of the area fraction of circular inclusions on both the effective mechanical properties and the percolation threshold of the composite material.

Area fraction of circles (%)	60	70	80	90	100
E (25%, GPa)	20.43	21.02	21.87	21.61	21.91
G (25%, GPa)	6.78	7.16	7.66	7.70	7.96
Percolation threshold	0.2229	0.2006	0.2007	0.1916	0.1928

an increase of the percolation threshold for a high fibre density. Thus, the percolation threshold varies from 0.1973 to 0.2609 while the fibre density varies from 35 to 85 and Young's and shear moduli decrease continuously. Therefore, the results illustrate both the narrow link between the percolation threshold and the effective mechanical properties, and the negative impact of the clustering phenomenon on the reinforcement of the material.

4.2. Impact of the area fraction of circles

The impact of the area fraction of circles on the effective mechanical properties is investigated under the hypothesis of a scale ratio set at 1. It deals with investigating the effect of the level of agglomeration on the effective mechanical properties. The study is similar to the previous one except we consider a new criterion to estimate the level of agglomeration. Thus, it consists in estimating both the effective Young's and shear moduli, and the percolation threshold for given area fractions of circles. We consider the same assumptions as previously used but we deliberately limit our survey to an area fraction of circles more than $a_c = 0.62045$ so that the probability of percolation of circles is more than 50%. Table 4 illustrates the influence of the area fraction of circles on both the effective moduli and the percolation threshold. First, one can notice that the estimated percolation threshold, for an area fraction of circles equal to the area of the RVE, is consistent with the estimated value for a homogeneous dispersion of fibres seen in Section 3.3 (0.1928 vs 0.1924). In addition, one can notice the real benefit of a homogeneous distribution of fibres on both the effective mechanical properties and the percolation threshold. Indeed, the greater the area fraction of circles is the greater the effective Young's and shear moduli are, and the lower the percolation threshold is.

4.3. Impact of the scale ratio on the percolation threshold

This section focuses on the close relationship between the state of dispersion of the fibre network, and the scale ratio. Thus, a scale ratio set at 1 induces the generation of a network of clustered fibres while a high scale ratio generates a real inhomogeneous dispersion of fibres without bundle. According to Jeulin and Moreaud [6] and Willot and Jeulin [33], the percolation threshold of a network of spherical inclusions in 3D decreases when the scale ratio increases, and tends to s^2_{hom}, where s_{hom} stands for the percolation threshold of a homogeneous distribution of spheres, when the scale ratio tends to ∞. Their investigations lead to two open questions about the effects of dispersion on the mechanical response of random fibre composites. The first issue is related to the effects of the scale ratio on the percolation threshold in the framework of randomly oriented fibres. The second one is related to the effects on the effective mechanical properties. The present investigation is dedicated to the impact of the scale ratio on the percolation threshold regardless to the effective mechanical properties.

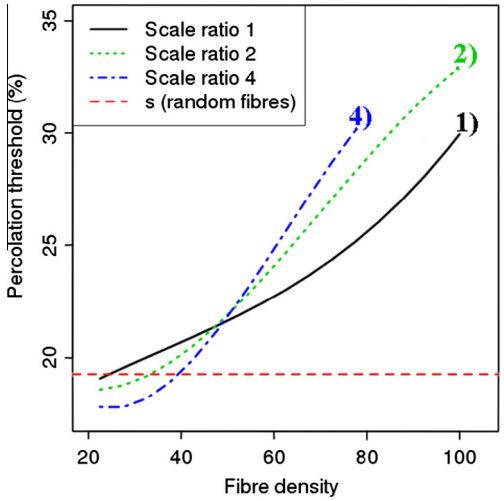

Fig. 9. Influence of the average fibre density on the percolation threshold of a network of inhomogeneously distributed fibres.

Fig. 9 exhibits the influence of the average fibre density on the percolation threshold for a scale ratio set at 1, 2 and 4 respectively. The percolation threshold of a homogeneous distribution of fibres is represented by a horizontal dashed red line. One can observe a change of behaviour around an average fibre density of 45. Thus, in a first interval for which the density is less than 45, the lower the scale ratio is the greater the percolation threshold is. The tendency is in the reverse order for a fibre density greater than 45. In addition, one can notice that for scale ratios greater than 1 the fitted curves are slightly located below the horizontal line. The issue of the size of RVE explains the phenomenon. Indeed, the RVE is larger for a higher scale ratio in order to respect the ratio between the dimensions of the pattern and the diameter of circles. Second, Fig. 10 illustrates the influence of the area fraction of circular inclusions on the percolation threshold for the same values of scale ratio. The horizontal dashed red line corresponds to the percolation threshold of a homogeneous distribution of fibres as well, and the vertical dashed pink line corresponds to the percolation threshold of a random generation of circular inclusions that was evaluated at $a_c = 0.62045$. We observe a sort of symmetry with the previous study. In the three cases, the minimum percolation threshold is provided when the area fraction of circles is close to 100%. In other words, in the present study, the percolation phenomenon is optimised when considering a homogeneous distribution of fibres. However, the investigation does not exclude a possible reduction of the percolation threshold for an area fraction of circles less than 100% and a scale ratio higher than 4. Unfortunately, our computational means do not enable us to check out this point.

4.4. Impact of the scale ratio on the effective Young's modulus

The previous investigation highlights the crucial importance of a homogeneous dispersion of fibres to keep a low percolation threshold of the fibre network. The purpose of the present investigation is to determine whether the increase of the percolation threshold is related to a real decrease in elastic properties when an inhomogeneous distribution of fibres is considered. For this

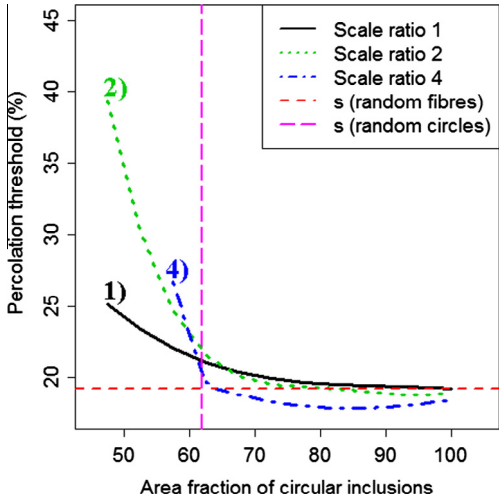

Fig. 10. Influence of the area fraction of circles on the percolation threshold of a network of inhomogeneously distributed fibres.

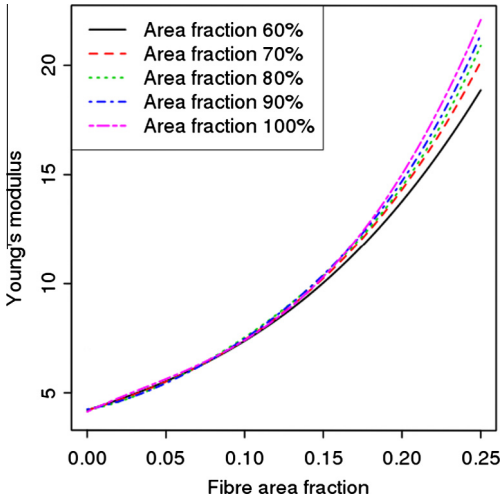

Fig. 11. Influence of the area fraction of circles on the effective Young's modulus under the hypothesis of a scale ratio set at 2.

purpose, first, we set up the same study as seen in Section 4.2 but we consider the assessment of the effective Young's modulus. In a second step, we link the present study to the previous one about the percolation threshold. Figs. 11 and 12 illustrate the evolution of the effective Young's modulus depending on the fibre area fraction for different area fractions of circles and a scale ratio set at 2 and 4 respectively. In both cases, one can notice a decrease in effective Young's modulus depending on the level of agglomeration whatever are both the fibre area fraction and the percolation threshold. Thus, the mechanical reinforcement does reflect the loss in percolation threshold observed in the previous Section 4.3.

Table 5 summarizes the influence of the scale ratio (sr) on both the effective Young's modulus (E) and the percolation threshold (s). Results are provided for different values of the area fraction of circular inclusions and a fibre area fraction set at 25% for which the discrepancies are relevant. One can notice a decrease of the mechanical property combined with an increase in percolation threshold depending on the scale ratio when the area fraction of circles is higher than a_c. However the results obtained under the hypothesis of a scale ratio set at 4 are affected by two phenomena. First, the sample of RVEs is less important, second the RVE is larger

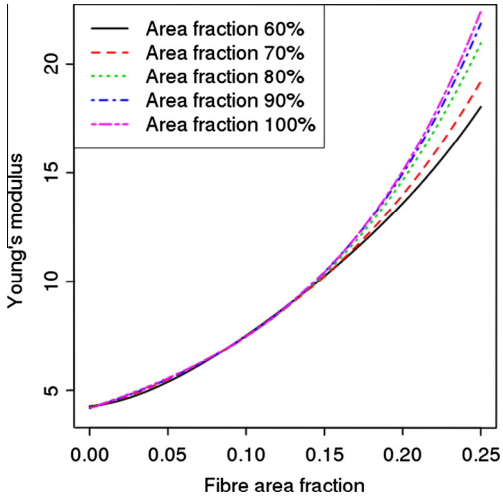

Fig. 12. Influence of the area fraction of circles on the effective Young's modulus under the hypothesis of a scale ratio set at 4.

than in the two other cases. Thus, for an area fraction of circles set at 100% which corresponds to a perfect homogeneous dispersion of fibres, the effective Young's modulus is slightly higher and the percolation threshold slightly lower in comparison with the two other configurations.

5. Effects of both the dispersion and the morphology of fibres

The present investigation is dedicated to the combined effects of dispersion and morphology of fibres. The purpose is to check out the conclusions of the previous section in the framework of specific configurations of the fibre network. We limit our study to the morphological features of orientation and aspect ratio and the scale ratio is set at 1. The modelling of the random fibre composite and the calculation of both the effective properties and the percolation threshold are performed according to the methodologies described in Sections 2 and 3. In addition, we consider the same hypotheses on the size of RVE, the ratio between the representative pattern and the inclusions, and the mechanical properties of both the fibres and the matrix as seen in Section 4.

5.1. Fibre alignment

First, a study of the impact of a network of aligned fibres on the mechanical response of a random fibre composite is set up in the framework of an inhomogeneous distribution of fibres. Large samples of RVEs in which the fibres are oriented according to a given orientation, so that the network of fibres is only composed of perfectly parallel inhomogeneities, are set up. Table 6 shows the influence of the area fraction of circular inclusions on both the Young's (E) and shear (G) moduli, and the percolation threshold of the composite material. The effective mechanical properties are estimated for a fibre area fraction set at 25%. In addition, the Young's modulus is assessed according to the preferential direction of the fibres. One can notice that the greater the area fraction of circles is, the greater the Young's modulus is, and the lower both the percolation threshold and the shear modulus are. However, the benefit in shear modulus is not significant. That is why, we can state that the conclusions of the Section 4 about the impact of an inhomogeneous dispersion of randomly oriented fibres remain similar in the framework of aligned fibres. An inhomogeneous dispersion of the heterogeneities undermines both the effective Young's modulus and the percolation of the fibre network.

Table 5
Influence of the scale ratio on both the effective Young's modulus and the percolation threshold of the composite material.

	Area fraction of circles (%)	60	70	80	90	100
sr = 1	*E* (25%, GPa)	20.43	21.02	21.61	21.87	21.91
	Percolation threshold	0.2154	0.1991	0.2026	0.1916	0.1928
	Number of realizations	16180	22756	21035	37557	25430
	Standard deviation	0.0015	0.0010	0.0016	0.0007	0.0004
sr = 2	*E* (25%, GPa)	18.86	20.16	20.89	21.40	22.07
	Percolation threshold	0.2329	0.1963	0.1920	0.1897	0.1882
	Number of realizations	6867	7602	7960	11310	13516
	Standard deviation	0.0042	0.0017	0.0008	0.0006	0.0004
sr = 4	*E* (25%, GPa)	18.03	19.19	20.96	21.85	22.41
	Percolation threshold	0.2956	0.1847	0.1793	0.1810	0.1810
	Number of realizations	701	1790	2258	3812	4096
	Standard deviation	0.0137	0.0033	0.0007	0.0003	0.0002

Table 6
Influence of the area fraction of circular inclusions on both the effective mechanical properties and the percolation threshold of the composite material.

Area fraction of circles (%)	60	70	80	90	100
E (Area fraction 25%)	40.62	45.59	49.82	52.02	53.69
G (Area fraction 25%)	2.48	2.43	2.43	2.42	2.40
Percolation threshold	0.3262	0.3150	0.3112	0.30.74	0.3047

Table 7
Influence of the area fraction of circular inclusions on both the effective Young's modulus and the percolation threshold of the composite material for different values of aspect ratio.

Area fraction of circles (%)	60	70	80	90	100
E (25%, Aspect ratio 10)	14.54	14.93	15.16	15.34	15.45
s (Aspect ratio 10)	0.3015	0.2877	0.2768	0.2751	0.2753
E (25%, Aspect ratio 20)	20.43	21.02	21.61	21.87	21.91
s (Aspect ratio 20)	0.2229	0.2006	0.2007	0.1916	0.1928
E (25%, Aspect ratio 50)	30.12	33.04	36.58	38.24	39.44
s (Aspect ratio 50)	0.1124	0.1043	0.1012	0.0983	0.0968
E (25%, Aspect ratio 100)	39.58	45.20	49.49	52.67	55.11
s (Aspect ratio 100)	0.0630	0.0581	0.0556	0.0549	0.0531

5.2. Fibre aspect ratio

A study of the combined impact of both the dispersion of the fibres and their aspect ratio is set up. We consider a network of random oriented fibres as studied in Section 4, and the fibre aspect ratio varies from 10 to 100. Table 7 shows the impact of the area fraction of circular inclusions on both the effective Young's modulus (*E*) and the percolation threshold (*s*). The Young's modulus is evaluated under the assumption of a fibre area fraction set at 25%. First, one can notice that the estimated percolation threshold obtained when considering an area fraction of circles of 100% is consistent with the values obtained in Section 3.3 in the framework of a homogeneous distribution of fibres. Then, one can observe that the greater the area fraction of circles is, the greater the effective Young's modulus is and the lower the percolation threshold is. This conclusion is in agreement with the ones of the Section 4 and the previous subsection, and remains checked out whatever the fibre aspect ratio is.

6. Conclusion

A numerical study of the effects of the state of dispersion of a 2D random fibre composite on both the effective mechanical properties and the percolation threshold has been set up. First, some calculations have been performed in the framework of a Boolean scheme of circles for which the scale ratio is set at 1 and leads to a clustered network of fibres. The results highlight the loss in both effective properties and percolation in this context whatever is the choice of the orientation and the aspect ratio of fibres. Second, the state of dispersion has been investigated by varying the scale ratio which leads to a real inhomogeneous distribution of fibres when tending to ∞. In our study, for which the scale ratio is limited to 4, our results highlight no benefit in both percolation threshold and mechanical reinforcement in comparison with a homogeneous distribution of fibres. In addition, the percolation threshold is scarcely affected by the scale ratio when considering an area fraction of fibres more than a_c.

Acknowledgments

The authors thank the conseil régional de Basse-Normandie for its financial support to Willy Leclerc's Ph.D. thesis and the High-Performance Computing Centre of Haute-Normandie (CRIHAN) for the computing means put at their disposal.

References

[1] X. Gong, J. Liu, S. Baskaran, R.D. Voise, J.S. Young, Chemistry of Materials 12 (2000) 1049–1052.
[2] L.Q. Liu, H.D. Wagner, Composites Science and Technology 65 (2005) 1861–1868.
[3] R. Guzmãn De Villoria, A. Miravete, Acta Materialia 55 (9) (2007) 3025–3031.
[4] D. Jeulin, M. Moreaud, Multi-scale simulation of random sphere aggregates – application to nanocomposites, in: 9th European Congress on Stereology and Image Analysis, Zakopane, Poland, 2005.
[5] D. Jeulin, M. Moreaud, Percolation of multi-scale fiber aggregates, in: S4G 6th International Conference, Prague, 2006.
[6] D. Jeulin, M. Moreaud, Percolation d'agrégats multi-échelles de sphéres et de fibres – application aux nanocomposites, in: Congrés matériaux, Dijon, 2006.
[7] P. Pötschke, I. Alig, S. Dudkin, Polymer 44 (2003) 5023–5030.
[8] M. Niklaus, H.R. Shea, Acta Materialia 59 (2011) 830–840.
[9] B. Fralick, E. Gatzke, S. Baxter, Probabilistic Engineering Mechanics 602 (2012) 1–8.
[10] L. Mishnaevsky Jr., K. Derrien, D. Baptiste, Composites Science and Technology 64 (12) (2004) 1805–1818.
[11] L. Mishnaevsky Jr., Acta Materiala 52 (14) (2004) 4177–4188.
[12] L. Mishnaevsky Jr., Materials Science and Engineering 407 (1–2) (2005) 11–23.
[13] W. Leclerc, P. Karamian, A. Vivet, Computational Materials Science 69 (2013) 481–493.
[14] E. Sanchez-Palencia, Non-Homogeneous Media and Vibration Theory, Berlin, vol. 127, 1980.
[15] A. Bensoussan, J.L. Lions, G.C. Papanicolaou, Asymptotic Analysis for Periodic Structures, amsterdam ed., Springer verlag, North Holland, 1978.
[16] W. Leclerc, P. Karamian, International Journal of Solids and Structures (2013), http://dx.doi.org/10.1016/j.ijsolstr.2013.04.014.
[17] D. Jeulin, Modeling heterogeneous materials by random structures, in: Invited LectureEuropean Workshop on Application of Statistics and Probabilities in Wood Mechanics. Bordeaux, 1996.
[18] D. Stoyan, K. Mecke, Space, Structure and randomness contributions in honor of georges matheron in the fields of geostatistics, random sets, and mathematical morphology, in: M. Bilodeau, F. Meyer, M. Schmitt (Eds.), The Boolean Model: from Matheron till Today, New-York, 2005, pp. 151–182.

[19] W.J. Drugan, J.R. Willis, Journal of the Mechanics and Physics of Solids 44 (4) (1996) 497–524.
[20] T. Kanit, S. Forest, I. Galliet, V. Mounoury, D. Jeulin, International Journal of Solids and Structures 40 (13–14) (2003) 3647–3679.
[21] M.J. Berger, P. Colella, Journal of Computational Physics 82 (1989) 64–84.
[22] M. Ostoja-Starzewski, Probabilistic Engineering Materials 21 (2006) 112–132.
[23] M. Ostoja-Starzewski, International Journal of Solids and Structures 35 (19) (1998) 2429–2455.
[24] K. Sab, European Journal of Mechanics 11 (5) (1992) 585–607.
[25] M.D. Rintoul, S. Torquato, Journal of Physics A 30 (1997) 585–592.
[26] J. Quintanilla, R. Ziff, Physical Review E 76 (2007) 051115.
[27] I. Balberg, C.H. Anderson, S. Alexander, N. Wagner, Physical Review B 30 (7) (1984).
[28] I. Balberg, Physical Review B 31 (6) (1985).
[29] A.L. Kalamkarov, A.V. Georgiades, S.K. Rokkam, V.P. Veedu, M.N. Ghasemi-Nejhad, International Journal of Solids and Structures 43 (22–23) (2006) 6832–6854.
[30] G.D. Seidel, D.C. Lagoudas, Mechanics of Materials 38 (8–10) (2006) 884–907 (Advances in Disordered Materials).
[31] C. Fan, Y. Liu, H. Chyanbin, Applied Physics A: Materials Science 95 (2009) 819–831.
[32] P.C. Ma, N.A. Siddiqui, G. Marom, J.K. Kim, Composites Part A: Applied Science and Manufacturing 41 (10) (2010) 1345–1367.
[33] F. Willot, D. Jeulin, Elastic and electrical behavior of some random multiscale highly-contrasted composites, International Journal of Multi-scale Computational Engineering 9 (3) (2011) 305–326.

International Journal of Solids and Structures 50 (2013) 2808–2816

Contents lists available at SciVerse ScienceDirect

International Journal of Solids and Structures

journal homepage: www.elsevier.com/locate/ijsolstr

Domain decomposition methods to evaluate effective elastic properties of random fibre composites in the framework of the double-scale homogenization

W. Leclerc, P. Karamian-Surville *

Université de Caen Basse-Normandie, UMR 6139 LMNO, F-14032 Caen, France
CNRS, UMR 6139 LMNO, F-14032 Caen, France

ARTICLE INFO

Article history:
Received 30 January 2013
Received in revised form 13 April 2013
Available online 9 May 2013

Keywords:
Domain decomposition
Homogenization
Parallel computing
RVE
Random fibre composites

ABSTRACT

The paper deals with the evaluation of the effective elastic properties in the framework of domain decomposition. The field of random fibre composites, for which the network of heterogeneities is complex and leads to several numerical shortcomings, is considered. 2D representative volume elements (RVEs) of the composite are generated and some elastic properties are estimated with the help of the double-scale homogenization. Such methodology is reliable but turns out to be potentially inefficient due to the required size of RVEs. Two adaptations of domain decomposition methods in the framework of double-scale homogenization are proposed to drastically reduce the calculation costs: a Schur complement method, and a mixed Schur complement and FETI-1 method. Several numerical tests are performed which highlight reliability and efficiency of the first one in the present context.

1. Introduction

Fibre composites could lead to interesting applications in the industrial field. Their lightness associated to a high stiffness, a good electrical conductivity and a low cost of production are major assets which arouse a great interest in the engineering community. Random fibre composites are composed of randomly distributed and oriented fibres. Experimental measurements are sometimes difficult to set up when, for example, we consider very small scales as in nanocomposites field. In the present paper, the framework of a numerical simulation of random fibre composites is considered in the prospect of the assessment of effective elastic properties. Such a kind of process requires the generation of representative volume elements (RVEs). An RVE can be defined as a volume V large enough to take into account enough informations on the microstructure of the medium (Hill, 1963; Hashin, 1983) and sufficiently small to limit the calculation cost and respect a minimum scale ratio with the macroscopic material (Kanit et al., 2003). Consequently, a key issue is related to the assessment of the dimensions of the RVE which strongly impact the validity of the numerical evaluation. Two methodologies are possible (1) One can construct a large RVE which includes a large number of heterogeneities, inclusions, voids, grains, fibres, . . .(2) One can generate a sampling of small RVEs for which effective properties are obtained from averaging the scope of results (Kanit et al., 2003; Pelissou et al., 2009). The second approach is known as being the most efficient (Leclerc et al., 2012; Leclerc et al., 2013) since large RVEs cannot be handled. However, a great care must be taken when choosing the dimensions of the small cells. Indeed an RVE has to be large enough to avoid a bias introduced by the boundary conditions (Sab, 1992; Ostoja-Starzewski, 1998) and ensure the accuracy of the macroscopic response (Drugan and Willis, 1996).

In the present work, our choice is to consider the second approach for which the size of the RVE is assessed according to the methodology of Kanit et al. (2003). A random draw of a complete set of morphological parameters, namely the length, diameter, orientation and spatial distribution of fibres, is set up to generate one RVE. In addition, intersections between two or more fibres are allowed which leads to a strongly entangled network of heterogeneities. Such a geometrical complexity requires a pixel-based finite element simulation to get round the tricky step of the mesh generation (Mishnaevsky, 2005). We consider the model with an n-order approximate geometry which was studied in this context and exhibited interesting results in calculation time (Leclerc et al., 2012; Leclerc et al., 2013). The basic idea consists in conceiving the mesh according to a structured grid of quadrangular elements the size of which is equal to the effective diameter of fibres. Thus, the critical shortcoming related to the complex geometry of the network of heterogeneities is a priori solved.

However, the required size of simulation grids are sometimes really important. For example, when the spatial distribution is

* Corresponding author at: Université de Caen Basse-Normandie, UMR 6139 LMNO, F-14032 Caen, France. Tel.: +33 2 31 56 74 61; fax: +33 2 31 56 73 20.
E-mail addresses: willy.leclerc@unicaen.fr (W. Leclerc), philippe.karamian@unicaen.fr (P. Karamian-Surville).

0020-7683/$ - see front matter © 2013 Elsevier Ltd. All rights reserved.
http://dx.doi.org/10.1016/j.ijsolstr.2013.04.014

inhomogeneous which leads to consider a large representative pattern to efficiently take into account the microstructure of the network of fibres (Jeulin and, 2005; Jeulin and Moreaud, 2006; Jeulin and Moreaud, 2006). The efficiency of the method is then drastically reduced causing the explosion of the calculation cost. One obvious solution in the current context of the fast development of multi-core computations is to use parallel strategies. Domain decomposition provides a solid mathematical framework which is modified to suit such a kind of process. Non-overlapping domain decomposition methods such as Schur complement (Agoshkov and Lebedev, 1985) and FETI-1 methods (Fahrat and Roux, 1227; Fahrat and Roux, 1994) have been extensively studied in this purpose during the last two decades. Thus, their robustness and scalability have been demonstrated and have led to numerous practical applications. Their great advantage is to reduce a global problem to an interface problem for which the degrees of freedom number is widely less important and the conditioning is improved. The Schur complement method is based on the displacements while the FETI-1 focuses on the Lagrange multipliers. Each concept has its own advantages and drawbacks.

The aim of the paper is to adapt the Schur complement and FETI-1 methods in the framework of the periodic double-scale homogenization (Bensoussan et al., 1978; Sanchez-Palencia, 1980). This latter is a powerful tool to assess effective elastic properties, particularly in the fibre composites field. Both domain decomposition methods are modified in such a manner that they directly provide mechanical coefficients such as Young's and shear moduli ones. Some numerical tests are performed on a set of 100 RVEs which are randomly generated depending on a complete set of morphological parameters. Each square representative pattern is subdivided into several similar subdomains for which the continuity on the inner interfaces and the periodicity on the outer ones are ensured. First the reliability of both methods is sequentially investigated. Results highlight their suitability in the context of high contrast heterogeneous media. Second C++ parallel algorithms are set up with the help of MPI libraries. Both issues of efficiency and ideal number of subdivisions are discussed. The paper is outlined as follows, (1) a reminder of both the theoretical framework of the double-scale homogenization and the associated optimization problem are done (2) A description of both modified domain decomposition methods is performed (3) Numerical results are provided to evaluate their reliability and efficiency in the framework of random fibre composites with a high contrast of properties.

2. Double-scale homogenization

This section is devoted to a reminder of the theoretical framework of the double-scale homogenization. We describe both the asymptotic principle which the method is based on and provide the associated variational formulation. Expression of homogenized elastic properties is provided in the context of domain decomposition.

2.1. Setting up

The variational formulation presented and proposed in this section is a generalization of the technique for the calculation of homogenized coefficients (Débordes, 1986) in an asymptotic framework (Bensoussan et al., 1978; Sanchez-Palencia, 1980). The basic idea consists in introducing an additional fictitious variable in test functions, which leads to a symmetric bilinear form taking into account two unknowns related to (1) the macroscopic strain field E (2) the microscopic strain field $e_{kly}(\mathbf{u})$. The artifice allows one to directly evaluate homogenized coefficients, but also amounts to introducing a field representing the macroscopic stress one Σ. Therefore, this term becomes a changeable data for the variational problem and has to be imposed in such a clever way so that this one leads directly to homogenized coefficients. The choice of the variational formulation is related to the fact that, as we will show thereafter, this one is well adapted to the domain decomposition technique. This remains true providing that great care is taken in the treatment of periodic boundary conditions and internal nodes common to different subdomains.

In the general context of periodic homogenization, strain e and stress σ fields are supposed Y-periodic where Y is a unit cell (Bornert et al., 2001; Magoariec et al., 1675). The strain field $e_{kl}(\mathbf{u})$ is then described as the sum of E regardless to local fluctuations, and a Y-periodic displacement $\mathbf{u}^{per}$ as follows,

$$e_{kl}(\mathbf{u}) = E + e_{kl}(\mathbf{u}^{per}) \tag{1}$$

where the average value of $e_{kl}(\mathbf{u}^{per})$ over Y is equal to zero.

In the context of linear elasticity and a periodic multi-scale approach, a localization problem for which E is given, leads to the following equation,

$$\begin{cases} -\mathrm{div}\,\sigma(\mathbf{u}^{\varepsilon}) = \mathbf{f} \quad \text{in} Y \ (+\text{periodic b.c. on } \partial Y) \\ \sigma_{ij}(\mathbf{u}^{\varepsilon}) = C^{\varepsilon}_{ijkh} e_{kh}(\mathbf{u}^{\varepsilon}) \end{cases} \tag{2}$$

where C^{ε}_{ijkl} is the local stiffness tensor, $\mathbf{f}$ is the loading and b.c. stands for boundary conditions. ∂Y represents the boundary of Y. From a theoretical point of view, ε is a positive real parameter which is supposed to tend to zero. Practically, this one is a very small parameter ($\varepsilon < 10^{-3}$) which is the ratio between a first scale called macroscopic and denoted as x, and a second one called microscopic and denoted as y. The displacement is denoted as $\mathbf{u}^{\varepsilon}$ expanded according to the ε parameter. We seek for an asymptotic expansion as the form,

$$\mathbf{u}^{\varepsilon}(x,y) = \mathbf{u}^0(x) + \varepsilon \mathbf{u}^1(x,y) + \varepsilon^2 \mathbf{u}^2(x,y) + o(\varepsilon^2) \tag{3}$$

Hence, after expanding and reordering, we deduce the following expression of the strain tensor,

$$\begin{aligned} e_{kl}(\mathbf{u}^{\varepsilon}) &= e_{klx}(\mathbf{u}^{\varepsilon}) + \frac{1}{\varepsilon} e_{kly}(\mathbf{u}^{\varepsilon}) \\ &= \underbrace{(e_{klx}(\mathbf{u}^0) + e_{kly}(\mathbf{u}^1))}_{e^0_{kl}} + \varepsilon \underbrace{(e_{klx}(\mathbf{u}^1) + e_{kly}(\mathbf{u}^2))}_{e^1_{kl}} + o(\varepsilon) \end{aligned} \tag{4}$$

with,

$$e_{klx}(\mathbf{u}^h(x)) = \frac{1}{2}\left[\frac{\partial u^h_k}{\partial x_l} + \frac{\partial u^h_l}{\partial x_k}\right], \quad e_{kly}(\mathbf{u}^h(x)) = \frac{1}{2}\left[\frac{\partial u^h_k}{\partial y_l} + \frac{\partial u^h_l}{\partial y_k}\right] \tag{5}$$

where h denotes the h-th component of the asymptotic expansion of $\mathbf{u}^{\varepsilon}$. In addition,

$$\sigma_{ij}(\mathbf{u}^{\varepsilon}) = \underbrace{C^{\varepsilon}_{ijkl}(e_{klx}(\mathbf{u}^0) + e_{kly}(\mathbf{u}^1))}_{\sigma^0_{ij}} + \varepsilon \underbrace{C^{\varepsilon}_{ijkl}(e_{klx}(\mathbf{u}^1) + e_{kly}(\mathbf{u}^2))}_{\sigma^1_{ij}} + o(\varepsilon) \tag{6}$$

thus,

$$e^h_{kl} = e_{klx}(\mathbf{u}^h) + e_{kly}(\mathbf{u}^{h+1}) \quad \forall h \in \mathbb{N} \tag{7}$$

$$\sigma^h_{ij} = C^{\varepsilon}_{ijkl}(e_{klx}(\mathbf{u}^h) + e_{kly}(\mathbf{u}^{h+1})) \quad \forall h \in \mathbb{N} \tag{8}$$

Let us remark that e^0_{kl} is then strongly analogous to the formulation of $e_{kl}(\mathbf{u})$ described in Eq. (1). Indeed, one can see $e_{klx}(\mathbf{u}^0)$ as the macroscopic strain field E and $e_{kly}(\mathbf{u}^1)$ as the microscopic periodic strain field the average over Y of which is equal to 0. In other words, the first order of the asymptotic expansion of $e_{kl}(\mathbf{u}^{\varepsilon})$ leads to the classical formulation of the strain field in periodic homogenization theory.

2.2. Homogenized coefficients

In the present work, we consider a second order asymptotic expansion of Eq. (2). The process leads to two formulations for each scale of the material. The first one called macroscopic and related to order (ε^0), in other words ε free terms, the equation reads,

$$-\mathrm{div}_x\sigma^0 - \mathrm{div}_y\sigma^1 = \mathbf{f} \tag{9}$$

then, by averaging on a Y periodic domain, we obtain,

$$-\mathrm{div}_x\tilde{\sigma}^0 - \frac{1}{|Y|}\int_{\partial Y}\sigma^1\mathbf{n}\mathrm{d}\Sigma_Y = \tilde{\mathbf{f}} \tag{10}$$

for which, $\mathbf{n}$ is the outer normal to ∂Y,

$\tilde{\cdot} = \frac{1}{|Y|}\int_Y .\mathrm{d}Y$ and $\frac{1}{|Y|}\int_{\partial Y}\sigma^1\mathbf{n}\mathrm{d}\Sigma_Y = 0$ due to periodicity. Finally, the macroscopic problem consists in finding $\mathbf{u}^0(x)$ such as,

$$\begin{cases} -\mathrm{div}_x\tilde{\sigma}^0(\mathbf{u}^0) = \tilde{\mathbf{f}} \\ \tilde{\sigma}^0_{ij}(\mathbf{u}^0) = C^{hom}_{ijkl}e^0_{kl}(\mathbf{u}^0) \end{cases} \tag{11}$$

One can notice a strong analogy between Eqs. (2) and (11). Hence the idea to find C^{hom}_{ijkl} the tensor of homogenized coefficients linking $\bar{\sigma}^0$ to e^0_{kl}. On the other hand a microscopic formulation of Eq. (2) related to order (ε^{-1}) is as follows,

$$-\mathrm{div}_y\tilde{\sigma}^0 = \mathbf{0} \tag{12}$$

and,

$$-\frac{\partial}{\partial y_j}\tilde{[}C^{\varepsilon}_{ijkl}(e_{klx}(\mathbf{u}^0(x)) + e_{kly}(\mathbf{u}^1(x,y)))\tilde{]} = 0 \tag{13}$$

Eq. (13) leads to consider $\mathbf{u}^1(x,y)$ as follows,

$$\mathbf{u}^1(x,y) = e_{klx}(\mathbf{u}^0(x))\boldsymbol{\kappa}^{kl}(y) \tag{14}$$

where $\boldsymbol{\kappa}^{kl}(y)$ is a Y-periodic function which only depends on the microscopic variable y. Thus, one can rewrite Eq. (13) depending on $\boldsymbol{\kappa}^{kl}(y)$ as follows,

$$-\frac{\partial}{\partial y_j}\tilde{[}C^{\varepsilon}_{ijpq}(\delta^k_p\delta^l_q + e_{pqy}(\boldsymbol{\kappa}^{kl}(y)))e_{klx}(\mathbf{u}^0(x))\tilde{]} = 0 \tag{15}$$

As $\mathbf{u}^0$ only depends on the macroscopic variable x, Eq. (15) can be rewritten as follows,

$$-\frac{\partial}{\partial y_j}[\tilde{[}C^{\varepsilon}_{ijpq}(\delta^k_p\delta^l_q + e_{pqy}(\boldsymbol{\kappa}^{kl}(y)))\tilde{]}\tilde{e}_{klx}(\mathbf{u}^0(x))] = 0 \tag{16}$$

hence, we can extract the following expression of homogenized coefficients,

$$C^{hom}_{ijkl} = \frac{1}{|Y|}\int_Y C_{ijpq}(y)[\delta^k_p\delta^l_q + e_{pqy}(\boldsymbol{\kappa}^{kl}(y))]\mathrm{d}Y \tag{17}$$

where the tensor is the sum of the mean of properties and a corrective term related to the local disruption at the microscopic scale. In addition, one must keep in mind that we have,

$$C_{ijpq}(y) = C^{\varepsilon}_{ijpq}(x) \tag{18}$$

2.3. Variational considerations for practical applications

We intend to show how one can practically evaluate effective elastic properties. Let us start with Eq. (12), we have,

$$-\frac{1}{|Y|}\int_Y\frac{\partial}{\partial_j}(\sigma^0_{ij})\boldsymbol{\psi}^{mn}(y)\mathrm{d}Y = 0 \quad \forall\boldsymbol{\psi}^{mn}\in\mathbb{H}^1_{per}(Y) \tag{19}$$

with,

$$\mathbb{H}^1_{per}(Y) = \{\boldsymbol{\psi}^{mn}\in\mathbb{L}^2/\mathbf{grad}_y\boldsymbol{\psi}^{mn}\in\mathbb{L}^2(+\text{periodic b.c.})\} \tag{20}$$

an integration by parts provides due to the symmetry,

$$\frac{1}{|Y|}\int_Y\sigma^0_{ij}e_{ijy}(\boldsymbol{\psi}^{mn})\mathrm{d}Y = 0 \quad \forall\boldsymbol{\psi}^{mn}\in\mathbb{H}^1_{per}(Y) \tag{21}$$

reporting the expression of σ^0_{ij} we then have,

$$\frac{1}{|Y|}\int_Y C_{ijpq}(y)(e_{pqx}(\mathbf{u}^0(x)) + e_{pqy}(\mathbf{u}^1(x,y)))e_{ijy}(\boldsymbol{\psi}^{mn})\mathrm{d}Y = 0 \quad \forall\boldsymbol{\psi}^{mn}\in\mathbb{H}^1_{per}(Y) \tag{22}$$

and, from Eq. (14), Eq. (22) reads,

$$\frac{1}{|Y|}\int_Y C_{ijpq}(y)(\delta^k_p\delta^l_q + e_{pqy}(\boldsymbol{\kappa}^{kl}))e_{ijy}(\boldsymbol{\psi}^{mn})e_{klx}(\mathbf{u}^0(x))\mathrm{d}Y = 0 \quad \forall\boldsymbol{\psi}^{mn}\in\mathbb{H}^1_{per}(Y) \tag{23}$$

Then Eq. (23) can be rewritten as follows,

$$\frac{1}{|Y|}\int_Y C_{ijpq}(y)(\delta^k_p\delta^l_q + e_{pqy}(\boldsymbol{\kappa}^{kl}))(\delta^m_i\delta^n_j + e_{ijy}(\boldsymbol{\psi}^{mn}))\mathrm{d}Y - \frac{1}{|Y|}\int_Y C_{ijpq}(y)(\delta^k_p\delta^l_q + e_{pqy}(\boldsymbol{\kappa}^{kl}))\delta^m_i\delta^n_j\mathrm{d}Y = 0 \quad \forall\boldsymbol{\psi}^{mn}\in\mathbb{H}^1_{per}(Y) \tag{24}$$

hence,

$$\begin{aligned}&\frac{1}{|Y|}\int_Y C_{ijpq}(y)(\delta^k_p\delta^l_q + e_{pqy}(\boldsymbol{\kappa}^{kl}))(\delta^m_i\delta^n_j + e_{ijy}(\boldsymbol{\psi}^{mn}))\mathrm{d}Y \\ &= \frac{1}{|Y|}\int_Y C_{ijpq}(y)(\delta^k_p\delta^l_q + e_{pqy}(\boldsymbol{\kappa}^{kl}))\delta^m_i\delta^n_j\mathrm{d}Y \\ &= \frac{1}{|Y|}\int_Y C_{mnpq}(y)(\delta^k_p\delta^l_q + e_{pqy}(\boldsymbol{\kappa}^{kl}))\mathrm{d}Y = C^{hom}_{mnkl} \quad \forall\boldsymbol{\psi}^{mn} \\ &\in\mathbb{H}^1_{per}(Y)\end{aligned} \tag{25}$$

Practically, Eq. (25) can not be directly used to determine effective properties since the right hand side C^{hom}_{mnkl} is unknown. An artifice consists in introducing $P^{k'l'}_{kl}$ and $Q^{m'n'}_{mn}$ two tensors which do not depend on the microscopic parameter y. Let us evaluate the product $C^{hom}_{mnkl}P^{k'l'}_{kl}Q^{m'n'}_{mn}$ as follows,

$$\begin{aligned}C^{hom}_{mnkl}P^{k'l'}_{kl}Q^{m'n'}_{mn} &= \frac{1}{|Y|}\int_Y C_{ijpq}[\delta^k_p\delta^l_qP^{k'l'}_{kl} + e_{pqy}(P^{k'l'}_{kl}\boldsymbol{\kappa}^{kl})][\delta^m_i\delta^n_jQ^{m'n'}_{mn} \\ &\quad + e_{ijy}(Q^{m'n'}_{mn}\boldsymbol{\psi}^{mn})]\mathrm{d}Y \\ &= \frac{1}{|Y|}\int_Y C_{ijpq}[P^{k'l'}_{pq} + e_{pqy}(P^{k'l'}_{kl}\boldsymbol{\kappa}^{kl})][Q^{m'n'}_{ij} \\ &\quad + e_{ijy}(Q^{m'n'}_{mn}\boldsymbol{\psi}^{mn})]\mathrm{d}Y \quad \forall\boldsymbol{\psi}^{mn} \\ &\in\mathbb{H}^1_{per}(Y)\end{aligned} \tag{26}$$

Let us introduce $\boldsymbol{\omega}^{k'l'}$ and $\boldsymbol{\phi}^{m'n'}$ be two unknowns equal to $(P^{k'l'}_{kl}\boldsymbol{\kappa}^{kl})$ and $(Q^{m'n'}_{mn}\boldsymbol{\psi}^{mn})$ respectively. It is verified that both only depend on microscopic parameter y since $P^{k'l'}_{kl}$ and $Q^{m'n'}_{mn}$ are constant tensors. Then, Eq. (26) can be expressed as follows,

$$\begin{aligned}C^{hom}_{mnkl}P^{k'l'}_{kl}Q^{m'n'}_{mn} &= \underbrace{C^{hom}_{ijpq}P^{k'l'}_{pq}}_{\Sigma^{k'l'}_{ij}}Q^{m'n'}_{ij} \\ &= \frac{1}{|Y|}\int_Y C_{ijpq}[P^{k'l'}_{pq} + e_{pqy}(\boldsymbol{\omega}^{k'l'})][Q^{m'n'}_{ij} \\ &\quad + e_{ijy}(\boldsymbol{\phi}^{m'n'})]\mathrm{d}Y \quad \forall\boldsymbol{\phi}^{mn} \\ &\in\mathbb{H}^1_{per}(Y)\end{aligned} \tag{27}$$

From Equations (12) and (16), one can notice that $\Sigma^{k'l'}_{ij}$ tensor is similar to the stress one $\tilde{\sigma}^0_{ij}$. After renaming k',l',m' and n' variables into k,l,m and n, Eq. (27) leads to the following variational formulation,

$$\begin{cases}\text{Find } (\boldsymbol{\omega}^{kl}, P^{kl}_{pq})\in\mathbb{H}^1_{per}(Y)\times\mathbb{L}^2 \text{ such that} \\ \frac{1}{|Y|}\int_Y C_{ijpq}[P^{kl}_{pq} + e_{pqy}(\boldsymbol{\omega}^{kl})][Q^{mn}_{ij} + e_{ijy}(\boldsymbol{\phi}^{mn})]\mathrm{d}Y = \Sigma^{kl}_{ij}Q^{mn}_{ij} \\ \forall(\boldsymbol{\phi}^{mn}, Q^{mn}_{ij})\in\mathbb{H}^1_{per}(Y)\times\mathbb{L}^2 \quad \& \ i,j,k,l,m,n,p,q\in\{1,2,3\}^8\end{cases} \tag{28}$$

The right hand side can be chosen in such a manner that it directly provides the compliance tensor which is the inverse of the effective stiffness tensor C^{hom}_{ijkl}. Indeed, we have,

$$C^{hom}_{ijpq} P^{kl}_{pq} = \Sigma^{kl}_{ij} \tag{29}$$

The choice of Σ^{kl}_{ij} is independent from C^{hom}_{ijpq} and P^{kl}_{pq}. Consequently, we consider the identity tensor $\delta^k_i \delta^l_j$ for which P^{kl}_{pq} is the effective compliance tensor. Thus, the variational formulation (28) directly provides homogenized coefficients. Practically, 6 *kl* independent systems in 3D (3 in 2D) have to be solved to completely determine P^{kl}_{pq} tensor.

2.4. Optimization problem

Some bilinear (a) and linear (b) forms can be associated to the variational formulation (28) as follows,

$$a((\boldsymbol{\phi}^{mn}, Q^{mn}_{pq}), (\boldsymbol{\phi}^{mn}, Q^{mn}_{ij})) = \frac{1}{|Y|}\int_Y C_{ijpq}[Q^{mn}_{pq} + e_{pqy}(\boldsymbol{\phi}^{mn})][Q^{mn}_{ij} + e_{ijy}(\boldsymbol{\phi}^{mn})]\mathrm{d}Y \tag{30}$$

and,

$$b((\boldsymbol{\phi}^{mn}, Q^{mn}_{ij})) = ((\mathbf{0}^{kl}, \delta^k_i \delta^l_j).(\boldsymbol{\phi}^{mn}, Q^{mn}_{ij})) = \delta^k_i \delta^l_j Q^{mn}_{ij} \tag{31}$$

Continuity and coercivity of the symmetric bilinear form a, and continuity of the linear form are checked out without difficulty knowing the positivity of C_{ijpq} and $\delta^k_i \delta^l_j$. Consequently, we satisfy the hypotheses of the Lax–Milgram theorem, and we obtain existence and uniqueness of the solution of the variational formulation (28). The solution $(\boldsymbol{\omega}^{kl}, P^{kl}_{pq})$is obtained from the following optimization problem,

$$(\boldsymbol{\omega}^{kl}, P^{kl}_{pq}) = \underset{(\boldsymbol{\phi}^{mn}, Q^{mn}_{ij}) \in \mathbb{H}^1_{per}(Y)\times\mathbb{L}^2}{Arg\ min} \quad \mathcal{J}(\boldsymbol{\phi}^{mn}, Q^{mn}_{ij}) \tag{32}$$

where $\mathcal{J}(\boldsymbol{\phi}^{mn}, Q^{mn}_{ij})$ is a convex function the expression of which is as follows,

$$\mathcal{J}(\boldsymbol{\phi}^{mn}, Q^{mn}_{ij}) = \frac{1}{2} a((\boldsymbol{\phi}^{mn}, Q^{mn}_{pq}), (\boldsymbol{\phi}^{mn}, Q^{mn}_{ij})) - b((\boldsymbol{\phi}^{mn}, Q^{mn}_{ij})) \tag{33}$$

2.5. Finite element discretization

A finite element discretization is built from variational formulation (28) to solve the optimization Problem (32). First local strain tensor $e_{ijy}(\boldsymbol{\phi}^{mn})$ is discretized as $[e]$,

$$[e] = B[\boldsymbol{\phi}] \tag{34}$$

hence we have,

$$[\boldsymbol{\omega}]^t \underbrace{\frac{1}{|Y|}\int_Y B^t C B \mathrm{d}Y}_{K}[\boldsymbol{\phi}] + [P]^t \underbrace{\frac{1}{|Y|}\int_Y C B \mathrm{d}Y}_{KE^t}[\boldsymbol{\phi}] + [\boldsymbol{\omega}]^t \underbrace{\frac{1}{|Y|}\int_Y B^t C \mathrm{d}Y}_{KE}[Q] + [P]^t \underbrace{\frac{1}{|Y|}\int_Y C \mathrm{d}Y}_{E}[Q] = \mathbb{I}_6[Q] \tag{35}$$

where $\mathbb{I}_6$ is the 6×6 identity tensor. K is the local stiffness tensor and E represents the mean of properties obtained without taking into account the corrective terms related to the microstructure. KE represents the coupling between both previous tensors. Finally the discretization leads to the following matrix system,

$$\begin{bmatrix} K & KE^t \\ KE & E \end{bmatrix} \begin{bmatrix} \boldsymbol{\omega}^{kl} \\ P^{kl}_{ij} \end{bmatrix} = \begin{bmatrix} \mathbf{0}^{kl} \\ \delta^k_i \delta^l_j \end{bmatrix} \tag{36}$$

The resolution of the previous matrix system is numerically performed for each *kl* problem. This directly provides P^{kl}_{ij} which is the effective compliance tensor.

3. Domain decomposition methods

Adaptations of Schur complement and FETI-1 methods are set up to yield homogenized elastic properties according to the double-scale homogenization. First both generation and partitioning of RVEs are described. Second a description of both modified methods is provided.

3.1. Generation of RVEs and partitioning

2D square RVEs are generated according to a random draw of a complete set of parameters. Each one corresponds to a morphological feature of the fibres, namely the length, diameter, orientation and spatial location. We suppose no curvature and the overlapping between two or more fibres is allowed. A preliminary treatment of each representative pattern enables one to ensure the periodicity of the cell. A direct mesh generation according to the boundaries of the network of heterogeneities is difficult because of its strongly entangled form. Hence, we preferred to use the model with an n-order approximate geometry to build meshes (Leclerc et al., 2012; Leclerc et al., 2013). Such a concept is suitable in the framework of domain decomposition due to the uniformity of the mesh. The main drawback of a double-scale process is intimately connected to the issue of the required size of RVEs. Two strategies are possible to choose the dimensions of the cell. We can set up either a small number of large patterns or a large sample of small ones. Some investigations exhibited that the second paradigm is more efficient in the present framework (Leclerc et al., 2013). However it turns out that the calculation cost is sometimes prohibitive whatever the choice of strategy is. The drawback is more noticeable when the density of fibres is important or the spatial distribution is inhomogeneous for which a higher minimum size of RVE is required.

A possible way to reduce the calculation cost is to subdivide the representative patterns and consider a parallel computing in the framework of domain decomposition. In the present work, the partitioning is performed by evenly subdividing RVEs into several square subdomains. Such a kind of process is realized without remeshing or, roughly speaking, by splitting the initial grid according to the boundaries of each domain. A subsequent treatment on the boundaries enables one to ensure the continuity of the medium on the inner interfaces. The similarity between the RVE and each subdomain leads us to denote them as sub-RVEs. Fig. 1 illustrates an example of partitioning of an RVE into four sub-RVEs. One can notice that we consider non-overlapping domains and both the periodicity and the continuity at the interfaces are checked out. Γ^i designates the set of inner boundaries, and Γ^o the set of outer boundaries. $\Gamma = \Gamma^i \cap \Gamma^o$ represents the gathering of both previous sets. Ω_n represents the area of the n-th subdomain.

3.2. Schur complement method

In a first approach, we consider the primal Schur complement method (Agoshkov and Lebedev, 1985) to evaluate effective properties of the composite material. The method is adapted to take into account additional terms related to homogenized coefficients. The process consists in reducing the initial problem to the interface one taking into account both the outer and inner boundaries, and the effective coefficients. The initial problem

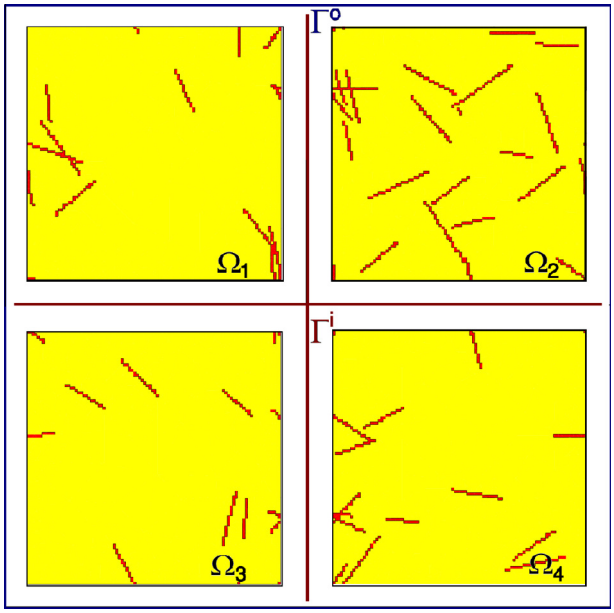

Fig. 1. Partitioning of an RVE into four sub-RVEs

consists in a renumbering of the matrix system (36) in the framework of domain decomposition. Thus, in the hypothesis of a subdivision into N sub-RVEs, K stiffness matrix is rewritten as follows,

$$K = \begin{array}{c} \\ 1 \\ \vdots \\ i \\ \vdots \\ N \\ \Gamma \end{array} \begin{array}{c} \begin{array}{cccccc} 1 & \dots & i & \dots & N & \Gamma \end{array} \\ \begin{bmatrix} K_1 & 0 & \dots & \dots & 0 & K_{\Gamma 1}^t \\ 0 & \ddots & \ddots & & \vdots & \vdots \\ \vdots & \ddots & K_i & \ddots & \vdots & K_{\Gamma i}^t \\ \vdots & & \ddots & \ddots & 0 & \vdots \\ 0 & \dots & \dots & 0 & K_N & K_{\Gamma N}^t \\ K_{\Gamma 1} & \dots & K_{\Gamma i} & \dots & K_{\Gamma N} & K_{\Gamma\Gamma} \end{bmatrix} \end{array} \tag{37}$$

Thus Stiffness matrix K is split into several K_i matrices for which i corresponds to the number of the subdomain. K_i is only composed of inner contributions. Indeed, interface contributions are gathered together in a $K_{\Gamma i}$ matrix for which Γ designates indistinctly both outer and inner interfaces. One must keep in mind that each interface node is only numbered once whatever the number of subdomains it belongs to. Moreover, $KE, \boldsymbol{\omega}^{kl}$ and $\mathbf{0}^{kl}$ are then as follows,

$$KE^t = \begin{bmatrix} KE_1^t \\ \vdots \\ KE_i^t \\ \vdots \\ KE_N^t \\ KE_\Gamma^t \end{bmatrix} \quad \boldsymbol{\omega}^{kl} = \begin{bmatrix} \boldsymbol{\omega}_1^{kl} \\ \vdots \\ \boldsymbol{\omega}_i^{kl} \\ \vdots \\ \boldsymbol{\omega}_N^{kl} \\ \boldsymbol{\omega}_\Gamma^{kl} \end{bmatrix} \quad \mathbf{0}^{kl} = \begin{bmatrix} \mathbf{0}_1^{kl} \\ \vdots \\ \mathbf{0}_i^{kl} \\ \vdots \\ \mathbf{0}_N^{kl} \\ \mathbf{0}_\Gamma^{kl} \end{bmatrix} \tag{38}$$

where $\boldsymbol{\omega}_i^{kl}$ is the microscopic displacement related to the ith subdomain, and $\boldsymbol{\omega}_\Gamma^{kl}$ the one related to the nodes located on the boundary Γ. The renumbering is easily performed whatever is the number of sub-RVEs. Thus, in the example of Fig. 1 for which we consider 4 ones, the renumbered matrix system is as follows,

$$\begin{bmatrix} K_1 & 0 & 0 & 0 & K_{\Gamma 1}^t & KE_1^t \\ 0 & K_2 & 0 & 0 & K_{\Gamma 2}^t & KE_2^t \\ 0 & 0 & K_3 & 0 & K_{\Gamma 3}^t & KE_3^t \\ 0 & 0 & 0 & K_4 & K_{\Gamma 4}^t & KE_4^t \\ K_{\Gamma 1} & K_{\Gamma 2} & K_{\Gamma 3} & K_{\Gamma 4} & K_\Gamma & KE_\Gamma^t \\ KE_1 & KE_2 & KE_3 & KE_4 & KE_\Gamma & E \end{bmatrix} \begin{bmatrix} \boldsymbol{\omega}_1^{kl} \\ \boldsymbol{\omega}_2^{kl} \\ \boldsymbol{\omega}_3^{kl} \\ \boldsymbol{\omega}_4^{kl} \\ \boldsymbol{\omega}_\Gamma^{kl} \\ P_{ij}^{kl} \end{bmatrix} = \begin{bmatrix} \mathbf{0}_1^{kl} \\ \mathbf{0}_2^{kl} \\ \mathbf{0}_3^{kl} \\ \mathbf{0}_4^{kl} \\ \mathbf{0}_\Gamma^{kl} \\ \delta_i^k \delta_j^l \end{bmatrix} \tag{39}$$

One can notice that E, the average of properties without corrective terms directly appears without being subdivided. Indeed, let us introduce E_i the counterpart of E for the i-th subdomain. We have,

$$E_i = \frac{1}{|\Omega_i|} \int_{\Omega_i} C \mathrm{d}Y \tag{40}$$

however,

$$E = \frac{1}{|\Omega|} \sum_i \int_{\Omega_i} C \mathrm{d}Y = \frac{1}{|\Omega|} \sum_i |\Omega_i| E_i \tag{41}$$

Thus the renumbering leads to directly take into account E tensor as the average of E_i tensors. Such decomposition directly provides P_{ij}^{kl} which corresponds to the effective compliance tensor associated to the complete domain. System (39) is subsequently reduced to an interface problem via the Schur complement matrix S. The purpose is to decrease the number of unknowns to the sum of the degrees of freedom on the boundaries, and the number of homogenized terms. The new system is as follows,

$$\begin{cases} S\mathbf{u}_\Gamma = \tilde{\mathbf{f}}_\Gamma^{kl} \\ S = \tilde{K}_\Gamma - \sum_i \tilde{K}_{\Gamma i} K_i^{-1} \tilde{K}_{\Gamma i}^t \end{cases} \tag{42}$$

where expressions of $\tilde{K}_{\Gamma i}, \tilde{K}_\Gamma, \tilde{\mathbf{f}}_\Gamma^{kl}$ and $\mathbf{u}_\Gamma$ are as follows,

$$\tilde{K}_{\Gamma i} = \begin{bmatrix} K_{\Gamma i} \\ KE_i \end{bmatrix} \quad \tilde{K}_\Gamma = \begin{bmatrix} K_\Gamma & KE_\Gamma^t \\ KE_\Gamma & E \end{bmatrix} \quad \tilde{\mathbf{f}}_\Gamma^{kl} = \begin{bmatrix} \mathbf{0}^{kl} \\ \delta_i^k \delta_j^l \end{bmatrix} \quad \mathbf{u}_\Gamma = \begin{bmatrix} \boldsymbol{\omega}_\Gamma^{kl} \\ P_{ij}^{kl} \end{bmatrix} \tag{43}$$

System (42) is finally solved by an iterative method, such as a preconditioned conjugate gradient one, and homogenized coefficients are directly estimated for each kl problem.

3.3. Mixed FETI-1 and Schur complement method

In a second approach, we consider an adaptation of the FETI-1 method (Fahrat and Roux, 1227; Fahrat and Roux, 1994) in the framework of the double-scale homogenization. The method is dual to the Schur complement one in the sense that the constraints are formulated in Lagrange multipliers and not in displacements on the boundaries. In the present work, we consider the basic form of the process called FETI-1. Several modifications have to be performed to adapt the method in the framework of the double-scale homogenization. First, the hypothesis of periodicity prevents the setting up of a complete dual problem. Indeed, such a boundary condition leads to an excessive number of rigid body modes when taken into account by Lagrange multipliers. A possible way to get round the drawback is to rewrite the problem in another base what involves the appearance of unsuitable coupling terms between subdomains. Our choice is to write the periodicity on the outer boundaries Γ^o by considering the displacements without duplicating the nodes like the Schur complement method. Hence, we talk about a mixed FETI-1 and Schur complement method since the inner connections are taken into account by Lagrange multipliers and

outer ones by displacements. Second, additional terms related to the homogenized coefficients have to be considered. The terms are added to the tensor describing the connections on the outer boundaries and consequently treated in the same way as in the Schur complement method. Finally, the only connections of inner boundaries are described by Lagrange multipliers. Thus, the initial problem is described by the following renumbering of the matrix system (36),

$$\begin{bmatrix} K_1 & 0 & 0 & 0 & K^t_{\Gamma^o 1} & KE^t_1 & C^t_1 \\ 0 & K_2 & 0 & 0 & K^t_{\Gamma^o 2} & KE^t_2 & C^t_2 \\ 0 & 0 & K_3 & 0 & K^t_{\Gamma^o 3} & KE^t_3 & C^t_3 \\ 0 & 0 & 0 & K_4 & K^t_{\Gamma^o 4} & KE^t_4 & C^t_4 \\ K_{\Gamma^o 1} & K_{\Gamma^o 2} & K_{\Gamma^o 3} & K_{\Gamma^o 4} & K_{\Gamma^o} & KE^t_{\Gamma^o} & \mathbb{O}^t_{\Gamma^i \Gamma^o} \\ KE_1 & KE_2 & KE_3 & KE_4 & KE_{\Gamma^o} & E & \mathbb{O}^t_{\Gamma^i E} \\ C_1 & C_2 & C_3 & C_4 & \mathbb{O}_{\Gamma^i \Gamma^o} & \mathbb{O}_{\Gamma^i E} & \mathbb{O}_{\Gamma^i} \end{bmatrix} \begin{bmatrix} \boldsymbol{\omega}^{kl}_1 \\ \boldsymbol{\omega}^{kl}_2 \\ \boldsymbol{\omega}^{kl}_3 \\ \boldsymbol{\omega}^{kl}_4 \\ \boldsymbol{\omega}^{kl}_{\Gamma^o} \\ P^{kl}_{ij} \\ \boldsymbol{\lambda}^{kl} \end{bmatrix} = \begin{bmatrix} \mathbf{0}^{kl}_1 \\ \mathbf{0}^{kl}_2 \\ \mathbf{0}^{kl}_3 \\ \mathbf{0}^{kl}_4 \\ \mathbf{0}^{kl}_{\Gamma^o} \\ \delta^k_i \delta^l_j \\ \mathbf{0}^{kl}_{\Gamma^i} \end{bmatrix} \tag{44}$$

Stiffness matrix K is split into several K_i matrices in the same manner as seen in the Schur complement method. Each K_i matrix takes into account only inner contributions. Indeed outer interface contributions of the i-th subdomain are represented by $K_{\Gamma^o i}$ matrix. Inner interface contributions are taken into account by Lagrange multipliers associated with linear relations which are provided by C_i matrix. C_i designates the signed matrix of connections composed of 1. KE_i represents coupling terms between K_i and E_i the expression of which is identical to Eq. (41). One can notice that E the mean of properties without corrective terms is not split because of the linearity of E_i tensors. $\boldsymbol{\omega}^{kl}_i$ is the microscopic displacement of the i-th subdomain, and $\boldsymbol{\omega}^{kl}_{\Gamma^o}$ the one related to outer interfaces. $\boldsymbol{\lambda}^{kl}$ is the vector of Lagrange multipliers. The renumbering leads to a direct evaluation of P^{kl}_{ij} the effective compliance tensor associated to the complete domain. As a result System (44) can be rewritten as follows,

$$\begin{bmatrix} K_1 & 0 & 0 & 0 & R^t_1 \\ 0 & K_2 & 0 & 0 & R^t_2 \\ 0 & 0 & K_3 & 0 & R^t_3 \\ 0 & 0 & 0 & K_4 & R^t_4 \\ R_1 & R_2 & R_3 & R_4 & K_R \end{bmatrix} \begin{bmatrix} \boldsymbol{\omega}^{kl}_1 \\ \boldsymbol{\omega}^{kl}_2 \\ \boldsymbol{\omega}^{kl}_3 \\ \boldsymbol{\omega}^{kl}_4 \\ \Lambda^{kl} \end{bmatrix} = \begin{bmatrix} \mathbf{0}^{kl}_1 \\ \mathbf{0}^{kl}_2 \\ \mathbf{0}^{kl}_3 \\ \mathbf{0}^{kl}_4 \\ \mathbf{f}^{kl}_R \end{bmatrix} \tag{45}$$

where the expressions of $R_i, K_R, \mathbf{f}^{kl}_R$ and Λ^{kl} are as follows,

$$R_i = \begin{bmatrix} K_{\Gamma^o i} \\ KE_i \\ C_i \end{bmatrix} K_R = \begin{bmatrix} K_{\Gamma^o} & KE^t_{\Gamma^o} & \mathbb{O}^t_{\Gamma^i \Gamma^o} \\ KE_{\Gamma^o} & E & \mathbb{O}^t_{\Gamma^i E} \\ \mathbb{O}_{\Gamma^i \Gamma^o} & \mathbb{O}_{\Gamma^i E} & \mathbb{O}_{\Gamma^i} \end{bmatrix} \mathbf{f}^{kl}_R = \begin{bmatrix} \mathbf{0}^{kl}_{\Gamma^o} \\ \delta^k_i \delta^l_j \\ \mathbf{0}^{kl}_{\Gamma^i} \end{bmatrix} \Lambda^{kl} = \begin{bmatrix} \boldsymbol{\omega}^{kl}_{\Gamma^o} \\ P^{kl}_{ij} \\ \boldsymbol{\lambda}^{kl} \end{bmatrix} \tag{46}$$

R_i is an interconnection matrix which takes into account the connections on both outer and inner boundaries for each subdomain i. K_R represents the matrix of connections between nodes located on outer boundaries. Λ^{kl} is the vector of solutions and $\mathbf{f}^{kl}_R$ is restricted to an identity tensor on the homogenized coefficients. System (45) cannot be directly solved by a conjugate gradient because of floating subdomains. An interface problem has to be performed for which a second level of multipliers is provided by n_{rbm} rigid body modes Fahrat and Roux, 1994, where $n_{rbm} = 3$ in 2D and 6 in 3D. We have,

$$\begin{bmatrix} F_I & G_I \\ G^t_I & \mathbb{O} \end{bmatrix} \begin{bmatrix} \Lambda^{kl} \\ \boldsymbol{\alpha}^{kl} \end{bmatrix} = \begin{bmatrix} \mathbf{f}^{kl}_R \\ \mathbf{0}^{kl} \end{bmatrix} \tag{47}$$

where,

$$\begin{cases} F_I = K_R - \sum_i R_i K^+_i R^t_i \\ G_I = [R_1 B_1 \dots R_{n_{nfd}} B_{n_{nfd}}] \end{cases} \tag{48}$$

F_I corresponds to the tensor of connections on both outer and inner interfaces. G_I stores the traces of rigid body modes and $\boldsymbol{\alpha}^{kl}$ is an amplification vector of the same rigid body modes. K^+_i is a generalized inverse meaning either a pseudo-inverse, if Ω_i is a floating subdomain, or else a classical one. n_{nfd} is the number of floating domains. One must keep in mind that a subdomain i is called floating if $\Gamma_i \cap \Gamma^o = \emptyset$ where Γ_i represents its boundaries. B_j ($j \in [1, n_{nfd}]$) is the rigid body modes matrix related to the j-th floating subdomain. The interface system is solved by a preconditioned conjugate projected gradient as in a classical FETI method and leads to a direct calculation of the homogenized coefficients for each kl problem.

3.4. Preconditioning

Gradient methods are performed to solve the interface problem. Such iterative processes are costly and require a preconditioning to speed up the convergence. A classical preconditioner for a primal domain decomposition resolution is the one of Neumann–Neumann's type. Its related condition number is bounded by $\mathcal{O}((1 + \log(H/h))^2)$, where the ratio H/h corresponds to the ratio between the dimensions of a subdomain and the size of elements. This latter is suitable in the framework of a homogenization process but turns out to be really expensive due to the non-zero number within each submatrix K_i. In addition, this latter only focuses on the local Schur complement $S^i = \tilde{K}_{\Gamma i} K_i^{-1} \tilde{K}^t_{\Gamma i}$ regardless of $\tilde{K}_\Gamma$ which contains E the average stiffness tensor and the main corrective terms related to the heterogeneities. That is why we prefer the cheaper following preconditioner M_S for which more emphasis is placed on $\tilde{K}_\Gamma$,

$$M_S = \tilde{K}_\Gamma - \sum_i \tilde{K}_{\Gamma i} (K^d_i)^{-1} \tilde{K}^t_{\Gamma i} \tag{49}$$

where K^d_i is the matrix composed of the diagonal terms of K_i. In the case of the mixed FETI-1 and Schur complement method, its two-fold nature prevents the use of classical FETI preconditioners as Dirichlet (Fahrat and Roux, 1994) and lumped (Fahrat et al., 1994) ones. Cheap preconditioners are then difficult to set up and often exhibit a low efficiency. This conclusion leads us to investigate the only Schur complement method in the sequel. The next section is dedicated to numerical tests for which preconditioner M_S is used.

4. Numerical results

Parallel algorithms of the two proposed methods have been implemented in C++ language with MPI libraries. The present section provides some numerical results in both reliability and efficiency for the Schur complement's one. First effective elastic properties are sequentially assessed and compared with a direct calculation without domain decomposition. Second the speed-up criterion is estimated for different numbers of subdomains.

4.1. Framework

A set of unit RVEs, for which the fibres are randomly oriented and spatially distributed, is set up. The length and the width of each heterogeneity are set at 1/12 and 1/240 the size of the RVE which is adimensional, respectively. These values are chosen in order to check out a minimum ratio between the size of RVEs and the dimensions of each fibre. Indeed this point is crucial to ensure the

validity of the assessment of effective properties and avoid a bias introduced by the boundary conditions (Sab, 1992; Ostoja-Starzewski, 1998). Each inclusion is supposed straight without curvature. In addition, the overlapping between two or more fibres is allowed so that the network of heterogeneities is strongly entangled. The number of realizations is evaluated according to the methodology described by Kanit et al. (2003) and Pelissou et al. (2009). This strongly depends on the ratio between the size of the RVE and the length of each reinforcement, the density of fibres, the contrast of properties, the material configuration and an expected relative error which is set at 0.002 % in the present case. Consequently, an assessment is realized for each investigated density of fibres since this one is, in the present study, randomly drawn between 0 and 30 fibres per unit cell. Such a range of values corresponds to an area fraction of between 0 and 25 %. Thus, for information purpose, the overall number of realizations is 100. Moreover, each RVE is subdivided into several non-overlapping sub-RVEs for which both the continuity of the medium and the hypothesis of periodicity are checked out. One heterogeneity can be located on several domains and crosses several inner and outer boundaries. An initial mesh is then generated according to the concept of 0-order approximate geometry. In other words, we consider quadrangular elements the size of which is equal to the diameter of the heterogeneities. The 0-order model leads to inaccurate results in comparison with an n-order greater than 1. The choice is mainly motivated by its convenience for generating RVEs with an acceptable quality and a reasonable calculation time. More details about the effects of the geometric approximation are provided in Leclerc et al. (2012) and Leclerc et al. (2013). After partitioning the domain, elastic properties are assessed with the help of the Schur complement method by double-scale homogenization. Homogenized elastic properties are finally obtained by taking the average of the complete set of results. Each fibre is supposed to follow a transverse isotropic behavior law. The longitudinal and transverse Young's modulus are set at 1050 and 600 GPa respectively. The shear modulus is set at 450 GPa. The matrix is an isotropic polymer resin with Young's and shear moduli set at 4.2 and 1.55 GPa respectively. We deliberately choose a high contrast of properties to maximize the conditioning of the matrix in the iterative resolution.

4.2. Reliability

In a first approach some tests are performed to check out the reliability of both proposed domain decomposition methods in the framework of random fibre composites. We consider the previous hypotheses and subdivide each RVE into 4, 9, 16 and 36 sub-RVEs. First, the basic idea consists in assessing homogenized elastic properties for each partitioning. Second a comparative study is done to validate the methods. Fig. 2 exhibits the evolution of the effective Young's modulus depending on the density of fibres for the different levels of partitioning. Mean curves represent the results obtained from the Schur complement method, and symbols depict some values estimated with the help of the mixed FETI-1 and Schur complement method. Confidence intervals are not represented since these ones are too small to be noticeable. A comparison is realized with a classical calculation performed on the same set of representative patterns without partitioning (curve in black). One must keep in mind that we keep the same grid of quadrangular elements for the complete domain whatever the level of subdivision is. The mesh of each subdomain then results from the splitting of the latter. Thus, the total degrees of freedom number is constant and independent of the number of sub-RVEs. Conversely the nodes number for each subdomain is reducing with increasing partitioning. Results exhibit three main points. First, both domain decomposition methods lead to the same values whatever the number of subdomains and the number of fibres are. Second, one can notice a quite good consistency of both methods according to the degree of partitioning. Indeed all curves fit together. Third, the greater both the number of fibres and subdomains are, the more noticeable some discrepancies are. Thus, a comparison between the calculation realized with 36 subdomains and the calculation performed without partitioning, for a density of fibres set at 30, yields a relative error of 3.39%. The gap could be related to the preliminary treatment of the connections on the inner boundaries. Indeed the process replaces the labeling of several quadrangular elements from matrix to fibre in order to ensure the continuity of the medium, and could consequently overestimate the homogenized coefficients. A direct calculation is set up to check out this hypothesis. This one is based on the following assumption, domain decomposition methods are not used but meshes are modified and treated in the same way as in the context of a partitioning. Thus, we generate and associate 5 meshes to each RVE in the prospect of a comparative survey with the previous outcomes seen in Fig. 2. Each mesh corresponds to a "virtual" partitioning into 1, 4, 9, 16 and 36 subdomains respectively. Fig. 3 exhibits the evolution of the effective Young's modulus depending on the density of fibres in the configuration of the direct calculation. One can notice that the discrepancies are very similar. This observation confirms the hypothesis of the critical impact of the treatment of continuity. Other surveys the results of which are not provided in the present paper, highlight that its impact strongly depends on the contrast of properties, the coarseness of the initial grid and the number of subdomains. However, except this issue, results are globally quite stationary and highlight the consistency of both domain decomposition methods when the fibres are strongly entangled and the contrast of properties is high.

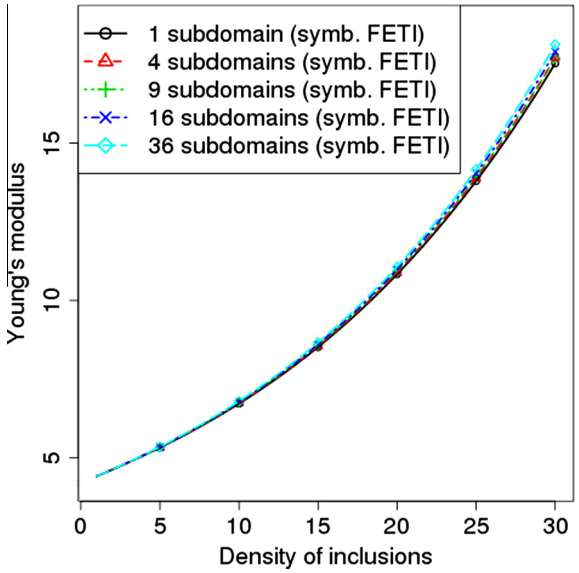

Fig. 2. Influence of the density of fibres on the effective Young's modulus: case of a domain decomposition method

4.3. Efficiency

Domain decomposition efficiency is investigated in the framework of the assessment of effective elastic properties of random fibre composites. We consider the 0-order approximate geometry for the mesh and the modified Schur complement method for the domain decomposition resolution. In a first approach, we set up a comparative study between three kinds of calculations: (1) the direct one, which is performed without subdividing the initial RVE, (2) the sequential domain decomposition and (3) the MPI parallel domain decomposition. In the last case, one must keep in mind that we associate one sub-RVE with one processor. Thus,

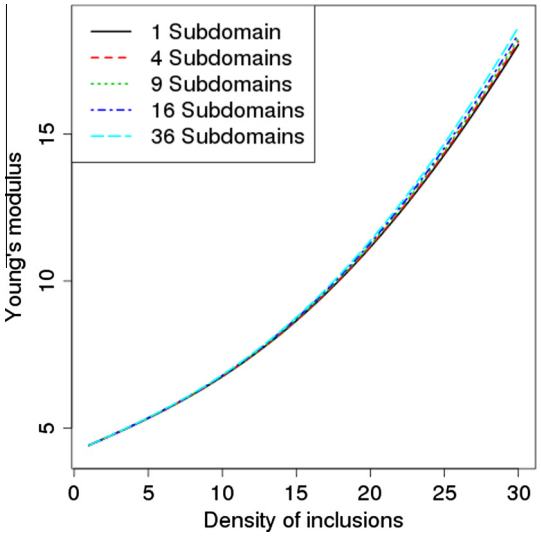

Fig. 3. Influence of the density of fibres on the effective Young's modulus: case of a direct method

the number of subdomains is equal to the number of processors. A sample of 100 unit RVEs is built according to the hypotheses of the subSection 4.1. Each is based on an initial grid composed of 57600 quadrangular elements. Figs. 4 and 5 depict the evolution of the calculation time depending on the density of fibres for 4 and 9 sub-RVEs respectively. The provided CPU time corresponds to the mean one to generate an RVE and evaluate associated elastic properties. The computations are performed with Intel Westmere EP @ 2.8 GHz processors. First, one can notice that the CPU time between the direct calculation and the sequential domain decomposition one is only reduced when the density of fibres is important. Consequently, this observation combined to the previous one related to the reliability issue leads to conclude that a domain decomposition approach is suitable to study composite materials based on a strongly entangled network of fibres. Second the efficiency of the method is widely improved by an MPI parallel calculation whatever the density of heterogeneities is. Thus the benefit of a parallel calculation is checked out independently of the complexity of the fibre network despite the high contrast of properties. This highlights the robustness of the method. Finally the calculation time is reduced between a subdivision into 4 and 9 subdomains respectively. Accurate results are provided by Fig. 6 to

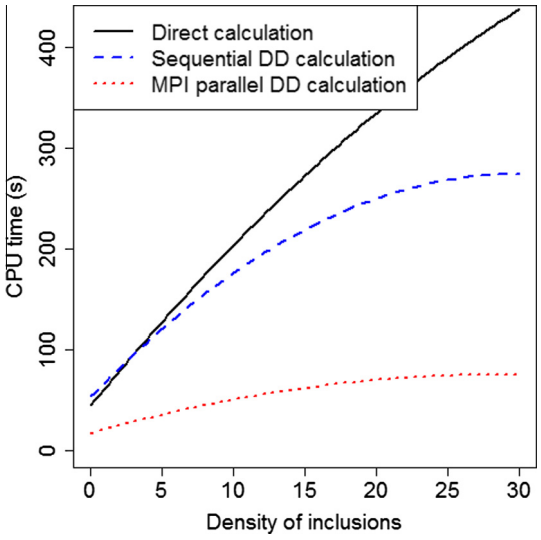

Fig. 4. Influence of the density of fibres on the CPU time for 4 sub-RVEs

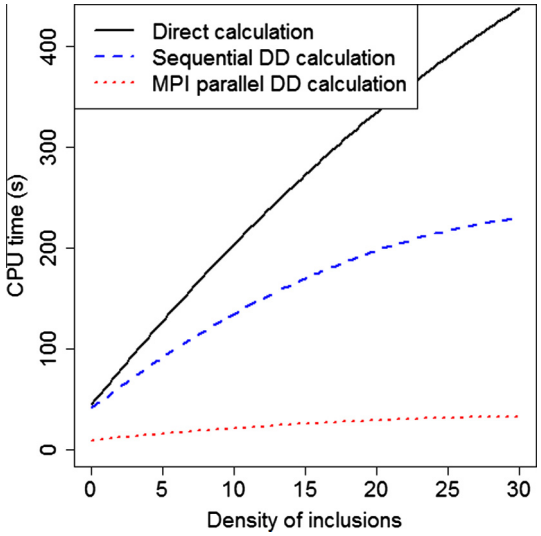

Fig. 5. Influence of the density of fibres on the CPU time for 9 sub-RVEs

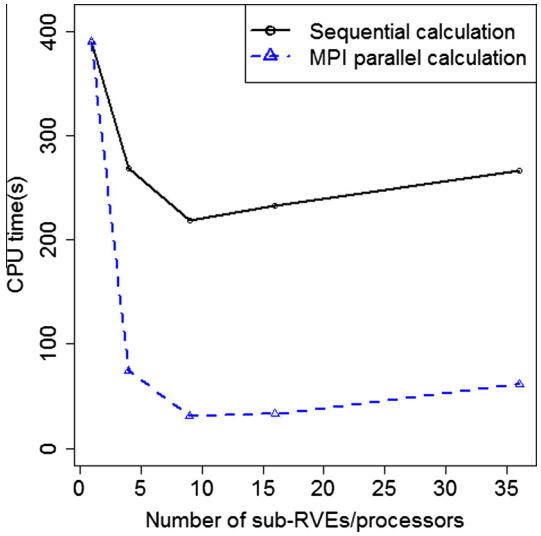

Fig. 6. Influence of the number of sub-RVEs on the CPU time

emphasize this point. The graph exhibits the evolution of the CPU time depending on the number of sub-RVEs. Subdivisions into 1, 4, 9, 16 and 36 subdomains are considered. One can observe that the calculation time is reducing well when the number of sub-RVEs is less than 9 but a stagnation is subsequently noticeable.

The last observation leads to the question of the parallel efficiency which can be estimated with the help of the speed-up criterion. This latter corresponds to the ratio between the sequential calculation time and the parallel one (Amdahl, 1967). Fig. 7 exhibits the evolution of the speed-up criterion depending on the number of processors. The continuous line in black corresponds to the ideal speed-up criterion which is equal to the number of processors. 4 other curves are drawn, namely,

- a blue[1] dashed line depicts the values obtained with the help of the 0-order model and 1-by-1 RVEs,
- a red dotted curve illustrates the results obtained with the help of the 0-order model and 2-by-2 RVEs,
- a pink dashed and dotted curve shows the results obtained with

[1] For interpretation of color in Fig. 7, the reader is referred to the web version of this article.

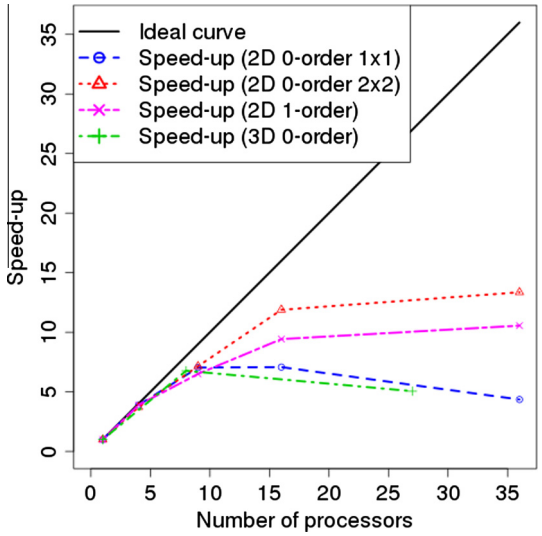

Fig. 7. Influence of the number of processors on the speed-up criterion

the help of the 1-order model and 1-by-1 RVEs,
- a green dashed and dotted line illustrates the results obtained with the help of the 0-order model and 1-by-1-by-1 RVEs in a 3D framework.

Each assessment is realized using a set of a hundred of RVEs except for the 3D case for which 20 RVEs are used since numerical calculations are much more costly. Results highlight that the speed-up criterion is only about 1 when the number of sub-RVEs is less than 9. In fact, it turns out that the drawback is related to the communication time between processors which becomes too important when both the number of processors is growing and the size of each sub-RVE is reducing. A fast calculation exhibits that the mesh of each sub-RVE has only 1600 nodes when we consider a subdivision into 36 sub-RVEs and a 2D unit (or 1-by-1) RVE. Other results obtained with 2D 2-by-2 RVEs lead to an improved behavior of the speed-up criterion. We assume that the larger the initial RVEs are the better the criterion is. Consequently the parallel efficiency of the modified Schur complement method strongly depends on the initial degrees of freedom number. This latter must be sufficiently important to ensure the relevance of a high level of partitioning. Effects of the geometric approximation are considered by a comparison between 0-order and 1-order models. One can notice that parallel efficiencies obtained with the 1-order model and a set of 2D 1-by-1 RVEs are quite close to the ones exhibited in the case of the 0-order model and a set of 2D 2-by-2 RVEs. This is due to the number of elements of the initial mesh which is the same for both cases. However, a small gap is noticeable and could be related to the difference of structure between both models. Finally, some results are provided in the context of 3D simulations for which the calculation time is prohibitive in a sequential approach. For example, a sequential calculation performed in order to generate and treat a 3D 1-by-1-by-1 RVE takes about 4 hours to be completed. Results highlight a behavior quite close to the one observed for 2D calculations. Consequently, no dimensional effect is exhibited in the present study.

5. Conclusion

A domain decomposition framework to evaluate effective elastic properties of random fibre composites has been investigated. Two methods have been proposed: the modified Schur complement and the mixed FETI-1 and Schur complement one. Both processes take into account additional terms related to the double-scale homogenization and directly yield effective coefficients. Numerical investigations have led to check out their reliability but the convergence speed of the second one is foiled by the lack of a cheap and efficient preconditioner. However, in the first case, MPI parallel computational tests have exhibited a drastic reduction of the calculation cost. A survey based on the speed-up criterion has highlighted the strong influence of the initial grid size on the optimum choice of partitioning.

Acknowledgments

The authors thank the conseil régional de Basse-Normandie for its financial support to Willy Leclerc's Ph.D. thesis and the High-Performance Computing Centre of Haute-Normandie (CRIHAN) for the computing means put at their disposal.

References

Hill, R., 1963. Elastic properties of reinforced solids: some theoretical principles. Journal of the Mechanics and Physics of Solids 11, 357–372.
Hashin, Z., 1983. Analysis of composite materials: a survey. Journal of Applied Mechanics 50, 481–505.
Kanit, T., Forest, S., Galliet, I., Mounoury, V., Jeulin, D., 2003. Determination of the size of the representative volume element for random composites: statistical and numerical approach. International Journal of Solids and Structures 40 (13–14), 3647–3679.
Pelissou, C., Baccou, J., Monerie, Y., Perales, F., 2009. Determination of the size of the representative volume element for random quasi-brittle composites. International Journal of Solids and Structures 46, 2842–2855.
Leclerc, W., Karamian, P., Vivet, A., Campbell, A., 2012. Numerical evaluation of the effective elastic properties of 2D overlapping random fibre composites. Technische Mechanik 32, 358–368.
Leclerc, W., Karamian, P., Vivet, A., 2013. An efficient stochastic and double-scale model to evaluate the effective elastic properties of 2D overlapping random fibre composites. Computational Science of Materials, 481–493.
Sab, K., 1992. On the homogenization and the simulation of random materials. European Journal of Mechanics 11 (5), 585–607.
Ostoja-Starzewski, M., 1998. Random field models of heterogeneous materials. International Journal of Solids and Structures 35, 2429–2455.
Drugan, W.J., Willis, J.R., 1996. A micromechanics-based nonlocal constitutive equation and estimates of representative volume element size for elastic composites. Journal of the Mechanics and Physics of Solids 44 (4), 497–524.
Mishnaevsky Jr., L., 2005. Automatic voxel-based generation of 3D microstructural FE models and its application to the damage analysis of composites. Material Science and Engineering A 407 (1–2), 11–23.
Jeulin, D., Moreaud, M., 2005. Multi-scale simulation of random sphere aggregates - application to nanocomposites. In: 9th European Congress on Stereology and Image Analysis, Zakopane, Poland.
Jeulin, D. Moreaud, M. 2006. Percolation of multi-scale fiber aggregates. In: S4G 6th international Conference, Prague.
Jeulin, D., Moreaud, M., 2006. Percolation d'agrégats Multi-échelles de Sphères et de Fibres – Application Aux Nanocomposites. Congrès matériaux, Dijon.
Agoshkov, V.I., Lebedev, V.I. 1985. The Poincaré-Steklov's operators and the domain decomposition methods in variational problems. Computational Processes and Systems, Nauka, pp. 173 – 227.
Fahrat, C., Roux, F.X., 1227. A method of finite element tearing and interconnecting and its parallel solution algorithm. International Journal of Numerical Methods in Engineering 32, 1205–1227.
Fahrat, C., Roux, F.X., 1994. Implicit parallel processing in structural mechanics. Computational Mechanics Advances, North Holland 2 (1), 1–124.
Bensoussan, A., Lions, J.L., Papanicolaou, G.C., 1978. Asymptotic Analysis for Periodic Structures, Amsterdam ed. Springer, North Holland.
Sanchez-Palencia, E., 1980. Non-homogeneous media and vibration theory, 127. Springer, Berlin.
Débordes, O., 1986. Homogenization computations in the elastic or plastic collapse range. Applications to unidirectional composites and perforated sheets. In: 4th. Int. Symp. Inn. Meth. in Eng.. Springer-Verlag, Atlanta, pp. 453–458.
Bornert, M., Bretheau, T., Gilormini, P., 2001. Homogénéisation en mécanique des Matériaux. Hermes Sciences Europe Ltd, Paris.
Magoariec, H., Bourgeois, S., Débordes, O., 1675. Elastic plastic shakedown of 3D periodic heterogeneous media: a direct numerical approach. International Journal of Plasticity 20, 1655–1675.
Fahrat, C., Mandel, C., Roux, F.X., 1994. Optimal convergence properties of the FETI domain decomposition method. Computer Methods in Applied Mechanics and Engineering 115, 365–385.
Amdahl, G., 1967. Validity of the single processor approach to achieving large-scale computing capabilities. AFIPS Conference Proceedings. Thompson books, Washington D.C., pp. 483–485.

Influence of morphological parameters of a 2D random short fibre composite on its effective elastic properties

W. Leclerc[a,b], P. Karamian-Surville[a,b,*], A. Vivet[c,d,e,f]

[a] *Université de Caen Basse-Normandie, UMR 6139 LMNO, F-14032 Caen, France*
[b] *CNRS, UMR 6139 LMNO, F-14032 Caen, France*
[c] *Université de Caen Basse-Normandie, UMR 6252, F-14032, France*
[d] *ENSICAEN, UMR 6252, CIMAP, F-14050, France*
[e] *CNRS, UMR 6252, F-14032, France*
[f] *CEA, UMR 6252, F-14032, France*

Abstract

The paper deals with the assessment of the influence of morphological parameters of a 2D random short fibre composite on its effective elastic properties. A double-scale 2D finite element approach is used and periodic representative volume elements are generated according to the model with an n-order approximate geometry. This one is a recent and powerful tool to generate meshes in the context of complex microstructures such as random fibre composites. Impact of three morphological features namely, aspect ratio, tortuosity of fibres and width of the interphase area, is investigated. Numerical results are provided for several contrasts of properties and volume fractions of fibres.

Keywords: Computational solid mechanics / short fibre composites / RVE / finite element analysis (FEA)

*corresponding author. Tel.:+33 2 31 56 74 61
Email addresses: philippe.karamian@unicaen.fr (P. Karamian-Surville), willy.leclerc@unicaen.fr (A. Vivet), philippe.karamian@unicaen.fr (A. Vivet), corresponding author. Tel.:+33 2 31 56 74 61 (A. Vivet), alexandre.vivet@unicaen.fr (A. Vivet)

1. Introduction

For several decades short fibre composites have been manufactured and used for industrial purposes. Their low cost of production associated to their excellent strength-to-weight ratio have led to numerous applications in many fields like aerospace, automotive engineering, and competitive sport. For instance, fibreglass is massively produced for building hulls in marine industry and carbon-fibre-reinforced composites are used for the retrofitting of old structures in civil engineering. The main issue is to assess their intrinsic mechanical properties in order to evaluate their ability to replace one-phase materials. Experimental measurements are sometimes difficult and costly to set up for this purpose. That is why analytical models are very useful for estimating effective properties. Mori-Tanaka micromechanics model [1] and self-consistent estimates [2] are classical tools for predicting elastic coefficients of two-phase heterogeneous media. However, accurate predictions of the mechanical response are difficult to obtain since this one strongly depends on several parameters such as orientation, shape and aspect ratio of heterogeneities. Thus, numerous micromechanics models have been proposed during the last decades for improving the accuracy of estimates, among which, the general self-consistent scheme [3] and the third-order approximation [4].

However, the range of validity of a micromechanics model is always restricted. Thus, there is no model for complex-shaped heterogeneities, for example tortuous fibres, for which no Eshelby's tensor is available. In this context, a numerical modelling is more convenient to evaluate effective properties. The basic idea consists in generating a Representative Volume Element (RVE) of the material either by a Random Sequential Adsorption (RSA) [5] for which distance constraints prevent the overlap between two or more heterogeneities, or a fully Monte-Carlo (MC) process [6]. Effective elastic properties are generally evaluated either with the help of a Fast Fourier Transformation [7], or more classically, by Finite Element (FE) analysis [8]. Unfortunately, in the context of random heterogeneous media, a FE approach is difficult to set up since the mesh generation is thwarted by several drawbacks related to the complex structure of the network of heterogeneities. Hence, a modelling of such a microstructure is often basic and unrealistic. However, the recent development of the model with an n-order approximate geometry [9] which is based on a grid approximation, has opened prospects for the generation of complex microstructures. In the present work, a FE approach using this

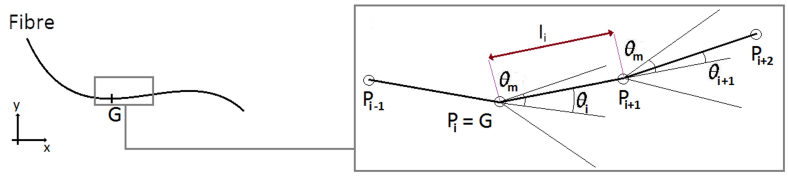

Figure 1: Parametrisation of the tortuosity of a fibre

concept is considered in order to assess elastic coefficients of a 2D random short fibre composite for which the microstructure is complex and strongly entangled. Influence of three morphological parameters namely, aspect ratio, tortuosity of fibres and width of the interphase area, is investigated.

2. Numerical modelling

2.1. Morphological parameters

2D microstructures are generated according to a set of random morphological parameters describing the complex geometry of a random fibre composite. Each parameter is either randomly drawn according to a given distribution law such as, for instance, the Gaussian law and uniform law, or a fixed one. On the one hand, both centroid spatial location and orientation of each heterogeneity are randomly drawn. One must keep in mind that we assume no distance constraint between two or more fibres so that the process can be seen as a MC one. Thus, all distribution laws are unbiased, and the overlap between two or more fibres is possible. On the other hand, other parameters are set at given values in order to be investigated in a deterministic way,

- the **aspect ratio** a_r of fibres which is the ratio between the length l and the diameter d of each heterogeneity,

- the parameter of **tortuosity** of fibres which describes the level of non-straightness of a heterogeneity. This one is defined by a maximum angle θ_m which has to be respected in the generation of a fibre in the same way as [10]. Fig. 1 illustrates how one set up a tortuous fibre. The process consists in building the reinforcement point by point starting from its centroid G. Thus, each new point P_{i+1} is obtained from its predecessors P_i and P_{i-1} considering the distance between two consecutive nodes l_i,

and an angle θ_i which is uniformly drawn between $-\theta_m$ and θ_m. l_i is chosen constant and sufficiently small to ensure the smoothness of the heterogeneity.

- the width w_{int} of the **interphase area**. This one is an area surrounding each reinforcement where the properties of the matrix are disrupted due to the presence of the heterogeneity. One must take care of not confusing interphase with interface which designates the boundary between soft and hard phases. In the present work, no decohesion is taken into account and perfect bondings are supposed.

2.2. RVE

The investigation of the dimensions of the RVE is a key issue from which representativeness, efficiency and validity of the numerical modelling strongly depend [11]. The size of an RVE is defined as s, the scale ratio between its width and the average length of each heterogeneity. s must be greater than a critical scale ratio s_r to check out the representativeness of a unit cell and avoid a bias introduced by the boundary conditions. Its assessment is realised according to the process described by [11] which leads to a compromise between accuracy of results and low cost of calculation. In the present work, an RVE is generated from the set of random and deterministic parameters described in 2.1. In addition, a specific treatment is performed to ensure the periodicity of the cell. Its principle consists in duplicating and translating the fibres intersecting the boundaries of the unit cell.

2.3. Mesh generation

A reliable, efficient and automated mesh generation of overlapping random heterogeneous media is particularly difficult to set up in a classical approach for which the mesh is directly generated from the boundaries of the network of fibres. The voxel-based FE approach [12] circumvents the drawbacks relative to the mesh generation. This one consists in approximating the boundaries of the network of fibres according to a grid of pixels in 2D or voxels in 3D. The concept is very suitable for a reliable and automated mesh generation but is poorly efficient. The last point is drastically improved in the context of a strongly entangled microstructure when using the model with an n-order approximate geometry [9]. This one is based on a 2-step mesh generation. First, one has to generate a grid of coarse elements the size of which is typically equal or greater than the diameter of fibres. Second, an adaptive mesh

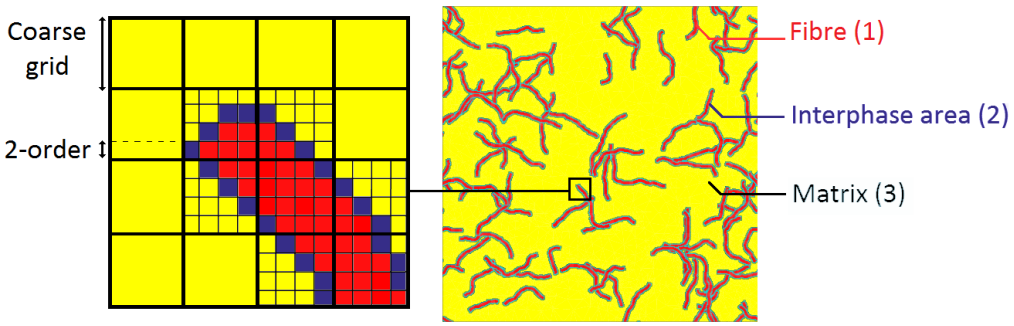

Figure 2: RVE obtained according to the model with a 2-order approximate geometry (100-by-100 coarse grid)

refinement (AMR) is performed in order to locally refine the boundaries of each heterogeneity according to an n-order parameter. This one is defined as the ratio between the diameter of fibres and the size of the smallest voxel, expressed in logarithm in base 2. Thus, a Delaunay triangulation constrained to the approximate boundaries enables a reliable and automated mesh generation. In addition, it was exhibited [9] that the n-order strategy leads to a tremendous reduction of the calculation cost in comparison with a classical approach without AMR. Fig. 2 illustrates an RVE obtained according to the model with a 2-order approximate geometry before meshing. The red phase (1) corresponds to the reinforcement, the blue one (2) corresponds to the interphase area and the yellow one (3) corresponds to the matrix phase. Morphological parameters are as follows, w_{int} is set at $d/4$, a_r is set at 20, θ_m is set at 40^o and s is set at 5. The number of heterogeneities is set at 100.

3. Influence of morphological parameters

An investigation of a set of morphological parameters, namely the aspect ratio, the tortuosity and the width of the interphase is set up under the following hypotheses. First, effective elastic properties are evaluated according to the asymptotic process described by [11]. This one consists of generating a complete sample of RVEs for which elastic coefficients are assessed by a homogenisation technique namely, in the present work, the double-scale approach [13]. Effective properties are then obtained from averaging the scope of results. Second, we consider networks of randomly distributed and oriented fibres. Each one follows an isotropic transverse behaviour law and the

soft phase is isotropic. Y_l^f, Y_t^f, μ^f and κ^f designate longitudinal and transverse Young's, shear and bulk moduli of each fibre respectively. Y^m, μ^m and κ^m are Young's, shear and bulk moduli of the matrix respectively. Poisson's ratios are equal to 0.25 and 0.35 for hard and soft phases respectively. In addition, we set $Y_l^f = 2Y_t^f$. κ^* is the normalised effective planar bulk modulus which is estimated as follows,

$$\kappa^* = \frac{1}{4\kappa^m} \sum_{\alpha,\beta \leq 2} C_{\alpha\alpha\beta\beta} \tag{1}$$

where $C_{\alpha\beta\gamma\delta}$ ($\alpha, \beta, \gamma, \delta \in \{1, 2\}^4$) is the effective stiffness tensor. In addition, interphase area is supposed isotropic with shear and Young's moduli equal to 0.5 times the ones of the soft phase. The contrast of properties c_r between hard and soft phases is defined as follows,

$$c_r = \frac{Y_l^f}{Y^m} = \frac{\mu^f}{\mu^m} \tag{2}$$

Finally, meshes are built according to the model with a 2-order approximate geometry, and the size of RVE s is set at 5 according to previous investigations [9].

3.1. Aspect ratio

First, a study is realised for a range of aspect ratios a_r between 5 and 50. θ_m is equal to 20 and w_{int} is equal to $d/4$. Several volume fractions of fibres are considered between 5 and 25 %. Fig. 3 (a) illustrates the influence of the aspect ratio on the normalised effective bulk modulus κ^* for a contrast of properties set at 10. One can notice that the greater the aspect ratio is the greater the bulk modulus is whatever the load rate is. Thus, κ^* varies from 1.2690 to 1.4529, for a volume fraction of fibres of 25 %, when the aspect ratio goes from 5 to 50. Results are similar with higher values in the case of a high contrast of properties (Fig. 3 (b), $c_r = 50$) for which κ^* varies from 1.5171 to 2.4033 for a volume fraction of fibres of 25 %. One can notice that the saturation is almost reached when c_r is equal to 10 while this one is barely noticeable for a high-contrast composite. This result is related to end effects which much more impact the mechanical response of the material when the contrast is important.

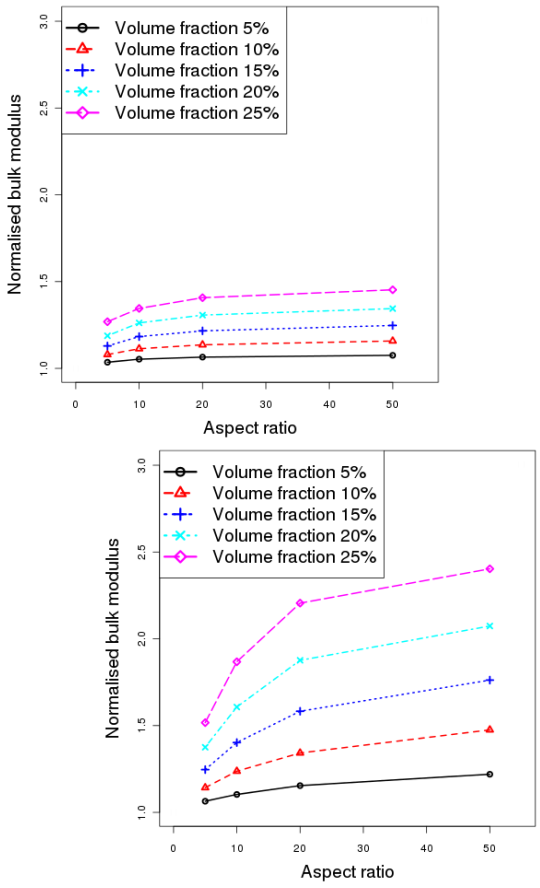

Figure 3: Influence of the aspect ratio on the normalised effective bulk modulus (a) $c_r = 10$ (b) $c_r = 50$

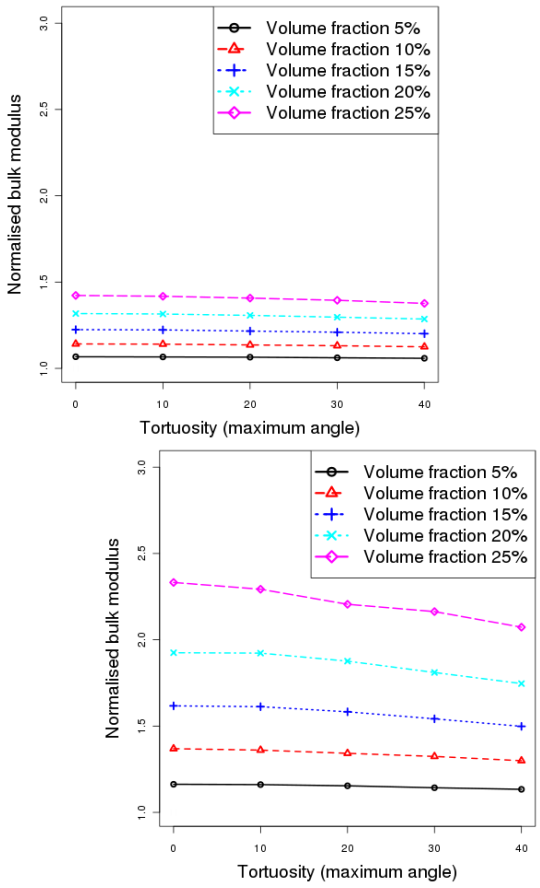

Figure 4: Influence of the maximum angle on the normalised effective bulk modulus (a) $c_r = 10$ (b) $c_r = 50$

3.2. Tortuosity

Second, the influence of the tortuosity of fibres is examined. Maximum angle θ_m is set at several values between 0 for which fibres are straight and 40^o for which fibres are strongly tortuous. a_r is set at 20, w_{int} is set at $d/4$ and several volume fractions of fibres are considered between 5 and 25 %. Fig. 4 (a) illustrates the influence of the tortuosity of fibres on κ^* for c_r set at 10. On the one hand, results highlight a slight negative impact of the tortuosity for a low contrast of properties. Thus, κ^* varies from 1.4226 to 1.3767 when θ_m goes from 0^o to 40^o and the volume fraction of fibres is 25 %. In addition, κ^* goes from 1.10587 to 1.0676 when θ_m varies from 0^o to 40^o and the volume fraction of fibres is 5 %. On the other hand, discrepancies are greater when the contrast of properties is higher (Fig. 4 (b), $c_r = 50$). Thus, κ^* varies from 2.3322 to 2.0730 when θ_m goes from 0^o to 40^o and the volume fraction of fibres is 25 %. However, the influence of the tortuosity is still slight when the load rate is low. Indeed, κ^* varies from 1.1630 to 1.1337 when θ_m goes from 0^o to 40^o, the volume fraction of fibres is 5 % and c_r is 50.

3.3. Width of the interphase area

Finally, the width of the interphase area is investigated. This one is chosen between 0 for which there is no interphase area and 0.75 times the diameter of fibres. One must keep in mind that a_r is set at 20, θ_m is set at 20 and several volume fractions of fibres are considered between 5 and 25 %. Fig. 5 (a) shows the influence of the width of the interphase area on κ^* for a contrast of properties set at 10. The wider the interphase area is the lower the properties are whatever the load rate of heterogeneities is, which is consistent with the fact that the interphase area is less stiff than the soft phase. Thus, κ^* varies from 1.5450 to 1.2240 when the volume fraction of reinforcements is 25 % and w_{int} varies from 0 and $0.75d$. The same one goes from 1.0907 to 1.0156 when the volume fraction of reinforcements is 5 %. In addition, Fig. 5 (b) depicts the influence of w_{int} on κ^* for a contrast of properties set at 50. Results are quite similar to the previous ones. Thus, κ^* varies from 2.4487 to 1.9358 when the volume fraction of fibres is 25 %.

4. Conclusions

An investigation of the influence of morphological parameters of a 2D random short fibre composite on its effective elastic properties has been set

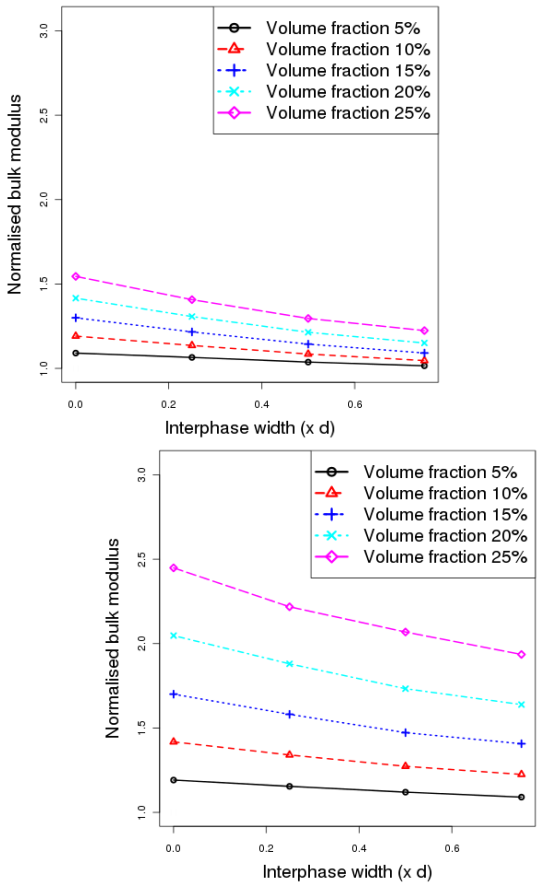

Figure 5: Influence of the width of the interphase area on the normalised effective bulk modulus (a) $c_r = 10$ (b) $c_r = 50$

up. Conclusions are as follows. First, results confirm the benefit of using long fibres rather than short ones. Second, non-straight fibres slightly affect the mechanical response, especially when both volume fraction of fibres and contrast are high. Finally, the interphase area drastically reduces the reinforcement of the material whatever the contrast of properties is.

Acknowledgements

The authors thank the conseil régional de Basse-Normandie for its financial support to Willy Leclerc's Ph.D. thesis and the High-Performance Computing Centre of Haute-Normandie (CRIHAN) for the computing means put at their disposal.

[1] T. Mori, K. Tanaka, Average stress in matrix and average elastic energy of materials with misfitting inclusions, *Acta Metallurgica* 21 (1973) 571-574

[2] R. Hill, A self-consistent mechanics of composite materials, *Physics of Solids* 13 (1965) 213-222

[3] R.M. Christensen, K.H. Lo, Solutions for effective shear properties in three phase sphere and cylinder models, *Journal of Mechanics and Physics of Solids* 27 (1979) 127-140

[4] S. Torquato, Random heterogeneous media : microstructure and improved bounds on effective properties, *Applied Mechanics Reviews* 44 (1991) 37-76

[5] J. Segurado, J. Llorca, A numerical approximation to the elastic properties of sphere-reinforced composites, *Journal of the Mechanics and Physics of Solids* 50(10) (2002) 2107-2121

[6] A.A. Gusev, P.J. Hine, I.M. Ward, Fiber packing and elastic properties of a transversely random unidirectional glass/epoxy composite, *Composites Science and Technology* 60 (2000) 535-41

[7] H. Moulinec, P. Suquet, A numerical method for computing the overall response of nonlinear composites with complex microstructures, *Computer Methods in Applied Mechanics and Engineering* 157 (1998) 69-94

[8] S. Kari, H. Berger, U. Gabbert, Numerical evaluation of effective material properties of randomly distributed short cylindrical fibre composites, *Computational Materials Science* 39(1) (2007) 198-204

[9] W. Leclerc, P. Karamian, A. Vivet, An efficient stochastic and double-scale model to evaluate the effective elastic properties of 2D overlapping random fibre composites, *Computational Materials Science* 69 (2013) 481-493

[10] F. Dalmas, R. Dendievel, L. Chazeau, J.Y. Cavaillé, C. Gauthier, Carbon nanotube filled polymer composites. Numerical simulation of electrical conductivity in 3D entangled fibrous networks, *Acta Materiala* 54(11) (2006) 2923-2931

[11] T. Kanit, S. Forest, I. Galliet, V. Mounoury, D. Jeulin, Determination of the size of the RVE for random composites: statistical and numerical approach, *International Journal of Solids and Structures* 40(13-14) (2003) 3647-3679

[12] L. Mishnaevsky Jr., K. Derrien, D. Baptiste, Effect of microstructure of particle reinforced composites on the damage evolution: probabilistic and numerical analysis, *Composites Science and Technology* 64(12) (2004) 1805-1818

[13] E. Sanchez-Palencia, Non-homogeneous media and vibration theory, Springer, Berlin, 1980.

TECHNISCHE MECHANIK, vol., is., (year), bbb– eee
submitted: month day, year

Numerical evaluation of the effective elastic properties of 2D overlapping random fibre composites

W. Leclerc, P. Karamian, A. Vivet and A. Campbell

We present a numerical investigation of the elastic coefficients of random fibre composites with high contrast of properties. Here we consider a numerical study based on the generation of representative volume elements (RVEs) with overlapping random fibre network. Such a concept requires an important Monte-Carlo draw of patterns as well as an accurate determination of RVE size. In this paper, this latter is done by estimating the evolution of the standard deviation according to the number of realizations for given values of RVE size. We consider the use of an appropriate model for an automatic, reliable and fast generation of RVEs : the model with an n-order approximate geometry that allows the construction of complex overlapping fibre network. It is well-established that the morphology of the microstructure greatly affects the mechanical response of such kind material. Some morphological features, namely orientation, aspect ratio and dispersion are investigated by considering them as random variables in the design of RVEs. The results are subsequently linked to the percolation phenomenon that occurs when fibres overlap and form some pathways inside the soft phase. This phenomenon influences effective properties of heterogeneous media, particularly in the case of a high contrast of properties.

1 Introduction

This paper is devoted to the evaluation of elastic properties of heterogeneous media with overlapping short fibre inclusions. Here, the fluctuations of the microstucture and the high contrast of properties thwart the accuracy of the usual bounds as Voigt and Reuss, and Hashin-Shtrikman's ones (Hashin and Shtrikman, 1963). That is why our approach is based on a numerical investigation related to the generation of a large number of RVEs. This latter can be defined as a volume V large enough to take into account the microstructure of the media and sufficiently small to limit the calculation cost and respect a minimal scale ratio with the macroscopic material. We invite the reader to refer to the article of Drugan and Willis (1996) on this subject. The notion of RVE has a crucial importance in the field of heterogeneous media and requires an accurate determination depending on the material configuration. Thus, Kanit et al. (2003) set up a statistical approach to evaluate the RVE size for a given absolute or relative error ε in the case of Voronoï mosaics. According to authors, a unique large RVE can be chosen as well as several smaller ones providing that the dimensions avoid the bias related to the boundary conditions. It turns out periodical conditions yield the best results in RVE size convergence because the bias is reduced in comparison with kinematic or static uniform boundary conditions (KUBC or SUBC). Hence our choice was to perform a asymptotic evaluation of the properties by considering a large number of small and periodical RVEs according to the double-scale method described by Sanchez-Palencia (1980) and, Bensoussan et al. (1978).

We consider random short fibre composites with high contrast of properties. Such a kind material can be related to high technology composites reinforced in carbon nanotubes (CNTs). Early observations of carbon fibres and CNTs by Oberlin et al. (1976) and later by Iijima (1991) have aroused a big interest among the industrialists. Thus, for example, in the mechanical field their extraordinary stiffness associated to a low density could enable a use as reinforcement element for polymer-based composite materials. Among the first experiments made in order to conceive such materials, the works of Shaffer and Windle (1999) introduced the critical question of the morphology of the CNT network. The consequent scientific effort made to study the impact of CNT and CNT network morphology has highlighted 4 key points to master in order to optimize the properties of CNT-based composites. First, Odegard et al. (2003), among others, studied the effect of alignment. Their results show a sizeable effect of reinforcement in the preferential direction with a loss in transverse properties. Second, effect of waviness and decohesion was checked out by several authors whose Fisher et al. (2003) and Shao et al. (2009).

Third, an important aspect ratio of inclusions is a well-known factor of reinforcement in fibre composites. This assumption stays true in the case of nanoparticles (see Odegard et al. (2003)). Finally, an important effect of morphology is related to the dispersion of inclusions inside the soft phase. In the example of CNTs, Van Der Waals interactions tend to agglomerate them in bundles. The resulting inhomogeneous distribution turns out greatly affecting the mechanical response of the composite (see Villoria and Miravete (2007), and, Seidel and Lagoudas (2006)). However, consider a uniform distribution as undermining the reinforcement is a premature conclusion. Jeulin and Moreaud (2005, 2006b,a); Moreaud (2006) investigated the clustering phenomenon by a two-level Boolean scheme of spheres. Their purpose was to quantify the percolation phenomenon that occurs when pathways are formed by inclusions inside the matrix. Their results showed low percolation thresholds that highlighted an effect of reinforcement for a heterogeneous distribution of fibres.

In this work, first, we introduce a modelling adapted to take into account the overlapping phenomenon that is crucial to consider effects of percolation inside the matrix : the model with an n-order approximate geometry. The idea is to approximate the geometry of fibres by considering a grid of quadrangular elements and an adaptive mesh refinement process introduced by Berger and Colella (1989). The paradigm is adapted to an automated, reliable and fast generation of random RVEs taking into account overlaps. Some comparisons in time and results with a classical geometry are given as well. Second, we put up the RVE size determination by a statistical approach based on the variance estimate. Results in number of realizations are provided for different values of the absolute error. Third, a direct comparison of effective Young's, bulk and shear moduli is carried out with Voigt and Reuss, and, Hashin-Shtrikman bounds (Hashin and Shtrikman, 1963) and, self-consistent Halpin-Tsai estimates (Halpin and Kardos, 1976), (Wall, 1997). In a fourth step, we consider the investigation of different morphological parameters, namely orientation, aspect ratio and dispersion. In this last case, we use a two-scale Boolean scheme of circles to model the agglomerates. The investigation is done for agglomerates of a size equals to fibre diameter and a range of circle area fraction f between 60 and 100 $\%$ of the RVE. Finally, we link our results with the percolation threshold that is evaluated for different configurations of CNT network with the help of the model by classifying described by Jeulin and Moreaud (2007).

2 Numerical modelling

The modelling we consider is based on a 2D periodical representative volume element (RVE). That deals with a representative pattern of an inhomogeneous material the size of which requires an accurate investigation. Indeed the pattern has to be small enough in comparison with the medium dimensions and sufficiently large to take into account enough informations on the microstructure and the network of fibres (Kanit et al., 2003). Here we considered periodic boundary conditions and the effective properties are evaluated by a Monte-Carlo draw of a large number of RVEs. The number of random draws greatly influences on the convergence of the homogenized properties and depends on the RVE size that will be subsequently investigated. The mesh and the geometry related to the representative patterns are created with the Cast3M software developed by the CEA. We consider plane and periodic RVEs for which the main morphological parameters of the inclusions namely, the fibre length, diameter, orientation and distribution are introduced as random variables. Each parameter can be fixed or follow a probability law as a Gaussian or a logarithmic-normal distribution. Each fibre considered in this article will be represented as a plane section of cylinder according to a straight or curved direction. In this section, RVE size is fixed to an adimensional value of 4, fibre length follows a Gaussian law around a mean value of 0.4 with a standard deviation of 0.08. Hence we have a mean scale factor of 10 between the dimensions of RVE and inclusions. The diameter of each fibre is fixed to 0.02 and we consider random oriented inclusions. Interactions between fibres are allowed and we suppose perfect bondings at the interface fibre/matrix.

2.1 RVE model with smooth boundaries

First we consider a RVE model with smooth boundaries. This model respects the hypotheses introduced previously with a fibre represented as smooth section of cylinder. Figure 1 exhibits an example of RVE with the exact geometry built from a program which we have coded in Cast3M. We can observe in light (yellow) the polymer matrix and in dark (red) some fibres.

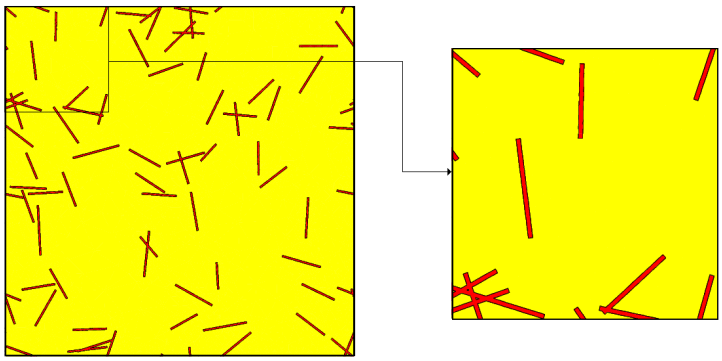

Figure 1. Periodical representative volume element of the CNT-reinforced polymer for the model with smooth boundaries.

Some calculations performed with this model highlight some drawbacks related to the mesh construction. The first defect is the CPU calculation time which is too long to generate RVEs. For example if we want to create a representative pattern with a 5 percent fibre area fraction the calculation time is near to 1 minute with a processor Intel(R) Xeon(R) W3520 @ 2.67 GHz. That is a severe drawback to evaluate homogenized properties by putting into place a sample of several thousands of RVEs. Second, the mesh design becomes very difficult when we have numerous inclusions. Indeed the hypothesis of overlapping requires to recreate the connected interface around each aggregate formed by the intersected fibres. This step becomes very difficult to set up when we have a lot of inclusions with complex intersections inside the RVE and affects drastically the reliability and the automation of the design of a large sample of representative patterns. Another problem is related to the triangular elements which can be very elongated with the model with the exact geometry for which the mesh is created by triangulation around the interfaces. This kind of structural defaults in the mesh cannot be neglected because they generate ill-conditioned matrices in the calculation of the homogenized properties. We conclude that the RVE model with smooth boundaries is not suitable to perform a large generation of representative patterns and consequently to evaluate the mechanical properties of heterogeneous media. We must conceive a new, suitable and reliable model to avoid the different defaults highlighted here.

2.2 RVE model with a 0-order approximate geometry

In reality the boundaries of the fibres are often discontinuous. Thus, for a CNT fibre, the edge is made of a discrete lattice structure of C-C bonds. An idea is to conceive a model for which the inclusions are not represented with smooth boundaries but with an approximate geometry according to a structured grid of quadrangular elements and a local adaptive mesh refinement process (L.A.M.R., see Berger and Colella (1989)). Such a kind concept enables a tremendous diminishing in calculation cost and allows a totally reliable generation of overlapping fibres. This modelling is called RVE model with an n-order approximate geometry and depends on an n-order related to the degree of approximation of the geometry compared to the model with smooth boundaries. It corresponds to the ratio in power of 2 between the fibre diameter and the size of the quadrangular elements. Hence, on one hand, ∞-order model is geometrically equivalent to the model with smooth boundaries. On the other hand, the 0-order provides a geometry for which the fibre diameter is equal to the size of elements, see Figure 2. This latter enables the fastest generation of RVEs and maintains a sufficient accuracy in the calculation of effective properties.

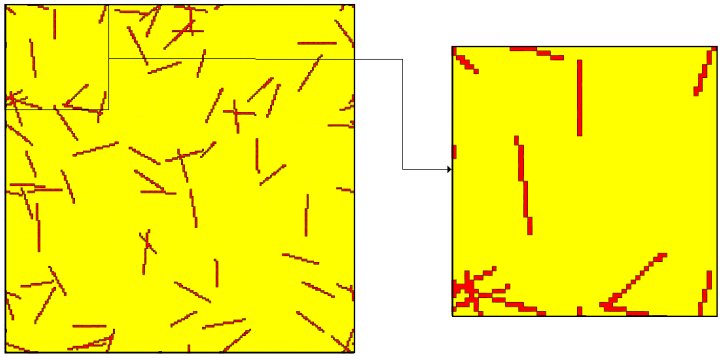

Figure 2. Periodical representative volume element of the CNT-reinforced polymer for the model with a 0-order approximate geometry.

2.3 Construction of the RVE model with a 0-order approximate geometry

Our modelling depends on an initial grid of elements for which the size is not equal to the fibre diameter but is several times larger, up to a multiplicative factor parameter chosen by the user. The locations of the centres of gravity are either randomly drawn or distributed according to a probability law as the Gaussian law. All morphological parameters are set up in the same way. First, each inclusion is represented as a segment subdivided according to the fibre diameter. The next step consists in determining the elements of the coarse grid intersecting the straight segments. Thus we get coarse overlapping fibre that we refine locally according to a L.A.M.R. method to obtain elements of the size equivalent to the fibre diameter. The process is finished when we have gathered the refined elements with a fibre label inside the boundaries of the coarse nanoparticle. In the last step we subdivide each quadrangular element into two triangular elements and create the mesh of the matrix by triangulation around the boundaries of the hard medium and the RVE.

2.4 Comparative study between approximate and smooth geometry

Here, we set up a comparative study in results and calculation time between the models with smooth boundaries and an approximate geometry. For this purpose, we consider the 0, 1 and 2-orders and the model with smooth boundaries for which the convergence in mesh refinement is achieved. Table 1 exhibits the CPU time t[1](in seconds) and the relative scatter of the effective Young's modulus (e_{rel}) obtained between the two models for the discussed orders.

	2%		4%		6%		8%		10%	
Model	e_{rel}	t	e_{rel}	t	e_{rel}	t	e_{rel}	t	e_{rel}	t
0-order	1.62	0'02"47	4.07	0'04"26	6.11	0'06"05	7.45	0'07"88	8.91	0'09"85
1-order	0.456	0'11"82	2.33	0'23'16	3.98	0'35"47	4.75	0'49"53	5.34	0'65"53
2-order	0.109	0'11"14	0.962	0'22'28	1.67	0'34"95	1.76	0'50"18	1.97	0'67"47
∞-order	–	0'09"49	–	0'23"28	–	0'55"90	–	2'09"00	–	4'31"00

Table 1. Comparison in CPU time t (in seconds) and relative scatter of Young's modulus (e_{rel}) of the two discussed models.

The results highlight an acceptable adequacy between the smooth and approximate geometries for a fibre area fraction less than 10%. The lower the order is, the greater the fibre area fraction is, the greater the relative scatter is. Thus, for an area fraction of 10 %, we obtain a relative scatter of 8.91 %. This value exhibits a sensitive effect of geometry which is diminished for a higher order. In the case of the CPU time, the results highlight the real contribution of the model with an approximate geometry. Thus, for a fibre area fraction fixed at 10% the calculation cost is decreased from 4 minutes and 31 seconds to only 9 seconds passing from smooth boundaries to the 0-order approximate geometry.

3 Determination of the RVE size

The crucial issue of the RVE size is investigated in this section. We use a statistical approach that was developed by Kanit et al. (2003) in the framework of Voronoï mosaics but we consider random fibres composites with high contrast of properties. For this purpose, an important Monte-Carlo draw of RVEs for different sizes is set up in the framework of the isotropy and the model with a 0-order approximate geometry. The question of the appropriate number of realizations is studied by considering an accurate study of the variance parameter. Furthermore, we assume fibres as a hard continuous medium with an isotropic transverse behaviour and the matrix as an isotropic one. Here the fibre length follows a Gaussian law around a mean value of 0.4 with a standard deviation of 0.08. The diameter of each fibre is fixed at 0.02 and the inclusions are randomly oriented. Interactions between fibres are allowed and we suppose perfect bondings at the interface fibre/matrix. Moreover, in the case of fibres, the longitudinal Young's modulus is fixed at 1050, the transverse one is 600 and the shear modulus is 450. As regards the matrix phase the Young's modulus is fixed at 4.2 and the shear one at 1.55.

[1]Quadricore Intel(R) Xeon(R) W3520 @ 2.67 GHz

3.1 Effects of RVE size

The RVE size must respect several conditions to respect the representativeness of the RVE in a homogenization process. First, a suitable RVE has to be large enough to take into account sufficient informations on the microstructure of the material. However a large RVE affects the calculation cost and loses its elementary aspect. Furthermore, an important drawback is related to the boundary conditions that introduce a bias in the calculation of the effective properties. The RVE area A can be linked to a given absolute error ε_{abs} and the standard deviation of the investigated effective property Y, $D_Y(A)$. Thus, for n independent realizations of area A, we have,

$$\varepsilon_{abs} = \frac{1.96 D_Y(A)}{\sqrt{n}} \tag{1}$$

In other words, the calculation of the interval confidence for large samples of RVEs yields the suitable RVE size for given number of realizations and absolute error ε_{abs}. Therefore, a critical point is related to the following question, do we have to consider a small number of realizations of large RVEs or a large number of realizations of small RVEs to obtain the expected error ε_{abs} ? As regards the calculation cost the second assertion gives the best performances. However too small RVEs widely affect the accuracy of the effective properties because a bias is introduced by the boundary conditions (Sab, 1992), (Ostoja-Starzewski, 1998). This latter can be reduced in the case of periodic conditions (Kanit et al., 2003) but still exists. Figure 3 b) illustrates the evolution of the mean effective Young's modulus for different values of RVE size between 1.5 and 4 and an area fraction fixed at 5 %. The number of realizations for each RVE size is obtained so that the relative error ε_{rel} is less than 0.002. We observe a convergence of the effective property according to the RVE size around a mean value of 5.6. Besides, the standard deviation $D_Y(A)$ slightly decreases in the same time.

3.2 Number of realizations and calculation cost

Figure 3 b) exhibits the evolution of the number of realizations according to the RVE size for an area fraction fixed at 5 %. Here, the relative error ε_{rel} is 0.005. The CPU time to carry out the corresponding realizations is illustrated on the same figure. We observe the greater the RVE is, the lower the number of realizations is, the greater the CPU time becomes. Thus the investigation of the calculation cost does not exhibit an optimal value of RVE size but a steady evolution according to the same parameter. Hence, the suitable size has to be chosen by considering the convergence of the effective property Y that describes the influence of boundary conditions. Here we have consciously limited our study to a RVE size of 4 for which, on the one hand, the convergence in Y is observed and, on the other hand, the calculation cost stays reasonable.

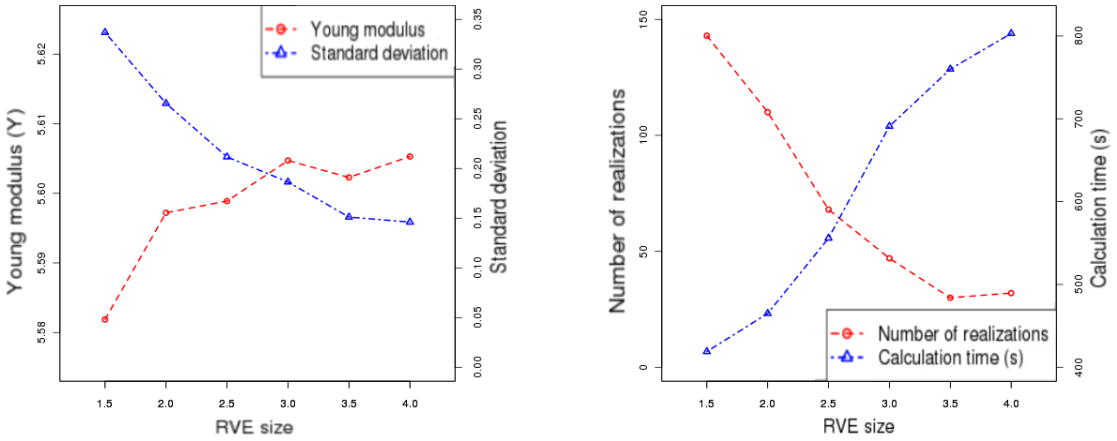

Figure 3. a) Parallel evolutions of the standard deviation and the Young's modulus according to the RVE size for a fibre area fraction fixed at 5%.
b) Parallel evolutions of the number of realizations and the corresponding calculation time according to the RVE size for a fibre area fraction fixed at 5% and a relative error of 0.005.

4 Comparison with bounds

Analytical bounds provide a limited approximation of the effective properties as bulk, shear and Young's moduli in the framework of the linear elasticity. Indeed microstructure and statistical informations are difficult to take into account in a micromechanics model. However, Hashin-Shtrikman's bounds (Hashin and Shtrikman, 1963), (Benveniste, 1987) as well as Halpin-Tsai's self-consistent estimates (Halpin and Kardos, 1976), (Wall, 1997) enable to perform an interesting comparison with numerical results. Here, we consider a comparative study with bounds under the hypotheses previously presented and the assumption of an effective isotropic medium.

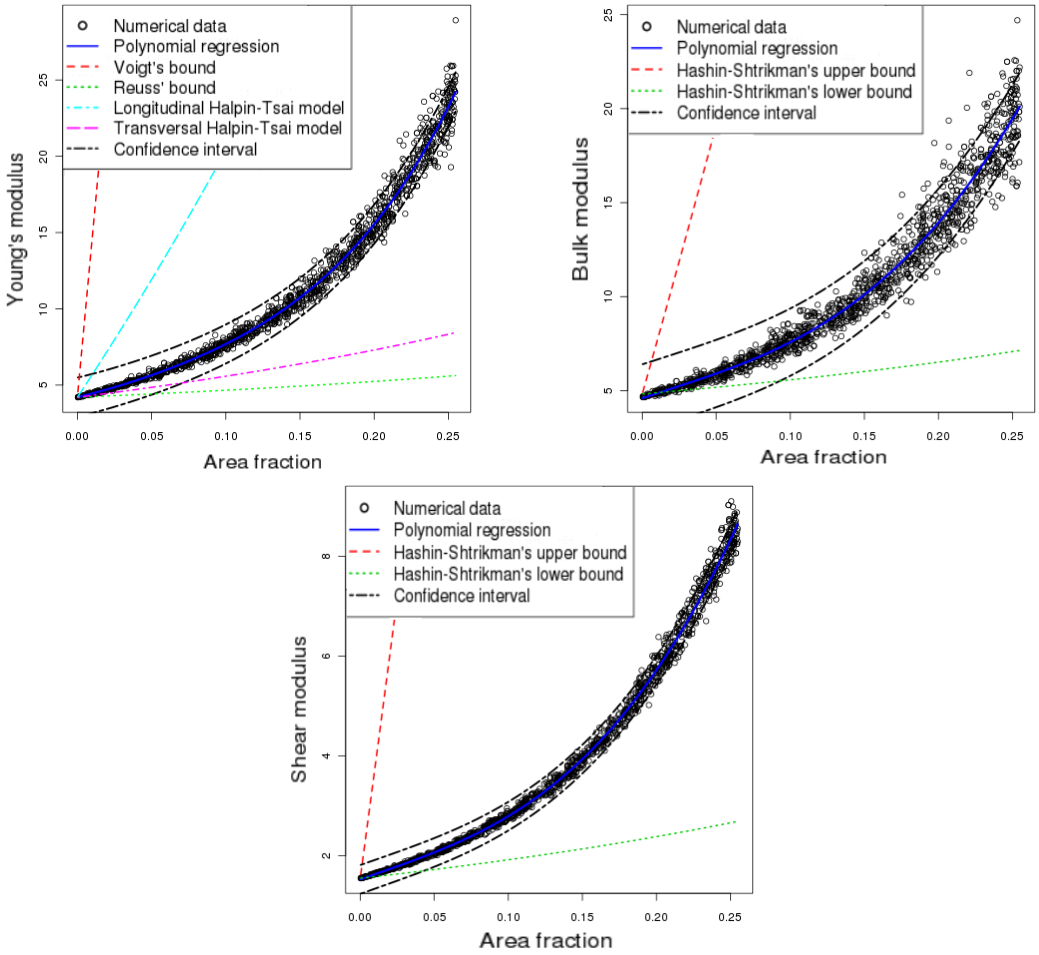

Figure 4. a) Evolution of the Young's modulus according to the fibre area fraction and comparison with Voigt and Reuss bounds and Halpin-Tsai estimates.
b) Evolution of the bulk modulus according to the fibre area fraction and comparison with Hashin-Shtrikman bounds.
c) Evolution of the shear modulus according to the fibre area fraction and comparison with Hashin-Shtrikman bounds.

First, the effective Young's modulus is investigated in comparison with Voigt and Reuss bounds and Halpin-Tsai's estimates (see Figure 4 a)) which are obtained by considering extreme cases of longitudinal and transversal orientations of the material (Villoria and Miravete, 2007). We notice that the mean curve increases continuously according to the load rate of fibres inside the RVE. All data are localized between the bounds and the interval confidence is very narrow around the fitting curve obtained by a multiple linear regression. Second, we consider a similar study for the effective bulk and shear moduli which are compared to Hashin-Shtrikman's bounds. Figures 4 b) and c) illustrate the evolutions of the two moduli according to the area fraction of fibres. We observe that our results are all localized between the bounds as well. Therefore, the comparisons allow us to suppose our results are conform to the bounds.

5 Results and discussion

In this section, the impact of some morphological features of fibres on the effective properties is studied. We consider the parameters of alignment, aspect ratio (or slenderness ratio) and distribution. According to several authors (Pötschke et al., 2003, 2004), (Jeulin and Moreaud, 2005, 2006b,a; Moreaud, 2006) the percolation phenomenon induces a significant improvement of effective properties. This phenomenon is related to the appearance of pathways inside the soft phase for a high load rate of fibres. This latter can be quantified by the statistical parameter of percolation threshold that corresponds to the required fibre area fraction to obtain 50% of RVEs for which the phenomenon is observed. Here, we evaluate both this parameter and elastic moduli for each discussed parameter. A final comparison of results is performed. It highlights a narrow link between percolation and reinforcement. Here, we consider RVEs for which both the representation and the material properties of fibres are the same as in the section 3.

5.1 Impact of fibre alignment

First, we suppose the fibres are not randomly oriented but perfectly aligned according to a preferential direction. In this case the composite material does not follow an elastic isotropic behaviour law anymore but an elastic orthotropic one according to the preferential direction. Contacts between inclusions are only allowed in their extremities. Figure 5 a) illustrates the evolution of the longitudinal Young's modulus according to the fibre area fraction, a comparison is made with the isotropic model and for three Gaussian models for which we consider a disruption of the alignment according to a Gaussian law. We remark that Young's moduli in the case of aligned fibres are drastically more important than for randomly oriented ones. Moreover, we can observe that the Gaussian models are scarcely affected by the amplitude of disruption (5, 15 or 25 degrees). The same figure exhibits the evolution for the shear modulus. In this case, the effective property is clearly diminished for aligned fibres and the disruption is much more significant. Thus the fibre alignment enhances the longitudinal effective properties to the detriment of transverse ones.

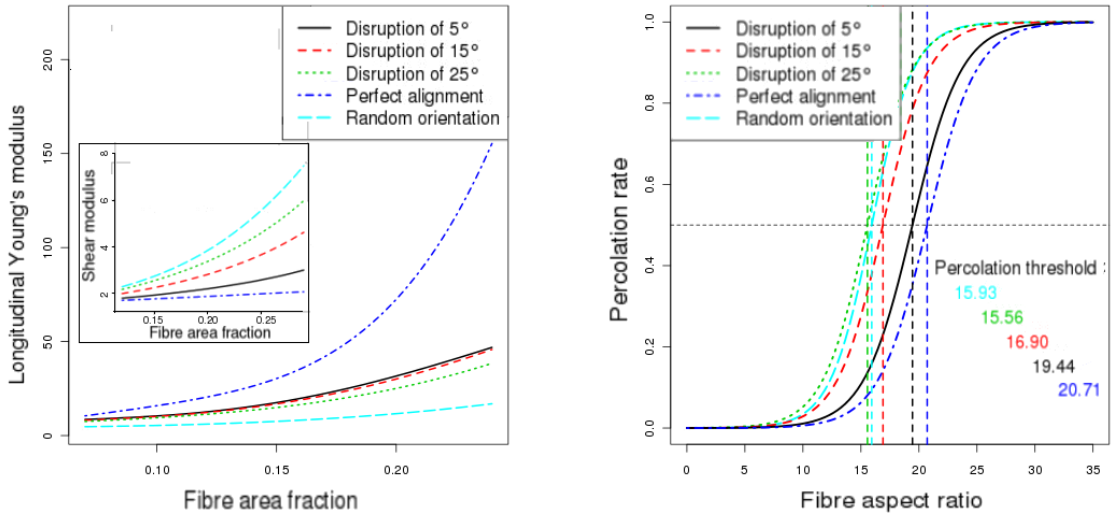

Figure 5. a) Evolution of effective Young's and shear moduli according to the fibre area fraction for aligned fibres.
b) Evolution of the percolation rate according to the fibre area fraction for aligned fibres.

An assessment of percolation rate was performed according to the method described by Jeulin and Moreaud (2006b) for the discussed models. A preliminary estimation was done in the case of an isotropic medium. The process consisted in generating a large data base of RVEs for which the percolation of the fibre network was subsequently evaluated. The results yielded a percolation threshold of 15.93 under the assumptions of randomly oriented fibres with aspect ratio 20. This value is near to different theoretical and empirical evaluations. Thus Sharma et al. (2006), in the framework of in-plane conductivity of spray metallic coatings, found a threshold close to 16. Other estimations done by Jeulin and Moreaud (Jeulin and Moreaud, 2006b, 2007) in the case of a 3D Boolean model of parallel cylinders gave percolation thresholds along axial and orthogonal directions of the axis of cylinders of 12.50 and 15.96. Their calculations for sphero cylinders with axis in the same plane and aspect ratio 5 yielded

percolation thresholds along axial and orthogonal directions of 12.94 and 16.125. Here, the estimations for aligned fibres give higher percolation thresholds except for the Gaussian model with a disruption of 25 degrees. Thus, the more the fibres are aligned the greater the percolation threshold is and the more the composite is strengthened along the preferential direction.

5.2 Impact of fibre aspect ratio

We investigate the parameter of aspect ratio that is the ratio between the length and the diameter of fibres. For this purpose, we suppose an isotropic medium of randomly oriented fibres. A calculation was performed on 4 values of aspect ratio : 10, 20, 50 and 100. Large samples of RVEs were constructed in each case for different lengths (and corresponding diameters) and area fractions. Furthermore, the RVE size is fixed at 4 except for the last value for which it is 8. Figure 6 a) exhibits the influence of the aspect ratio on the Young's modulus for different fibre area fractions. We observe that the more the fibres are slender the more the composite is reinforced. Besides, we remark that the RVE size affects our results if not properly chosen. Thus, the calculation of the effective Young's modulus is undermined in the case of an aspect ratio of 100 for which the RVE size is 4 and the fibre length is fixed at 1. A new calculation performed with RVEs of size 8 yield results in agreement with the linear behaviour of the effective property according to the aspect ratio.

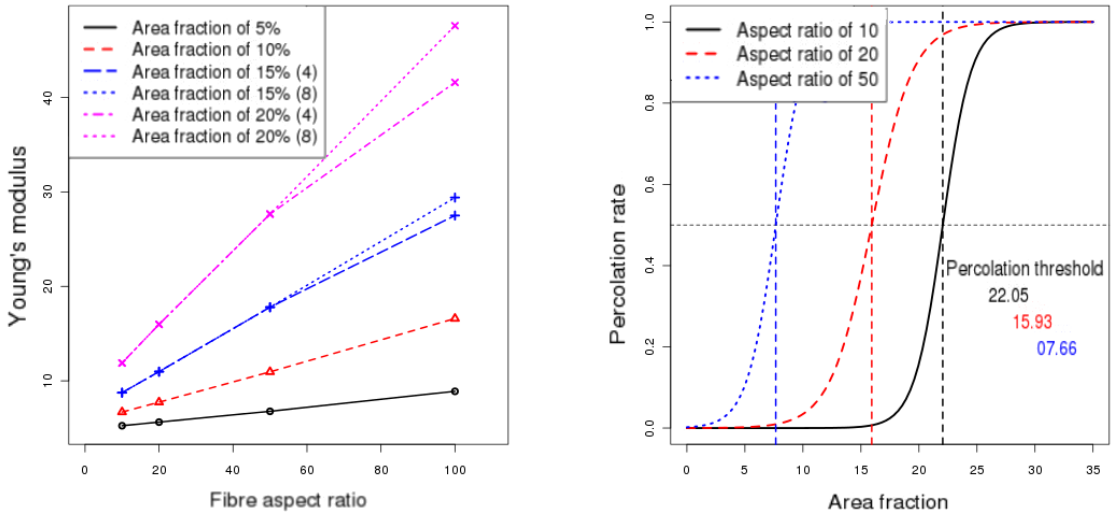

Figure 6. a) Evolution of the Young's modulus according to the fibre aspect ratio for different fibre area fractions.
b) Evolution of the percolation rate according to the fibre area fraction for different aspect ratios.

Figure 6 b) illustrates the influence of the aspect ratio on the percolation rate. The more the fibres are long and thin, the more the percolation phenomenon appears. Thus, the percolation threshold is multiplied by three, from 7.66 for aspect ratio of 50 to 22.05 for aspect ratio of 10. It turns out that the enhancement of effective Young's modulus is simultaneous to the appearance of percolation phenomenon.

5.3 Impact of fibre dispersion

A heterogeneous distribution of fibres inside the soft phase is well-known to influence the effective properties of fibre composites (Villoria and Miravete, 2007; Seidel and Lagoudas, 2006). The key issue is related to the real impact of the dispersion. Indeed, according to Jeulin and Moreaud (2007); Willot and Jeulin (2009, 2011), a suitable arrangement of 3D agglomerates inside the matrix enhances the effective properties of the material. Their works were based on a 2-scale Boolean scheme of spheres that models the distribution of clusters of fibres inside RVEs. Numerical estimations of percolation threshold performed by the authors in the case of heterogeneous media highlighted a simultaneous improvement of percolation and reinforcement. Here, we use the Boolean scheme to generate heterogeneous RVEs but we limit our study to circles with diameter equal to fibres' one. In other words, the scale factor between the inclusions and the agglomerates is fixed at 1. Figure 7 a) illustrates the scheme for which the RVE size is 4 and fibres are randomly oriented. The length of inclusions is fixed at 0.4 and the diameter at 0.02 so that the aspect ratio is 20. Figure 7 b) shows the corresponding final RVE with a mesh of 3-node triangular elements.

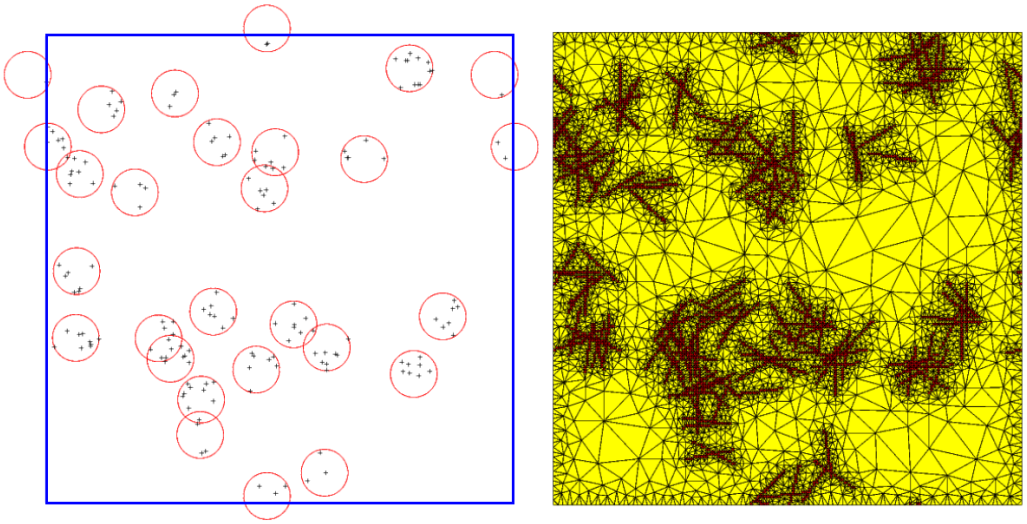

Figure 7. a) Boolean scheme of circles with centres of gravity of fibres.
b) Final RVE with mesh.

In a first step the percolation threshold of the Boolean scheme of circles was evaluated under the assumption of a random distribution of overlapping circles. A value of $a_c = 62.045$ was found that is largely higher than the one estimated in the case of spheres in 3D (28.95 according to Rintoul and Torquato (1997)). However the assessment is close to the threshold estimated by Quintanilla and Ziff (2007) in the case of 2D overlapping circles (67.635). Thus, the dispersion of fibres was investigated for an area fraction of circles more than a_c so that the percolation phenomenon might be possible. Figure 8 a) shows the impact of the area fraction of circles on the evolution of the Young's modulus according to the fibre area fraction. We observe that the lower the area fraction of circles is the lower the effective Young's modulus is. Moreover, figure 8 b) illustrates the influence of the dispersion of fibres on the percolation rate. The calculation of percolation thresholds yield values more than the one estimated in the case of a homogeneous distribution of inclusions. However the results obtained here are restricted to a scale factor fixed at 1 while the benefit of a fibre dispersion is only checked out for higher ratios according to Jeulin and Moreaud (2005, 2006b,a); Moreaud (2006).

6 Conclusions

The evaluation of effective elastic properties of 2D overlapping random fibre composites by Monte-Carlo draws of RVEs requires an accurate preliminary investigation. First, the RVE size can affect the results if not properly chosen. This one has to be sufficiently large to be representative of the heterogeneous material. Second, the minimal number of realizations has to be estimated by considering the evolution of the variance for a given expected error. Third, the representativeness of the pattern is related to the spatial arrangement, the morphology of fibres, the contrast of properties and the hypotheses of construction of the fibre network such as the authorization of overlaps. Therefore, the preliminary study must be repeated for each discussed configuration of fibres and fibre network.

The effective properties widely depends on the morphology of fibres. Thus, the alignment, the aspect ratio and the dispersion of fibres have a significant effect on the mechanical response. The dependance of properties on the configuration of fibres can be related to the percolation phenomenon which appears when fibres overlap and form some pathways inside the soft phase. This latter is quantified by the percolation threshold that is the required percolation rate to get 50 $\%$ of RVEs for which the phenomenon is observed. The calculation of the threshold for the discussed configurations highlight a narrow link between the enhancement of effective properties and the percolation. For example, long and thin fibres improve the phenonemon as well as they strengthen the material. However, this conclusion is only true for isotropic media. Thus, in the case of an alignment of fibres, the enhancement of longitudinal properties is simultaneous to an increase of percolation threshold.

The issue of the fibre dispersion is a key point to investigate. Here, we considered a Boolean scheme of circles to introduce a heterogeneous distribution of inclusions. A scale ratio between the RVE size and the diameter of circles was fixed at 10. Different parameters such as the scale factor between the size of agglomerates and the length of fibres, and the area fraction of circles inside each RVE affect the effective properties. Here the survey was restricted to a scale factor of 1 and an area fraction of circles from 60 $\%$ to 100 $\%$. The results showed a sensitive

diminishing of effective properties as well as an increase of percolation threshold under these hypotheses. However, a 2D inhomogeneous dispersion of fibres is more suitably simulated by considering higher scale factors. Thus, an in-depth study of this parameter is required as well as a 3D setting of the model with an n-order approximate geometry to detect possible dimensional effects.

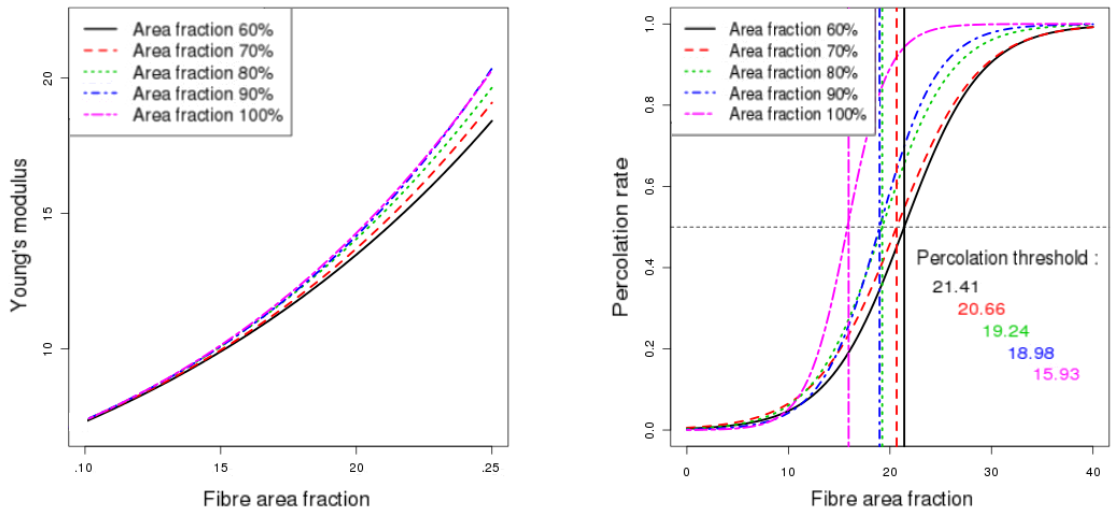

Figure 8. a) Evolution of the Young's modulus according to the fibre aspect ratio for different area fractions of circles.
b) Evolution of the percolation rate according to the fibre area fraction for different area fractions of circles.

Acknowledgments The authors wish to thank the regional council of Lower-Normandy for its financial support to Willy Leclerc's PhD.

References

Bensoussan, A.; Lions, J.; Papanicolaou, G.: *Asymptotic analysis for periodic structures*. Springer verlag, north holland, amsterdam edn. (1978).

Benveniste, Y.: A new approach to the application of mori-tanaka's theory in composite materials. *Mechanics of Materials*, 6, 2, (1987), 147 – 157.

Berger, M. J.; Colella, P.: Local adaptive mesh refinement for shock hydrodynamics. *J. Comput. Phys.*, 82, (1989), 64–84.

Drugan, W.; Willis, J.: A micromechanics-based nonlocal constitutive equation and estimates of representative volume element size for elastic composites. *Journal of the Mechanics and Physics of Solids*, 44, 4, (1996), 497 – 524.

Fisher, F. T.; Bradshaw, R. D.; Brinson, L. C.: Fiber waviness in nanotube-reinforced polymer composites–i: Modulus predictions using effective nanotube properties. *Composites Science and Technology*, 63, 11, (2003), 1689 – 1703, modeling and Characterization of Nanostructured Materials.

Halpin, J.; Kardos, J.: The halpin-tsai equations : a review. *Polymer Engineering and Science*, 16, 5, (1976), 344 – 352.

Hashin, Z.; Shtrikman, S.: A variational approach to the theory of the elastic behaviour of multiphase materials. *Journal of the Mechanics and Physics of Solids*, 11, 2, (1963), 127 – 140.

Iijima, S.: Helical microtubules of graphitic carbon. *Nature*, 354, (1991), 56 – 58.

Jeulin, D.; Moreaud, M.: Multi-scale simulation of random sphere aggregates - application to nanocomposites. 9th European Congress on Stereology and Image Analysis, Zakopane, Poland, (2005).

Jeulin, D.; Moreaud, M.: Percolation d'agrégats multi-échelles de sphères et de fibres - application aux nanocomposites. Congrés matériaux, Dijon, (2006).

Jeulin, D.; Moreaud, M.: Percolation of multi-scale fiber aggregates. S4G 6th international Conference, Prague, (2006).

Jeulin, D.; Moreaud, M.: Percolation of random cylinder aggregates. *Image Anal Stereol*, 26, (2007), 121 – 127.

Kanit, T.; Forest, S.; Galliet, I.; Mounoury, V.; Jeulin, D.: Determination of the size of the representative volume element for random composites: statistical and numerical approach. *International Journal of Solids and Structures*, 40, 13–14, (2003), 3647 – 3679.

Moreaud, M.: *Propriétés morphologiques multi-échelles et prévision du comportement diélectrique de nanocomposites*. Ph.D. thesis, Ecole des Mines de Paris, Centre de Morphologie Mathématique, Fontainebleau (2006).

Oberlin, A.; Endo, M.; Koyama, T.: Filamentous growth of carbon through benzene decomposition. *Journal of Crystal Growth*, 32, 3, (1976), 335 – 349.

Odegard, G. M.; Gates, T. S.; Wise, K. E.; Park, C.; Siochi, E. J.: Constitutive modeling of nanotube-reinforced polymer composites. *Composites Science and Technology*, 63, 11, (2003), 1671 – 1687, modeling and Characterization of Nanostructured Materials.

Ostoja-Starzewski, M.: Random field models of heterogeneous materials. *International Journal of Solids and Structures*, 35, 19, (1998), 2429 – 2455.

Pötschke, P.; Alig, I.; Dudkin, S.: Dielectric spectroscopy on melt processed polycarbonate-multiwalled carbon nanotube composite. *Polymer*, 44, 17, (2003), 5023 – 5030.

Pötschke, P.; Bhattacharyya, A. R.; Janke, A.: Melt mixing of polycarbonate with multiwalled carbon nanotubes: microscopic studies on the state of dispersion. *European Polymer Journal*, 40, 1, (2004), 137 – 148.

Quintanilla, J. A.; Ziff, R. M.: Asymmetry in the percolation thresholds of fully penetrable disks with two different radii. *Phys. Rev. E*, 76, (2007), 051115.

Rintoul, M. D.; Torquato, S.: Precise determination of the critical threshold and exponents in a three-dimensional continuum percolation model. *Journal of physics A.*, 30, (1997), 585 – 592.

Sab, K.: On the homogenization and the simulation of random materials. *European journal of mechanics*, 11, 5, (1992), 585 – 607.

Sanchez-Palencia, E.: *Non-homogeneous media and vibration theory*, vol. 127 (1980), berlin.

Seidel, G. D.; Lagoudas, D. C.: Micromechanical analysis of the effective elastic properties of carbon nanotube reinforced composites. *Mechanics of Materials*, 38, 8-10, (2006), 884 – 907, advances in Disordered Materials.

Shaffer, M.; Windle, A.: Fabrication and characterization of carbon nanotube/poly (vinyl alcohol) composites. *Advanced Materials*, 11, 11, (1999), 937 – 941.

Shao, L. H.; Luo, R. Y.; Bai, S. L.; Wang, J.: Prediction of effective moduli of carbon nanotube-reinforced composites with waviness and debonding. *Composite Structures*, 87, 3, (2009), 274 – 281.

Sharma, A.; Gambino, R. J.; Sampath, S.: Anisotropic electrical properties in thermal spray metallic coatings. *Acta Materialia*, 54, 1, (2006), 59 – 65.

Villoria, R. G. D.; Miravete, A.: Mechanical model to evaluate the effect of the dispersion in nanocomposites. *Acta Materialia*, 55, 9, (2007), 3025 – 3031.

Wall, P.: A comparison of homogenization, hashin-shtrikman bounds and the halpin-tsai equations. *Application of Mathematics*, 42, 4, (1997), 245 – 257.

Willot, F.; Jeulin, D.: Elastic behavior of composites containing boolean random sets of inhomogeneities. *International Journal of Engineering Science*, 47, 2, (2009), 313 – 324, dedicated to Valery Levin's 70th Birthday.

Willot, F.; Jeulin, D.: Elastic and electrical behavior of some random multiscale highly-contrasted composites. *International Journal of Multi-scale Computational Engineering*, 9, 3, (2011), 305 – 326.

Address: Willy Leclerc, Philippe Karamian, Alexandre Vivet and Alain Campbell,
University of Caen Lower-Normandy, Mathematics laboratory Nicolas Oresme, Campus 2, Bld maréchal Juin, 14032 Caen.
email: willy.leclerc@unicaen.fr; philippe.karamian@unicaen.fr.